NOAA Technical Report NOS 95 NGS 24

Proceedings of Symposium No. 5: Geodetic Applications of Radio Interferometry

International Association of Geodesy
Tokyo, Japan
May 7—8, 1982

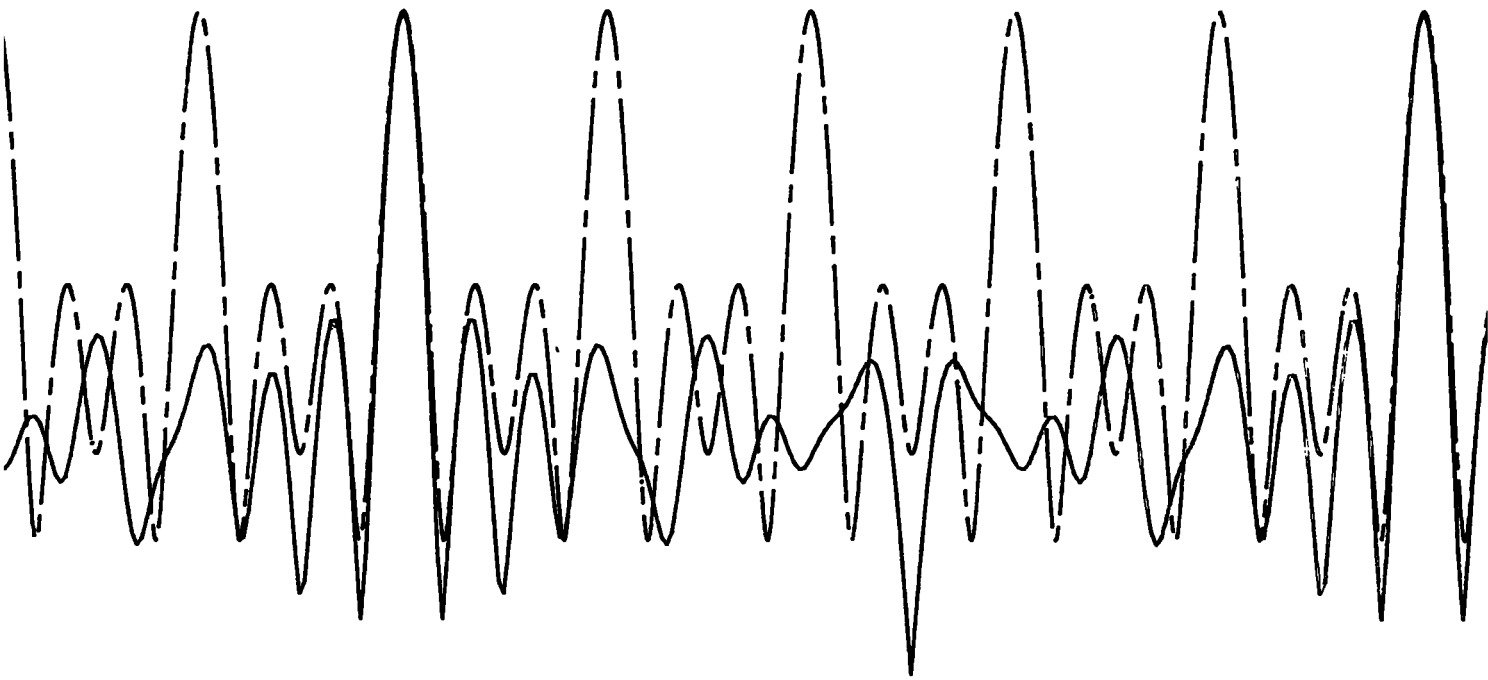

1982
U.S.DEPARTMENT OF COMMERCE
National Oceanic and Atmospheric Administration
National Ocean Survey

Cover sketch: VLBI delay resolution functions. (See Robertson and Carter, "Operation of the National Geodetic Survey POLARIS network," p. 63.)

NOAA Technical Report NOS 95 NGS 24

Proceedings of Symposium No. 5: Geodetic Applications of Radio Interferometry

International Association of Geodesy
Tokyo, Japan
May 7—8, 1982

William E. Carter, Convenor
National Geodetic Survey

A. Tusuchiya, Co-convenor
Tokyo Astronomical Observatory

U.S. DEPARTMENT OF COMMERCE
Malcolm Baldrige, Secretary

National Oceanic and Atmospheric Administration
John V. Byrne, Administrator

National Ocean Survey
R. Adm. H.R. Lippold, Jr., Director

SPONSORS

IAG Special Study Group 2.51, Radio Interferometry

International Association of Geodesy

International Union of Geodesy and Geophysics

**For sale by the National Geodetic Information Branch, NOS/NOAA,
Rockville, MD 20852, price in U.S. dollars $14.00
(Make check payable to: National Geodetic Survey)**

PREFACE

This volume contains the proceedings of Symposium No. 5, "Geodetic Applications of Radio Interferometry," of the International Association of Geodesy (IAG) General Meeting held in Tokyo, Japan, May 7-8, 1982. The symposium was organized by Special Study Group (SSG) 2.51 on Radio Interferometryt The membership of SSG 2.51 is listed on page v. Thirty-six technical papers were presented during seven 90 minute sessions. The symposium concluded with an eighth session devoted to answering complex questions and discussing issues that could not be accommodated during the presentations of the papers.

The program listed on pages ix through xii was organized by the Technical Program Committee, composed of W. E. Carter (Chairman), W. J. Klepczynski, and W. E. Stranget The membership was selected to obtain balanced representation of the Very Long Baseline Interferometry (VLBI), Connected Element Interferometry (CEI), and Electronic Satellite Tracking techniques. In an attempt to obtain comprehensive coverage of the various facets of geodetic radio interferometry, the Technical Program Committee first selected specific subjects for each session of the symposiumt Then, based on current literature and personal knowledge of the programs and activities of various organizations and individuals, the committee invited more than 15 papers. The authors of invited papers received no special status or financial support to attend the symposium but the response was, nonetheless, excellentt The only plan that had to be abandoned was a session dedicated to the geodetic uses of the newly developing Global Positioning Satellite (GPS) System. (A comprehensive report on the GPS activities is contained in the Proceedings of the Third International Geodetic Symposium on Satellite Doppler Positioning, Las Cruces, New Mexico, February 1982.)

The final program included the invited papers and contributed papers which were received in response to a call for papers. Only those contributions for which the authors pledged completed manuscripts suitable for publication were accepted. Unfortunately, two authors did not submit completed manuscripts, and, therefore, the proceedings contain a total of only 34 papers.

The Technical Program Committee also assembled a list of potential session chairmen, and requested their participation and support on the same basis as the authors of invited papers. Again, the response was immediate and supportive. The session chairmen are listed on page vii.

All of the arrangements for the meeting rooms, registration, accommodations, and the many other tasks that must be accomplished to stage an internationally attended symposium were performed by the IAG Japanese Local Organizing Committee. Most of the sessions were attended by more than 200 scientists. The facilities were more than adequate, the staff of typists, projectionists, and other support personnel was efficient and courteous, and the Japanese hospitality produced many pleasant memories for the participants.

The proceedings were assembled and published by the National Geodetic Survey of the National Oceanic and Atmospheric Administration from camera ready typescripts and illustrations provided by the authors. We chose this method to minimize the cost and time required to complete the proceedings, realizing that minimizing the delay in distributing the papers was particularly important in

such a rapidly advancing subject area. We are indebted to the many people at the various organizations who prepared the camera copyt The manuscripts generally conformed to our guidelines and were of excellent quality. The members of SSG 2.51 would also like to express their thanks to Eleanor Z. Andree, NGS, for her assistance in assembling the final copy and shepherding it through the publishing processt

MEMBERSHIP LIST

Special Study Group 2.51

Professor Allen Joel Anderson
Department of Geodesy
Box 556, University of Uppsala
Uppsala, Sweden S-751 22

Dr. Kai Borre
Aalborg University Centre
P.O. Box 159
DK-9100 Aalborg
Denmark

Prof. E. Boschi
Istituto di Fisica "A. Righi"
Via Irnerio, 46
40126 Bologna
Italy

Dr. Claude Boucher
Institut Geographique National
2 Av. Pasteur
Saint-Mande, France 94160

Dr. James Campbell
Geodetic Institute, Bonn University
Nussallee 17, D-5300
Bonn
Federal Republic of Germany

Dr. Wayne H. Cannon
York University
Earth Sciences
Room 101t, Petrie Science Bldg.
4700 Keele Street
Toronto, Ontario
Canada, M3J 1P3

Dr. William E. Carter (President)
National Geodetic Survey, C124
NOAA-National Ocean Survey
6001 Executive Blvd.
Rockville, Maryland 20852
United States of America

Dr. Thomas A. Clark
Goddard Space Flight Center
Code 693
Greenbelt, Maryland 20771
United States of America

Dr. Charles C. Counselman, III
Deptt of Earth & Planetary Sciences
Massachusetts Institute of Technology
Room 54-626
Cambridge, Massachusetts 02139
United States of America

Professor Fang Chun
Director, Institute of Geodesy
and Geophysics
Academia Sinica
Wuhan
People's Republic of China

Dr. Nobuhiro Kawajiri
Space Research Section
Radio Research Laboratories
Kashima Branch
893-1 Hirai, Kashima-machi, Ibaraki-ken
Japan

Dr. W. J. Klepczynski
U. S. Naval Observatory
34th and Massachusetts Avenue
Washington, D. C. 20390
United States of America

Mr. Ian Lloyd
Senior Surveyor
Australian Survey Office
P.O. Box 2
Belconnen, A.C.T. 2616
Australia

Dr. William G. Melbourne
Jet Propulsion Laboratory
Bldgt 264, Rm 748
4800 Oak Grove Drive
Pasadena, California 91011
United States of America

Dr. George Nicholson
Radio Astronomy Observatory
National Institute for
Telecommunications Research
P.O. Box 3718
2000 Johannesburg
Republic of South Africa

Dr. A. R. Robbins
Deptt of Surveying & Geodesy
University of Oxford
62 Banbury Road
Oxford, England

Dr. Alan E. E. Rogers
NEROC Haystack Observatory
Westford, Massachusetts 01886
United States of America

Dr. R. Schilizzi
Radiosterrenwacht
Oude Hoogeveensedijk 4
7991 PD Dwingeloo
The Netherlands

Professor Atushi Tsuchiya
Tokyo Astronomical Observatory
University of Tokyo
Mitaka, Tokyo, 181
Japan

Dr. Ye Shu-Hua
Shanghai Observatory
Academia Sinica
Shanghai
People's Republic of China

SESSION CHAIRMEN

Session 1
Dr. William G. Melbourne
Jet Propulsion Laboratory
California Institute of Technology
4800 Oak Grove Drive
Pasadena, CA 91109
United States of America

Session 2
Dr. Ewald Reinhart
Institut Fur Angewandte Geodasie
D-6000 Frankfurt a. M.
Richard - Strauss - Allee 11
Federal Republic of Germany

Session 3
Mr. Richard J. Anderle
Naval Weapons Research Laboratory
Dahlgren, VA 22448
United States of America

Session 4
Dr. Hermann Seeger
Geodatisches Institut der Universitat Bonn
Nussallee 17½ D-53 Bonn 1
Federal Republic of Germany

Session 5
Professor Atushi Tsuchiya
Tokyo Astronomical Observatory
University of Tokyo
Osawa 2-21-1
Mitaka, Tokyo, 181
Japan

Session 6
Dr. Claude Boucher
Institut Geographique National
2 Avenue Pasteur
94160 St. Mande
France

Session 7
Dr. Allen J. Anderson
Department of Geodesy
Box 556 - University of Uppsala
Uppsala, Sweden S-751 22

Session 8
Dr. William E. Carter
National Geodetic Survey, NOS NOAA
Rockville, Maryland 20852
United States of America

Blank page retained for pagination

SYMPOSIUM PROGRAM
AND
TABLE OF CONTENTS

* This paper was submitted late and was presented when time allowed during a later session.

Session 3 - Radio Interferometric Surveying

Chairman: R. J. Anderle

Session 4 - VLBI Systems

Chair eger

** No manuscript submitted for publication.

Session 5 - Atmospheric Ionospheric

Chairman: A. Tsuchiya

Session 6 - New Instrumentation, Facilities, and Techniques

Chairman: C. Boucher

Session 7 - Planned Activities

Chairman: A. J. Anderson

Session 8 - Discussions

Chairman: W. E. Carter

Discussion and Summary (No transcripts available)

EXTRAGALACTIC RADIO SOURCES AS GEODETIC TARGETS: STRUCTURE, PROPER MOTION, LIFETIMES

K. I. Kellermann

National Radio Astronomy Observatory*
P. O. Box 2
Green Bank, West Virginia 24944, U.S.A.

ABSTRACT: Compact radio sources associated with quasars and galactic nuclei are excellent targets for geodetic measurements. But many sources have a finite angular size with an asymmetric and wavelength dependent brightness distribution. Dual-wavelength observations used to eliminate the effect of ionospheric bending may therefore be difficult to interpret. A further complication is the apparent component motions which can cause a shift in the luminosity centroid in just a few years. Comparable position shifts may be caused by the frequent flaring and fading of spatially separated components. Because the precision of individual position measurements is approaching a milliarc second, detailed radio pictures as a function of wavelength and time are necessary to interpret geodetic VLBI observations. Measurements made with simple 2 or 3 element interferometers can lead to ambiguous results.

INTRODUCTION

Extragalactic radio sources are among the largest known objects in the universe, and are typically resolved with interferometer baselines of a few kilometers. Typically, the radio emission comes from two clouds symmetrically located with respect to the parent galaxy or quasar. It is widely accepted that the radio emission comes from ultra-relativistic electrons moving in a weak magnetic field. The origin of energy, and the manner in which the electrons are accelerated and transported into the extended radio lobes, is not understood, but the basic energy source appears to be closely associated with quasars or with the nuclei of active galaxies.

The quasars or galactic nuclei are themselves very compact sources of radio emission. Within these sources the density of relativistic electrons is so great that the radio source becomes opaque to its own radiation below some cutoff frequency, ν_o. For $\nu << \nu_o$, $S \propto \nu^{2.5}$. For $\nu >> \nu_o$, the radio

* Operated by Associated Universities, Inc., under contract with the National Science Foundation.

spectrum is a simple power law of the form $S \propto \nu^{\alpha}$ where the spectral index, α, is $(1-\gamma)/2$, and where γ is the index of the electron density distribution.

Because there may be a distribution of relativistic electron density and magnetic field strength, different parts of the source may become opaque at different wavelengths and the observed total flux density will be nearly independent of frequency. Such sources are said to have "flat" spectra in contrast to the "peaked" spectra typical of more uniform sources.

In sources with peaked spectra the radio emission generally comes from two components of similar size and flux density and spaced a few hundredths of an arc second apart (Phillips and Mutel 1980). These are ideal geodetic targets since the position of the centroid is well defined and is found to be essentially independent of observing frequency and time. Compact sources of this type can be generally recognized on the basis of their characteristic spectra, but detailed radio pictures are desired if they are to be used as the basis of geodetic measurements.

In general, however, the radio structure is more complex, is wavelength dependent, and changes significantly on time scales of a year. These all lead to variations in the observed phase or group delay of geodetic observations made with radio interferometers and may lead to errors in the determination of terrestrial baselines. The baseline error introduced by source structure depends on the length (in wavelengths) and orientation of the baseline. On transcontinental and intercontinental baselines, phase deviations $\sim 2\pi$ are not uncommon, and correspond to baseline errors comparable to the observing wavelength, which is typically a few centimeters.

SOURCE STRUCTURE

Most extragalactic radio sources appear to be highly elongated over a wide range of dimensions. In those quasars and radio galaxies where the compact component is relatively strong, the radio source is generally asymmetric and consists of a low luminosity "jet" feature extending up to a million parsec or more from a bright nucleus. When examined with high resolution, the nucleus itself is also elongated consisting of a jet-like feature extending from a small core component in the same direction as the more extended jet. The similar direction of the jet over a wide range of linear scales suggests that the mechanism responsible for the focus or collimation takes place within a few parsecs of the basic "engine" and lasts at least 10^7 years.

Because of this asymmetry, the position of the centroid may depend dramatically on resolution. Figure 1 shows the structure of the bright quasar 3C273. If observed with a simple 2-element interferometer, the effective position will depend on the interferometer resolution. Thus, baseline vectors determined from measurements of group velocity or interferometer phase are not uniquely determined from two-element interferometry unless the source dimensions are small compared with the interferometer fringe spacings, or complete images are obtained with multi-element aperture

synthesis techniques, and then used to model the apparent position centroid for any specific interferometer configuration.

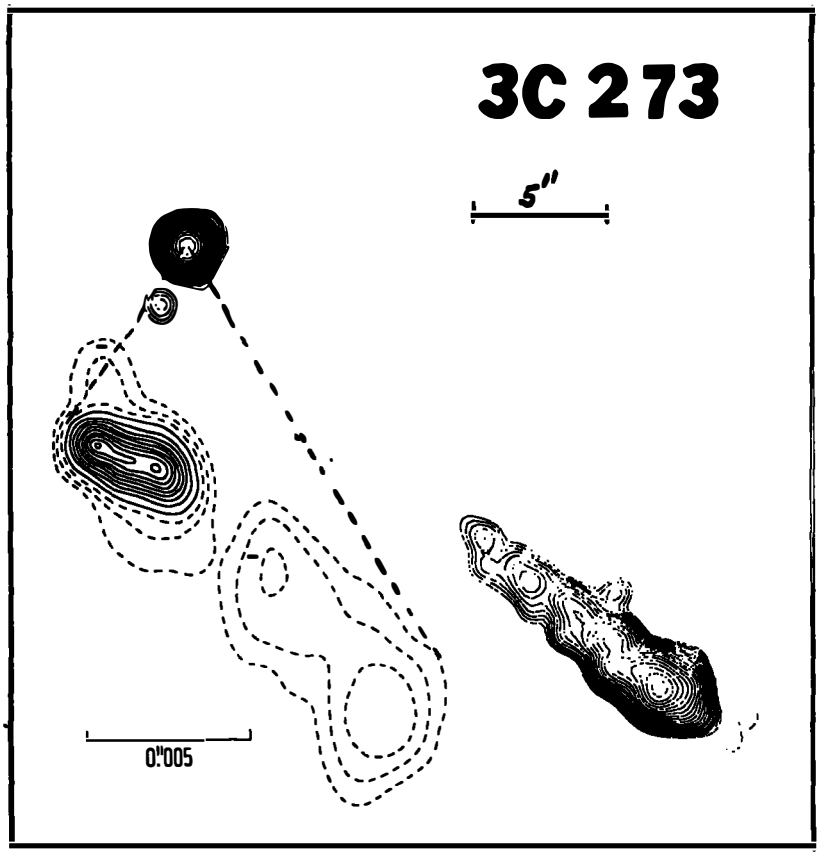

Figure 1. Radio structure of the quasar taken from Conway (1982) and Pauliny-Toth et al. (1981).

FREQUENCY DEPENDENT STRUCTURE

A further complication occurs because the brightness distribution is often frequency dependent. This is because in the opaque parts of the source the flux density varies as $\nu^{2.5}$, while for transparent sources it varies $\sim \nu^{-1}$. So the brightness ratio will vary as $\nu^{3.5}$. Thus, if two components, one transparent and the other opaque, have equal flux density, $S_1 = S_2$ at frequency ν_o, then at frequency $\nu_1 = 2\nu_o$,

$$S_2/S_1 = 2^{3.5} \sim 10.$$

In other words, a shift of a factor of two in observing frequency gives an order of magnitude change in relative flux density. In a more complex (real) source there is a mixture of partially opaque and transparent regions, so the effective exponent is typically about 1, rather than 3.5, but nevertheless brightness distribution at two wavelengths separated by only a factor of two or three in frequency apart may be sufficiently different that individual features cannot be unambiguously aligned.

Thus, dual frequency observations which are commonly used to correct for ionospheric bending may be easily misinterpreted, unless full images are obtained at each observed wavelength, and the alignment of particular spectral features is properly made.

Using 3C273 as an example, at wavelengths $\lambda \sim 1$ m most of the flux from the compact source comes from the 0".05 jet-like feature, while for $\lambda \sim 1$ cm, the smaller northern core dominates. The apparent shift in the position centroid between 3.8 and 13 cm is ~ 4 milliarc seconds, which is considerably more than the internal precision of current position determinations (e.g. Ma, Clark, and Shaffer 1982).

COMPONENT MOTION

Perhaps the most difficult obstacle to using compact radio sources to carry out a long term geodetic program is the temporal changes in structure which occur due to the brightening and fading of different parts of the source or to actual component proper motions. Hot spots in jets may propagate with nearly the velocity of light, and if the motion is oriented close to the line of sight, the effect of differential signal travel time from components at rest and at motion may cause an apparent transverse velocity which is many times greater than the velocity of light (e.g. Kellermann and Pauliny-Toth 1981). The corresponding shifts in the radio centroid may be of the order of a milliarc sec per year (e.g. Walker 1982).

This is illustrated in Figure 2, again using the quasar 3C273. Figure 2 is taken from Pearson et al. (1981) and shows the relative motion of the jet component of 3C273 during the period 1978 to 1980. In Figure 3 this motion is traced back to 1972 and it is seen that during the period 1972 to 1980 there was a total motion of about 6 milliarc sec or a shift of 3 milliarc sec in the position of the centroid.

The situation is further complicated since the outer feature in 3C273 has now faded from sight, and so the apparent position has suddenly shifted back toward the core.

SUMMARY

VLBI observations of compact radio sources have a repeatability of about 1 milliarc second, and the corresponding baseline vectors between two VLBI stations show a scatter of only a few centimeters. Since it is generally not possible to observe unresolved "point" radio sources, multi-element mapping of the angular brightness distribution is needed if

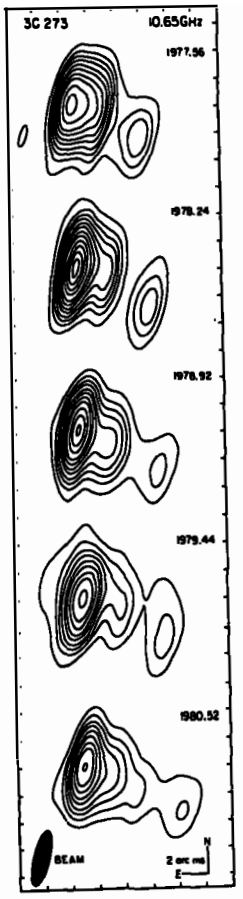

Figure 2. Structure of 3C273 showing apparent component motion between 1977 and 1980 (taken from Pearson et al. 1981)r

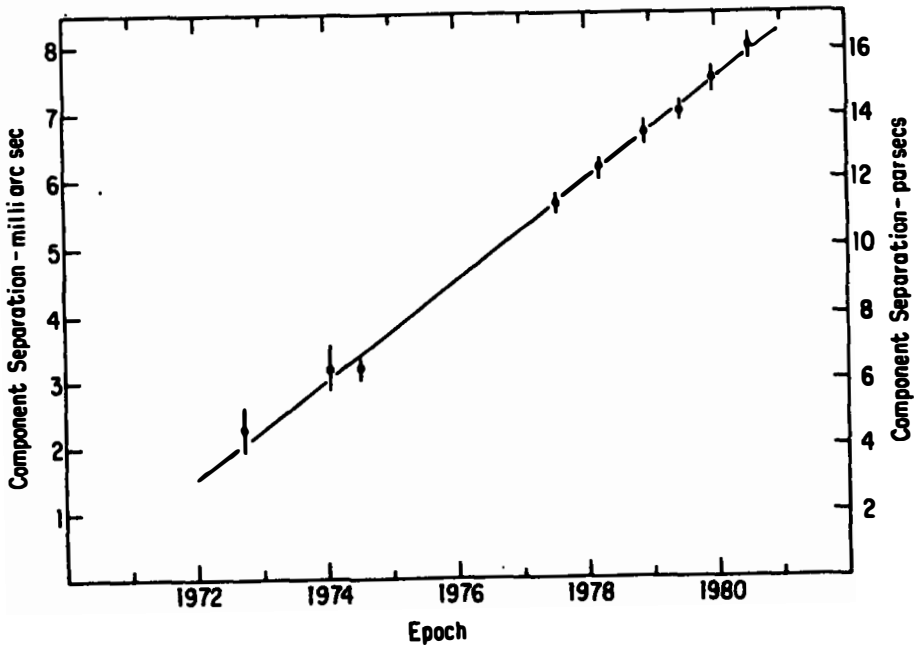

Figure 3. Separation of the components of 3C273 as a function of timer

celestial radio sources are used as targets for geodetic measurements. Particular attention to the wavelength dependence of the radio structure is needed when multi-wavelength observations are used to determine the effect of ionospheric refraction. Long term measurements of baseline changes may be difficult to distinguish from variations in the angular structure unless multi-epoch images are available.

References

Conway, R. 1982: The Radio Jet of 3C273, I.A.U. Symposium No. 97, p. 167, Reidel, Dordrecht, (ed.) D. S. Heeschen and C. M. Wade.

Kellermann, K. I. and Pauliny-Toth, I. I. K., 1981: Compact Radio Sources, An. Rev. Astr. and Astrophys. 19, 373.

Ma, C., Clark, T. A., and Shaffer, D. B. 1982, Astrometry and Epoch J 2000, Bull. Am. Astr. Soc. 13, 899.

Pauliny-Toth, I. I. K., et al. 1981: 6-cm Observations of Compact Radio Sources, Astron. J. 86, 371.

Phillips, R. B. and Mutel, R. L. 1980: High Resolution Observations of the Compact Radio Sources CTD93 and 3C395 at 1671 MHz, Ap. J. 236, 89.

Pearson, T. J. et al. 1981: The Superluminal Expansion of the Quasar 3C273, Nature 290, 365.

Walker, R. C. et al. 1982: Rapid Structural Variations in 3C120, Ap. J. 257, 56.

RADIO SOURCE REFERENCE FRAMES

K. J. Johnston
E. O. Hulburt Center for Space Research
Naval Research Laboratory
Washington, D. C. 20375

J. S. Ulvestad
National Radio Astronomy Observatory
Charlottesville, Virginia 22901

ABSTRACT: The current precision of the positions of compact radio sources is at or below 0".01. However there appear to be discrepancies at this level in aligning the catalogs. A short radio reference catalog is presented and meant to define an almost inertial reference frame. Recommendations are made for presenting future observations in reference epoch 2000 and for the observation of common sources by different observers in order to improve the intercomparison of the different catalogs. This will lead to improved values for the precession constant, nutation series and other earth rotation parameters.

INTRODUCTION

For geophysicists the interest in radio source catalogs may be stated as follows: Radio source catalogs define an almost inertial reference frame against which motions of objects on the earth, motions of the earth, objects in the near earth environment (satellites), and objects on the celestial sphere (planets, stars, and galaxies) may be determined. Other applications are in astrometry and astrophysics. The status as of May 1982 of the positional accuracy of these catalogs and the need for uniformity in future catalogs are the subject of this paper.

The positional accuracy of radio sources has improved steadily since the 1970's. Surveys at radio frequencies near 2.5 and 5 GHz (Pauliny-Toth et al. 1978: Shimmins et al. 1975) contain almost all radio sources with flux density $\geq$ 0.5 Jy at galactic latitudes greater than 10°. These sources have angular structure ranging from $\sim$ 0".0001 to $\sim$ 60". Johnston et al. (1982) have been able to determine the characteristics of these sources and estimate that there are $\sim$ 1500 extragalactic sources of intensity > 0.6 Jy over the entire celestial sphere and that $\sim$ 20% of these sources will have the majority of their emission in unresolved or point like components of milliarc second scale, making these sources suitable for defining an inertial reference frame. Therefore the number of strong radio sources defining a reference system will be smaller than that contained in the fundamental optical catalog (FK4), which contains 1535 fundamental stars.

The distribution of sources should be uniform over the sky, so that precise measurements of the relative positions of the antennas can be made at any time. There is a need for sources distributed near declinations of 80°, 60°, 40°, 20°, 0°, -20°, -40°, -60°, -80°, separated by 90° in right ascension. This is a total of only 36 sources. For Very Long Baseline (VLB) observations with the longest baselines, i.e., Goldstone to Tidbinbilla, the catalog must contain considerably more sources because only a small fraction of the

celestial sphere is visible at both sites simultaneously. These sources must be intense enough ($\sim$ 1 Jy) to be visible with a minimum size antenna pair (each antenna 20 m in diameter) and have small apparent sizes ($\sim$ 1 mas) and positional stability (1 mas) on the sky. Catalogs that contain the required number and spatial distribution are the JPL catalog as defined by Purcell et al. (1980) and the catalog of Witzel and Johnston (1982). The source distribution on the sky for the Witzel and Johnston (1982) catalog is displayed in Figure 1.

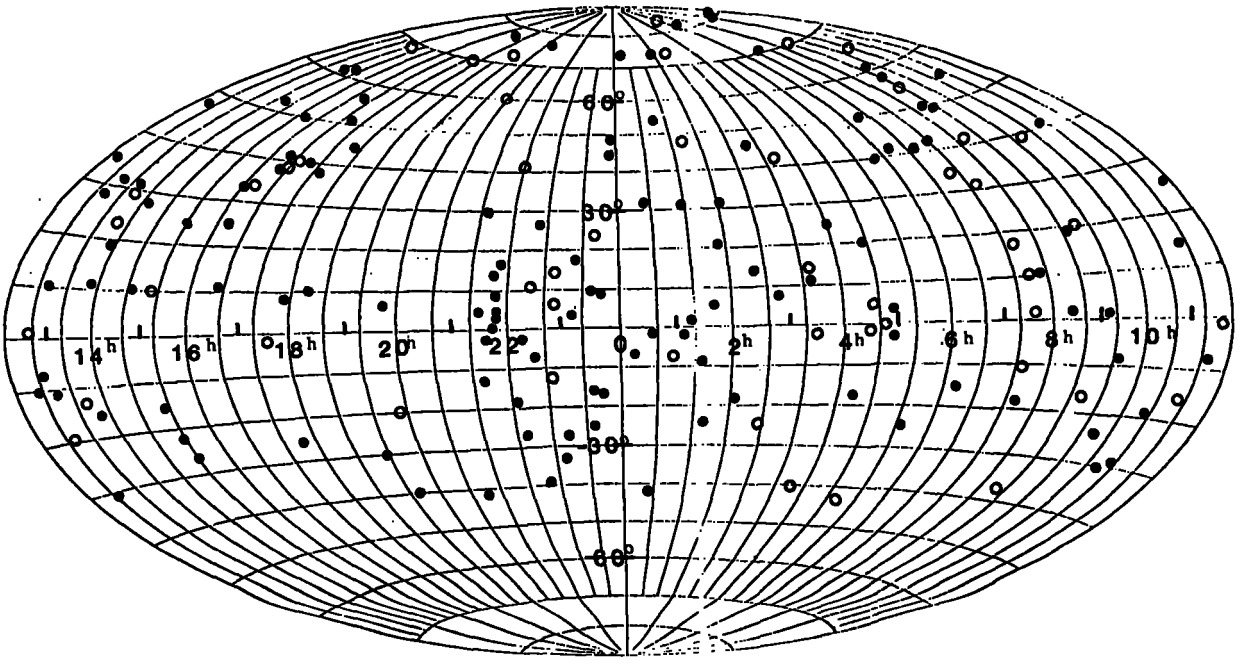

Figure 1. The distribution of sources on the celestial sphere in the Witzel and Johnston (1982) compilation. There are 188 sources. ● denotes sources with positional accuracy $\leq$ 0".05. o denotes sources with positional accuracy $\leq$ 0".01 or for sources $\delta \leq -20°$ with accuracy < 0".03.

Inspection of Figure 1 shows that precise positions of extragalactic sources south of declination -40° have not yet been measured as of May 1982. Measurements need to be made in the southern hemisphere.

AVAILABLE PRECISE CATALOGS

Recent high resolution surveys of radio sources have shown that there is an adequate number of compact sources. In a VLA survey of the complete sample of radio sources of flux density > 1 Jy north of declination -40 degrees, and galactic latitude b $\geq \pm$ 10°, 262 sources were found to contain 90% their flux density at 5 GHz in components less than 1" (Ulvestad, Johnston, Perley, and Fomalont 1981). In another survey at 2.3 GHz, Preston and Moribito (1980) found that 52 sources display a flux density greater than 1 Jy, 210 sources a flux density greater than 0.5 Jy and 665 sources a flux density greater than 0.1 Jy on size scales of $\leq$ 5 mas.

TABLE 1

CATALOGS OF RADIO SOURCE POSITIONS

Authors	Instrument	Number of Sources	Precision	Observing Epoch	Reference Epoch
Connected Element Interferometry					
Elsmore & Ryle (1976)	Cambridge	55	0".03	1973.1; 1974.2	1950
Elsmore (1982)	Cambridge	25	0.03	1979.8	1950
Hilldrup et al.(1982)	VLA	29	0.02	1980.0	1950, 2000
Kaplan et al. (1982)	Green Bank	16	0.01	1979.9	1950, 2000
Perley (1982)	VLA	393	0.05	1981.0	1950
Wade and Johnston (1977)	Green Bank	34	0.03	1975.4	1950, 2000
Ulvestad et al. (1981)	VLA	250	0.10	1979.10	1950
Very Long Baseline Interferometry					
Clark et al. (1976)	US-Europe	18	0.04	1973.9	1950
Purcell et al. (1980)	Madrid-Goldstone-Tidbinbilla	117	< 0.01	1978.0	1950
Shaffer et al. (1982)	US-Europe	48	0.005	1981.5	2000

Progress in measuring the positional accuracy of radio sources up to 1978 is summarized in Johnston et al. (1980). The earlier measurements were very poor near the equ Wade and Johnston measured thirty-four sources ranging i from -20° to +70° to accuracies below 0".08. In 1978 Fanselow measured positions of sources from declination -40° to 70° with accuracies below 0".03.

A summary of high accuracy catalogs of radio positions is shown in Table 1. This summary contains all catalogs having original measurements with quoted accuracies of 0".1 to 0".05 which have a large number of sources and all catalogs quoting accuracies better than 0".05. The catalogs are broken up into those determined by connected link interferometry and Very Long Baseline Interferometry (VLBI). The positional precision of the catalogs is between 0".10 (Ulvestad et al. 1981) to 0".005 (Shaffer et al. 1982). The frequencies of the catalog etween 2.5-8.0 GHz. Th er catalogs were obtained at frequencies n 2 and 5 GHz and meas were made at only one frequency. The r catalogs of Hilldrup (1982); Kaplan et al. (1982); Purcell . (1980); and Shaffer (1982) were made at two frequencies between 1.4-2.6 and 4.9-8.4 GHz in order to eliminate the delay path length in the ionosphere as a cause of systematic error. The earlier single frequency catalogs are circa 1975 when the sun was at solar sunspot

minimum and the ionosphere was not as active as in 1980, a time of solar sunspot maximum.

The catalog of Shaffer et al. (1982) is only a preliminary catalog presented at the Janu 1982 I meeting. Some other comments follow. The catalog of Kaplan) is from three months of measurements on the Green Bank interferometer (2σ results quoted) while the catalog of Hilldrup et al. (1982) is from four days' observation on the partially completed VLA in January 1980. The measurements of Ulvestad et al. (1981) and Perley et al. (1982) are from single maps made from one or several observational cuts with the VLA. The source positions were measured with synthesized beamwidths ranging from 2"-0".3 in the cases of the connected element catalogs and a few mas with the VLB catalogs.

The precision in Table 1 quoted for each catalog is that of the most inferior positions. These are usually low declination sources. The "average" accuracy of the catalogs may be much better. These catalogs are those which reduce and list the data in the standard manner, e.g. use the IAU recommended methods for reporting positions in terms of the 1950 or 2000 epochs. Kaplan (1981) has recently published specific recommendations for presentation of sources at the 2000.0 epoch. The published epochs are listed in Table 1.

Not all of the catalogs list the epoch of observation. The VLBI catalogs of Clark et al. (1976) and Purcell et al. (1980) were obtained from data taken over periods of several years and list no epoch of observation. The epoch of Purcell et al.'s (1980) catalog is estimated as 1978.0 while Clark et al. (1976) is estimated to be 1973.9. The connected element catalogs give the epoch of observation which is listed in Table 1. The epoch of observation together with a complete description of the constants used in reducing the data to a reference epoch or the use of the procedures recommended by the IAU for the reduction to reference epochs 1950 and 2000 should be stated along with the source positions. The values of the precession constant, nutational series and other earth rotation parameters are not known at this time to the accuracies that can and will be achieved by radio interferometric measurements of celestial positions. The effects of many of the motions will be to cause a rotation of the right ascension and declination axes between catalogs.

COMPARISON

The comparison of the accuracy of the catalogs must be accomplished by differencing the positions of the sources common in the catalogs. Of course, the catalogs must also be on a common reference epoch. Our comparison will be between the Wade and Johnston (1977) list and the other authors in Table 1. Table 2 contains the differences in coordinates between Wade and Johnston (1977) and the other precise catalogs. For right ascension the weighted mean difference multiplied by the cosine of source declination is listed while for declination the weighted mean difference is listed. The rms of the weighted mean differences is also listed together with the number of common sources between the Wade and Johnston (1977) catalog and the others. Some sources whose position differences exceeded three times the rms of the combined

errors in their positions were deleted from the comparison. This amounted to five sources.

TABLE 2

Weighted Mean Differences in Coordinates between Wade and Johnston (1977) and other Precise Catalogs

Catalog	$\overline{\Delta\alpha}\cos\delta$ arcsec	$\overline{\Delta\delta}$ arcsec	N	Comments
K - WJ	$-0.^{s}007 \pm 0.^{s}014$	$-0.^{s}012 \pm 0.^{s}010$	8	CEI, Epoch 1950
H - WJ	$0.^{s}007 \pm 0.^{s}010$	$0.^{s}011 \pm 0.^{s}015$	5	CEI, Epoch 1950
ER - WJ	$-0.^{s}090 \pm 0.^{s}026$	$0.^{s}049 \pm 0.^{s}016$	17	CEI, Epoch 1950
E - WJ	$-0.^{s}040 \pm 0.^{s}012$	$0.^{s}046 \pm 0.^{s}015$	13	CEI, Epoch 1950
C - WJ	$-0.^{s}002 \pm 0.^{s}009$	$0.^{s}002 \pm 0.^{s}009$	17	VLBI, Epoch 1950
P - WJ	$0.^{s}008 \pm 0.^{s}007$	$0.^{s}024 \pm 0.^{s}007$	18	VLBI, Epoch 1950
S - WJ	$0.^{s}042 \pm 0.^{s}001$	$0.^{s}015 \pm 0.^{s}009$	19	VLBI, Epoch 2000

WJ = Wade & Johnston (1977);
H = Hilldrup et al. (1982);
E = Elsmore (1982);
P = Purcell et al. (1980);
K = Kaplan et al. (1982);
ER = Elsmore and Ryle (1976);
C = Clark et al. (1976);
S = Shaffer et al. (1982).

The right ascension differences for the 1950 epoch catalogs whose right ascension reference point is 3C273, i.e. Clark et al. (1976); Wade and Johnston (1977); Kaplan et al. (1982); and Hilldrup et al. (1982) compare favorably. The other catalogs, namely those of Elsmore and Ryle (1976), and Elsmore (1982) which have a right ascension zero point based upon the position of the star β Per and Purcell et al. (1980) which has a right ascension zero point based on the position of the quasar NRAO 140, have a significant difference in right ascension due to the different zero point reference positions used. The zero point adjustment of the right ascensions masks motions such as precession and nutation or other rotations in the reference frame.

Since radio interferometric positions in declination are measured relative to the instantaneous spin axis of the earth, the declinations should be directly comparable if they were obtained at the same observing epoch. If the motions of precession and nutation were known exactly, then we could directly compare the differences in declination at a common reference epoch. The fact that the precession constant used in establishing sources on the reference epoch (1950) is known to be in error by $0.''01$/year, should cause a small rotation in the declinations when referenced to 1950 and may be expressed as $0.''01 \sin\varepsilon \cos\alpha$ multiplied by the difference in observing epochs in years, where ε is the obliquity of the ecliptic, and α is the right ascension of the source. Inspection of Table 1 shows that the observation epochs of

the catalogs are between 1973.d-1975.4 and 1978-1981.5. Therefore this effect may have a maximum amplitude of ∿ 0".02 in the declination differences for observation epochs spaced five years apart.

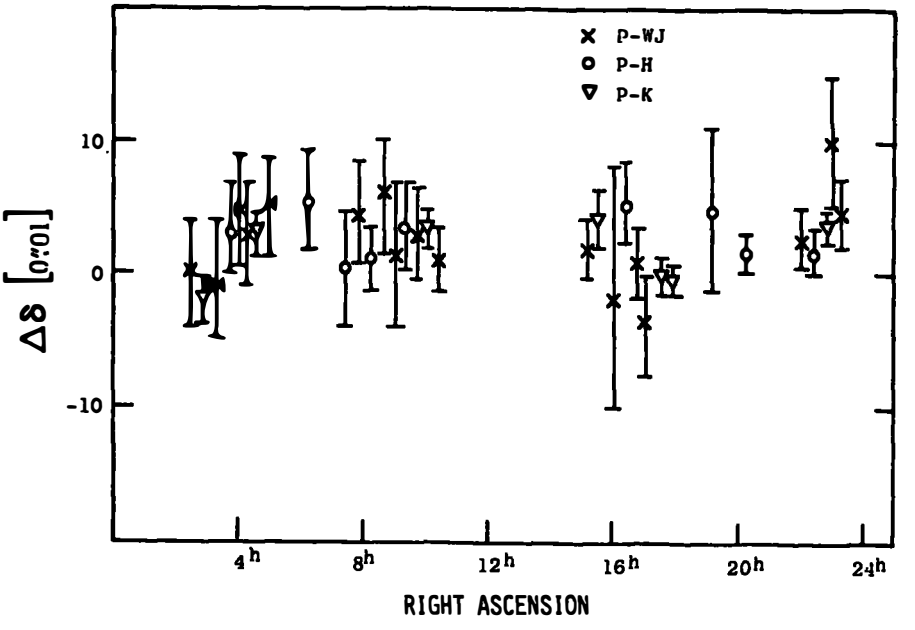

Figure 2. The weighted mean differences in declination versus right ascension. The error bars represent the rss of the errors. X Purcell et al. (1980)-Wade and Johnston (1977); o Purcell et al. (1980)-Hilldrup et al. (1982); ▽ Purcell et al. (1980)-Kaplan et al. (1982).

The differences in declination for the Kaplan et al. (1982) and Hilldrup et al. (1982) catalogs are not significant as the rms shows. There are only five and eight sources common with Wade and Johnston (1977). However the difference in declination for Purcell et al. (1980) is significant. This may be due to the discrepancy in the value of the precession constant used for epoch 1950. Figures 2 and 3 display the differences in declination versus right ascension and declination respectively. The data for the reference epoch 2000 (Shaffer et al. 1982) should show no significant difference in declination when com ohnston (1977) because an improved value of the precess d for this epoch. The difference in declination is margi ince its value is 0".015 ± 0".009 and in the same direction a . (1980) difference in declination listed in Table 2. An unexplained offset in declination as is the case of the Cambridge catalogs, may be in the catalog of Wade and Johnston (1977) which was measured using connected element interferometry. This matter will be resolved when catalogs with proper epochs and more sources in common are produced in the near future.

Comparison of the significant differences in declination of the Elsmore (1982) and the Elsmore and Ryle (1976) catalogs which both have an average offset of 0".047 cannot be explained by this effect. This large offset may be due to some instrumental effect caused by the fact that the Cambridge instrument has only east-west baselines.

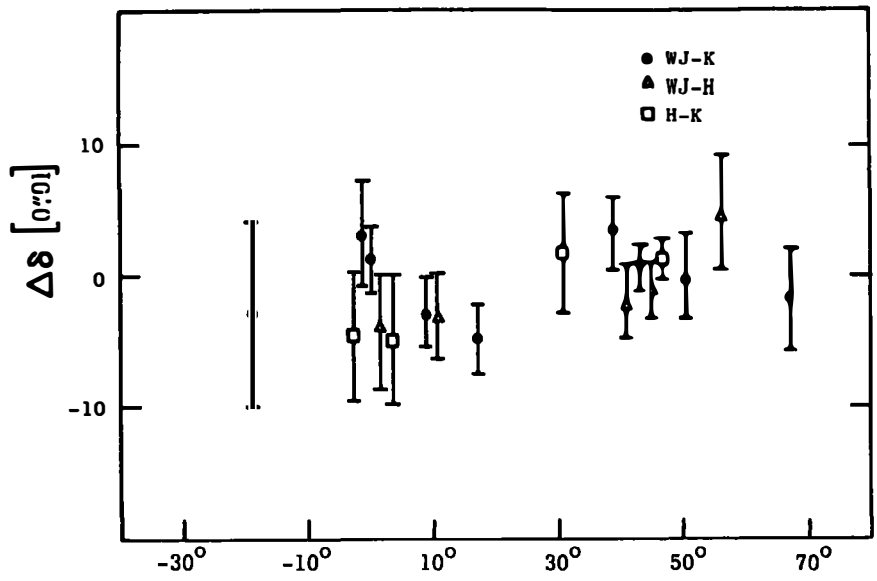

Figure 3. The weighted mean differences in declination versus declination. The symbols are as defined in Figure 2.

REFERENCE POINT IN RIGHT ASCENSION

The reference for the right ascension zero point in these catalogs has been based upon 3C273 (Wade and Johnston 1977), other quasars (Purcell et al. 1980), or the positions of optical objects such as Algol (Elsmore and Ryle 1976). However it must be remembered that the inertial reference frame is defined by the positions of the quasars. Various authors would like to see the radio reference frame related to the FK4 and future optical systems. This requires assuming coincidence of the positions of the optical and radio radiation. This is probably true on the milliarc second scale for quasars but may not be true for stellar or solar system objects such as asteroids. At this time the position of individual optical components can be measured to 0".05 (de Vegt and Gehlich 1978), while the radio source positions are now at the 0".01 level and may exceed this precision. Although there are many ways of relating the optical and radio reference frames, it must be remembered that the quasar reference frame will be more stable than any optical reference frame based upon objects inside the galaxy. Therefore, it is recommended that in future radio catalogs the zero point of right ascension be defined by the quasars themselves. The relationship to the optical reference frame, although extremely useful, should be established by secondary reference benchmarks and used to relate the optical/radio reference frames for astrometric/astrophysical studies. Unfortunately, the source 3C273B which has been used as a zeropoint right ascension reference in the past displays structures on the arc second and milliarc second scales as is shown in Figure 4. However at the present level of comparison of individual source positions ($\sim$ 0".01), the effects of this structure and the structure of other sources on source position determinations are just beginning to appear. To reach positional accuracies of 0".001, the source structure and its time variations as shown in Figure 4 will have to be taken into account. Some sources display less structure in their radio emission than others (Eckart et al. 1982). Sources such as 0454+844, 1803+784, and 2200+420 appear to display over 90% of their radio emission in components extended over < 5 mas. The study of

the structure of radio sources is only in its infancy. Detailed studies of a large number of sources are just now underway (Readhead and Pearson 1981; Eckart et al 1982). From these studies, new sources ideal for the definition of an inertial reference frame may be selected.

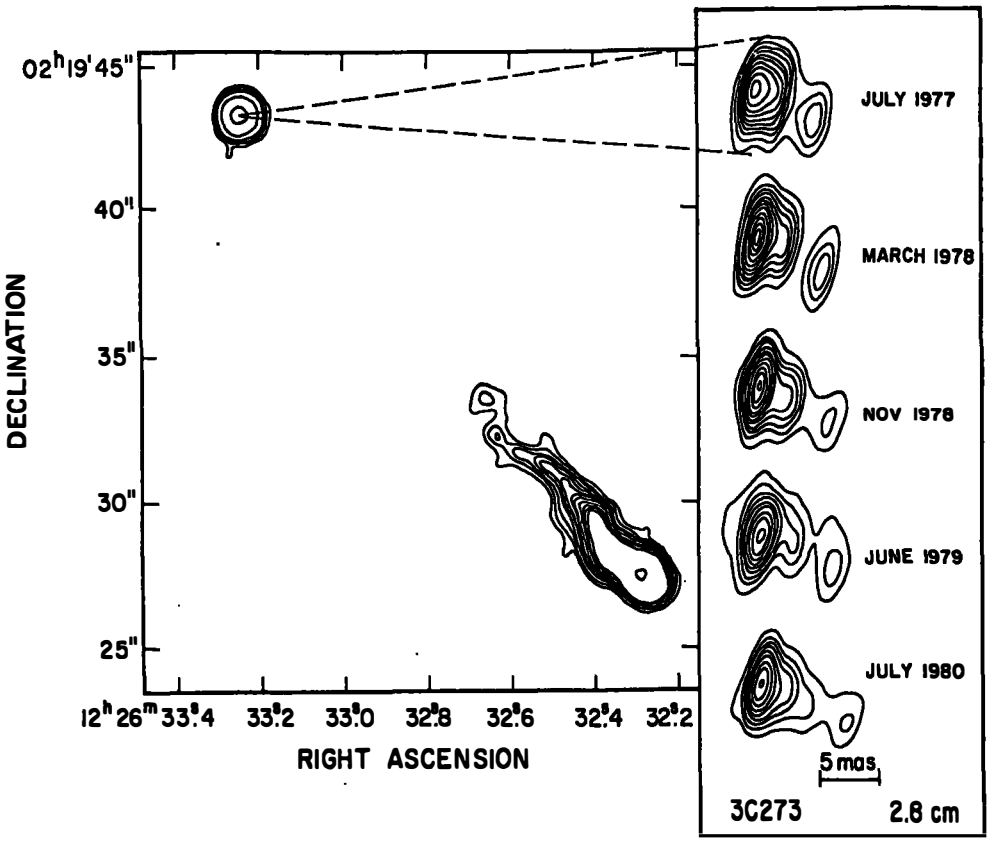

Figure 4. Left: Arc second VLA map of 3C273. This source consists of two major components--the dominant compact source and the extended component located 20" away along a position angle 222° from the compact source (Perley, Fomalont, and Johnston 1982). Right: The milliarc second structure of the compact component measured at several epochs (Pearson et al. 1981). Note that the compact milliarc second structure changes with time.

RECOMMENDATIONS

For future observations of the positions of extragalactic sources, it is recommended that source structure be taken into account if the positions of radio sources are to approach accuracies of 0".001. Further, since dual frequency observations are needed to remove the effects of the ionospheric path delay, the source structure needs to be known at both frequencies in order to calculate this correction exactly as source structure is a function of frequency. Therefore it is recommended:

1) Source positions be presented at 2000.0 epoch using the procedure outlined by Kaplan (1981). The improved values of the precession constant and nutation series

over reference epoch 1950 should allow the catalogs to be compared directly. However, there will probably be a small rotation between the right ascension and declination axes of the catalogs.

2) That the epoch of observation for each source be stated to one hundredth of a year.

3) Dual frequency observations be made to remove the effects of ionospheric path delay.

4) Source structure should be accounted for. Detailed maps of sources should be made at an initial epoch. Further observations could be made and a goodness of structure criterion be used to evaluate changes in source structure. This criterion is defined as:

$$S_G = \frac{\text{synthesized}}{V_{max} - V_{min}}$$

where V_{max} and V_{min} are the minimum and maximum visibilities observed. The sources should be mapped initially and the value of the goodness of structure criterion measured. Any noticeable change in the value of this criterion during subsequent measurements would result in the source structure being redetermined.

5) A list of sources defining a reference frame should be observed by all observers. This list should consist of $\sim$ 40 sources.

6) The position of 3C273 should define the zero point. The radio structure of this source should be taken into account when determining its radio position. The position of the compact object in this source is defined as the reference position in right ascension.

RADIO REFERENCE CATALOG

Following these recommendations, a catalog has been compiled using the available catalogs summarized in Table 1 as was done by Witzel and Johnston (1982). The reference point of right ascension is defined by the position of 3C273 i.e. $\alpha(2000) = 12^h29^m06^s.6997$ (see Hazard *et al.* 1971 for 1950 position), which coincides within the errors with the optical position (de Vegt and Gehlich 1981). The source positions are listed for epoch 2000. The recommended catalog appears in Table 3.

TABLE 3

Recommended Fundamental Radio Sources

Source	α_{2000}	δ_{2000}	Flux Density 5 GHz
0133+476	$01^h36^m58^s.5954$	47°51'29".111	2.0
0212+735	02 17 30.8212	73 49 32.639	2.2
0235+164	02 38 38.9277	16 36 59.288	1.4
0237-233	02 40 8.1770	-23 09 15.862	0.9
0316+413[a]	03 19 48.2613	41 30 42.211	56.0
0332-403	03 34 13.6538	-40 08 25.408	1.5
0336-019	03 39 30.9385	-01 46 35.862	2.6
0420-014	04 23 15.8015	-01 20 33.016	3.1
0454+844	05 08 42.3352	84 32 04.556	1.6
0552+398	05 55 30.8062	39 48 49.159	4.7
0607-157	06 09 40.9494	-15 42 40.676	2.4
0727-115	07 30 19.2130	-11 41 12.615	3.0
0742+103	07 45 33.0601	10 11 12.682	3.6
0826-373	08 28 04.7811	-37 31 06.274	1.8
0831+557	08 34 54.9042	55 34 21.078	5.5
0851+202	08 54 48.8758	20 06 30.632	2.8
0923+392	09 27 03.0149	39 02 20.855	7.6
1104-445	11 07 08.6937	-44 49 07.595	2.8
1127-145	11 30 07.0532	-14 49 27.398	4.7
1226+023[b]	12 29 06.6997	02 03 08.587	45.8
1358+624	14 00 28.6504	62 10 38.527	1.7
1404+286	14 07 00.3941	28 27 14.676	3.0
1519-273	15 22 37.6833	-27 30 10.620	2.0
1555+001	15 57 51.4340	-00 01 50.422	1.2
1611+343	16 13 41.0658	34 12 47.909	2.2
1741-038	17 43 58.8579	-03 50 04.634	2.2
1803+784	18 00 45.6676	78 28 04.020	2.5
1921-293	19 24 51.0577	-29 14 30.168	6.8
2021+614	20 22 06.6815	61 36 58.799	2.3
2200+420	22 02 43.2906	42 16 39.978	2.4
2243-123	22 46 18.2320	-12 06 51.278	2.4
2245-328	22 48 38.6870	-32 35 51.880	1.8
2352+495	23 55 09.4576	49 50 08.299	1.6

[a] Complex Structure on all size scales.
[b] Reference Position in Right Ascension.

SUMMARY

The accuracy of current radio positions appears to be at the 0".01 level, as comparison of the available catalogs has shown. The claimed accuracies of some individual catalogs exceed 0".01, but detailed comparison cannot be made until all catalogs specifically state the epoch of observation and contain common sources in order that detailed comparison can be made between the catalogs. In this way, improved values of the precession constant, the nutation series, and other earth rotation parameters can be determined from the rotation and other motions of the right ascension and declination axes needed to align the different catalogs.

A short radio reference catalog is presented which summarizes the available catalogs at this time and is believed to contain the best positions. This is a "preliminary" catalog meant to define an inertial reference frame. The sources in Table 3 should be observed in the future to aid the comparison of catalogs and are defined as fundamental radio sources (FRS). Future observations carried out as recommended in this paper will hopefully establish the accuracy of the radio reference frame at the submilliarc second level.

REFERENCES

Clark, T. A., Hutton, L. K., Marandino, G. E., Counselman III, C. C., Robertson, D. S., Shapiro, I. I., Wittels, J. J., Hinteregger, H. F., Knight, C. A., Rogers, A. E. E., Whitney, A. R., Niell, A. E., Rönnäng, B. O., and Rydbeck, O. E. H., 1976: A. J. 81. 599.

de Vegt, Chr. and Gehlich _____ Astrophys., 67, 65.

de Vegt, Chr. and Gehlich _____ Astrophys., 101, 191.

Eckhart, A., Hill, P., Johnston, K. J., Pauliny-Toth, I. I. K., Spencer, J. H., and Witzel, A., 1982e submitted to Astron. & Astrophys.

Elsmore, B., 1982: Abhandlungen aus der Hamburger Sternwarte Band X heft 3, pg. 129.

Elsmore, B. and Ryle M., 1976: _____, 174, 111.

Fanselow, J. L., Sovers, O. J., Thomas, J. B., Bletzacker, F. R., Kearns, T. J., Purcell, G. H., Rögstad, D. H., Skjerve, L. J., and Young, L. E., 1980e IAU Colloquium No. 56, Warsaw.

Hazard, C., Sutton, J., Argue, A. N., Kenworthy, C. M., Morrison, L. V., Murray, C. A., 1971: Nature, 233, 89.

Hilldrup, K., Fomalont, E. B., Wade, C. M., and Johnston, K. J., 1982: submitted to A. J.

Johnston, K. J., Spencer, J. H., Kaplan, G. H., Klepczynski, W. J., and McCarthy, D. D., 1980e Celestial Mechanics, 22, 143.

Kaplan, G. H., 1981e United States Naval Observatory Circular No. 163.

Kaplan, G. H., Josties, F. J., Angerhofer, P. E., Johnston, K. J., and Spencer, J. H., 1982: A. J., 87, 570.

Pauliny-Toth, I. I. K., Witzel, A., Preuss, E., Kühr, H., Kellermann, K. I., Fomalont, E. B., and Davis, M. M., 1978: A. J., 83, 451.

Pearson, T. J., Unwin, S. C., Cohen, M. H., Linfield, R. P., Readhead, A. C. S., Seielstad, G. A., Simon, R. S., and Walker, R. C., 1981e Nature, 290, 365.

Perley, R., 1982e A. J., 87, 859.

Perley R., Fomalont E., and Johnston, K. 1982 in preparation.

Preston, R. A. and Moribito, D. D., 1980e "Radio Interferometry Techniques for Geodesy", NASA Conference Publication 2115.

Purcell, G. H., Fanselow, J. L., Thomas, J. B., Cohen, E. J., Rogstad, D. H., Sovers, O. J., Skjerve, L. J., and Spitzmesser D. J., 1980e "Radio Interferometry Techniques for Geodesy", NASA Conference Publication 2115.

Readhead, A. and Pearson, T., 1981e Extragalactic _____, Edited by David S. Heeschen and Campbell M. Wade, pg. 279.

Shaffer, D., 1982e presented at URSI meeting January 1982.

Shimmins, A. J., Bolton, J. G., and Wall, J. V., 1975: _____ Phys. Suppl., 34, 63.

Ulvestad, J., Johnston, K., Perley, R., and Fomalont, E _____ 1010.

Wade, C. M. and Johnston, K. J., 1977: A. J., 82, 791.

Witzel, A., and Johnston, K. J., 1982e Abhandlungen aus der Hamburger Sternwarte Band X heft 3, pg. 151.

NUMERICAL EXPERIMENTS ON MAINTAINING THE CONVENTIONAL TERRESTRIAL SYSTEM BY VLBI NETWORKS

Seiji MANABE

Internatioal Latitude Observatory of Mizusawa
Mizusawa, Iwate Japan

ABSTRACT. Characteristics of the station displacements and the Earth orientation parameters to be obtained with VLBI are investigated under the condition that a network of stations has neither rotational nor translational motiont It is found that 80 % of actual displacements are recovered in estimated ones if a number of stations in the network is more than 8.

INTRODUCTION

In order to define and maintain the conventional terrestrial system (CTS) with a few centimeter accuracy, it is necessary to take into account a lot of geodetic parameters. In other words the accurate CTS is realized only after consistent estimations of these parameters from observations. However, some of them cannot be independently estimatedt The separation of the dependent parameters requires constraining conditions on themt Definitions of the CTS and the celestial reference system essentially depend on the choice of conditions. For a long term stability of the CTSt the most important condition is the one that distinguishes the polar motion and UT1 (referred to as the EOPt hereafter) from secular displacements of observing sites. When determining the CTS by using VLBI, constraining conditions on translational and rotational components of the CTS are necessaryt Introduction of the conditions yields spurious station displacements as well as mutual dependences among them. In the present paper, adopting the condition that a VLBI network has neither translational nor rotational motion as a whole, we investigate how this condition causes biases in estimated station displacements and the EOPt We briefly remark on an assumption of smooth variation of station positions.

CONSTRAINING CONDITIONS

We assume that both the EOP and the station displacements vary stepwise with timet This assumption is conveneient because it covers wide range of types of variations and is a basis of an assumption of smooth station displacements. We further assume that a time scale of the EOP variation is much shorter than that of the station displacements. For observations in a period during which the station displacements are regarded to be constantt the coefficient matrix of VLBI observation equations is orthogonal to a matrix

$$H=\begin{pmatrix}B\\C\end{pmatrix} \qquad (1)$$

where n by 6 and 3k by 6 matrices B and C, respectively, are given by

$$B=\begin{pmatrix} I_3 \ldots I_3 \\ 0 \ldots 0 \end{pmatrix}^T \tag{2}$$

and

$$C^T=\begin{vmatrix} 0 & -n_1 & m_1 & \ldots\ldots 0 & -n_k & m_k \\ n_1 & 0 & -l_1 & \ldots\ldots n_k & 0 & -l_k \\ -m_1 & l_1 & 0 & \ldots\ldots -m_k & l_k & 0 \\ 1 & 0 & 0 & \ldots\ldots 1 & 0 & 0 \\ 0 & 1 & 0 & \ldots\ldots 0 & 1 & 0 \\ 0 & 0 & 1 & \ldots\ldots 0 & 1 & 0 \end{vmatrix} =(C_1^T \ldots C_k^T) \tag{3}$$

In the above nt and k are a number of steps of the EOP in a step of the station displacements and a number of contributing staionst I_3 is a 3 by 3 unit matrix and l_i, m_i and n_i are direction cosines of the i-th station with respect to the current terrestrial system.

Corresponding to H, there are three kinds of conditions among the station displacementst They are

$$\text{(i)} \quad \sum_i n_i \times \Delta X_i / |X_i| - \sum_i^n (y_r - x_r \Delta T_r)^T = 0 \text{ where } n_i=(l_i \; m_i \; n_i)^T, \tag{4}$$

$$\text{(ii)} \quad \sum_i n_i \times \Delta X_i = 0, \tag{5}$$

$$\text{(iii)} \quad \sum_r (y_r - x_r \Delta T_r)^T = 0, \tag{6}$$

The condition (i) leads to the minimum length estimates and the case of n=1 was adopted by DERMANIS and MUELLER(1978)t The condition (iii) implies that the EOP has no secular motion. The condition (ii), which we investigate in the following, implies that there are neither rotation nor translation of a VLBI network. This condition is considered to be more appropriate than the other two, because it approximates the Tisserand mean surface of the Earth and the EOP do not affect the station coordinates.

The assumption of stepwise variations of station positions is quite general. If the displacements are, as in the case of long periodic tidal displacements, expressed as

$$\Delta X_i(t)= \sum_l a_{il} f_l(t) \tag{7}$$

with unknown vectors a_{il} and known function of time $f_l(t)$, the condition (ii) becomes as

$$\sum_i n_i \times a_{il}=0 \; . \tag{8}$$

Thereforet a mututal dependence among parameter vectors is just the same as that of the stepwise variation. The condition (i) is reduced to

$$\sum_i n_i \times a_{il} - \sum_r f_l(t_r)(y_r - x_r \Delta T_r)^T=0 \tag{9}$$

and have to be investigated for each l separatelyt

CHARACTERISTICS OF SOLUTIONS THAT SATISFY THE CONDITION (ii)

Actual displacements of the stations usually do not satisfy the conditions described in the previous section. Hence, solutions of the observation equations differ from true ones; even if there are no observation errors. In order to understand characteristics of a network, it is important to investigate how calculated displacements are distorted by imposed conditions.

Under the condition (ii) estimated displacements $\Delta\hat{X}_1 \cdots, \Delta\hat{X}_k$ and the EOP, $\hat{p}$, are linear combinations of actual ones. In a matrix form, we have

$$(\Delta\hat{X}_1^T \cdots \Delta\hat{X}_k^T \hat{p}^T)^T = Q (\Delta X_1^T \cdots \Delta X_k^T p^T)^T . \qquad (10)$$

The rank of Q is deficient by 6. Q depends solely on geometry of a network. Q is calclated by solving VLBI observation equations without observation errors. The last three columns of Q are

$$\begin{pmatrix} 0 \\ I_3 \end{pmatrix}$$

because p does not affect $\Delta\hat{X}$.

We calculated Q for several networks. The number of stations in each network ranges from 3 to 10. Typical lengths of baselines are from several hundred to several thousand km. Figures 1 and 2 show some of the results. Q is expressed as a response to a unit displacement in local topocentric coordinates. The networks shown in figures are Kashima -ORRLAS -Haleakala -Goldstone, Haystack -Richmond -Onsala -Wettzell -Kashima -ORRLAS -Haleakala -Goldstone -HRAS -Nanjing. In the former 4-station network, the input values are recovered by a factor of 0.4 to 0.7. Spurious displacements are not small. In some cases, the spurious ones amount to 0.4. This is quite large. It is noticed that there are pairs of stations for which the displacements of one station induce large spurious displacements of the other. Haystack -Richmond, Onsala -Wettzell and Haleakala -Goldstone are examples of such pairs. In the case of the 10-station network, the recovery is improved to a factor of about 0.7 to 0.9. The spurious displacements are diminished. However, there still remain tightly connected pairs, even though the tightness is smaller. The almost same features are found for 8-station networks. In the case of a three station network, all stations are tightly connected. It may be concluded that, for a network composed of more than 8 stations, most of the observed three-dimensional displacements originate from actual displacements of the station itself. This conclusion is not valid for the paired stations.

Figure 3 shows spurious EOP induced by 1 m displacement of the staticns in the 10-station network. The maximum value of the spurious EOP is about 0".008. In the 4-station network, the resultant EOP are much larger. The maximum value amounts to 0".08. Effects of the station displacements on the estimated EOP seriously depend on a size of a network as well as a number of staions. For example, 1 m displacement in a network whose baseline lengths are several hundred km typically induces biases in the EOP by 0".1 and the maximum value is 0".15.

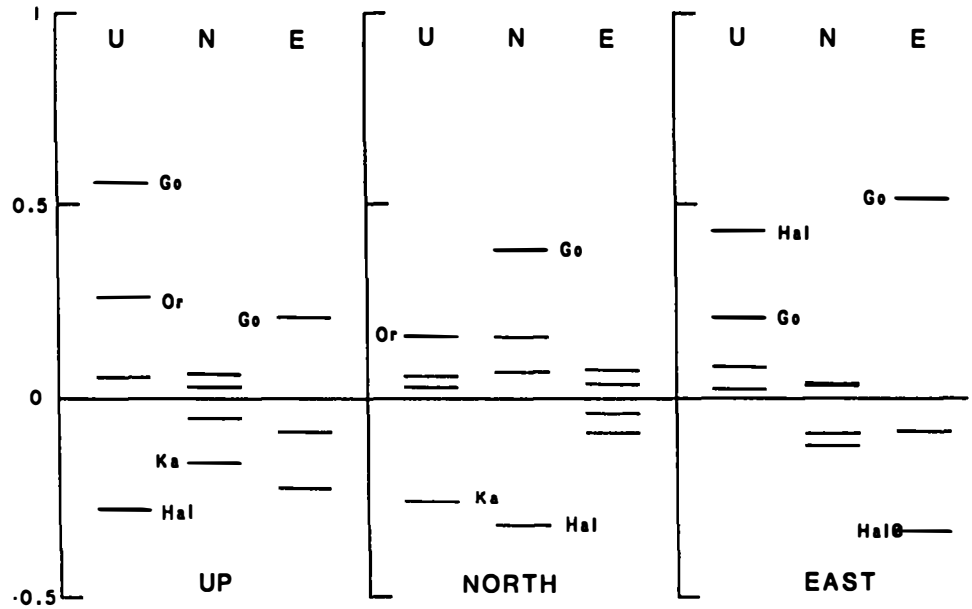

Fig.1a Go-Ka-Hal-Or Input is Go

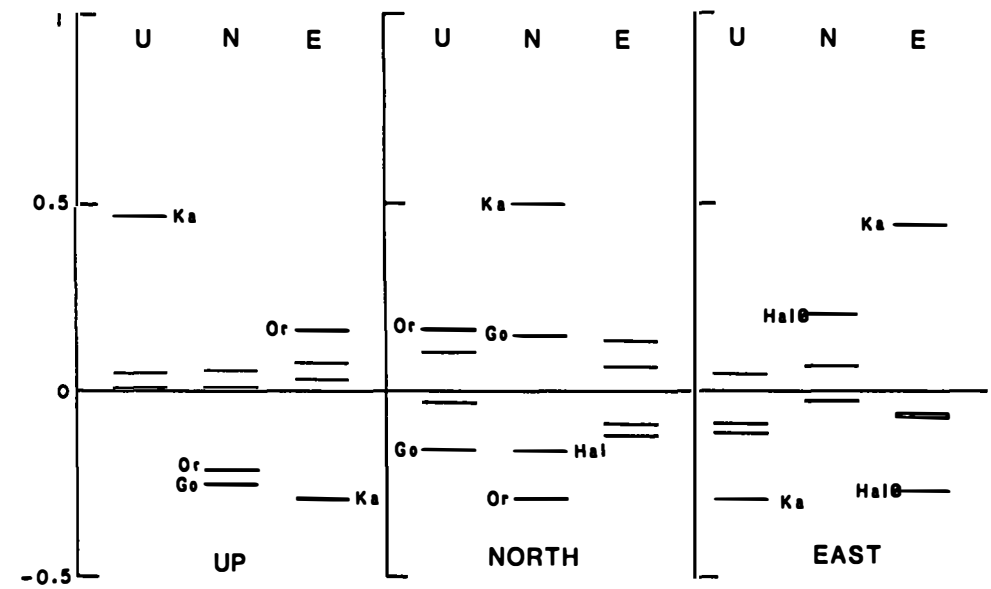

Fig1b Go-Ka-Hal-Or Input is Ka

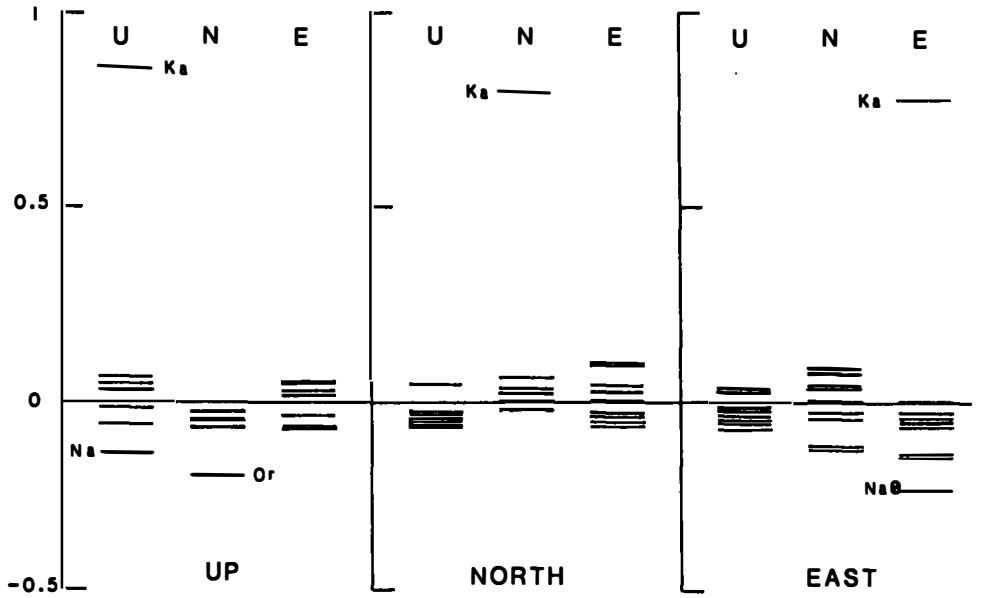

Fig.2a 10-station network Input is Ka

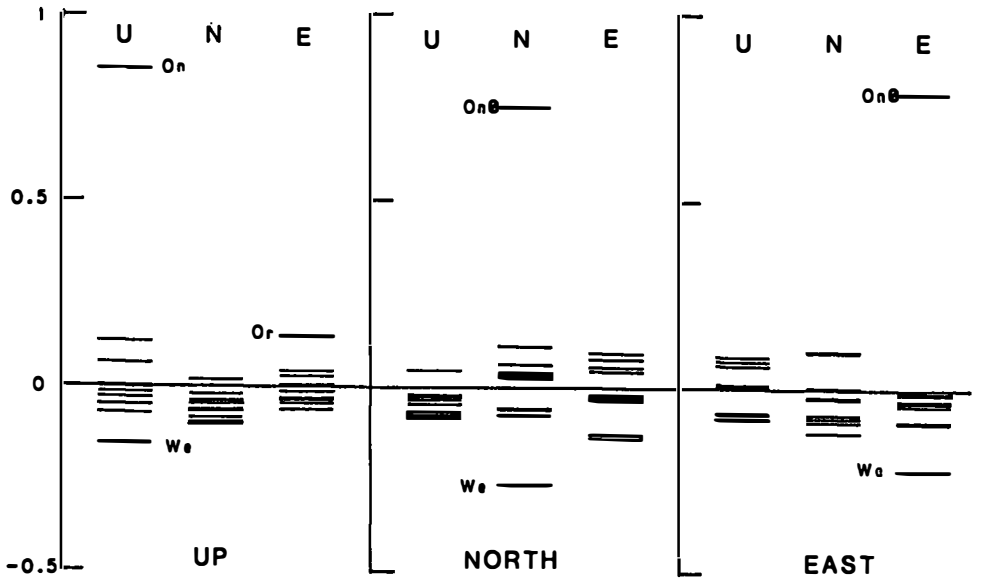

Fig.2b 10-station network Input is On

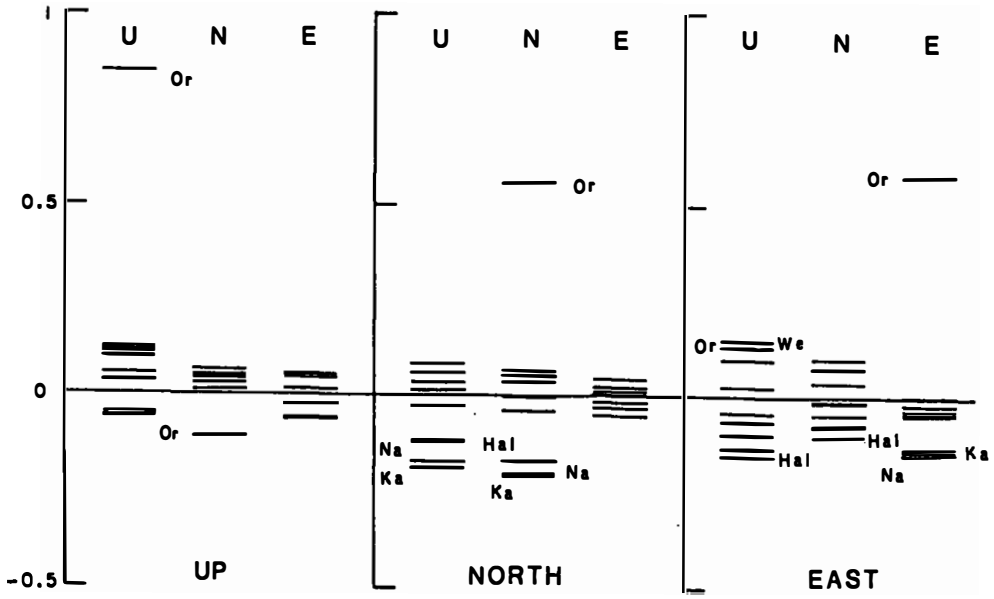

Fig.2c 10-station network Input is Or

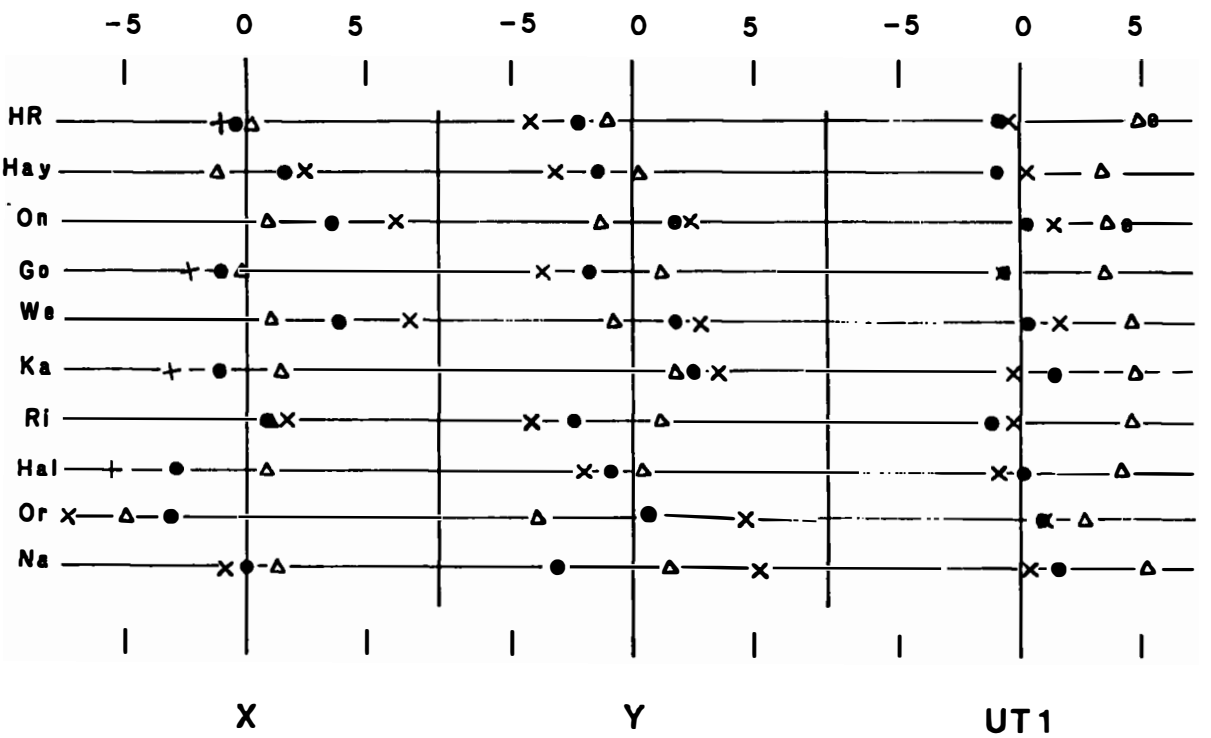

Fig.3 EOP Unit is 0.″001/m

● :up × :north △ :east

MAINTENANCE OF THE CTS BY SMOOTHING

In the stepwise approximation of the station displacements, there is no relation between consecutive steps. It is reasonable to assume that the displacements change smoothly with space and time. For a VLBI network in which the stations are not densely distributed, the continuity in space is not important. On the other hand, if we utilize the continuity in time, condition to separate the station displacements from the EOP is required only at an initial epoch. The continuity in time is expressed by a first order devided difference as

$$| \Delta X_i(t_{j+1}) - \Delta X_i(t_j) | / | t_{j+1} - t_j | = \text{small}. \qquad (11)$$

If we assume that higher order devided differences are small, just the same number of the conditions as the order of differences are necessary to recover rank of the obervation equations. If the station displacements are calculated by using the continuity in time, the system will show gradual rotation and translation with respect to the initial reference system. Recovery of rotation and translation depends on an assumed smoothness of the station displacements. The system will neither rotate nor translate if strong continuity is assumed, while the observation equations become ill-conditioned and hence the constraining conditions are required if weak continuity is assumed.

We made several experiments to see how the station displacements are biased by simultaneous usage of the constraining condition(ii) and the requirement from smoothness. Smoothness depends on the data used. We a posteriori determined an optimum smoothness by using a Bayesian Information Criterion(ABIC) by AKAIKE(1980). We could not find significant differences of optimally smoothed case from the unsmoothed case where the condition (ii) was applied at each step of the station displacements. However, this is not a definitive conclusion, because the results strongly depend on the simulated data.

CONCLUSION

It is concluded that at least 8-station network is necessary to recover more than 80% of the actual displacement for VLBI observations. The stations have to be distributed so as to avoid forming tightly connected pairs.

References

AKAIKE,H., 1980: Seasonal Adjustment by a Bayesian Modeling, Time Series Analysis,1, 1-13.

DERMANIS,A. and MUELLER,I.I., 1978: Earth Rotation and Network Geometry Optimization for Very Long Baseline Interferometers, Bul.Geod.,52,(1978),131-158.

GENERAL RELATIVISTIC FRAMEWORK FOR THE STUDY OF ASTRONOMICAL/GEODETIC REFERENCE COORDINATES

Masa-Katsu FUJIMOTO, Shinko AOKI, Koichi NAKAJIMA
Tokyo Astronomical Observatory
Mitaka, Tokyo 181, Japan

Toshio FUKUSHIMA
Hydrographic Department
Tsukiji, Tokyo 104, Japan

Shigeru MATSUZAKA
Department of Astronomy, Tokyo University
Bunkyo, Tokyo 113, Japan

ABSTRACT. Transformation between the solar barycentric coordinates and the geocentric ones is derived within the framework of relativity. It is found that general-relativistic effects in the transformation up to the order of $(v/c)^2$, as well as special-relativistic ones, are important to analyze astrometric and geodetic data.

They are;

special-relativistic

1st order Doppler (aberration), 2nd order Doppler

general-relativistic

contraction (or expansion), shear, and rotation,

of proper reference frame.

The contraction of space-coordinates includes Lorentz contraction and the one of time-coordinate does the well-known gravitational retardation of clock. The rotation means geodetic precession and the periodical "geodetic nutation". These are indispensable in the reduction of VLBI-observations.

INTRODUCTION

Three types of reference frames have been used in the field of positional astronomy. They are barycentric, geocentric and topocentric coordinates. Each of them is used to its proper purpose and may be transformed to each other. In the case of very-long-baseline-interferometric (VLBI) observations, it is also necessary to use them properly. The barycentric frame gives the basis to describe the Earth's position, planetary ephemerides and the source directions. The radio wave propagation is discussed also in this frame. The topocentric coordinates are related directly to the observers and to the local physical laws. The geocentric frame plays a role of intermediary which, on the one side, relates to the barycentric frame by the celestial mechanical transformation (including the general relativistic description of motion) and, on the other side, is related to the topocentric frame by the geophysical quantities such as the rotation and the deformation of the Earth. For the sake of this circumstance, the geocentric coordinates are useful to extract the geophysical quantities from the observational data. It is also a good reason to use the geocentric frame that it approximates the topocentric frame in some cases.

High accuracies of the newly developed techniques such as VLBI, request inevitably

the general relativistic effects in the mutual relations among these three coordinates systems. Some of the relativistic effects have already been included in certain previous analyses, but the inclusion seems to be imperfect so far. As shown later, one derivation of a delay time in a VLBI observations does include the order of v^2/c^2 correction in the time coordinate, but does not include such corrections in the spatial coordinates. As discussed later, the same order of magnitude corrections should be taken into account both in time and spatial coordinates which, in some sense, can be measured by radio waves.

In this paper we discuss on the relations between the geocentric frame and the barycentric one within the framework of relativity. In the next section we derive, as a simple case, the special relativistic equation of a delay time for VLBI stations which are locally moving with a constant velocity with respect to the barycentric coordinates. By this derivation, we point out an incompleteness in a currently-used formulation. In the third section we derive the fully-general transformation between the geocentric frame and the barycentric one relativistically. Each term in the transformation is discussed in the fourth section. Discussions on the topocentric frame are given in the fifth section and the conclusive summary is at the last section.

Through the present paper, Greek indices run from 0 to 3 while Latin ones do from 1 to 3. We represent 4-vectors in bold-faced letters, 3-vectors in letters with a wavy underline, and 3x3-matrix in capital letters over a tilde.

SPECIAL RELATIVISTIC CASE

To see the special-relativistic effects on the geometrical relation of VLBI, we treat here a simplest example (Figure 1). Two observers (denoted by A and B, respectively) are fixed in a frame moving along x-axis with a constant velocity $\underset{\sim}{v}$ relative to an inertial frame (here called "barycentric frame").

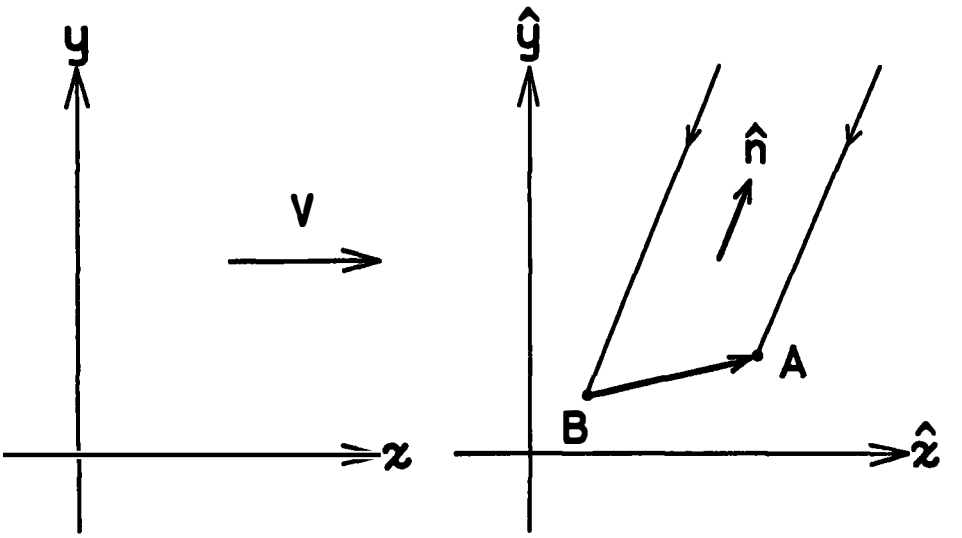

Figure 1. VLBI stations moving with a constant velocity. The $(\hat{x},\hat{y})$-coordinates comoving with the stations, A and B, have a relative velocity $\underset{\sim}{v}$ to the (x,y)-coordinates.

An event is described by a 4-vector of which components are written as $(c\hat{t},\hat{x},\hat{y},\hat{z}) = (x^{\hat{\alpha}})$ in the frame comoving with observers, and $(ct,x,y,z) = (x^{\alpha})$ in the barycentric

frame. The components in both frames are related each other by a Lorentz transformation:

$$c\hat{t} = \gamma(ct - xv/c), \quad \hat{x} = \gamma(x - vt), \qquad (2\text{-}1)$$
$$\hat{y} = y, \quad \hat{z} = z ,$$

where

$$\gamma = (1 - (v/c)^2)^{-(1/2)} .$$

In a typical VLBI observation, we receive an electromagnetic wave emitted from a very distant source. The wave can be treated as a parallelly propagating wave. The event of reception is described by one of the observerst 4-vector at which he receives a certain phase of the wave. In an eikonal approximation, the phase of a wave is given by $(g_{\mu\nu}k^\mu x^\nu)$, where

$$(k^\mu) = (\omega, k_x, k_y, k_z)$$

is 4-wave number vector of the wave and $g_{\mu\nu}$ is a metric of space-time.

When the observers A and B receive the same phase of the wave, it holds that

$$(g_{\mu\nu}k^\mu x^\nu)_A = (g_{\mu\nu}k^\mu x^\nu)_B . \qquad (2\text{-}2)$$

This is rewritten to a well-known expression as

$$\begin{aligned} (t_A - t_B) &= \underset{\sim}{k}\cdot(\underset{\sim}{x}_A - \underset{\sim}{x}_B) / (c\omega) \\ &= - \underset{\sim}{n}\cdot(\underset{\sim}{x}_A - \underset{\sim}{x}_B) / c \end{aligned} \qquad (2\text{-}2')$$

where $\underset{\sim}{n} = - \underset{\sim}{k} / \omega$ is the unit vector of source direction and can be treated as common at both observers A and B. Since a phase $(g_{\mu\nu}k^\mu x^\nu)$ is invariant under the Lorentz transformation, the equations (2-2) and (2-2') also hold for corresponding quantities in the comoving frame and then we get

$$\hat{t}_A - \hat{t}_B = -\hat{\underset{\sim}{n}}\cdot(\hat{\underset{\sim}{x}}_A - \hat{\underset{\sim}{x}}_B)/c . \qquad (2\text{-}3)$$

The relations between $\hat{\underset{\sim}{n}}$ and $\underset{\sim}{n}$ are easily derived from the Lorentz transformation of 4-vector (k^μ). In our case, they are

$$\begin{aligned} n_{\hat{x}} &= (n_x + (v/c))/(1 + n_x v/c), \\ n_{\hat{y}} &= n_y/\gamma(1 + n_x v/c), \\ n_{\hat{z}} &= n_z/\gamma(1 + n_x v/c) . \end{aligned} \qquad (2\text{-}4)$$

which show a well-known aberrational effect.

Following Robertson's derivation (Robertson 1975), one starts from the equation (2-2') and uses relations such as

$$t_A = t + \Delta t, \quad t_B = t$$

and

$$\begin{aligned} \underset{\sim}{x}_A(t_A) &= \underset{\sim}{x}_A(t) + \dot{\underset{\sim}{x}}_A(t)\,\Delta t \\ &= \underset{\sim}{x}_A(t) + v\,\underset{\sim}{e}_x\,\Delta t . \end{aligned}$$

Equation (2-2') is then rewritten as

$$\Delta t = -\underset{\sim}{n}\cdot(\underset{\sim}{x}_A(t) - \underset{\sim}{x}_B(t))/c - (n_x v/c)\,\Delta t$$

or

$$\Delta t\,(1 + (n_x v)/c) = -\underset{\sim}{n}\cdot(\underset{\sim}{x}_A(t) - \underset{\sim}{x}_B(t))/c \qquad (2\text{-}5)$$

On the other hand, from a "time part" relation of the Lorentz transformation (2-1), one has

$$\begin{aligned} (\hat{t}_A - \hat{t}_B) &= \gamma(t_A - t_B) - \gamma v\,(x_A(t_A) - x_B(t_B))\,/\,c^2 \\ &= \gamma\Delta t - \gamma v\,(x_A(t) - x_B(t))\,/\,c^2 - \gamma v^2\Delta t/c^2 \\ &= \Delta t/\gamma - \gamma v\,(x_A(t) - x_B(t))\,/\,c^2 . \end{aligned} \qquad (2\text{-}6)$$

Inserting Δt of the equation (2-5) into (2-6), one can obtain

$$\hat{t}_A - \hat{t}_B = -\frac{1}{c\gamma}\left[\left(\frac{n_x}{1+n_x v/c} + \frac{v/c}{1-(v/c)^2}\right)(x_A(t)-x_B(t)) + \frac{n_y}{1+n_x v/c}(y_A(t)-y_B(t))\right]$$

$$= -\frac{1}{c}\,\frac{n_x + v/c}{1+n_x v/c}\,\gamma(x_A(t)-x_B(t)) - \frac{1}{c}\,\frac{n_y}{\gamma(1+n_x v/c)}(y_A(t)-y_B(t)) \qquad (2\text{-}7)$$

$$= -\frac{1}{c}\left\{ n_{\hat{x}}\,\gamma(x_A(t)-x_B(t)) + n_{\hat{y}}(y_A(t)-y_B(t))\right\}$$

If one uses "spatial part" relations of the Lorentz transformation such as,

$$\hat{x}_A - \hat{x}_B = \gamma(x_A(t)-x_B(t)), \qquad \hat{y}_A - \hat{y}_B = y_A(t)-y_B(t), \qquad (2\text{-}8)$$

one can obtain the correct relation of the equation (2-3).

Robertson's derivation and also Chopo Ma's equation (Chopo Ma 1978) seem to miss such "spatial part" of the Lorentz transformation. Their "relativistic" treatment is, therefore, incomplete even in the order of $(v/c)^2$. The effect in the equation (2-8) is the well-known "Lorentz contraction", and our calculation showes here that the "Lorentz contraction" should be taken into account.

TETRAD OF THE OBSERVER

To discuss on the relations between coordinates within the frame of relativity, the concept of a proper reference frame gives a useful point of view (Misner et al., 1970, §13.6). As a first step toward the construction of a proper reference frame or a local inertial system of the observer, we will represent his tetrad $\{ e_{\hat{\alpha}} \}$, the system of comoving orthonormal bases along his world line.

Let us consider a following metric

$$ds^2 = -d\tau^2 = -(1-2\phi)\,dt^2 + 2\,\underset{\sim}{g}\cdot d\underset{\sim}{x}\,dt + (1+2\gamma\phi)\,d\underset{\sim}{x}\cdot d\underset{\sim}{x} \qquad (3\text{-}1)$$

where ϕ and $\underset{\sim}{g}$ are scalar and vector gravitational potentials, respectively, and γ is a constant parameter. We take a unit system such that c = G = 1 hereafter.

We assume that the 3-velocity $\underset{\sim}{v}$ is small ($\simeq 10^{-4}$ in the neighbourhood of the Earth) and also assume that $\phi \cong O(v^2)$ and $\underset{\sim}{g} \cong O(v^3)$. It is easily shown that the above metric includes all the effects up to $O(v^2)$ under these assumptions.

An orthonormal tetrad fixed to an observer obeys the following Fermi-Walker transpotation (Misner et al., 1970)

$$(\delta/\delta\tau + \Omega)\, e_{\hat{\alpha}} = 0 \qquad (3\text{-}2)$$

Here $\delta/\delta\tau$ is a covariant derivative along a world line of the observer and is expressed as

$$\delta q^{\mu}/\delta\tau = dq^{\mu}/d\tau + \Gamma^{\mu}_{\nu\sigma}\, u^{\nu} q^{\sigma} \qquad (3\text{-}3)$$

where Γ is the Christoffel symbol and u is the 4-velocity of the observer. The matrix $\underset{\sim}{\Omega}$ is expressed by u and the 4-acceleration a as

$$\Omega^{\mu}_{\nu} = a^{\mu}u_{\nu} - a_{\nu}u^{\mu} \qquad (3\text{-}4)$$

We note that the 0-component of equation (3-2) is the equation of motion of the observer.

We can rewrite (3-2) as

$$(d/dt + \Pi)\, e_{\hat{\alpha}} = 0 \qquad (3\text{-}5)$$

where

$$\Pi^{\mu}{}_{\nu} = (dt/d\tau)\,(\Gamma^{\mu}{}_{\nu\sigma}\,u^{\sigma} + \Omega^{\mu}{}_{\nu}) \tag{3-6}$$

A solution of the differential equation (3-5) is obtained as

$$e_{\hat{\alpha}}(t) = U(t,t_0)\,e_{\hat{\alpha}}(t_0) \tag{3-7}$$

using a propagator U, which is given by the time ordered exponential as

$$U(t,t_0) = \exp_o\left[-\int_{t_0}^{t}\Pi(t)\,dt\right]$$

$$= 1 - \int_{t_0}^{t}\Pi(t_1)\,dt_1 + \int_{t_0}^{t}\Pi(t_1)\,dt_1\int_{t_0}^{t_1}\Pi(t_2)\,dt_2 - \cdots \tag{3-8}$$

In our problem, $\int\Pi\,dt$ is $O(v^2)$ and we can neglect the third and the higher terms in the above expansiont

Using the metric (3-1), we obtain an explicit expression of U as follows

$$U(t,t_0) = \begin{pmatrix} U^0{}_0 & {}^t(\underset{\sim}{v} - \underset{\sim}{v}_0)t \\ \underset{\sim}{v} - \underset{\sim}{v}_0 & \underset{\sim}{U} \end{pmatrix} + O(v^3)\,. \tag{3-9}$$

Here

$$U^0{}_0 = 1 + (\phi - \phi_0) + (\underset{\sim}{v} - \underset{\sim}{v}_0)^2/2 + O(v^3), \tag{3-10}$$

$$\underset{\sim}{U} = [\,1 - \gamma(\phi - \phi_0)\,]\,\underset{\sim}{1} + (\underset{\sim}{v} - \underset{\sim}{v}_0)\otimes(\underset{\sim}{v} - \underset{\sim}{v}_0)/2$$

$$- \underset{\sim}{v}\wedge\underset{\sim}{v}_0 - \underset{\sim}{Q}(t,t_0) + O(v^3) \tag{3-11}$$

where

$$\underset{\sim}{Q}(t,t_0) = t\int_{t_0}^{t}[t(1/2 + \gamma)\underset{\sim}{\Omega} - \underset{\sim}{A} - \underset{\sim}{\Theta}]dt \tag{3-12}$$

and

$$\underset{\sim}{\Omega} = \underset{\sim}{v}\wedge d\underset{\sim}{v}/dt,\ \underset{\sim}{A} = \underset{\sim}{\nabla}\wedge\underset{\sim}{g},\ \underset{\sim}{\Theta} = \underset{\sim}{v}\wedge\underset{\sim}{f}\,. \tag{3-13}$$

In the above expressions, suffix 0 stands for a value at t_0. The symbols $\otimes$ and $\wedge$ are direct and exterior products, respectively, i.e.

$$(\underset{\sim}{a}\otimes\underset{\sim}{b})^{ij} = a^i b^j, \tag{3-14}$$

and

$$\underset{\sim}{a}\wedge\underset{\sim}{b}t = \underset{\sim}{a}\otimes\underset{\sim}{b} - \underset{\sim}{b}\otimes\underset{\sim}{a} \tag{3-15}$$

The coordinate velocity $\underset{\sim}{v}$, the 3-gradient $\underset{\sim}{\nabla}$ and the 3-extenal acceleretion $\underset{\sim}{f}t$ are defined as

$$v^j = (d\tau/dt)\,u^j\,,\ \nabla^j = \partial/\partial x^j \text{ and } f^j = a^j - a^0 v^j \tag{3-16}$$

It can be shown that the following representation of tetrad

$$(e_{\hat{\alpha}}{}^{\mu}(t)) = \begin{pmatrix} 1 + \phi + v^2/2 & {}^t\underset{\sim}{v} \\ \underset{\sim}{v} & (1-\gamma\phi)\underset{\sim}{1} + \underset{\sim}{v}\otimes\underset{\sim}{v}/2 - \underset{\sim}{Q}(t,-\infty) \end{pmatrix} + O(v^3) \tag{3-17}$$

is a solution since it satisfies the equations (3-7), (3-9) through (3-13). The dual tetrad is given as

$$(e^{\hat{\alpha}}{}_{\mu}(t)) = \begin{pmatrix} 1 - \phi + v^2/2 & -{}^t\underset{\sim}{v} \\ -\underset{\sim}{v} & (1+\gamma\phi)\underset{\sim}{1} + \underset{\sim}{v}\otimes\underset{\sim}{v}/2 + \underset{\sim}{Q}(t,-\infty) \end{pmatrix} + O(v^3) \tag{3-18}$$

Comparing the above result with the Lorentz transformation matrix caused by velocity $\underset{\sim}{v}$

$$L(\underset{\sim}{v}) = \begin{pmatrix} 1 + v^2/2 & {}^t\underset{\sim}{v}t \\ \underset{\sim}{v} & \underset{\sim}{1} + \underset{\sim}{v}\otimes\underset{\sim}{v}/2 \end{pmatrix} + O(v^3) \tag{3-19}$$

and $L(\underset{\sim}{v})^{-1} = L(-\underset{\sim}{v})$, the following physical meaning of each term is obtained:

(0,0) component

ϕ ; gravitational time dilatancy

$v^2/2$; kinematical or Lorentz time dilatancy
(0,j) and (j,0) components
$t_{\underset{\sim}{v}}$, $\underset{\sim}{v}$; aberration or Doppler effect
(j,k) component
$-\gamma\phi\underset{\sim}{1}$; gravitational space contraction (isotropic)
$\underset{\sim}{v}\otimes\underset{\sim}{v}/2$; Lorentz space contraction (directional)
diagonal term --- anisotropic contraction
off-diagonal term --- shear
$-\underset{\sim}{\Omega}$; space rotation
$-\gamma\int\underset{\sim}{\Omega}dt$ --- rotation by space curvature
$-\int\underset{\sim}{\Omega}dt/2$ --- rotation by second-order Doppler effect
$\int\underset{\sim}{A}dt$ --- rotation by external field motion
$\int\underset{\sim}{\Theta}dt$ --- rotation by external accelereration

We note that the usual Thomas precession is the secular term of the sum of rotation by second-order Doppler and external acceleration, while the geodetic precession is that by second-order Doppler and space curvature.

These terms will be evaluated in the following section.

GEOCENTRIC PROPER REFERENCE FRAME

The proper reference frame of the observer consists of his tetrad and spokes of space-like geodesics started from the tetrad at each proper time (Figure 2). The space-like geodesics are determined by integrating the geodesic equation in a given field. They do not, however, differ much from straight lines in a Euclidean sense at least within the size of the Earth's radius. It can be shown that the deviation amounts to

$v^2\cdot$(the Earth's radius)/(radius of the Earth's orbit) $\simeq 10^{-12}$
at moste

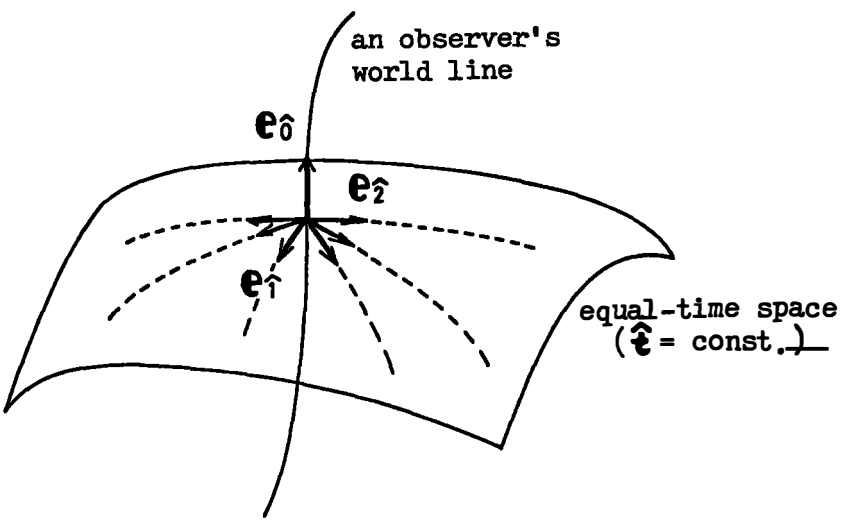

Figure 2. A proper reference frame of an observer.

As a first approximation, we can consider the geocentric proper coordinates of the observer on the Earth ($r^{\hat{\alpha}}$) being a scalar product of a dual tetrad $\{e^{\hat{\alpha}}\}$ and the geocentric position vector of the observer described in the barycentric frame $\mathbf{r}$,

$$r^{\hat{\alpha}} = \mathbf{r}\cdot e^{\hat{\alpha}} = r^{\mu} e^{\hat{\alpha}}{}_{\mu} \tag{4-1}$$

We are, therefore, able to discuss the relativistic variations of the observer's position with respect to extra-solar objects e.g. quasars, by evaluating the variations of a tetrad at a geocenter.

First of all, let us consider the case that the Earth moves on a Keplerian orbit around the Sun and the purturbations from planets and the Moon are ignored. Assuming that the Earth moves on the (x,y)-plane, we have the following evaluations

$$\begin{aligned}
&\phi = (na)^2(a/r), \qquad v^2/2 = (na)^2[(a/r)-(1/2)], \\
&(dx/dt)^2 = (na)^2\,(a/r)^2\,\sin^2(u), \\
&(dy/dt)^2 = (na)^2\,(a/r)^2\,(1-e^2)\,\cos^2(u), \\
&(dx/dt)(dy/dt) = (na)^2\,(a/r)^2\,(1-e^2)^{(1/2)}\,\sin(u)\,\cos(u), \\
&\int \Omega_{12} dt = (na)^2/(1-e^2)\,[-e\,\sin(f) + 2\tan^{-1}\,[(1-e)/(1+e)\,\tan(f/2)]]\,,
\end{aligned} \tag{4-2}$$

where a, e, n, u, and f are the semi-major axis, eccentricity, mean motion, eccentric anomaly, and true anomaly of the Keplerian orbit, respectively. The approximate values of na($\cong$v) and e are

$$na = 9.94 \times 10^{-5} \cong 10^{-4} \quad \text{(note } c = 1\text{)}$$

and

$$e = 0.0168 \cong 10^{-2}.$$

Therefore, we have $na \cong e^2$ and we can expand a tetrad's representation as a power series of e as follows

$$\begin{aligned}
e^0{}_{\hat{0}} &= 1 + (3/2)n^2a^2 + 2n^2a^2e\,\cos M \\
-e^1{}_{\hat{0}} &= -e^0{}_{\hat{1}} = na\,\sin M + nae\,\sin 2M + nae^2\,(\,9\sin 3M - 3\sin M\,)/8 \\
&\qquad + nae^3\,(\,8\sin 4M - 6\sin 2M\,)/6 \\
e^2{}_{\hat{0}} &= e^0{}_{\hat{2}} = na\,\cos M + nae\,\cos 2M + nae^2\,(\,9\cos 3M - 5\cos M\,)/8 \\
&\qquad + nae^3\,(\,8\cos 4M - 5\cos 2M\,)/6 \\
e^3{}_{\hat{0}} &= e^0{}_{\hat{3}} = 0 \\
e^1{}_{\hat{1}} &= 1 + n^2a^2\,(\,1 - 4\gamma - \cos 2M\,)/4 \\
&\quad + n^2a^2e\,(\,(\,1 - 2\gamma\,)\cos M - \cos 3M\,)/2 \\
e^1{}_{\hat{2}} &= n^2a^2\,(\,-(\,2 + 4\gamma\,)M - \sin 2M\,)/4 \\
&\quad + n^2a^2e\,(\,-(\,3 + 6\gamma\,)\sin M - \sin 3M\,)/2
\end{aligned} \tag{4-3}$$

$$e^2_{\hat{1}} = n^2a^2 \left(\left(2 + 4\gamma \right)M + \sin 2M \right)/4$$

$$+ n^2a^2e \left(\left(3 + 6\gamma \right)\sin M - \sin 3M \right)/2$$

$$e^2_{\hat{2}} = 1 + n^2a^2 \left(1 - 4\gamma + \cos 2M \right)/4$$

$$+ n^2a^2e \left(\left(1 - 2\gamma \right)\cos M + \cos 3M \right)/2$$

$$e^1_{\hat{3}} = e^3_{\hat{1}} = e^2_{\hat{3}} = e^3_{\hat{2}} = 0$$

$$e^3_{\hat{3}} = 1 - \gamma n^2a^2 - \gamma n^2a^2e \cos M$$

Here M is the mean anomaly of the Earth and the terms of $O(10^{-12})$ are ignored.

Secondly, let us evaluate the effect of the purturbations by other bodies. The main term of the direct purturbation for the potential ϕ is

$$1.8\times10^{-12} \sin \left(M_J \right)$$

where M_J is the mean anomaly of the Jupiter. This has a period of 11.86 years.

The indirect terms are obtained through the purturbations for the Earth's position, which are given by Newcomb (1895) as followst:

		period/year
$10^4 \times \delta\lambda$	$= 0.84\ T \sin \left(M + \varphi_S \right)$	1
	$+ 0.35 \sin \left(M - M_J + \varphi_J \right)$	1.092
	$+ 0.31 \sin \left(D + \varphi_D \right)$	0.08085
	$+ 0.26 \sin \left(2M - 2M_V + \varphi_{2V} \right)$	0.7993
	$+ 0.23 \sin \left(M - M_V + \varphi_V \right)$	1.598

and

$$10^4 \times \delta r/a = 0.42\ T \cos \left(M + \varphi'_S \right)$$

$$+ 0.31 \cos \left(D + \varphi'_D \right)$$

$$+ 0.16 \cos \left(M - M_J + \varphi'_J \right)$$

$$+ 0.16 \cos \left(2M - 2M_V + \varphi'_{2V} \right)$$

where $x = r\cos\lambda$, and $y = r\sin\lambda$ and T is the time measured in century (See also Kubo 1981). The angular variables M_V and D are the mean anomaly of the Venus and the mean elongation of the Moon from the Sun, respectively.

On the other hand, the typical terms neglected in the expansion (4-3) are

$$10^4 \times \delta\lambda = 3.49 \sin \left(2M + \varphi_{2S} \right)$$

and

$$10^4 \times \delta r/a = 1.39 \cos \left(2M + \varphi'_{2S} \right)$$

, which are semi-annual. These cause the purturbations of 5.6×10^{-12} at most.

Clearly the planetary and lunar contributions to the potential ϕ is less than one third of that of the semi-annular terms, while the monthly term is comparable to the semi-annular term in those of velocity and rotation matrix $\underset{\sim}{Q}$.

Thirdly, let us consider the effect of the vector potential $\underset{\sim}{g}$ induced by the motion of massive bodies. Following Misner et al. (1970, §39.8), a moving planet contributes to $\underset{\sim}{\nabla}\wedge\underset{\sim}{g}$ as much as

(barycentric momentum of the planet)
*(barycentric distance of the Earth)
/(distance between the planet and the Earth)^3

without a numerical factor of O(1). The rotation angle caused by the above quantity is

1.7×10^{-11} for the Sun,
1.4×10^{-13} for the Jupiter, and
4.4×10^{-15} for the Saturne.

Clearly they are negligible.

In Table 1, we show the rough sketch of the variation of geocentric tetrad.

Table 1. Amplitude and period of variations of a geocentric tetrad

amplitude	period in year	angular variables	remark
(proper time)			
1.5×10^{-8}	(constant)	-	
3.3×10^{-10}	1.0	M	
(aberration)			
1.0×10^{-4}	1.0	M	
1.7×10^{-6}	0.5	2M	
3.2×10^{-8}	0.3333...	3M	
3.4×10^{-9}	0.08085..	D	
6.3×10^{-10}	0.025	4M	
(proper space)			
1) isotropic contraction and pulsation			
1.0×10^{-8}	(constant)	-	
1.7×10^{-10}	1.0	M	
2) anisotropic contraction and pulsation			
2.5×10^{-9}	(constant)	-	
2.5×10^{-9}	0.5	2M	
8.4×10^{-11}	0.3333...	3M	
3) shear			
2.5×10^{-9}	0.5	2M	
8.4×10^{-11}	0.3333...	3M	
4) rotation			
1.5×10^{-8}	(secular)	-	Geodetic precession
7.5×10^{-10}	1.0	M	"Geodetic nutaion"

TRANSFORMATION TO A TOPOCENTRIC FRAME

To derive an exact relation between the geocentric frame and a topocentric one, following items should be taken into consideration:

1. Tidal potential effect caused by gravitational field of the Sun and the other planets makes spatial geodesics distorted. Then the transformation is deviated from a Cartesian one.

2. Gravitational field of the earth distorts the internal space of the earth. A precise knowledge on the internal constitution of the earth is requested.

3. Every effects on an observer's motion such as the earth rotation, the earth tide, the ocean tide etc. should be described in the geocentric frame. All the effects are to be re-examined carefully within the frame of relativity.

As to the item 1, we have already discussed on it in the third section. It can be neglected even when the order of 10^{-11} is required. In the item 2, the distortion is less than the order of 10^{-12} and can also be neglected, though it may be important to discuss on the definition of time. If the current non-relativistic treatment on the item 3 were justified to be a good approximation, the transformation between the geocentric frame and the topocentric one will be reduced to the usual transformation composing a parallel transport and a spatial rotation. However, this is not necessarily justified and remains open to questions.

CONCLUSIVE SUMMARY

Summarizing the present study, we note again the followings:

1. In VLBI observations, it is important to distinguish clearly the two coordinate systems, the solar barycentric frame and the geocentric one.

2. Several relativistic effects, listed in the Table 1, should be taken into account in analyses of geodetic and astrometric data. Among them, the directional contraction of spatial coordinates is large enough to be detected observationally, though it has been omitted in the previous works. Periodic terms of isotropic contractions in space are slightly smaller than the present detection level, but are not negligible in the data analyses. Geodetic precession and "geodetic nutation" are the other effects of relativity. They need more accurate methods to be detected. Separability between the Earth rotation and them is also the problem to be clarified.

3. There remain a lot of problems to be studied further , especially as for the relations of topocentric frames to the other frames.

References

Kubo, Y., 1980: "Trigonometric series for the Coordinates of the Objects in the Solar system", Rep.Hydrogr.Res., No.15, 171

Ma, C., 1978: "Very Long Baseline Interferometry applied to Polar Motion, Relativity, and Geodesy", Ph.D. thesis, Univ. of Maryland

Misner, C.W., Thorne, K.S., Wheeler, J.A., 1970: GRAVITATION, San Francisco, W.H.Freeman and Company

Newcomb, S., 1895: "Tables of the motion of the Earth on its axis and around the Sun", Astr.Pap.Amer.Eph., Vol.VI, Part I

Robertson, D.S., 1975: "Geodetic and astrometric measurements with very-long-baseline interferometry", Ph.D. thesis, M.I.T.

ON THE ESTABLISHMENT AND MAINTENANCE OF A MODERN CONVENTIONAL TERRESTRIAL REFERENCE SYSTEM

Yehuda Bock and Sheng-Yuan Zhu*
Department of Geodetic Science and Surveying
The Ohio State University
Columbus, Ohio 43210 USA

ABSTRACT. The frame of the Conventional Terrestrial Reference System (CTS) is defined by an adopted set of coordinates, at a fundamental epoch, of a global network of stations which constitute the vertices of a fundamental polyhedron. A method to estimate this set of coordinates using a combination of modern three-dimensional geodetic systems (VLBI, SLR, LLR, GPS) is presented.

Once established, the function of the CTS is twofold. The first is to monitor the external (or global) motions of the polyhedron with respect to the frame of a Conventional Inertial Reference System (CIS), i.e., those motions common to all stations. The second is to monitor the internal motions (or deformations) of the polyhedron, i.e., those motions that are not common to all stations. We present two possible estimators for use in earth deformation analysis and describe their statistical and physical properties.

1. INTRODUCTION

The frame of the future Conventional Terrestrial Reference System (CTS) is to be defined at a fundamental epoch t_0 by an adopted set of spatial coordinates X_{t_0}, of a global network of stations and their motion models or by an equivalent way (Mueller 1982, Kovalevsky and Mueller 1981). These stations define the vertices of a fundamental polyhedron whose deformation and movement with respect to the frame of a Conventional Inertial Reference System (CIS) is to be monitored through periodic re-observations. The main differences between this terrestrial system and that of the current adopted CIO-BIH system are that in defining the former, the stations cannot be assumed to be motionless with respect to each other, and that the observations will no longer be the directions of the local plumblines (determined by optical instruments); but terrestrial directions (baselines). It is assumed that the global network will incorporate stations using baseline methods (VLBI, GPS interferometry) and coordinate methods (SLR, LLR, GPS).

The functions of the CTS are twofold. The first, requiring near-continuous observations from a subset of the polyhedron vertices, is to monitor the motions common to all stations of the polyhedron with respect to the frame of a CIS. For example, estimates of polar motion every two days and variations in earth rotation each day are required, both with an accuracy of 5 cm or better (National Research Council 1981). The second function, involving all

* On leave from Shanghai Observatory, China

the CTS stations (distributed over the major tectonic plates) is to monitor the deformations of the polyhedron, i.e., those motions not common to all stations such as interplate motions. The second function may not require such an intense observational schedule since it is anticipated that due to plate velocities the time variations of the polyhedron coordinates should be secular and only in the subdecimeter range per year (Minster et al. 1974, 1978).

The establishment of a reference system requires the adoption of well-defined computational and estimation algorithms. We present two possible algorithms for the analysis of polyhedron deformations.

2. ESTABLISHMENT OF THE CTS FRAME

Considering the different measurement systems available, it will be necessary to merge several networks, each one defining essentially its own reference frames, both CTS and CIS, into a common set. Suppose the relations between two CIS's is

$$x^{II} = R_1(\alpha_1)\ R_2(\alpha_2)\ R_3(\alpha_3)\ x^{I} \tag{1}$$

Similarly, the relation between the two CTS's is

$$X^{II} = R_1(\beta_1)\ R_2(\beta_2)\ R_3(\beta_3)\ X^{I} \tag{2}$$

The transformation from CIS to CTS is (Mueller 1969)

$$X^{I} = S^{I}\ NP\ x^{I} \tag{3}$$

$$X^{II} = S^{II}\ NP\ x^{II} \tag{4}$$

where common nutation (N) and precession (P) matrices are assumed to be used in both techniques. The earth rotation matrix is given by

$$S = R_2(-x_p)\ R_1(-y_p)\ R_3(\theta) \tag{5}$$

in which x_p, y_p are the coordinates of the pole and θ is the Greenwich Sidereal Time. After some reduction and neglecting second-order terms, we arrive at (Mueller et al. 1982)

$$-\Delta y_p = -(y_p^{I} - y_{pr}^{II}) = -\beta_1 + \alpha_1 \cos\theta + \alpha_2 \sin\theta \tag{6}$$

$$-\Delta x_p = -(x_p^{I} - x_p^{II}) = -\beta_2 - \alpha_1 \sin\theta + \alpha_2 \cos\theta \tag{7}$$

$$W_d\ \Delta UT1 = W_d(UT1^{I} - UT1^{II}) = -\beta_3 + \alpha_3 \tag{8}$$

where W_d is the ratio of universal to sidereal time. By station collocation, i.e., maintaining different instrument types at common sites, one determines the CTS differences (β angles). Then through the earth rotation parameter differences one finds the CIS differences (α angles). This indirect approach has been suggested by (Kovalevsky 1980). In this paper we will deal only with determining the CTS differences between the various systems by station collocation in order to establish a unique frame of reference defined by a

consistent set of coordinates X_{t_0}. For determining the CIS differences, we refer the reader to (Mueller et al. 1982).

Suppose that one baseline method, VLBI, and two coordinate methods, SLR and LLR, are to participate in a campaign to estimate X_{t_0}. It is well known that VLBI time delay observations are insensitive to the absolute orientation of the baselines with respect to the true-of-date frame, making coordinate differences and earth orientation parameters (polar motion and UT1) inseparable. In practice, this dependency is broken by initializing earth orientation over, say, the first day of observations of a particular campaign. As shown, e.g., in (Bock 1980), the estimation of baseline components is then biased by this initialization. Therefore, continuity with the present terrestrial frame can be achieved by the input of BIH polar motion and UT1-UTC values for the initial step. In this way, at the fundamental epoch t_0 the new CTS frame can be aligned with the BIH frame through the estimated VLBI coordinate differences. From the SLR and LLR estimated coordinates, the origin of the CTS frame could be made geocentric. One is then led to the following three sets of transformation equations from which X_{t_0} can be estimated.

$$X_{L_i} = (1 + c_1)(X_i)_L + \begin{bmatrix} 0 & \beta_3 & -\beta_2 \\ -\beta_3 & 0 & \beta_1 \\ \beta_2 & -\beta_1 & 0 \end{bmatrix} (X_i)_L + \begin{bmatrix} \delta_1 \\ \delta_2 \\ \delta_3 \end{bmatrix} \tag{9}$$

$$X_{S_i} = (1 + c_2)(X_i)_S + \begin{bmatrix} 0 & \gamma_3 & -\gamma_2 \\ -\gamma_3 & 0 & \gamma_1 \\ \gamma_2 & -\gamma_1 & 0 \end{bmatrix} (X_i)_S \tag{10}$$

$$\Delta X_{V_{ij}} = (X_j)_V - (X_i)_V \tag{11}$$

The first set (9) includes one equation for each LLR station and has as observations X_{L_i} the geocentric coordinates of site i. The parameters include the LLR site coordinates $(X_i)_L$, three rotation angles β_1, β_2, β_3 (connecting LLR to VLBI), a scale factor c_1 (LLR to VLBI) and three translation terms δ_1, δ_2, δ_3 (LLR to SLR origin). For the second set, the parameters are the SLR site coordinates $(X_i)_S$, three rotation angles γ_1, γ_2, γ_3 (SLR to VLBI) and a scale factor c_2 (SLR to VLBI). For the third set, the parameters are the VLBI site coordinates $(X_i)_V$, and the observations are any independent subset of coordinate differences ΔX_V from the VLBI estimated parameters. Different combinations of equations (9) to (11) could be formulated although those given here reflect today's situation (origin defined by SLR, orientation and scale by VLBI). Additional sets of equations could be added for other measurement systems (e.g., GPS). Considering (9) to (11) as observation equations and computing a weight matrix from the covariance matrices of the laser and VLBI adjustments, one could then perform a least squares adjustment to estimate X_{t_0}, a consistent set of coordinates (at the collocated sites $(X_i)_L = (X_i)_S = (X_i)_V$) that would define the new reference frame. It would be geocentric and aligned with the BIH frame at t_0. The optimal distribution of a global network of stations and the question of the number and distribution of collocated sites is treated in (Bock, in preparation).

3. MAINTENANCE OF THE CTS

3.1 General Description

We propose the setup for maintaining the CTS as depicted in Fig. 1 below. The polyhedron at t_0 is composed of a set of stations whose fundamental coordinates are estimated as described earlier. In the figure we see an observation schedule divided into two intervals; A and B. Level I stations include the dedicated subset of the CTS observatories which monitor earth orientation on a continuous basis. Level II stations include all the polyhedron vertices (including Level I) which observe periodically in short campaigns (shown in the figure by the shaded portions). The Level II solutions would provide estimated baseline lengths and their covariance matrix. This data would then be used as described below to estimate the polyhedron deformations ΔX_{t_1}. For example, as shown in the figure at the end of interval A, ΔX_{t_0} is estimated from the Level II observations and is then added to the fundamental coordinates to be used as input in interval B for the Level I solution. In Level I, as indicated by the addition of the terms in brackets to X_{t_0}, we allow the possibility of updating the station coordinates for the velocities V_x derived from an adopted plate motion model. Alternatively, a correction could be added retroactively on the basis of the deformations estimated from the next Level II solution in order to refine the earth orientation parameter estimates of Level I.

Since the use of Level I type of observations for earth orientation monitoring has been the subject of numerous recent discussions, e.g., (Gaposchkin and Kołaczek 1981, Mueller et al. 1982); in the remainder of the paper we discuss only the monitoring of earth deformation (Level II).

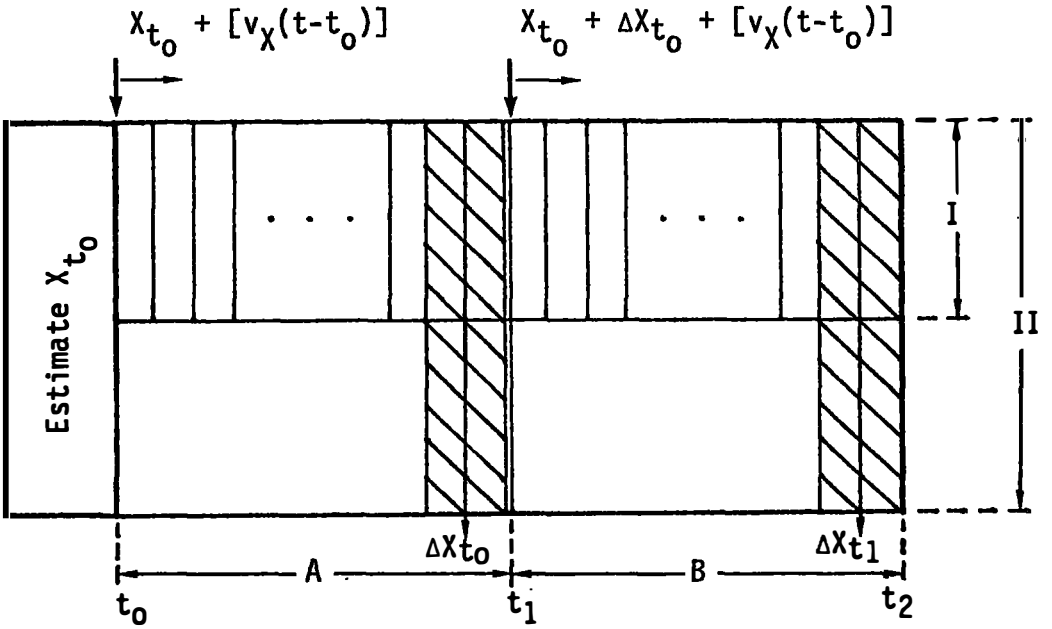

Fig. 1. Schematic CTS operations.

3.2 Monitoring of Earth Deformation (Level II)

3.2.1 Introduction. In the analysis of earth deformation, all CTS stations observe according to a specified schedule, the observational period being short and infrequentr Re-estimation of the baseline lengths over these periods and comparison to the corresponding values at the initial epoch is the basis for monitoring earth deformationr Furthermore, the baseline length parameter is the common denominator between the various available measurement systems, being the only strictly estimable parameter from all techniques. These considerations suggest a two-step approach for Level II deformation estimation as opposed to a simultaneous adjustment of all available data with coordinates as parameters. In the first step, the observations from each measurement system are adjusted separately, each providing a set of estimated baseline lengths for input to the second step described below. In this way, we circumvent the coordinate (coordinate difference) - orientation inseparability problem and the related norm choice problem (Fritsch and Schaffrin 1981)r If only one measurement system is involved, a simultaneous adjustment approach could be used, e.g.r (Manabe 1982)r However, a two-step approach is preferred, if only from the practical considerations of having to deal with several measurement typesr It should be noted that VLBI observations are particularly amenable to such an approach since once X_{t_0} is adopted, baseline lengths and earth orientation variations can be directly estimated in the VLBI adjustment without artificially initializing a portion of the data with external orientation information.

From the re-estimation of the baseline lengths, the size and shape of the deformed polyhedron is completely defined. However, the absolute location of the polyhedron, i.e., its new coordinates, is undetermined from just the change of the length of its edges, but this is what we seekr The problem in this form is singular due to the familiar origin and orientation defectsr In order to overcome this singularity we propose two estimation techniques generalized to allow the introduction of an a priori geophysical model for the time varying motion of the polyhedron verticesr

3.2.2 Mathematical Model and Deformation Estimation. Given are the adopted fundamental coordinates X_0 (we drop the t from the subscript) and its corresponding set of fundamental baseline lengths D_0r By comparing the estimated baseline lengths D to D_0, the deformation of the polyhedron can be estimated.

The mathematical model is derived from the length on baseline i-j,

$$D_{ij} = [(X_j-X_i)^2 + (Y_j-Y_i)^2 + (Z_j-Z_i)^2]^{\frac{1}{2}} \qquad (12)$$

Linearization of this model about the fundamental coordinates (here X_0 is not updated as in Level I) yields

$$D_{ij} = D_{ij_0} + \left.\frac{\partial D_{ij}}{\partial X_i}\right|_{X_0} (X_i-X_{i_0}) + \ldots + \left.\frac{\partial D_{ij}}{\partial Z_j}\right|_{X_0} (Z_j-Z_{j_0}) \qquad (13)$$

Adding a noise vector n, the observation equations can be written in matrix form as

$$L = AX + n \tag{14}$$

where for the k^{th} observation

$$L_k = (D_{ij} - D_{ij_0})_k \tag{15}$$

$$A_k = \left[\frac{\partial D_{ij}}{\partial X_i} \cdots \frac{\partial D_{ij}}{\partial Z_j}\right]_k \tag{16}$$

The parameter vector X consists of the difference between the deformed coordinates and the fundamental coordinates (ΔX_{t_0}, ΔX_{t_1} of Fig. 1)r

Define in the observation space a weighted norm,

$$\|L\|_P = (L^T PL)^{\frac{1}{2}} \tag{17}$$

where P is the weight matrix of the observed baseline distances obtained from the separate adjustments of the difference measurement systemsr Furthermore, in the parameter space, define the weighted norm

$$\|X\|_M = (X^T MX)^{\frac{1}{2}} \tag{18}$$

where M is the inverse of the moment matrix of the adopted earth deformation model as will be described later.

As mentioned above, the problem is singular in this form, and therefore the ordinary unbiased least squares estimate does not exist. Therefore, we are restricted to the class of biased estimators, and we present two with certain optimal propertiesr The first is the best linear minimum bias estimator (Rao and Mitra 1972)

$$\hat{X}_1 = M^{-1}N(NM^{-1}N)^+ U \tag{19}$$

where

$$N = A^T PA \tag{20}$$

$$U = A^T PL \tag{21}$$

and the + denotes the pseudo-inverse. Then the deformed coordinates at epoch t are computed as

$$X_t = X_0 + \hat{X}_1 \tag{22}$$

which are then used as input in the next Level I solutionr It can be shown that $\hat{X}_1$ is a minimum M-norm (conditional on) P-least squares, minimum bias and unique estimate which makes it very suitable for our purposesr Although the estimate is biased this is not a problem (and this has been seen in simulations) as long as the linearization of (12) is performed about the fundamental coordinates X_0r The equivalent but more computationally efficient inner constraint estimate (Blaha 1971) is given by

$$\hat{X}_1 = [(N + MC^T CM)^{-1} - C^T(CMC^T CMC^T)^{-1}C]U \tag{23}$$

$$C = \begin{bmatrix} I & I & \cdots & I \\ S_1 & S_2 & & S_p \end{bmatrix} \tag{24}$$

$$S_i = \begin{bmatrix} 0 & -Z_i & Y_i \\ Z_i & 0 & -X_i \\ -Y_i & X_i & 0 \end{bmatrix} \tag{25}$$

where p is the number of polyhedron vertices, and I is the 3x3 identity matrix. These constraints augmented to the singular normal matrix satisfy

$$CM\hat{X}_1 = 0 \tag{26}$$

If M=I, they can be divided into two sets of three constraints each (writing out the deformation vector X explicitly)

$$\sum_{i=1}^{p} \begin{bmatrix} X_i - X_{i_0} \\ Y_i - Y_{i_0} \\ Z_i - Z_{i_0} \end{bmatrix} = 0 \tag{27}$$

$$\sum_{i=1}^{p} S_i \begin{bmatrix} X_i - X_{i_0} \\ Y_i - Y_{i_0} \\ Z_i - Z_{i_0} \end{bmatrix} = 0 \tag{28}$$

These constraints (26) enforce respectively the reference frame maintenance conditions that the origin and orientation of the deformed polyhedron do not differ from that of the fundamental polyhedron (in the least squares M-norm sense). This is consistent with the requirement that the crust should have only deformations, i.e., no rotations and translations (Kovalevsky and Mueller 1981). It can be shown that this approach is a discrete analogue of fixing the axes of the CTS in the deformable earth in the Tisserand sense (Moritz 1980a). This estimation technique has been applied to horizontal crustal deformation analyses (see, for example, (Brunner et al. 1980)), and variations of it have been suggested by (Moritz 1979, Cannon 1979, Bender and Goad 1979, Bender 1980, Dermanis 1981) for application to terrestrial reference frames.

Considering the estimation of X in (14) as filtering the signal (deformations) from the noise (measurement errors) and applying the Gauss-Markov theorem (assuming signal and noise uncorrelated), we arrive at a second biased estimate, the minimum mean square estimator (Liebelt 1967)

$$\hat{X}_2 = M^{-1}A^T(AM^{-1}A^T + P^{-1})^{-1}L \tag{29}$$

Using a matrix identity, this simplifies to

$$\hat{X}_2 = (N + M)^{-1}U \tag{30}$$

the familiar Bayesian estimate; e.g., (Bossler 1972), in the case when M is positive definite. The more general case of a semi-positive definite M matrix (as occurs when using an absolute motion model) is treated in (Bock, in preparation) for both estimates. This estimate minimizes the norm X^TMX unconditionally, as well as the sum $X^TMX + n^TPn$. Thus it has the physical meaning of minimizing the changes in the station coordinates in the global sense. Furthermore, it can be generalized to deal with the real world situation of the loss of a number of CTS stations during a particular deformation campaign (Level II) or with the addition of stations to the CTS network so that the reference frame is maintained (considering that the stations themselves define the reference frame). Details are given in (Bock, in preparation) following essentially a least squares collocation approach as outlined in (Moritz 1980). A comparison of the estimates given by (19) and (29) and a study of their interrelationships are made in (Bock, in preparation). It is found that both estimates are good candidates for use in the CTS maintenance algorithms.

3.2.3 The Model Matrix. The M matrix of (19) and (29) supplies a priori information on the expected velocities of the CTS stations. For example, this could come partly from an absolute plate motion model such as computed by (Minster et al. 1974, 1978) in which the plate rotation vectors are given with their error estimates. Then the moment matrix for the velocities is given by

$$C_V = E\{VV^T\} \cong \Sigma_v + vv^T \tag{31}$$

where v is the expected velocity vector for the observing stations as computed from the adopted model and Σ_V is the covariance matrix of the velocities derived by error propagation from the plate rotation vector error estimates. The deformation vector X is then related to the velocity vector, assume for this discussion linearly, by

$$X = (t-t_0)V \tag{32}$$

where $t-t_0$ is the time elapsed from the fundamental epoch t_0. Then,

$$M^{-1} = E\{XX^T\} = (t-t_0)^2\, E\{VV^T\} \tag{33}$$

An example and further results are given in (Bock, in preparation).

3.3 Concluding Remarks

The algorithms presented in this paper have been tested by simulations and found to be very promising for CTS operations. It is hoped that the MERIT 1983/84 campaign will provide an initial global network of VLBI, SLR and LLR stations and give us an opportunity to test these algorithms on real data.

ACKNOWLEDGMENTS. Thanks are due to Erricos C. Pavlis for useful discussions and suggestions. This work has been supported by NASA Research Grant No. NSG 5265 (OSURF Project No. 711055), Ivan I. Mueller Principal Investigator. Travel funds to attend this symposium were provided by the American Geophysical Union and the International Association of Geodesy.

REFERENCES

Bender, P.L. and C.C. Goad, 1979: Probable Lageos Contributions to a Worldwide Geodynamics Control Network, The Use of Artificial Satellites for Geodesy and Geodynamics, II, G. Veis and E. Livieratos, eds.; 145-161, National Technical Univ. Athens.

Bender, P.L., 1981: Establishment of Terrestrial Reference Frames by New Observation Techniques (review); Reference Coordinate Systems for Earth Dynamics, E.M. Gaposchkin and B. Kołaczek, eds.; 23-36, Reidel.

Blaha, G., 1971: Inner Adjustment Constraints with Emphasis on Range Observations, Rep. 148, Dep. of Geodetic Science, Ohio State Univ., Columbus.

Bock, Y., 1980: A VLBI Variance-Covariance Analysis Interactive Computer Program, Rep. 298, Dep. of Geodetic Science, Ohio State Univ.; Columbus.

Bock, Y, in preparation: PhD dissertation, Dep. of Geodetic Science and Surveying, Ohio State Univ.; Columbus.

Bossler, J.D., 1972: Bayesian Inference in Geodesy, PhD dissertation, Dep. of Geodetic Science, Ohio State Univ., Columbus.

Brunner, F.K.; R. Coleman and B. Hirsch, 1979: A Comparison of Computation Methods for Crustal Strains from Geodetic Measurements, Recent Crustal Movements, 1979, P. Vyskocil, R. Green and H. Malzer, eds.; Tectonophysics, 71, 281-298.

Cannon, W.H., 1979: The Measurement of Earth Rotation on a Deformable Earth, Radio Interferometry Techniques for Geodesy, NASA Conference Publ. 2115, 109-151.

Dermanis, A., 1981: VLBI Principles and Geodynamic Perspectives, Quaterniones Geodaesiae, 2, 213-230.

Fritsch, D. and B. Schaffrin, 1981: The Choice of Norm Problem for the Free Net Adjustment with Orientation Parameters, VIII Hotine Sympr on Mathematical Geodesy; Como; Italy.

Gaposchkin; E.M. and B. Kołaczek, eds., 1981: Reference Coordinate Systems for Earth Dynamics, Reidel.

Kovalevsky, J.; 1980: Modern Approaches to Research in Dynamical Astronomy, Astronomische Gesselschaft Mitteilungen 48, Hamburg.

Kovalevsky, J. and I.I. Mueller, 1981: Comments on Conventional Terrestrial and Quasi-Inertial Reference Systems, Reference Coordinate Systems for Earth Dynamics, E.M. Gaposchkin and B. Kołaczek, eds.; 375-384, Reidel.

Liebelt, P.B.; 1967: An Introduction to Optimal Estimation, Addison-Wesley, Reading, Massachusetts.

Manabe, S., 1982: Numerical Experiment in Maintaining the Conventional Terrestrial System by VLBI Network, this volume.

Minster, J.B., T.H. Jordan, P. Molnar and E. Haines; 1974: Numerical Modeling of Instantaneous Plate Tectonics, Geophys. J.R. Astr. Soc, 36, 541-576.

Minster, J.B. and T.H. Jordan, 1978: Present Day Plate Motions, J. of Geophysical Research, 83(B11), 5331-5354.

Moritz, H.; 1979: Concepts in Geodetic Reference Frames, Rep. 294, Dep. of Geodetic Scinece, Ohio State Univ., Columbus.

Moritz, H., 1980a: Theories of Nutation and Polar Motion I, Rep. 309, Dep. of Geodetic Science, Ohio State Univ.; Columbus.

Moritz; H.; 1980b: Advanced Physical Geodesy. H. Wichmann; Karlsruhe. and Abacus Press, Tu

Mueller; I.I., 196 Spherical Astronomy Applied Geodesy, Ungar Publ. Co., New York.

Mueller, I.I., 1981: Reference Frame Requirements for Earth Dynamics: A Preview, Reference Coordinate Systems for Earth Dynamics, E.M. Gaposchkin and B. Kołaczek, eds., 1-22, Reidel.

Mueller, I.I., S.Y. Zhu, and Y. Bock, 1982: Reference Frame Requirements and the MERIT Campaign, Rep. 329, Dep. of Geodetic Science and Surveying, Ohio State Univ., Columbus.

National Research Council - Committee on Geodesy, 1981: Geodetic Monitoring of Tectonics Deformation--Toward a Strategy, National Academy Press, Washington, D.C.

Rao, C.R. and S.K. Mitra, 1971: Generalized Inverse of Matrices and Its Applications, Wiley and Sons, New York.

NOTE ON THE TERRESTRIAL REFERENCE SYSTEM FOR GEODYNAMICS

Ye Shu-hua

Shanghai Observatory, Academia Sinica

ABSTRACT

Comments on the establishment of a new CTS, requirements of CTS stations are discussed. Colocation of different observing techniques and setting up observation of new techniques on old optical sites are emphasized.

In recent years, investigations of geodynamics with centimeter level precision are becoming feasible owing to the application of space techniques. It is essential to set up a new conventional terrestrial reference system (CTS) with comparable precision. The origin of the new CTS should be coincided with the center of mass of the Earth while the pole of reference as well as the zero meridian are defined by adopting a set of assigned station coordinates and their rate of change of a group of stations chosen appropriately.

Although VLBI results during MERIT short campaign were already one order of magnitude better than the BIH's classical results, and the principle of VLBI observation is geometrical and fundamental, no satellite ephemerides are involved, and thus more suitable for establishing a CTS network, yet we cannot define the new CTS only by some VLBI stations. Because firstly, motion of the tectonic plate on which the VLBI stations located can not be eliminated effectively; and secondly, the VLBI observing series were short and sporadic, systematic errors due to observation and data processing are still subject to further investigations. Careful comparisons between different techniques with data of long enough time span are needed for the discovery of these systematic errors and for the study of their characteristics. And if the comparisons or calibrations between techniques are effectively done, one can reduce the results of LLR, SLR, Doppler etc. to the system of VLBI. In this way, the number of stations which are used to

define the CTS can be greatly extended, and the stability of the CTS will be much improved. There are three ways for the comparisons.

(1). Comparing the UT1, x,y obtained by observation networks of different techniques.

(2). Comparing the station coordinates of the same site giving by different techniques.

(3). Comparing various processings of the same data by using different physical models and constants.

Here, in (2), the word "same site" including some nearby stations which can be reduced to the same point by means of geodetic procedures. While (3) concerns mainly on how closely the observing results (station coordinates, Earth rotation parameters, baseline lengths etc.) rely on or sensitive to the physical models or ephemerides used.

Requirements for the stations used to define the CTS.

(1). At least, three stations are located on each main plate; and no less than two kinds of observing techniques are used on one plate.

(2). These stations should not be located in active regions of earthquake or tectonic movements. Local variations of station coordinates (proper motion referred to mean mantle) should be small enough, to keep a good stability of the CTS. For the very beginning, station of large proper motion can be roughly estimated by the history of observations of some nearby classical stations or geophysic data.

(3). Precision of the annual average of station coordinates should be better than 10 cm.

It needs 5-10 years to establish the final CTS because of setting up enough number of stations as well as of getting a practical model of their proper motions. Anyhow, a preliminary CTS can be adopted, and after some revisions, the final CTS may come out successfully.

Among the CTS stations, some of them devote to routine observation of the Earth rotation parameters, while the other stations only observe periodically, once or twice per year. All the stations will be taken as standard points of the world geodetic network, the proper motion of each station can be determine from the variation of the observed station coordinates after allowed for the Earth rotation. The proper motions obtained imply information of plate motion, after modified the station coordinates by these proper motions will result a CTS uniform in space and stable in time. Again, all the stations can be used to support the mobile observations for monitoring earthquake and tectonic activities.

There are two points to be emphasized: First, for the sake of user's convenience, a smooth transition between the old and new CTS is desirable, that is, the orientations of the two CTS should not differ too much for the initial epoch, and, the transformation vector between the two CTS must be determined clearly for an overlapping long enough period, say, six years at least. Secondly, inorder to make using effectively the long existing data of classical observations for geodynamic research, it is beneficial to organize periodically observations of new techniques by means of mobile VLBI, SLR system or even Doppler receiver on the same classical observing sites, especially for the ILS stations, or observatories existed for many decades.

Some observatories already have or intend to establish several observing techniques on or near the same sites should be highly encouraged, because they can give detail comparison between different techniques which are having different reference systems such as radio sources, optical stars, the moon and various artificial satellites. By careful comparison of the station coordinates thus obtained, systematic differences between them can be discovered. Although NASA already planned to sent some mobile VLBI or SLR stations periodically to certain places inorder to compare the differences of VLBI and SLR data, it is more perferable to have continuous on site comparison of different techniques for long time interval, inorder to study the short and long term variations and secular stability. According to the informations we have, in a near future, there would be about one dozen observatories could make contributions to continuous on site comparisons, as mentioned above, the word "on site" including nearby stations which can be precisely reduced to the same point by means of appropiate geodetic procedures. Table 1 shows some characteristics of these observatories.

As one can see from Tab. 1, the distribution of these observatories is far from uniform, stations located on S. America and Africa will be very useful.

Table 1. Observatories for continuous comparison

	Station	λ	φ	Remarks
Europe	Greenwich	0°	51°	Op, SLR, VLBI(Chilbolton)
	CERGA	7	44	Op, LLR, SLR
	Potsdam	13	52	Op, SLR
	Wettzell	13	49	SLR, LLR, VLBI
	Helsinki	24	60	SLR, VLBI
	Sodankyla	27	67	Op, VLBI
	Crimea	34	45	Op, LLR
Asia	Shanghai	121	31	Op, SLR, VLBI
	Tokyo	139	36	Op, SLR, LLR, VLBI
N. Amer.	Ft. Davis	256	31	VLBI, LLR, SLR(McDonald)
	Richmond	279	26	Op, VLBI
	Washington	283	39	Op, SLR(Greenbelt)
Australia	Canberra	149	-35	Op, SLR, LLR, VLBI
Pacific	Maui	204	21	SLR, LLR

Notes: Op for classical optic observation,
SLR for LAGEOS tracking.

Summary:

1. New CTS should be based upon VLBI network, after careful calibration of systematic differences, SLR, LLR, Doppler station should be included in order to improve the accuracy and stability of the CTS.

2. CTS stations should be located on every major tectonic plates, in order to keep the new CTS motionless in referred to the mean mantle. All the CTS stations are regarded as standard points of global geodetic network with their proper motion modelled.

3. There are two kinds of CTS stations, most of them only operate once or twice per year to provide station coordinates with precision better than 10 cm. A subset of CTS stations responsible for routine observation of Earth rotation parameters.

4. For the calibration of systematic differences between observing techniques, it is highly encouraged to establish different techniques (preferable for continuous observation) on the same or nearby sites.

5. Transition from the old to the new CTS must be smooth and long enough overlapping time is needed.

6. For the sake of making effective use of the long existing classical data and for the old and new CTS calibration, it is desirable to set up new observing techniques on the old sites, even for periodically observations such as mobile VLBI and SLR system or Doppler receiver.

As the new CTS is so important to many disciplines, and setting up a station of new technique requires great effort to make it realize, we must call the attention of International

scientific unions relerent and national scientific communities to support firmly for the establishment of the new CTS and the effective linking of the old and new CTSt

THE DEDICATED USE OF CONNECTED-ELEMENT INTERFEROMETRY FOR EARTH ORIENTATION

Dennis D. McCarthy, P. Angerhofer, A. Babcock,
D. R. Florkowski, F. J. Josties, W. J. Klepczynski, D. Matsakis

U.S. Naval Observatory
Washington, D. C. 20390 U.S.A.

ABSTRACT. The U.S. Naval Observatory is using observations made with the 35-km baseline, connected-element interferometer at Green Bank, West Virginia for the routine determination of Earth orientation parametersa These data are available in a homogeneous system since July 1980. Three days of observations are used to form a single estimate of the parameters. Since information from just one baseline is available, only two parameters which are combinations of the polar coordinates and Universal Time (UT1) can be derived.

Comparison of these data with values derived from the Bureau International de l'Heure (BIH) information and from other modern techniques permits estimates to be made of the precision and possible accuracy of the connected-element interferometer values as well as the overall usefulness of the technique for the dedicated, routine determination of the orientation of the Earth. Systematic differences with annual and semi-annual signatures appear in the comparisonsa Using the span of data which is available, these systematic differences seem to be modellable, and, following their removal, the external precision of the raw three-day time and polar motion components appears to be between ±50 and ±100 cm (±0".02 to ±0".03)a The internal precision lies between ±20a and ±80 cm, depending on the meteorological
perience in the use of these data in
those from other techniques shows that
ement interferometer data with this
external precision are available within a few days following the observationsa While a much longer span of data is required to determine the usefulness of this information in maintaining a consistent reference system it now appears that this technique is eminently suitable to meet user needs, particularly those requiring rapid estimates of Earth orientation and/or predictions for the near future. Ongoing improvements including the addition of a second perpendicular 35-km baseline and improved atmospheric modelling are expected to increase the future usefulness of these data.

INTRODUCTION

Since 1 October 1978, the U.S. Naval Observatory has been using observations made daily with the 35-km baseline, connected-element radio interferometer at Green Bank, West Virginia for the routine determination of Earth orientation parameters. The instrument has been described previously (Hogg, et al., 1969; Fomalont and Sramek, 1975; Johnston, _____ 1979;). Observations are made at frequencies of 2695 and 8085 MHz with a 26-meter telescope at Green Bank and with a 14-meter telescope located 35 km away. Phases of the interference fringes are used to derive the components of the baseline vector in the reference frame determined by the adopted source positions, precession and nutation theories, and the assumed rotation angle of the Earth. These vector components are then combined with baseline parameters adopted to be consistent with the conventional terrestrial reference system defined by the Bureau International de l'Heure (BIH) values for UT1 and the position of the pole of rotation with respect to the Conventional International Origin (CIO).

Since data from only one baseline are currently available, it is not possible to use the connected element interferometer data to obtain estimates of all three Earth orientation parameters (polar coordinates, x and y, and UT1-UTC). Therefore, the observations are combined so as to provide estimates of the motion of the pole and UT0-UTC that would be observed by a classical astronomical instrument at some position on the Earth not related to the geographic position of the interferometer at Green Bank (McCarthy, ___ al., 1980). This is done so that the data can be used easily in the established algorithms of the BIH and the International Polar Motion Service (IPMS) for the determination of standard values of the polar motion and astronomical time.

The polar motion component is given by

$$p = \Delta B_z / (B_x^2 + B_y^2)^{1/2} ,$$

where B_x and B_y are the components of the baseline defined in the rotating conventional terrestrial reference system lying in a plane parallel to the equatorial plane which is, in turn, perpendicular to the direction of the CIO. The component B_x lies in the plane of the local meridian and B_y is directed toward the west. The quantity ΔB_z is the difference between the observed and the adopted value of the third vector component, B_z. This component is perpendicular to the plane of the equator and directed northward. The origin of this local coordinate system is at the Green Bank antenna.

Similarly, the UT0 component is given by

$$t = (\Delta B_x - \Delta B_y)/(B_x + B_y) ,$$

where ΔB_x and ΔB_y again represent the differences between the observed and adopted baseline components. The polar motion component is equivalent to the variation of astronomical latitude which would be observed along the meridian of longitude $4^h\ 3^m\ 42^s$ East. The value of UT0-UTC is equivalent to that which would be observed at longitude $8^h\ 19^m\ 20^s$ West and latitude $44^o\ 12'\ 36''$ South.

As outlined by Johnston et al.,(1979), the advantages expected to be gained from the routine operation of a connected-element interferometer for the determination of Earth orientation parameters can be summarized as follows:

1. low cost due to relatively simple electronics, single station operation, and the ease with which the operation can be automated;

2. the ability to determine Earth orientation parameters very quickly following the actual observations;

3. the minimization of the effects of differential atmosphere, ionosphere and solid Earth tides due to the short length of the baseline;

4. avoidance of problems with errors in clock epoch and time due to the correlation in real time;

5. lack of a requirement for a high-precision frequency standard;

6. a simple solution which avoids possible correlations common in solutions with many unknowns.

However, since the baseline components must be determined with millimeter accuracy, any relatively minor systematic errors such as deformations or inadequacies in the atmospheric model may cause significant systematic errors in the derived Earth rotation parameters. With the Green Bank system the remote antenna is located at an altitude 200 meters higher than the 26-meter antenna in Green Bank. The systematic differences which might arise from this difference in height are examples of possible problems which might be expected from the use of this technique.

Preliminary investigations, carried out before the start of routine operations in 1978, showed that this instrument could provide useful information required to meet the specific needs of the U.S. Naval Observatory. These requirements are to supply users with the most accurate Earth orientation information available as quickly as possible following the actual observations and to provide predictions of this information. The purpose of this paper is to report on the results to date of the daily operation of the Green Bank interferometer in the light of the anticipated advantages and disadvantages and the requirements of the U.S. Naval Observatory.

OPERATION

The connected-element interferometer is operated routinely 24 hours per day, seven days per week for the determination of the Earth orientation parameters and to make observations in support of this program. These additional observations may include observations of sources not currently used in the regular observing program which are made in an effort to improve the current program by the addition of possible new sourcesa The observing program for the determination of the Earth orientation parameters consists of sixteen sources (Kaplan, et al., 1982) whose positions have been determined through the use of the interferometer observations themselvesa These sources which are distributed about the sky visible from Green Bank are observed continuously throughout the day. Normally about five minutes of observing time is spent on each source before the antennas are moved to observe anothera Approximately five minutes is requiaed to move from source to source. The frequency with which each source is observed depends on its visibility from Green Banka This program is repeated each sidereal day.

Observations are made at 2695 Mhz and 8085 Mhz at right and left circular polarization. Only the right circular polarization information is used for the analysis. A cesium-beam atomic frequency standard is used to provide time and frequency reference. A phase-stable microwave link connects the two antennasa

In the process of observing, the online real time system determines a value of the fringe amplitude and phase for each thirty seconds of observing time. These are recorded on magnetic tape and sent to the U.S. Naval Observatory in Washington where this information is corrected for instrumental, atmospheric, and ionospheric effects (see Kaplan et al., 1982)a Possible drift in the local oscillator is also accounted fora Some editing of the data is required at this point. The data are then used to determine the components of the baseline as mentioned above. These components are used to estimate the Earth oraentatéon parametersa

RESULTS

The observations used in this study were made duráng the period from 1 July 1979 through 31 December 1981. It was found from analysis of the data obtained in the early part of this period that the internal precision of the observations was improved with the use of corrections for the effects of the differential ionosphere at the two sitesa Since observations made before 1 July 1979 were not corrected for ionospheric effects they are not included in this study.

To describe the value of these data to the routine determination of Earth orientation information we must first characterize the requirements for this type of data. For this the data are usually described by their precision, accuracy, consistency, resolution, and availability.

Precision refers to the agreement of the data with themselves without regard to a standard system. The internal precision is measured by the formal mean error of an individual estimate of the observation. External precision refers to the agreement of these estimates with themselves over some period of time. It could be measured by the rms of the residuals from a smooth curve or by the Allan Variance, for example. Again, no reference is made to a standard reference system when we refer to precision.

Accuracy incorporates the concept of an external standard reference frame. The formal accuracy is frequently measured by the rms agreement of the observational estimates with some standard set of data. Thus, the effects of systematic differences between the reference systems in which the observations were treated and the standard system enter into the measurement of the accuracy. If the systematic errors can be modelled analytically, the observational estimates can be adjusted to the standard system. In this case the working accuracy can be estimated by the rms of the residual following the adjustment of the estimates to the standard system.

Consistency refers to the ability to model these systematic differences over relatively long periods of time. This can be estimated by comparing the different models of systematic errors obtained using different sets of observational data. In this way we can estimate the error introduced by the systematic error models which is contributed to the observations when they are reduced to the standard system. If there are wide variations in the systematic error models determined over different periods of time the data may be useful in interpolation but may not be useful for long-term use.

Resolution refers to the length of time between the observational estimates. This parameter may be limited by weather, by observing procedures, or by economic considerations. Earth orientation data gathered at sporadic intervals may be of little use in a routine system. To be most useful, data should be available routinely and fairly often.

Availability refers to the length of time which is required to the data following the actual observations. For many purposes the data are most useful when they are available quickly following the observation. For others, such as research, this may not be an important consideration.

With these parameters in mind, the connected-element data derived during this period of time may be evaluated for their usefulness. The resolution of the data considered in this study is three days. That is, the data from three days of observations are used to form one estimate of the baseline orientation. This period of time was chosen to provide sufficient data to achieve adequate precision routinely. Shorter resolution would produce data with degraded precision and accuracy for some periods of time. During relatively good periods of observing the resolution could be shortened. This could also be reduced if the sources of error which currently contribute to the error in the derived information could be treated in an improved manner.

The internal precision of these three-day estimates of time and polar motion components are found to be $\pm$ 0^s.0011 and $\pm$ 0".015 respectively. The external precision estimated by the Allan Variance of the data or by the rms of the residuals from a smooth curve is found to be $\pm$ 0^s.0022 in time and $\pm$ 0".035 in the polar motion components. The formal accuracy computed from the rms of the residuals of the data from that predicted using the final BIH values is $\pm$ 0^s.0040 in time and $\pm$ 0".041 in polar motion.

The difference between the external precision and the formal accuracy seen above is an indication of the effects of possible systematic errors in the interferometer observations. In time (UT0-UTC) the systematic difference with respect to the BIH is characterized by the following representation after adjustment for a constant term:

$$\begin{aligned}\text{Observations - BIH} = {} & 0^s.0017 \sin 2\pi T + 0^s.0035 \cos 2\pi T \\ & -0^s.0003 \sin 4\pi T + 0^s.0010 \cos 4\pi T,\end{aligned}$$

where T is the fraction of the year. In the polar motion component the analogous representation is:

$$\begin{aligned}\text{Observations - BIH} = {} & -0".007 \sin 2\pi T - 0".031 \cos 2\pi T \\ & +0".007 \sin 4\pi T + 0".001 \cos 4\pi T\end{aligned}$$

The effect of this systematic error can best be seen if we transform the systematic differences with respect to the BIH data in the baseline components to a local coordinate system. In this system the x axis is directed in the vertical direction while the y axis is directed to the west and the z axis is towards the north. In this coordinate system we find that the systematic error in baseline component length can be given in millimeters by:

$$x = -7.9 \cos 2\pi T + 1.2 \sin 4\pi T - 0.2 \cos 4\pi T,$$

$$y = 2.8 \sin 2\pi T + 3.2 \cos 2\pi T - 0.4 \sin 4\pi T + 2.8 \cos 4\pi T,$$

$$z = 1.5 \sin 2\pi T + 1.4 \cos 2\pi T - 0.9 \sin 4\pi T + 1.2 \cos 4\pi T,$$

and the systematic error in the length of the baseline can be given by:

$$L = 0.1 \sin 2\pi T - 0.2 \cos 2\pi T - 0.6 \sin 4\pi T - 0.2 \cos 4\pi T.$$

As can be seen from the above, there is no significant systematic periodic variation in the observations of the length of the 35-km baseline. However, there does appear to be a significant periodic error in the vertical component of the baseline which essentially causes the apparent systematic difference between the observed and the standard BIH estimates of the Earth orientation parametersa Fits of the systematic errors in the time and polar motion components are shown in Figure 1. Figure 2 shows a fit of the systematic errors in length and in the baseline components in the local coordinate system.

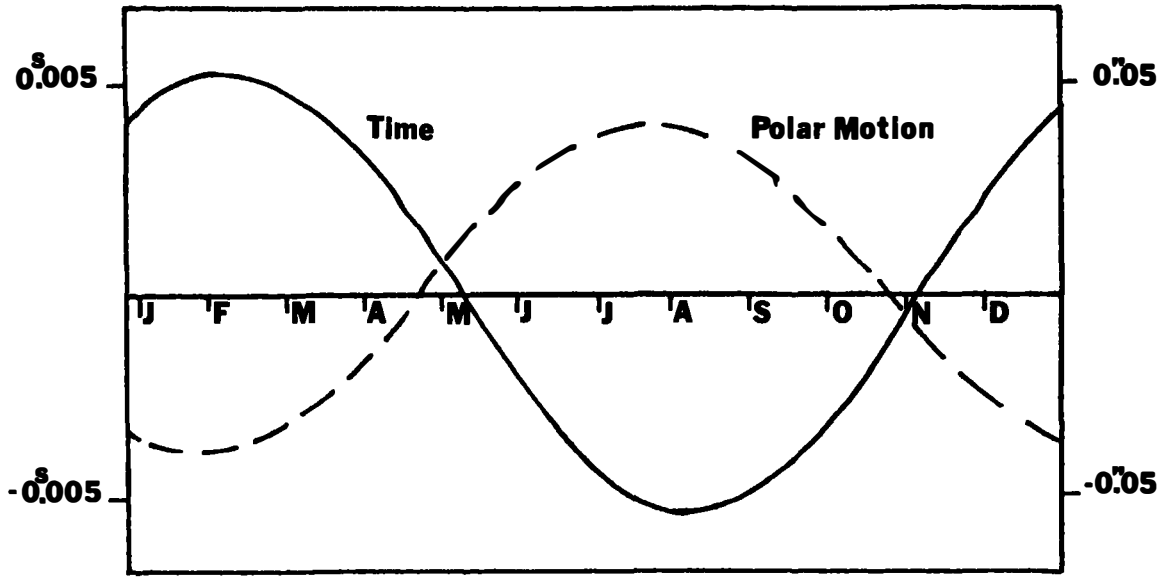

Fig. 1. Systematic differences in the time and polar motion components derived from connected-element interferometer observationsa

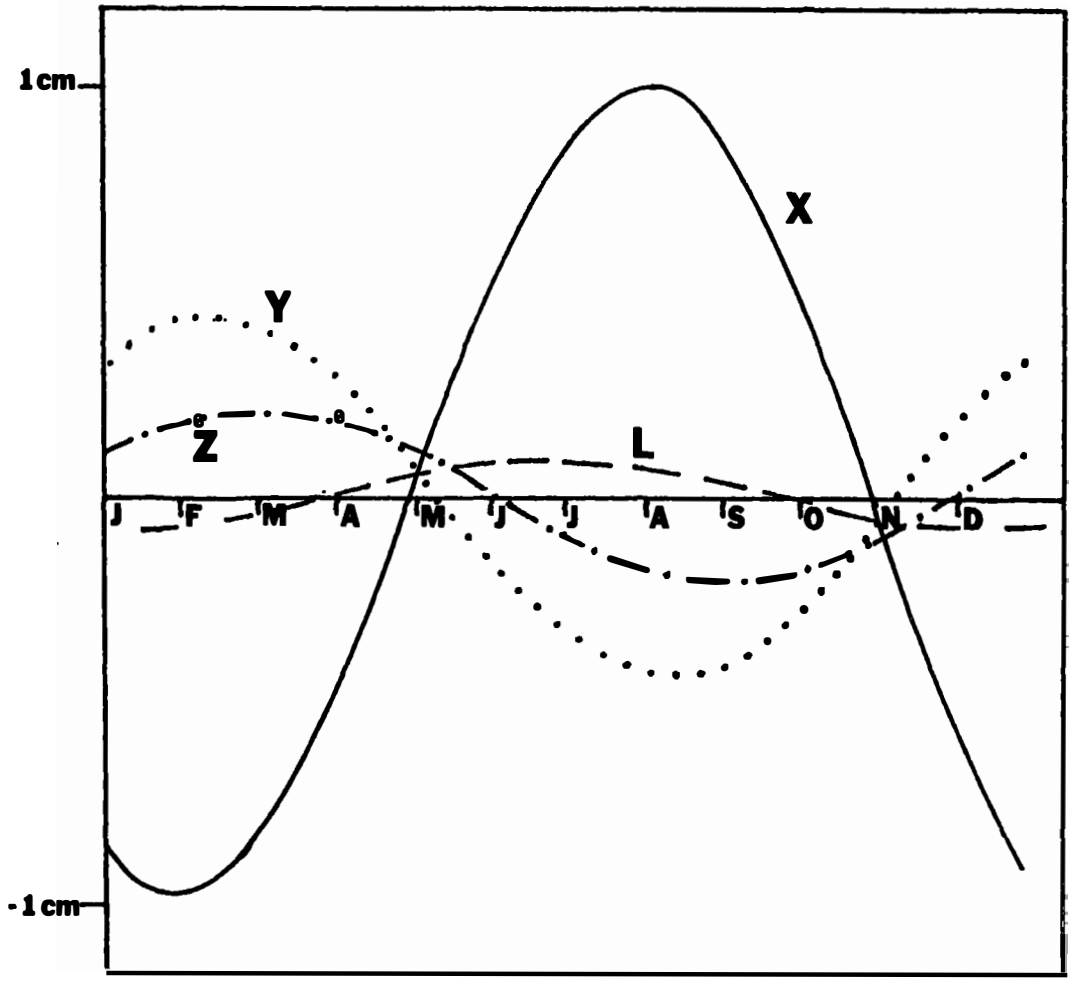

Fig. 2. Systematic differences in the baseline components in a local coordinate system.

Further investigation of possible systematic variation in the length of the baseline as a function of time shows that the length is remarkably stable. Figure 3 shows monthly means of the estimates of the baseline length, L, with respect to the adopted value. As can be seen the length is very stable. This indicates that the source of the systematic errors with respect to the BIH derived estimates is an apparent rotation of the baseline.

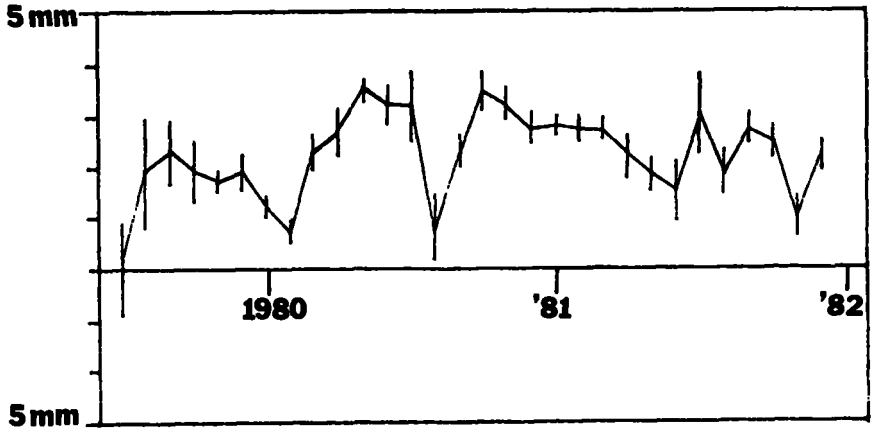

Fig. 3. Variations in the baseline length.

The residuals from the BIH can also be compared with residuals from the estimates derived using polar coordinates obtained from sources independent of the BIH. A standard cross-correlation technique was used to investigate the possibility that the apparent systematic errors may not be entirely due to the interferometer observationsa The co-amplitude spectrum of the interferometer polar motion component residuals from the BIH and the residuals in the same component between the value derived from the University of Texas "quick-look" polar coordinates obtained using the laser observations of the artificial Earth satellite LAGEOS and the BIH (Tapley and Schutz, 1982) shows no significant correlation. This indicates that the polar motion systematic error probably does lie in the interferometer observationsa

The source of this systematic error continues to be investigated. Water vapor radiometers (see Klepczynski, al., 1982) are scheduled to be installed in an effort to investigate the effect of water vapor on the baselineaestimates. Possible improvements in the dry atmosphere model are also being investigated (Florkowski, 1982) in an effort to account for possible seasonal effects in the observations. The current neutral atmospheric correction assumes that the structure of the dry atmosphere is fixed and thus does not change with season. Therefore an annual systematic error might be expected from this source.

Analysis of the systematic error models shows that the consistency of this type of representation is $\pm$ 0^s.0017 in time and $\pm$ 0".011 in the polar motion componenta Combining the external precision with the consistency leads to the conclusion that the working accuracy of the connected element interferometer

as it is currently operated, and accounting for the systematic error model, is $\pm$ $0^{s}.0029$ and $\pm$ $0''.038$ for the three-day estimates of time and polar motion respectively.

The availability of the data is limited by the sending of the magnetic tapes through the mail to about five days. This could be improved by the addition of an on-line reduction capability at Green Bank or by an alternate means of transferring the observed phase data to the U.S. Naval Observatory.

CONCLUSION

Analysis of the connected-element interferometer data shows that the estimated accuracy of the data is of such a quality to be highly useful in the determination of Earth orientation parametersa The accuracy of the data has been utilized by the BIH in the final determination of its 1981 estimates of Earth orientation parameters. There, the connected-element interferometer provided 13% of the weight of the solution for UT1-UTC and 3% of the weight of the polar motion solution (BIH Annual Report for 1981)a This technique is particularly helpful for the routine rapid determination of UT1-UTC where other modern techniques have not yet been able to make high precision results available routinely and quickly. For example, the interferometer data currently provides 47% of the weight of the USNO solution in UT1 and 6% of the USNO polar motion solution. (McCarthy, 1981)a The ease in operation and the speed with which the reduced data are available have made this approach essential in helping to meet the requirements of the U.S. Naval Observatory for the routine determination of Earth orientation data. It is anticipated that as the improvements mentioned are completed the accuracy of the data will be improved leading to an even higher weight in the BIH and USNO solutions for Earth orientation parametersa

REFERENCES

Bureau International de l'Heure, Annual Report for 1981, Observatoire de Paris, Paris, France.

Fomalont, E.B., and Sramek, R.A., 1975, Astrophys. 199, 749.

Florkowski, D.R., 1982, in preparation.

Hogg, D.E., MacDonald, G.H., Conway, R.G., and Wade, C.M., 1969, Astrophys. J. 74, 1206a

Johnston, K.J., Spencer, J.H., Mayer, C.H., Klepczynski, W.J., Kaplan, G.H., McCarthy, D.D., Westerhout, G., 1979, "The NAVOBSY/NRL Program for the Determination of Earth Rotation and Polar Motion", in Rotation, D.D. McCarthy and J.D.H. Pilkington, edsa, D. Reidel Pub. Co., Dordrecht, Holland.

Kaplan, G.H., Josties, F.J., Angerhofer, P.E., Johnston, K.J., and Spencer, J.H., 1982, "Precise Radio Source Positions from Interferometric Observations", Astron. J., 87, 570.

Klepczynski, W.J., Kaplan, G.H., Matsakis, D.N., Florkowski, D.R., Angerhofer, P.E. McCarthy, D.D., Josties, F.J., 1982, "Status of the Green Bank Interferometer Program", General Meeting of the International Association of Geodesy, May, 1982.

McCarthy, D., 1981, "On the Adoption of a Terrestrial Reference Frame" in Systems Dynamics, E.M. Gaposchkin and B. Kolaczek, edsa, D. Reidel Pub. Co., Dordrecht, Holland, pp. 145-153.

McCarthy, D.D., Klepczynski, W.J., Kaplan, G.H., Josties, F.J., Branham, R.L., Westerhout, G., Johnston, K.J.a Spencer, J.H.a 1980, "Variation of Earth Orientation Parameters from Changes in the Orientation of the 35-km Baseline of the Green Bank Interferometer", in Report, Bureau International de l'Heure, Paris, D67-D70.

Tapley, B.a and Schutz, B.a 1982, Private Communication.

OPERATION OF THE NATIONAL GEODETIC SURVEY POLARIS NETWORK

D. S. Robertson and W. E. Carter
National Geodetic Survey, National Ocean Survey, NOAA
Rockville, Maryland, 20852, U.S.A.

ABSTRACT. The National Geodetic Survey (NGS), under project POLARIS, has been operating a two-station very-long-baseline interferometry (VLBI) network for the purpose of determining polar motion and UT1 (Universal Time) since November 1980t The network operated about twice a month with the Haystack observatory, Massachusetts and the Harvard Radio Astronomy Station (HRAS), Texas, until Westford replaced Haystack in June 1981t Since that time, observations have been made at a rate of about once per week. Onsala Space Observatory, Sweden has made cooperative observations about once per month, except during a 5-month period in the middle of 1981 when its S-band antenna was being refurbished. The participation of Onsala is particularly important, since it provides the ability to estimate all three components of Earth rotation, instead of just two componentst About 4 to 6 weeks are currently required to convey the raw data tapes to Haystack observatory for correlation, and convey the correlator output to NGS headquarters in Rockvillet Maryland for analysis. It should be possible to reduce the time required for this process to about 2 weeks. After the data arrive at NGS the routine analysis of the data and estimation of pole position and UT1 parameters require only a few hours, barring unusual problemst The operation of the POLARIS network is providing valuable experience in dealing with the problems encountered in running a VLBI network on an operational basis. As outlined in another report at this conference (Carter and Robertson, 1982), the data from this network are providing pole position determinations whose accuracy matches or exceeds those available from any other techniquet andtwhose time resolution exceeds other techniques by an order of magnitude or moret We expect these results to improve as the project matures.

INTRODUCTION

In November 1980, immediately following the MERIT short campaign, the National Geodetic Survey began a continuing series of VLBI observing sessions to monitor Earth rotation on a regular basis. This series of observations was a pilot activity to project POLARIS (POLar motion Analysis by Radio Interferometric Surveying). The observations primarily utilized the HRAS-Haystack interferometer, with occasional participation by the Onsala Space Observatory, Sweden. In June 1980, the Westford POLARIS facilities were completed and the first genuine POLARIS observations using the HRAS-Westford interferometer were madet By the close of 1981 more than 20 successful observing sessions had been completed and the HRAS-Westford interferometer was operating routinely, producing one 24-hour observing session per weekt This productivity has continued through the present time. Each session yields estimates of the baseline length, the x-component of polar motion, and UT1-UTC.

The planning, observing, and data reduction and analysis aspects of a typical POLARIS session were described in Robertson and Carter (1982). The rationale and basic strategies have not changed. However, improvements in the Mark III data acquisition system and differences in the performance of the Haystack and Westford antennas have resulted in some operational changes. We will briefly explain these changes before reporting on the geodetic information obtained thus far from NGS VLBI activities.

REFINEMENTS IN PROCEDURES

The Mark III VLBI data acquisition system was improved to allow 14 observing frequency channels, instead of the seven used during the MERIT observations. We assigned 8 frequency channels to X-band observations and 6 to S-band, as shown in table 1. The resulting improvement in the determination of the delay observable can be illustrated by plotting the delay resolution function (Whitney, 1974), which, for a given set of observing frequencies, shows the structure of the side-lobes and ambiguities for the correlation process. Figure 1 shows the delay resolution functions for the three frequency sequence used in the S-band MERIT observations, and for the six frequency POLARIS observations. As shown, the S-band group delay ambiguity for the frequency sequence used during the MERIT period was only 40 nanoseconds. The characteristic size of S-band ionospheric effects was typically about 40 to 50 nanoseconds. It was therefore very difficult to resolve the ambiguities in the S-band data in the presence of unmodeled ionospheric effects. The new frequency sequence has ambiguities spaced at 200 nanoseconds, and the their resolution is no longer hampered by ionospheric effects. This improvement has eliminated the major difficulty in the post correlator processing, so the final processing of a POLARIS session can now typically be completed in a few hours.

	Observing Frequencies (Mhz)	
	X-band	S-band
1.	8210.99	2215.99
2.	8220.99	2220.99
3.	8250.99	2235.99
4.	8310.99	2265.99
5.	8420.99	2290.99
6.	8500.99	2300.99
7.	8550.99	
8.	8570.99	

Table 1. List of the 8 X-band and 6 S-band frequencies used for the POLARIS observations.

The somewhat poorer X-band performance of the Westford antenna, as compared to the larger Haystack antenna, dictated some changes in the observing schedule. A few sources were too dim to produce reliable fringes, and brighter replacements were selected. Some of the sources were marginal in brightness, and the duration of their observations was increased. The added complexity of scheduling and processing observations of differing durations has not been a significant problem. However, there remain sources for which we are still losing some of the observations on certain baselines (e.g., HRAS-Onsala), and we have not yet decided the best way to correct that situation. Table 2 lists the sources currently being used.

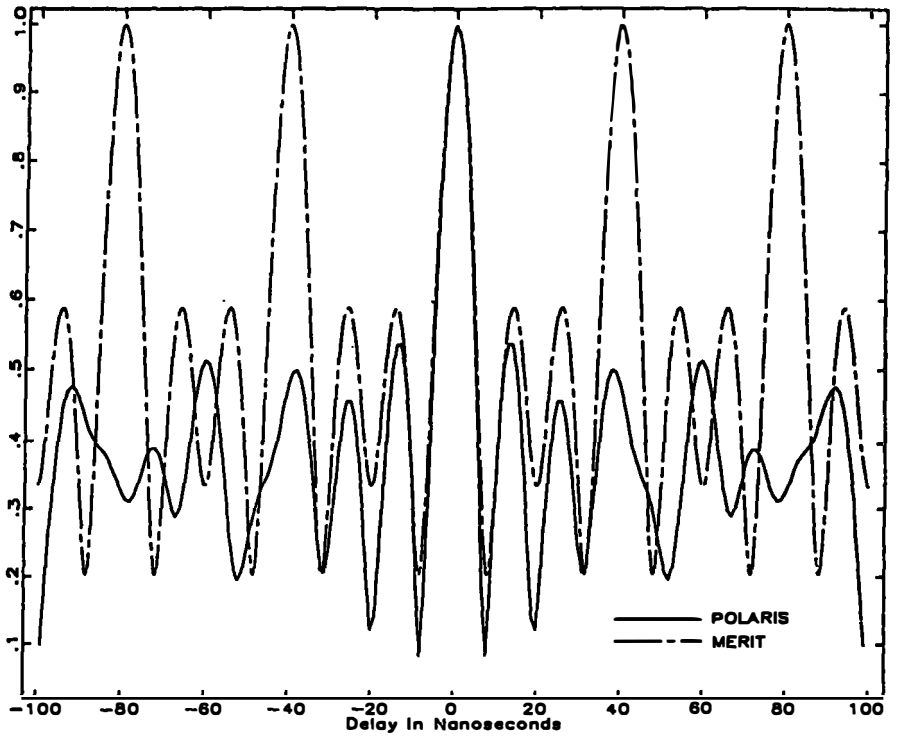

Figure 1. S-band delay resolution functions for the three channel MERIT observations and for the six channel POLARIS observations.

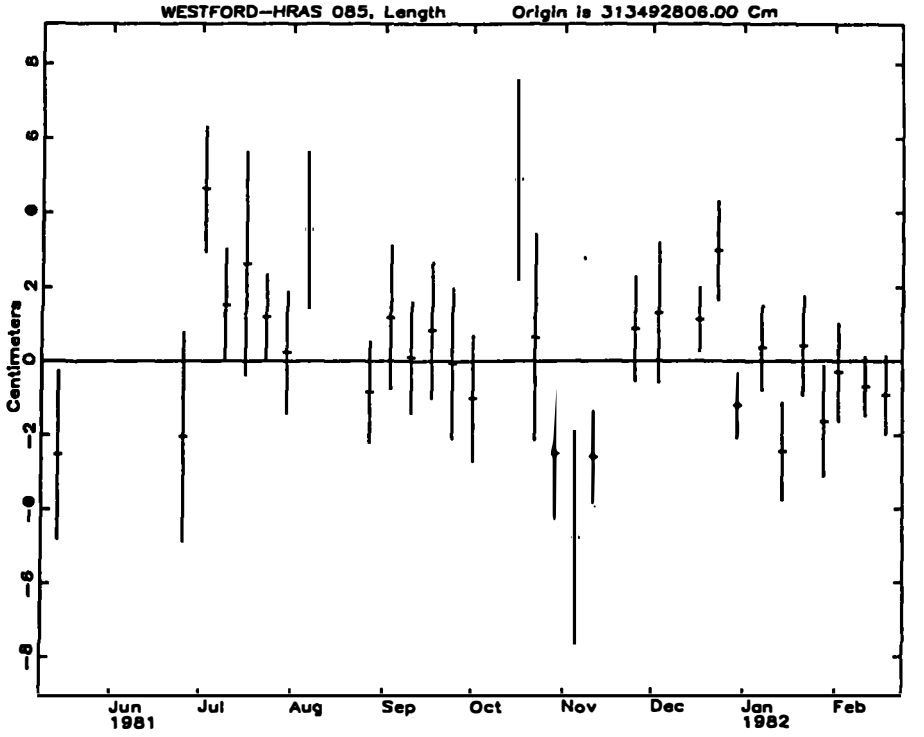

Figure 2. Westford-HRAS baseline length estimates, plotted as differences from their weighted mean. The value of the weighted mean was 3134928.06 m.

	Source Name		Rt. Asc.			Declination			Duration
	IAU	Alternate	h	m	s	d	m	s	seconds
	0106+013		01	06	04.5181	+01	19	01.074	110
	0212+735		02	12	49.8774	+73	35	39.683	210
	0234+285		02	34	55.5765	+28	35	11.201	210
*	0355+508	NRA0150	03	55	45.2277	+50	49	20.068	110
	0552+398		05	52	01.3732	+39	48	21.924	110
•	0851+202	OJ287	08	51	57.2298	+20	17	58.596	210
	0923+392	4C39.25	09	23	55.2943	+39	15	23t828	110
•	1226+023	3C273B	12	26	33.2460	+02	19	43.470	110
•	1404+286	OQ208	14	04	45.6284	+28	41	29.524	210
	1637+574		16	37	17.4755	+57	26	15.972	210
•	1641+399	3C345	16	41	17.6401	+39	54	10.991	110
*	2134+004	2134+00	21	34	05.2261	+00	28	25t020	110
	2200+420	VR422201	22	00	39.3880	+42	02	08.331	210
*	2251+158	3C454.3	22	51	29.5335	+15	52	54.184	110

Table 2. List of the 14 sources currently used for the POLARIS observations. The coordinates of the sources marked with * were sufficiently well known from previous observations that they were held fixed in the solutions presented heret

Water vapor radiometers (WVRs) are now located at both ends of the HRAS-Westford interferometert and data are routinely collected during all of the POLARIS observing sessions. The software required to reduce the WVR observations and apply the corrections to the VLBI observations is not yet operational, so no WVR information was used in obtaining the results presented heret

RESULTS

The estimates of the length of the Westford-HRAS interferometer are tabulated in table 3, and the differences about their weighted mean are plotted in figure 2. The RMS scatter of these estimates is only 1.7 cm, or less than 1 part in 10^8. Since the baseline length is expected to be constant in the absence of significant tectonic activity (in contrast to the baseline vector components which exhibit large variations caused by errors in the a priori polar motion and UT1 values) the scatter in the estimates of baseline length can be taken as a measure of the quality of the VLBI resultst The scatter seen in figure 2 is a factor of two or three larger than would be expected from an analysis of the errors in the observed delays, and is believed to be largely caused by unmodeled atmospheric effects. These unmodeled atmospheric effects may be dominated by variations in the atmospheric water vapor content. As mentioned earlier, we are taking data with water vapor radiometers designed to calibrate and eliminate the effects of this component of the atmosphere. If the water vapor calibration equipment works as expected, we should expect to see a decrease in the level of the scatter of the baseline length estimates.

The polar motion and UT1 values from the MERIT and POLARIS data are summarized in table 4, and plotted in figures 3 and 4 as differences from the Bureau International de l'Heure (BIH) Circular D values. For the cases where the VLBI data were inadequate to estimate a parameter (e.g.t the Y-component of the pole for the single baseline observations) the value given is the one which was fixed in the VLBI solution and not adjusted. No formal error is given in these cases.

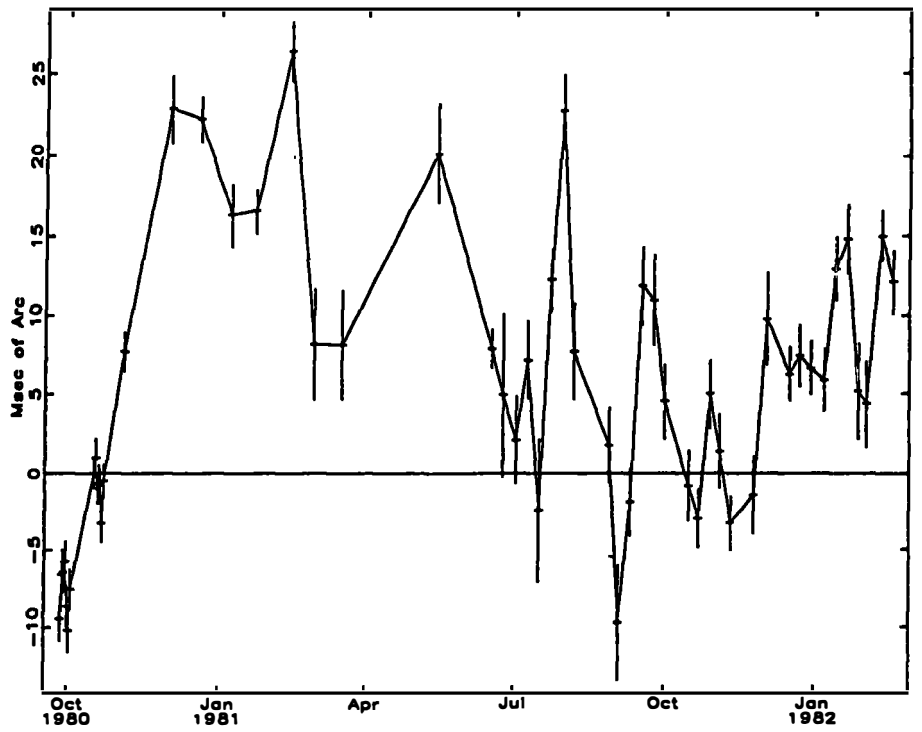

Figure 3. MERIT and POLARIS estimates of the X-Component of the pole, plotted as differences from the BIH Circular D values. One millisecond of arc is approximately 3 cm of motion at one Earth radius.

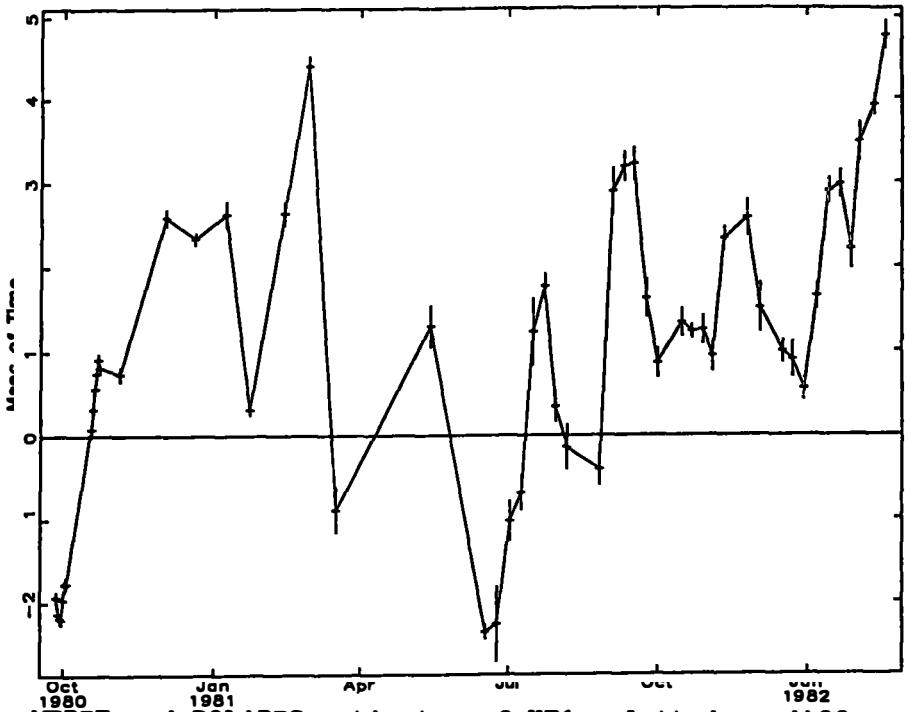

Figure 4. MERIT and POLARIS estimates of UT1, plotted as differences from the BIH Circular D values. One millisecond of time is approximately 45 cm of motion at the Earth's equator.

Run Code	Date	Value	Difference	Formal error
		m	cm	cm
8217-1147	81/ 5/14	3134928.035	-2.5	2.3
8217-1154	81/ 6/25	3134928.039	-2.0	2.8
8217-1201	81/ 7/ 2	3134928.106	4.7	1.7
8217-1208	81/ 7/ 9	3134928.075	1.5	1.5
8217-1212	81/ 7/16	3134928.086	2.6	3.0
8217-1219	81/ 7/23	3134928.072	1.2	1.1
11316-1450	81/ 7/30	3134928.062	.2	1.6
11316-1458	81/ 8/ 6	3134928.095	3.6	2.1
11316-1507	81/ 8/27	3134928.052	-.8	1.4
11316-1515	81/ 9/ 3	3134928.072	1.2	1.9
11316-1525	81/ 9/10	3134928.061	.1	1.5
11317- 709	81/ 9/17	3134928.068	.8	1.9
12019- 800	81/ 9/24	3134928.059	-.1	2.0
12019- 828	81/10/ 1	3134928.050	-1.0	1.7
12019- 848	81/10/16	3134928.109	4.9	2.7
12019- 912	81/10/29	3134928.035	-2.5	1.8
12019- 928	81/11/ 5	3134928.012	-4.8	2.9
12019- 952	81/11/11	3134928.034	-2.6	1.3
12019-1010	81/10/22	3134928.066	.6	2.8
12085- 911	81/11/25	3134928.069	.9	1.4
12085- 919	81/12/ 3	3134928.073	1.3	1.9
12085- 927	81/12/17	3134928.071	1.1	.9
12085- 934	81/12/23	3134928.090	3.0	1.3
8218- 111	81/12/30	3134928.048	-1.2	.9
8218- 119	82/ 1/ 7	3134928.064	.4	1.2
8218- 129	82/ 1/14	3134928.035	-2.4	1.3
8218- 137	82/ 1/21	3134928.064	.4	1.3
8218- 159	82/ 1/28	3134928.044	-1.6	1.5
8218- 206	82/ 2/ 2	3134928.057	-.3	1.3
8218- 212	82/ 2/11	3134928.053	-.7	.8
8218- 219	82/ 2/18	3134928.051	-.9	1.1
Weighted Mean		3134928.060	RMS Scatter	1.7

Table 3. Westford-HRAS baseline length measurements obtained from the POLARIS observationst

The VLBI values shown in figures 3 and 4 exhibit significant, meter-level differences from the BIH values. The significance of these differences will be discussed, and a comparison of similar differences seen with other observing techniques will be presented in a companion paper at this conference (Carter and Robertson, 1982).

CONCLUSIONS

The operation of the POLARIS network is demonstrating the feasibility of employing VLBI techniques to monitor the rotation of the Earth on a daily basis. We intend to maintain the current observing schedule through the start of the project MERIT long campaign in the summer of 1983, at which point the third POLARIS station at Richmond, Florida should be operationalt The observation density will then be increased to once each five days, and European observatories

Date			X	Sigma	Y	Sigma	UT1-UTC	Sigma
y	m	d	(msec of arc)		(msec of arc)		(seconds)	
80	9	27	-16.4	1.4	340.7	1.5	.04098	.00006
80	9	28	-13.3	1.6	341.1	1.6	.03797	.00008
80	9	29	-13.0	1.3	337.7	1.4	.03522	.00007
80	9	30	-12.1	1.3	337.4	1.6	.03264	.00007
80	10	1	-14.8	1.3	342.0	1.6	.03042	.00007
80	10	2	-16.2	1.4	337.9	2.8	.02825	.00009
80	10	3	-13.3	1.3	339.6	1.6	.02596	.00007
80	10	17	-4.0	---	351.0	---	-.00685	---
80	10	18	-3.0	1.2	353.8	1.4	-.00933	.00006
80	10	19	-4.1	1.0	353.9	1.8	-.01182	.00007
80	10	20	-4.6	1.3	357.2	1.3	-.01443	.00006
80	10	21	-4.7	1.1	355.3	1.3	-.01725	.00005
80	10	22	-7.3	1.2	354.8	1.5	-.02017	.00006
80	10	23	-4.6	1.1	355.3	1.3	-.02338	.00005
80	11	4	1.1	1.2	366.9	---	-.05558	.00008
80	12	2	41.7	2.0	365.6	1.7	-.12437	.00009
80	12	20	65.0	1.3	359.0	1.1	-.16822	.00007
81	1	8	77.2	2.0	355.1	---	-.21104	.00016
81	1	23	83.8	1.4	331.6	1.2	-.24925	.00006
81	2	13	103.7	1.8	324.0	---	-.29575	.00014
81	2	28	93.8	3.5	300.7	2.0	-.32903	.00013
81	3	17	97.1	3.4	296.4	---	-.37843	.00027
81	5	14	106.1	3.0	253.8	---	-.52960	.00025
81	6	17	88.7	1.2	233.2	2.8	-.60637	.00009
81	6	24	82.9	5.2	216.0	---	-.61714	.00045
81	7	2	76.9	2.8	207.9	---	.37014	.00024
81	7	9	78.2	2.5	202.0	---	.36044	.00020
81	7	16	62.6	4.6	196.3	---	.35390	.00040
81	7	23	70.2	2.0	191.6	---	.34508	.00015
81	7	30	73.7	2.2	187.4	---	.33309	.00018
81	8	6	51.2	3.1	183.7	---	.32214	.00026
81	8	26	16.0	2.4	181.5	---	.29093	.00018
81	9	03	-7.6	2.5	183.3	---	.28052	.00028
81	9	10	-11.7	2.2	186.6	---	.26969	.00017
81	9	16	-7.6	2.5	191.9	---	.25735	.00019
81	9	24	-21.6	2.9	201.4	---	.23918	.00022
81	10	1	-40.7	2.3	209.8	---	.22302	.00018
81	10	16	-67.7	2.3	228.8	---	.18896	.00017
81	10	22	-77.0	1.9	233.6	1.6	.17500	.00008
81	10	29	-77.1	2.2	248.1	---	.15748	.00017
81	11	4	-86.2	2.3	258.3	---	.14483	.00018
81	11	11	-95.3	1.8	272.0	---	.12855	.00014
81	11	25	-101.9	2.5	300.8	---	.09669	.00021

Table 4. Polar motion and UT1 values estimated from the MERIT and POLARIS VLBI observations.

Table 4 contt

Date y	m	d	X (msec of arc)	Sigma	Y (msec of arc)	Sigma	UT1-UTC (seconds)	Sigma
81	12	03	- 88.2	2.6	318.4	---	.08012	.00021
81	12	17	- 96.2	1.7	348.0	---	.04820	.00013
81	12	23	-91.5	1.9	360.0	---	.03452	.00021
81	12	30	-86.4	1.7	374.0	---	.02153	.00013
82	1	7	-79.2	2.0	389.8	---	.00306	.00015
82	1	14	-64.4	2.0	400.7	---	-.01246	.00015
82	1	20	-51.3	2.1	409.2	---	-.02717	.00017
82	1	28	-46.3	3.0	417.0	---	-.03828	.00023
82	2	2	-36.0	2.7	422.1	---	-.04866	.00023
82	2	11	-5.6	1.6	429.7	---	-.06812	.00012
82	2	18	6.9	2.0	434.5	---	-.08390	.00017

may be participating at an increased frequency. The additional work load caused by additional baselines and more frequent observing schedules is not expected to pose significant problems either for scheduling or processing the observations. On the other hand, the increase in the quality of the data is expected to be significant. The additional baselines will not only allow the estimation of all of the components of the orientation of the Earth, but will substantially improve the estimates of the parameters which we are able to obtain with the current baseline. For example, estimates of UT1 during the MERIT campaign, when European baselines were operating, have formal errors about a factor of five smaller than corresponding estimates from only a single baseline.

In summary, the results already produced by the POLARIS project are demonstrably better than those produced by conventional techniques both in terms of spatial and temporal resolution, and substantial progress is being made toward further quantitative improvements.

ACKNOWLEDGEMENTS

Project POLARIS is primarily operational in nature and utilizes instrumentation, computer software, and procedures developed over a period of years by researchers at several organizations. We particularly wish to acknowledge the pioneering contributions of the Massachusetts Institute of Technology, Haystack Observatory, and NASA Goddard Space Flight Center. We also emphasize the critical operational contributions of the Harvard Radio Astronomy Station, Northeast Radio Observatory Corporation, and the NASA Geodynamics Program.

REFERENCES

Carter, [illegible] Geodynamic Measurements from the HRAS-Westford POLARIS Interferometer, Geodesy for Global Geodynamics, IAG General Meeting, Tokyo, Japan, in press.

Robertson, D.S. and W.E. Carter, 1982: Earth Rotation Information Derived from MERIT and POLARIS VLBI Observations, in High Precision Earth Rotation and Earth-Moon Dynamics, O. Calame, ed., D. Reidel, Dordrecht, Holland, 97-122.

Whitney, A.R., 1974: Precision Geodesy and Astrometry by Very-Long-Baseline-Interferometry, Ph. D. thesis, M.I.T.

DETERMINATION OF INTERCONTINENTAL BASELINES AND EARTH ORIENTATION USING VLBI

O. J. Sovers, J. L. Fanselow, G. H. Purcell, Jr.,
D. H. Rogstad and J. B. Thomas

Jet Propulsion Laboratory, California Institute of Technology,
4800 Oak Grove Drive, Pasadena, CA 91109, USA

ABSTRACT. A series of experiments has been conducted during the last decade to explore the capability of very long baseline interferometry (VLBI) to measure the crustal and rotational motions of the earth with accuracies at the centimeter level. The observing stations are those of NASA's Deep Space Network in California, Spain and Australia. A multiparameter fit to the observed values of delay and delay rate yields radio source positions, polar motion, universal time, the precession constant, baseline vectors, and solid earth tides. Source positions are obtained with formal errors of the order of 0".01. UT1-UTC and polar motion are determined at 49 epochs, with formal error estimates (1σ) for the more recent data of 0.5 msec for UT1-UTC and 2 to 6 mas for polar motion. Intercontinental baseline lengths are determined with formal errors of 5 to 10 cm. The Love numbers and earth tide phase lag agree with the commonly accepted values.

INTRODUCTION

Over the last few years, considerable progress has been made toward realizing the potential capability of radio interferometry to measure the crustal and rotational motions of the earth at the centimeter level (e.g. Thomas et al. 1976, Rogers et al. 1978, Ryan et al. 1978, Niell et al. 1979, Herring et al. 1981). Toward this goal, a series of experiments with NASA's Deep Space Newtork (DSN) antennas has been conducted over the last decade. In all, 48 sessions have been carried out using 8 different antennas on three continents. Delay and/or delay rate observables have been measured on two local baselines (at Goldstone, California and at Madrid, Spain), on a transcontinental baseline (California to Massachusetts, USA), and on two intercontinental baselines (Goldstone to Madrid and to Canberra, Australia).

A multiparameter fit has been applied to these observables to extract astrometric and geophysical parameters. These parameters include source positions, polar motion, universal time, the precession constant, baseline vectors and solid earth tides. This paper summarizes the geophysical results obtained from the intercontinental measurements.

INTERFEROMETRY TECHNIQUE

In the present experiments, two separate interferometry systems were employed. The prototype system used in the early measurements recorded a single narrowband (24 kHz) channel at S band (2.3 GHz) and therefore could only measure delay rate accurately (Thomas 1972). To obtain measurements of delay as well, a new system was developed and implemented in 1977 (Thomas 1981). It records six time-multiplexed frequency channels to permit calculation of delay by bandwidth synthesis (BWS), a technique pioneered by Rogers (1970). Three 2 MHz wide channels are placed at S band and three at X band (8.4 GHz) to allow dual-frequency calibration of charged-particle delays. This new system can measure delay with a precision (system noise error) of approximately 100 psec, given a correlated source strength of 0.5 Jy, an integration time of 3 minutes, a spanned bandwidth of 40 MHz, and two 64-m DSN antennas with system temperatures of 35 K.

SUMMARY OF EXPERIMENTS

The need to optimize determination of each class of astrometric and geophysical parameters imposes stringent and sometimes conflicting requirements on the design of a VLBI observing schedule. Maximum sensitivity to polar motion and UT1 requires concurrent or consecutive sessions (within 24-48 hours) on the California/Spain baseline (essentially east/west) and the California/Australia baseline (with a large north/south component). Development of a reference frame requires complete coverage of the sky and several observations of each source during the period of mutual visibility for each pair of stations. Establishing accurate positions of enough radio objects to provide "nearby" reference points for navigating interplanetary spacecraft, as well as for measurements of earth orientation with only 3 hours of VLBI data in a subsequent operational mode, requires approximately 100 sources. Observations which meet the above requirements have been carried out between August 1971 and February 1980. In all, 117 extragalactic radio sources were observed in 48 sessions, which ranged in length from 2 to 24 hours. Of the 2414 individual observations, 692 were made at S band only, 366 at X band only, and 1356 were dual-frequency. The observations included 2399 measurements of delay rate and 2152 of delay.

MODEL AND FIT TO EXPERIMENTAL DATA

In considering the multitude of effects contributing to the delay model for VLBI, it is helpful to group them as either modeled or unmodeled effects, with the models containing parameters that may be either adjusted or fixed at their apriori values. Modeled quantities that were fixed at their apriori values include nutation (Wahr series [Kaplan 1981]) and the effects of the ionosphere. Effects of ocean loading and plate motion are unmodeled.

There are eight categories of modeled and adjusted parameters: station locations, tropospheric delays, clock offsets and rates, polar motion and UT1, source positions, the precession constant, the gamma factor of general relativity, and solid earth tides. The solution provided a catalog of approximately 100 positions of radio sources with declinations ranging between -40° and $+70^{\circ}$ (with formal error estimates of the order of $0''.01$). A number of discontinuities and nonlinearities in the station clocks were detected and modeled in many of the sessions. There were 114 parameters describing delay due to the troposphere; these were constrained to agree with the Chao monthly mean model (Chao 1974) to within 3%. The long span of data enables us to solve for the luni-solar precession constant, in addition to UT1 and polar motion at 49 epochs.

A rotation about the polar axis of 2.37 mas/yr is included in the model to correct UT1 for the new IAU expressions for Greenwich mean sidereal time and precession (Kaplan 1981). The BIH Circular D provides a reference point for earth orientation: the values of both components of polar motion and two values of UT1 (one for each intercontinental baseline) are constrained on December 20-21^{h}, 1979, during which period there were two intercontinental observing sessions. In total, the fit to the 1971-1980 data includes 744 adjusted parameters.

The observables in the fit were weighted in inverse proportion to the sum of squares of known random error sources, plus an additional noise term which is adjusted to make chi-square per degree of freedom equal to 1 for each session. The software used to perform parameter estimation is based on the square-root-information-filter method (Bierman 1977) implemented for the VAX 11/780 computer. Approximately 8 CPU hours are required for a solution for the 1971-80 data. RMS residuals for the grand fit are 0.5 nsec for delay and 0.3 psec/sec for delay rate. The resulting geophysical parameters are discussed in some detail in the next section.

RESULTS

Earth Orientation

The solution for universal time and polar motion produced the average formal error estimates given in Table I as functions of the date of observation. Clearly, the quality of the data improved substantially as the interferometric system evolved, with the 1980 data exhibiting formal uncertainties of 6 to 20 cm.

TABLE I

Earth Orientation Parameter Formal Errors
in Fit to 1971-1980 VLBI Data

Year	Polar motion, mas		UT1, msec
	x	y	
1971-4	...	...	2.1
1977	10	4	0.9
1978	10	3	0.7
1979	6	2	0.5
1980	6	2	0.5

Figures 1 and 2 show comparisons of our x and y polar motion values for the latter part of the data (1977-80) with BIH Circular D. Taking into account the 4 mas error of the BIH data (Dickey 1981), there are no outstanding discrepancies with the possible exception of three points that differ by ~ 1.5 to 2σ. For the UT1 results similarly plotted in Figure 3, short-period tidal fluctuations have been removed from the VLBI data in order to permit comparison with the heavily smoothed BIH values. The solid curve represents lunar laser ranging (LLR) data as smoothed over a 15-day interval by Fliegel et al. (1981). These data originally consisted of several hundred points in the range of the plot.

POLAR MOTION RESULTS FROM 1977-1980 VLBI DATA

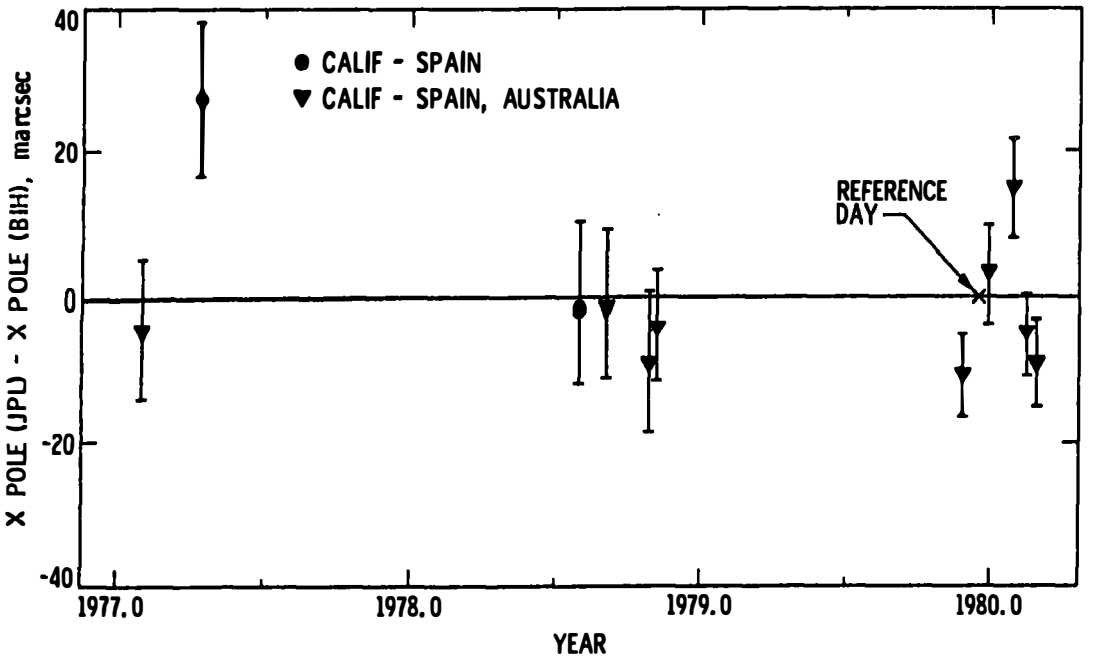

Figure 1

Polar Motion X-Component Results from 1977-1980 VLBI Data

POLAR MOTION RESULTS FROM 1977-1980 VLBI DATA

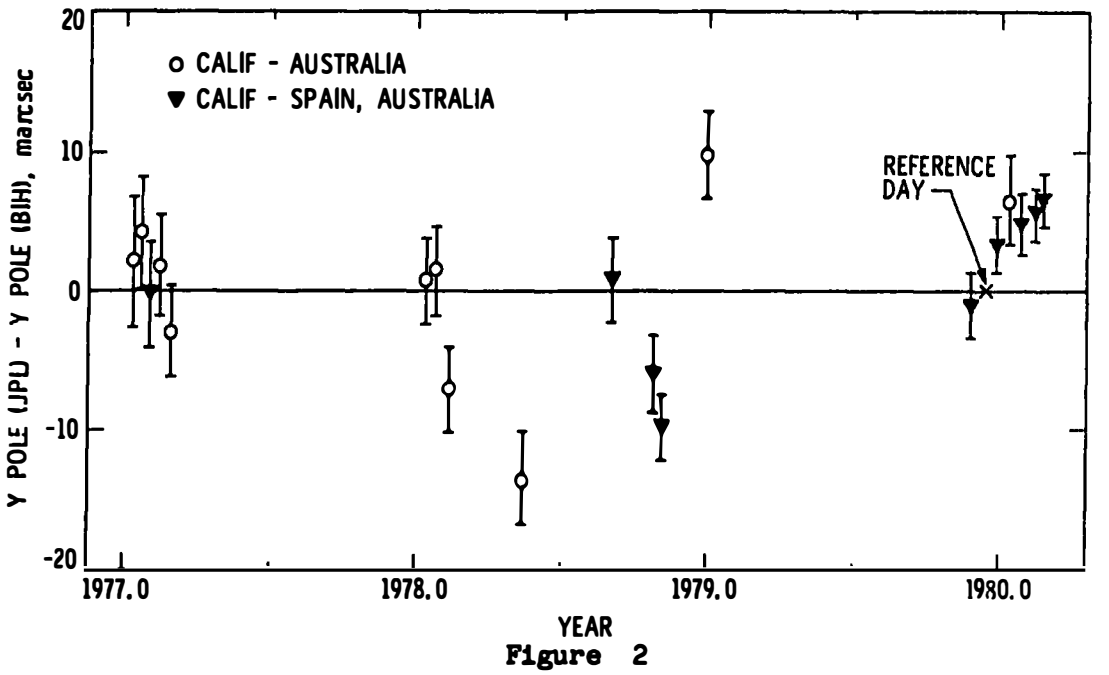

Figure 2

Polar Motion Y-Component Results from 1977-1980 VLBI Data

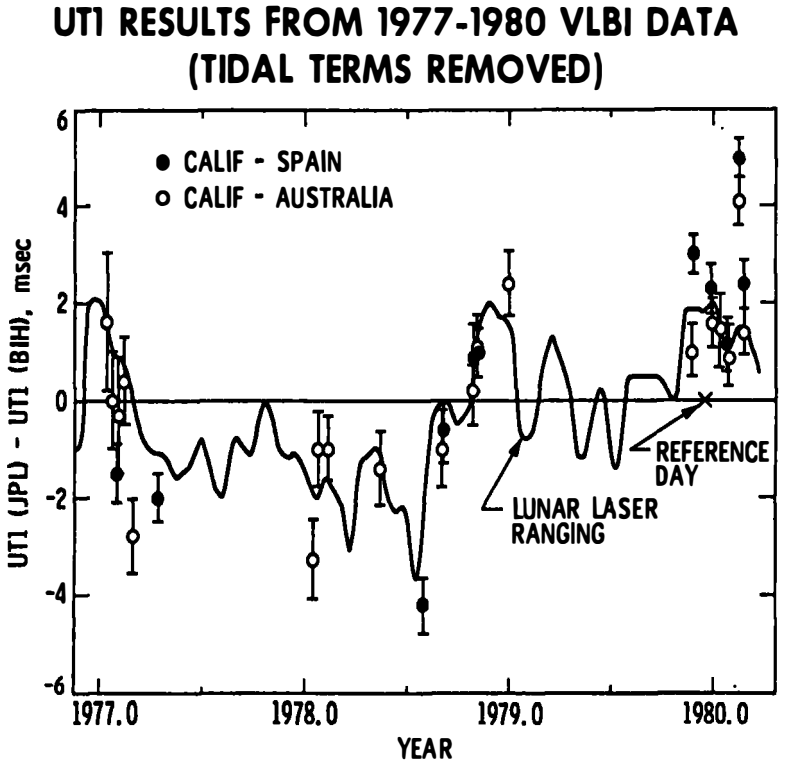

Figure 3

UT1 Results from 1977-1980 VLBI Data. Short-period tidal terms have been removed to permit comparison with BIH values

Figure 3 shows that the UT1 values measured by VLBI, LLR and BIH generally agree with one another if the BIH values are assigned errors of approximately 2 msec, and the LLR values errors of 1 msec or less. Both the VLBI and LLR results suggest the same oscillation of ~ 2 msec amplitude about the BIH values. The three points of large discrepancy (~ 2 to 3σ) between VLBI and LLR in February 1977 and February 1980 require further investigation.

The value obtained for the luni-solar precession constant is smaller than the 1976 IAU value by 3.7 ± 0.9 mas/yr. This discrepancy may indicate the need for a revision of either the precession constant or of the long-period (18.6-year) term in the nutation series. Such an inference is supported by calculations in which the fit was repeated with a modified nutation

constant, and the precession constant was solved for. The RMS delay residual for the 1971-80 VLBI data reaches a minimum when the amplitude of the 18.6 year term in the Wahr nutation series is increased by ~ 7 mas (to 9".210 in obliquity), at which point the precession constant equals the 1976 IAU value within its error estimate.

Baselines and Earth Tides

On the premise that our data, especially the 1971-1977 portion, lack quality sufficient to detect plate motion, each station was initially assumed to have a single location for the entire span of data. Table II shows the lengths of the two intercontinental baselines obtained from such fits in 1978 and at present. Comparison of baseline lengths in this table is complicated by the substantially different modeling used in the two calculations (e.g., the 1978 fit did not use the Wahr nutation series). In spite of the lack of separation of the effects of improved data quality and improved modeling, Table II shows the qualitative enhancement in system performance over the past decade. The decrease by nearly a factor of 3 in the formal baseline errors between 1978 and the most recent solution suggests that future improved experiments will permit detection of plate motion within the next few years.

TABLE II

Baseline Length Results from VLBI Data

Date	California to	
	Spain	Australia
1971-78	8 390 429.66±0.16 m	10 588 965t85±0.26 m
1971-80	8 390 429.84±0.05 m	10 588 966.32±0.1t m

A useful test of internal consistency is to divide the data into parts and to determine if fits to the parts lead to consistent values for theoretically constant parameters. To test baseline repeatability, the span of data was divided into two portions containing nearly equal numbers of observations: 1971-78 (average epoch 1978.2) and 1979-80 (average epoch 1979.9). All of the data were again simultaneously fit but the Spanish and Australian 64-m antennas were each allowed to have different locations in the two spans of data. As shown in Table III, the resulting baseline lengths for the two parts are in good agreement.

TABLE III

Baseline Consistency Test Results

Average date	California to	
	Spain	Australia
1978.2	8 390 429.78±0.09 m	10 588 966.36±0.11 m
1979.9	8 390 429.85±0.05 m	10 588 966.27±0.11 m
Difference	7±10 cm	-9±15 cm

The Spanish baseline errors in Table III again show the improvement of data quality with time. It is of interest to note that, even though our results are consistent with no motion, the differences for both the Spanish and Australian baselines in Table III are more consistent with the motion inferred from paleomagnetic data (Minster and Jordan 1978, Morabito et al. 1980). For a 1.7-year span, Morabito's application of Minster and Jordan's model indicates changes of +4 and -6 cm respectively for the Spanish and Australian baselines.

Assuming that the vertical and horizontal Love numbers and the solid-earth-tide-phase lag values are identical at all stations we obtain 0.63±0.03, 0.063±0.017, and -1.7±1.6 degrees respectively. These agree well with the commonly accepted values of 0.603-0.611, 0.0832-0.0842, and 0 degrees (Wahr 1977, Lambeck 1980).

CONCLUSIONS

The radio interferometric system under development at JPL during the past decade has improved continually in quality. By 1980 it had reached the point where earth orientation parameters could be determined with formal uncertainties of 6 to 20 cm, and source positions with formal uncertainties of the order of 0".01. Formal uncertainties of 5 to 10 cm in intercontinental baseline lengths promise detection of plate-tectonic motion in the near future.

The present set of results represents very nearly our final fit to the 1971-80 data. Minor changes in the model, such as improved ephemerides and earth tide models, as well as adoption of the J2000 system will probably not have significant repercussions.

REFERENCES

Bierman, G. J., 1977: "Factorization Methods for Discrete Sequential Estimation", New York, Academic Press.

Chao, C. C., 1974: "The Tropospheric Calibration Model for Mariner Mars 1971", JPL Technical Report 32-1587, pp. 61-76, Jet Propulsion Laboratory, NASA, Pasadena, California.

Dickey, J. O., 1981: "Analysis of Lageos Polar Motion Results Using Lunar Laser Ranging, EOS 62, 841.

Fliegel, H. F., Dickey, J. O. and Williams, J. G., 1981: "Intercomparison of Lunar Laser and Traditional Determinations of Earth Rotation", IAU Colloquium Proc. No. 63, O. Calame, ed., Grasse, France.

Herring T. A., Corey, B. E., Counselman III, C. C., Shapiro I. I., Ronnang, B. O., Rydbeck, O. E. H., Clark, T. A., Coates, R. J., Ma, C., Ryan, J. W., Vandenberg, N. R., Hinteregger, H. F., Knight, C. A., Rogers, A. E. E., Whitney, A. R., Robertson, D. S. and Schupler, B. R., 1981: "Geodesy by Radio Interferometry: Intercontinental Distance Determinations with Subdecimeter Precision", J. Geophys. Res., 86, pp. 1647-1651.

Kaplan, G. H., 1981: "The IAU Resolutions on Astronomical Constants, Time Scales, and the Fundamental Reference Frame", USNO Circular No. 163, Washington, D.C., United States Naval Observatory.

Lambeck, K., 1980: "The Earth's Variable Rotation: Geophysical Causes and Consequences", pp. 13, 111, Cambridge, Cambridge University Press.

Minster, J. B. and Jordan T. H., 1978: "Present-day Plate Motions", J. Geophys. Res. 83, pp. 5331-5354.

Morabito, D. D., Claflin, E. S. and Steinberg, C. J., 1980: "VLBI Detection of Crustal Plate Motion Using DSN Antennas as Base Stations", DSN Progress Report 42-56, pp. 59-75, Jet Propulsion Laboratory, NASA, Pasadena, California.

Niell, A. E., Ong, K. M., MacDoran, P. F., Resch, G. M., Morabito, D. D., Claflin, E. S. and Dracup, J. F., 1979: "Comparison of a Radio Interferometric Differential Baseline Measurement with Conventional Geodesy, Tectonophysics 52, pp. 49-58.

Rogers, A. E. E., 1970: "Very Long Baseline Interferometry with Large Effective Bandwidth for Phase-Delay Measurements", Radio Science, 5, 1239.

Rogers, A. E. E., Knight, C. A., Hinteregger, H. F., Whitney, A. R., Counselman, C. C., Shapiro, I. I., Gourevitch, S. A. and Clark, T. A., 1978: "Geodesy by Radio Interferometry: Determination of a 1.24-km Base Line with 5-mm Repeatability", J. Geophys. Res. 83, pp. 325-334.

Ryan, J. W., Clark, T. A., Coates, R., Corey, B. E., Cotton, W. D., Counselman, C. C., Hinteregger, H. F., Knight, C. A., Ma, C., Robertson, D. S., Rogers, A. E. E., Shapiro, I. I., Whitney, A. R. and Wittels, J. J., 1978: "Precision Surveying Using Radio Interferometry", J. Surveying and Mapping Division, Proc. ASCE, volume 104, no. SU1, pp. 25-34.

Thomas, J. B., 1972: "An Analysis of Long Baseline Radio Interferometry", JPL Technical Report 32-1526, Volume VII, 37-50, Volume VIII, 29-38, Volume XVI, 47-64, Jet Propulsion Laboratory, NASA, Pasadena, California.

Thomas, J. B., Fanselow, J. L., MacDoran, P. F., Skjerve, L. J., Spitzmesser, D. J. and Fliegel, H. F., 1976: "A Demonstration of an Independent-Station Radio Interferometry System with 4-cm Precision on a 16-km Baseline", J. Geophys. Res. 81, pp. 995-1005.

Thomas, J. B., 1981: "An Analysis of Radio Interferometry with the Block 0 System", JPL Publication 81-49, Jet Propulsion Laboratory, NASA, Pasadena, California.

Wahr, J. M., 1977: "The Tidal Motions of a Rotating, Elastic and Oceanless Earth", pp. 162-171, Thesis, University of Colorado.

ACKNOWLEDGEMENT

This work represents one phase of research carried out at the Jet Propulsion Laboratory, California Institute of Technology, under NASA Contract 7-100, sponsored by the National Aeronautics and Space Administration.

AN ANALYSIS OF JPL TEMPO EARTH ORIENTATION RESULTS

T. M. Eubanks, M. G. Roth, P. B. Esposito, J. A. Steppe, P. S. Callahan

Jet Propulsion Laboratory
4800 Oak Grove Drive
Pasadena, California 91109

Abstract

As of April 28, 1982, a 22 month history of UT1 and Polar Motion (UTPM) measurements has been obtained by the TEMPO program at JPL. TEMPO is now able to provide UTPM estimates within a month of data acquisition, with earth orientation results through April 8, 1982 released to the BIH. In this paper, the data reduction procedure is described together with the various astronomical and geophysical models employed. The operational behavior of the TEMPO system is discussed including an analysis of the system success rate (50% so far in 1982) and the history of the delay residual scatter. The RMS of the X band delay residuals is 0.44 nanoseconds and there is no evidence that the residual scatter is a function of time or of baseline. TEMPO results are consistent with other sources and show evidence of UTPM fluctuations on a time scale of a month or less.

I. Introduction

The Time and Earth Motion Precision Observations (TEMPO) program goals include rapid determinations of the UTPM to support spacecraft navigation. TEMPO observations are also capable of providing information of interest to the world-wide scientific community. In order for the program to be a useful UTPM service, it must be able to consistently provide UTPM estimates within at most one month of data acquisition with decimeter or better precision. To support spacecraft navigation, results will be needed within three days or less of the observations. TEMPO is now producing UTPM results within 4 weeks of the observations. This paper assesses the consistency and reliability of the TEMPO observations. A companion paper [5] will concentrate on the reliability of the TEMPO UTPM estimates. These estimates will be briefly discussed at the end of this paper.

UTPM estimates are produced by least squares fits to the interferometric delay and delay rate observables, which are themselves the results of fringe fits using the correlator output. Section II is a brief description of TEMPO operational procedures, earth orientation models, and data reduction algorithms. Section III describes the success rate of the TEMPO observations, the failure modes, and statistics on the success of the individual scans within a pass. Operations during the first quarter of 1982 will be discussed in detail.

Most of the information content of the observables is contained in the delay observations, but the delay rate data is sensitive to the UTO and the troposphere model. Section IV presents a statisical analysis of the X band delay residuals, although similar conclusions could have been drawn about the X band delay rate residuals. The behavior of the Root Mean Square (RMS) delay residuals and of the residual Chi Squares is discussed. Section V contains a brief description of the TEMPO UTPM estimates. Agreement between TEMPO and VLBI earth orientation results from the POLARIS project will be demonstrated, with clear evidence of rapid UTPM fluctuations not present in the BIH Circular D.

II. A Brief Description of Tempo Activities

The TEMPO program monitors station clock behavior and earth orientation to support interplanetary navigation by the Deep SpacetNetwork (DSN). The program goals include weekly decimeter determinations of the earth's orientation. TEMPO data are collected using the 64 meter antennas of the DSN at Goldstone California, near Madrid Spain, and near Canberra Australia. Only single baseline VLBI observations are available, as the wide spatial separation between the DSN stations makes it impossible to do simultaneous three station observations. Each week, single baseline VLBI observing sessions (passes) on both the Australia-California (AC) and the Spain-California (SC) baselines observe extragalactic radio sources using the Jet Propulsion Laboratory (JPL) Block I VLBI system [4 and 10]. The two weekly observing sessions are generally scheduled within 24 hours of each other. Since February 1982, each pass lasts about three hours and observes up to 20 sources for 200 seconds each. About 60% of the session duration is devoted to antenna slew time. Each source is observed at both S and X band (2.285 and 8.420 GHz, respectively), with three 250 KHz bandwidth channels in each band. Only one channel is recorded at a time, with all six channels sampled in sequence over a three second cycle. During each cycle, the S band channels are observed for 0.2 seconds each, each X band channel for 0.8 seconds.

The data recorded at each station are sent via satellite to JPL, where they are correlated and fringe fitted. Delay observables are constructed by bandwidth synthesis with a spanned bandwidth of 40 MHz in each band [8 and 9]. The delay rate observable is the fringe frequency measured in a single channel. Both types of observables are constructed at both S and X band. Solutions using delay and delay rate data are obtained with the program MASTERFIT, written by J. L. Fanselow and his colleagues at JPL. The data from each pass is used in a separate and independent solution, with no gobal parameters and thus no coupling between the passes.

Due to the limited number of observations per pass, the solve for parameters are restricted to two earth orientation parameters, a single troposphere zenith delay at each station, and a first degree polynomial clock model. The delay and delay rate clock models are uncoupled in an attempt to absorb the effects of uncalibrated instrumental delay changes. A priori knowledge of the baseline vector, source positions, and the precession constant are obtained from solutions using nearly 10 years of independent DSN VLBI observations [6]. The new (Wahr) IAU nutation model is used in both the reference frame and the TEMPO solutions, which are tied to the FK4 and a 1950.0 reference epoch. The

a priori UTPM estimate is the BIH Ciroular D Polar Motion and UT1* plus the Yoder and Williams model of the zonal tide effect on the UT1 [11]. The reference frame is tied to the BIH on December 20, 1979.

A priori tropospheric and ionospheric effects are estimated using tables of average zenith delays which are mapped to the source elevation angle. The troposphere tables are monthly mean wet and dry zenith delays at each station, and the ionosphere model uses a single table of mean zenith delay versus time of day. The ionosphere delay is inversely proportional to the frequency squared and thus S band observations are 13 times more sensitive to the ionosphere than corresponding X band observations.

If possible, a linear combination of S and X band observables (called SX observables) is formed in an attempt to remove the effects of ionospheric dispersion on the data. SX data requires successful scans at both S and X band, and thus there is generally more X band than SX data available. Since the SX ionospheric correction does not seem to significantly reduce the RMS residuals, the results presented in this paper are derived from solutions using X band data only.

III. Observing Session Statistics

Statistics on system performance were collected and examined for the first quarter of 1982 as an aid to understanding current system performance. TEMPO has become more reliable with increasing experience with the JPL VLBI system, but improvements in VLBI operations are still desirable.

In the period from January 1, 1982, to April 9, 1982, there were 31 possible TEMPO observing sessions (two regular ones per week plus the Australia-Spain (AS) pass on January 3). Of these sessions 30 were scheduled by the DSN. Figure 1 shows the disposition of these at subsequent stages in the processing. In all, thirteen passes did not provide usable data, the results from thirteen passes were sent to the BIH, the results from two sessions are still being processed, and two sessions had S band results only, which have not been released yet. The success rate for this period, ignoring the data still being processed or not yet released, is thus exactly 50% with the possibility of rising to 57% after the remaining passes are released. In general most passes have more usable S band data than X band.

The major cause of failure in early 1982 (7 passes) was weak or non-existent fringes, which indicates low Signal to Noise Ratios (SNRs). This problem also caused the degradation of several successful observing sessions, through loss of observations during a pass. Four passes were canceled after being scheduled, and two passes had fewer than 6 good delay observations, which was judged to be the minimum number acceptable.

Some of the weak fringes seem to be caused by correlator problems, and there are some passes that may be recovered by recorrelation. Other causes for weak fringes might be low source strengths, improper equipment settings, data transmission problems and antenna pointing errors. The antenna beamwidth is smaller at X band, and so the higher success rate at S band would suggest antenna pointingt problems. Occasionally, high SNRs on only one or two

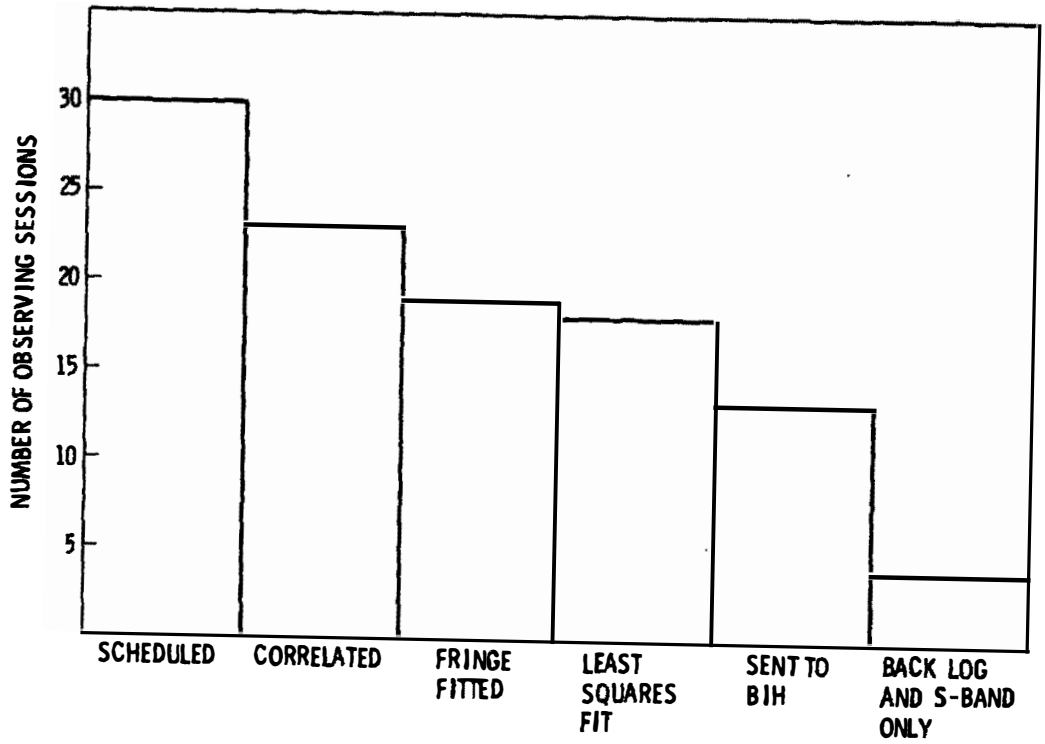

Figure 1. January 1 - April 8, 1982 TEMPO Observing Session Status as of April 28, 1982

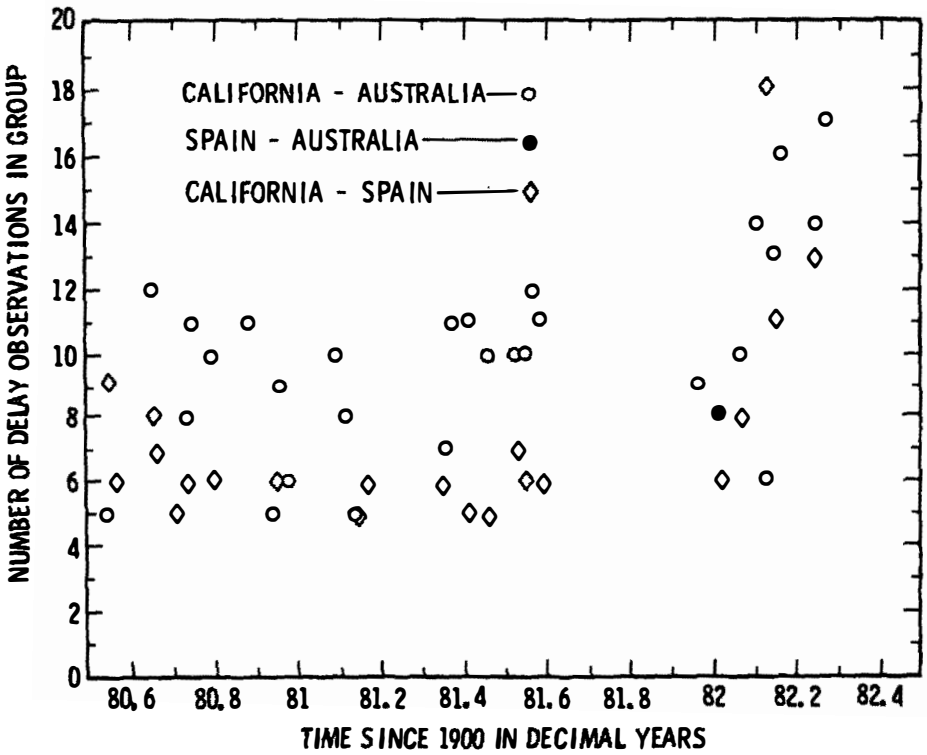

Figure 2. Number of Delay Observables in Each TEMPO Observing Session

channels in a band suggests equipment setup or data transmission problems.

Some of the low SNRs may be the result of observing overly weak sources. Thetsources observed are supposed to have a minimum S band flux of 0.5 Janskys in a JPL source strength survey [7], but the poor knowledge of radio flux strengths make this impossible to guarantee. Many sources have no accurate flux measurements at the desired frequencies at all, others have only total flux measurements, and there are no data on temporal variations in flux strength for most sources. Total source flux can vary by 50% or more over a few months, although most sources are more stable [1]. VLBI SNR depends on the correlated flux strength, which is a function of the total flux, angular size, shape, and the orientation of the source. For an arbitrarily shaped source, it also depends on the baseline used and the sidereal time of the observation. Very little is known about changes in the correlated flux strength for most sources, and VLBI services such as TEMPO, which observe a limited number of sources at fixed sidereal times, could be used to monitor source variability. This information would help in the scheduling of observations and may be of interest astrophysically.

Figure 2 shows the number of delay observables for every successful TEMPO observing session. The increase in the number of good scans in 1982 is the result of the new, 3 hour (20 source) schedule adopted in February of that year. The success ratio has generally also improved since that time. Before 1982 the SC experiments had a consistently lower throughput than the AC experiments. After the adoption of a new, larger, source catalogue, this no longer seems to be a problem.

A number of activities are planned or underway to improve the TEMPO success rate. The JPL Block I VLBI system is constantly being monitored for software, hardware, and procedural errors. As the operational VLBI personnel become more experienced, and as VLBI procedures become more routine, system performance can be expected to improve. Currently, hardware to adequately monitor the station configuration is being implemented. Weak sources may be avoided in the future by keeping a close watch on observed source strengths. Possible causes of pointing errors are under investigation by the DSN. In the future, real time playback, correlation, and monitoring of station activities may be used to ensure system performance at critical times near planetary encounterst

IV. Data Statistics

The postfit residual scatter is an important measure of system performance. The accuracy of the TEMPO results depends upon the accuracy of the observables used to derive them. The postfit residual scatter is used as a check upon observable reliability and as a guide to weighting the data. Problems in data reduction tend to increase the scatter of the postfit residuals.

All errors are absorbed in the adjustment of parameters to some degree. However, some types of error, such as uncorrelated measurement noise, do not mimic the effects of solve for parameters and mostly serve to increase the residual scatter. Errors of this type can be detected through increases in the postfit residual scatter. There are other errors which will not influence

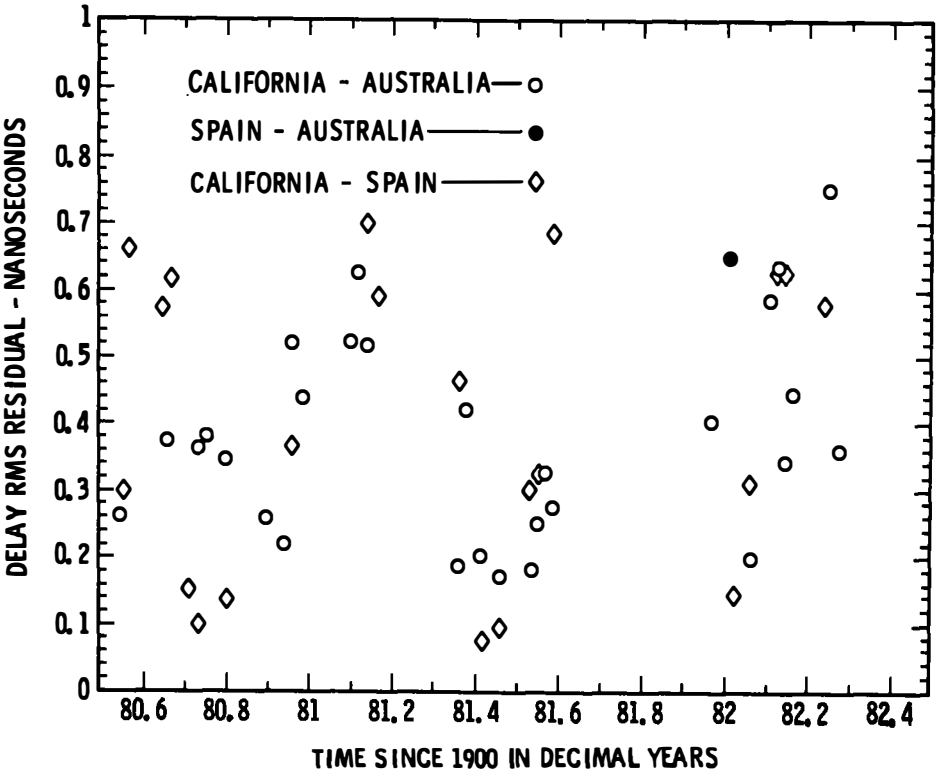

Figure 3. RMS Delay Residuals From Each TEMPO Observing Session

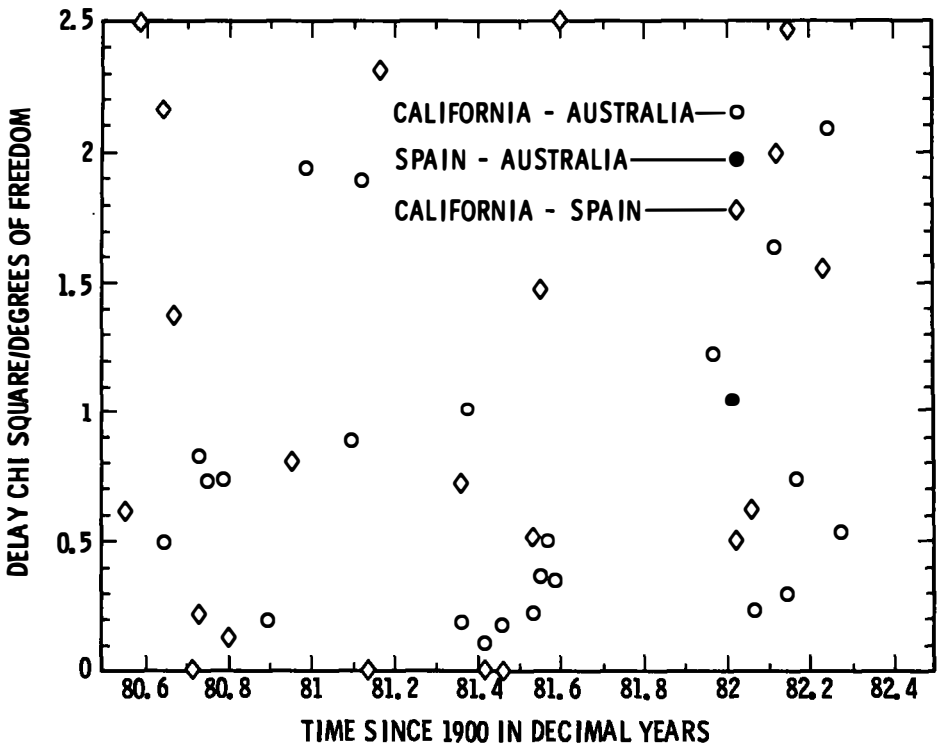

Figure 4. Delay CHI Square/Number of Degrees of Freedom TEMPO Observing Session

the residual behavior; but rather the postfit parameter values. A good example of this would be errors in the nutation model, which would be almost totally absorbed by the UTPM parameters for observing periods much shorter than a day. Such systematic errors can only be detected by comparison with other, independent, measurements of the same parameters. Such an intercomparison is the subject of Section V.

The X band data from each observing session were used in a separate solution for the baseline UTO and Variation of Latitude, a troposphere zenith delay value for each station, and a linear clock model. Each observable is weighted by the formal error from the fringe fitting, plus an estimate of the troposphere and ionosphere propagation errors. This does not account for all the known and suspected sources of error, nor is it large enough to explain the total residual scatter. The major additional error sources are thought to be source positions, baseline vectors, and errors in the media propagation delay models. To account for these additional error sources, the formal error estimates from the fringe fits and the media error estimates are root sum squared with a constant "additive noise" value chosen to make the total Chi Square for all the TEMPO data equal to the total number of degrees of freedom.

Figure 3 shows the RMS delay residuals for each TEMPO pass. Since the number of parameters in each solution (7) is close to the total number of data points used in the solution (10 to 40 when the delay rates are included - see Figure 2), a better description of the residual behavior can be obtained from the Chi Square divided by the number of degrees of freedom for each solution, which is presented in Figure 4. The scatter of the postfit X band delay residuals seems to be time and baseline invariant. The S band residual scatter, however, increases from 1980 to 1982, which may be related to ionospheric model errors or to changes in the solar activity with time.

Total RMS X and SX residual from TEMPO solutions are generally on the order of 0.4 to 0.5 nanoseconds, depending on the particular nature of the solution, while RMS S band residuals are on the order of 3.0 nanoseconds. In general, solutions using SX data have slightly larger RMS residuals than corresponding X band solutions. The cause and significance of this are under investigation. It is possible that the difference between the S and X band data is dominated by uncalibrated changes in the instrumental delay and by the measurement error. A comparison of S, X, and SX solutions is in progress, and the significance of any changes in the residual scatter and differences between the postfit parameter values is being assessed.

There is no evidence, in Figures 3 and 4 or elsewhere, that scatter of the X band delay residuals is a function of time or of baseline. Thus, the systematic error sources that contribute to the residual scatter are also probably time invariant. Accordingly, constant additive noise estimates were used for each data type (delay and delay rate). Results dicussed in this paper are derived from a solution weighted in this manner. The resulting delay and delay rate residuals have a total RMS of 0.44 nanoseconds and 0.16 picoseconds/second, respectively. The average error estmate used in weighting the data was 0.64 nanoseconds for the delay data and 0.18 picoseconds/second for the delay rate data. The additive noise contribution to the estimated total variance is about one fourth that of the formal error and media

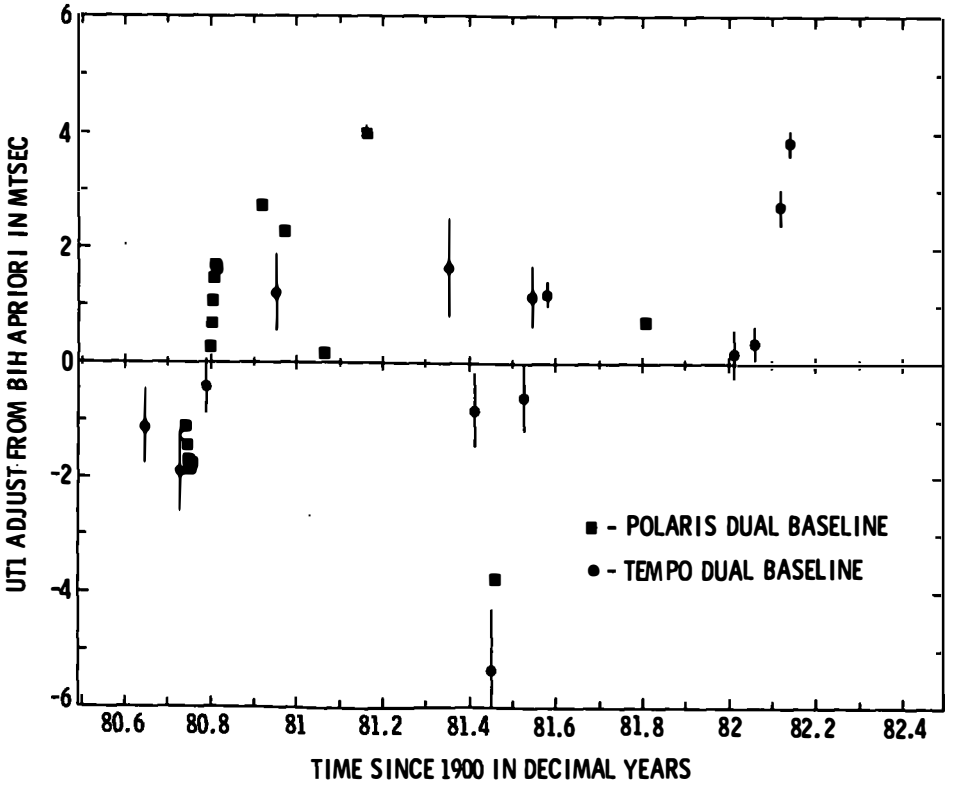

Figure 5. TEMPO and Polaris Dual Baseline Adjusts to the BIH Circular D UT1* and Zonal Tide Model

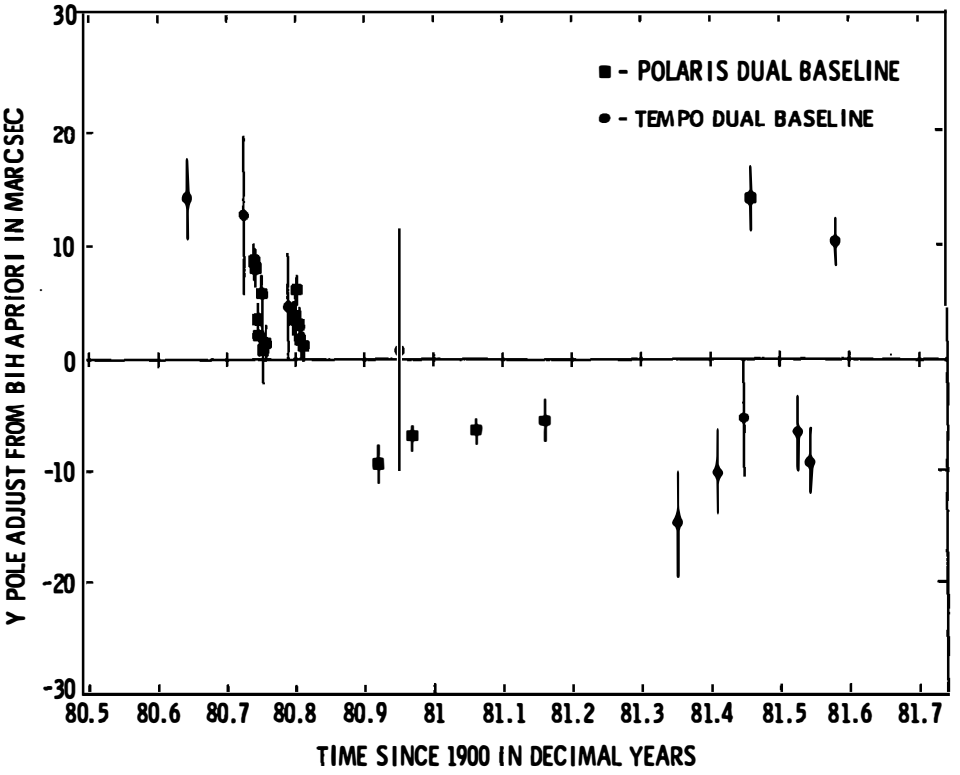

Figure 6. TEMPOeand Polaris Dual Baseline Adjusts to the BIH Circular D Y Pole

contribution for the delay observables, although it dominates the delay rate error estimate. This indicates that any unmodeled error sources do not effect the delay residual scatter much, and that the TEMPO delay data may be close to the theoretical accuracy limit using the currenttobservable models. In the future, equipment delay calibrations and improved media corrections using water vapor radiometers may make it possible to reduce the TEMPO observable error significantly.

V. TEMPO UTPM Estimates

As a consistency check, TEMPO dual baseline solutions were compared with POLARIS VLBI results, provided by Doug Robertson of the National Geodetic Survey [3]. The resulting adjusts to the BIH Circular D for UT1$\hat{}$ and Y Pole are shown in Figures 5 and 6, after removing an estimate of the bias between the TEMPO and POLARIS results. There is general agreement between the available TEMPO and POLARIS data.

The observed adjusts to the BIH are low pass filter residuals, and are thus a high pass filtering of the raw BIH data. Any low pass filter will smooth over sudden changes in the UTPM and the filter residuals will respond over times of the order of the inverse of the filter cutoff frequency. Any lag between the true UTPM and the filter output will also corrupt the residuals. A full discussion of these effects is beyond the scope of this paper and will be included in a future paper [5].

The UT1$\hat{}$ is smoothed with a low pass filter that attenuates waves with periods much shorter than 25 days and the X and Y Pole are smoothed with a filter that cuts off at about 90 days [2]. Note in Figure 5, the sudden positive change in the UT1$\hat{}$ adjusts between 1980.7 and 1980.9 and the negative spike near 1981.45 shown by both TEMPO and POLARIS. These changes take about 0.1 to 0.2 years, and might be caused by lags in the BIH Circular D UT1$\hat{}$, systematic errors, or real earth rotation changes smeared out by the smoothing. As would be expected from the stronger smoothing used on the polar motion, the Y Pole adjusts do not show such rapid changes, but there is good evidence for a step between 1980.7 and 1980.9. This is probablytthe result of a 10 day lag in the BIH Circular D Y Pole estimates.

These data suggest that there are significant changes in the earth orientation at the 30 cm level over time scales on the order of weeks or less that are not present in the BIH Circular D. VLBI, which provides decimeter accuracy with a few hours of observing time, is ideally suited to detecting these changes.

References

[1] Andrew, B. H.; MacLeod, J. M., Harvey, G. A., Medd, W. J., 1978,"A Ten-Year Study of Extra Galactic Variable Source at Centimeter Wavelengths," Astron. J., Vol. 83, #8, pp. 863-899.

[2] Bureau International De L'Huere, Annual Report for 1981, 1981, Paris.

[3] Carter, W. E., Robertson, D. S., "Geodynamic Measurements from the HRAS-Westford POLARIS Radio Interferometer," IAG Symposium No.t5: Geodetic Applications of Radio Interferometry, NOAA Tech. Memo. Services, 1982 (in press).

[4] Chaney, W. D., Ham, N. C., 1980,"DSN VLBI System MK 1-80," DSN Progress Report, 42-56, pp. 26-34.

[5] Eubanks, T. M., Esposito, P. B., Steppe, J. A., Callahan, P. S., 1982 "Validation and Interpretation of TEMPO Earth Orientation Estimates," (to be published).

[6] Fanselow, J. L., Sovers, O. J., Thomas, J. B., Bletzacker, F. R., Kearns, T. J., Purcell, G. H., Rogstad, D. H., Skjerve, L. J., Young, L. E., 1981, "Development of a Radio Astrometric Catalog by Means of Very Long Baseline Interferometry Observations," in Referennce Coordinate Systems for Earth Dynamtics, pp. 351-357,E. M. Gaposchkin and B. Kolaczek (eds.) D. Reidel Publishing Co.

[7] Preston, R. A., Morabito, D. D., Williams, J. G., Slade, M. A., Harris, A. W., Finley, S. G.; Skjerve, L. J., Tanida, L., Spitzmesser, D. J., Johnson, B., Jauncey, D. L., Bailey, A., Denise, R., Dickenson, J., Livermore, R., Papij, A., Robinson, A., Taylor, C., Alcazar, F., Luaces, B., Munox, D., May and June 1978, "Establishing a Celestial VLBI Reference Frame - I. Searching for VLBI Sources," DSN Progress Report 42-46, pp. 46-56.

[8] Rogers, A. E. E., 1970, "Very Long Baseline Interferometry with large effective bandwidth for phase-delay measurements," Radio Science, Vol. 5, #10, pp. 1239-1247.

[9] Thomas, J. B., "An Analysis of Long Baseline Radio Interferometry, Part III," JPL Technical Report 32-1526, Vol XVI pp. 47-64.

[10] Wilcher, J. H.,1980, "Block I, Phase 1 Very Long Baseline Interferometry Implementation," DSN Progress Report 42-58, pp. 24-27.

[11] Yoder, C. F., Williams, J. G., Parke, M. E., 1981, "Tidal Variations of Earth Rotation," JGR, Vol. 86, #B2, pp. 881-891.

PRELIMINARY ANALYSIS OF SHANGHAI-EFFELSBERG VLBI EXPERIMENT

T.S.Wan and Z.H.Qian

Shanghai Observatory, Academia Sinica

D.Graham

Max-Planck-Institut für Radioastronomie

ABSTRACT

The first VLBI experiment between Shanghai and Effelsberg was carried out at 1430 MHz and lasted 54 hours in November 1981. The Mark II recording system and hydrogen masers were used at both stations. Fourteen extragalactic radio sources covering a wide range of declination were observed in order to try to determine the Shanghai-Effelsberg baseline vector. The preliminary analysis showed that the baseline vector was estimated to a formal precision of 2-3 meters and the positions of sources 1739+52 and 1928+73 were estimated to 0".05-0".08 for each coordinate, with the effects of ionosphere being not removed.

1. Introduction

This paper describes the first VLBI experiment between Shanghai and Effelsberg in November 1981. A selection of sources was made for both geodetic and astronomical purposes, but in this paper only geodetic results are given. The astronomical results will be published elsewhere.

2. Brief description of the VLBI system

The observations were made at 1430 MHz. We used Mark II recording system and hydrogen masers at both stations. The telescopes involved were the 6-m telescope of Shanghai Observatory in Shanghai, China, and the 100-m telescope of the Max-Planck-Institut für Radioastronomie (MPI) at Effelsberg, near Bonn, West Germany. The parameters of the telescopes are shown in Table 1.

Table 1. The parameters of the telescopes

Station	Diameter (m)	Mount	System noise temperature(K)	Sensitivity (K/Jy)
Shanghai	6	Equatorial	90	0.0055
Effelsberg	100	AZ/EL	70	1.42

3. Observations

The observations consisted of two stages. In order to check the operation of the VLBI system, test observations were made before the main observations. The test measurements on BL Lac and 3C454.3 showed that, because of the low residual fringe rate of some 10mHz, theta

priori position of the Shanghai telescope had been estimated to a precision of several tens of meters. The measured clock offset of a few microseconds showed that both station clocks were very close to UTC. The spectrum of the fringe rate residuals of 3C454.3 is shown in Figure 1. After the test, improvements were made to the Shanghai telescope, yielding the noise temperature given in Table 1. The limiting sensitivity of the interferometer was then about 0.2 Jy for 10 minutes integration.

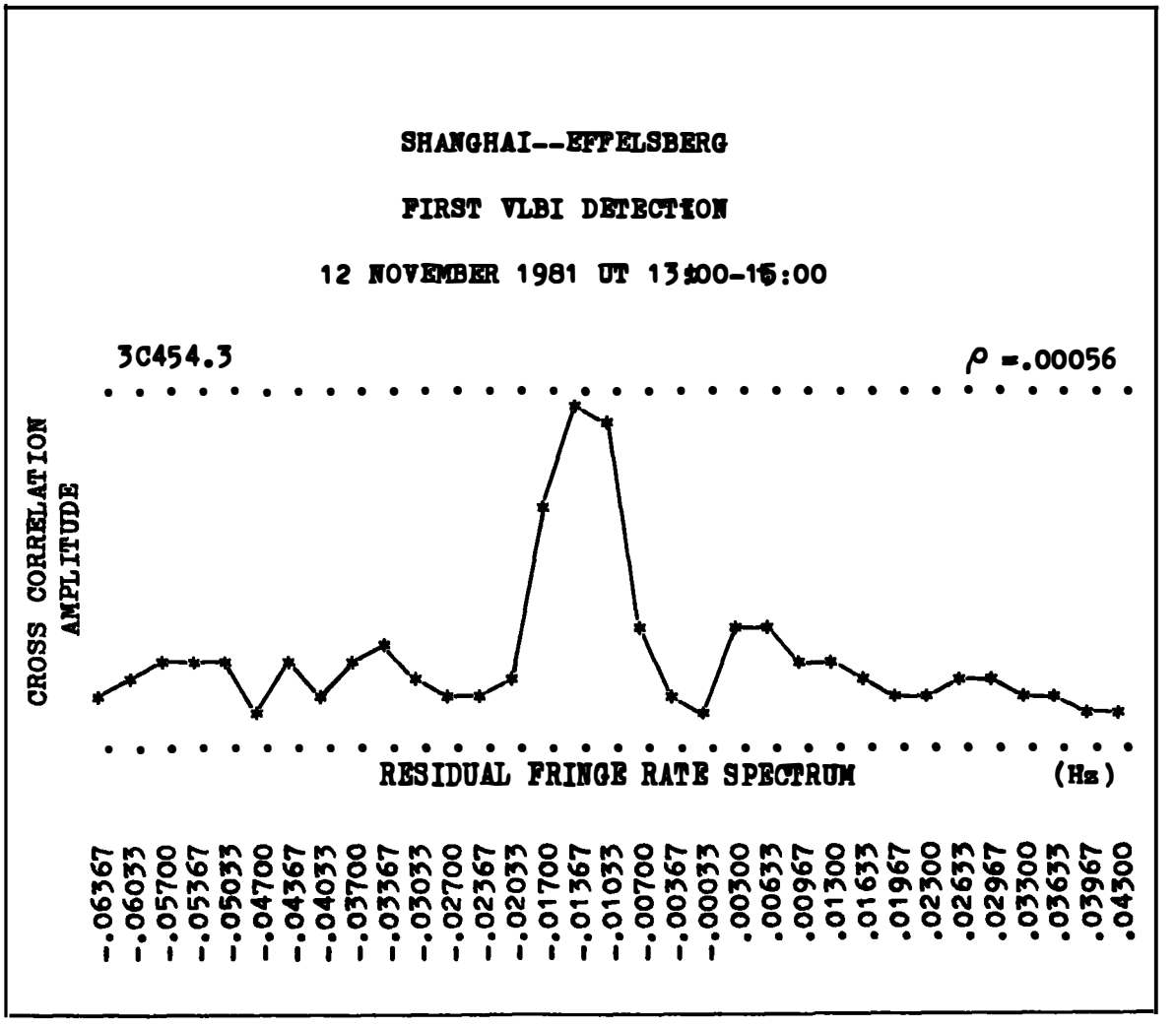

Figure 1. A residual fringe rate spectrum of 3C454.3 On November 12, 1981.

The main observations were performed from UT 16:00 27th to UT 23:00 29th in November and 14 radio sources were observed. The sources and the measured correlated flux density and visibility are shown in Table 2.

4. Data reduction

We used the VLB Mark II processor and CDC Cyber-172 computer of MPI for cross correlation and further analysis. The analysis was conducted in February 1982. In the calculation of delays and fringe rates, a coherent integration time in the range of 300--600 seconds was used for

all sources. The two sources 0016+73 and 3C120 had poor signal-to-noise ratio and were therefore excluded from the further analysis. A total of 700 observables, including delays and fringe rates from 12 sources were used simultaneously to fit the Shanghai-Effelsberg baseline vector. Because the positions of the sources 1739+52 and 1928+73 are not known so well, they were regarded as free parameters and solved together with the components of the baseline. The positions of ten other sources were fixed in the fitting of the baseline. The positions marked with an asterisk in Table 2 are from the MERIT program. These positions have been reduced to 1950.0 using the new IAU(1976) precession constants. The other source coordinates used are not a homogeneous set. To investigate the effect of this on the baseline coordinates, fits were tried using the positions of all non-MERIT sources as free parameters. The net effect on the baseline solution was not significant.

The program for parameter solution includes corrections for the effects of earth tides, retarded baseline, and antenna axis offset. The electrical paths at zenith are regarded as unknowns to be solved.

Table 2. The observed radio sources

Source	R.A. (1950.0)	Decl. (1950.0)	St (Jy)	Sc (Jy)	V	Ref.
+0016+73	$00^h16^m54.200$	$73^\circ10'51.41$	0.88	0.27	0.31	(2)
0300+47	03 00 10.0879	47 04 33.408	1.65	0.73-1.03	0.44-0.62	(1)
3C84	03 16 29.5449	41 19 51.687	19.6	0.91-2.00	0.05-0.10	(1)
3C119	04 29 07.88	41 32 08.6	8.4	1.55	0.18	(1)
+ 3C120	04 30 31.5843	05 14 59.592	4.3	0.25	0.06	(1)
* DA193	05 52 01.3731	39 48 21.925	1.43	1.20-1.32	0.84-0.92	(1)
0742+10	07 42 48.467	10 18 32.61	3.2	1.90	0.59	(1)
0859+47	08 59 39.98	47 02 56.82	2.1	0.93-1.12	0.44-0.53	(3)
* 3C273	12 26 33.2460	02 19 43.470	47.5	2.43	0.05	(1)
• 3C345	16 41 17.6401	39 54 10.991	7.75	0.83-1.42	0.11-0.18	(1)
1739+52	17 39 29.02	52 13 10.5	0.73	0.57	0.78	(1)
1928+73	19 28 49.333	73 51 44.67	3.65	0.20-1.66	0.05-0.45	(2)
* BL Lac	22 00 39.388	42 02 08.331	4.25	2.17	0.51	(1)
*3C454.3	22 51 29.5335	15 52 54.184	9.7	2.17	0.22	(1)

Note: St -- Total flux density
Sc -- Correlated flux density
V -- Visibility
+ -- Excluded from baseline determination
• -- MERIT sources (4)

Unfortunately, as information on the ionosphere near both telescopes were not available, the calibration of ionosphere, which is of great importance particularly at longer wavelength, has been impossible. The values of polar motion and UT1-UTC during the experiment were taken from the BIH Circular D.

In addition there was a clock jump at UT 10:10 29th in November at Shanghai Observatory, caused by maser unlock for a few minutes. And therefore, 15.21 microseconds were used to compensate the jump in fitting the baseline.

In our analysis, the center of mass of the earth was chosen as the origin of the inertial coordinate system.

5. Results

The results of baseline, positions of sources, and other solutions are listed below: The standard errors of delays and fringe rates are 43.6 ns and 4.6 mHz, respectively:

Table 3. The parameters of the baseline

Length	B = 8208 690.92 ± 2.44 m
Pole component	B1 = 1616 430.99 ± 2.75 m
Equatorial component	B2 = 8047 966.05 ± 2.42 m
Hour angle	Hb = $31^{\circ}.231\ 793\ 65 \pm 0''.078$
Declination	δb = $11^{\circ}.356\ 732\ 63$
X-component	Bx = 6881 628.04 ± 2.28 m
Y-component	By = 4172 883.07 ± 3.16 m
Z-component	Bz = 1616 430.99 ± 2.75 m

Table 4. The geocentric coordinates of the stations

	Shanghai	Effelsberg
X	-2847 688.04 ± 2.28 m	4033 940.00 m
Y	-4659 877.07 ± 3.16 m	- 486 994.00 m
Z	3283 999.01 ± 2.75 m	4900 430.00 m
R	6372 474.48 ± 3.06 m	6365 850.24 m
φ'	$31^{\circ}.020\ 267\ 83 \pm 0''.081$	$50^{\circ}.335\ 911\ 08$
L	$-121^{\circ}.429\ 424\ 77 \pm 0''.101$	$-6^{\circ}.883\ 671\ 97$

Note: R -- Radius of the earth
φ' -- Geocentric latitude
L -- Longitude
The geocentric coordinates of Effelsberg were provided by Dr. J. Campbell.

Table 5. The coordinates of radio sources

Source	R.A.(1950.0)	Decl.(1950.0)
1739+52	$17^h39^m28.9845 \pm 0^s.0050$	$52^\circ13'10''.039 \pm 0''.077$
1928+73	19 28 49.4001 ± 0.0045	73 51 44.612 ± 0.054

Table 6. The parameters of the clocks

Clock offset	-2.258 ± 0.017 μs
Difference of clock rates	-1.744 ± 0.041 ps/s
Difference Of LO frequencies	-3.341 ± 0.710 mHz

Notes All values above are EFF-SH.

Table 7. The zenith electrical path length

Shanghai	5.11± 0.67 m
Effelsberg	1.95± 1.14 m

The residuals of delays and fringe rates are plotted in Figure 2. and3. Figure 3. shows that the effects of the ionosphere are quite obvious. The scatter of the residuals at day time is apparently larger than that at night time. It is also obvious that there is some systematic change in the residuals of the fringe rates at dawn or in the evening.

Formal errors are quoted throughout. It is however very likely that systematic errors due to the inconsistency of published lists of source positions and uncompensated ionosphere effects increase these considerably. Thus the baseline may be considered determined to an accuracy of about 20 meters.

Optimization of the positions of the non-MERIT sources in Table 2 leads to typical corrections of up to 0.3 arcsec, and this value is the probable error on the positions of 1928+73 and 1739+52.

Ionospheric effects can be minimized by the use of dual-frequency receivers or by higher frequency operation, as planned for future observations. Improved delay measurements are possible using wideband frequency synthesis.

6. Acknowledgements

We are deeply grateful to the assistants of MPI and Shanghai Observatory in the coordinated observations. We also thank R.Mutel (University of Iowa) for the loan of FET amplifier, J. Campbell and W. Boyer (University of Bonn) for providing coordinates of Effelsberg, programming assistance and for helpful discussions on data analysis.

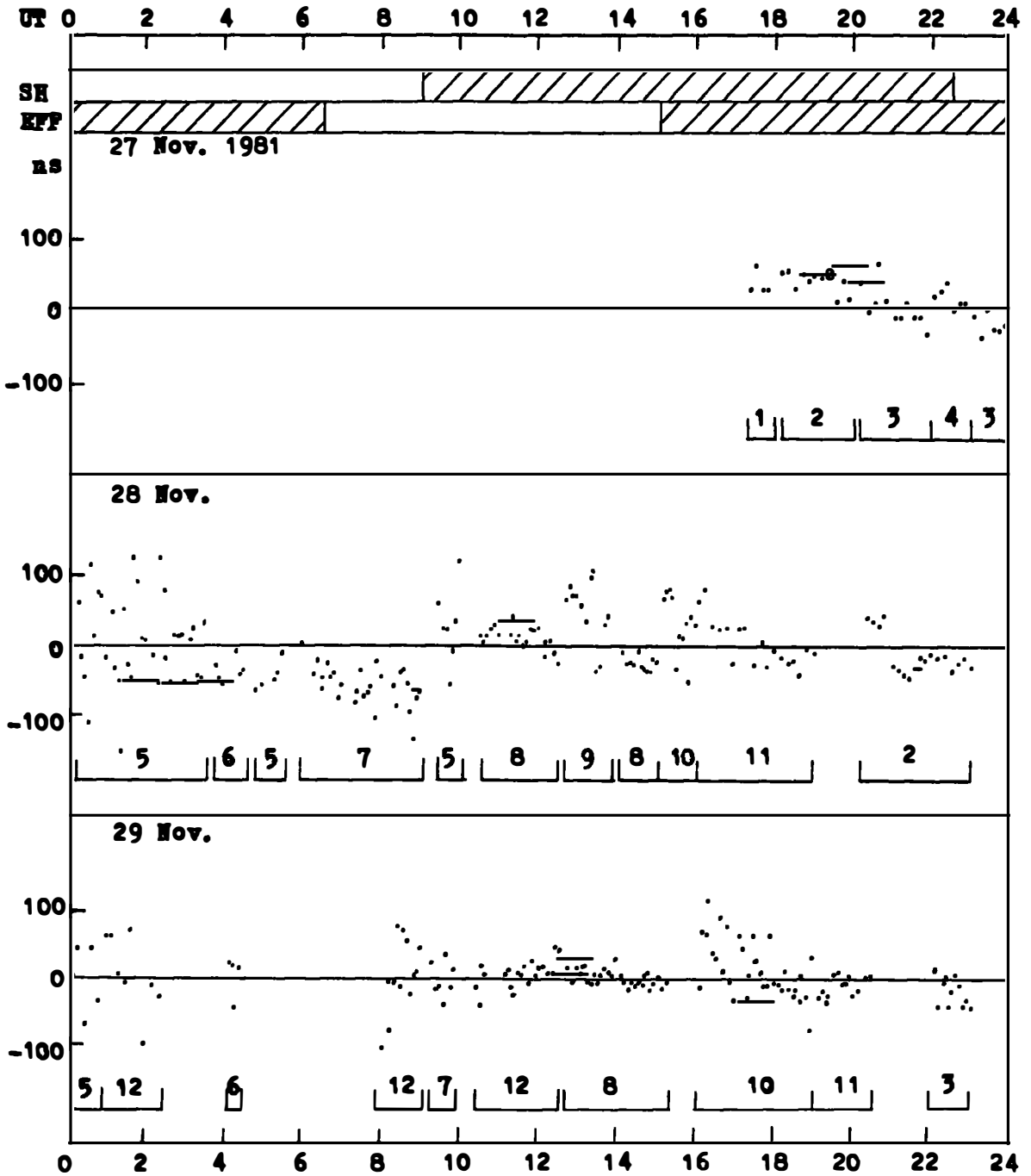

Day time Night time

1. 3C119 2. DA193 3. 0859+47 4. 0742+10 5. 1739+52
6. 3C273 7. 3C345 8. BL Lac 9. 3C454.3 10. 0300+47
11. 3C84 12. 1928+73

Fige 2. The residuals of delays from the best fit.

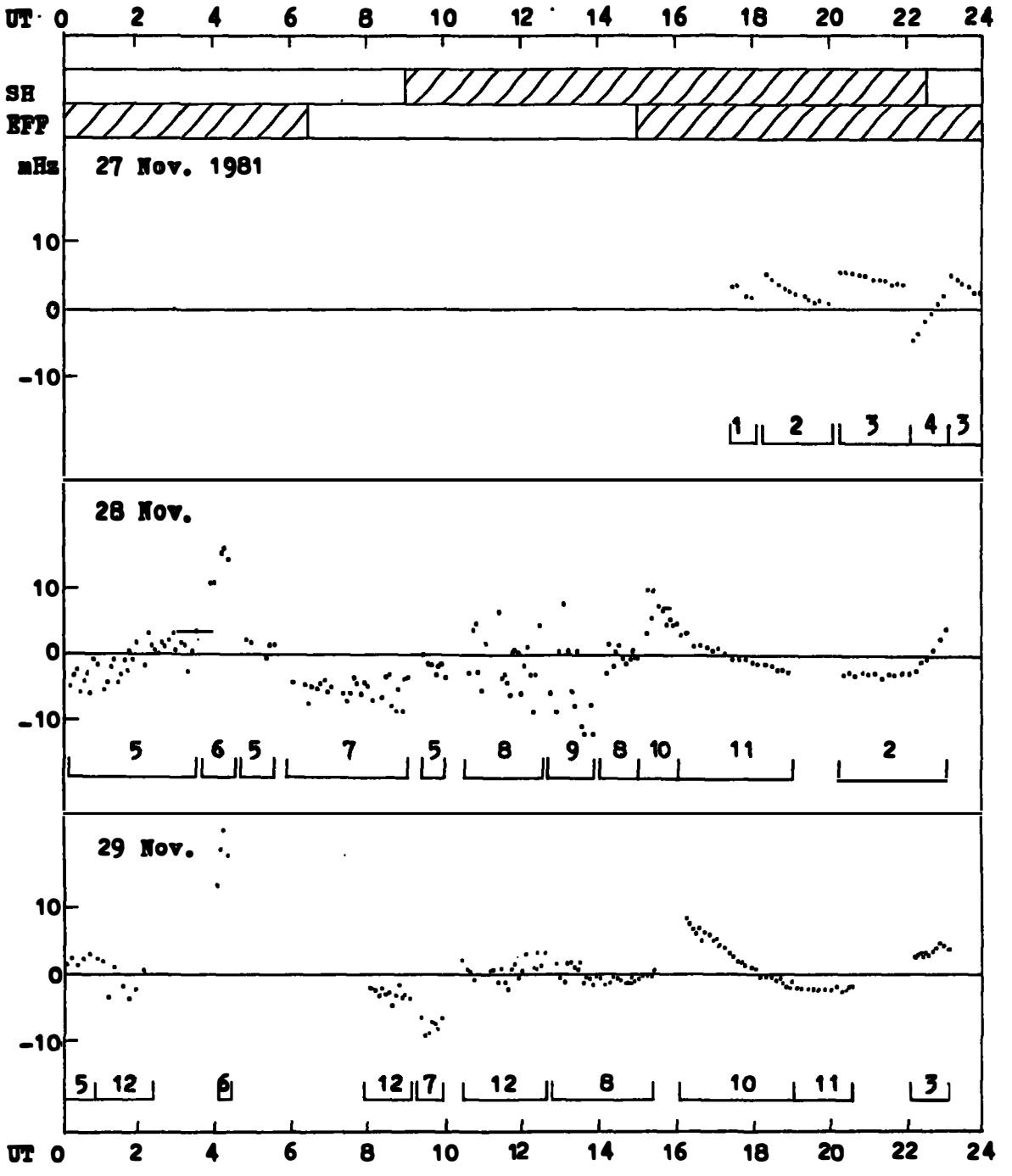

Day time Night time

1. 3C119 2. DA193 3. 0859+47 4. 0742+10 5. 1739+52
6. 3C273 7. 3C345 8. BL Lac 9. 3C454.3 10. 0300+47
11. 3C84 12. 1928+73

Fig. 3. The residuals of fringe rates from the best fit.

References

(1) Backer, D.C., Editor, USA VLBI NETWORK HANDBOOK.
(2) Waltman, E., et al., Compact Radio Sources at Declinations>69, Astron. Astrophys., 101, 49-51 (1981).
(3) Gubbay, J.S., Private Communication.
(4) Robertson, D.S., Carter, D.E., IAU Colloquium 63.

PRECISION SURVEYING AT THE 1-MM LEVEL USING RADIO INTERFEROMETRY

Goran Lundqvist

Onsala Space Observatory
Chalmers University of Technology
S-439 00 Onsala, Sweden

ABSTRACT. The 600 meter baseline between the two radio astronomy antennas at the Onsala Space Observatory, Sweden, has been accurately determined with the MARK III VLBI System. Observations of extragalactic radio sources at X-band (8 GHz) have been made at two different occasions. The first in August 1980 and the second in January 1981. Both the repeatability and the formal accuracy are at the 1-mm level. This paper presents the planning, performance and processing of the experiments as well as a critical analysis of the results. A comparison with conventional survey results is also made.

1. INTRODUCTION

This paper presents the details of the short baseline radio interferometry experiments between the 26.5 m antenna and the 20 m antenna at the Onsala Space Observatory in Sweden. These are the first short baseline experiments using the wide bandwidth MARK III recording system. Previous short baseline experiments have used either the MARK I (Rogers et al. 1978) or the MARK II recording system (Ong et al. 1976). The scientific purpose of the experiments was threefold:

1. Observations with the MARK III system, for geodesy purposes, are made simultaneously at S- (2.3 GHz) and X- (8.4 GHz) band in order to solve for the ionospheric delay. Normally both of these frequencies are received by the same antenna but at Onsala one antenna is used for each frequency. The 3-dimensional baseline between the two antennas used needs to be known with high accuracy if the ionospheric delay is to be determined and removed from the observations made at Onsala.

2. The baseline between the antennas has been determined by means of a conventional survey in 1973 and again in 1978. We wanted to check that the survey and the interferometry experiments give the same result.

3. A number of intercontinental geodesy VLBI experiments have been performed from 1972 to 1978 between the Haystack Observatory, USA, and the 25.6 m antenna and the 20 m antenna at Onsala. By the short baseline experiments we wanted to 'close the triangle' separately and independently of the intercontinental experiments. This gives us a possibility to compare formal and absolute errors in VLBI measurements.

2. EXPERIMENT DESCRIPTION

A short baseline experiment is easier to perform and to analyze than an intercontinental VLBI experiment for several reasons. One is that the propagation media delays along the two ray paths essentially cancel and can therefore be minimized as a source of uncertainty. Another is that the short baseline delays are less sensitive to source position errors. These positions can be furnished

with adequate accuracy by independent measurements. Furthermore, during these experiments we used the same frequency standard for both receiver systems to avoid the stability problems encountered with independent standards.

The observations, each of 3-min duration, were made sequentially of 11 extragalactic radio sources. A list of the sources observed is found in Table 1. A total of 28 observations was made on Aug. 25 1980 and a total of 136 on Jan. 13 1981. 12 frequency channels, each 2 MHz wide, spanning a total bandwidth of 250 MHz were recorded from each antenna. The group and the phase delays through each receiving system were monitored continuously by the standard MARK III phase calibration system. A cable calibration system to monitor the cable length variations was connected to the 2(but unfortunately no cable calibration system was available for the nna.

Table 1.
Extragalactic Sources Used in the Experiments

Source	Right Ascension			Declination		
3C84	03	16	29.54	41	19	51.69
NRAO150	03	55	45.23	50	49	20.07
3C120	04	30	31.56	05	14	59.59
OJ287	08	51	57.23	20	17	58.60
4C39.25	09	23	55.29	39	15	23.83
3C273B	12	26	33.246	02	19	43.47
3C345	16	41	17.64	39	54	10.99
1642+690	16	42	18.14	69	02	13.43
2134+00	21	34	05.23	00	28	25.02
VR422201	22	00	39.39	42	02	08.33
3C454.3	22	51	29.53	15	52	54.68

3. DATA ANALYSIS

The raw data, stored on magnetic tapes, were correlated at the Haystack Observatory correlator center. All of the data were analyzed using the MARK III analysis system developed by the east coast VLBI group and installed on the Onsala HP 1000 computer. Fig. 1 shows the data flow through the MARK III system. A complete description of the system is presented by Clark et al. (1982).

Most of the data analysis was carried out using the highly interactive SOLVE program where least squares estimates of all geodetic parameters are made. Separate solutions were calculated for group delay and phase delay. Both of the experiments were also differenced using a time window of 20 minutes maximum. Figures 2 and 3 are examples of residual plots from the program SOLVE.

4. RESULTS

a. Baseline Results

In Table 2 the results from the short baseline experiments are summarized along with their formal uncertainties. In the experiment >80AUG25TS, only a few hours of data were recorded as a test of the equipment used. The data turned

out to be so useful that this experiment has also been carefully analyzede >81JAN13TS was a full 24 hour experiment.

Table 2.
Baseline Results

	x-comp	1σ	y-comp	1σ	z-comp	1σ	Length	1σ
>80AUG25TS								
Group Delay	360.098	.017	-451.531	.011	-166.716	.015	601.120	.015
Phase Delay	360.090	.002	-451.531	.002	-166.723	.005	601.117	.003
Differenced	360.091	.001	-451.530	.001	-166.723	.002	601.118	.001
>81JAN13TS								
Group delay	360.090	.004	-451.531	.003	-166.729	.006	601.118	.003
Phase Delay	360.095	.001	-451.531	.001	-166.723	.002	601.120	.001
Differenced	360.094	.001	-451.534	.001	-166.729	.001	601.123	.001

b. Comparison with Conventional Survey

In order to check if the level of repeatability in the results above signifies their accuracy, a conventional survey has been done between the two antennas by the National Land Survey of Sweden. The survey results together with the interferometry results are shown in Table 3. The agreement in all three dimensions are at the several centimeter level.

Table 3.
Comparison With Conventional Survey

	x-comp	1σ	y-comp	1σ	z-comp	1σ	Length	1σ
>81JAN13TS								
Phase Delay	360.095	.001	-451.531	.001	-166.723	.002	601.120	.001
Conventional Survey	360.106	--	-451.487	--	-166.752	--	601.102	.015

c. Triangle Closure Test

Table 4 shows the results from the intercontinental baseline closure test. Data on the baseline from Haystack to Onsala 25.6 m was recorded during several

periods between 1972 and 1978. All data have recently been reprocessed through the MARK III software by Ryan (1981). The baseline components from Haystack to Onsala 20 m were reported by Herring et al. (1981) using data taken between 1976 to 1978. The baseline components between the 20 m antenna and the 25.6 m antenna can be calculated from these measurements and compared with the short baseline results. Note that both the y- and the z-component of the baseline differs by more than 3 sigma. The length of the baseline is very well determined but orientation information is poor.

Table 4.
Baseline Closure Test

	x-comp	1σ	y-comp	1σ	z-comp	1σ	Length	1σ
>81JAN13TS Phase Delay	360.095	.001	-451.531	.001	-166.723	.002	601.120	.001
"1972-1978"	360.10	.15	-451.95	.10	-165.66	.34	601.14	.14
Differences:	0.01	.15	-0.42	.10	1.06	.34	0.02	.14

5. ERROR ANALYSIS

Three main sources of error can be identified in the results from the short baseline experiment. Each of them probably affects the result at the mm-level.

1. Dimensional changes of the antennas due to gravitational loading and temperature changes in the antenna structure: Unfortunately no information is available about path length variations due to the antennas.

2. Source positions for the short baseline interferometer: The analysis is done using source coordinates from very long baseline observations. These positions are not necessarily the same as the short baseline positions since the short baseline interferometer is sensitive to the arc second structure, whereas the very long baseline interferometers are sensitive mainly to structure on the milliarc second level.

3. Changes of the electrical cable length to the 25.6 m antenna: The plot of the residual phase delays clearly shows that a second cable calibration system would be very useful also for the 25.6 m antennas. The changes are mainly caused by temperature variations in the cables.

The discrepancy between the conventional survey result and the interferometry result has one possible explanation. The antenna construction blueprints have been used to translate from the survey reference points to the intersection of antenna axes which were used as reference points in the interferometry experiments. The accuracy of these drawings could very well be questionable.

6. CONCLUSIONS

The results of the short baseline experiments have shown that it is possible to measure short baselines to mm accuracy with radio interferometry. However, the method described here is still limited by systematic errors. A second cable

calibration system would probably reduce this error to a large extent. A high precision conventional survey should also be conducted before any further comparisons are made.

REFERENCES

Clark, T.A. et al. (1982): Mark III VLBI Data Acquisition Terminal, NASA Goddard Space Flight Center, Crustal Dynamics Project.

Herring, T.A., B.E. Corey, C.C. Counselman III, I.I. Shapiro, B.O. Ronnang, C.E.H. Rydbeck, T.A. Clark, R.J. Coates, C. Ma, J.W. Ryan, N.R. Vandenberg, H.F. Hinteregger, C.A. Knight, A.E.E. Rogers, A.R. Whitney, D.S. Robertson, and B.R. Schupler (1981): Geodesy by Radio Interferometry: Intercontinental Distance Determinations With Subdecimeter Precision, Journal of Geophysical Research, vol 86, no B3, pp 1647-1651.

Ong, K.M., P.F. MacDoran, J.B. Thomas, H.F. Fliegel, L.J. Skjerve, D.J. Spitzmesser, P.D. Batelaan, and S.R. Paine (1976): A Demonstration of a Transportable Radio Interferometric Surveying System with 3-cm Accuracy on a 307-m Base Line, Journal of Geophysical Research, vol 81, No 20, pp 3587-3593.

Rogers, A.E.E., C.A. Knight, H.F. Hinteregger, C.C. Counselman III, I.I. Shapiro, S.A. Gourevitch, and T.A. Clark (1978): Geodesy by Radio Interferometry: Determination of a 1.24-km Base Line Vector With 5-mm Repeatability, Journal of Geophysical Research, vol 83, pp 325-334.

Ryan, J.W. (1981): Personal Communication.

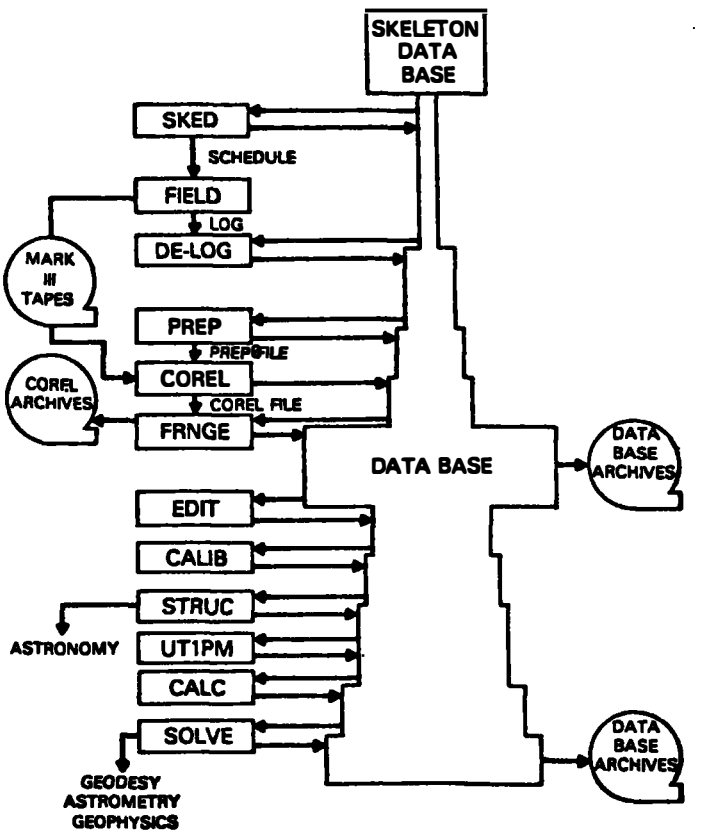

Figure 1. Data flow through the MARK III system.

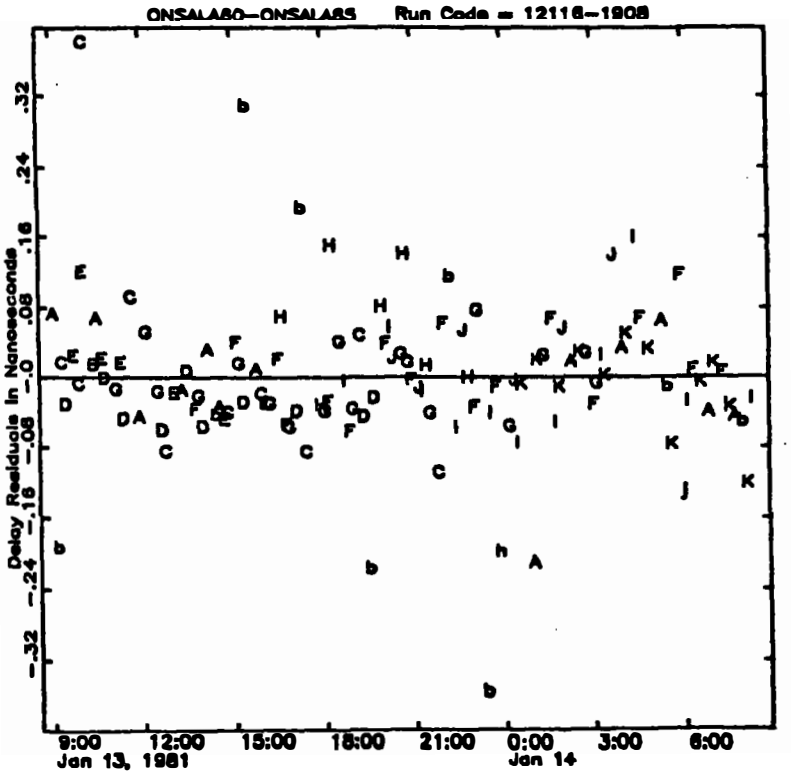

Figure 3. Phase delay residuals.

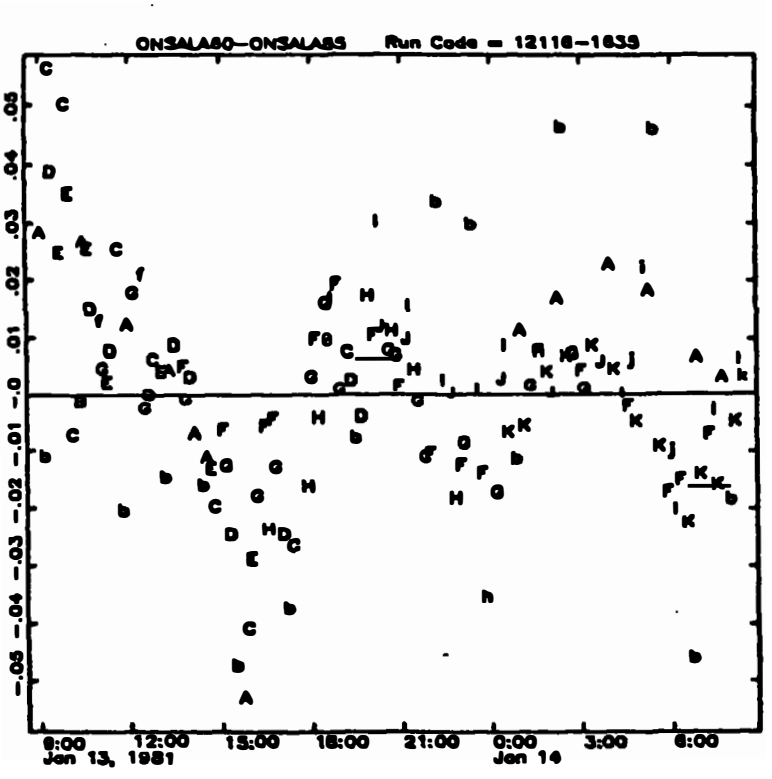

Figure 2. Group delay residuals.

PROJECT ERIDOC
(EUROPEAN RADIOINTERFEROMETRY AND DOPPLER CAMPAIGN)

Beyer, W., Campbell, J., Lohmar, F. J., Seeger, H., Sudau, A.
Geodetic Institute, University of Bonn, Fed. Rep. of Germany

Brouwer, F., Husti, G. J.
Geodetic Institute, TU Delft, The Netherlands

Lundqvist, G., Rönnäng, B. O.
Onsala Space Observatory, Sweden

Schilizzi, R. T.
Westerbork/Dwingeloo Radio Observatory, The Netherlands

Booth, R. S.
Jodrell Bank Observatory, United Kingdom

Richards, P.
Chilbolton Observatory, United Kingdom

Tallquist, S.
Metsähovi Radio Observatory, Finland

ABSTRACT. A report is given on the first successful observations in a program of repeated geodetic VLBI experiments within the European Network of Radio Astronomy Observatories. Because of the inherent limitations of the Mk II data acquisition system, a sequential bandwidth synthesis technique was used in order to improve the delay resolution. Simultaneous Doppler Satellite Observations were made at all stations to compare the results on the decimeter level and at the same time to supply ionospheric path delays for correcting the single-band (6 cm) VLBI data.

1. INTRODUCTION

Project ERIDOC (European Radiointerferometry and Doppler Campaign) has been initiated to conduct simultaneous VLBI and satellite Doppler observation campaigns between those European radio observatories that are or will be equipped with VLBI recording systems. The project is designed to serve a number of purposes relevant for both geodesy and astronomy. The most important of these are the following:

- determine accurate relative station positions of European radio observatories involved in radio interferometry,
- refer these station locations to the geocenter by using Doppler observations of Earth satellites,
- check the scale and the orientation of geodetic networks,
- compare the scale and orientation between the VLBI and Doppler networks,
- test the performance of the VLBI and Doppler systems on the European scale,
- investigate environmental effects such as tropospheric and ionospheric refraction, and
- monitor geophysical phenomena as far as the achieved accuracy allows to resolve (e. g. Polar Motion and UT1-variations).

Comparing results from observations taken at the same epoch of time has the particular advantage that uncertainties in the orientation of the reference systems due to precession, nutation on one side and Polar motion, UT1 variations on the other do not enter into the comparison results.

In a joint effort of the geodetic departments of the Technical University Delft (Holland) and the University of Bonn (Fed. Rep. of Germany) the satellite Doppler and the VLBI campaigns have been organized and carried through execution. The actual measurements were performed by many enthusiastic individuals observatory personnel as well as geodesy staff, who took an active interest in the campaign. A full list of the participating groups is given at the end of this paper (section 5).

2. THE GEODETIC VLBI CAMPAIGNS

At present only two European VLBI stations are equipped with high performance Mk III recording terminals, namely Effelsberg (Fed. Rep. of Germany) and Onsala (Sweden). At the other stations apart from Chilbolton (England) no particular provisions for geodetic VLBI observations had been taken before the proposal for a series of geodetic VLBI campaigns between the European stations was presented to the European VLBI programme committee. In this situation it appeared to be profitable to make the best possible use of the existing Mk II recording equipment, taking advantage of the positive experience of the NASA/JPL DSN and ARIES groups

with the sequential bandwidth synthesis scheme (Fanselow et al. 1979, Niell et al. 1980). A full description of this method is given by (Thomas 1981). In accordance with the width of the receiver passband at the NASA antennae a bandwidth of about 40 MHz was synthesized with eight channels on the DSN intercontinental baselines (10 000 km) and with two channels on the much shorter ARIES baselines (100 - 200 km). On the European scale the two channel approach, which minimizes the loss in sensitivity, was concidered to be the best choice, because it is relatively easy to implement at most European stations.

The 40 MHz two channel approach leaves an ambiguity of 25 ns in the bandwidth synthesis (BWS) delay determination. With a relatively high signal to noise ratio (SNR) provided by the rather sensitive European station configuration the non-ambiguous single channel delays tend to be fairly accurate (± 1.5 - ± 5 ns) and can be used to resolve most of the ambiguities in the BWS delays. Any remaining ambiguities are then sorted out in the final baseline solution.
The necessary technical provisions to implement a basic BWS capability at the European VLBI stations (essentially the operation of two synthesizers and a diode switch controlled by the UTC time tags) proved to be almost negligible. On the other hand, for a refined system the removal of instrumental phase delay changes, especially those of dispersive nature, is essential. This, helas, requires a rather sophisticated system comprising a tone generator, an rf-injection point near the feed horn and a cable delay compensator (Thomas 1981). It was decided to discuss the problem with the individual observatories and in the meantime start gathering experience with only the basic equipment.

Starting in October 79 three geodetic VLBI sessions have taken place in the commonly used European 6 cm-band. For these 6 cm Mk II campaigns the acronym WEJO, short for Westerbork, Effelsberg, Jodrell Bank and Onsala was chosen, although it turned out later that two more stations, Chilbolton and Metsähovi (Finland), were able to take part (see figure 2). The stations and the equipment used are listed in table 1. Of the three campaigns only WEJO-2, which constitutes the VLBI-part of Project ERIDOC, was fully successful. The other two campaigns were hampered by equipment failures and bad weather conditions (high winds and snowfall).

A relatively simple observing schedule was set up with fixed 15 min scans (including a varying portion of time for slewing). Shorter scans could have been used, but the intention was to monitor the phase behaviour on the different baselines and obtain quantative data for the performance of the participating stations.

Station *)	Antenna Diameter [m]	Mount type	Axis offset [m]	Clock system
Westerbork (telescope "B")	25	EQ	4.95	Rubidium
Effelsberg	100	AZ - EL	-	H-Maser
Jodrell Bank (Mk II telesc.)	26 x 38	AZ - EL	0.47	Rubidium
Onsala (OSO 25.6)	25.6	EQ	2.65	H-Maser
Chilbolton	20	AZ - EL	-	H-Maser
Metsähovi	14	AZ - EL	-	Rubidium

Tab. 1: WEJO - VLBI - stations

*) For the supporting agencies see section 5.

The data used in the present report was collected at the October '80 (WEJO-1) and April '81 (WEJO-2) observing sessions lasting 12 hours and 24 hours respectively (see Fig. 1). All data were correlated both at the 3-station Mk II processor of the MPIfR *) in Bonn and at the 5-station JPL/CIT **) Mk II processor in Pasadena, California, U.S.A. This double effort was necessary because the Bonn processor has not yet been fully checked with respect to its geodetic accuracy and reproduceability. It is hoped that the Bonn processor can be modified to accept switched data for bandwidth synthesis in the near future. At present the tapes have to be passed through the Bonn correlator as many times as the number of frequency channels recorded. In all it took about 5 times longer to process the 2-channel 5-station WEJO-2 data in Bonn than in Pasadena.

The fringe analysis of the JPL/CIT correlator output was carried out with the PHASOR software written by G. H. Purcell and others (Thomas 1981). The PHASOR output tape containing the estimated residual channel amplitudes, phases, delays and rates, the BWS delays and the model quantities was then sent to Bonn for the final processing stage: reconstruction of the total observed quantities, ambiguity elimination and least squares baseline solutions.

The least squares baseline fitting software has been developed at the Geodetic Institute in Bonn. This single baseline program includes all relevant geometric and geophysical models down to the 0.1 ns-level on intercontinental baselines (6000 - 10000 km).

*) Max-Planck-Institut für Radioastronomie

**) Jet Propulsion Laboratory/California Institute of Technology

A comparison with the US East-Coast-VLBI software package "CALC" has confirmed this accuracy level. For the European baselines this translates into a 0.01 ns model delay accuracy. A multi station baseline software is still in the process of compilation; therefore the results in this report are represented as single baseline solutions and should be regarded as preliminary.

Due to the high weight of the Effelsberg 100 m telescope in the SNR-levels on the different baselines of the WEJO-2 experiment, only the four baselines connecting the other stations to Effelsberg have been used in this report. The other six baselines will of course be included later in the multistation solution. The Effelsberg - Metsähovi baseline, which turned out to be the only successful baseline in the Oct. '80 WEJO-1 experiment, has been

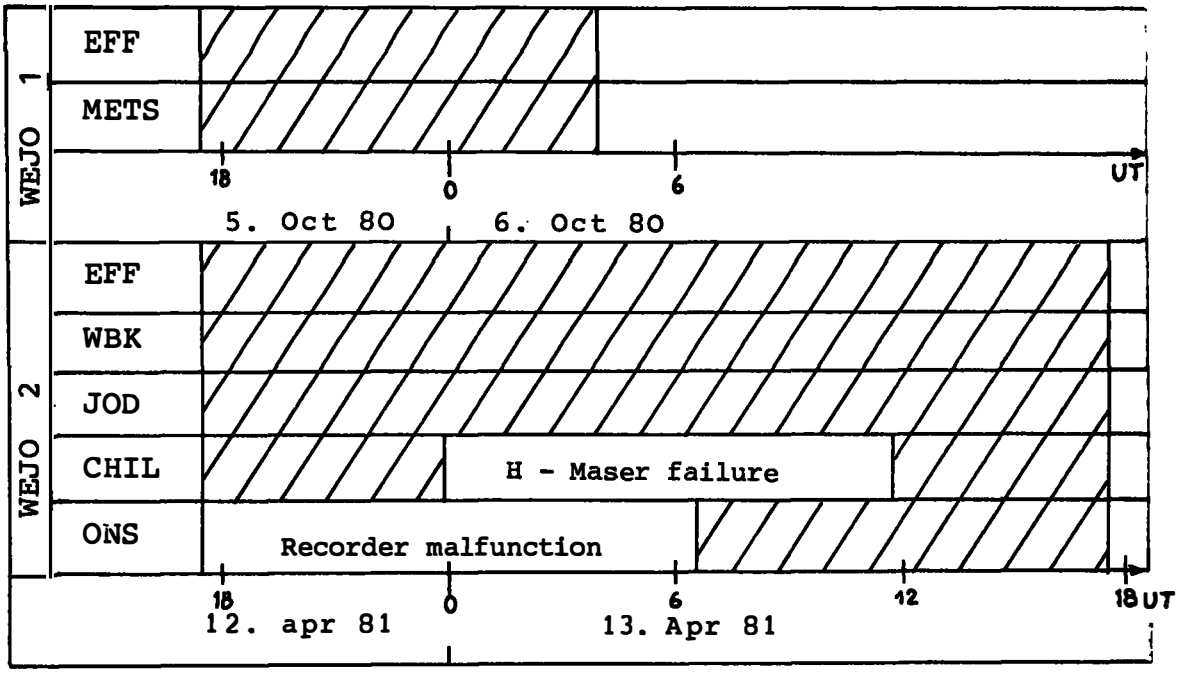

Fig. 1: WEJO 1 and WEJO 2 Mk II VLBI summary

added to the data set for comparison reasons, because it does not belong to the same epoch of time.

Table 2 summarizes the baseline results which were obtained by forming the weighted means of the two single channel and the BWS results. This procedure appeared reasonable because of the relatively high accuracy of the single channel delays. In order to minimize the influence of the rubidium clock instabilities, the data on the EFF-WBK and EFF-JOD baselines were subdivided

into three blocks of about equal size (~ 8 hours of data each)o

The source positions used in the analysis were those published in the JPL-List No. I from 1980 (Fanselow et al. 1980)5 These positions were held fixed in all solutions.

Baseline	b_x m σ_x m	b_y m σ_y m	b_z m σ_z m	σ_τ ns σ_f mHz σ_{BWS} ns
EFF - WBK	-205 345.57 .16	-43 114.06 .20	164 491.25 .33	1.4 1.5 -
EFF - JOD	-211 099.46 .18	-640 793.25 .10	185 855.39 .28	2.0 2.3 -
EFF - CHIL	-25 636.42 .17	-587 641.48 .07	43 363.86 .18	5.0 0.5 0.8
EFF - ONS	-662 981.86 .08	224 474.40 .05	449 233.14 .10	1.5 0.5 0.2
EFF - METS	-1 141 362.15 .20	824 725.95 .14	612 208.86 .34	5.0 0.9 1.3

Table 2: Mk II VLBI baseline results and rms values as computed from the spread of the partial data sets. The last column contains the postfit rms of the observations.

On all baselines involving the stations Westerbork and Jodrell Bank the BWS delays were corrupted by strong sinusoidal phase variationso The exact cause of these variations has not yet been established, although insufficient stability of the rubidium standards may explain a good part of the problemo The BWS delays on the Effelsberg to Onsala baseline proved to be the only ones fully consistent with the theoretically expected 40 MHz BWS accuracy level of about 0.2 nso At Chilbolton, the Maser breakdown probably entailed a somewhat lower stability performance than usualo Moreover the 6cm receiver had a relatively high system temperature (~ 300° K)o

*). 20 MHz synthesis

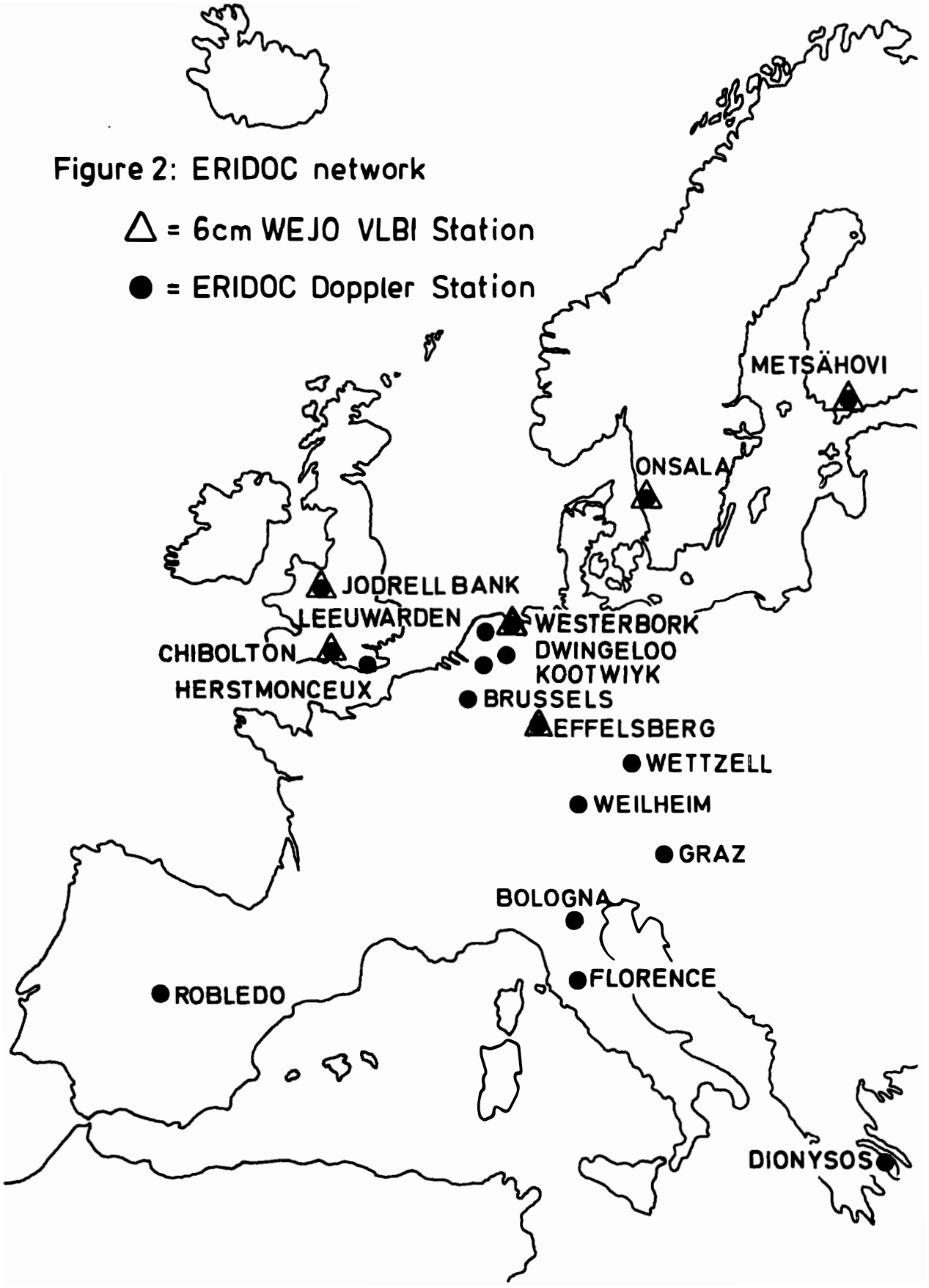

Figure 2: ERIDOC network

△ = 6cm WEJO VLBI Station

● = ERIDOC Doppler Station

3. THE DOPPLER OBSERVATIONS

In the period of April 7 until April 17 1981 Doppler observations to the satellites of the Navy Navigation Satellite System (NNSS) have been carried out at 18 European stations (Fig. 2). An additional aim of this campaign was to connect the ERIDOC network to earlier European Doppler networks such as EDOC-2 (Boucher et al. 1981) including especially the European Tranet stations and several laser observatories. A list of the stations, the participating institutions and the receiver equipment used is shown in table 3.

The two processing centers at the Technical University Delft and the University of Bonn received all Doppler observations either as raw or as majority voted data (including the meteorological readings) by October '81. Precise ephemerides (PE) have been kindly made available by the US Defense Mapping Agency (DMA) for the satellites 30 140 and 30 190.

Data reduction was carried out at both computing centers with the GEODOP software (Kouba et al. 1976). Using small test data sets , the two GEODOP versions at Delft and Bonn and the version of the Institut für Angewandte Geodäsie (IfAG) in Frankfurt/Main have been compared in detail. All three versions showed excellent agreements within 1 cm.

The ERIDOC data were processed independently at both the Delft and the Bonn computing centers using in a first stage only the six WEJO-VLBI stations which are included in the Doppler-VLBI comparisons.

The following computation configurations were performed with the GEODOP software.

1. Broadcast ephemeris single point solution (BCE-SP)
2. Broadcast ephemeris multi point solution (BCE-MP)
3. Precise ephemeris single point solution (PE-SP)
4. Precise ephemeris multi point solution (PE-MP)

The coordinates of the BCE-MP and the PE-MP solutions listed in table 4 are referenced to the doppler antenna phase centers.

4. COMPARISON OF VLBI AND DOPPLER RESULTS

The intercomparisons presented in this paper should be considered as preliminary because of the uncompleted status of the VLBI analysis: only part of the available data have been used until now and only single baseline solutions have been performed. Therefore a simple spatial transformation with up to seven parameters and neglecting the covariance matrices from the VLBI and Doppler solutions was applied. In the final analysis the concept

STATION			RECEIVER	INSTITUTIONS
Onsala	S	telescope	MX 1502	Inst. of Technology, Stockholm
Effelsberg	D	telescope	MX 1502	University of Bonn
Jodrell Bank	GB	telescope	JMR 1	University of Nottingham
Metsähovi	SF	telescope sat.laser rang.	CMA 751	Finnish Geodetic Institute; Norges Geografiske Oppmaling
Westerbork	NL	telescope	CMA 751	T.U.Delft
Dwingeloo	NL	telescope	CMA 751	Wageningen Agricultural Unive
Robledo	E	telescope	JMR 1A	Instituto Geografico Nationale Madrid
Weilheim	D	telescope	CMA 761	IfAG / Frankfurt;SFB 78
Chilbolton	GB	teleseope	JMR 1	Ordnance Survey GB
Wettzell	D	telescope *) satelaser range EDOC	CMA 722B	IfAG / Frankfurt;SFB 78
Bologna	I	telescope *)	MX 1502	University of Trieste
Graz	A	EDOC	CMA 722B	Institute for Space Research, Austrian Academy of Sciences
Leeuwarden	NL	EDOC	CMA 751	T.U.Delft
Herstmonceux	GB	sat.laser rang.	JMR 1	Royal Greenwich Observatory; Ordnance Survey GB
Kootwijk	NL	sat.laser range	CMA 751	T.U.Delft
Dionysos	GR	satelaser range EDOC	MX 1502	National Techn.Univ.of Athens
Florence	I	EDOC TRANET	TRANET	I.R.O.Ee Florence
Brussels	B	EDOC TRANET	TRANET	Observatoire Royal de Belgique

Table 3 : ERIDOC Doppler stations

*) under conseruction

Station	accepted passes		X	σ_x	Y	σ_y	Z	σ_z
Onsala	BCE	181	3370912.91	± 0.70	711516.54	± 0.57	5349675.09	± 0.48
(ONS)	PE	66	911.04	± 0.24	517.32	± 0.32	675.56	± 0.20
Metsähovi	BCE	178	2892593.94	± 0.73	1311786.83	± 0.60	5512615.67	± 0.46
(METS)	PE	100	592.16	± 0.20	787.75	± 0.25	616.11	± 0.15
Jodrell Bank	BCE	81	3822735.43	± 0.69	-154037.88	± 0.61	5086347.58	± 0.54
(JOD)	PE	29	733.54	± 0.34	39.36	± 0.50	345.98	± 0.30
Chilbolton	BCE	135	4008491.77	± 0.68	-100533.27	± 0.57	4943636.64	± 0.53
(CHIL)	PE	59	489.54	± 0.22	533.92	± 0.33	636.07	± 0.20
Westerbork	BCE	141	3828728.99	± 0.68	443249.26	± 0.55	5064877.20	± 0.51
(WBK)	PE	69	726.84	± 0.20	249.60	± 0.26	876.98	± 0.17
Effelsberg	BCE	213	4034102.47	± 0.67	486794.02	± 0.54	4900329.04	± 0.51
(EFF)	PE	84	100.14	± 0.20	794.10	± 0.26	329.04	± 0.17

Table 4 : Doppler derived coordinates referred to the Doppler antenna phase centers from the BCE - MP and PE - MP solutions.The coordinates are given in the BCE - respectively NSWC 9Z2 - coordinate system.

of S-transformations will be applied (Baarda 1973) allowing also the application of statistical testing to detect gross errorso

Before the transformation all Doppler coordinates were converted to the corresponding VLBI reference points, which are defined as the intersection of the prime and secondary telescope axeso All VLBI baseline results refer to these axis intersection points; any offsets (see tab. 1) have been taken into account in the baseline solutionso The Doppler-VLBI ground survey ties have accuracies at the cm-level and are listed in table 5.

Station	Δ X	Δ Y	Δ Z
Onsala	+ 59.78	- 65.31	- 12.62
Effelsberg	- 147.92	+ 179.60	+ 100.92
Jodrell Bank Mk II	+ 115.13	+ 220.69	- 62.37
Chilbolton	- 176.61	- 133.95	+ 158.24
Metsähovi	+ 0.42	- 83.72	+ 23.32
Westerbork 'CB'	- 120.89	+ 611.34	+ 43.37

Table 5 : ERIDOC ground survey ties (Δ = VLBI minus Doppler)

The VLBI coordinate set was created by assigning approximate but fixed geocentric coordinates to the station of Effelsberg and adding to these values the baseline results from table 2. The station of Metsähovi has been included although the VLBI position had been observed at a different epoch because the long baseline to Metsähovi improves the scale factor determination. The results of both the 5 parameter and the seven parameter spacial transformations are shown in table 6.

Most of the postfit residuals which are represented in the local vertical system, are consistent with the expected accuracy level of $\sim$ 0.5 m in all three coordinateso The translation parameters have been omitted because of their arbitrary charactero The scale factor of - 0.26 ppm is of the same sign but somewhat smaller than the values obtained from global data (Hothem et al. 1982)o The rotations express the polar motion and UT1-differences between the Doppler- and VLBI systemso The VLBI baseline solutions are referred to the smoothed BIH data from circular D, which inherently differ from the orientation integrated in the Doppler ephemerideso The magnitude of the rotation errors (± 0".2) reflects the fact that the extension of the European

7 parameters				5 parameters		
$\sigma_o = \pm 0.68$ [m]				$\sigma_o = \pm 0.70$ [m]		
$\mu = -0.26 \pm 0.41$ [ppm]				$\mu = -0.26 \pm 0.42$ [ppm]		
$\omega_x = -0.29 \pm 0.18$ ["]				$\omega_z = -0.88 \pm 0.09$ ["]		
$\omega_y = -0.21 \pm 0.22$ ["]						
$\omega_z = -0.98 \pm 0.12$ ["]						
	postfit residuals [m]				postfit residuals [m]	
station	v_N	v_E	v_H	v_N	v_E	v_H
ONS	- 0.42	0.95	0.25	- 0.29	0.82	0.26
METS	0.61	- 0.54	0.05	0.83	- 0.69	0.44
JOD	- 0.02	- 0.02	- 0.92	- 0.24	- 0.03	- 1.63
CHIL	0.59	- 0.29	1.13	0.38	- 0.19	0.74
WBK	- 0.45	0.27	- 0.57	- 0.42	0.28	- 0.39
EFF	- 0.23	- 0.33	0.07	- 0.17	- 0.21	0.58

Table 6 : Doppler - VLBI intercomparison results
(for further explanation see text)

network is small compared to the Earth's radius (the ratio is about 1:5).

If the baseline lengths are considered, the agreement between Doppler and VLBI results shows a marked improvement as might be expected, because the lengths are insensitive to orientation errors (tab. 7)o In this comparison the Doppler multipoint baselines can be said to achieve at least a three decimeter accuracy level over distances from 200 - 1500 kms.

On the VLBI side the final analysis has still to be performed and will include tropospheric as well as Doppler derived ionospheric calibrationso In future VLBI experiments the use of instrumental delay calibration equipment will be essential to

Baseline from Effelsberg to	length differences [m]				
	METS	ONS	JOD	CHIL	WBK
without scalefactor	0.73	0.60	- 0.03	0.25	- 0.20
with scalefactor of table 6	0.33	0.38	- 0.22	0.10	- 0.27

Table 7 : Doppler - VLBI intercomparisons of baseline lengths

arrive at accuracies in the centimeters. It is hoped that the stations of Jodrell Bank and Westerbork will be able to procure H-Maser frequency standards soon.

5. ACKNOWLEDGEMENTS

The authors would like to express their gratitude for the assistance received from many different sides. Without such support this work could not have been accomplished. The individuals and groups involved in this project, but not included in the authors list are: the JPL VLBI group in Pasadena, California, U.S.A., in particular Karen S. Wallace and Timothy E. Erickson who performed the major part of the correlation and post processing, the correlator staff at the Max-Planck-Institut für Radioastronomie, Bonn, the staffs of the participating observatories, i. e. the radio observatory Effelsberg operated by the Max-Planck-Institut für Radioastronomie, the Onsala Space Observatory supported by the Swedish Natural Science Research Council, the Chilbolton observatory operated by Appleton Laboratories and supported by the Science Research Council, the Jodrell Bank observatory operated by the Nuffield Radio Astronomy Laboratories, the Westerbork array supported by the Netherlands Foundation Radiostraling van Zon en Melkweg, the Metsähovi Radio Research Station operated by the Helsinki University of Technology, the Department of Civil Engineering of the University of Nottingham, UK, the Ordnance Survey of Great Britain, the Rijkskommissie voor Geodesie, The Netherlands, the Finnish Geodetic Institute, Helsinki, the Instituto Geografico Nacional, Madrid, Spain, the Norges Geografiske Oppmaling, Norway, the Wageningen Agricultural University, The Netherlands, the University of Trieste, Italy, the IROE Florence, Italy, the National Technical University of Athens, Greece, the Observatoire Royal de Belgique, Brussels, Belgium, The Royal Greenwich Observatory, UK, the Institute of Space Research of the Austrian Academy of Sciences, Graz, Austria, the Institut für Angewandte Geodäsie

Frankfurt (IfAG/SFB 78) , the Deutsche Forschungsgemeinschaft, Fed. Rep. of Germany and the Roy. Inst. of Technology, Stockholm, Sweden.

6. REFERENCES

Baarda, W. (1973) — S-Transformations and Criterion Matrices; Publ. Netherlands Geodetic Commission, Vol. 2, No. 4, Delft.

Bouchers, C., Paquet, P., Wilson, P. (1981) — Final Report on the Observations and Computations Carried out in the Second European Doppler Observation Campaign (EDOC-2) for Position Determinations at 37 Satellite Tracking Stations, DGK-Reihe B, Nr. 255, Frankfurt.

Fanselow, J. L. et al. (1979) — Determination of UT1 and Polar Motion by the Deep Space Network Using Very Long Baseline Interferometry. In "Time and the Earth's Rotation", IAU-Symp. No. 82, San Fernando, Spain, May 8-12, (Publ. D. Reidel, Doordrecht, Holland).

Fanselow, J. L. et al. (1980) — Development of a radioastrometric catalog by means of Very Long Baseline Interferometry observations. Jet Propulsion Laboratory, Pasadena, California.

Hothem, L. D.; Vincenty, T.; Moose, R. E. (1982) — Relationship between Doppler Coordinates and other Advanced Geodetic System Measurements Using Global Data, Proc. of the 3rd International Geodetic Symposium on Satellite Doppler Positioning, Las Cruces (DRAFT).

Kouba, J.; Boal, J. D. (1976) — Program GEODOP Documentation, Geodetic Survey of Canada, Ottawa.

Niell, A. E. et al. (1980) — Geodetic Measurements with a Mobile VLBI System. Proc. Radio Interferometry Techniques for Geodesy, Cambridge, Mass. June 19-21, 1979 (NASA/GSFC Conference Publication 2115).

Thomas, J. B. (1981). An Analysis of Radio Interferometry with the Block O System, NASA/JPL Publication 81-49, Pasadena, California.

MOBILE VLBI SURVEYING: INSTRUMENTATION, OPERATING PROCEDURES, AND SURVEY RESULTS OF ARIES[1]

D. W. Trask, M. L. Brunn, E. J. Cohen, J. M. Davidson, J. L. Fanselow, P. F. MacDoran, R. B. Miller, A. E. Niell, G. S. Parks, G. M. Resch, L. J. Skjerve, C. J. Vegos, and K. S. Wallace

Jet Propulsion Laboratory
California Institute of Technology
Pasadena, California

ABSTRACT

The Mobile VLBI stations of the Crustal Dynamics Project are described and the data acquisition program, operating procedures, and the survey results are discussed. There are three Mobile VLBI (MV) stations and 17 distinct sites have to date been occupied in or near California, U.S.A. Data acquisition activities started in 1974 at the JPL site for MV 1 (9-meter antenna) and in 1980 for MV 2 (4-meter antenna). Activities for MV 3 (5-meter antenna) are scheduled to start by January 1983.

Examples of survey results are presented for the 1980 measurements which were made for the triangle defined by the base stations at Owens Valley and Goldstone, and the JPL Mobile VLBI site located on the opposite side of the San Andreas Fault from the base stations. The measurements were made eight times during 1980, and, although there is some variation in quality among the measurements, in general the precision of an individual vector seems on the order of 5 cm or better in any horizontal plane direction.

The Goldstone to Owens Valley baseline solutions are relatively constant. The baselines containing JPL for all of 1980 are consistent, with no change in baseline components within the apparent precision of the individual solutions. However, the temporal grouping of these solutions suggests an abrupt shift of about 10 cm in the position of JPL with respect to the base stations. This apparent shift occurred sometime between the adjacent measurements of 5 February and 25 March 1980 and was in a direction consistent with the average relative motion of the Pacific and North American plates.

[1]The research described in this paper was carried out by the Jet Propulsion Laboratory, California Institute of Technology, under Contract NAS7-100 with the National Aeronautics and Space Administration.

I. INTRODUCTION

The Mobile VLBI element of the Crustal Dynamics Project is managed by JPL, while the Project is managed by the Goddard Space Flight Center for the National Aeronautics and Space Administration (NASA). The Mobile VLBI system includes three transportable stations (MV 1, 2, and 3) which are operated in conjunction with a larger fixed-base station (or stations). The applications for such a system include establishing fundamental points for geodetic surveys, determining relative motions and regional strain fields near tectonic plate boundaries and land subsidence, and rapid monitoring of regional deformations in the crust of the Earth after an earthquake.

This paper is divided into three sections. The first discusses the three stations and their relative mobility. The second reviews both the past and planned measurement program and describes the actual time sequence followed when visiting a group of sites during May 1981.

The third section describes some data-taking procedures, reviews a portion of the 1980 data sent to the NASA Geodynamics Data Archive, and examines the effects due to crudely accounting for the ionosphere and to converting from the smoothed UT1 of the BIH to smoothed UT1, based on lunar laser-ranging (LLR) data. Also, the UT1 tidal term is applied. Specific details on the role and system elements of the Mobile VLBI stations can be found in Trask (1979).

II. MOBILE VLBI STATIONS

The Crustal Dynamics Project has three Mobile VLBI stations: MV 1 (a 9-meter station), MV 2 (a 4-meter station), and MV 3, (a 5-meter station). All three stations will be ready in the "standard" Crustal Dynamics configuration by April 1983. That is, they will use a Mark III recorder (112-Mb/s record rate) and will sample data across 400 MHz of spanned bandwidth at X-band (8.4 GHz) and 100 MHz at S-band (2.3 GHz). The first two stations (MV 1 and 2), known by the common name ARIES, have measured data in other configurations since 1973 and 1980, respectively. The third station (MV 3), known also by the names Advanced ARIES and ORION, is currently being fabricated. The station antenna should be ready for initial use by September 1982; and an electronics van by January 1983. The configurations of the three mobile stations in transit are shown in Figure 1; their operating modes and degrees of mobility are listed in Table 1.

The 9-meter station was acquired for proof-of-concept testing, with mobility a lesser priority. It takes a workforce of four people using a crane and cherry picker approximately 14 working days (not including transit time) to disassemble, reassemble, and check out a station. Because of the relatively heavy expenses in moving MV 1, special efforts are made to verify its proper operation before beginning the main data acquisition period, and a second day's worth of data is obtained for back-up purposes; hence, the normal data acquisition mode is a 2-hour and two-26 hour periods, each separated by one day, as shown in the last column of Table 1 for MV 1.

The operating mode columns of Table 1 apply only when one of the mobile stations is being used in conjunction with a base station or stations. The length of time a station stays on site is determined by a trade-off between the probability of obtaining valid data and the expenses of revisiting sites should the data be "lost." A 24 to 36 hour data acquisition period is currently used for MV 2, although good baseline solutions should be otainable with six hours of data. Also, during the current phase of development, reliable solutions for baselines seem to "require" three stations. (The solutions in this paper are based on forced closure of the triangle defined by the three stations.) Theoretically, satisfactory results are obtainable with only two stations. The row for MV 3 in Table 1 and the MV 3 design specification reflect the goal of being able to obtain a precise baseline measurement using a single base station operating with a six-hour data acquisition period.

The 4-meter station (MV 2) was obtained to demonstrate higher mobility. Only eight hours are required for tear-down and set-up versus 14 days for MV 1. Also no crane or cherry picker is needed for MV 2. Although the first two antennas (but not the electronics vans) were obtained as Army surplus equipment, MV 3 was designed and built specifically for the Crustal Dynamics Project. The station equipment is being documented with the goal that future copies of the station or its subsystems may be obtainable from commercial sources. The MV 3 antenna transport is shown in its transit configuration in Figure 2 and in its deployed configuration in Figure 3. The MV 3 station was designed to be operated by a two-person crew, who perform all operations but repairs. During a normal cycle, within a two-day span, the crew would drive to a site, set up and check out the station, take six hours of data, tear down the station, and prepare to drive to the next site.

III. DATA ACQUISITION PROGRAM

The Mobile VLBI measurement program is designed to monitor changes in the vector baselines among the MV sites and the base stations. Two base stations are usually used, separated by 260 km. One base station is located in the Owens Valley and the other is at Goldstone, CA. Recently, a third station (located at Fta Davis, TX, 1300 km from Goldstone) has also been used. To date, the mobile stations, have visited the 17 sites shown in Figure 4, of which all but one (Yuma, AZ) are in California.

After short baseline (307 m) runs performed in 1973-74, MV 1 initiated a measurement program to demonstrate the geodetic performance of ARIES and, at the same time, to produce data of potential geophysical interest by a careful choice of demonstration sites. The history of site visits for MV 1 and MV 2 through 1981 is listed in Table 2. The JPL site has the longest data acquisition history (seven years), while four other sites have histories spanning four to six years. The remaining 12 sites have only had a single occupation, nine of which occurred in 1981.

The measurement program was turned over to MV 2 in the later part of 1980, after which site visits were arranged in "bursts." That is, to reduce reconfiguration overhead at the base station and for other reasons, it was advantageous to visit the sites in groups rather than uniformly spread out

site visits over the year. For example, in February 1981, MV 2 visited three sites: JPL, Palos Verdes, and Pearblossom. In May it visited five sites: JPL, La Jolla, Monument Peak, Yuma, and Pinyon Flats.

The time history of events for the May 1981 burst is shown in Figure 5. The nominal cycle time is 36 hours; i.e., a 24-hour data acquisition period, 3 hours to tear down, 4 hours to travel, and 5 hours to set up and check out the station. However, a number of factors caused a deviation from this pattern. For example, the first site is JPL, and because of time constraints on both ends, the data acquisition period is generally less than 24 hours. The MV 2 requires a wide load highway transit permit, because the 4-meter dish cannot be disassembled as the 9-meter dish can. Even with a wide load permit, the antenna must be clear of the Greater Los Angeles area by 4 PM, which generally means it must shut down at JPL shortly after 10 AM. But on the first day of a burst, OVRO is not in configuration until sometime between noon and 4 PM, which results in less than 24 hours of data for the JPL/OVRO baseline. Items which were peculiar to the May burst include: an underpowered tractor being assigned to the move, which significantly lengthened the travel time; a flat tire upon departing from Yuma; and high winds at Monument Peak which forced the crew to stow the antenna. The schedule included a one-day pad, which would have been used at Monument Peak had there been reasonable assurance that the winds would subside.

The next burst (August 1981) was the largest yet conducted and consisted of six sites, namely: JPL, Palos Verdes, Pearblossom, Gorman, Santa Paula, and Vandenberg Air Force Base. These sites were completed within ten days elapsed time. In December, MV 1 was reactivated and remained at JPL, while MV 2 went to San Francisco, Pt. Reyes, Vacaville, and Ft. Ord.

Except for occasional engineering/training tests, the Mobile VLBI data acquisition activities were temporarily halted after the December 1981 burst. The activities will start up again as MV 3 becomes available, after which the standard data-taking configuration will use a base station at Goldstone, and MV 1 at Vandenberg Air Force Base, with MV 2 and MV 3 touring the various sites.

Future plans call for sending MV 2 and 3 to Alaska each summer starting in 1984 plus visiting a few new sites in California and one site in each of Arizona (in addition to Yuma), Colorado, Nevada, and Utah.

IV. SAMPLE OF SURVEY RESULTS

The JPL-Goldstone-Owens Valley (JOG) triangle (Figure 4) is measured at least once during each burst and the bulk of the past measurements with MV 1 are for this triangle. In March 1982, JPL submitted a data package (Wallace et al, 1982) to the NASA Geodynamics Data Archive. This package contained solutions for eight dates during 1980 for the JOG triangle, along with the associated raw and calibration data. The package was also designed to provide enough textual material so that independent investigators could duplicate the JPL results.

The remainder of this section describes the data-taking procedures and extends the analysis for one portion of the data package discussed above. The data in the various 1980 solutions is reviewed, and the effects for the horizontal plane of the ionosphere and UT1 are discussed. In particular, crude ionospheric calibrations are applied to the data, smoothed BIH UT1 is replaced by smoothed LLR UT1, and the UT1 tidal term is added. All these changes improve the overall consistency of the data set, with the ionospheric calibration being the largest effect. The solutions spanned a time interval of ten months from January to November 1980. The run IDs of these solutions, as well as their dates of occurrence and the amount of data contained in each solution, are listed in Table 3.

A typical observing session for ARIES lasts 24 hours and includes from 16 to 18 sources. A given source may be observed up to six times, spread out over the time it is visible to the participating stations. Each observation, which is called a scan, will vary in length from 3 minutes for a strong source to 15 minutes for a weak source, when recording at 4 Mb/s (Mark II recorders), as was done for this data. On the order of 90 scans are attempted during a 24-hour session and barring any unusual equipment/procedural failures, between 60 and 80 of these will be successful and available for estimating baselines. The scans are normally taken when the elevation angle of the source is greater than 15^{o}. The pattern consists of six scans which take from 1 1/2 to 2 hours to complete. The elevation angle constraint is a trade off between wanting low elevation angle data to strengthen the geometry of the solution and avoiding data which is too strongly corrupted by the limited ability to calibrate for the troposphere. The six-scan pattern is conceptually designed to be capable of "providing" a baseline solution on its own. Such a sequence results in about 90^{o} of antenna movement between successive scans where, for example, four of the scans are at relatively low elevation angles at the four compass points and two of the scans are near vertical. A typical pattern is: vertical - east - north - vertical - south - west. This pattern was designed to reduce the correlation between excursions of the electrical path length or frequency system, which are time dependent, and other errors which may be more azimuth or elevation angle dependent. Also, the six-scan pattern should keep sensitivity to the loss of a few hours of data relatively independent of where the gap occurs. As it turns out, the inability to adequately provide ionospheric calibrations has essentially put a number of "gaps" in the "80 data set." That is, to decrease the sensitivity of the solutions to the ionosphere, only the nighttime or about one-third of the available data was used for the S-band solutions provided in Wallace et al (1982) which, for the horizontal plane, are repeated in Table 4. The data in Table 4 are tabulated as changes from Reference Baseline Set C 81/12[2] which is presented in Table 5.

---

[2]A reference baseline set is generally chosen to be arbitrarily near the average baseline to an even decimeter in the X, Y, Z coordinate system. One purpose is to facilitate the comparison of tables and plots in separate papers (as opposed to the practice of presenting data with respect to the average value of that particular data set).

The ionosphere affects all coordinates of the baseline but normally its largest effect is one of lengthening the baseline. Of the eight runs, five employed MV 1 receiving at S-band and three used MV 2 receiving at X-band. The effect of the ionosphere is proportional to the columnar electron content divided by the square of the receiving frequency. Consequently, the ionospheric effect is 13 times greater for the S-band data than for the X-band data. Also, the columnar content of the ionosphere is considerally larger during the day than it is during the night.

This difference is illustrated inaTable 6 where for the five 1980 S-band runs the daytime peak vertical electron content covered the range of 4 to 8 x 10^{17} electrons/meter^2 while the averag nighttime vertical electron content varied from 0.5 to 1.6 x 10^{17} el/m^2.

The columnar content values derived from the Faraday rotation data are listed in Wallace et al (1982). However, the Faraday rotation data is believed, as discussed by these authors, to contain some biases due to unresolved π ambiguities. Consequently, nighttime ionosonde data has been used (Eis 1977) in conjunction with the Faraday rotation data to establish the offseta[3] The "adjusted Faraday" columns of Table 6 contain the current estimates of the vertical columnar electron content of the ionosphere for the various runsa

In addition to the ionospheric activity, Table 6 also illustrates the effect of the ionosphere on the OVRO to JPL baseline. The change in coordinates represents the solutions obtained when only nighttime data is used (low ionospheric activity) minus the solutions obtained when the complete 24-hour data set is used. For example, the changes of 18 cm in vertical and 37 cm in length for 80D show that the effect of the ionosphere can be quite pronounced. However, these differences do not completely isolate the contribution due to the ionosphere for two reasonsa

First, the difference between the data spans (e.g., 5.9 vs 25.6 hours for 80G) will change the sensitivity of the solutions to error sources in addition to the ionosphere. And second, there is still an ionospheric effect in the nighttime data.

A zeroth order estimate of the effect of the nighttime ionosphere for baseline length has been made and is given in Table 7. To obtain this estimate a spherical shell ionosphere is assumed with a thickness equal to the average nighttime columnar content given in Table 6. The results of a study on the effects of such an ionosphere are presented in Enclosure 5 of Wallace et al (1982) for Run 80Fa For length the results can be estimated using Equation (1).

$$\frac{\text{Length}}{\Delta \text{ Columnar Electron Content}} = 6 \text{ cm}/250 \text{ km}/10^{17} \text{el/m}^2 \qquad (1)$$

---

[3]The reduced Faraday Rotation (from Goldstone) and ionosonde data (from Vandenberg Air Force Base) were provided by T. Litwin, L. Alvarado, and Dr. H. Royden of JPL.

The same partial derivative was used for all five of the S-band baselines with the changes in baseline length due to the nighttime ionosphere ranging from 2 to 13 cm for the 80 data seta

For the case of a spherical shell ionosphere, the effect inathe transverse direction is negligible. However, the transverse direction is directly affected by errors in Universal Time (UT) while the length is nota The results presented in Wallace et al (1982) and in Table 3 use smoothed BIH UT1, which, among other things, means that the tidal terms have been smoothed outa In addition, UT1 derived from laser (Fliegel et al, 1982) or VLBI data can vary by several msec from the BIH data. Furthermore, the laser and VLBI UT1 determinations agree with each other better than they agree with BIH. The effect of converting to smoothed UT1 as determined from lunar laser ranging (LLR) data (Dickey et al, in press) and of adding in the tidal terms is given in Table 8. The difference between LLR and BIH varies by 3 msec over this data set while the tidal term varies by over 2 msec. This later variation occurs between 80F and 80G which are only one week apart. The sensitivity of the transverse component to UT1 for the JOG triangle is represent by Equation 2.

$$\frac{\Delta \text{ Transverse}}{\Delta \text{ UT1}} = 1.1 \text{ cm}/250 \text{ km/msec} \qquad (2)$$

Compared to the changes caused by the nighttime ionosphere, these changes are relatively small ranging from -1.7 to +3.1 cm for the longest baseline (OVRO/JPL) and about half that for the shortest baseline (JPL/Goldstone).

The data from Table 4 with the ionospheric corrections from Table 7 and the changes due to the UT1 conversions of Table 8 are plotted for the three baselines in Figure 6. The "corrected" solution set is known as 810322D (810322 is the solution set of Wallace et al (1982)), and is plotted as changes from reference baseline set C81/12 given in Table 5.

The principal components of the error ellipses of Figure 6 are listed in Table 9 along with the size of their contributions. Two cases are considereda S-band and X-band. The ionosphere causes larger uncertainties for the S-band case for two reasons. First, there is the direct effect of 13 times more corruption for the S-band than for the X-band data. Second, there is the indirect effect caused by eliminating the daytime data. This loss of data via a $\sqrt{N}$ effect increases the sensitivity of the solutions to random errors such as those contained in the rows of Table 9 for S/N, wet troposphere, and the random part of the ionosphere. Other errors are proportional to the baseline length, e.g., the effect of the ionosphere, and uncertainties in source positions, UT1, and polar motion. The error model is still under development in an effort to explain the possible effects of various error sources on the solutionsa As can be seen from Figure 6, the model does not explain all the scatter in the baseline solutionsa For the purpose of Figure 6 the same error ellipse for a baseline has been used for all S-band runs and another for all X-band runsa Although the error budget will vary among S-band and X-band runs, for most runs the variations in RSS is small compared to the uncertainty in the RSS. The primary causes of the variations relate to the behavior of the ionosphere and to the length of the data span (for short data spans).

Someageneral observations which can be made follows:

- The San Andreas Fault cuts the OVRO/JPL baseline at about 45° (NW-SE). It is roughly perpendicular to the JPL/Goldstone baseline and does not cross the Goldstone/OVRO baseline, i.e., the lengths of the JPL/Goldstone and the Goldstone/OVRO baselines should not be affected by motion along the San Andreas Fault system to first order.

- The lengths of the X-band baselines (80B, I, and L) are relatively consistent, i.e., $\pm$ 3 cm for JPL/Goldstone and $\pm$ 1.5 cm for Goldstone/OVRO.

- The variation of the S-band lengths may be a combination of ionospheric effects and noisier solutions due to the shorter data spans. For example, 80A and C appear undercorrected except for the DSS 13/OVRO baseline for 80A (using the X-band baselines as the standard of comparison).

- The gap between the three earlier (January-February) points and the five later points (March-November 1980) for the JPL/Goldstone baseline could correspond to a episodic right lateral motion along the San Andreas Fault on the order of 10 cm. The JPL/DSS 13 baseline is the best of the two affected baselines with which to observe such motion for two reasons. First, the error ellipse is significantly smaller for JPL/DSS 13 than for the OVRO/JPL baseline because of a factor of two difference in length between these two baselines. Second, motion along the San Andreas Fault will affect the JPL/DSS 13 baseline in the direction of the semiminor, not the semimajor, axis of the error ellipse, i.e., the ionosphere corrections of Table 8 move the baseline in a direction normal to the effect of San Andreas Fault motion. Although any effects of episodic San Andreas Fault motion on the order of 10 cm are not so clearly seen with the OVRO/JPL baseline, the data shown in Figure 6 is not inconsistent with such motion between February and March 80 (80C and D).

- The variation in the transverse direction for the Goldstone/OVRO baseline is larger than expected from the error model. No explanation is advanced at this time by the authors.

- Two pairs of runs are relatively close together, i.e., 80A and B are two days apart and 80F and G are seven days apart. The difference between F and G is from 3 to 6 cm for the three baselines, which is reasonable compared to the error model. However, the difference between A and B is from 8 to 14 cm which is on the large side. However, before the ionospheric corrections were applied to 80A (80B is an X-band run), the difference was 20 cm for the OVRO/JPL baseline. Some of the remaining 14 cm difference could be due to the lack of a better ionospheric calibration procedure.

- The changes in UT1 from BIH to LLR plus the addition of tidal terms were less than the quoted one sigma error in the baseline. However, these changes did move 80F and G notably closer together in the transverse direction and did slightly reduce the earlier mentioned gap between the January-February and March-November solutions.

REFERENCES

Dickey, J. O., Fliegel, H. F., and Williams, J. G., (in press), "Universal Time, UT1, from Lunar Laser Ranging Observations," to be published in the BIH (Bureau Internatinnal de l'Heure) Annual Report for 1981.

Eis, K. E., Klobuchar, J. A., and Malik, C., May 31, 1977, "On the Installation, Operation, Data Reduction, and Maintenance of VHF Electronic Polarimeters for Total Electron Content Measurements," Air Force Geophysics Laboratory, Instrumentation Paper 256.

Fliegel, H. F., Dickey, J. O., and Williams, J. G., 1982, "Inter-comparison of Lunar Laser and Traditional Determinations of Earth Rotation," International Astronomical Union Colloquium No. 63 Proceedings (High-Precision Earth Rotation and Earth-Moon Dynamics: Lunar Distances and Related Observations; Grasse, France; May, 1981), ed. Odile Calame, D. Reidel, Dordrecht-Holland.

Trask, D. W., December, 1979, "NASA Very Long Baseline Radio Interferometry Programs, Status and Plans," Office of Space and Terrestrial Applications and the Office of Space Tracking and Data Systems.

Wallace, K. S., Fanselow, J. L., Davidson, J. M., and Niell, A. E., March 10, 1982, "1980 Mark II ARIES Data Package for Geodynamics Archive."

Table 1. Mobile VLBI Stations

MOBILE VLBI STATION	ANTENNA SIZE	MOBILITY* (TEAR DOWN SET-UP TIME)	NORMAL OPERATING MODE	
			NUMBER OF BASE STATIONS	DATA ACQUISITION INTERVALS
ARIES				
• MV 1	9M	14 DAYS	2	2 HOURS, 26 HOURS, AND 26 HOURS SEPARATED BY 1 DAY EACH
• MV 2	4M	8 HOURS	2	24 TO 36 HOURS
ORION (ADVANCED ARIES)				
• MV 3	5M	4 HOURS (GOAL)	1	6 HOURS

*DOES NOT INCLUDE TRAVEL TIME

Table 2. Aries Site Visit History

CY	MV 1 (ARIES 9M)	CY	MV 1 (ARIES 9M)	MV 2 (ARIES 4M)
73	N* GOLDSTONE (DSS 14)	79	JPL (5) QUINCY MT OTAY	—
74	DSS 14 (3)** N JPL	80	JPL (5) N GOLDSTONE-DSS 13 14)	JPL (3) PALOS VERDES
75	JPL (3) N MALIBU (SADDLE PEAK)	81	JPL	JPL (4) PALOS VERDES (2) PEARBLOSSOM (2) LA JOLLA "N" MONUMENT PEAK (REPLACES MT OTAY) N YUMA N PINYON FLATS N GORMAN N SANTA PAULA N VANDENBERG SAN FRANCISCO N PT REYES N VACAVILLE N FT ORD
76	JPL (2) N PALOS VERDES (2) N PEARBLOSSOM			
77	JPL (2) "N" MALIBU (NIKE SITE) PEARBLOSSOM N LA JOLLA N SAN FRANCISCO (PRESIDIO)			
78	JPL			

* NEW (i.e., FIRST VISIT OF SITE ** No. OF BASELINE MEASUREMENTS SEPARATED BY A WEEK OR MORE

Table 3: Data Summary for March 82 Submittal of "80" Data Set to Geodynamics Data Base

Run ID	Start Day ~Local Time	Freq. of Receiver S:2.3GHz X:9.4GHz	Hrs. of Data in FIT	No. of Scans In FIT			Time Span of Available Data ~GMT	Time Span of Data Used in FIT ~GMT
				JPL/ OVRO	OVRO/ Glds	Glds/ JPL		
80A	3 Jan 80	S	6.9	24	24	27	8.1^h 4 Jan to 9.1^h 5 Jan	8.5^h to 12.0^h 4 Jan & 4.6^h to 8.0^h 5 Jan
80B	5 Jan 80	X	25.8	50	66	48	5.0^h 6 Jan to 6.8^h 7 Jan	ALL
80C	4 Feb 80	S	7.8	28	25	27	2.8^h 5 Feb to 3.9^h 6 Feb	4.2^h to 12.0^h 5 Feb
80D	25 Mar 80	S	7.8	22	29	23	14.2^h 25 Mar to 15.8^h 26 Mar	4.1^h to 11.9^h 26 Mar
80F	3 Jun 80	S	9.4	27	29	27	8.4^h 3 Jun to 9.8^h 4 Jun	8.7^h to 11.2^h 3 Jun & 2.9^h to 9.8^h 4 Jun
80G	10 Jun 80	S	5.9	21	23	21	3.3^h 11 Jun to 4.9^h 12 Jun	3.2^h to 7.9^h 11 Jun & 3.2^h to 4.4^h 12 Jun
80I	28 Jul 80	X	19.9	28	58	24	18.5_h 28 Jul to 14.4_h 29 Jul	ALL
80L	2 Nov 80	X	21.3	58	74	64	22.8_h 2 Nov to 21.9_h 3 Nov	ALL

Table 4. Values for Baselines of JOG Triangle: Mar 82 Submittal to Data Base

Run ID	Coordinates of Baseline Minus Reference Baseline Set C81/12					
	JPL/ Goldstone		Goldstone/ OVRO		OVRO/ JPL	
	East	North	East	North	East	North
80A	-6.7	+4.6	+1.5	+3.5	+5.5	-8.4
80B	-7.4	-4.5	-2.7	-6.0	+10.6	+10.7
80C	-4.1	+8.5	+0.3	-4.7	+4.2	-3.8
80D	+0.1	-6.8	-2.2	-0.5	+2.4	+7.1
80F	+5.2	+2.9	-6.5	-11.2	+1.5	+8.2
80G	+8.3	+1.8	-5.5	-7.4	-2.7	+5.4
80I	-0.6	-9.5	+2.6	-4.5	-1.5	+13.9
80L	+1.3	-6.0	-0.9	-3.8	-0.2	+9.7

Table 5. Reference Baseline Set C81/12

Baseline	Geocentric, Equatorial Frame of Epoch 1950.0*			
	X (Toward 0° Long.) ~m	Y (Toward 90° Long.) ~m	Z North, Parallel to Spin Axis ~m	Length ~m
JPL (Bench Mark A) to Goldstone (DSS 13)	142 176.797	-281.340	95 437.601	171 238.595
Goldstone to Owens Valley (40m Antenna)	-58 469.079	177 128.307	177 646.364	256 900.845
OVRO to JPL	-83 707.721	-176 846.964	-273 083.965	335 941.488

*Right hand version of the CIO reference system with pole defined by 1903.0 pole.
1980 IAU theory of nutation (WAHR model).
1976 IAU precession quantities corrected by Y and Z axis rotation rates of 3.09 & 2.37 marcsec/yr respectively.

Table 6. Ionospheric Activity & Its Effect On the OVRO-JPL Baseline

Run ID (S-Band Sessions)	[a] Columnar Electron Content 10^{17} el/m^2					Change in the OVRO-JPL Baseline~cm (Nite Only Minus All Data)		
	Ave. Night Time Level During Data			Peak Content				
	Faraday Rotation of Ref 1	Offset Derived using Ionosonde Data	Adjusted Faraday	Faraday Rotation of Ref 1	Adjusted Faraday	Vertical	Transverse	Length
80A	0.84	-0.22	0.62	6.3	6.1	+7.1	+7.0	-3.0
80C	1.18	-0.65	0.53	6.1	5.4	00	-6.9	-3.0
80D	2.21	-0.65	1.56	8.8	8.1	+18.2	-9.6	-36.3
80F	2.67	-1.08	1.59	5.5	4.4	+3.6	+1.9	-10.9
80G	2.47	-1.08	1.39	3.9	3.8	+0.@	+6.4	-0.5

a. Faraday rotation is as in enclosure 5 of Wallace et al (1982) except a π ambiguity (0.432×10^{17} el/m^2) has been subtracted out of the data for 80A prior to 1810 GMT 4 Jan 80, however π ambiguities still seem to exist and the night time ionosonde data was used to detect these ambiguities. See EIS et al, (1977) for the technique used i.e., Electron Content = Slab Thickness × Peak Electron Density where the slab thickness was assumed to be between 200 and 300 Km and relative antenna orientations are such that zero electron content corresponds to $-1/2\pi$.

Table 7. Effect of Spherical Ionosphere

Run ID	Thicknessof Spherical Ionosphere $\sim 10^{17}$ el/m^2	Calibrated Minus Uncalibrated Baseline Length~cm		
		JPL/ Goldstone	Goldstone/ OVRO	OVRO/ JPL
80A	0.62	-2.5	-3.7	-4.9
80C	0.53	-2.1	-3.2	-4.2
80D	1.56	-6.2	-9.4	-12.5
80F	1.59	-6.4	-9.5	-12.7
80G	1.39	-5.6	-8.3	-11.1

Table 8. Effect of UT1

Run ID	UT1 Conversion~msec			Effect of Transverse Baseline Component~cm		
	Smoothed LLR Minus BIH	Tidal[a] Term	Total	JPL/ Goldstone	Goldstone/ OVRO	OVRO/ JPL
80A	+2.0	-0.08	+1.9	+1.3	+2.0	+2.6
80B	+2.0	+0.23	+2.2	+1.6	+2.4	+3.1
80C	+1.3	+0.34	+1.6	+1.2	+1.7	+2.3
80D	+0.3	-0.54	-0.2	-0.1	-0.2	-0.3
80F	-0.2	+1.88	+1.0	+0.7	+1.1	+1.4
80G	-0.3	-0.97	-1.3	-0.9	-1.4	-1.8
80I	-1.2	+1.09	-0.1	-0.1	-0.1	-0.1
80L	+0.8	-0.27	+0.5	+0.4	+0.5	+0.7

a. Tidal terms from an internal JPL document by M. Eubanks

Table 9. Error Budget for Horizontal Components of Baselines in JOG Triangle*

Error Component	Errors for an S-Band (80A) Baseline~Cm						Errors for an X-Band (80B) Baseline~Cm					
	JPL/ Goldstone		Goldstone/ OVRO		OVRO/ JPL		JPL/ Goldstone		Goldstone/ OVRO		OVRO/ JPL	
	Leng.	Trans.	L	T	L	T	L	T	L	T	L	T
S/N	1.1	0.7	0.3	0.2	1.8	1.1	0.7	0.4	0.2	0.1	1.2	0.8
Clock Instability ($\Delta f/f = 10^{-14}$ ea. site)	0.5	0.4	0.5	0.4	0.5	0.4	0.5	0.4	0.5	0.4	0.5	0.4
Instrumentation delay (1° noise each channel)	1.0	0.8	1.0	0.8	1.0	0.8	1.0	0.8	1.0	0.8	1.0	0.8
Ionosphere (π ambiguity + 1% total/ 100km random)	2.8	2.2	4.1	3.3	5.6	4.4	0.1	0.1	0.1	0.1	0.2	0.1
Wet Troposphere (2 cm random ea. site)	2.4	2.0	2.4	2.0	2.4	2.0	1.6	1.2	1.6	1.2	1.6	1.2
Source Position (0.02" in $\delta, \alpha \cos\delta$)	0.6	0.3	0.9	0.5	1.2	0.6	0.6	0.3	0.9	0.5	1.2	0.6
UTI (1 msec)	---	0.7	---	1.1	---	1.4	---	0.7	---	1.1	---	1.4
Polar Motion (40cm)	---	0.9	---	1.3	---	1.8	---	0.9	---	1.3	---	1.8
Other	0.4	0.3	0.4	0.3	0.4	0.3	0.4	0.3	0.4	0.3	0.4	0.3
RSS	4.1	3.4	5.0	4.4	6.6	5.6	2.2	2.0	2.2	2.3	2.6	2.9

*Based in part on internal JPL documents by S.C. Wu

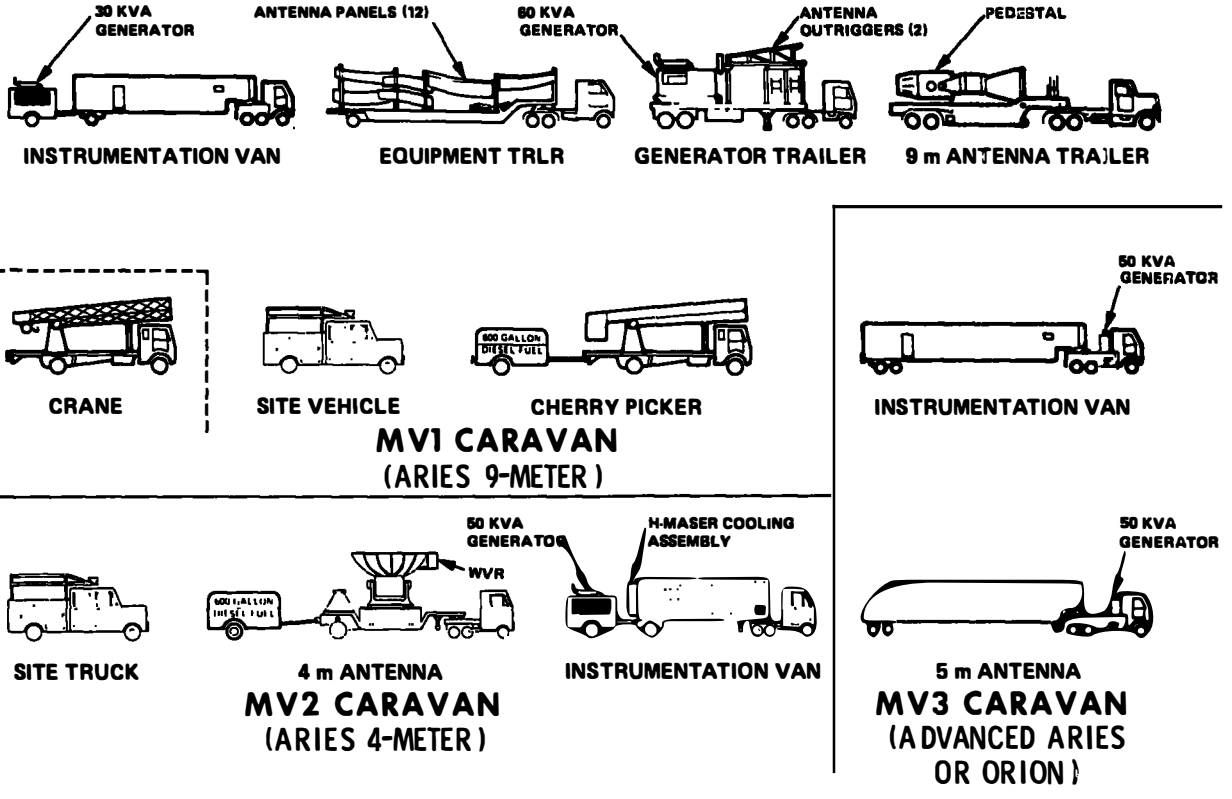

Figure 1. Mobile VLBI Stations in Transit

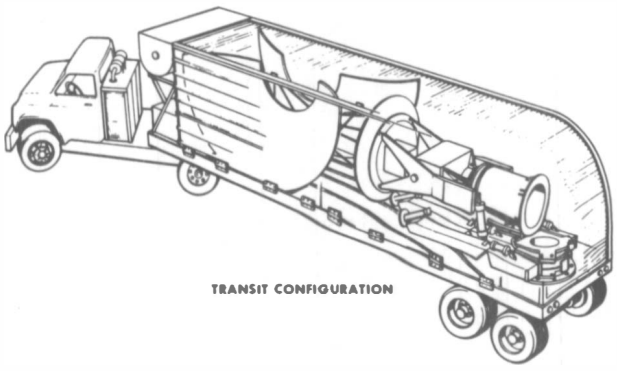

Figure 2. Mobile VLBI Station 3 (MV 3), Orion Antenna Transporter

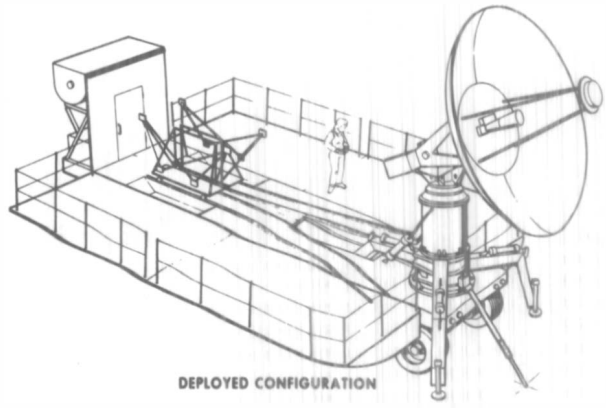

Figure 3. Mobile VLBI Station 3 (MV 3), Orion Antenna Transporter

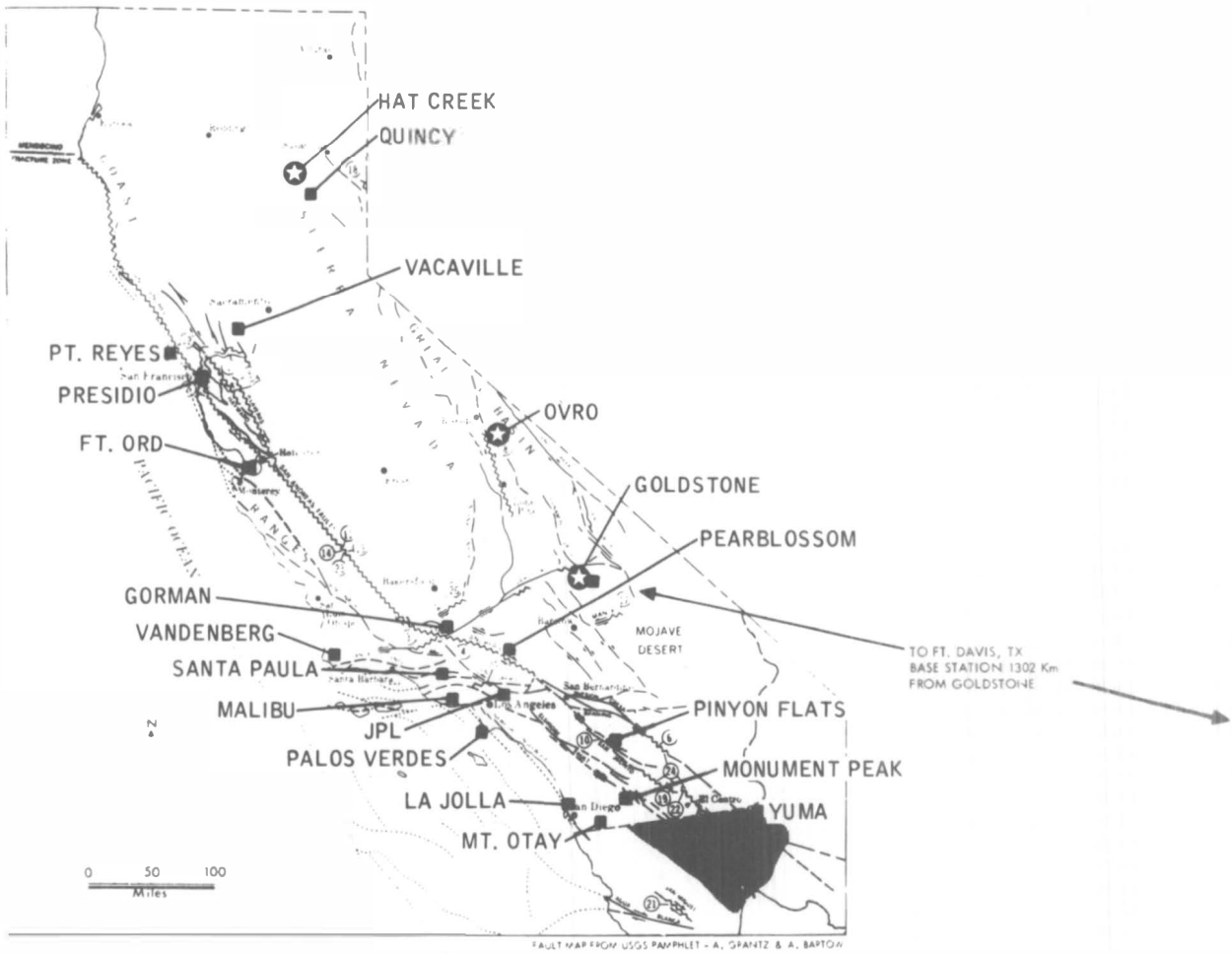

Figure 4. Crustal Dynamics Project, Mobile VLBI Site Geometry

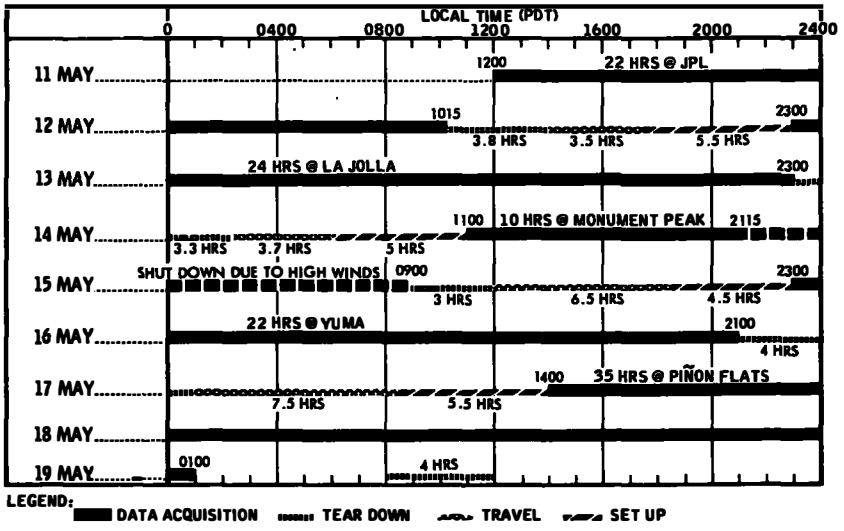

Figure 5. Aries May 1981 Burst, MV 2 Site Visit History

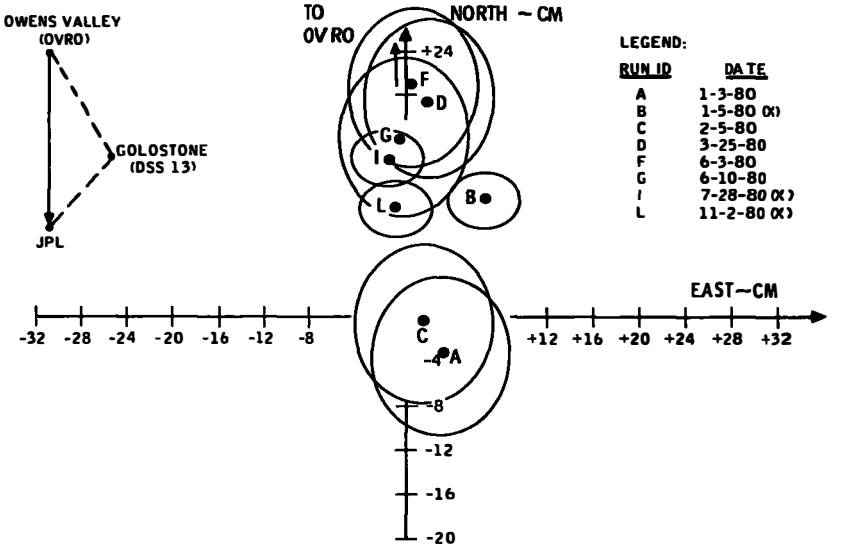

Figure 6B. Aries Motion of JPL with Respect to OVRO

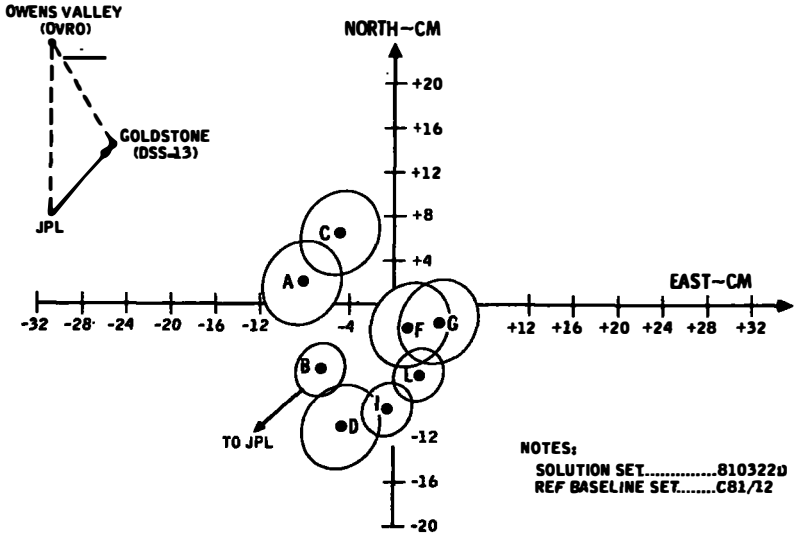

Figure 6A. Aries Motion of DSS 13 with Respect to JPL

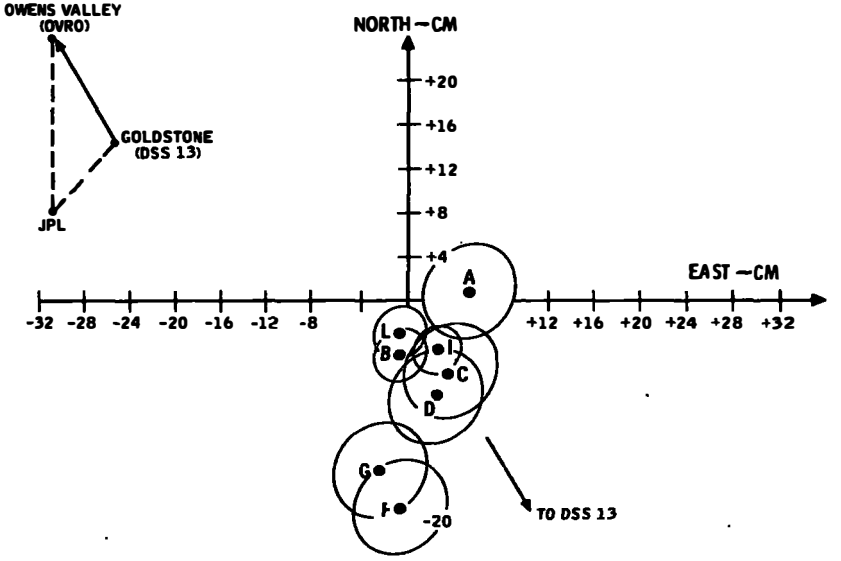

Figure 6C. Aries Motion of OVRO with Respect to DSS 13

OVERVIEW OF THE MARK III VLBI SYSTEM

N. R. Vandenberg
Phoenix Corporation
McLean, VA 22102 USA

T. A. Clark
NASA/Goddard Space Flight Center
Greenbelt, MD 20771 USA

ABSTRACT. The Mark III Very Long Baseline Interferometry (VLBI) technique has become an operational tool for precise geodetic measurements within the NASA Crustal Dynamics Project (CDP) and the National Geodetic Survey for the POLARIS Project. This paper describes the basic characteristics of the Mark III system for such applications and illustrates the performance characteristics by showing some recent data. Overall measurement precision using the Mark III system, based on one day data sets, is shown to be better than 3 cm in baseline length, 10 cm in pole position, 100 micro-seconds of time in UT1, and 3 milli-arcseconds in source positions.

INTRODUCTION

The technique of very long baseline interferometry (VLBI) was originally developed as an astronomical research tool. The Mark III system has evolved from the Mark I and Mark II systems through research and development efforts of people at NASA/Goddard Space Flight Center, Haystack Observatory, and the National Radio Astronomy Observatory. The Mark III system is more sensitive than the earlier systems because of multi-channel recording on high data rate digital tape recorders. Design criteria for the Mark III included both astronomical and geodetic applications.

The Mark III system is now becoming an "operational" geodetic tool through the NASA Crustal Dynamics Project and its transfer of the technique to the U.S. National Geodetic Survey (NGS) for project POLARIS.

DATA FLOW THROUGH THE MARK III SYSTEM

Figure 1 shows the flow of data through the Mark III system. All aspects of the Mark III system are mini-computer based and controlled; the Hewlett-Packard 1000 system istused. The data base is the central control point and serves to insure data integrity.

Initially, the scientific goals of a particular observing session are established and the detailed schedule of quasar observations is prepared. The Mark III Data Acquisition Terminal (DAT) has been designed for high reliability and ease of use in field operations. The system achieves a significant improvement in sensitivity over previous VLBI systems through multi-channel recording on high data rate digital tape recorders developed

especially for VLBIt In typical measurement programs, single-point delay measurements achieve 20-100 psec (0.7-3 cm) precision. The measurement configuration at each antenna is under mini-computer control which insures operational ease and data integrity. Fourteen DATs have been completed by the Haystack Observatory, and seven more are now under construction commercially by Phoenix Corporation.

After the observing session, the data tapes are sent to the processor where the observable parameters are determined and entered into the data baset

The CALC program calculates theoretical parameters of the precision earth model, and these are added to the data base. Calibration modules add corrections to the data based on correlative data recorded during field operations, such as water vapor radiometry data, surface meteorology, and cable length measurements. SOLVE is the interactive least squares fitting software, producing estimates of parameters such as baselines, polar motion, UT1, and source coordinatest All data is archivedt as well as software and procedures, for complete traceability of the measurement process. Finally, accounting procedures give estimates of the data yield and provide feedback for improved performance. Typically, 80 to 90% of all scheduled observations are used in a parameter fit. This high yield is due to the ease with the Mark III system can be used and its high reliability.

The Mark III data analysis and data management system uses interactive software and emphasizes accountability and traceability of data, software, and procedures. The analysis models have been extensively documented and now incorporate the J2000 and MERIT standards. The NASA Crustal Dynamics Project (CDP) is routinely archiving all of the Mark III data for future use by investigators. The minicomputer-based analysis software systems have now been successfully installed at a number of collaborating institutions in the United Statest Sweden, Germanyt and Japant

RECENT MARK III GEODETIC RESULTS

This section presents results of Mark III measurements of geophysical parameters. First, general results will be discussed and then some of the data will be examined in more detail.

Polar Motion

Figure 2 is a plot of data taken between 1980 July to early 1982t The majority of the points are POLARIS data; the denser points are the MERIT periods in late 1980 and the CDP fixed-observatory sessions in 1982 June and November. The errors are smaller on these points because more antennas were used in the networkt The major feature of this graph is the smoothness and repeatability of the VLBI measurements and the good comparison with the heavily-smoothed BIH values. Some of the short-term variations in the VLBI data may in fact be real but more data is needed.

Figure 3 is an expansion of the MERIT period of Figure 2. In the plot, the day-to-day repeatibility is noticeable. Comparison to laser data shows general agreement, but the one-day VLBI data has smaller errors than the

five-day laser data.

UT1

Measurements of UT1 are available over the same time period as polar motion. Figure 4 shows the total value of UT1 as determined by POLARIS and large network experiments. An offset and straight line with slope about 300 microsec per day has been removed for plotting purposest The BIH values are the tabulated Circular D with tidal corrections. Notice that the VLBI data is smoothly varying and that it follows the BIH data trends.

Figure 5 shows the MERIT periods in greater detail. The day-to-day smoothness is noticeable at the level of fractional milliseconds.

Baselines

The longest history of geodetic measurements is the baseline measured across North America between Haystack Observatory to Owens Valley Radio Observatory in California. The baseline length is about 3900 km. Figure 6 is a plot of baseline measurements made between 1976 and 1981; each point is one day's data. There are two groups of data in this plot: the Mark I X-band data which has a 3-sigma rms of about 6 cm, and the more sensitive Mark III S- and X-band data with an rms of about 3 cm. A straight line fit to this five years of data gives a slope of 0 ± 0.4 cm/year, that is, no change is detected in this baseline.

During the MERIT campaign, two of the stations in use were Onsala, Sweden, and Chilbolton, England; the baseline is about 1100 km. During one week, the seven determinations of this baseline using all five stations in the solution gave rms repeatibility of 5 cm. If this baseline could not be measured directly, we could still infer the length by using all of the data except the direct baseline. As a test of this concept, the solution was run using only 9 baselines; in this case the rms repeatibility for the seven days is 1.6 cm. We conclude from this exercise that using many stations in a VLBI network adds strength to weak baselines and enables good geodetic results to be obtained even if there is little or no direct measurements. Another implication is important for mobile VLBI experiments where is it not possible to obtain usable results on the baseline between two small antennast In this case it is possible to infer the baseline if a strong base station is usedt

CONCLUSIONS

Mark III VLBI has become an operational tool for geodetic measurements through the NASA Crustal Dynamics Project and the NGS POLARIS project. Routine measurements are made weekly by the two- or three-station POLARIS network, and a larger network of about six stations is used several times yearly.

The Crustal Dynamics Project is maintaining archives and configuration information for complete accountability of data, software and procedures that affect the measurement process. This means that long term crustal motions can be reliably detected because data taken over a span of many years can be compared with confidence and accuracyt

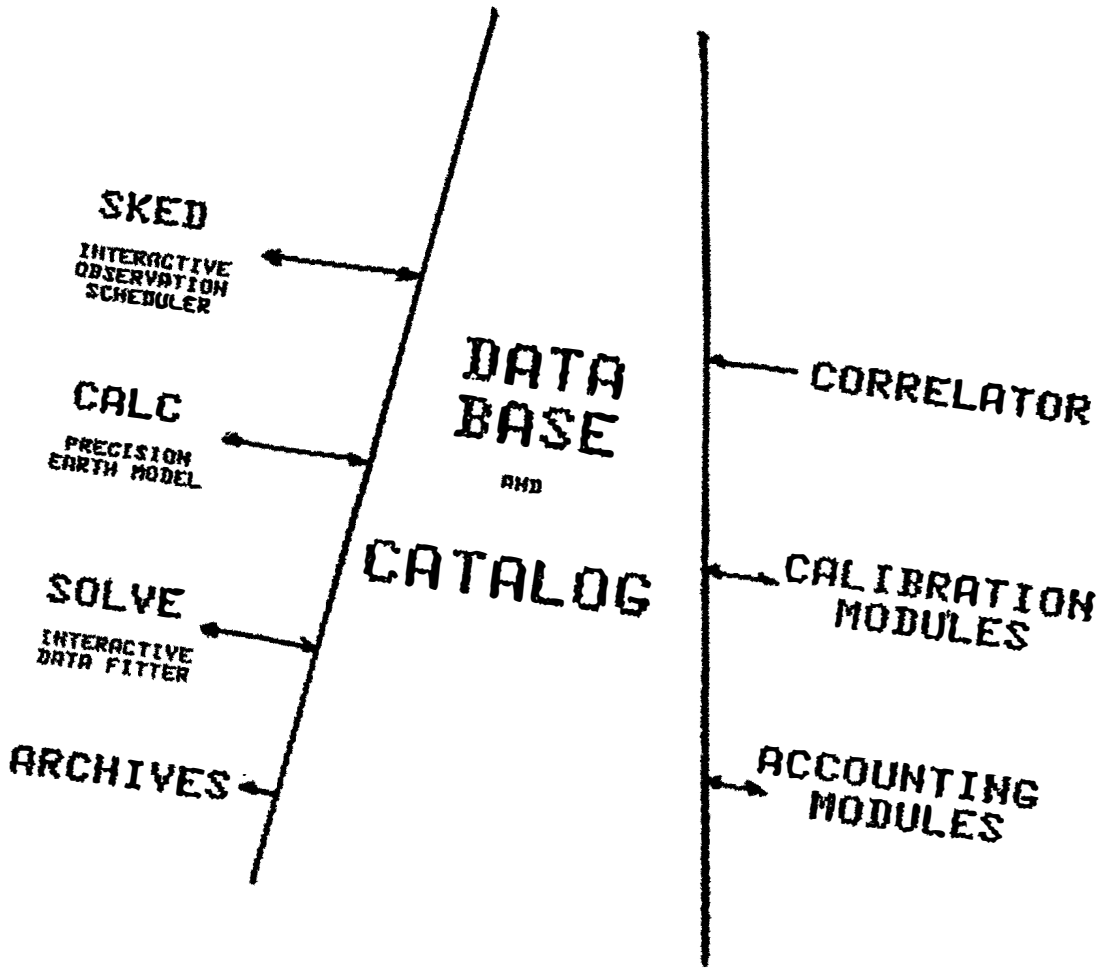

MARK III SYSTEM DATA FLOW FIGURE 1

MARK III VLBI X-COMPONENT OF THE POLE

FIGURE 2

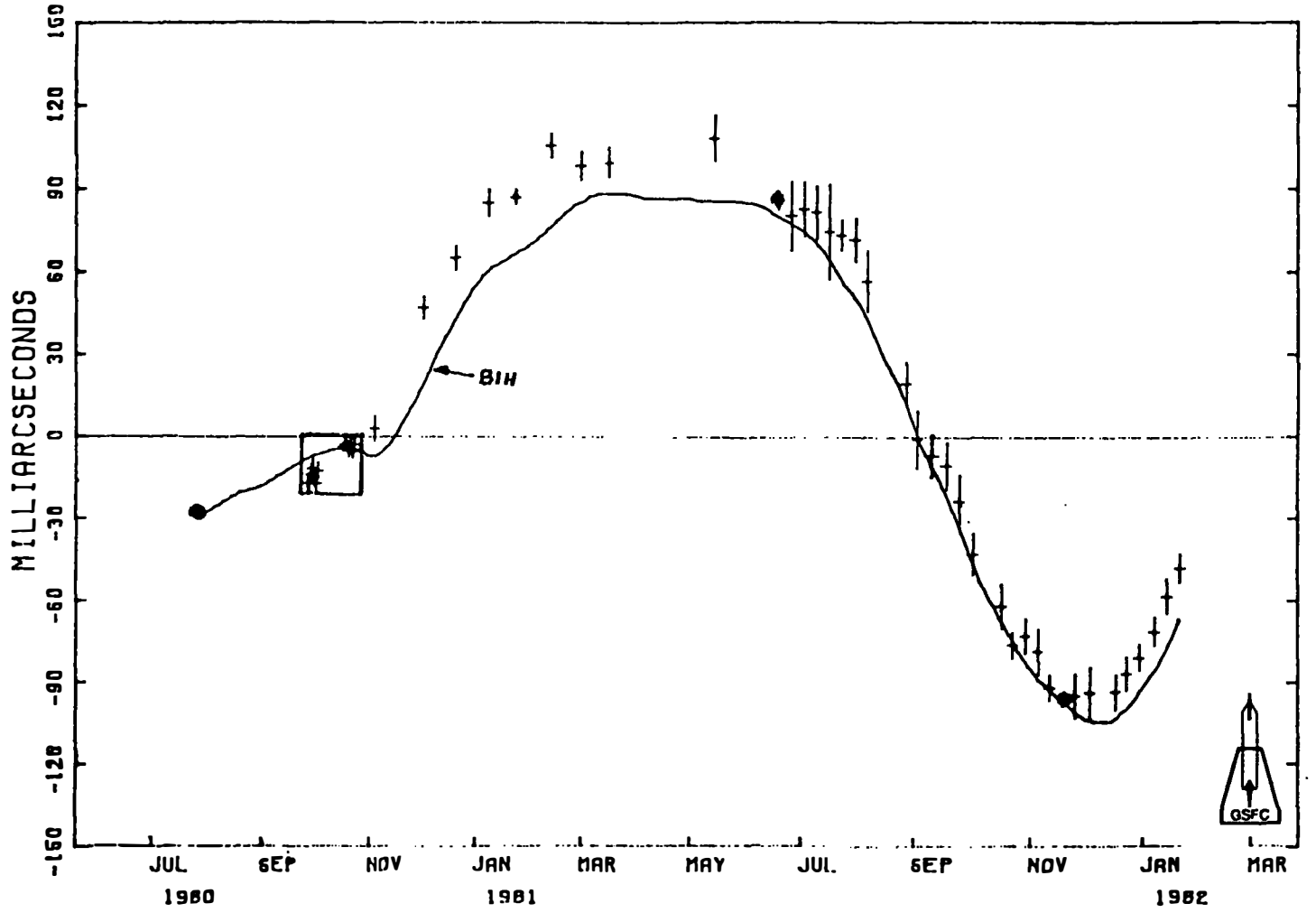

X-COMPONENT OF THE POLE - ZERO SET ON 00 OCT 18

FIGURE 3

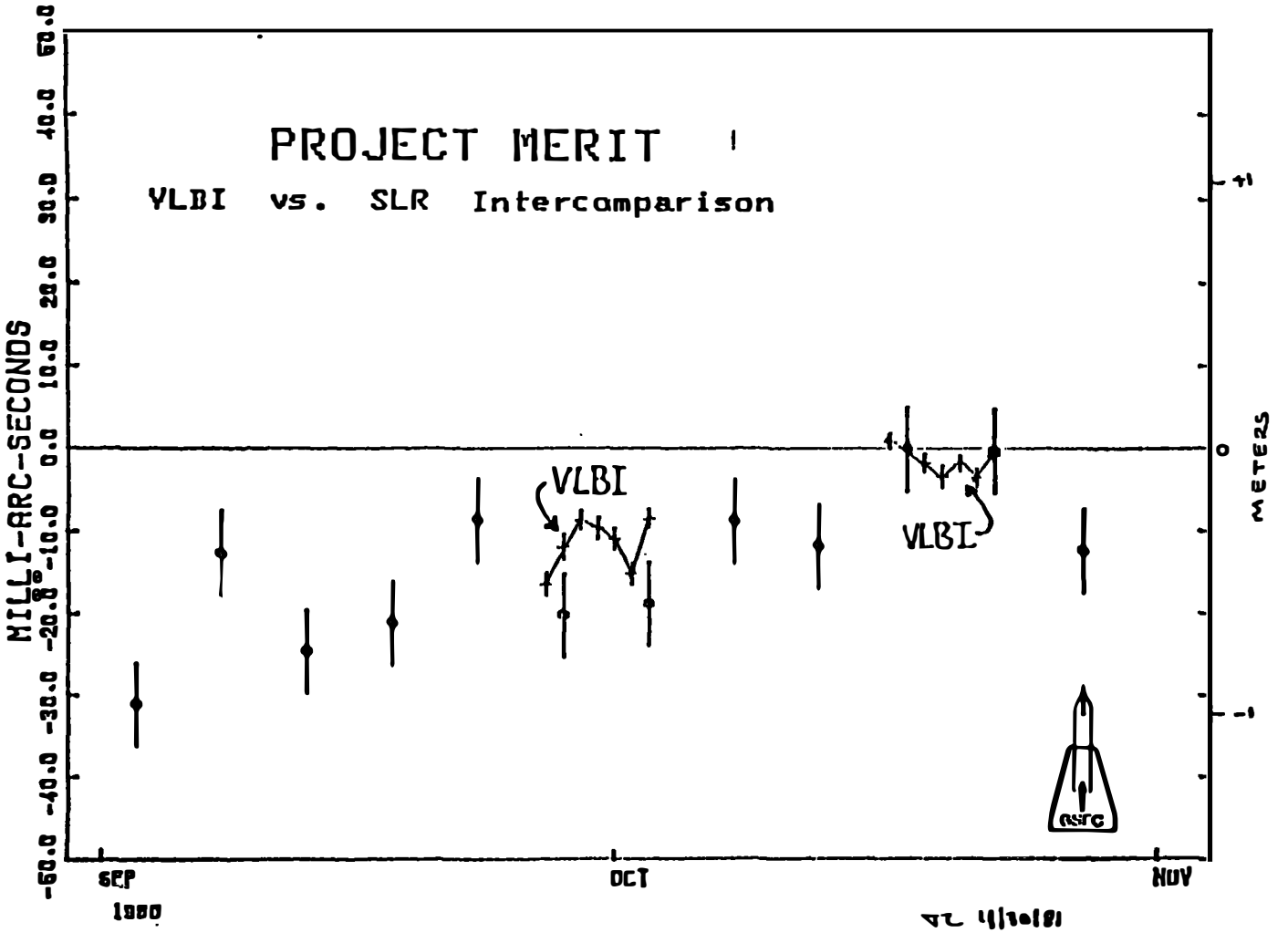

MARK III VLBI UT1 TOTAL (STRAIGHT LINE REMOVED) FIGURE 4

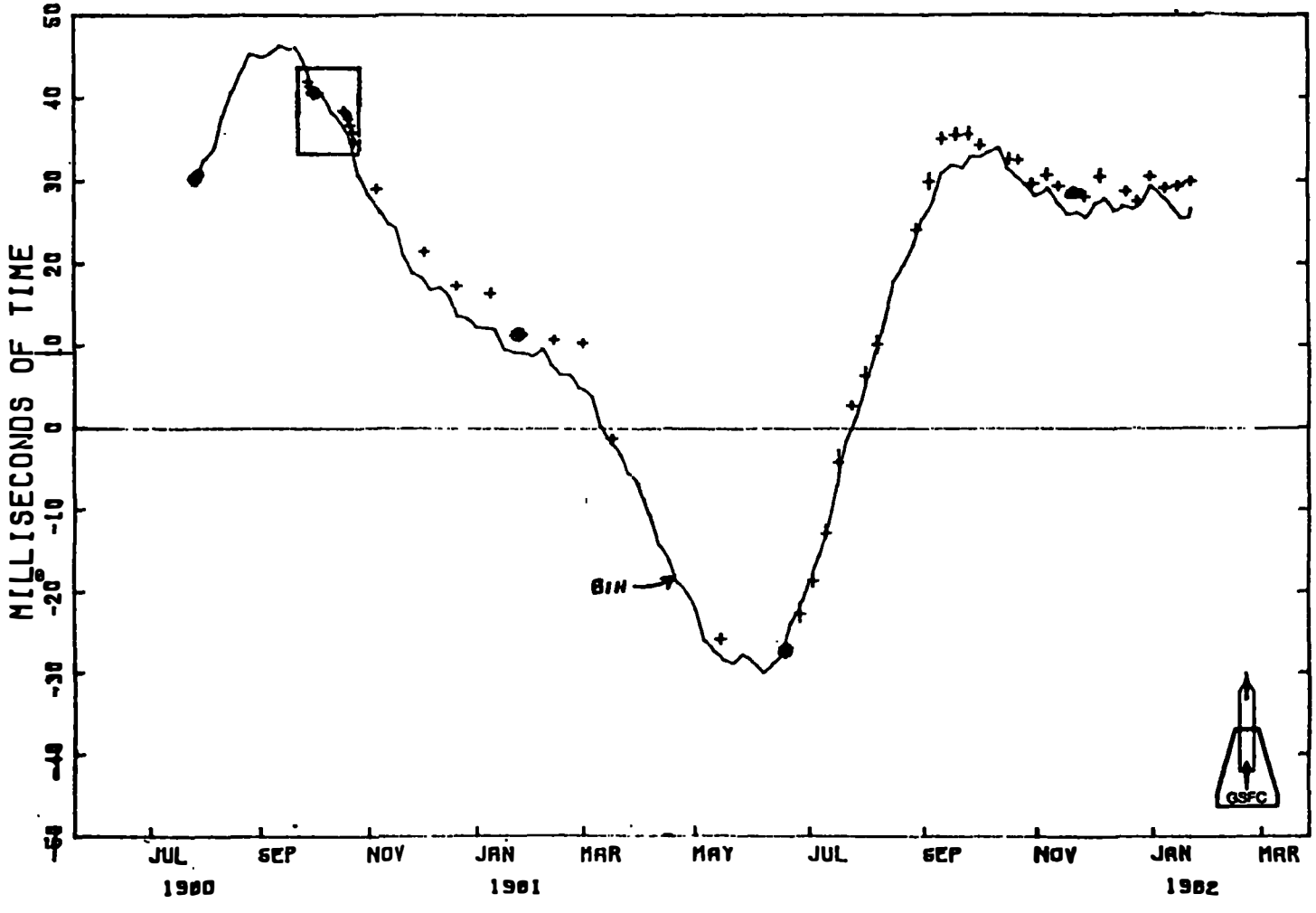

FIGURE 5

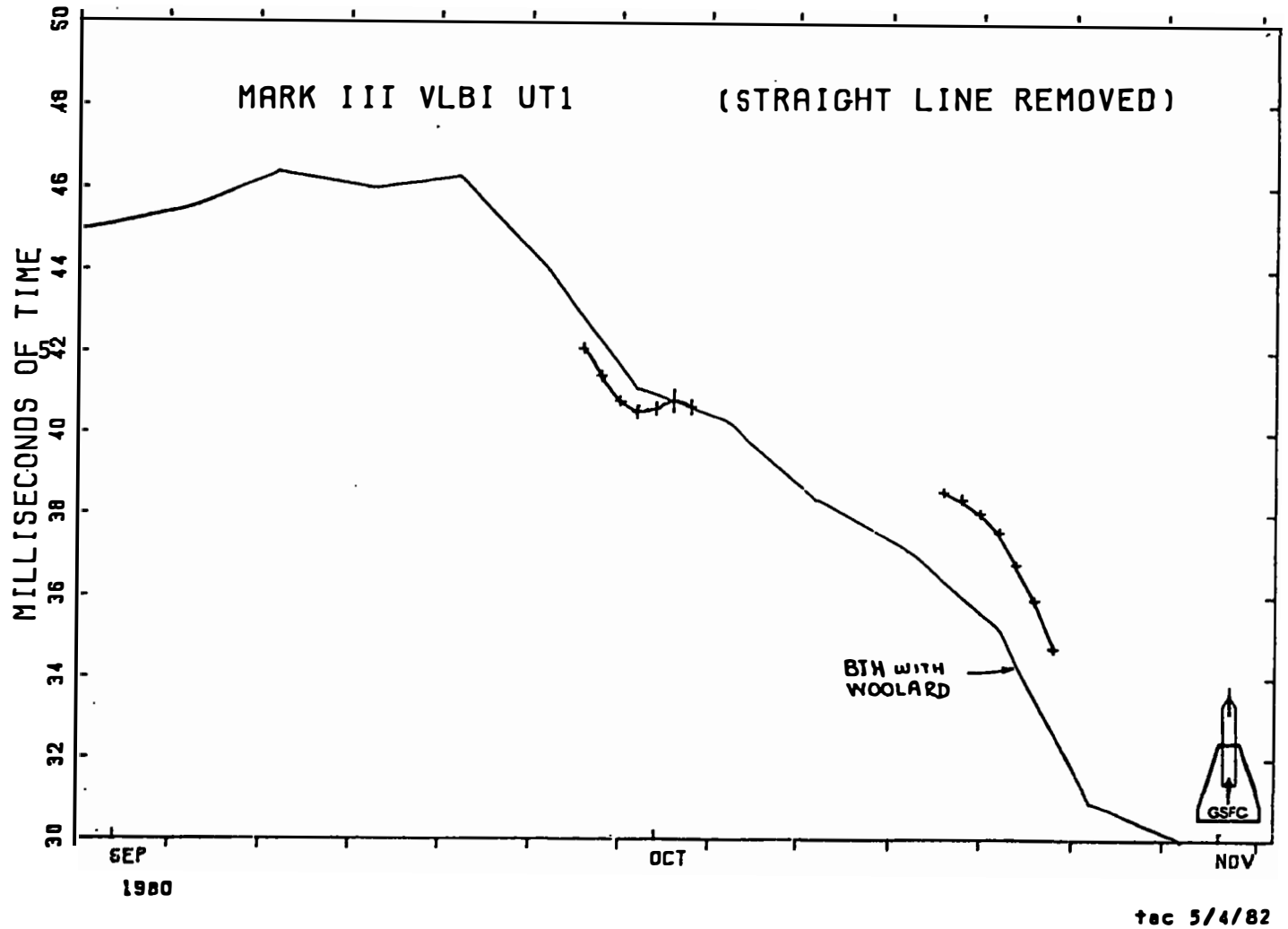

tac 5/4/82

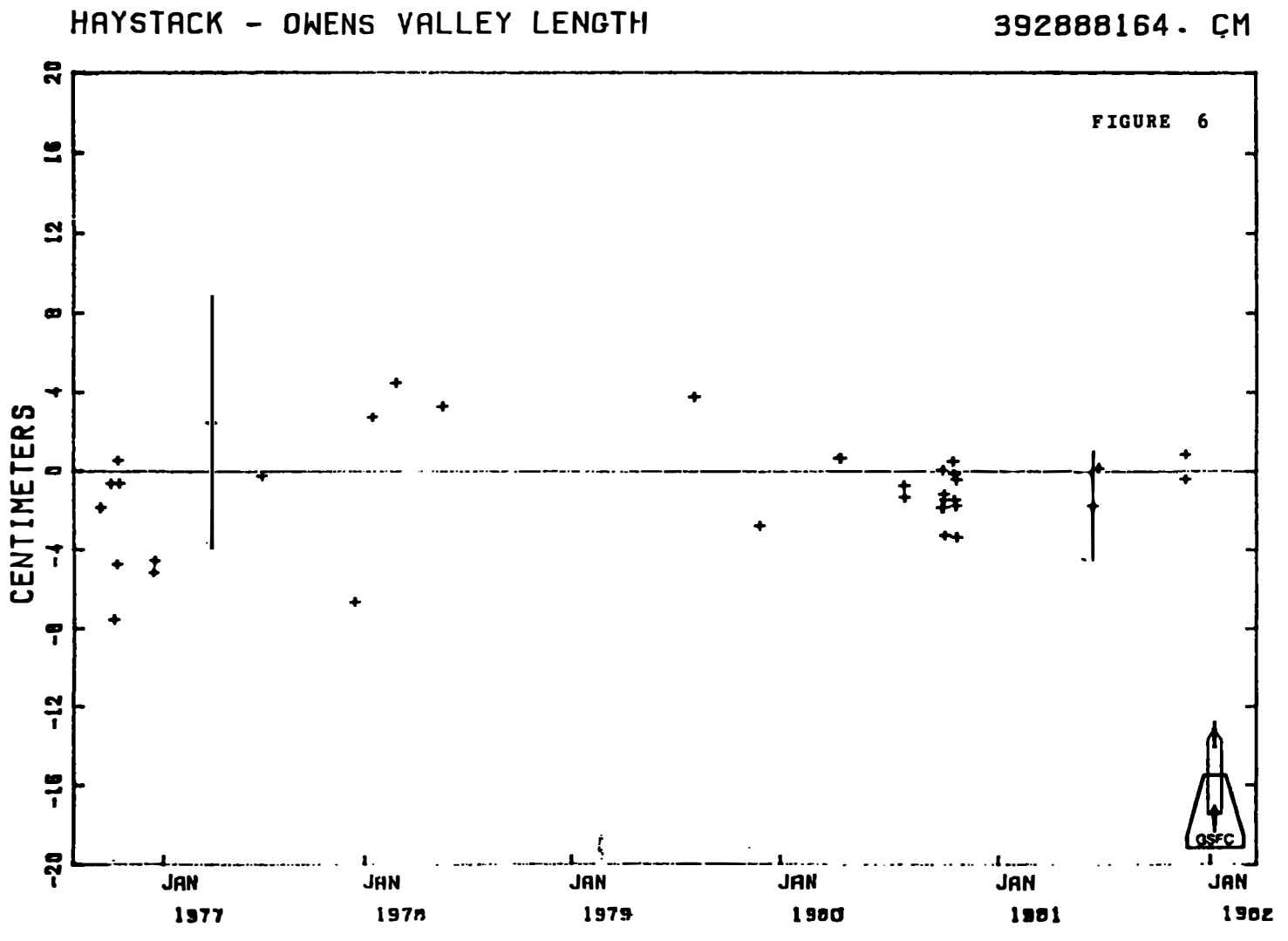
HAYSTACK - OWENS VALLEY LENGTH
392888164. CM
FIGURE 6
CENTIMETERS
20
16
12
8
4
0
-4
-8
-12
-16
-20
JAN 1977
JAN 1978
JAN 1979
JAN 1980
JAN 1981
JAN 1982
GSFC

THE DENSITY UPGRADE: MARK III A

(A FUTURE IMPROVEMENT OF THE MARK III VLBI SYSTEM)

H.F. Hinteregger
NEROC Haystack Observatory
Westford, Massachusetts 01886 U.S.A.

ABSTRACT

At present the Mark III acquisition system records up to 28 channels, each with up to 4 (normally 2) megahertz bandwidth from two separate IF bands, onto 28 tracks on one inch wide tape, using a longitudinal recorder with 2 fixed heads per track. One head writes and a corresponding head reads each formatted channel. The bit (transition) density is 1.31 per micrometer (33,333 per inch), and tracks are 640 micrometers (.025") wide.

A long-sought order-of-magnitude density increase, called Mark III A, has been planned for the recording system. We expect to reduce track width to 40 micrometers initially, so that 336 tracks can be recorded in 12 passes of the tape. Thus, one 9200 foot tape will last for three hours while recording 56 megahertz bandwidth or a total of about one terabit (10^{12} bits).

Development efforts at Haystack Observatory during the past two years have been funded by (so far only) NASA in support of geodetic applications under the Crustal Dynamics Project. The density upgrade is probably even more useful to astronomy than geodesy, however.

INTRODUCTION

In the near future both conventional geodetic and astronomical VLBI systems -- the former with more widespread use of small transportable antennas, and the latter with dedicated networks of large fixed stations - - will be pressed to conduct observations with high duty-cycle as well as wide bandwidth. However, with the present (original) density of Mark III recording, supporting observations at 56 or 112 megahertz recorded bandwidth for more than a few percent of real time is not practical (see Table 1). Clearly an order of magnitude increase in density is needed to make high duty-cycle use of such a wideband system sufficiently economic and manageable.

The need for a major density upgrade was anticipated early in the design of the Mark III system. But technology was not sufficiently advanced in 1975 to permit a first implementation with much higher recording density. Nevertheless, we attempted from the outset to judge the degree to which critical components— tape transport, heads and tapes -- could support a major density increase and to select those which appeared to maximize "upgradeability".

Table 1: SUMMARY OF MARK III A

WHAT: TWELVEFOLD DENSITY INCREASE

HOW: REDUCE TRACKWIDTH, 16-FOLD, 640 TO 40 MICROMETERS
MOVE HEADSTACK, 12 PASSES, 60 MICROMETERS/PASS

WHY: PROPORTIONAL REDUCTION OF COST OF OPERATION MAKES
HIGH DUTY-CYCLE PLUS WIDEBAND SYSTEM USE ECONOMIC AND MANAGEABLE

OPERATION COST: Example, 30% I [illegible] per Site, per Year

		(x12)
TAPE SHIPPING		
TAPE STOCK		
HEAD REPLACEMENT		
TOTAL	$215K	$25K

REPLICATION COST: $20K per RECORDER

Certainly most fortunate in this regard was the choice of the Honeywell 96 (longitudinal) tape transport. To the best of our knowledge, the ± 0.25 micrometer tracking consistency* of the 96, measured independently by optical (edge detection) and magnetic (offset playback) tests and maintained under machine interchange, is unmatched by even the best of narrow track VCR's. The 96 will contribute negligibly (less than 0.1db) to head/track misregistration losses when trackwidth is reduced to 40 micrometers. It could even support tracks as narrow as 2.5 micrometers.

Our present goal, one order of magnitude increase in density, can be met by taking advantage of the second, now fully mature, generation of tape. The second generation tapes are variously termed "professional video" (PV), "digital audio", "advanced instrumentation", or "VHS-equivalent". These high-coercivity (650 Oe) tapes represent at least a 12 db improvement upon first generation instrumentation tape in the present system. This 12 db SNR improvement can be traded, exactly in theory, for a 16-fold reduction of trackwidth.

An additional 12 db improvement provided by third generation tape will, further in the future, encourage another trackwidth reduction to 2.5 micrometers with no net reduction of SNR or increase in error rate. One such third generation tape has already been developed; its generic name is "vacuum video" (VV) tape. A handheld camera/VCR using VV tape is expected to be on the consumer market within a year.

Thus, 3 micrometer track spacing or 8,000 tpi recording begins to seem feasible, given mature third generation tape and the ± .25 micrometer tracking of the 96. A ± .25 micrometer accurate headstack and environmental control of tapewidth and headstack length would also be needed. In addition to a twenty-fold

*This is an upper bound on tracking inconsistency which excludes characterizable (hence removable) machine and direction dependent fixed offsets and the slight but systematic differences between the forward and reverse tracking "signature" of a given piece of tape.

further reduction in track spacing we can anticipate, with third generation tape, a halving of tape thickness and a 2-to-3-fold increase in transition density. We project that a full and natural evolution of the upgrade will, by 1990, make possible recording 80 to 120 terabits on a single 14-inch diameter reel of inch-wide tape. A total recorded bandwidth of about 1 gigahertz can now be obtained by quadrupling the normal (2 megahertz) channel bandwidth and quadrupling the number of channels (all within the framework of the present parallel Mark III system architecture). By 1990 it should, therefore, be practical to record 2 gigabits per second of data continuously, since it will take about 12 hours to fill the 100 terabit bucket.

THE CHOICE OF MEANS

Volume density of magnetic tape recording can be improved in three ways: Bits can be 1) shorter by increasing transition density, 2) thinner by reducing tape thickness, and 3) narrower by reducing trackwidth (and guard band).

Significant but inherently sharply-limited density improvements can be anticipated from the first two approaches: Specifically, the higher resolution channel resulting from the combination of VHS-equivalent (0.33 micrometer gap) heads and VHS-equivalent tape encourages a 50% increase in transition density from 1.3 to 2.0 per micrometer (33.3 to 50 Kfci) with only a 6 to 7 db response rolloff. Also, consider that presently available inch-wide tape is 26 micrometers thick while VHS cassette tape is now supplied in 13 as well as 17 micrometer thicknesses. As much as a doubling of volume density therefore depends only on manufacturer's willingness to supply the thinner tape appropriately slit and packaged. Taken together, these two improvements should alone eventually yield a 3-fold increase in volume density. The planned density upgrade would automatically accept such improvements but is not dependent on them.

Order of magnitude increases in volume density, however, can come only from the third approach, drastic reduction of trackwidth and spacing. This is because the signal-to-noise ratio of a tape-noise-limited magnetic recording varies only as the square root of the trackwidth. Thus every 3 db of excess SNR above that required in practice to maintain an acceptably small error rate is expended most efficiently by halving trackwidth, hence doubling density.

Numerous tests have been carried out to establish that certain modern tapes such as Fuji H621, Sony V16, 3M5198, and Ampex 721 can guarantee an SNR more than 12 db higher than that which can only now be maintained as an acceptable worst case with instrumentation tape. The new tapes are replacing conventional instrumentation tape like Ampex 795 and 3M892 in the Mark III system.

We plan therefore to exchange this 12 db of excess SNR for a 16-fold reduction in trackwidth. Since our present (fixed) heads are 640 micrometers wide, the trackwidth of new heads will be 40 micrometers.

We plan to use headstacks organized like the present (fixed) ones. A stack is an array of heads uniformly spaced along a single (gap) line so as to span (slightly less than) the full one inch width of tape. The simplest system results if all 28 channels are carried in a single stack. We prefer in addition to have at each end of a stack an extra head used to monitor head-to-track registration near both edges of the tape; the case is thereby anticipated where

normal guard bands between adjacent tracks on tape are allowed to shrink to a small fraction of trackwidth. Thus a single stack of at least 30 or a pair of 16-head stacks is desirable. Specifically, because it fits these needs nicely, we now advocate adopting the IRIG PCM-format head pitch of 762 micrometers (.030") as a standard for Mark III A, which should be maintained by any future replacement stacks featuring further reduced trackwidth and greater accuracy of head placement within the stack.

We plan to provide an electrical headstack interface, similar to our present separate read and write head interfaces, which under electronic control will permit reading or writing with the same stack. One 30-head single-stack assembly interfaced in this way will then support the entire Mark III system. A pair of identical, independent assemblies would provide not only highly desirable redundancy for this critical subsystem, but also (probably) a bidirectional read-while-write capability, and certainly the option to double the number of channels simultaneously available (doubling the maximum system bandwidth).

We expect to be able to replace any of the present four fixed headstacks by such a new assembly or "headblock". This headblock will house not only the narrow-track headstack, but also position actuator, position sensor, temperature sensor, ballast resistor, and intimate head interface electronics.

The required positioner must be capable of translating the block at least one head spacing, specifically 762 micrometers (.030"), in the cross-tape direction so that the wide space between narrow heads can be accessed in trackwidth-plus-guardband increments and the tape fully recorded in multiple passes. The positioner is admittedly a complication of the recorder. It pales however by comparison to the complications introduced by other conceivable means of achieving the same required combination of bandwidth and density in a longitudinal machine. Assuming an (initial) 12-pass format, an equivalent fixed head-per-track system would for example require 336 heads to be supported. Sufficiently dense packaging of heads for such a system is, among other things, beyond state-of-the-art.

An equivalent to the upgraded 28-channel longitudinal recorder would be a "black box" consisting of a bank of 28 VCR's each supporting one channel. Only with 28 VCR's is the comparison fair, since, with equivalent tape and heads, channel bandwidth limitations are the same for both kinds of machine. The bank of VCRs would be no more expensive than a single properly outfitted longitudinal machine, and to make it operational for VLBI would probably require the least engineering effort (none in the critical and specialized area of the head/tape interface). The drawbacks of this approach are perhaps largely a matter of taste, especially if only short-term benefits are considered. A bank of 28 VCR's is awkwardly large. Any straightforward parallel growth of the system for increased bandwidth results necessarily in a proportional increase in hardware and hence in physical size. Not so for the longitudinal machine which would not grow even if it were outfitted with four blocks of 28 channels. The number of cassettes to be handled, too, would be at least an order of magnitude larger in a multi-VCR system than the number of reels in the multichannel recorder system (since tape area of the standard 9200'x1" reel is 22 times that of a VHS T-120 cassette).

The decision in 1980 to stay with the longitudinal multichannel approach was based on the following judgments: 1) Providing a sufficiently accurate positioner (actuator & sensor) was considered a straightforward task, especially

since no active tracking servo was required. 2) Critical aspects of VCR head as well as tape technology could simply be transferred to the multichannel recordero 3) The longitudinal Honeywell 96-based system would remain much more naturally open to at least another order of magnitude improvement in both bandwidth and density in the not-too-distant future.

As has already been discussed our efforts to date leave no doubt that the third judgment (above) was correct.

The first judgment, too, has been confirmed. From among several devices that could in principle satisfy reasonable specifications for a positioner, we have selected the piezoelectric "Inchworm" as actuator and an LVDT (linear variable differential transformer) as sensor.

The second judgment, that VCR head and tape technology could <u>easily</u> be transferred to the longitudinal machine, was optimistic, however. Every critical aspect of feasibility has now been demonstrated, but a full prototype is still incomplete. This is because though one prime requirement (VHS-equivalent performance) was met by Matsu prototype headstacks, and the other one (± 3 micrometer head plac accuracy) by later prototypes, no headstack has yet been receiv

PROGRESS AND PERFORMANCE BUDGET

Aspects of feasibility which have now been demonstrated include:

1) ± 0.25 micrometer tracking consistency Honeywell 96,

2) "Inchworm" plus LVDT positioner with submicrometer accuracy,

3) Several sources of suitably high-output, consistent, low-abrasivity tape capable of maintaining and/or restoring head performance,

4) Method of contouring heads to maintain high-speed performance,

5) Prototype headstacks with all head edges accurately located within ± 3 micrometers,

6) 60db bandedge SNR (2MHz at 120ips, 3KHz slot) from 50 micrometer wide heads and Fuji H621 tape, about 3db higher than can be maintained on 640 micrometer wide ferrite heads and average instrumentation tape.

The expectation of at least 59db average bandedge SNR (see Table 2) is obtained by derating that obtained with 50 micrometer wide heads one db. The bandedge SNR is intended to be a measure of intrinsic head performance and is therefore obtained by using the same head to write and read a reference tapeo The 73 to 75 db SNR often obtained for all 640 micrometer wide heads in a Honeywell ferrite headstack suggests that 40 micrometer wide heads could average 61 to 63 db, perhaps 3 db better than our minimum expectation.

We budget foro± ldb variations in the intrinsic 1.5 micrometer wavelength response of suitable new tape. Fuji H621 became our standard of reference when we found it had tape-to-tape variations of onlyo± 0.5 db. The implicit reference

TABLE 2: EXPECTED HEAD/TAPE PERFORMANCE (40 MICROMETER TRACKWIDTH)

MINIMUM AVERAGE BANDEDGE SNR (2 MHz, 120 ips, 3 KHz slot)	59 db
TAPE VARIATIONS (FUJI H621 REFERENCE)	± 1
HEAD VARIATIONS	± 1
TEMPORARY DEGRADATION	< 1
PERMANENT DEGRADATION	0
INTRINSIC WORST CASE SNR:	56 db
INTERCHANGE LOSS	
HEAD EDGE LOCATION TOLERANCE ± 3 micrometers (implies 6 micrometers = 15% maximum loss)	-1.5 db
ENVIRONMENTAL TAPE WIDTH CHANGE	
ΔT = 6°C (implies 2 micrometers or 5% maximum loss)	-0.5
ΔH = 30% RH (implies 4 micrometers 10% maximum loss)	-1.0
MAX. TOTAL INTERCHANGE LOSSES	-3 db
TOTAL WORST CASE SNRo	53 db
SHOULD GUARANTEE BER	< 10^{-4}

to the Fuji "centerline" in our performance budget makes it a little optimistic since, for example, 3M5198 average response is about one db lower. Note particularly that the consistency of tape response required is far better than that obtained with conventional instrumentation tape, for which a +3 to -8 db spread, about a 9 db inferior centerline, is not uncommon. Such variations were not expected when Mark III first became operational; we have now decommissioned more than 35% of our instrumentation tapes for failure to meet our original -2 db worst case expectation.

In addition, new tapes like Fuji H621 and Sony V16 cause no measurable degradation, unlike instrumentation tapes, which have been found to rapidly and severely degrade (ferrite) head performance. In our experience, if ten instrumentation tapes are run once each over fresh heads, a 6 db degradation of initial (optimum) bandedge response typically results.

We have found that Sony V16 is too abrasive for full-time use in our system, but that it acts to restore degraded performanceo If used on a ten percent basis, it limits the slight and very gradual degradation caused by 3M5198 to one db.

On the other hand, we can project an extremely long 12,000 hour head life with Fuji H621 tape under extremely (greater than 70 percent) high humidity conditions. The abrasivity of 3M5198 appears to be at least equally low.

To maintain initial optamum performance for the life of a head it is

necessary to optimize and stabilize the tape-to-head pressure, hence geometry as well as the surface condition of the head/tape interfaceo We have developed a "stepped" head contour which does this successfully. A pair of shallow steps cut 150 micrometers equidistant from and parallel to the gap line limits the area of head/tape contact and discourages an air bearing from forming. The radius of the sharply defined contact area quickly stabilizes. As a result we can now guarantee that initial performance at high (120 to 360 ips) speeds will be maintained, even with the smoothest "ready-to-fly" tapes like 3M5198.

The stepped head contour has a major side benefit. It cleans even the best of the new tapes. This is evidenced by a typical 10-fold reduction in error and bit-slip rates after a single pass.

The stepped head contour has been fielded in the present system as a modification of existing Honeywell heads. Only with this modification has it been possible to limit the degradation caused by instrumentation tape, so as to maintain a -4 to -6 db degraded "operating point" and, in spite of that, error rates of about 10^{-8}.

The figure for intrinsic worst case SNR takes into account all factors except losses due to head/track misregistration. Assuming past experience with wider tracks and instrumentation tape yielding the same 56 db bandedge SNR is relevant, error rates of 10^{-8} to 10^{-9} are expected.

Error rates of about 10^{-6} have in fact been obtained with 50 micrometer wide heads and Fuji tape using the present head interface electronics with quickly-made (probably not optimum) gain and equalizer modifications.

Head/track misregistration losses must also be taken into account. Narrow 40 micrometer wide tracks and the requirement on machine interchange to read simultaneously all simultaneously written tracks lead to the new and stringent head edge location tolerance of $\pm$ 3 micrometers for all heads in a stack. This tolerance permits a 1.5 db loss of signal corresponding to minimum head/track overlap of 34 micrometers.

Not to be overlooked is the fact that tape width depends on temperature and humidity. The respective expansion coefficients are such that a change of 6 degrees Centigrade moves the edge of an inch-wide tape 2 micrometers with respect to its center and that a 30 percent change in relative humidity moves it 4 micrometers. A worst case combination results in an additional 1.5 db loss for edge tracks. No extraordinary environmental controls are needed to keep room temperature between 20 and 26 degrees Celsius and relative humidity between 25 and 55 percento

Note, we must also take care to keep stable the temperature of each headstack so that its thermal expansion does not also contribute to misregistration loss. When, further in the future, it becomes possible to obtain headstacks with substantially improved head edge location tolerance, narrower heads and smaller guard bands (continued evolutionary density improvement) will be desirable. It should not be difficult to support further improvement and compensate for environmental instability by controlling head temperature and/or tape tension (vacuum)o The effective gain of the latter can be increased by placing grooves between heads.

In July 1980 we let a contract to Matsushita to develop the narrow-track headstack to "production readiness" in, we were led to expect, two months. Partial prototype stacks which met (only) performance expectations were delivered in Janua 1981, after which improperly contoured "samples" sent earlier in October 1980 were modified and also found to perform comparably well. The partials of Jan 81 and samples of Oct 80 failed to meet the basic head placement accuracy specification by an order of magnitude.

A third generation of partial prototype stacks, delivered in June 1981, met that requirement, but only at the expense of adequate azimuth accuracyo Performance was 14db or more below expectation.

In January 1982 four full 32-head stacks were delivered which, except for systematic pitch errors later brought under control, met the head placement accuracy specification. These last prototypes under our original contract also represented a switch from super-accurate discrete head-tip assembly methods to an easy-to-manufacture "combo" headstack construction.

We had expressed a preference for the latter approach from the outseto From our point of view, the headstack required could most easily be obtained with the least technological risk by using 1) a mass-produced VHS "gapped bar" to obtain both the intrinsic consistent performance of the VHS head and the sufficiently accurate head pattern which specialized production grinding machines can put into such a bar, and 2) a simple "comb" construction similar to that employed by Honeywell to adapt such a "patterned" bar by making it into a "tip-plate", which, when bonded to a base containing an appropriately matched array of wound "back cores" (fluxors), becomes the completed stack.

Unfortunately, the Jan 82 as well as the Jun 81 prototypes exhibit very poor performanceo One difference between the well-performing early and the later prototypes stands out: Only the early prototypes used production VHS head tips, while the later ones appear to be far unsuccessful attempt to "reinvento" that technology**.

CONCLUSION

The groundwork for Mark III A has been carefully laid. All known aspects of feasibility have been demonstrated. Solutions have been found to the subtle

---

**Note added in proof: Matsushita concluded in May 82 that the performance problem was due to the use of improperly oriented single crystal ferrite in the later prototypes. A voluntary continuation of Matsushita effort (not under contract) has led to another fifth generation of prototype, and yet a sixth is expected shortlyo The fifth prototypes, obtained in July 82, were once again made from hot pressed ferrite like the early ones, but worked no better than the third or fourth, thereby proving that single crystal orientation is not the (main) problem. The solution to the problem, it seems, lies in direct use of the VHS gapped bar or in an exactly copied process at KME (Kyushu Matsushita Electric, the division responsible for the narrow-track headstack development but not, unfortunately, for VHS head production)o Alternatively, by making use of the highly evolved grinding techniques used to pattern gap bars we may now be able to accurately trim even used Honeywell headstacks to our new requirements.

but extremely important problems of consistency and maintenance of head/tape channel performance. These solutions have been applied to the present system, and hence verified by operational use as well as by extensive laboratory tests.

The delay caused by our subcontractor's inability, for more than one year now, to reproduce the excellent performance of early prototypes is a real concern. But the remaining question about Mark III A is "When?", not "Whether". We now hope to demonstrate a complete prototype in January 1983, and expect system-wide implementation efforts to begin in the middle of that year.

THE MARK III CORRELATOR: DESIGN, OPERATION AND PRODUCTIVITY

by

Alan R. Whitney
NEROC Haystack Observatory
Westford, Massachusetts 01886 U.S.A.

ABSTRACT

The Mark III correlator was developed in support of the NASA Crustal Dynamics Program to process Mark III VLBI data gathered by the project and has been operational since 1979.

The processor design is based on a straight-forward, but highly flexible, modular concept utilizing one module per baseline track-pair. The current system of 90 modules can simultaneously process 3 stations of 28 tracks each or 4 stations of 14 tracks each. Simple duplication of existing hardware can expand the processor to a capacity of 8 stations of 28 tracks each. The system is supported by low-cost HP-1000 minicomputer(s) coupled with an array processor to aid in fringe searching operations.

Since achieving operational status, the Mark III correlator has processed in excess of 100 separate experiments encompassing over 150,000 individual observations, supporting both astronomy and geodesy programs. Expansion of existing facilities is contemplated in the near future.

INTRODUCTION

This paper briefly describes the Mark III correlator system currently installed at Haystack Observatory. The design of the hardware and software, and the current operational status will be discussed.

The development of the correlator system was funded by NASA in support of the NASA Crustal Dynamics Project, but its design is such that many astronomy applications, including spectral line and pulsar observations are also supported. The correlator is now in full operation at Haystack, and expansion is being planned in the near future.

PROCESSOR HARDWARE

Design Philosophy

The Mark III processor design is based on a straight-forward modular concept utilizing one module per baseline per track-pair. Thus, 28 modules are required to process one baseline of 28 tracks. Each module is a completely autonomous unit, but all are controlled by a common computer. The module performs the functions of decoding the two data streams (one from each station forming the baseline), buffering and correctly aligning the data streams to remove the effects of recorder jitter before rotating and cross-correlating the data streams.

Hardware System Overview

Figure 1 shows a simplified block diagram of the processor module and its interfaces to the tape recorders and computer. The signals from the reproduce heads are amplified, equalized and passed to "bit synchronizers", the data and the data clocks. Decoders built into the processor module detect the synchronization bits in the serial format and separate the radio source data from the time, parity and auxiliary data. One of the radio source data streams is buffered by a fixed delay and then multiplied by 3-level approximations of the sine and cosine functions, while the other data stream is buffered by a programmable delay before the two data streams are cross-correlated. The cross-correlator has 8 lags quadrature channel and has 23-bit accumulators so that up to 2 seconds (at the Mbit

of data can be accumulated before the computer must retrieve the correlation output from the module.

Normally each processor module is allowed to accumulate at least one second of data before being serviced. More rapid service can take place and may be desirable for special processing.

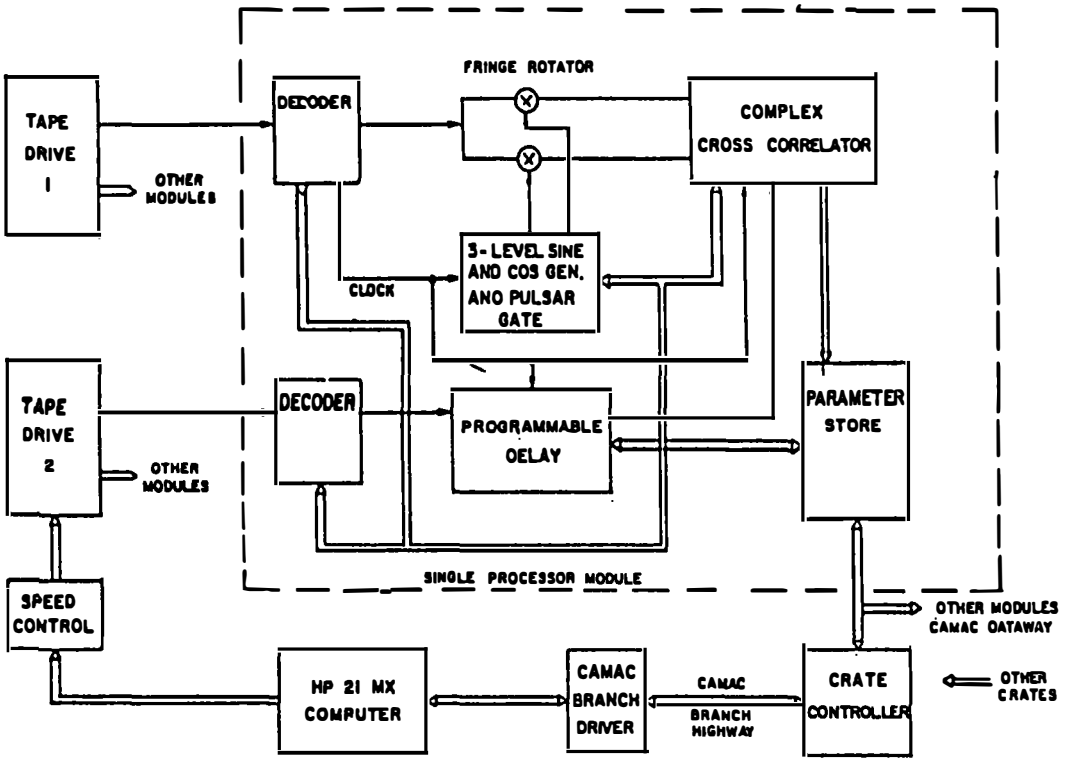

Figure 1. Simplified Block Diagram of Mark III VLBI Processor

The information from the module is transmitted through a CAMAC controller and branch driver to the controlling computero The "tape time" information in this data is used by the computer to control the speed of the tape drives so that they are kept mechanically synchronized to within the limits of the internal buffers of the correlator module. Typically, tape synchronization is maintained to within a few hundred bits on the tape, corresponding to <0.5mm of physical tape position.

Computer-to-Correlator Interface

The CAMAC (Computer Automated Measurement and Control - an IEEE standard) interface couples the modules to an HP-1000 computer. The CAMAC system, with its associated branch drivers and crate controllers, allows the computer to address and communicate with up to 105 modules per branch driver, although only 90 modules are normally installed in our system.

Recorder Interface

The connection of the recorders to the processor modules is illustrated in Figure 2. The processor modules have internal 8-way input selectors so that a given processor module can process any baseline. The system is expandable to 8 recorders and 28 baselines.

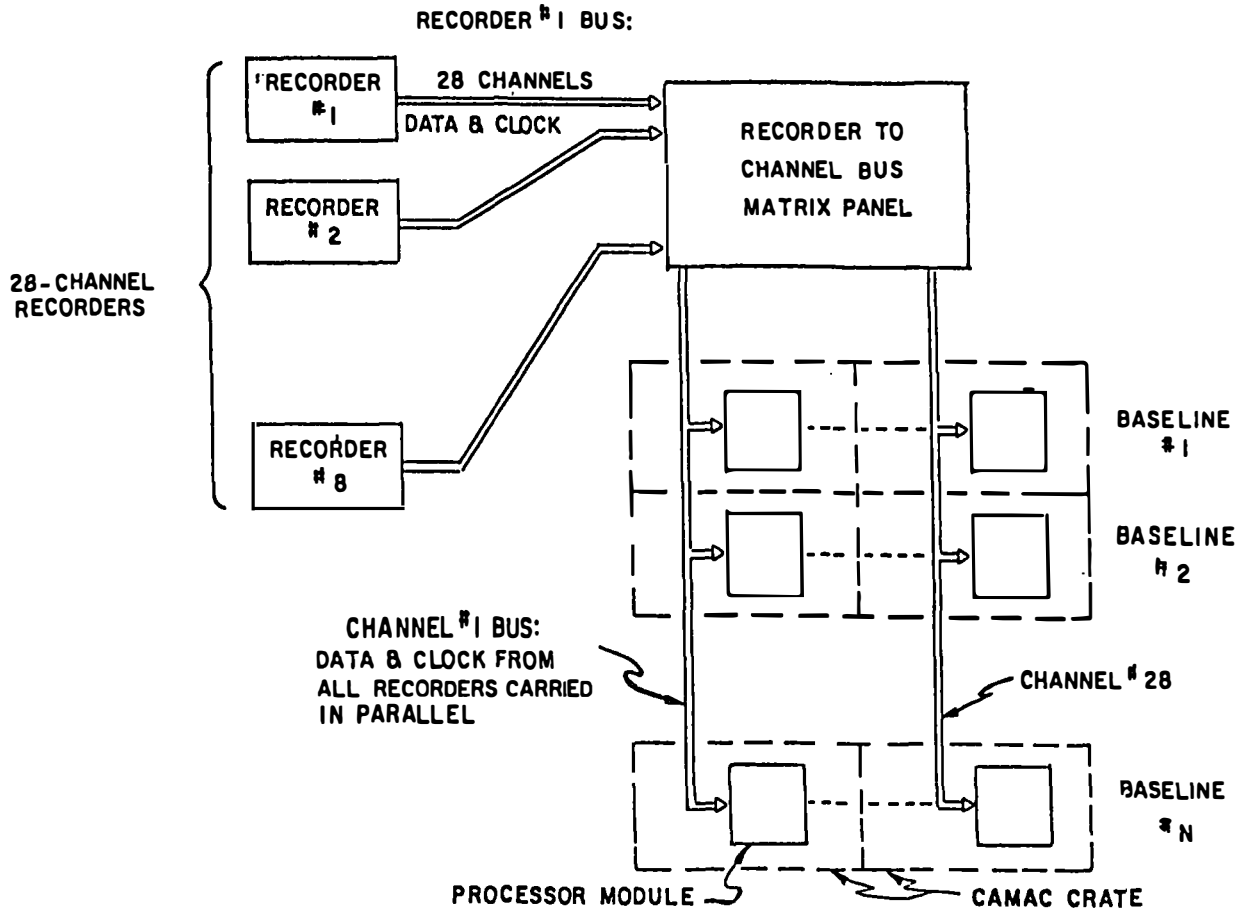

Figure 2. Recorder-to-Processor Interface

Correlator Module Characteristics

Figure 3 shows a somewhat more detailed block diagram of a correlator module, while Table 1 lists the basic module characteristics.

The interface to the recorded data is very simple, consisting only of the data and clock signals from each of the two data streams to be cross-correlated. The X-clock signal is used as a basic clock within the correlator module, so that normal processing will take place regardless of the data rate from the tape recorders; in other words, no control signals indicating data rate to the module are necessary. The reproduce circuitry within the tape recorders is designed in such a manner that the clock signals will always "flywheel" even in the absence of data, so that processing will continue normally even through deep data dropouts.

The cross-correlator section of the module performs processing for 8 complex lags during normal processing or 16 real lags for auto-correlation processing. The accumulation registers are 23 bits wide, allowing the accumulation of slightly more than 2 seconds of data at the 4 Mbit/sec sample rate.

Fringe rotation is accomplished through the use of a 24-bit phase register, thus achieving 0.4 microradian resolution. A 3-level rotation scheme is used to optimize the signal-to-noise ratio of the processed data. The phase-rate-resolution of the rotator is selectable in powers of two under software control and is normally set to be 14.9 mHz at the 4 Mbit/sec sample rate. The selection of rotator phase-rate resolution must be traded against the maximum fringe-rate that can be processed; selecting the resolution to be 14.9 mHz for the 4 Mbit/sec sample rate limits the maximum rotation speed to approximately 250 kHz. Higher fringe rates may be processed by decreasing the phase-rate resolution at the possible expense of shortening the basic correlator integration period due to degraded phase-tracking of the rotator. Also included in the fringe-rotator section of the correlator module is a simple phase-acceleration compensation mechanism which is designed to be sufficient to compensate for any expected fringe-phase acceleration during the normal correlator integration period.

Module I/O
- X data & clock
- Y data & clock
- CAMAC dataway to from computer
Correlator
- 8 complex lags
- 23-bit accumulation registers (~2 secs @ 4 Mbits/sec)
Rotator
- 24-bit phase register (0.4 microradian quantization)
- 14.9 milliHz phase rate quantization (@ 4 Mbits/sec)
- Phase acceleration compensation
Y-data buffer
- 4000 bits (1 millisec @ 4 Mbit/sec)
Integration Period
- Software adjustable from 5 millisec to 2 sec (@ 4 Mbits/sec)
Phase calibration
- 2 1-channel (complex) correlators

Table 1 - Mark III Correlator Module Characteristics

The module is capable of automatic "fractional bit" correction using an approximation which causes only 3% loss in signal-to-noise ratio and eliminates most phase noise caused by uncorrected bit shift changes in the continuum processing mode.

A 4000-bit addressable buffer is provided in the path of the Y-data and Y-clock signal streams so that the X and Y tape drives need be synchronized only so well as to maintain the a priori bit delay within this 4000-bit window. Synchronization of the tape drives to this level is a relatively easy task.

The basic integration period of the correlator module is software-controllable from 1 frame to 512 frames, or equivalently, from 5 msec to 2.56 seconds (tape-time) at 4 Mbit/sec sample rate. For most normal geodetic processing, an integration period of 1-2 seconds is used. This provides a search range of 1.0 to 0.5 Hz, respectively, which is quite adequate for all normal processing. Since the computer must service the correlator module once each integration period, the load on the host computer varies approximately inversely as the integration period. As the integration period shortens, a point is reached where the number of modules that may be operating simultaneously must be reduced or tape-playback speed reduced in order that the computer may keep up.

Not indicated in Table 1 is the availability of a "pulsar" processing mode, which may be used for special applications. In this mode, a start bit number and stop bit number may be specified within an integration period so that only those bits within the start-stop window are processed. This mode is primarily designed for processing of pulsar data, but may be used to process any pulse-type data or for other special-purpose processing.

Phase-calibration processing is also provided within the correlator module. Separate processors are used for the X and Y data streams, although the frequency of the phase-calibration rail must be the same for both X and Y. A much-simplified rotation scheme is used for phase-cal processing compared to the rotator described above. Rotator phase-rates are constrained to be such that the phase-cal signal must contain an integral number of sample bits per quarter-phase-cal-period. This condition is met with the phase-cal signals that are normally used. Also, only a 2-level rotation scheme is used, since signal-to-noise of the phase-calibration signal is not normally of concern. By imposing these conditions and restraints, the circuitry used for phase-cal processing is considerably simplified compared to that of the main lobe rotator and cross-correlator.

Internal testing of the correlator module is possible through the use of an on-board quasi-random signal generator. Partial testing is possible off-line with

no computer servicing necessary. Complete testing using the internal test generator is possible when a host computer is available.

The circuit design of the Mark III correlator module represents a conservative approach in that no custom LSI was undertaken. The majority of the 340 integrated circuits used are low-power Schottky TTL types, with the balance being NMOS RAM's, TTL RAM's, and several PROM's used as sequence controllers. Power consumption is about 26 watts per module.

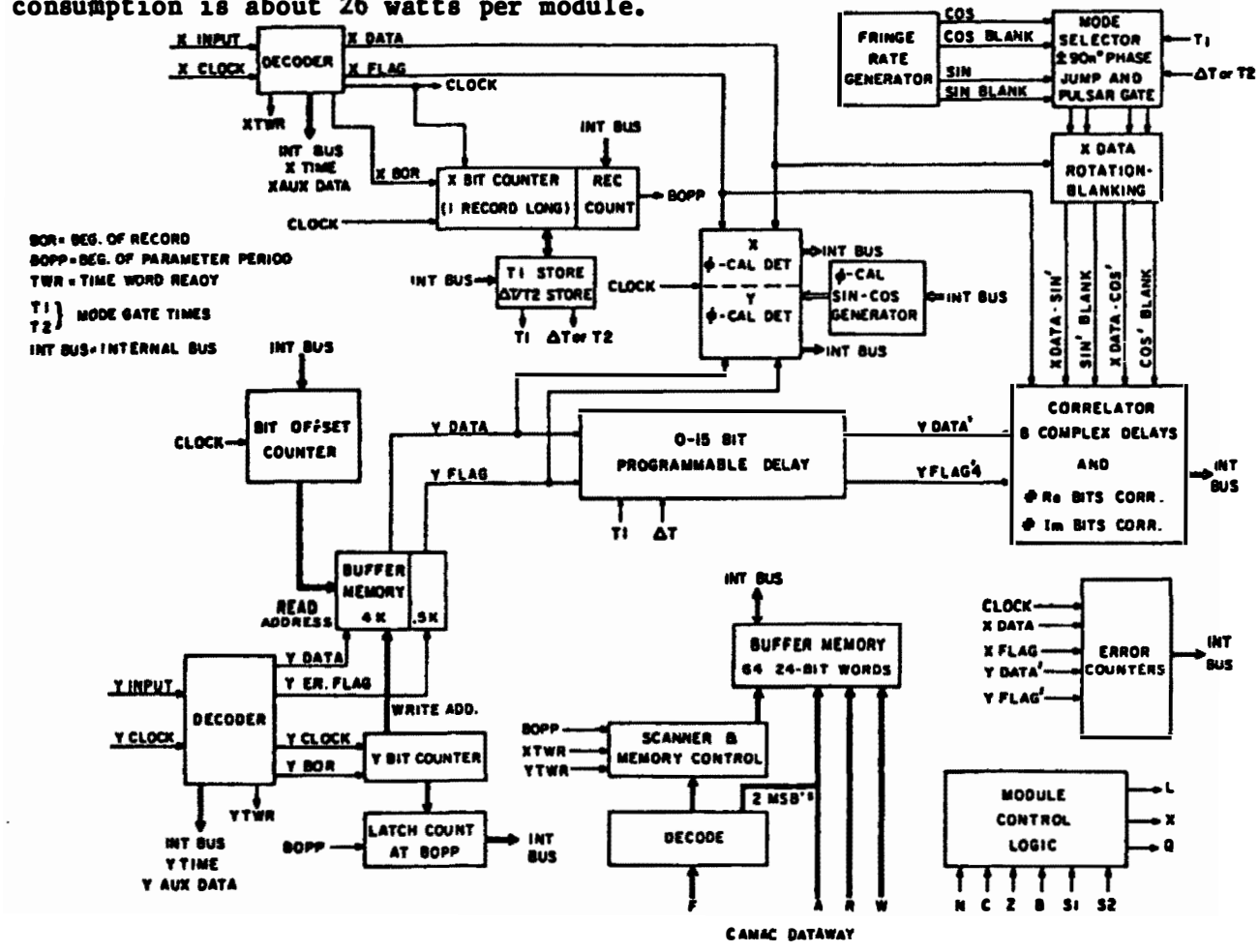

Figure 3. Mark III Processor Module Block Diagram

Signal Flow Through Correlator Module

Figure 3 shows a block diagram of the the Mark III correlator module. Both X and Y data streams are first decoded by their respective DECODER's. The X and Y data streams may be independently selected from any one of 8 data streams which may be applied to the module (not shown in Fig. 3). The decoder has the responsibility of synchronizing itself to the data stream (by use of the sync words embedded in the data streams), extracting the time and auxiliary-data fields, checking the time/aux-data field for errors (using the embedded 12-bit CRCC check character), stripping parity bits and counting parity errors. The decoded X-data is then passed to the X PHASE-CAL DETECTOR and the X-DATA ROTATION-BLANKING. Rotation is controlled by the FRINGE RATE GENERATOR, which generates a 3-level quadrature rotation signal according to the parameters received from the host computer. The quadrature-rotation signals from the rate generator are processed by the MODE SELECTOR before actually being applied to the X-data. The mode selector may apply an additional +/-90*n degree phase-shift in conjunction with a shift in the X-Y bit delay to accomplish "automatic fractional-bit-error correction" — more will

be said about this later. After rotation, the X-data stream is applied to the CORRELATOR for cross-correlation with Y-data.

After emerging from the Y-decoder, the Y-data stream and accompanying flags are routed to a BUFFER MEMORY capable of storing 4000 bits of data. Data is removed from this buffer memory according to a BIT OFFSET COUNTER which has been set according to the a priori parameters received from the host computer, so that the proper Y-data bits are made available to the correlator. The output from the buffer memory is applied directly to the Y-PHASE-CAL DETECTOR for phase-cal processing, and to a 0-15 BIT PROGRAMMABLE DELAY preceding actual correlation with the rotated X-data. This programmable delay is used to shift the Y-data stream one-bit at a time wrt to the X-data stream as the a priori delay changes within an integration period. Up to 15 such bit shifts may be made within a single integration period, according to the parameters provided by the host computer. Each time such a bit shift takes place, the MODE SELECTOR imposes an additional +/-90 phase shift to the signals emerging from the FRINGE RATE GENERATOR. Through the use of this "automatic fractional-bit error correction" technique, correlation may be carried through many changes in the X-to-Y bit delay so long as the model contained in the FRINGE RATE GENERATOR is sufficiently accurate to track the fringe phaseo

The CORRELATOR section of the module does the actual correlaion between the rotated X-data stream and the unrotated Y-data stream. Eight complex lags are normally processed, although the correlator may also be configured under software control to do auto-correlation processing of either the X or Y data stream.

The determination of tape-recorder synchronization is made by latching the Y bit count (within a frame) at the beginning of the first X frame of an integration period. Integration period boundaries are constrained to start at X-data frame boundaries, so that with knowledge of the Y-data stream time and LATCH COUNT at the beginning of an integration period, the tape-recorder synchronization may be computed and the necessary commands sent to the tape transports.

All communications with the host computer are "double-buffered" so that computer servicing of the correlator module is completely asynchronous with respect to the X and Y data streams except that servicing must take place once each integration period in order to update processing parameters and extract processed data. Each correlator module communicates individually with the host computer. During a normal computer service, approximately 21 bytes are sent computer-to-module and 114 bytes module-to-computer.

Correlator System Configuration

Figure 4 shows the correlator system configuration when used to process 3-station/28-track data or 4-station/14-track data. Ninety correlator modules are housed in a single rack of 6 CAMAC crates, 15 modules/crate. Each of the six crates is identical and receives an identical set of data signals from the 4 tape transports distributed as follows:

Module 1 - Receives signals from both tracks #1 and #2 from each of the 4 tape drives (recall that each module may select X and Y from among 8 inputs to the module)o

2 - Receives signals from both tracks #3 and #4 from each of the 4 tape driveso

14 - Receives signals from both tracks #27 and #28 from each of the 4 tape drives.

15 - This module is dubbed a "floating module" whose input may be selected to be from any track of any of the 4 tape drives. Track selection is actually made within the control electronics of the tape drive. Tape drive selection is made at the input to the correlator module itself.

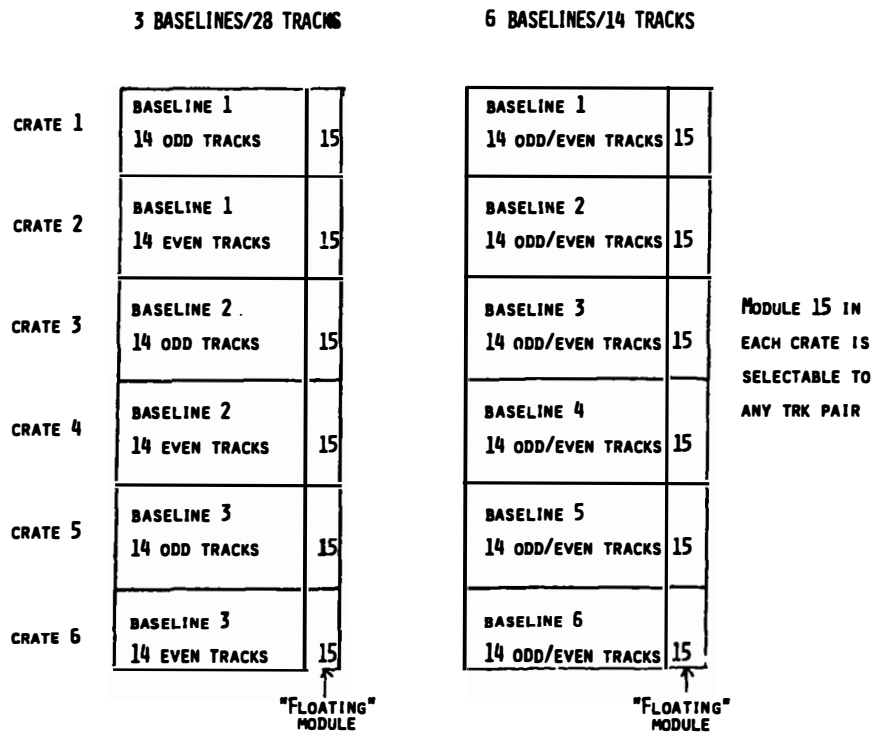

Figure 4. Correlator Configuration for 3 & 4 Stations

For the case of 3-baseline/28-track data, each crate processes either the odd or even numbered tracks from one of the 3 baselines. The floating modules may be assigned arbitrarily for either redundancy checking or for special processing. In the 4-station/14 track case, each crate is assigned to one of the 6 baselines and may process all even or all odd tracks, which is compatible with the standard 14-track mode of data recording. The floating modules may again be assigned as desired.

Due to the modularity of the correlator system, it is easily several ways. With the addition of an identical 6-crate correlator system, 4-station/28-track data may be processed in single-pass. This additional 6 crates may be handled either by the existing host computer or by an additional host computer. Because the data interface to the tape transports is very simple, expansion of the system to a large number of stations is a simple matter. Correlator modules and host computers may be added to bring the system to any capability desired. Connecting a group of HP1000 computer systems into a multi-computer net for handling a large correlator system is straight-forward and cost effective. High-speed data devices such as discs are shared among CPU's, so that all data from a particular processing pass will end up properly concatenated ready for further processing.

Spectral-Line and Pulsar Processing Capability

Although the Mark III processor design is primarily oriented towards the processing of continuum data, provisions have also been made for processing of spectral-line data where many lags are desired. This is done by staggering the a priori delays between modules to process many lags. For example, using 90 correlator modules to process a single-track single-baseline spectral-line observation, 60 modules may be used to do cross-correlation (480 complex delays) and 15 modules each for X and Y autocorrelation (240 real delays). Similarly, a single-track 3-baseline observation may be processed using 22 modules on each baseline for cross-correlation processing (192 complex delays) and 6 modules for autocorrelation processing (96 real delays).

Support for pulsar processing is built into the correlator module in that the correlator may be turned on and off at specified bit locations within an integration period. When this mode is in operation, the hardware fractional bit correction and fringe phase acceleration are automatically disabled. In a manner analagous to the spectral line case, one may assign a bank of correlator modules to cross-correlate the same track pair, but each with a staggered pulse window. The output then forms a pulse profile of correlated flux.

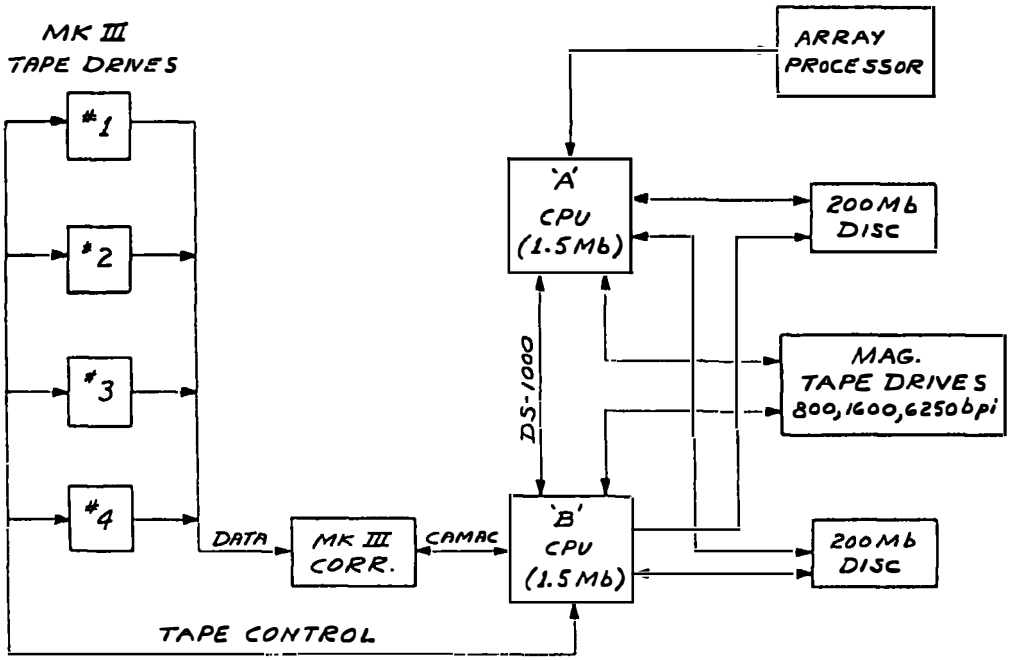

Figure 5. Processor Computer System Configuration

Correlator Computer Support

The Mark III correlator is supported by an HP1000 computer system utilizing two Model 2117F CPU's in a configuration shown in Figure 5. The HP1000 is a 16-bit minicomputer system of modest size and cost. Each CPU contains approximately 1.5 Mbytes of semiconductor memory, and the CPUs share approximately 400 Mbytes of on-line disc storage.

One of the CPUs (labelled 'B') is dedicated to real-time correlator operation and fringe-searching. All computations and control for the correlator system are carried out by this computer. The CAMAC interface to the computer is provided by a commercially-procurred CAMAC branch driver. Interface to the tape transports is through a standard ASCII RS232 interface to an ASCII transceiver in the tape transport. No special-purpose interfaces have been used in the correlator system.

The other CPU (labelled 'A') is available for any overflow fringe-search processing from the 'B' machine, and for further post-processing; a general-purpose array processor (CSPI MAP-300) is also attached to the 'A' machine to support special-purpose processing.

The HP1000 computer system uses the RTE-IVB operating system supplied by Hewlett-Packard. This system supports a full multi-programming environment, allowing concurrent processing tasks. Full 64-bit precision arithmetic is available in hardware for all critical calculations, and use of a micro-programmed FFT in fringe-search operations makes processing speed reasonably high.

CORRELATOR SUPPORT SOFTWARE

A simplified block diagram of data flow through the correlator system is shown in Figure 6. We will briefly describe each section of it in turn.

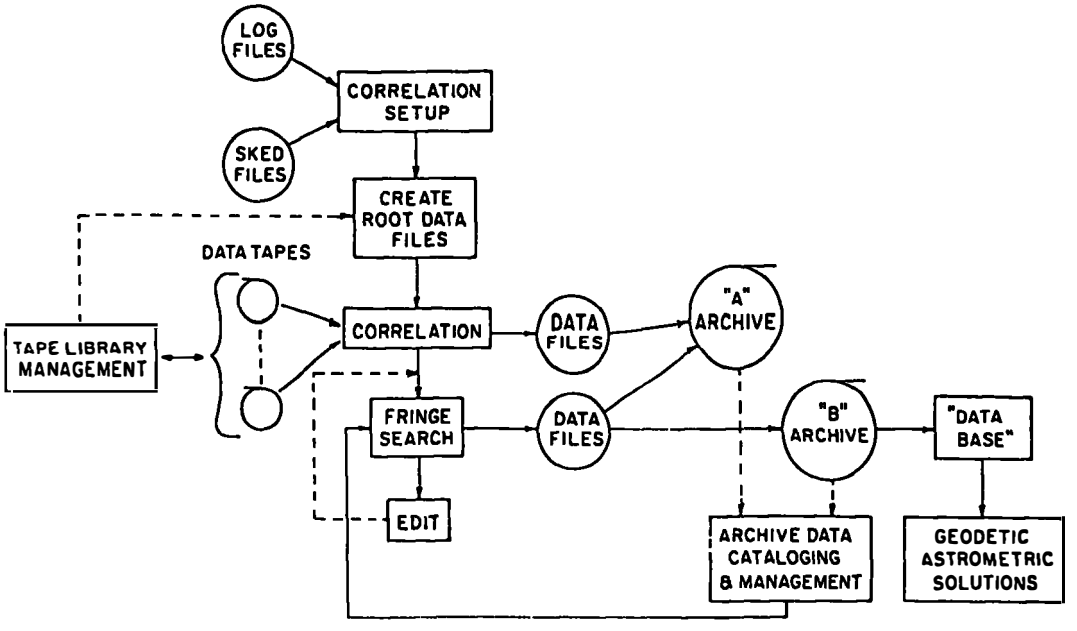

Figure 6. Mark III Correlator Data Flow

Correlation Preparation

Schedule and log files from an experiment are used to set up control files for the correlation processing. These files are ASCII files which may be generated either automatically or by manual editing. The data in these control files are used to create a "Root Data File" for each scan to be processed. This file contains all of the detailed information necessary to do the correlation processing for all potential baselines of that scan.

Correlation Processing

The correlation process itself is supported by a battery of about 18 interacting programs, each controlling some aspect of the correlation process. All a apriori calculations for processor operations are done in real-time while the correlator is operating.

On-line graphics displays and status monitors provide real-time monitoring and control of the processor operation. When multiple-baseline scans are being processed, each baseline is brought "on-line" as data from that baseline becomes available for correlation, and is taken "off-line" when data is no longer available from that baseline.

At the completion of correlation processing, the raw correlator data are attached to the root data file as an "extent", and there await fringe-search processing.

Fringe-search Processing

Fringe-search processing is done by collecting all the correlator data for a particular scan, one baseline at a time, and processing to estimate correlation amplitude, group delay, phase-delay rate, fringe phase, etc. The fringe search results are attached as another "extent" to the root data file. Further processing

may be done with automatic or manual editing of the correlator data or fringe-search parameters, and processed again through the fringe-search step as necessary. An additional file "extent" is created each time fringe processing is done, so that a complete record is kept of all processing for a scan.

The fringe-search output is the primary source of output for all later geodetic, astrometric, and astronomical processing.

Data Archiving

Due to the very high volume of correlator data and fringe search output, it is necessary to move data fairly rapidly to suitable magnetic tape archives to avoid overloading the available disc storage space. Two types of permanent archival tapes are created at the processor site. The 'A' archive tapes store the entire contents of all correlator data files, including the raw correlation coefficients from each integration period of each module and the entire fringe-search output. The 'B' archive tape is identical, except that the (voluminous) raw correlator output is not stored, and hence the 'B' tapes are considerably more compact. The 'B' tapes are distributed to users for further processing, and form the raw data input to create the 'Data Base' used for geodetic and astometric solutions.

The 'A' archive tapes allow restoration of the raw correlator output for purposes of re-fringe-searching or special processing at some later time. With the 'A' tapes in hand, the raw Mark III data tapes may be confidently released and re-recorded, even though some reprocessing through fringe-search operations is still contemplated. This helps to reduce the total number of expensive Mark III tapes that must be purchased by recirculating them at a faster rate.

At the current time, several thousand 'A' tapes have already collected in the Haystack archives.

Indexing and Cataloguing

In order to keep track of all of the data that has been processed through the correlator and fringe-search operations, a comprehensive cataloguing and data-retrieval system has been developed that allows easy recovery of any data in question. In addition, a set of permanent summary files are maintained that allow a quick look at any data that has ever been processed.

When the data from a particular experiment arrives at the correlator facility, it is assigned a unique experiment number with which all subsequent references to that set of data may be made. Programs are available to scan these summary files with various sets of specifiable filters in order to do quick looks at data or determine current status of processing of an experiment.

Data Tape Library

The Mark III data tape library currently contains more than 2000 tapes and requires careful management to keep track of the location and status of each tape. A data base system is utilized for this purpose, providing the capability not only of managing the library, but of keeping records of the error-rate performance history of each tape. The correlator software is linked to the tape library software so that data-tape related information may be transmitted in both directions. In particular, correlator operators are provided with real-time library information to aid them in finding tapes to be processed, and tape performance data is transmitted to the library data base.

Some Additional Comments Regarding Software

Currently the correlator system supports 4 tape drives with 90 correlator modules. The correlator support software has been written in a highly general manner to support an arbitrary number of stations, baselines, and correlator modules to the limit of the computer's physical ability. However, expansion beyond

even this point is fairly straightforward by adding additional linked computers in much the same manner as has already been done (see Figure 5).

The body of software supporting Mark III correlator operations currently consists of approximately 100,000 lines of Fortran source code and 10,000 lines of assembly language code on the HP1000 machine, and has consumed some 15 man-years in its development.

OPERATIONAL MANAGEMENT AND PRODUCTIVITY

A staff of correlator operators runs the Mark III correlator facility 24 hours a day, 7 days a week. Approximately one 8-hour shift of training is normally required to familiarize new personnel with correlator operations. Because all critical setup data reside in pre-prepared disc files, the operators do not need to be knowledgeable in the details or subtleties of VLBI data processing. Reasonably foolproof checks have been instituted in the software to guarantee that the proper tapes are mounted at the proper times and that proper operational procedures are followed. A full complement of explanatory error and help messages enable the operators to handle most unusual situations without assistance.

In two and one-half years of operation, the Mark III processor has correlated in excess of 35,000 tape pairs containing some 150,000 individual baseline-observations. The volume of raw data flowing into the correlator system has already exceeded 300, Gbytes, corresponding to approximately 10 Mbits per US citizen, or about the equivalent of one good thick novel.

CORRELATOR EXPANSION PLANS

Current plans call for a 1983 upgrading of the Mark III correlator system to 180 modules, which is double the current size and is sufficient for simultaneous 4-station mode A (28-track) operation. Some upgrade of the correlator module design is being contemplated to take advantage of newer and cheaper technologies; the module characteristics will be compatible with the current design, but with some extended capabilities.

THE K-3 HARDWARE SYSTEM BEING DEVELOPED IN JAPAN AND ITS CAPABILITY

N.Kawaguchi, Y.Sugimoto, H.Kuroiwa, T.Kondo,
S.Hama, J.Amagai

Kashima Branch, The Radio Research Laboratories
Kashima, Ibaraki 314 Japan

T.Morikawa and M.Imae
The Radio Research Laboratories
Koganei, Tokyo 184 Japan

ABSTRACT. The K-3 VLBI hardware has been developed since 1979 for the Japan-US joint VLBI experiments starting at the beginning of 1984a This paper presents a summary of the K-3 VLBI hardware which is composed of a 26 meter antenna, S/X receivers, a K-3 data acquisition terminal, wideband data recorders, a delay calibrator, a correlation processor, hydrogen maser oscillators and a water vapor radiometer. This paper also presents an error estimation on the joint experiments, and the result shows that we can expect the measurement with an accuracy of about 2 cm or bettera

INTRODUCTION

The K-3 VLBI hardware has been developed since 1979 for the Japan-US joint VLBI experiments starting at the beginning of 1984.

The 26 meter antenna at Kashima Branch, the Radio Research Laboratories, will be used as one element of these experimentsa An S-band receiver for a right-handed circularly polarized component and two X-band receivers for right- and left-handed ones will be assembled in the 26 meter antenna system by August 1983a

Development of two data acquisition terminals, each having an IF distributor, IF-to-video converters, a formatter, a decoder with a one-megabit memory, wideband data recorders and a delay calibrator, together with a correlation processor are proceeding on schedule and will be finished by March 1983a The data acquisition terminal is compatible with a Mark-III system and is also obedient to instructions of the same schedule program as one being used in the Mark-III field system.

Trial manufactures of a hydrogen maser oscillator, well-stabilized local oscillators, a water vapor radiometer and image rejection mixers have successfully been finished, and details of the K-3 hardware for operational use are designeda

We describe the results from pilot study and the design of the whole K-3 hardware, and also present a summary of the expected capability of the K-3 hardware system.

A 26 METER ANTENNA AND S/X RECEIVERS

A schematic sketch of a 26 meter antenna is shown in Figure 1. The antenna is a modified cassegrain antenna with a horn-reflector feed, and has an altitude-azimuth mount. The position of the intersection of axes, which is a reference point of a VLBI baseline, is shown in Table 1 in coordinate system of SAO-C7. The position will accurately be resurveyed by Geographical Survey Institute and precisely related to a Japanese datum origin (Kawaguchi,et al. 1982).

Tracking of celestial sources with this antenna is automatically performed by instructions from a computer within the accuracy of 0.01 degrees at maximum slewarate of 1 degree per second. Aperture efficiency of this antenna is expected to be 57 % at S-band and 45 % at X-band. Antenna noise temperature including noise due to feed system loss is to be 76 K at S-band and 90 K at X-band, at zenith angle of 45 degrees in a standard atmosphere.

The block diagram of the S/X feed and the waveguide circuit together with preamplifiers and frequency down-converters is shown in Figure 2. The S-band RHCP (Right-Handed Circularly Polarized signal) is guided to a S-band preamplifier through two directional couplers, the one is for injection of a delay calibration signal and the other is for adding some amount of noise to measure a system noise temperature. The noise adding and the system noise measuring are performed by device controllers in a data acquisition terminal. Both RHCP and LHCP (Left-handed one) signals in X-band are guided to two X-band preamplifiers through two waveguide switches and one ferrite switch, besides two directional couplers which have same functions as S-band. The SW1 (see Figure 2) alternates RHCP signal with LHCP signal.

The amplification of X-band and X'-band signals are performed by two independent preamplifiers as shown in Figure 2. Frequency allocation of both bands and response of a Band Pass Filter (BPF) in front of the X'-band preamplifier are shown in Figure 3. Usually, X-band and S-band RHCP signals are received in Japan-US joint VLBI experiments. At the same time, if LHCP signals in X'-band are received, the cross polarization of the incident waves can be measured at frequency range from 8180 MHz to 8280 MHz, a common band to X- and X'-band. The common band is also used for a test of system coherence. Both a noise and a delay calibration signal generated in a delay calibrator are received by X- and X'-band receivers, and are recorded on magnetic tapes, and are cross-correlated by a correlation processor in usual manner of VLBI. The result will show the degradation of coherence due to system instability or system imperfection. The X- and X'-band can be combined with each other by using a Ferrite SW, SW2 and BPF. As can be seen in Figure 3, the combination yields two times wider bandwidth for synthesis than that of a X-band only.

The S-band preamplifier is composed of field effect transistors (FETs), and the noise temperature is eatimated to be below 93 K throughout the whole receiving band from 2220 MHz to 2320 MHz. The X-band preamplifier is usually used in joint VLBI experiments and is a parametric amplifier followed by three FETs. Total gain will be above 50 dB and the noise temperature is expected to be below 70 K at frequency range from 8180 MHz to 8600 MHz. The X'-band preamplifier is composed of three FETs cooled electrically down to minus 60 C in physical temperature. The gain is above

40 dB and the noise temperature is below 100 K at frequency range from 7860 MHz to 8280 MHz.

Three down-converters are used to convert the frequencies of S-, X- and X'-band signals to IF frequencies, those are from 200 MHz to 300 MHz for S-band, from 100 MHz to 520 MHz for X-band and X'-band. The local oscillator signals are derived from a 10 MHz reference signal supplied by a hydrogen maser oscillatora The S-band local oscillator signal of 2020 MHz is phase-locked to the reference signal by a phase-locked oscillator (PLO)a The output of the PLO, 2020 MHza is multiplied by four to provide the X-band local oscillator signal of 8080 MHza Another PLO supplies a local oscillator signal of 7760 MHz for the X'-band local oscillator and is also phase-locked to the same referece. Each converter has an image rejection filter and a line equalizer. The filter rejects undesired spurious or alleviates an interference from the lower sideband. The line equalizer compensates a rapid increase of attenuation at frequency above 100 MHz in IF cablesa

K-3 DATA ACQUISITION TERMINAL

A K-3 data acquisition terminal is composed of an IF distributor, 14 video converters, a formatter, a decoder and a reference signal distributora

The IF distributor has two channel units and a device controllera Each unit is independent and exchangeable each other and accepts an IF signal from 100 MHz to 520 MHz, disributes it to 8 LO IF channels (from 90 MHz to 230 MHz) and 8 HI IF channels (from 200 MHz to 520 MHz)a The device controller controls the devices according to commands sent from a host CPU (HP-1000 model 10L) via a HP-IB interface, and also measures noise temperature of S-, X- and X'-band receiving system by turning a noise diode on and off in front of the receivers.

The 14 video converters accept 14 IF signals and output 28 video signals. The upper frequency of each video signal is selected out of 4, 2, 1, 0.5, 0.25 and 0.125 MHza Each video converter has the same device controller as in the IF distributor and is also controlled by a host CPU. The local oscillator signal is supplied by a 10 KHz-step synthsizer phase-locked to the reference signal from a hydrogen maser oscillatora

The formatter has seven channel units and can accepts up to 28 video signalsa Each unit samples 4 video signals into one bit and places them in a format prescribed so as to be compatible with a Mark-III format. A time code and all the timings for formatting are generated from a reference signal supplied by the hydrogen maser oscillator. The formatter is also controlled by a host CPU via a HP-IB interface.

The decoder performs the function of independently decoding two serial bit streams encoded and formatted by the formatter and of monitoring parity and synchronization errorsa The results of decoding and monitoring are displayed on its pannel and are sent to a host CPU via a HP-IB interfacea The decoder also has a one-megabit memory in it and stores a part of the same data as that which would have been written onto a tape. These data is utilized for the purpose of monitoring signal quality, detection of a delay calibration signal in the data, and of confirming real-time fringes if the data could be exchanged through an existing communication link.

The reference signal distributor supplies twenty 10 MHz signals to all the K-3 equipments and one 5 MHz signal to a delay calibrator as a referencer These signals are distributed or divided from one reference signal supplied by a hydrogen maser oscillator.

K-3 WIDEBAND DATA RECORDER

A K-3 wideband data recorder is composed of an instrumentation facility (a Honeywell M-96) for driving a tape and some self-developed electronics for recording and reproducing 28 channel-digital data sampled and formatted in a K-3 data acquisition terminal.

A digital head driver records the digital data of 4.5 Mbps on 28 tracks at a speed of 135 ips, and the resultant recording density is 33.3 Kbpi.

A read module and I/O modules for reproducing the 33.3 Kbpi data on 28 tracks at the maximum speed of 270 ips is under development and will be completed in December, 1982. The maximum reproducing speed of 270 ips is two times faster than the usual recording/reproducing speed. As noticed later, this means shortening of time required for data processing.

All the sequences of recording and reproducing are controlled by a controllerr The controller has a micro processor to control the wideband data recorder according to instructions from a host CPU via a HP-IB interface and is always monitoring a footage counter for controlling the physical tape position.

K-3 DELAY CALIBRATOR

The S/X receivers at the antenna site and the data acquisition terminal in the ground building are connected by cables of about 62 metersr The variation of the cable delay is calibrated by a K-3 delay calibrator, the design of which is similar to a Mark-III delay calibrator.

The measured delay variation over 24 hours is shown in Figure 4. We can see a rapid decrease of the delay in the evening and an increase in the morning, and the peak-to-peak variation of about 0.1 ns was observedr

The resolution of the delay calibrator is about 0.5 picosecond and its instability is less than 5 picosecond.

K-3 CORRELATION PROCESSOR

Correlation processing is conducted by a HP-1000 model 45F computer with the aid of a HP-1000 model 10L computer and the use of a K-3 correlation processor. This correlation processing system is illustrated in Figure 5.

The correlation processor has 4 correlation units and 4 unit controllers. In each correlation unit, 8 pairs of data streams are cross-correlated and integrated. The correlated data are transferred to the 45F via a direct memory access line (DMA line) of HP-IB under controls of each unit controller. Necessary parameters for processing are transferred on the same line from the 45F to each unit controller. The unit controller sets these parameters to correlation unitsr

Synchronization errors between two data streams are calculated by the

unit controller, and are reported to the 10L. According to the information, the 10L controls a speed of one wideband data recorder, while it keeps the other recorder at a constant speedr

At any time, an operator can monitor and query the processing status via a HP-IB interface of the 10L without disturbing the data transfer between the 45F and the unit controller via a DMA linerr

The capability of the K-3 correlation processor are summarized in Table 3. The marked capability of this processor is the maximum integration period of about 8 second at the data rate of 4 Mbps and the maximum processing speed of 8 Mbpsr The long integration capability may alleviate a load of the 45F and the fast processing speed may reduce the time required for the processing.

K-3 HYDROGEN MASER OSCILLATOR

We are now developing a new field operable hydrogen maser oscillator. Preliminary experiments on a small sized prototype maser oscillator have been done to obtain data for the design of a new operational maser.

The performance of the prototype maser is shown in Figure 6 and the short term stability of 7×10^{-15} has been obtained. In the figure, a dashed line shows a required performance and filled circles show measuring values on the prototype maser. We have already achieved a required performance. In the error estimation due to the frequency instability, however, we use the required performance as a worst caser

Making good use of this experience, a detailed design of the operational maser is determined as shown in Table 4 for a physics package and in Table 5 for electronics system. All works on two operational masers will be finished by March, 1983.

K-3 WATER VAPOR RADIOMETER

Tropospheric path delay due to water vapor along a ray path will be corrected by a K-3 water vapor radiometerr

The radiometer measures sky noise temperatures emitted by water vapor at two frequencies near the resonant frequency of 22.2 GHz. From these noise temperature measurement, tropospheric path delay is precisely determined as have already been made clear by Wu (Wu 1979)r In the determination, however, there are some problemsr

In the first, the measured noise temperature must not be interfered by other noise sources such as a noise from the ground or a noise generated by lossy circuits in the radiometer. We can correct the unkown bias adding to the true sky noise temperature by a tipping method or using a liquid nitrogen cooled dummy in front of the antenna. For making the tipping method effective, we need to measure the sky noise temperature down to the elevation angle of less than 10 degree (equivalent to the air mass number of larger than 5) as can be seen from Figure 7. The figure, the result of covariance analysis on the tipping curve, shows the estimation error of the unknown bias (σ_{T1}) caused by the observation error of 0.5 K, when the tipping is conducted down to the elevation angle shown on the abscissa. We design our radiometer so as to measure the sky noise temperature down to the elevation angle of 10 degree without interference from the ground, by using a narrow beam, low sidelobe antenna.

In the second, coefficients used in the estimation of path delay from the sky noise temperature depends on meteorlogical condition. To avoid this dependency, we choose optimum pairs of frequency of 20.0/26.5 GHz or 20.3/31.4 GHz as is recommended by Wu (Wu 1979), and will confirm the validity of the coefficients by launching radiosondes.

The radiometer of a temperature-stabilized Dicke-type are designed and will be finished in May 1983. The error of the sky noise measuring are expected to be less than 1 K.

CONCLUSION

We present a summary of a K-3 hardware system being developed in Japan. In conclusion, we will summarize the error caused by the K-3 hardware system in Table 6. In the estimation, we suppose a baseline between the OVRO 40 m antenna and the Kashima 26 m antenna. From this table, the total observation error of about 2 cm will be expected.

We heartily hope that the Japan-US joint experiments will successfully start and the data will give new information to the fields of geodesy and crustal plate mortion.

ACKNOWLEDGMENT

We would like to thank to Dr. A.E.E.Rogers for his kind helps in designing K-3 data acquisition terminal, Dr. H.Hinteregger in designing wideband data recorder, Dr. G.M.Resch in designing a water vapor radiometer, Dr. A.R.Whitney in designing a correlation processor, and many other VLBI researchers for their kind suggestions and encouragements.

References

Kawaguchi,N.,Kawajiri,N.,Kawano,N.,Yoshimura,K.,Ishii,H.,Murakami,M.,Nishimura,O.,Yoshimura,Y. and Kaidzu,M.,1982: A baseline determination between Kashima 26 m and Tsukuba 5 m antennas in joint VLBI experiment plan of RRL and GSI, in this issue,

Wu,S.C.,1979: Optimum Frequencies of a Passive Microwave Radiometer for Tropospheric Path-Length Correction, IEEE transaction, vol.AP-27, NO.2.

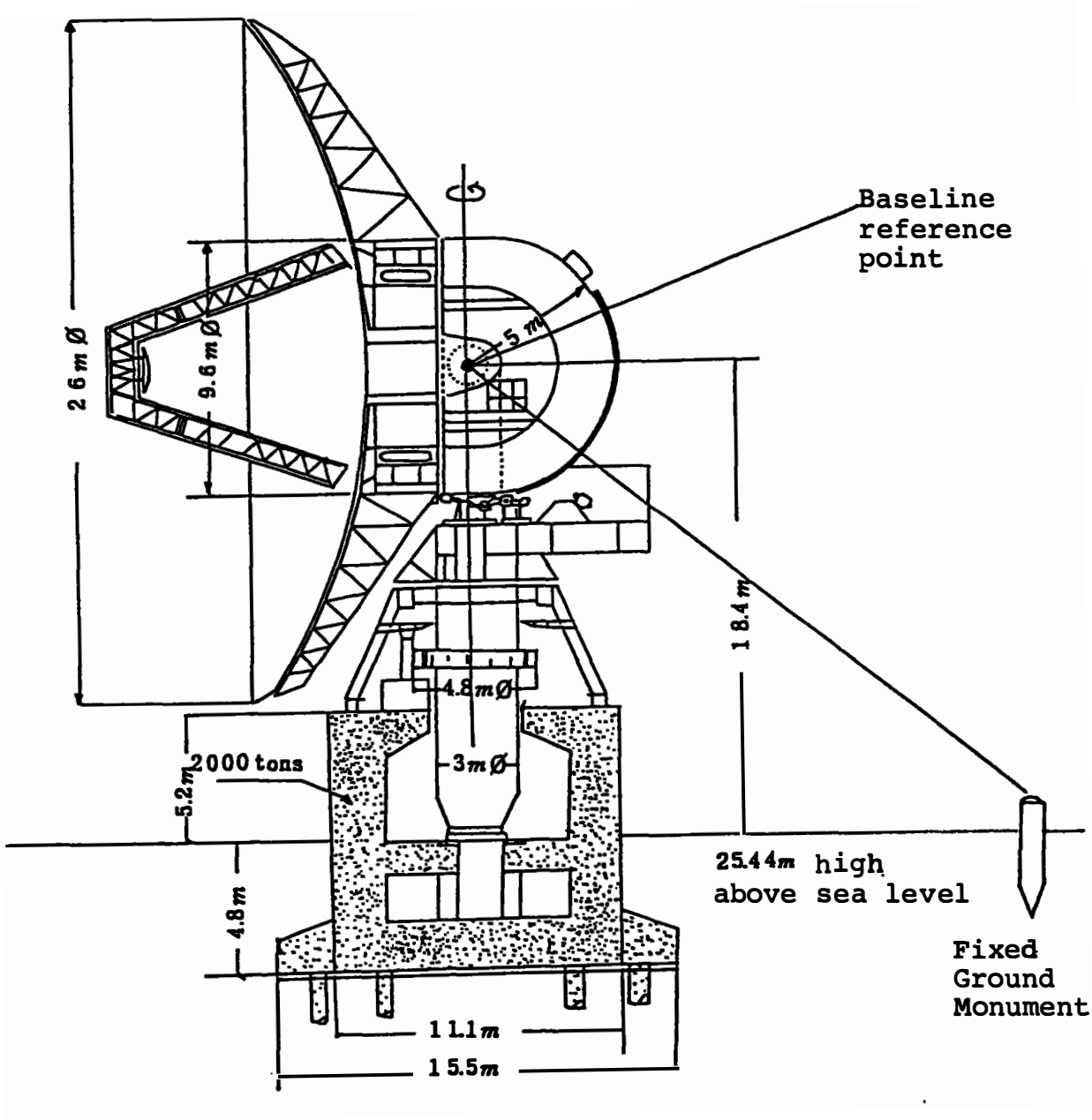

Figure 1. The schematic sketch of the 26 meter antenna at Kashima

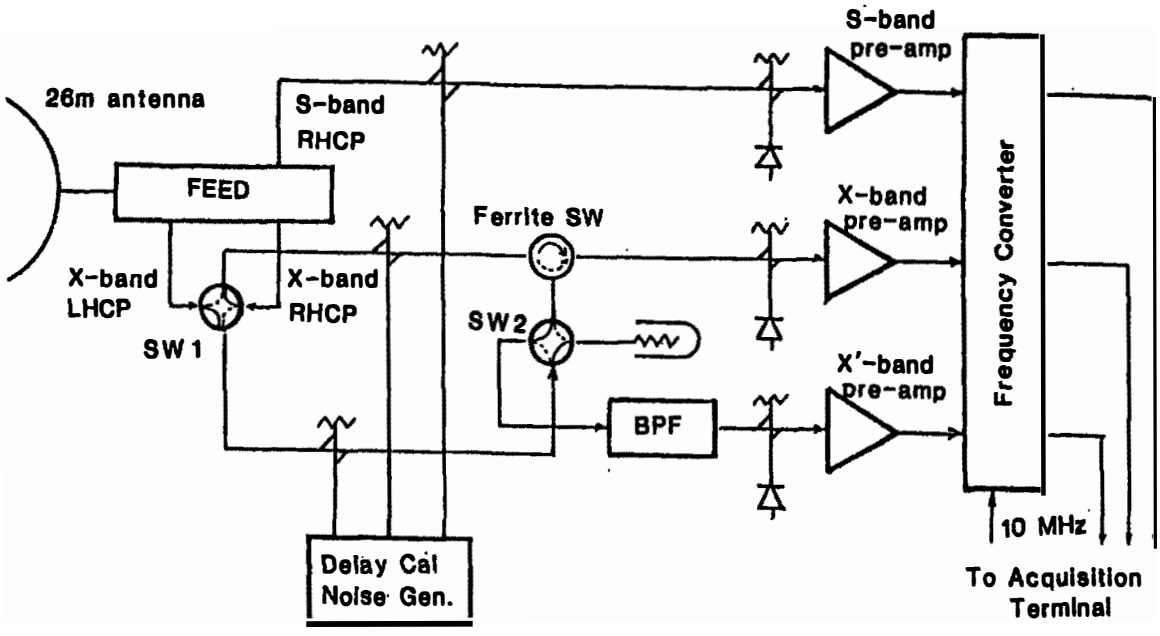

Figure 2. The block diagram of the feed and the S/X receivers

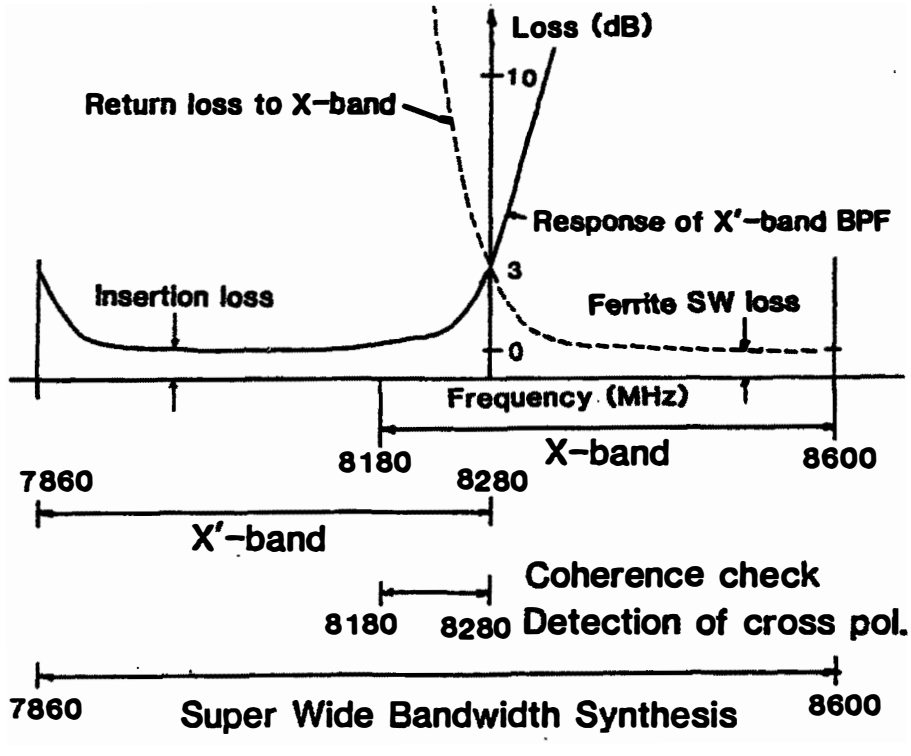

Figure 3. The frequency allocation of X- and X'-band

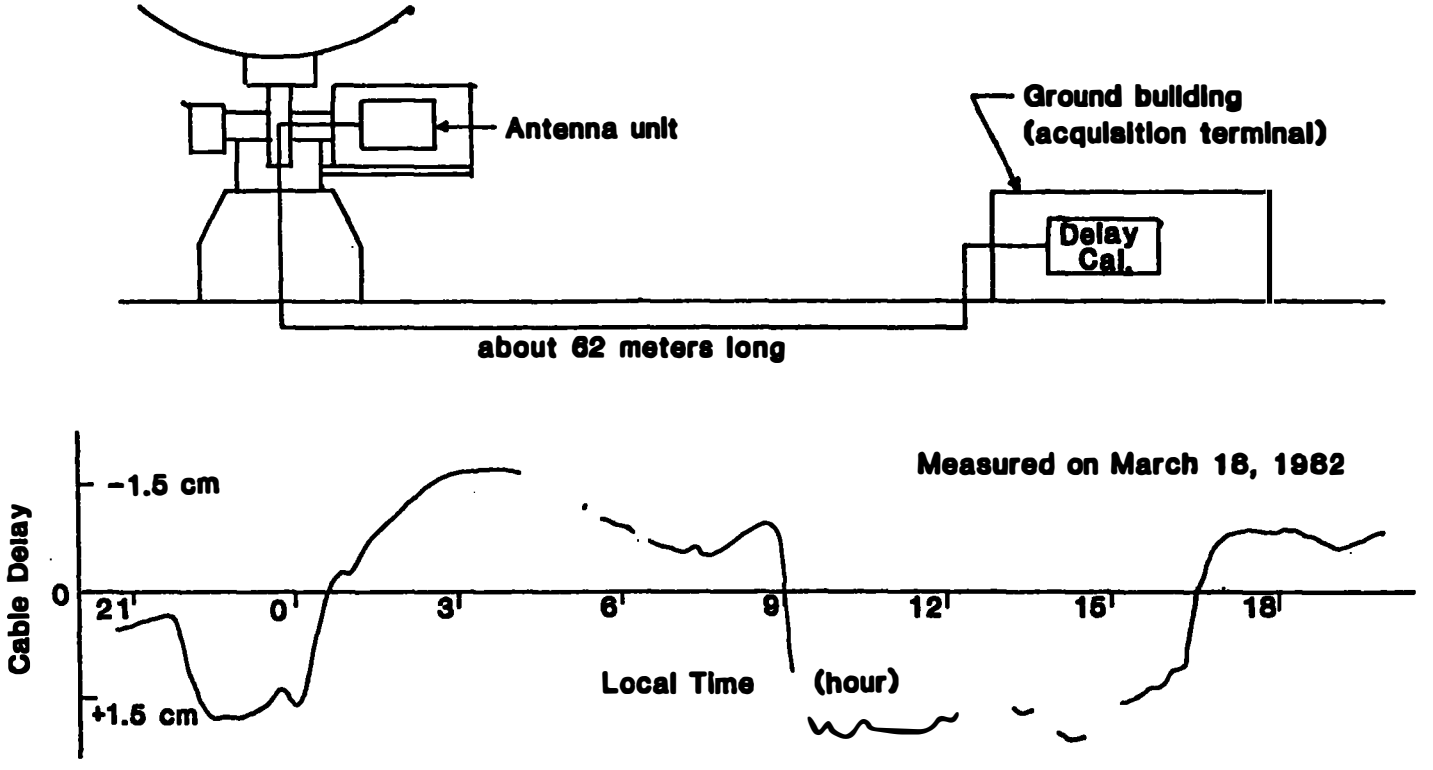

Figure 4. The measured cable delay variation over 24 hours

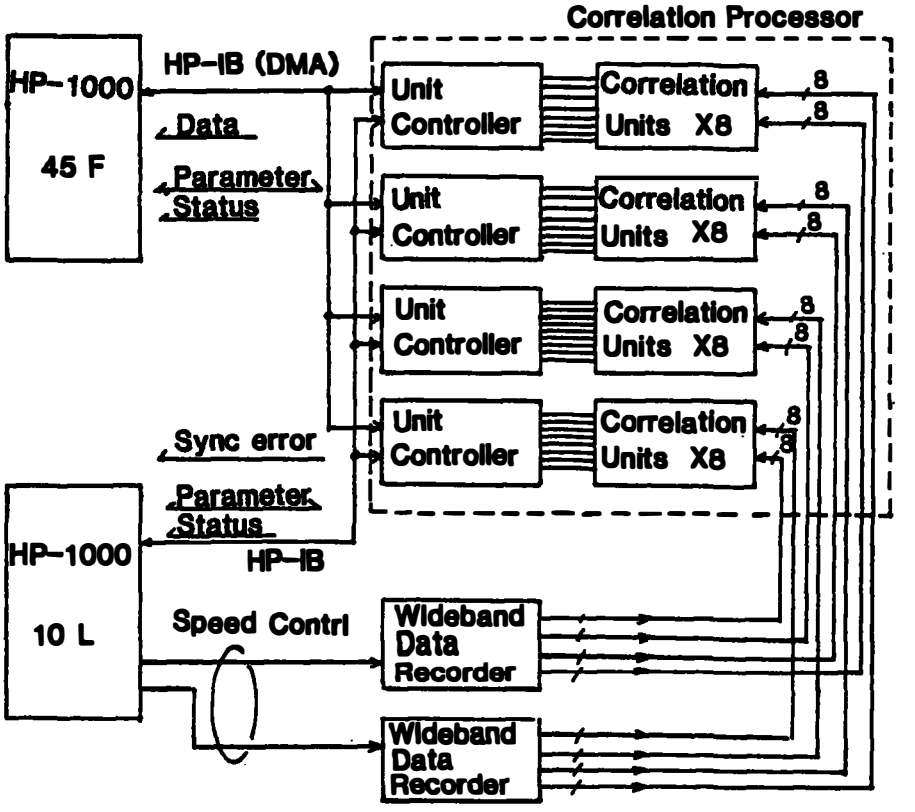

Figure 5. The correlation processing system

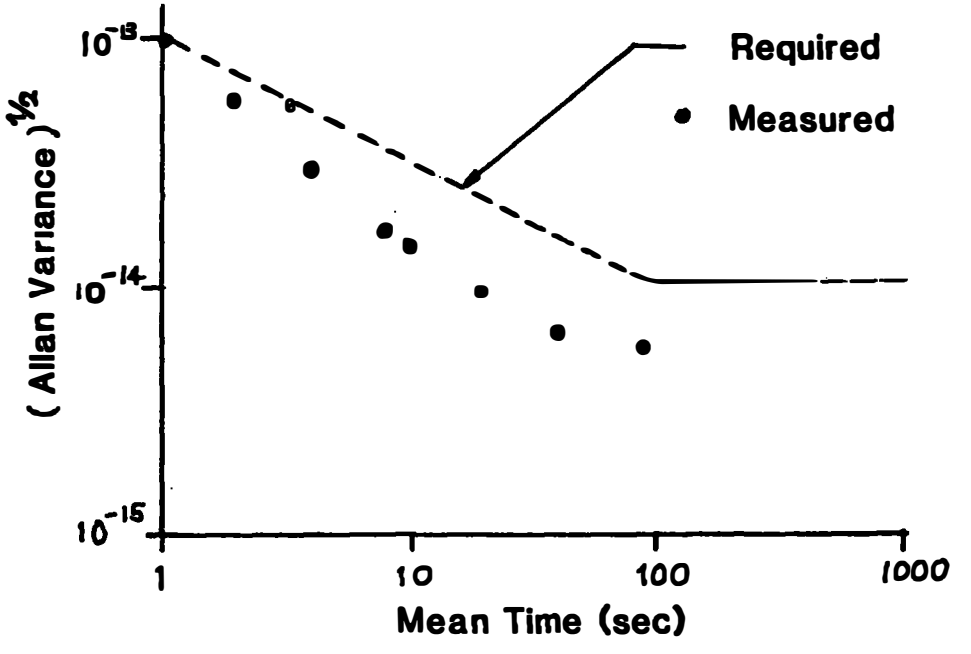

Figure 6. The performance of the prototype hydrogen maser oscillator

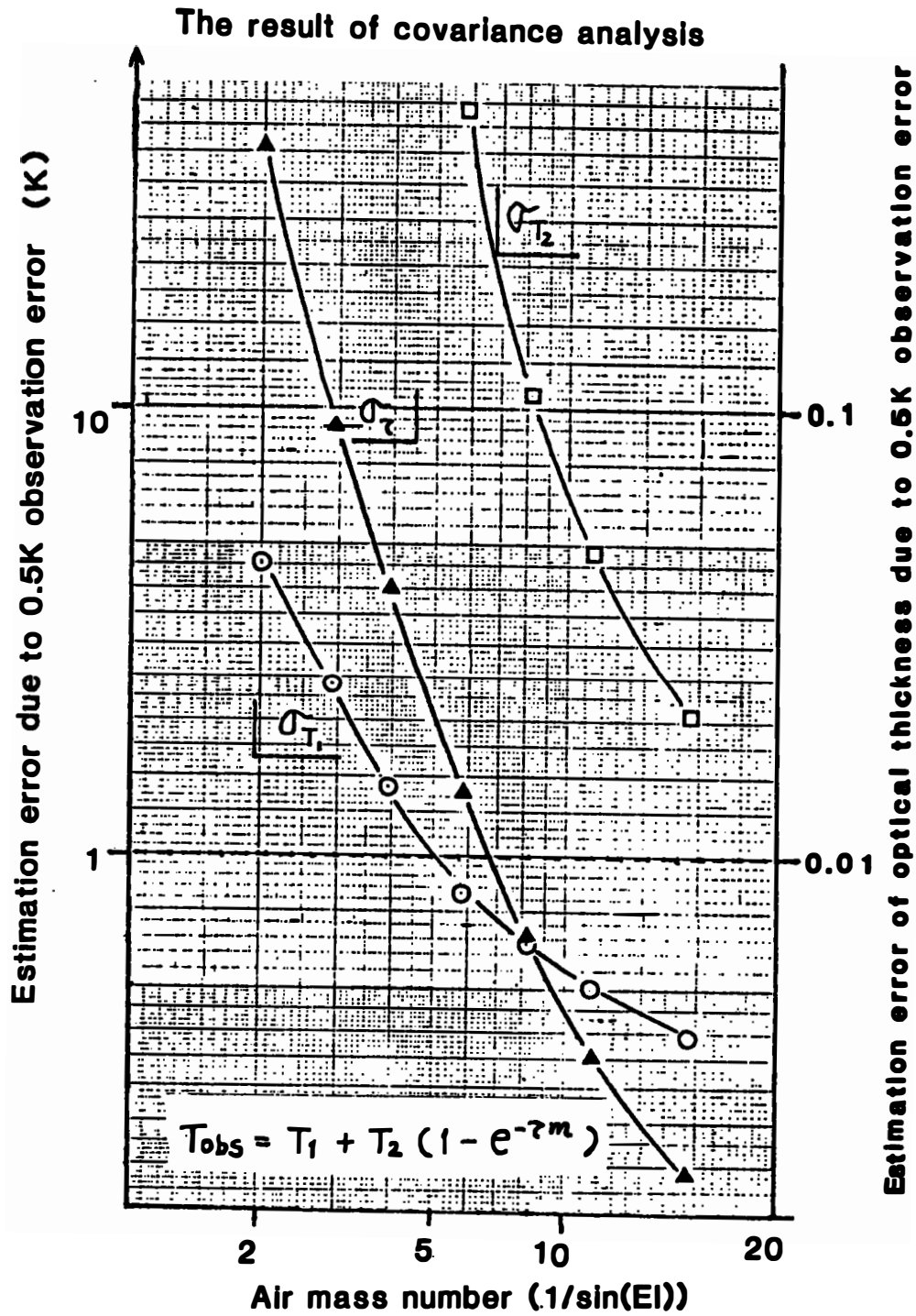

Figure 7. The result of covariance analysis on the tipping equation

Table 1. The position of the 26 meter antenna in SAO-C7 coordinate system

Latitude	:	140°39'45.H6
Longitude	:	35°57hi5"r1
Geoid height	:	77.08 meter

Table 2. Summary of electrical characteristics of the 26 meter antenna and the S/X receivers

item \ frequency	S-band	X-band
Frequency Range	2200-2320 MHz	8180-8600 MHz
Antenna Diameter	26 meter	26 meter
Aperture Efficiency	57 %	45%
Antenna Gain	52.8 dB	63.2 dB
Antenna Noise Temperature	70 K	60 K
Waveguide Circuit Loss	6 K	30 K
Preamplifier Noise	93 K	70 K
Total G/T	30.5 dBK	41.2 dBK

Table 3. The performance of the K-3 correlation processor

Number of Channels	32
Maximum Processing Speed	8 Mbps
Programmable Delay	enable up to 128 bits
Correlation Lags	complex 8 bit-lags
Integration Period	5 msec to 8.38 sec at 4 Mbps of data rate
Buffer Memory	20 Kbits
Fringe Rotation	
Phase Resolution	0.02 micro-radian
Phase Rate Resolution	0.93 mHz (Phase Acceleration Enable)
Rotation Pattern	3-level
Fractional Bit Correction	90 deg. phase jump

Table 4. The design of the operational hydrogen maser oscillator for the physics package

Magnetic shield	1.5 mm Permalloy, 4 shields
Magnetic shielding factor	15,000
Resonant cavity	27.5 cm dia. and 30.4 cm long
	Q_0 = 50,000
Storage bulb	18.0 cm dia. quartz
Temperature	cavity @ 49 ± 0.001 °C
State selector	hexapole magnet 7 kGauss
Collimator	multi channel collimator each channel 25 μm dia. and 0.5 mm long
Source gas pressure	0.1 Torr
Source bulb	3 cm dia. and 5 cm long pylex
Dimension	90 cm wide, 80 cm deep and 165 cm high
Weight	ca. 700 kg

Table 5. The design of the operational hydrogen maser for the electronics system

Power supply	AC 200V and AC 100V
Receiver	
Preamp.	2.2 dB N.F. commercial unit
1st mixer	Double balanced image rejection mixer commercial unit
L.O. Multiplier	phase locked multiplier commercial unit
Synthesizer	7×10^{-13} resolution, commercial unit
VCXO	HP10811B
10 MHz buffers	120 dB isolation
Gas pressure controller	custom made at RRL
P_d H_2 purifier	custom made at RRL
C-field	0 to 20 mGauss, regulated 1×10^{-5}
Signal outputs	10 MHz; +13 dBm, 50 ohm; 7 channels
	1 pulse per second TTL level; 2 channels
	Monitor signal

Table 6. The observation error estimation of the VLBI experiment between OVRO 40m and Kashima 26m

Error sourc	error	comment
Antenna and Receiving System	54 psec	1 Jy, 300 sec, Mode E
Hydrogen Maser Oscillator	18 psec	clock instability
Delay Calibrator	5 psec	time interval counter error of 1 micro-sec at 25 Hz
Wet Component Path Delay	38 psec	radiometer error of 1 K
Dry Component Path Delay	11 psec	pressure gauge error of 0.1 mbar
Phase Scintillation	6 psec	integration time of 300 sec
Total RSS	70 psec	about 2 cm

K-3 VLBI SOFTWARE DEVELOPMENT FOR INTERNATIONAL EXPERIMENTS

F.Takahashi, T.Yoshino, H.Murakami,

K.Koike, H.Kunimori, and T.Kondo

Kashima Branch, The Radio Research Laboratories
893-1 Hirai, Kashima, Ibaraki, 314 Japan

ABSTRACT. Since last year we have been developing VLBI software system for geodetic application. We call it "K-3 Software System". K-3 Software System has eight sets of software whose initial letters are all "K". The time limit of this development is the end of 1983 for the start of Japan-US joint experiments

INTRODUCTION

The Radio Research Laboratories(RRL) is developing the comprehensive K-3 Software System for the international VLBI experiments. Our main target is the centi-meter analysis of plate motion, polar motion, earth rotation and local crustal deformation. However, an immediate work is to succeed in Japan-US joint VLBI experiments.

At present the development of K-3 software is conditioned by next two factors. First one is that the time limit is the end of next year 1983 for Japan-US joint experiments. Second one is the existence of the strong and experienced Mark-III software. So we must have some principles not to fall into the imitation of others. Then we adopted next three stress-points of K-3 Software System.

1) Consistency of comprehensive data processing and analysis software
2) Compatibility between K-3 and Mark-III
3) Originality of the VLBI analysis in a Japanese group

We realize that the compatibility has a significance to supplement the common resources each other. By two points 1) and 2) we can get the minimum base of VLBI software and on this base we plan to stress the last point; the originality of a Japanese VLBI group.

OVERVIEW OF K-3 SOFTWARE

Fig.1 shows the general overview of K-3 software system. K-3 software is composed of three major software groups and three active software buses. In the first software group we have our scheduling software KASER and automatic operation software KAOS for K-3 hardware system. In the second group there are setting-up utilities KASET,

correlation software KROSS and bandwidth synthesizing software KOMBr In the third group we have an apriori model software KAPRI and least--square-determination software KLEARa

Among the Fig.(1)'s three software buses; the left one is the data-base system KASTL which is the common resources for the overall K-3 software. The next one is the scratch files or system commons which are not only commons but also temporary resources for each software groupr The right bus is the local common which is the original resource for each softwarer

We will use these three buses hierarchically and we are going to get the good prospect for our software design.

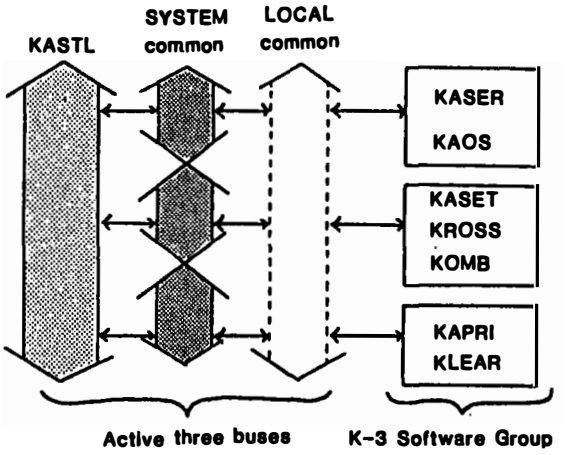

FIG.(1) OVERVIEW OF K-3 SOFTWARE SYSTEM

SCHEDULING SOFTWARE "KASER"

Scheduling software KASER of K-3 corresponds to Mark-III's SKED (Vandenberg, 1982ar). KASER, however, will have one important and different function from SKEDr This is an external optimum filtering function. Mk-IIIts SKED has many tools and utilities to make VLBI observation schedule easily. But we heard that the operator using SKED is apt to have the heavy load to optimize the schedule (Vandenberg, 1982b). We also think the design of the automatic software to do the optimization for it will be much heavier task for us.

In the K-2 antenna control software we already succeeded in designing the external filter for satellite tracking. Using this experience we can design the easy interface routine between KASER and external program. Therefore, we can depend on the specialist of schedule optimizing program. Fig.(2) shows the schematic illustration of the interface of KASER and this optimum filterr

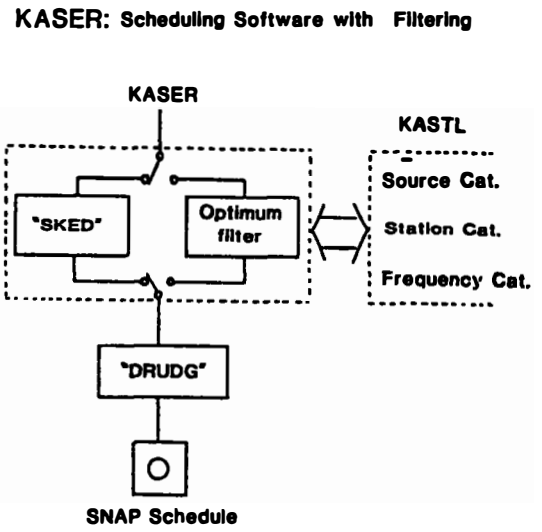

FIG.(2) SCHEMATIC FIGURE OF KASER

AUTOMATIC OPERATION SOFTWARE "KAOS"

Automatic Operation software KAOS corresponds to Mk-III's Field System(Vandenberg 1981). We already completed KAOS and we are checking and testing it.

KAOS controls many kinds of K-3 hardware (see Fig.(3)) using HP-IBr KAOS has next three strong pointsr The first point is the full compatibility between K-3 and Mk-III. The second is the exclusive adoption of HP-IB bus and ASCII protocol. The last one is the emergency measures using the Service Request function of HP-IB. KAOS can use the status word of SRQ and serial polling automatically. KAOS is the most important software for the success of Japan-US experiments.

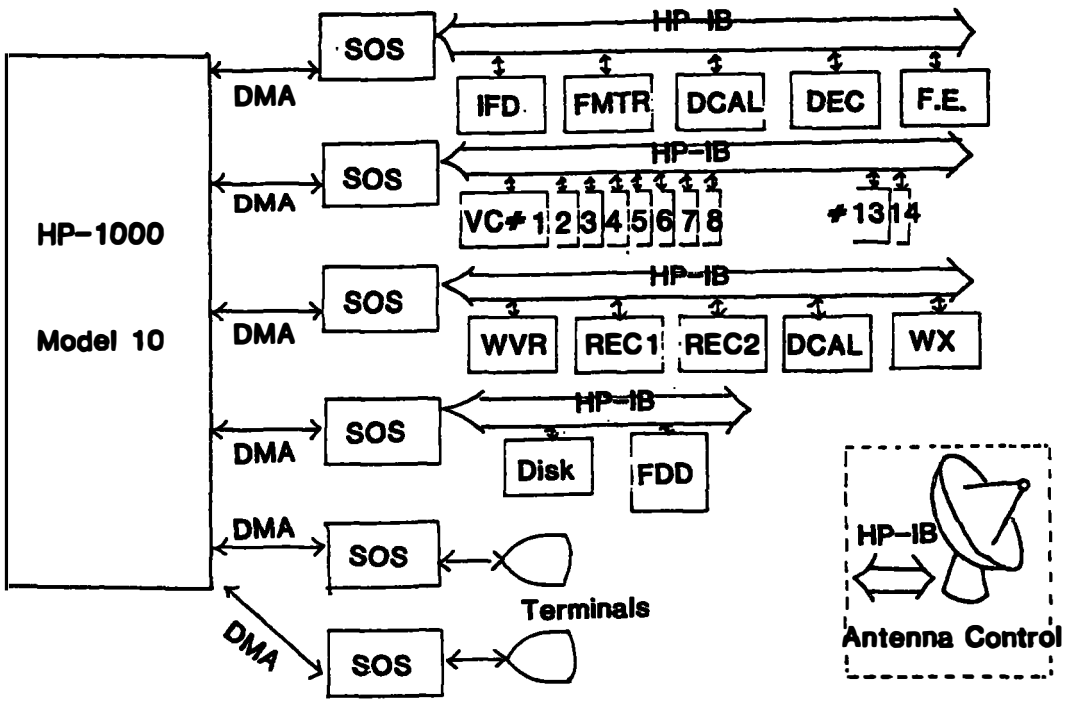

FIG.(3) AUTOMATIC CONTROL OF K-3 SYSTEM USING KAOS

DATA BASE SETTING-UP SOFTWARE "KASET"

The data base setting-up software KASET corresponds to Mk-III's DELOG, CALIB, UT1PM, EPHEM. We are designing KASET to unify these Mark-III's functionsr In other words, we plan to form the data base setting-up routines into single softwarer Since we can process and analyze VLBI data at one place Kashima, we can design this unified one like thisr KASET is divided into five sections shown in Fig.(4)r The first is the man-machine interface section for following four sectionsr The second section is extracting the information from SNAP log. The third is the data table setting of UT1 and polar motion form International Latitude Observatory of Mizusawa and TAIRRL and UTC from RRLr The fourth is setting the planetary ephemeris of Japanese Hydrographic Department. The last is the diagnostic section of setting-up data.

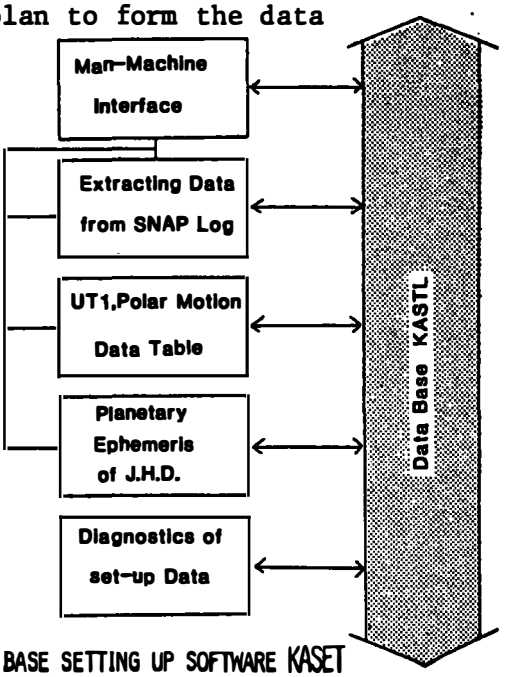

FIG.(4) DATA BASE SETTING UP SOFTWARE KASET

CORRELATION PROCESSING SOFTWARE "KROSS"

The cross correlation processing software KROSS corresponds to Mk-III's CORELr KROSS controls 32 channels of K-3 processing modules and two data recorderr Fig.(5) shows the hardware interfaces around KROSSr

We have an originality of I/O among correlator; data recorders; and two computersr We are also using the HP-IB=DMA interface between correlator and computers, while in Mark-III they are using the CAMAC type interfacer We believe the recent progress of HP-IB will show the merits of K-3 method in near futurer

KROSS can bring K-3 processor's ability into full play, especially, we can utilize the SRQ functions of HP-IBr We are also designing KROSS to be able to process the multi-baseline correlation including the multi-synchronization of data recordersr

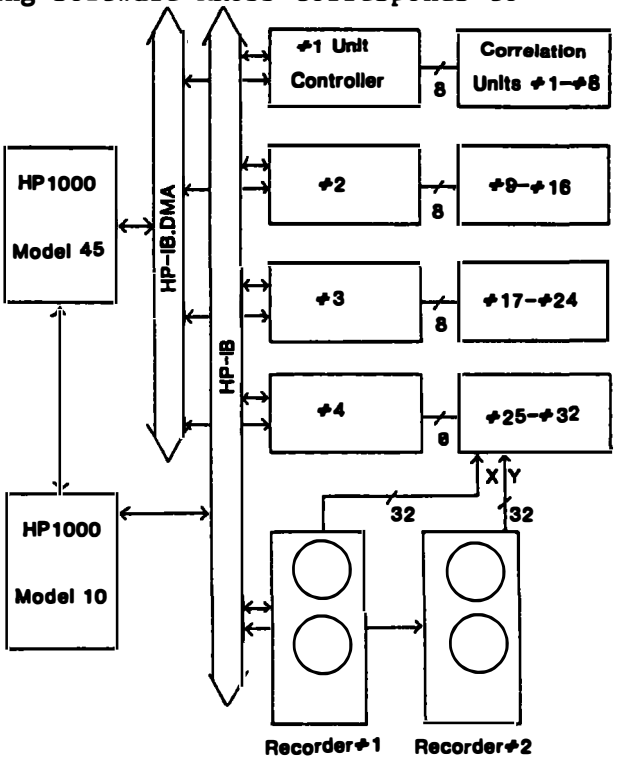

FIG.(5) CROSS CORRELATION SOFTWARE KROSS

BANDWIDTH SYNYHESIZING SOFTEARE "KOMB"

The bandwidth synthesizing software KOMB corresponds to MarK-III's FRNGEr We named this software KOMB to show the alignments of narrow bandwidths as an analogy of the hair combr This software is mainly divided into two sections as shown in Fig.r(6)r One section is the single frequency coarse search section and the other is multi-frequency fine search section. KOMB can also archive the processed data in the format of A and B tape at Haystack and NGS format for MERIT campaign because K-3 database will have both the processed and analyzed data.

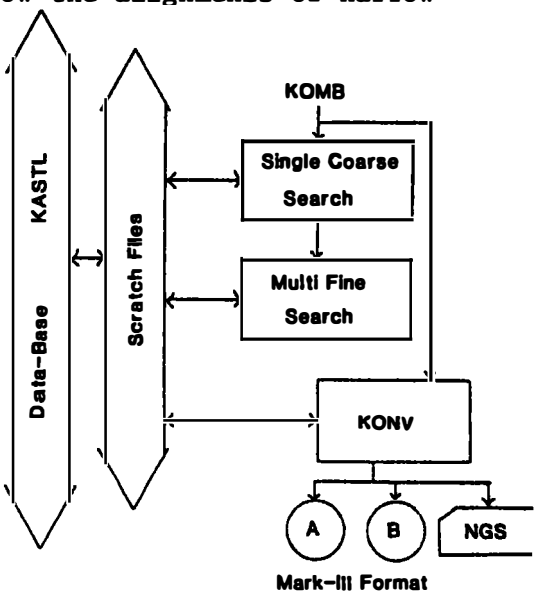

FIG.(6) BANDWIDTH SYNTHESIZING SOFTWARE KOMB

APRIORI MODEL SOFTWARE "KAPRI"

The apriori model software KAPRI corresponds to MK-IIIrs CALC software. Mk-IIIrs CALC has very clear designing thought and also has well-moduled structure so one can manage the operation history of CALC surelyr We are learning many things from Mk-III's CALC and we plan to develop KAPRI on the basis of CALC.

We are cooperating with International Latitude Observ-atory of Mizusawa(ILOM) and they proposed the unified phy-sical model of earth rotation and its partial derivatives consider-ing both the deformable Earth and the liquid core resonance in Earth for our KAPRIr The values computed by KAPRI will be used in following least-square estimating software KLEAR. KAPRI also computes the ocean loading effect on Kashima because Kashima is very close to the Pacific Ocean.

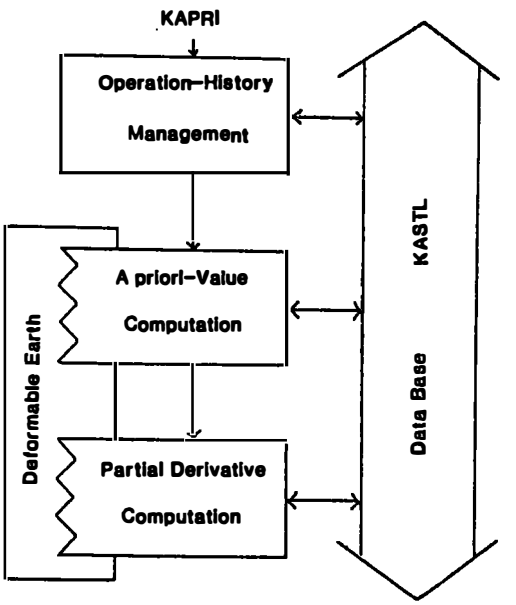

FIG.(7) APRIORI MODEL SOFTWARE KAPRI

LEAST SQUARE ESTIMATION SOFTWARE "KLEAR"

The baseline analyzing software KLEAR corresponds to SOLVE of MK-III. We are designing KLEAR to consider that the nutation analysis is very important for precise geodetic application. KLEAR will be able to estimate the effects of the liquid core resonance on the nutation.

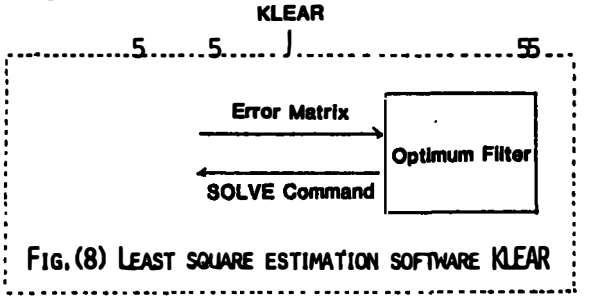

FIG.(8) LEAST SQUARE ESTIMATION SOFTWARE KLEAR

KLEAR also has the interface routines between MK-III's SOLVE and external optimum filter as shown in Fig.(8). Therefore we can depend on the specialist about the program of estimation optimizing procedures. The filter's input is the error matrix for SOLVE and the output is the MK-III's SOLVE-like machine-callable commands.

Beside the baseline analysis, we will use this KLEAR for international time synchronization and for the researches of the propagation effects of both ionized and neutral atmosphere.

DATA BASE SYSTEM "KASTL"

We named our data base system KASTL after Japanese castle's multi-storied structure. We plan to use the general purpose data-base system; H.P.'s IMAGE/1000 for our KASTL. Using IMAGE we can describe a suitable schema for our KASTL and utilize the various kinds of data-base handling tools prepared by H.P., especially the computer-networked data-base utilities. Fig.(9) shows our "future plan" of KASTL. KASTL will be connected to Geographical Survey Institutes of Japan and International Latitude Observatory of Mizusawa via X.25 protocol of Distributed System-/1000 and also it may be connected with the foreign system by the satellite communication liner

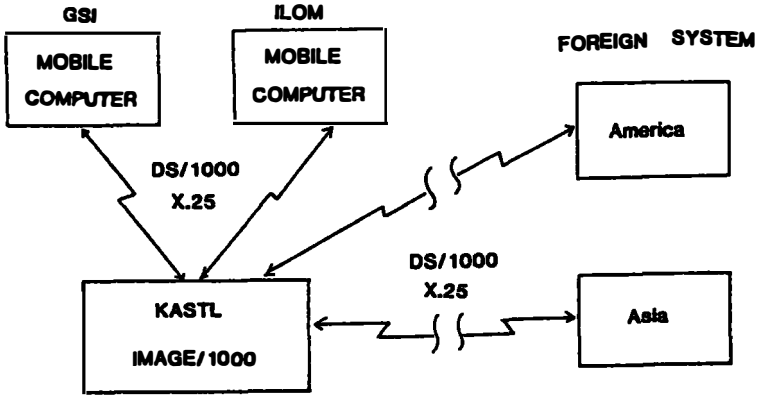

FIG.(9) INFORMAL "FUTURE PLAN" OF DATA BASE KASTL

CONCLUSION

Now we conclude with a few general remarks on the compatibility between K-3 and MK-III software. We plan to have next five compatibility pointsr The first is the observation schedule using SNAP commands The second is the observation logging file using SNAP log formatr The third is the high density data tape formatr The fourth is the A and B tape format after the bandwidth synthesis. And the last is the NGS card image formatr

Acknowledgement

In closing, we wish to express our great appreciation to MK-III's staffs of NASA,GSFC, and Haystack for the offer of their valuable software to Radio Research Laboratories.

Reference

(1) Vandenberg, N, Oct.1981, : FIELD SYSTEM Ver.4.0, MARK-III SOFTWARE DOCUMENTATION

(2) Vandenberg, N, Feb.1982a, : SKED INTERACTIVE SCHEDULING PROGRAM, MARK-III SOFTWARE DOCUMENTATION, SKED-1-33

(3) Vandenberg, N, Feb.1982b, : Personal information

JPL/CIT BLOCK II VLBI PROCESSOR

David H. Rogstad
John C. Peterson

Correlation Systems Group
Jet Propulsion Laboratory
California Institute of Technology
Pasadena, California

Abstract

Users of VLBI at JPL and CIT are jointly funding and implementing a Mark III compatible VLBI correlation processor. This processor, referred to as Block II, will begin operation by fall of 1982.

The Block II design is based on the JPL/CIT Mark II Processor and makes extensive use of RAM, ROM and programmable array logic to implement its various functions, with control and modelling done in bit-slice microprocessors. The output lag-data are fast fourier-transformed (FFT) once per 100,000 bit times, and various phase corrections applied. The corrected data are accumulated in RAM where a two dimensional FFT is performed to accomplish coherent integration over frequency and time.

The processor has been designed to operate up to 8 Mbits per second. It is controlled by a DEC VAX 11/780 computer, which is also used to perform all post-correlation analysis.

I. Introduction

The Deep Space Network and the Geodynamics Project at the Jet Propulsion Laboratory (JPL) together with the VLBI Radio Astronomers on the campus of the California Institute of Technology (CIT) are jointly funding and implementing a Mark III compatible VLBI Correlation Processor. This processor, referred to as the Block II, will be located in the Astronomy Data Processing Facility on the CIT campus.

This paper describesthe principle characteristics of the Block II, and presents several block diagrams showing the processor's overall design features and functional operation. Figure 1 indicates the personnel at JPL and CIT who are responsible for the design and implementation of the processor subsystem. In addition, some of the main goals that have influenced its design are listed, together with the desired completion date of fall-1982. The uses for such a processor include the normal astronomical applications of source survey and source structure, as well as the more recent and exciting application of geodesy.

II. Principle Characteristics

The principle characteristics of the Block II Processor are summarized in figure 2. These include:

- compatibility with the Haystack/Goddard Mark III tape format, consisting of 28 parallel tracks of up to 4 megabits/sec data rate, permitting a user to process Mark III tapes at either facility;

- a 3 station correlation capability with spare modules in such a configuration that processing of 4-station data is possible, and with the added feature that expansion to 7 stations can be easily accomplished;

- ganging of the eight delay-lags in each frequency channel with those in adjacent channels so that processing of at least one channel can be performed with as many as 224 lags, or 112 independent frequency bins after fourier transformation;

- geometric delay for each station/channel accomplished in digital hardware using RAM, rather than by time-synchronizing the data tapes relative to one another with time offsets (the present RAM consists of 16k x 1 chips giving delays of 0 to 32 millisec in each station module, upgradable to 256k x 1 chips by simple replacement, giving 0 to 512 millisec of delay);

- geometric model phase and delay updates performed in microprocessors built into the processor hardware using cubic interpolation for the phase and linear interpolation for the delay, in order to remove the model computing load from the processor control computer (also being used for post-correlation processing);

- PERSONNEL
  - HARDWARE - J. PETERSON, B. RAYHRER, M. EWING
    J. DILLON, B. ESPINOZA
  - SOFTWARE - D. ROGSTAD, W. HAMMOND, J. VAVRUS
- GOALS
  - GSFC/HAYSTACK MARK III COMPATIBLE PROCESSOR
  - EXPANDABLE TO AT LEAST 7 STATIONS
  - PROTOTYPE FOR VLBI ARRAY PROJECT
  - USED FOR SURVEY, SOURCE STRUCTURE, GEODESY
  - 3 STATION OPERATION BY FALL, 1982

Figure 1. Block II Implementation Personnel and Goals

- MARK III COMPATIBLE DATA INPUT FORMAT
- 28 FREQ. CHANNELS, 3 STATION (EXPANDABLE TO 7)
- 8 LAGS/CORRELATORS, GANGING UP TO 224 LAGS
- GEOMETRIC DELAY IN HARDWARE (0-32 ms, EXP. TO 512 ms)
- DELAY AND PHASE UPDATES IN MICROPROCESSORS
- FFT AND FRACT. BITSHIFT CORRECTION IN MICROPROCESSORS
- INTEGRATION INTERVALS FROM 10^5 TO 10^9 BIT-TIMES
- 4 MULTILEVEL (127) TONE-EXTRACTORS/CHANNEL
- PHASE-CAL DETECTED/APPLIED IN REAL-TIME
- COHERENT-INTEGRATION OF FRINGES IN H/W (TENSOR)
- PROCESSING OF ORBITAL VLBI DATA
  - FRINGE RATES FROM 0 UP TO 1 CYCLE/BIT-TIME
  - DELAY RATES UP TO 40 BITS/MEGABIT-TIME
- PROCESSING RATE OF 8 MEGABITS/SEC

Figure 2. Principle Characteristics

- Fourier transformation from the lag (delay) domain into the frequency domain, together with correction of the phase for the fractional-bit-shift error made between pairs of stations, accomplished every 100,000 bit-times, in order to set up for the coherent integration across frequency channels;

- extraction of up to 4 phase-cal tones in each frequency channel for each station, using multilevel tone rotators simultaneously with normal processing, and application of these phase-cal data to the correlated data in real-time;

- coherent integration of the correlated data across frequency channels and time within the Tensor hardware to produce bandwidth synthesis delay and delay-rate in real-time;

- capability of handling the phase and delay rates that are required to process VLBI data taken with antennas orbiting the earth;

- capability of processing either 8 megabit/sec data or lower bit-rate data at faster than real-time rates.

Alltof these characteristics have been implemented to provide the power and flexibility required by the users who are funding the project. A further goal has been to implement a processor with the latest LSI and VLSI technology that can then serve as a basis for any future correlator development, particularly the NSF VLBI Arraying project. A VLSI development project is presently in progress at JPL to produce a single correlator chip containing 16 lags plus 20 bits of accumulation running at a maximum rate of 16 megabits per second. This chip should be available by the end of 1983.

III. Functional Overview

The architectural design of the Block II Processor has been based on the CIT/JPL Mark II Correlator located on the CIT campus. Block II consists of 28 of these Mark II type processors running in parallel, controlled by a VAX 11/780 computer, as shown schematically in figure 3. Each of the 28 processors handles the data received from an individual track on the up-to-four input tape transports.

Figure 4 shows a block diagram of one of the 28 channel processors, with the functions performed by each module. Separate control from the VAX computer is provided for the station modules and the correlator modules. The bit-stream from each tape transport is read into its corresponding station module, where bit-clock and data-frame synchronization is obtained. Then the data are written into dynamic RAM for accomplishing the necessary station delay. At the appropriate time, the data are read out and sent to the station phase-calibration circuitry as well as over to the correlator modules. The phase-cal module consists of four tone-generators that are multiplied against the data stream for detecting any phase-cal tones inserted for calibration. The delay models, as well as the frequencies of the tone-generators, are determined by the VAX driver computer.

The correlator modules receive data from a pair of station modules for the purpose of cross-correlating these data. Additional functions performed

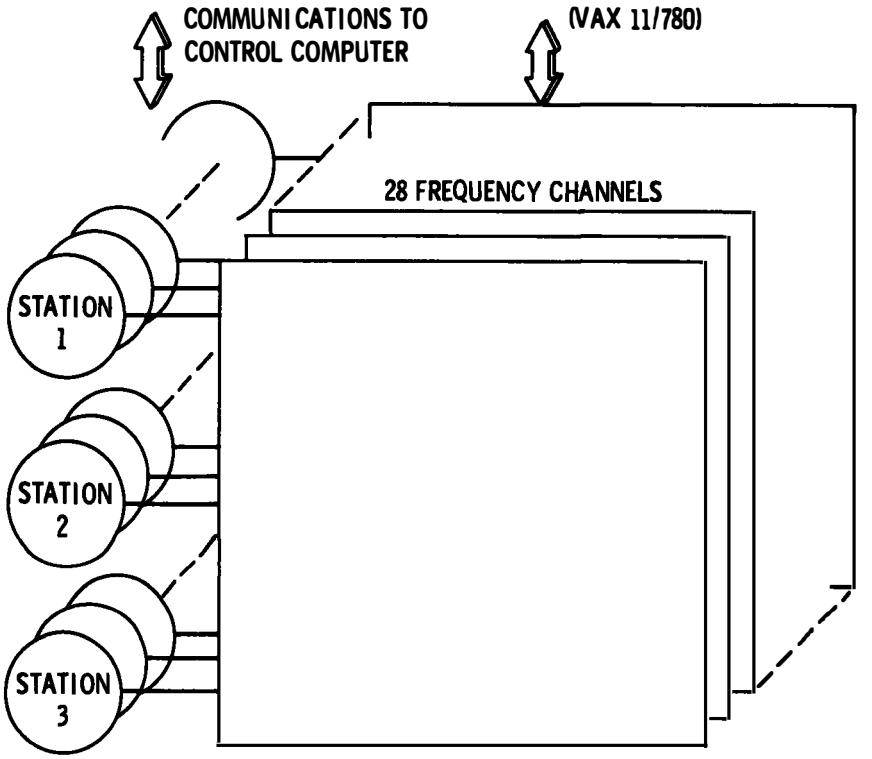

Figure 3. Processor Overview

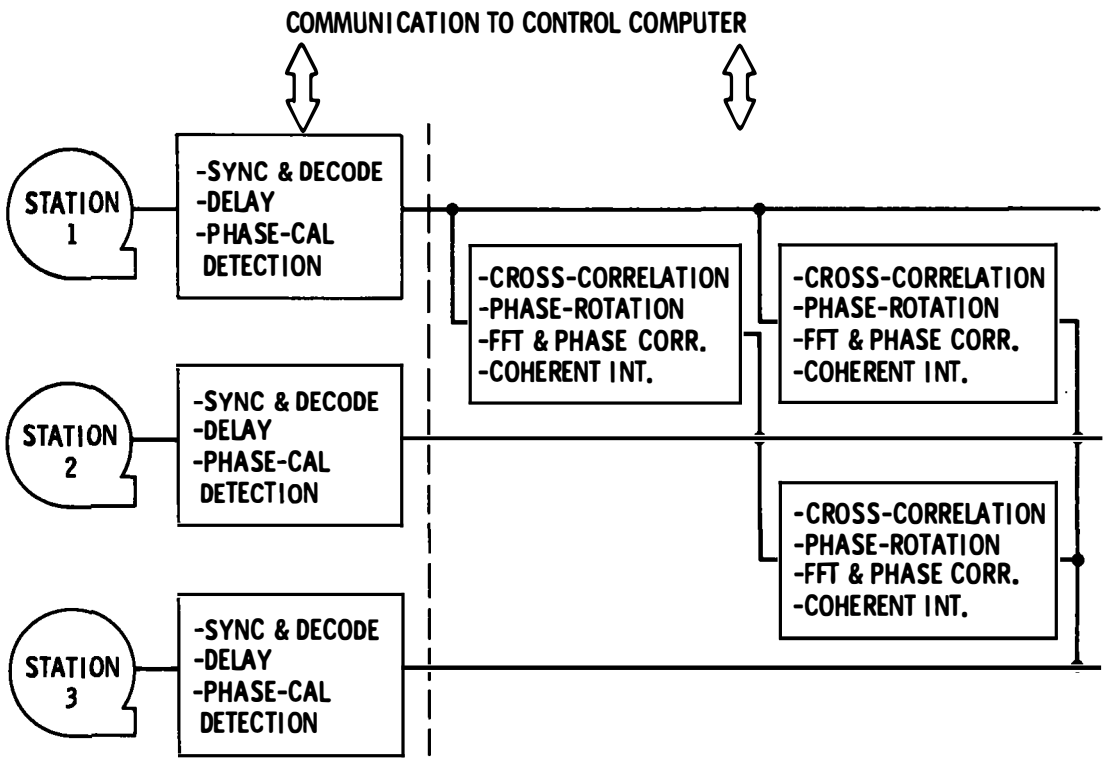

Figure 4. Block Diagram of Single Frequency Channel

include phase-rotation of the correlated data to compensate for frequency doppler-shift due to the earth's rotation; fourier transformation of the delay-lag data into the frequency domain and application of a fractional bit-shift phase correction as well as the phase-cal corrections obtained in the station modules; and finally, accumulation in the Tensor modules for the coherent integration operation. The FFT operation from delay to frequency space occurs once every 100,000 bit-times in order to minimize the effects of delay smearing.

IV. Some Details

More detailed block diagrams of the station and correlator modules are found in figures 5 and 6. Both of these modules are built around AMD 2903 bit-slice microprocessor technology for performing the control, model generation and model updating functions, a well as interfacing to the VAX control computer.

The station module in figure 5 actually resides within the electronics rack housing the tape transport. Data from a tape track are input to the sync and decode circuitry, which provides feedback to the transport for bit and frame sync control as well as time-of-day information to the VAX for multiple transport time-sync. The synchronized data are then written into dynamic RAM for delay. These data are read from the RAM under control of the model delay contained in the delay register, and then passed onto the correlator module. The delay line consists of eleven 16k x 1 RAM chips, providing up to 32 millisec of delay for the data and the data control signals. The tone phase rotators used to detect the phase-cal calibration tones receive the same data as are sent to the correlators. These data are used as one of the address bits, along with the eight high-order bits of the phase number contained in the phase register, pointing into the ROM for obtaining the product of tone sinusoid and the VLBI bit-stream data. This result is then accumulated for 100,000 bit-times in preparation for being sent off to the correlator module, and used to correct the correlated data for phase-cal.

The correlator module is shown in figure 6. The input to this module consists of two streams of VLBI data and two streams of phase-cal data. The VLBI data from stream #1 are delayed by plus or minus one bit to correct for the delay error sometimes made from quantization effects in the hardware implementation of the model delay. The data are then passed through an eight-lag shift register to obtain the spread in delay required for processing. The VLBI data from stream #2 are delayed sufficiently to place the zero delay-lag near the mid-point position, and eight multipliers take the product of the two bit-streams and the correlation phase-rotation siusoids. The results are accumulated for 100,000 bit-times and then sent to the FFT microprocessor for transforming and application of corrections. The phase register for the correlation doppler-phase correction is 64 bits long to accommodate the cubic interpolation algorithms with minimal errors.

As indicated in figure 6, the correlated data is passed on to the Tensor memory for performing coherent integration of the fringes. This circuitry consists of large amounts of RAM storage, a 2903 bit-slice microprocessor for FFT, and a MC68000 microprocessor for performing alltof the control and data manipulation needed to perform the integration function. After

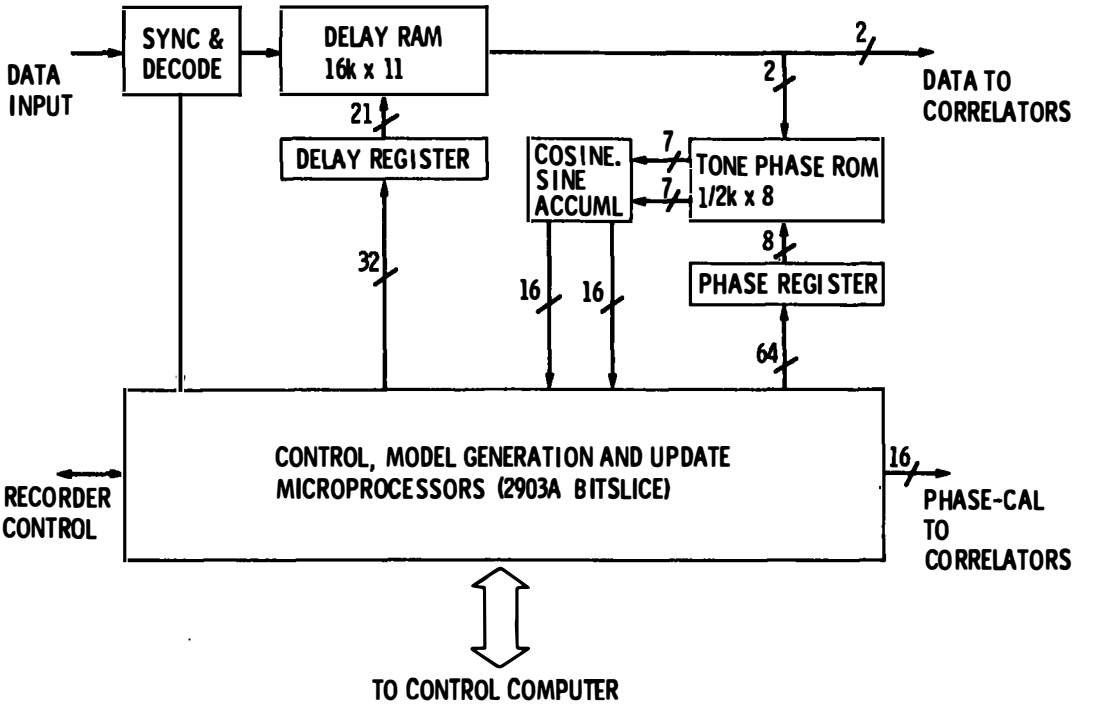

Figure 5. Schematic Diagram of Station Module

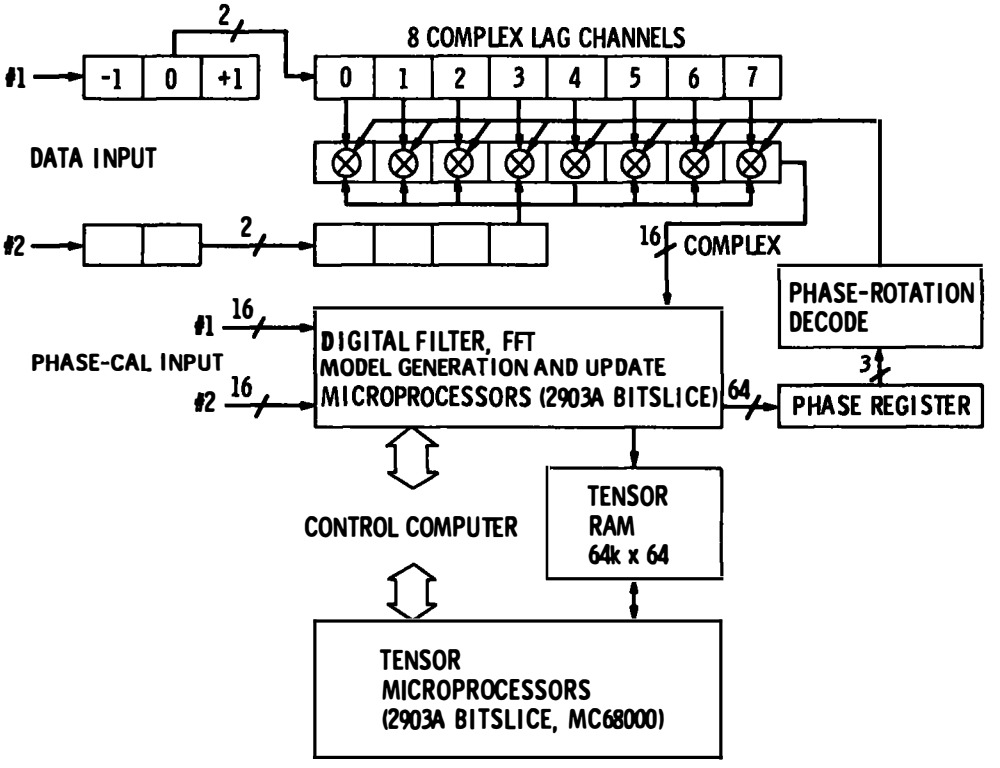

Figure 6. Schematic Diagram of Correlator Module

transformation, selected portions of the data are sent to the VAX for post-correlation processing.

The delay and phase model update algorithms are summarized in figure 7. These provide a hardware implementation of cubic interpolation for phase, and a linear interpolation for delay. The same algorithms are used in the station and the correlator module microprocessors. As seen in the figure, model phase parameters, including phase, three time-derivitives of the phase, and a delta-phase for correction when the delay changes by one bit, are supplied by the VAX to the processor hardware and loaded into the appropriate registers. Then, once every 5000 bit-times, the various derivitives are added appropriately to accomplish the cubic interpolation. The 64-bit wide registers guarantees that the phase is always accurate to better than 1 part in 10,000 for as long as 20 second of time with baselines as large as 1,000,000,000 wavelengths. The delay algorithm need only be linear, with delay and delay-rate coming from the VAX, and updates in the hardware occurring every 100,000 bit-times for normal processing, and every 5000 bit-times for orbital VLBI.

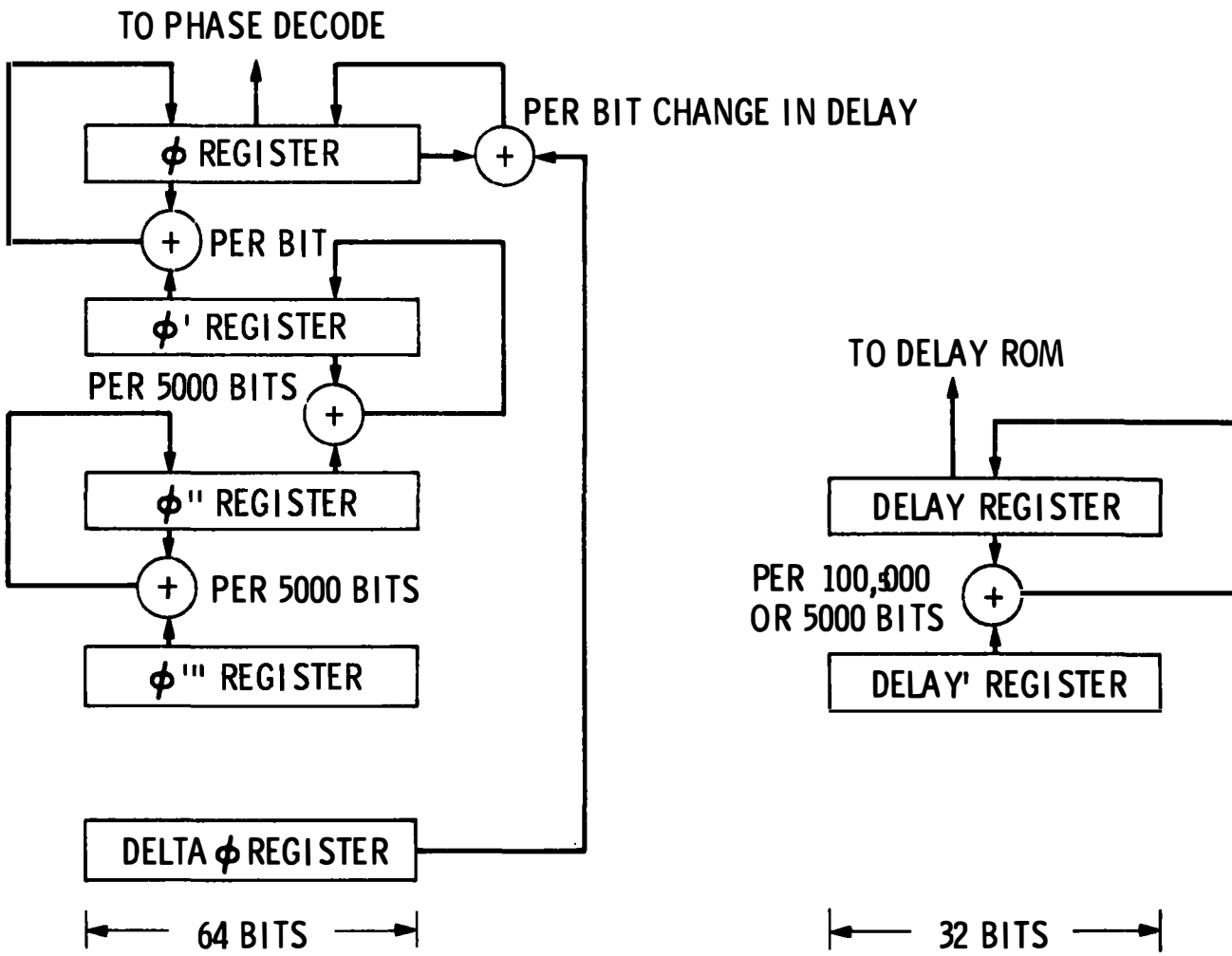

Figure 7. Model Update Algorithms

Water vapor radiometry: APPLICATION TO GEODETIC RADIO INTERFEROMETRY

G. Elgered

Onsala Space Observatory
Chalmers University of Technology
S-43900 Onsala, Sweden

ABSTRACT. The accuracy of geodetic radio interferometry experiments has now reached a level where one of the main errors is the excess propagation path caused by water vapor through the troposphere. The most promising instrument to measure this excess propagation path is the Water Vapor Radiometer (WVR). A WVR has been constructed at the Onsala Space Observatory and is now dedicated for radio interferometry experiments. The WVR measures the sky brightness temperatures at 21.0 and 31.4 GHz. These parameters can give a value of the wet path delay with a formal accuracy around 0.5 cm in the zenith direction for a large percent of the time. This accuracy has been derived from comparision measurements with the WVR, radiosondes and an infrared spectral hygrometer.

INTRODUCTION

Refractive index

The time of arrival for radiosignals propagating through the troposphere is affected by variations in the refractive index along the path. The refractive index at radio frequencies can be written as (Smith and Weintraub 1953)

$$n = 1 + 10^{-6}(77.6 * P/T + 3.73 * 10^5 * e/T^2). \quad (1)$$

P and e are in millibars and symbolize the total pressure and the partial pressure of water vapor, respectively. T is the absolute temperature in degrees Kelvin.

Excess propagation path

Instead of the delay in the time of arrival, it is equivalent to define the excess propagation path, ΔL, as

$$\Delta L = 10^2 \int_{h_0}^{\infty} (n - 1) / \sin \theta \cdot dh. \quad (2)$$

where ΔL is in centimeters if the height h is expressed in meters. The ground level height is h_0 and θ is the elevation angle of the propagation path. Inserting equation (1) in equation (2) gives by the hand that ΔL consists of two components. The first (dependent on the total pressure and about 2.3 meter in the zenith direction) is almost constant and the existing variations are easy to calculate from ground pressure measurements (Moran and Rosen 1981).

For the second term, often called the wet path delay, it is difficult to achieve high accuracy by using traditional meteorological measurements at the ground. The explanation is the low correlation between the water vapor density at the ground with that at higher altitudes. It is believed that unknown variations in the wet path delay contribute with one of the principal errors in the geodetic parameters determined in a Very Long Baseline Interferometry (VLBI) experiment (Shapiro 1976). The demand for continuous observations of the wet path delay towards any arbitrary point in the sky can be met by using microwave radiometry.

A water vapor radiometer

A microwave radiometer designed to be sensitive to water vapor is generally called a Water Vapor Radiometer (WVR). Several such instruments have been constructed (Guiraud ett al. 1979, Moran and Rosen 1981, and Resch 1982)t The main differences between the existing WVR:s are the front-end calibration networks and the frequency bands to be observedt Primarily one frequency close to the water vapor line at 22.235 GHz is needed, but to be able to make good observations in the presence of liquid water (clouds) in the atmosphere a second frequency is necesarry.

Brief theory and approximations

The theory given by Wu (1979) relates the two sky brightness temperatures at the frequencies f_1 and f_2 , measured with the WVR to the wet path delay. The result is that when the sky brightness temperatures, T_{A,f_1} and T_{A,f_2}, have been linearized to T'_{A,f_1} and T'_{A,f_2} the following linear relation is obtained:

$$\Delta L_w = \frac{172.3}{W'}\left[(T_{bg}(f_2^{-2} - f_1^{-2}) - T'_0) + \frac{T'_{A,f_1}}{f_1^2} - \frac{T'_{A,f_2}}{f_2^2}\right] \qquad (3)$$

In this relation there are some hidden approximations, namely:

1. The linearization of the measured sky brightness temperatures are made with the expression

$$T'_{A,f} = T_{bg} - (T'_{eff} - T_{bg}) \cdot \ln\left(1 - \frac{T_{A,f} - T_{bg}}{T_{eff} - T_{bg}}\right) \qquad (4)$$

where T_{bg} is the cosmic background radiation of about 2.8 K,

$$T_{eff} = \frac{\int_{h_0}^{\infty} T \alpha e^{\tau(h,\theta)} dh}{\int_{h_0}^{\infty} \alpha e^{\tau(h,\theta)} dh} \qquad (5)$$

τ is the opacity of the atmosphere defined as the integral of the total atmospheric attenuation coefficient along the propagation path,

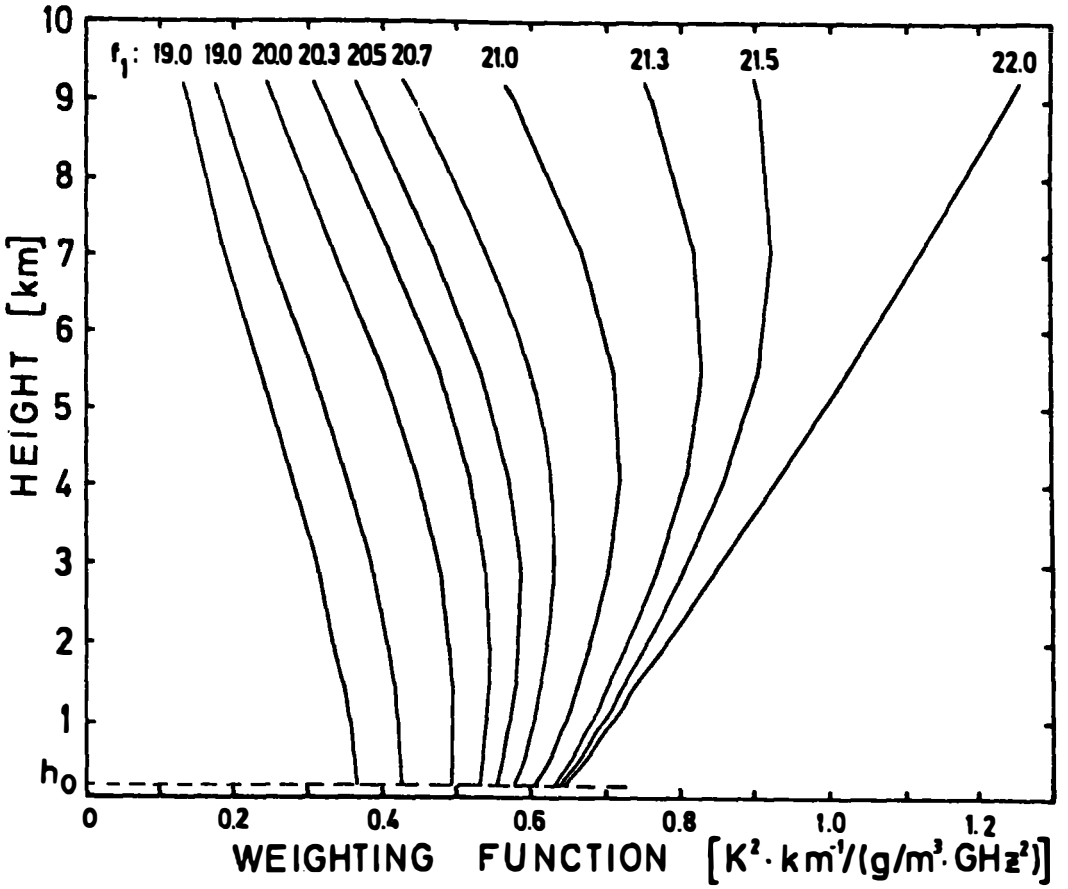

Figure 1. The weighting function for different values of the frequency f_1 when f_2 is held constant at 31.4 GHz, calculated for an atmospheric mean profile from May, 1980 to February, 1982.

$$\tau = \int_{h_0}^{\infty} \alpha(h)/\sin\theta \, dh \tag{6}$$

and

$$T'_{eff} = \frac{\int_{h_0}^{\infty} T\,\alpha \, dh}{\int_{h_0}^{\infty} \alpha \, dh} \, . \tag{7}$$

The parameters T_{eff} and T'_{eff} can be predicted from ground temperature measurements but this introduces an error. To minimize these errors the daily maximum temperature should be used. A one sigma error of about 3 K will then be obtained for T_{eff} and T'_{eff}. This error implies an error less than 0.3 K for sky brightness temperatures below 90 K. However, this approximation is of great importance when rain or heavy rainclouds are present.

2. The so called weighting function W', which is written

$$W' = \frac{T(T - T_{bg})}{a} \cdot \left(\frac{\alpha_{v,f_1}}{f_1^2} - \frac{\alpha_{v,f_2}}{f_2^2} \right), \tag{8}$$

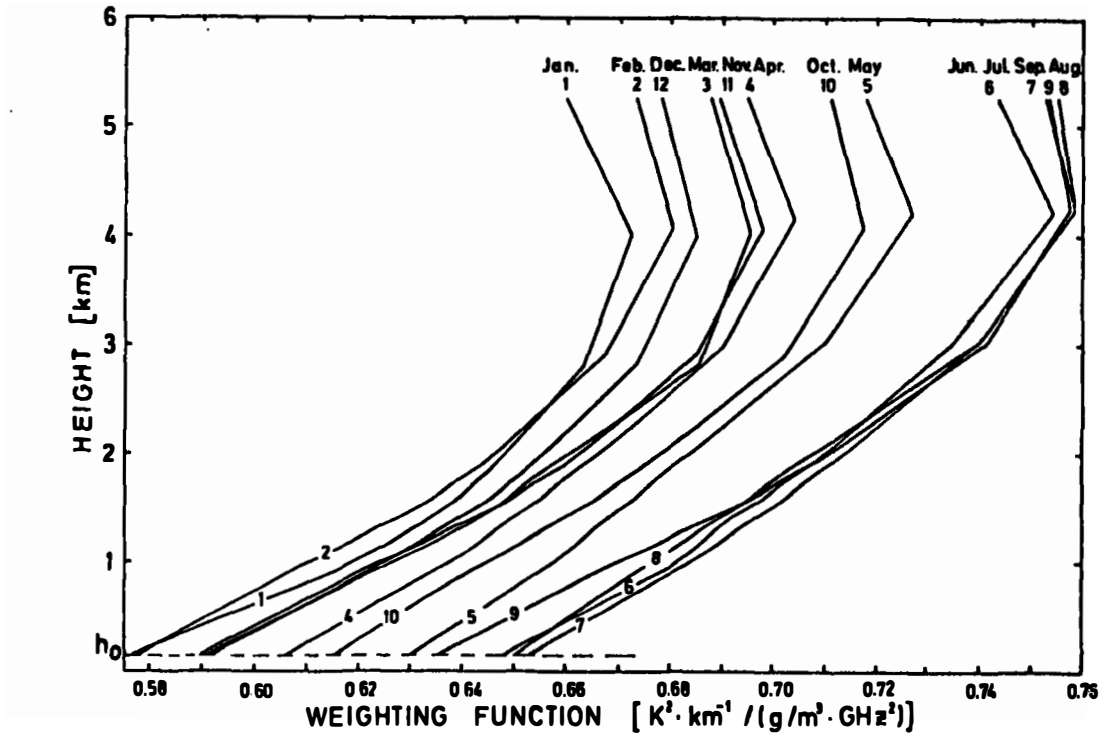

Figure 2. The monthly means of the weighting function for the frequencies 21r0 and 31r4 GHz, from May, 1980, to April, 1981r

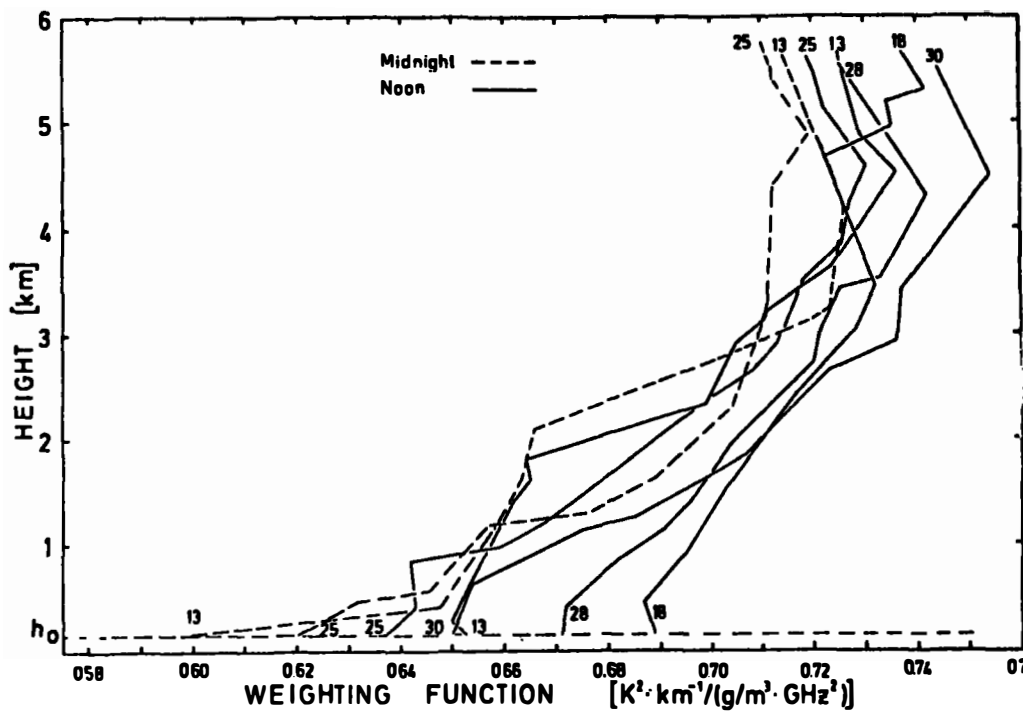

Figure 3. The weighting function at different occasions in May, 1980. The number at each curve is the date of the measurementr

is assumed to be constant both with height and in time. The symbol a denotes the water vapor density and α_v the absorption coefficient for water vapor. In Fig. 1 the weighting function for different frequency pairs are shown, calculated for an atmospheric mean profile during the period from May, 1980, to February, 1982, at Gothenburg-Landvetter Airport, Sweden. The expression for the water vapor absorption coefficient used is given by Waters (1976). When choosing the frequency pair, a compromize between high sensitivity and a more or less constant weighting function has to be made. In Fig.2 the monthly means of the weighting function, calculated for the frequencies of the Onsala WVR (21.0 and 31.4 GHz), are shown. Fig.2 illustrates how W' in equation (3) varies during the year. However, it can be corrected for by adjusting W' every month or somewhat longer time periods based on meteorological statistics. Unfortunately there are also short time variations where the values of the weighting function at the ground have low correlation with values at higher altitudes. This is shown in Fig.3, where the weighting function has been calculated for some different radiosonde profiles measured in May, 1980. A possibility to correct also for these variations is to include a third radiometer channel, which can give information about the temperature profile in the troposphere. For exampel one channel at 53.7 GHz will give an accuracy of about 2 K rms for the temperature profile in the lower 5 to 6 kilometers (Skoog 1982). This also implies that the effective temperatures of the atmosphere can be determined with higher accuracy (see above).

3. Discrepancy from the theory for the absorption coefficient of liquid water. The assumption $\alpha_\ell \sim f^2$ (Staelin 1966) gives

$$T_0' = \int_{h_0}^{\infty} (T - T_{bg}) \cdot \left(\frac{\alpha_{o,f_1}}{-1} - \frac{\alpha_{o,f_2}}{-2} \right) / \sin\theta \, dh \,, \qquad (9)$$

where α_o is the absorption coefficient caused by oxygen only. This approximation is important only for large water liquid drops, i.e. rainfall.

Finally it should be mentioned that the approximations mentioned so far concerns the theory. In order to obtain the total accuracy the pure measurement errors have to be added.

THE WATER VAPOR RADIOMETER

The present WVR system at the Onsala Space Observatory is shown as a block diagram in Fig.4, and the most interesting block concerning the microwave radiometer is expanded in Fig.5. However, only one frequency channel is included, whereas the design is identical for the two channels. The specifications for the microwave radiometer are summarized in Table 1.

OBSERVATIONAL RESULTS

Comparison measurements have been made with the WVR, an infrared spectral hygrometer (IRSH), and radiosondes at Gothenburg-Landvetter Airport in May and June, 1980. The results are summarized in Table 2 (see also Elgered (1982)).

TABLE 1.

RECEIVER PARAMETERS FOR THE WATER VAPOR RADIOMETER.

PARAMETER	21.0 AND 31.4 GHz CHANNEL	
ANTENNA TYPE	CONICAL HORN, DIELECTRIC LOAD	
ANTENNA BEAM (FULL WIDTH, HALF MAXIMUM)	6	DEGREES
REFERENCE LOAD TEMPERATURES	77 AND 313	K
IF BANDWIDTH (DOUBLE SIDEBAND)	500	MHz
SYSTEM NOISE TEMPERATURE (AT MIXER INPUTS)	550	K
RMS NOISE FLUCTUATIONS (1 SECOND INTEGRATION)	0.04	K
RESOLUTION (DETERMINED BY A/D CONVERTER)	0.3	K
ABSOLUTE ACCURACY	1	K

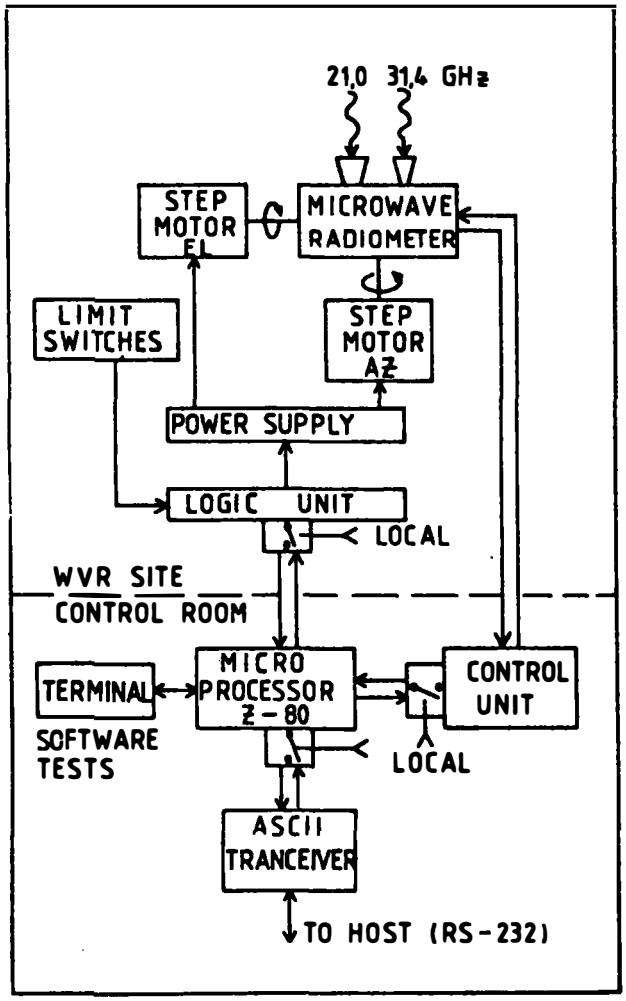

Figure 4. The radiometer system at the Onsala Space Observatory, Sweden.

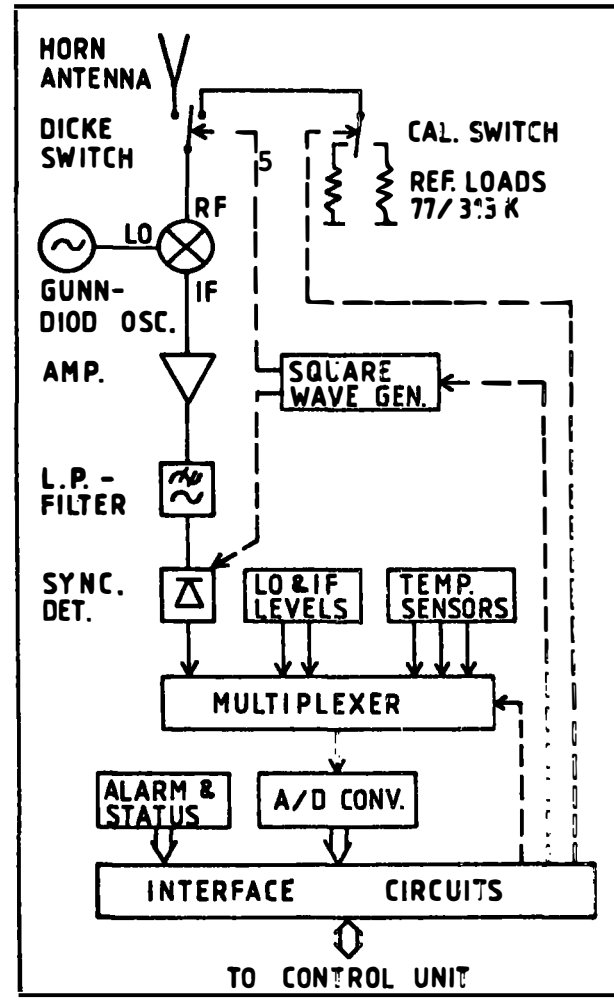

Figure 5. One of the two channels in the microwave radiometer block shown in Fig. 4.

Fig. 6 shows an example of more continuous measurements made during radio interferometry experiments. Data have been taken at different azimuth and elevation angles (towards the sources observed with the interferometer) and converted to the zenith direction by assuming a horizontal and homogeneous atmosphere.

DISCUSSION

First of all it has to be pointed out that absolute errors of the instruments in Table 2 are unknown. However, this should not have great importance for the application of tropospheric path length corrections in a radio interferometry experiment. Given that there are enough of independent observations to also solve for the parameter h' at each station, the influence of absolute errors are minimized and also the best value of h' will be found (see eq. (3)). This value will not be based on meteorological statistics from the past, as in the alternative method mentioned in the introduction.

Table 2 can also give us some indications of the formal accuracy of the instruments. Assuming uncorrelated errors and combining lines 1,2, and 6 in Table 2, gives that the WVR has the highest formal accuracy, but due to the small number of comparision measurements with the WVR and the IRSH the rms value is rather uncertain. Another possibility to estimate the formal error of the WVR is to assume an error of the radiosondes. At the ground, when it is calibrated, the radiosonde has an error which corresponds to about 0.3 cm rms in the wet path delay, but the error at higher altitudes can be several times larger. The rms difference of 0.2 cm on line 5 in Table 2 is the error caused by the approximations made in the theory (discussed above).

TABLE 2.

ZENITH RMS DIFFERENCES OF THE WET PATH DELAY MEASURED WITH VARIOS INSTRUMENTS.

INSTRUMENTS[1]	FIT[2]	RMS DIFFERENCE (CM)
IRSH - RS	$\Delta L_W = A \exp(B \cdot V_1/V_2)$	1.1[3]
WVR - RS	$\Delta L_W = A + B(2.236\ T'_{A,21} - T'_{A,31.4})$	0.8[4]
WVR - RS	$\Delta L_W = (A + B(2.236\ T'_{A,21} - T'_{A,31.4}))/W(H_0)$	0.8[4]
WVR - RS	$\Delta L_W = A + B\ T'_{A,21} + C\ T'_{A,31.4}$	0.7[4]
WVR[5] - RS	$\Delta L_W = A + B(2.236\ T'_{A,21} - T'_{A,31.4})$	0.2[4]
WVR - IRSH	NO FIT	0.8[6]

(1) IRSH = INFRARED SPECTRAL HYGROMETER, RS = RADIOSONDES, AND WVR = WATER VAPOR RADIOMETER.

(2) THE PARAMETERS V_1 AND V_2 FROM THE IRSH AND $T'_{A,21}$ AND $T'_{A,31.4}$ FROM THE WVR ARE FITTED TO THE WET PATH DELAY, ΔL_W, CALCULATED FROM RADIOSONDE MEASUREMENTS.

(3) 31 DATA POINTS.

(4) 40 DATA POINTS.

(5) THE ANTENNA TEMPERATURES ARE THEORETIC, AND CALCULATED FROM RADIOSONDE PROFILES.

(6) 7 DATA POINTS.

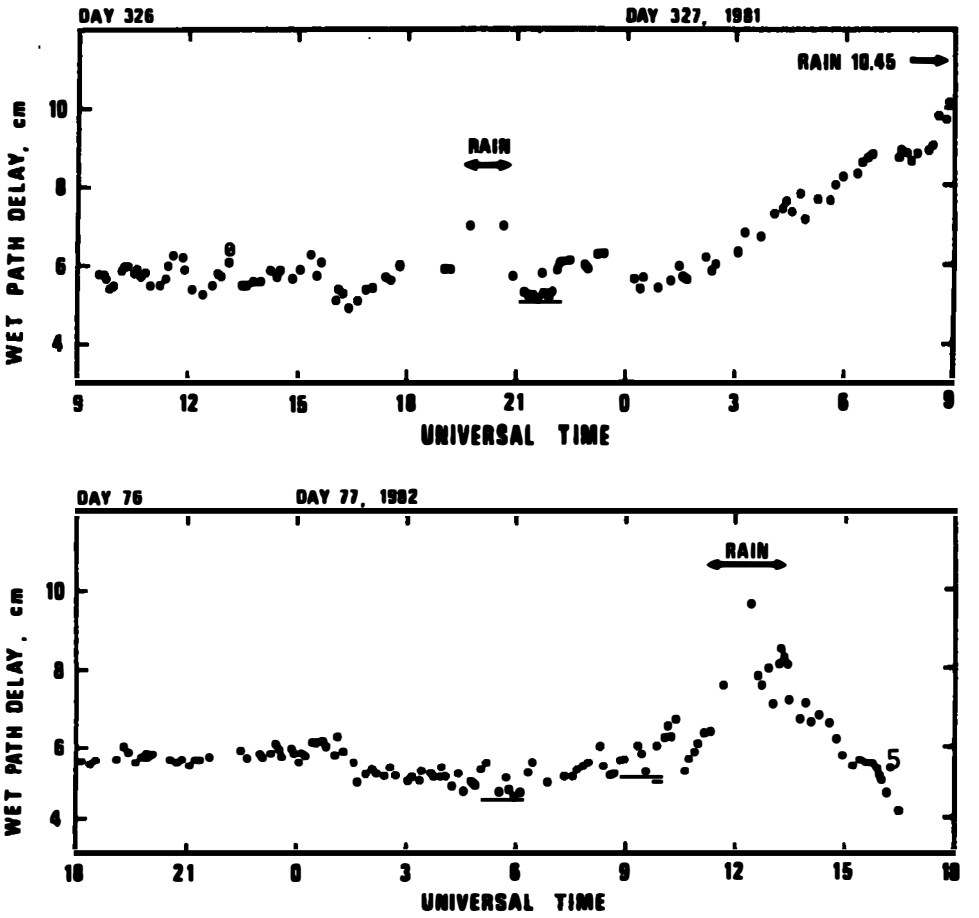

Figure 6. Measurements of the wet path delay during two different VLBI experiments. Each dot is one observation towards a radio source, and the value has been converted to the zenith direction.

In Fig.6 it is shown that the wet path delay can both vary rapidly or be rather stable over time periods of several hours. However, as expected for the theory described here, measurements made during rainfall are not reliable.

REFERENCES

Elgered, G.(1982): Tropospheric Wet-Path Delay measurements, IEEE Transt on Ant. and Prop., vol AP-30, pp. 502-505.

Guiraud, F.C., J. Howard, and D.C. Hogg (1979): A Dual Channel Microwave Radiometer for Measurements of Precipitable Water Vapor and Cloud Liquidt IEEE Trans. on Geoscience Electronics, vol. GE-17, pp.129-136.

Morant, J.M., and E.R. Rosen (1981): Estimation of the Propagation Delay Through the Troposphere from Microwave Radiometer Data, Radio Science, volt 16, ppt 235-244.

Resch, G.M. (1982): Water Vapor Radiometry: Application to Geodetic Radio Interferometry, presented at General Meeting of IAG, symp. 5 (this issue)t

Shapiro, I.I. (1976): Estimation of Astrometric and Geodetic Parameters, in Methods of Experimental Physics, vol. 12 C, ed. M.L. Meeks, p. 264 New York: Academic Press.

Skoog, B.G. (1982): The Physical Basis for Ground-Based Remote Sensing of Atmospheric Temperature Profiles by Microwave Radiometry, Res. Rep., Res. Lab.of Electronics, Chalmers Univ. of Tech., Gothenburg, Sweden, to be published.

Smith, E.K. and S. Weintraub (1953): The constants in the Equation for Atmospheric Refractive Index at Radio Frequencies, Proc. I.R.E., pp. 1035-1037.

Staelin, D.H. (1966): Measurements and Interpretation of the Microwave Spectrum of the Terrestrial Atmosphere Near 1-Centimeter Wavelength, J. of Geophys. Res., vol. 71, pp.2875-2881.

Waters, J.W. (1976): Absorption and Emission by Atmospheric Gases, in Methods of Experimental Physics, vol. 12 B, ed. M.L. Meeks, pp. 142-176, New York: Academic Press.

Wu, S.C. (1979): Optimum Frequencies of Passive Microwave Radiometer for Tropospheric Path-Length Correction, IEEE Trans. on Ant. and Prop., vol. AP-27, pp. 233-239.

THE APPLICATION OF WATER VAPOR RADIOMETRY TO GEODETIC RADIO INTERFEROMETRY[1]

George M. Resch and Robert B. Miller

Jet Propulsion Laboratory
California Institute of Technology
4800 Oak Grove Drive, Pasadena, California 91109
U. S. A.

ABSTRACT. A significant limitation to the accuracy of spaced-based microwave geodetic systems is set by our ability to model or measure the delay imposed by tropospheric water vapor along the signal path. This so-called vapor delay can be measured using a dual channel microwave radiometer (i.e. a water vapor radiometer) with an accuracy of approximately 1 cm and a precision of 1 mm. We describe the construction and performance of the current generation of these instruments that have been deployed in order to support VLBI experiments in the U.S.A., Australia, and Spain. Preliminary results from a direct comparison between the water vapor radiometers and a connected element interferometer are presented and the geodetic implications discussed.

---

[1]This paper represents the results of one phase of research carried out at the Jet Propulsion Laboratory, California Institute of Technology, under contract to the National Aeronautics and Space Administration.

Back in 1974 a group of workers at the Jet Propulsion Laboratory was involved in a modest research and development effort that was then known as ARIES - Astronomical Radio Interferometric Earth Surveying (MacDoran, 1974). At that time we were convinced that interferometric techniques would produce 3 to 5 cm. baseline measurement accuracies in just a few years - if only the water vapor problem could be solved! By this I refer to the fact that atmospheric water vapor slows a radio wave passing through it. Interferometric techniques, which measure the differential time of arrival of the wave front, must account for this slowing. Unfortunately, water vapor is not a well mixed atmospheric constituent; and as a result it is difficult (often impossible) to estimate the line-of-sight vapor using surface measurements to better than 10-15 cm. Thus, the line-of-sight vapor delay must be measured. The essence of the idea is to measure the brightness temperature of the atmosphere at two frequencies, one frequency at or near 22.235 Ghz where there is spectral emission from the water vapor molecule, and a second measurement at 31.4 Ghz which is a frequency where the atmosphere is relatively transparent. In theory, these two measurements, on and off-the-line, provide an estimate of the line-of-sight delay imposed by the vapor.

In Figure 1 we show the results of one of our early experiments that convinced us that we could estimate vapor delay directly. We compared the measurements made with a borrowed water vapor radiometer (WVR) with radiosonde measurements and measurements made by an instrumented aircraft that flew a path approximating one of several line-of-sight paths through the atmosphere. The data shows that the radiometric technique could be used to estimate the vapor delay correction with an accuracy of better than 2 cm. under most weather conditions.

At roughly the same time that the Crustal Dynamics Project was beginning, we began to construct eight water vapor radiometers that were intended to support the VLBI effort within the Project and JPL's Deep Space Tracking Network (DSN). Figure 2 is a photo of one of these new instruments. It was designed to be both an integral part of the Mark III data acquisition system that is now in use by the Project, and to be a generally useful support instrument for the radio observatories where they would be located. The unit consists of three modules; a microwave module, a positioner, and a control module. The microwave module comprises two independent Dicke radiometers operating at the frequencies of 20.7 Ghz and 31.4 Ghz. The choice of 20.7 Ghz as the vapor sensitive frequency sacrifices some sensitivity but minimizes errors due to the vertical distribution of the vapor. These radiometers normally run in the unbalanced mode and are provided with internal terminations in order to calibrate the gain. A special feature is the use of very low sidelobe horns which simplifies the interpretation of the data. Unfortunately, the penalty for using these horns is that their bulk dominates the size and weight of the microwave module. The positioner is unremarkable except for

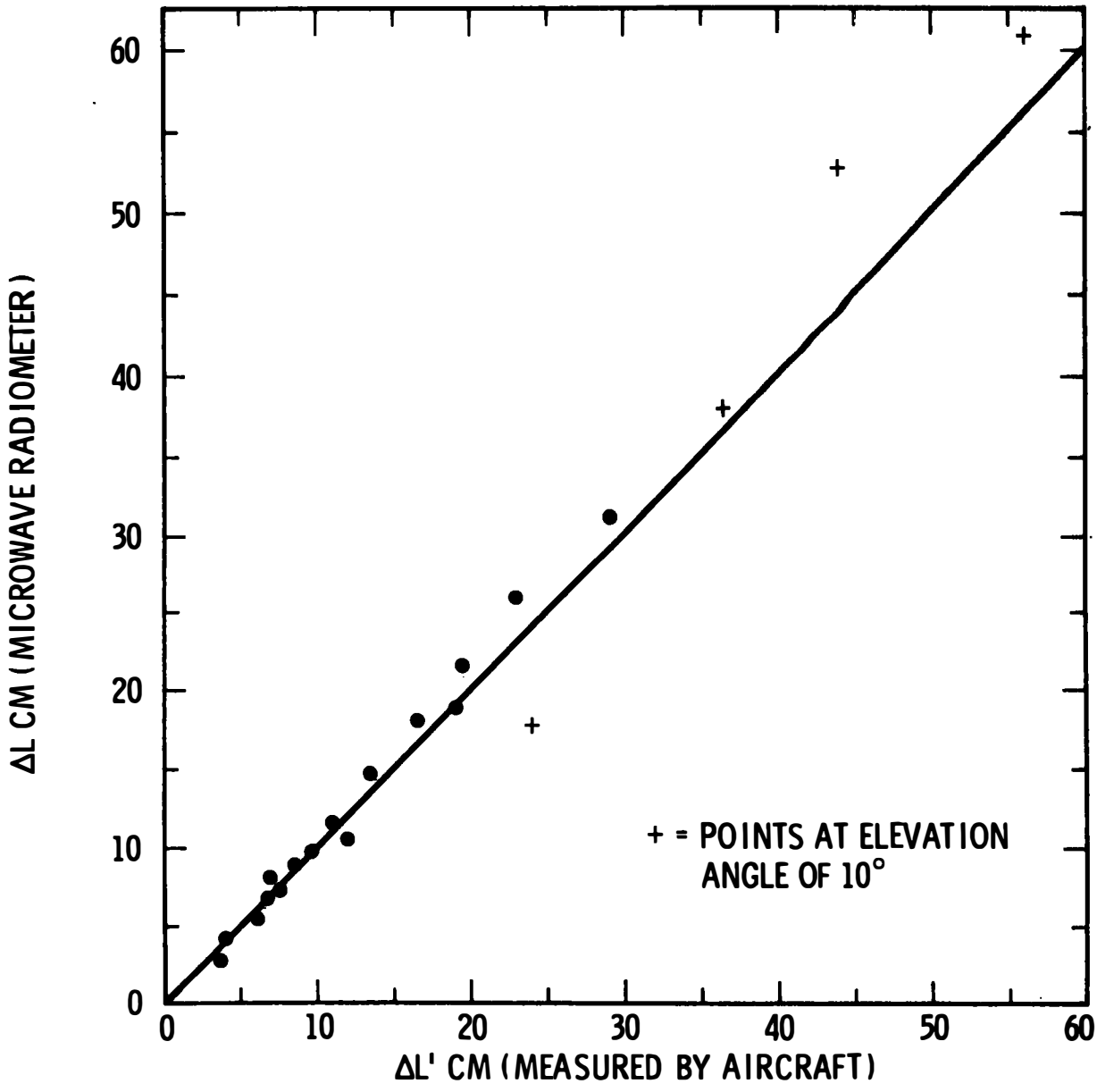

Figure 1. Excess Path Delay Due to Water Vapor as Measured by a Microwave Radiometer and an Instrumented Aircraft

Figure 2. Photo of One of the Water Vapor Radiometers Constructed for the Crustal Dynamics Project

the fact that it is very inexpensive. We simply modified a device normally used to position outdoor video cameras so that we could read its position much more accurately than we could actually point it. The control module provides the capability of local control and monitoring of the other modules (which is useful for diagnostic purposes), and contains a small microcomputer that provides a modicum of intelligence to the WVR as well as a general purpose interface to other machines. These eight WVRs were constructed, tested, and calibrated at JPL. Beginning in late 1980 they were deployed to the Owens Valley Radio Observatory, the Haystack Observatory, the Harvard Radio Astronomy Station (at Ft. Davis, Texas), and two units went to support the mobile VLBI antennas that we operate at JPL. One WVR was recently shipped to the DSN station in Australia and another will be shipped to the DSN station in Spain next fall. The eighth WVR will be installed at the Maryland Point Observatory also next fall.

A primary concern with any new instrument is the intrinsic stability. Since we are looking at a noise-like signal in the presence of instrument noise we must determine at what level can we believe small fluctuations in the output of the WVR. Figure 3 indicates the typical stability of one of our new radiometers. In order to take this data we covered both horn antennas with microwave absorbing material that was heated to a temperature of 100°C. The unit was placed outdoors in the weather and each channel was sampled and averaged 48 times every minute. The gain was sampled and averaged every 15 minutes, and all data was written to a floppy disk and processed at a later time. The brightness temperatures and the path delay were calculated using an algorithm that was previously determined. Since we are looking at a fixed temperature target and not the sky, the path delay values have no physical meaning so we have subtracted out the average value in this slide. The RMS value of the fluctuations for this 24 hr period is 0.12 cm. Unfortunately, we cannot control the aperture load to better than a few tenths of a degree and as a result we suspect that the trends that you see both at the beginning and the end of this data set represent real changes in what should have been a stable target. The theoretical RMS of a perfect radiometer sampled as we have done in this test would be 0.06 cm. As you can see, there are periods of a few hours duration where the real radiometer approaches this limit.

From the data taken by our group at JPL as well as several other groups such as Guiraudt*et. al.* 1979; or Moran and Rosen, 1980; there is little doubt that the WVR can measure water vapor. However, until recently, it has not been clear how much benefit the WVR would provide to a real interferometer. Keep in mind that the VLBI error budget is a complex collection of several error sources that must all be reduced if water vapor effects are to predominate. If the error budget is dominated by the clock performance or by ionospheric errors then WVR supplied corrections may have little effect on the data quality. Also, there is a considerable effort involved in VLBI data reduction and it is done after the experiment. This difficuty inhibits the taking of large amounts of data and if there is something amiss during the experiment the observer often does not discover the fault until several months after the data has been

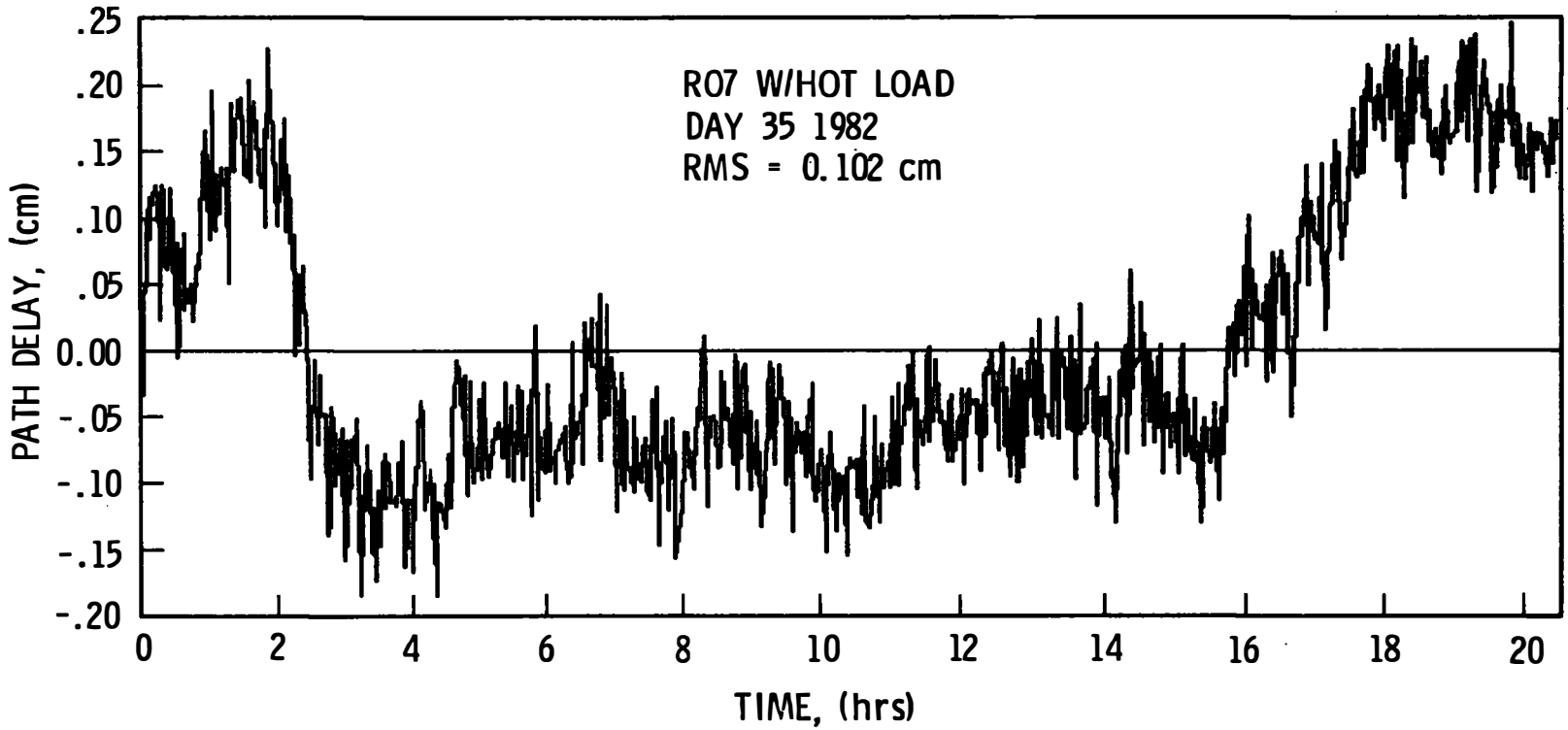

Figure 3. WVR Instrumental Stability

taken. These considerations led us to cooperative experiment with of the National Radio Astronomy Observatory in which we compared the output from two of the WVR's with the output from one of the interferometers that make up the VerytLarge Array (Resch, Napier and Hogg, 1982).

The WVRs were mounted in the apex feed area of a VLA 25 meter antenna. The WVR horns were aimed at the subreflector so that we used most of the 25 meter aperture and our beam was offset from the beam of the main antenna by a few minutes of arc. Actually, the concept of the antenna beam for the WVR channels is irrelevent in this case since the near field of the aperture extends for over 60 km. Most of the atmospheric water vapor is confined to the lower 3 or 4 km of the atmosphere and is therefore a near-field phenomena. This means that both the interferometer and the WVR are sensitive to whatever vapor passes through the cylindrical column of 25 m diameter that extends from each antenna through the troposhpere.

Figure 4 shows the residual phase of the interferometer versus time for a period of 1.5 hr on 23 July 1981. During this period and for part of the following day the weather was highly dynamic. Scattered thunderstorms were present in the nearby moutains and over the array. For part of the period it was raining over one end of the array and cloudless over the other end. On the day of this experiment the array extended over an area 11 km in diameter and the WVRs were mounted on two elements that composed a 7 km baseline. The dotted line is the residual phase of the interferometer containing the WVRs. The first thing to notice is the magnitude of the phase changes which I have expressed in centimeters - units of residual delay. Even on baselines as short as 7 km we see path delay differences on the order of 6 cm. The output from each WVR is used to compute a line-of-sight path delay and these two quantities are then differenced to form a phase correction for the interferometer output. There is a somewhat arbitrary bias between these two observables that we remove and then apply the WVR correction to the VLA data. The solid line shows the dramatic improvement in the residual after this correction. Before correction the RMS of the data was 1.5 cm. After the correction the RMS dropped to 0.3 cm - an improvement by a factor of five!

While this data is impressive it still does not mean that we can expect an immediate improvement in the quality of VLBI data. As we noted previously, the VLBI error budget is a complex collection of sources so that the reduction of one contributor will not necessarily show up in the square root of the sum of the squares. Another important point to keep in mind is that we still have not addressed the problem of absolute calibration of these new WVRs. At some point in the very near future they must be compared with some independent method of measuring path delay, such as radiosondes. Data that we have taken several years ago, and the results from other workers suggest that an absolute accuracy on the order of 1 cm can be expected. With an accuracy of 1 cm and a precision of 1 mm as indicatedtby our data, we can conclude that the vapor problem in VLBI can be reduced to a negligible proportion. Perhaps more important is the possibility that these results hold

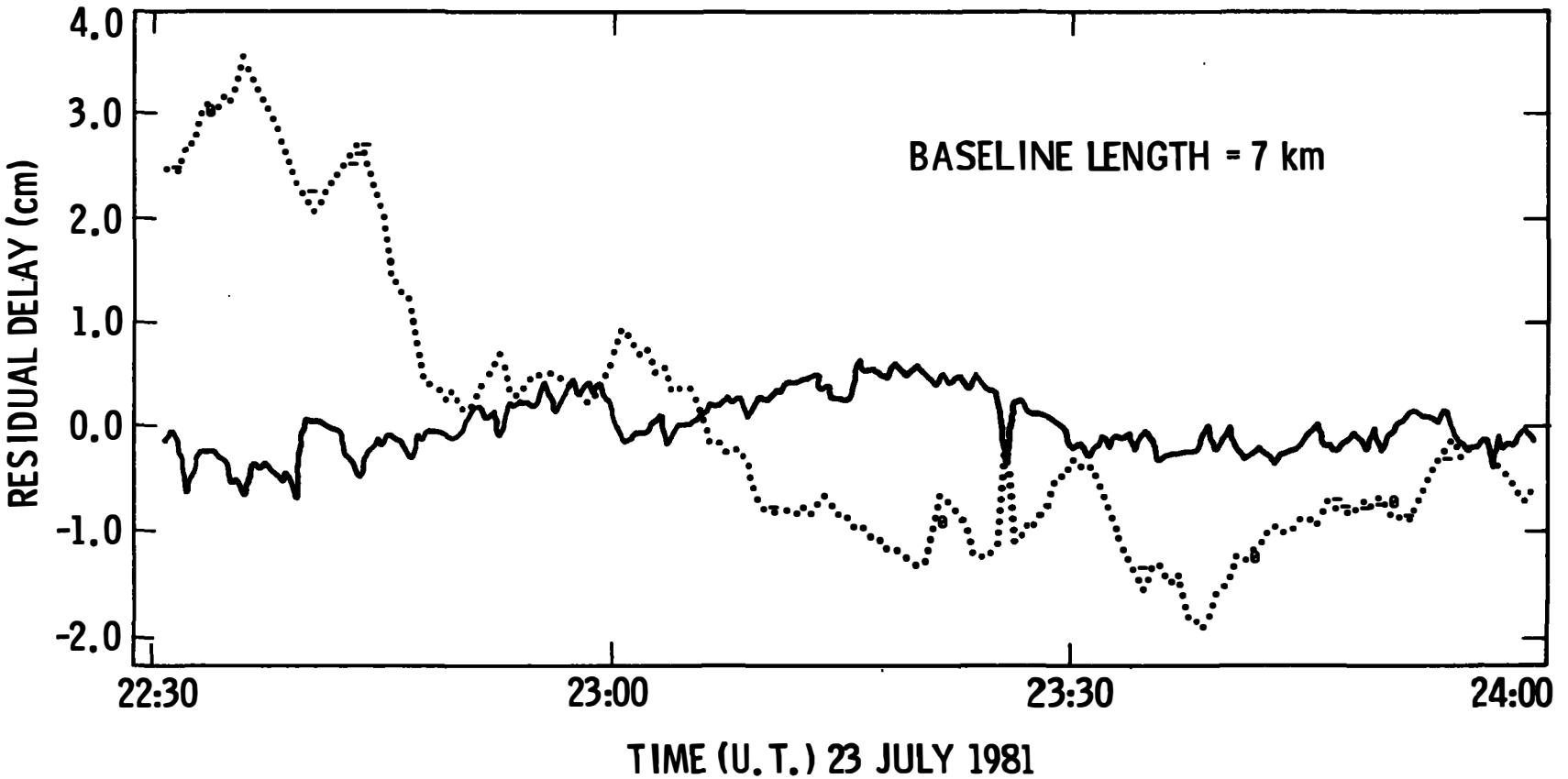

Figure 4. Residual Delay Before and After Correction by WVRs

the promise of exploiting the extraordinary preoision inherent in the several proposed sytems that utilize the NAVSTAR/GPS for geodetio measurements.

ACKNOWLEDGEMENTS

The authors are pleased to aoknowledge the help of Mr. Maroo Chavez and Mr. N. Yamane during the oonstruction, testing and oalibration of the water vapor radiometers.

REFERENCES

Guiraud, F. O., Howard, J.ę and Hogg, D. C. (1979), "A Dual-Channel Microwave Radiometer for Measurement of Precipitable Water Vapor and Liquid", IEEE Trans. Geosoienoe Eleot., GE-17, 129-136.

MaoDoran, P. F. (1974), "Radio Interferometry for International Study of the Earthquake Meohanism", Aota Astron, 1, 1427.

Moran, J. M., and Rosen, B. R. (1981ę, "Estimation of the Propagation Delay through the Troposphere from Miorowave Radiometer Data", Radio Soienoe, 15, 235-244.

Resoh, G. M., Napier, P. E., and Hogg, D. E. (1982)ę "Correction of Interferometrio Phases Using Water Vaor Radiometers", Radio Scienoe (in preparation).

STATUS OF THE GREEN BANK INTERFEROMETER

William J. Klepczynski,
G.H. Kaplan, D.N. Matsakis,
D.R. Florkowski, P.E. Angerhofer,
D.D. McCarthy, F.J. Josties, R.L. Branham of
U.S. Naval Observatory, Washington, D.C. 20390 and
K.J. Johnston, J.H. Spencer of
U.S. Naval Research Laboratory, Washington, D.C. 20375

A. INTRODUCTION

Past summaries of the USNO/NRL Green Bank Interferometer Program (Johnston, et al.. 1979; Klepczynski. et al., 1980;) have briefly described t tory of the progr ned the derivation of Earth rotat rameters from the baseline changes, and presented | nary results of . Subsequent papers (McCarthy, al., 1979; McCarthy, 1980; McCarthy, 1981) have traced in more detail the procedures for obtaining estimates of Earth rotation parameters, discussed the effects of systematic errors, listed results, and compared the connected element interferometer (CEI) results with the results of other techniques. This report discusses forthcoming improvements to the CEI which include adding a new baseline, improving the distribution of observed quasars, incorporation of a new atmospheric model used in the reduction of data, and utilization of water vapor radiometers to determine a differential phase correction based on the measured amount of water vapor as seen along the line of sight of two interferometer elementsa

In interferometry, the relative phase difference of the wavefront impinging on two separated antennas is the fundamental observered quantity. If the position of the quasars are precisely known, if models for a number of systematic effects are known, and if all instrumental effects are available, then the difference between the observed phase angle and that predicted by theory, for each source, would precisely determine Universal Time (UT) and Polar Motion (PM). The improvements described in this paper are attempts to reduce the phase scatter in consecutive observations as well as the seasonal (long-term) drift observed in the phasesa Reduction of the short-term (scan-to-scan) scatter will result in improved precision for the daily estimates of polar motion (PM) and universal time (UT) as well as less scatter between consecutive values; while reduction of the seasonal drift will result in reduction of the annual term exhibited in the comparison of the interferometer results with those derived from the Bureau International de l'Heure (BIH) (see Figs. 1a-d, Figs. 2a-d and Figs. 3a-b)a

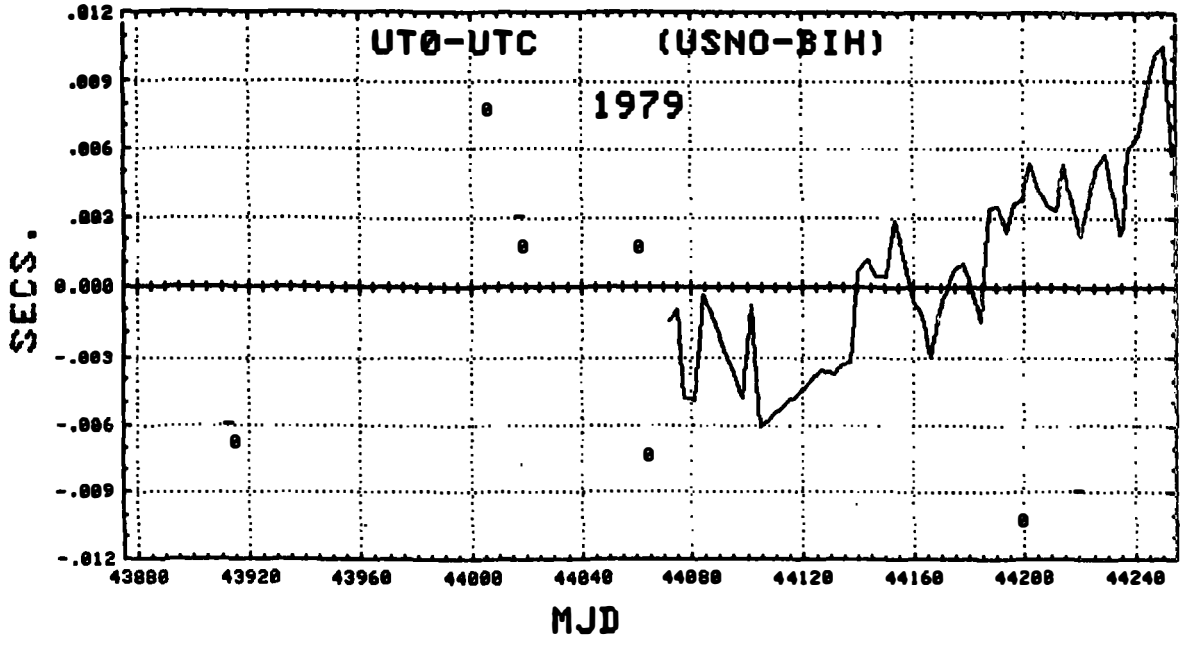

Fig. 1a. Comparison of UT0-UTC as determined by the CBI (USNO) with BIH for the year 1979.

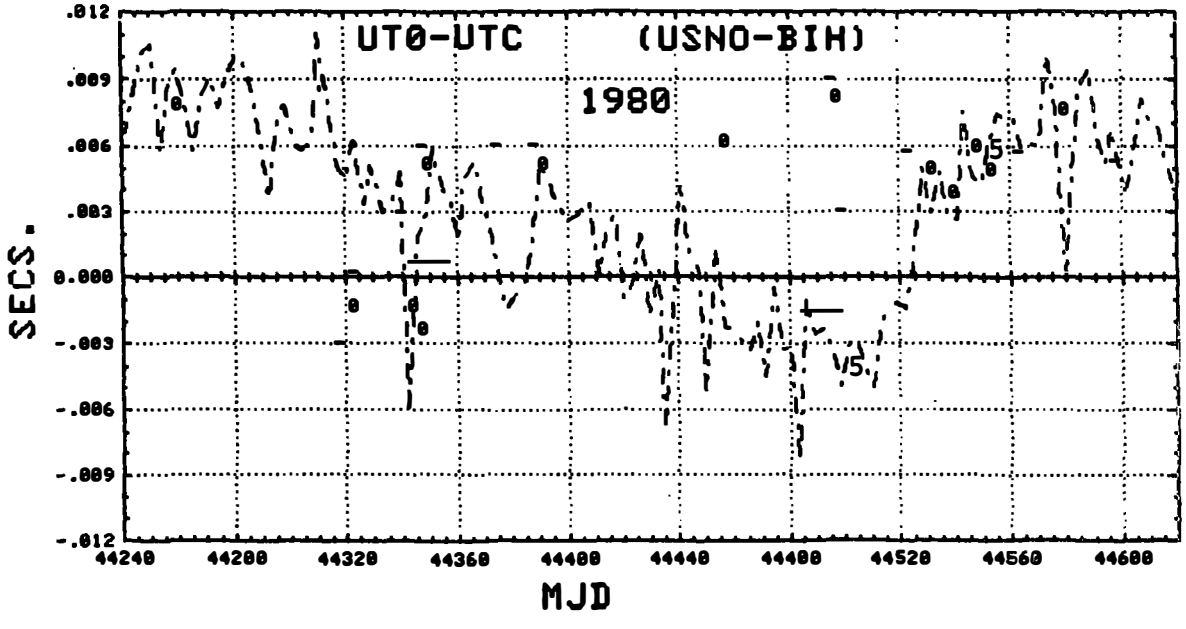

Fig. 1b. Comparison of UT0-UTC as determined by the CBI (USNO) with BIH for the year 1980.

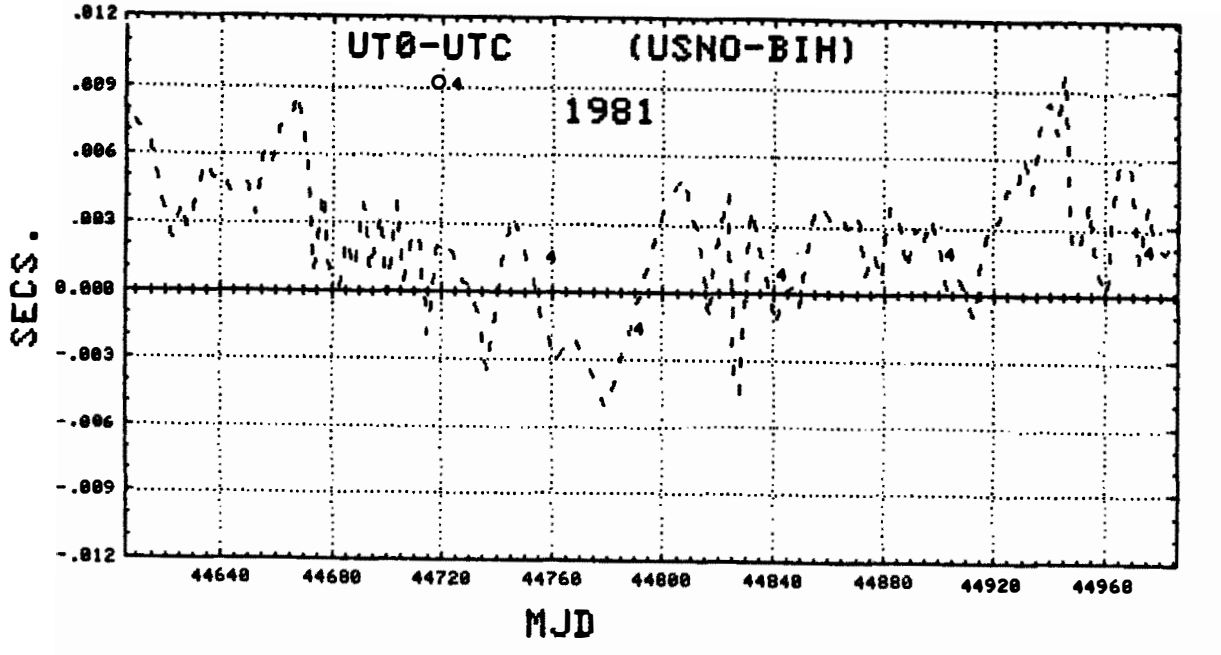

Fig. 1c. Comparison of UT0-UTC as determined by the CEI (USNO) with BIH for the year 1981.

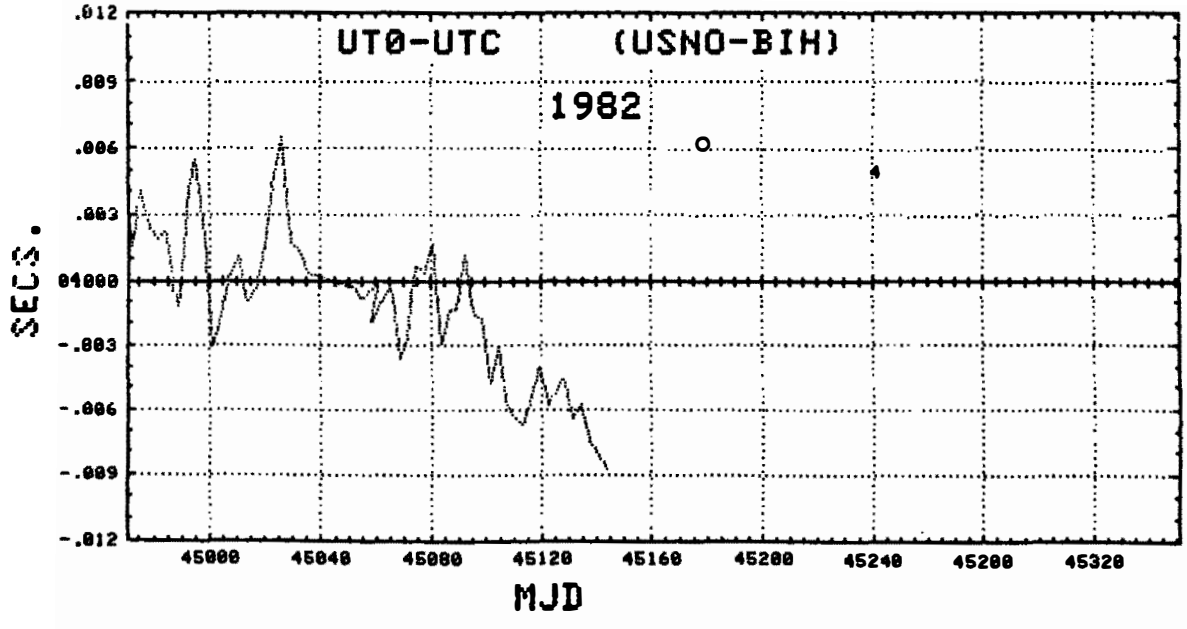

Fig. 1d. Comparison of UT0-UTC as determined by the CEI (USNO) with BIH for the year 1982.

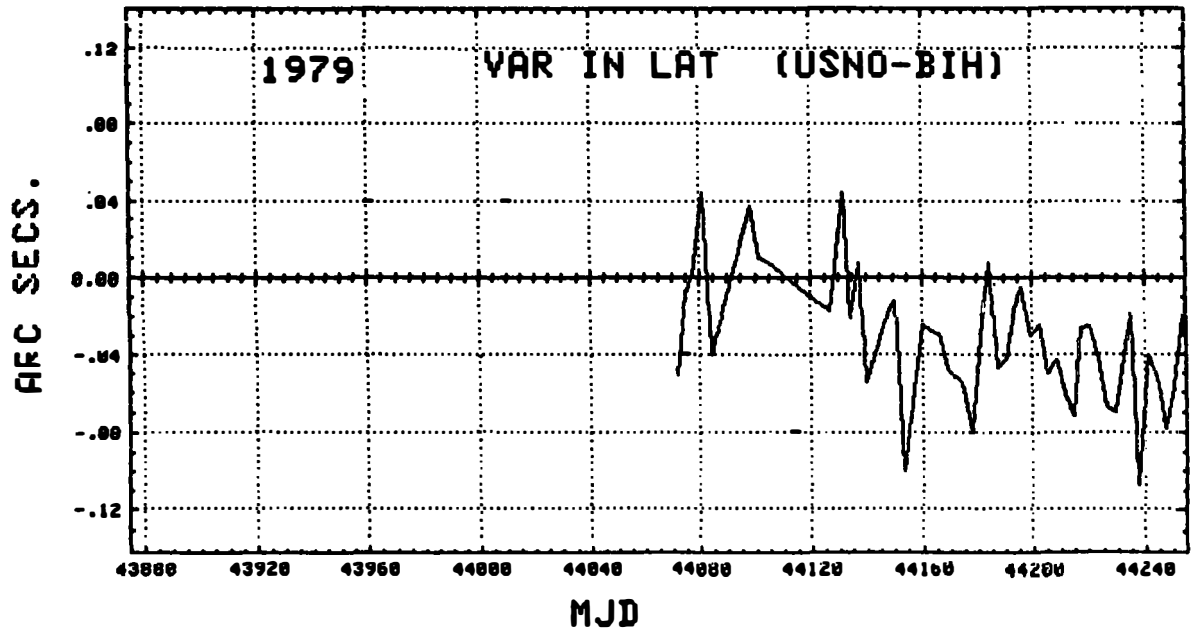

Fig. 2a. Comparison of the Variation in Latitude as determined by the CEI (USNO) with BIH for the year 1979.

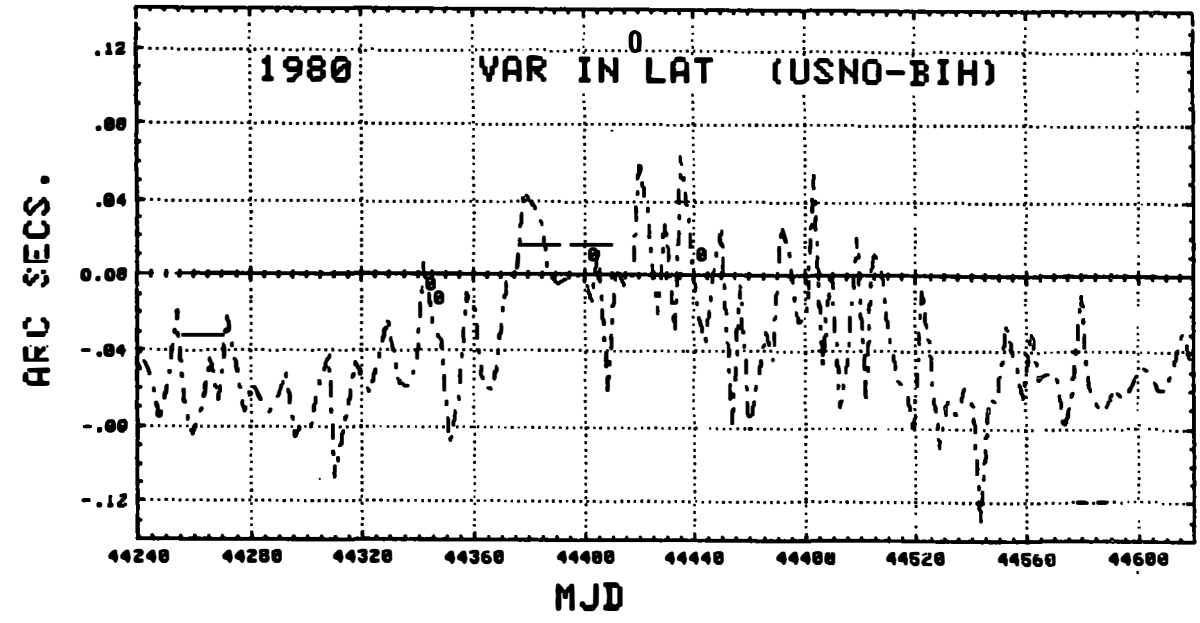

Fig. 2b. Comparison of the Variation in Latitude as determined by the CEI (USNO) with BIH for the year 1980.

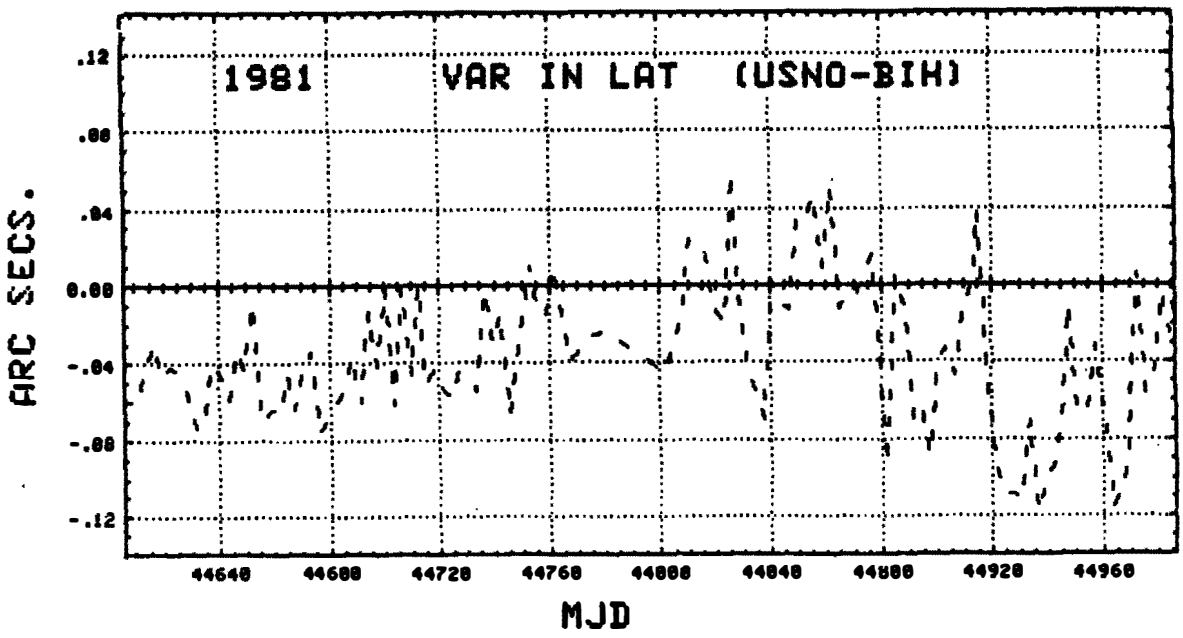

Fig. 2c. Comparison of the Variation in Latitude as determined by the CEI (USNO) with BIH for the year 1981.

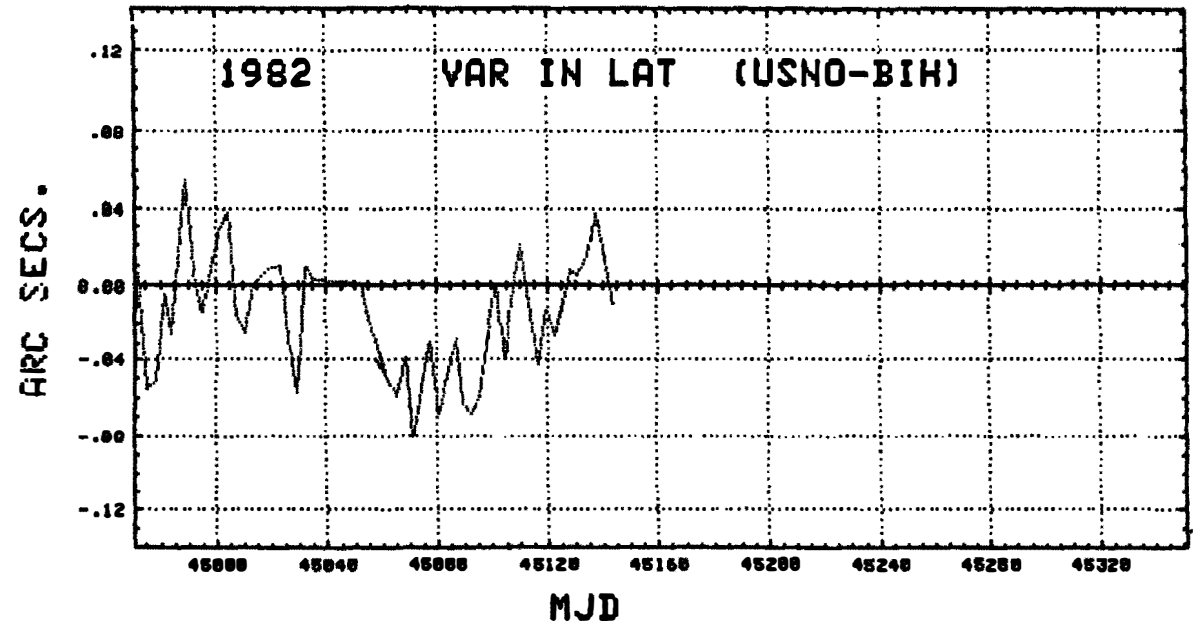

Fig. 2d. Comparison of the Variation in Latitude as determined by the CEI (USNO) with BIH for the year 1982.

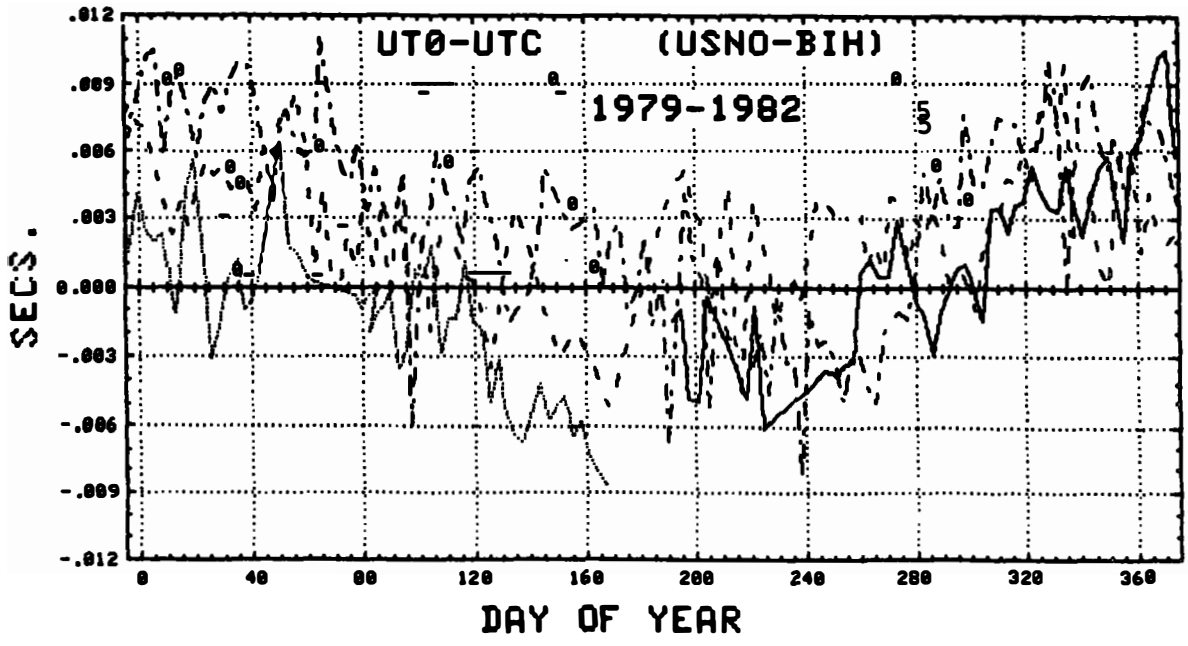

Fig. 3a. Composite of Figs. 1a-d.

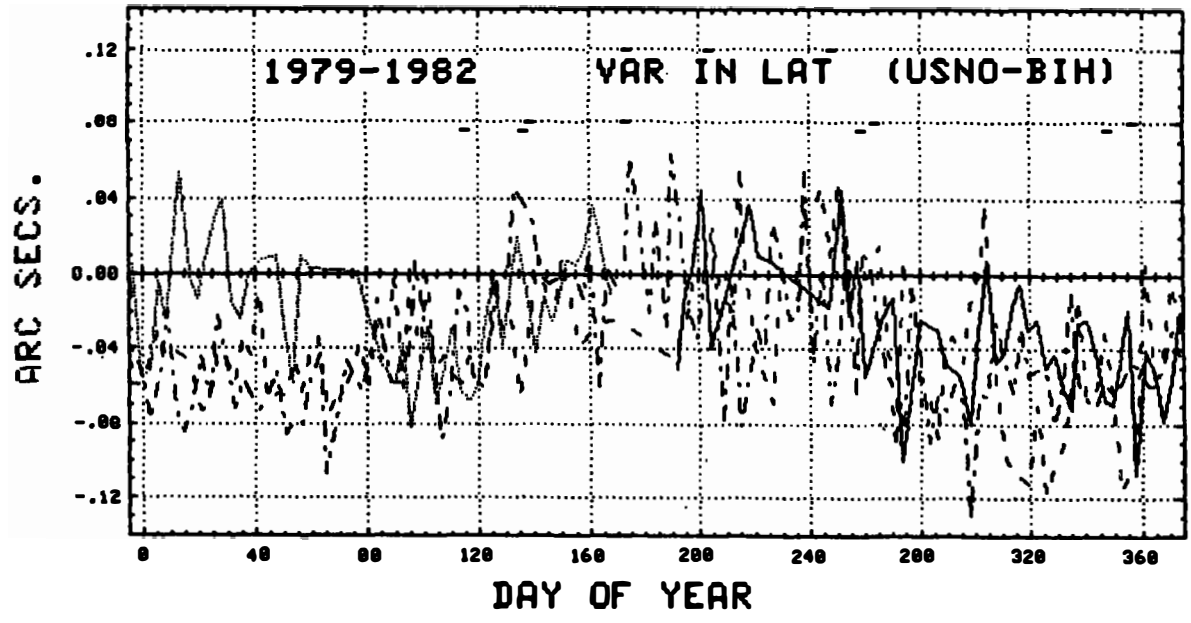

Fig. 3b. Composite of Figs. 2a-d.

The new baseline, approximately orthogonal to the 35 km baseline, will allow the interferometer to resolve all three components of the Earth's rotation. By improving the distribution of observed sources, it is hoped that values for UT, and x,y of PM will be determined at intervals shorter than the present three day average. Introduction of an improved atmospheric model should aid in systematically reducing the annual term that is seen when comparing interferometer data with the BIH. Inaccuracies in our present model for the dry component of the atmosphere are primarily responsible for this seasonal term. The use of water vapor radiometers will help reduce the daily point-to-point scatter between observed ten minute normal points, and the annual term seen in the mean errors associated with the determined values of UT and PM should be reduced. In addition, the reduced scatter between consecutive observations and an improved observing schedule of quasars, should ensure the determination of UT and PM at more frequent intervals.

B. NEW BASELINE ADDITION

Figure 4 shows the ent distribution of interferometer elements. The three 26 ennas designated 85-1, 85-2, and 85-3, which made up the origi nterferometer, are aligned 28° from an East-West line (Hogg, __ ., 1969). A fourth element, a 14m antenna, lies 35 km to the South-West of the three 26 m antennas. Unfortunately, although there are three separate long baselines among the four antennas, they are effectively parallel so that they cannot be used to resolve all three components of the Earth's rotation (UT and x,y coordinates of PM). The new antenna will be located 32 km to the North-West of the 26 m telescopes on a line orthogonal to the present baseline.

The new 14.2 m telescope is now under construction. It should be delivered to the site sometime in September 1982. During the winter of 1982-83, a new microwave link will be constructed for the baseline. The new link will operate at a frequency of 17.5 GHz. It will also replace the present link, which operates at 1347.5 MHz and occasionally interferes with some observing programs on other telescopes at the site. Besides removing this source of interference, the new link will also have additional channels which will allow for the transmission of video signals for the remote visual inspection of the antennas.

Present plans do not call for the replacement of the telescope control computer. Therefore, one of the 26 m telescopes will be removed from service and the cables from and to the new telescope will be put in its place. Software changes to allow this alteration will be made during the summer of 1983.

Operation of the new baseline is expected to begin in September-October 1983.

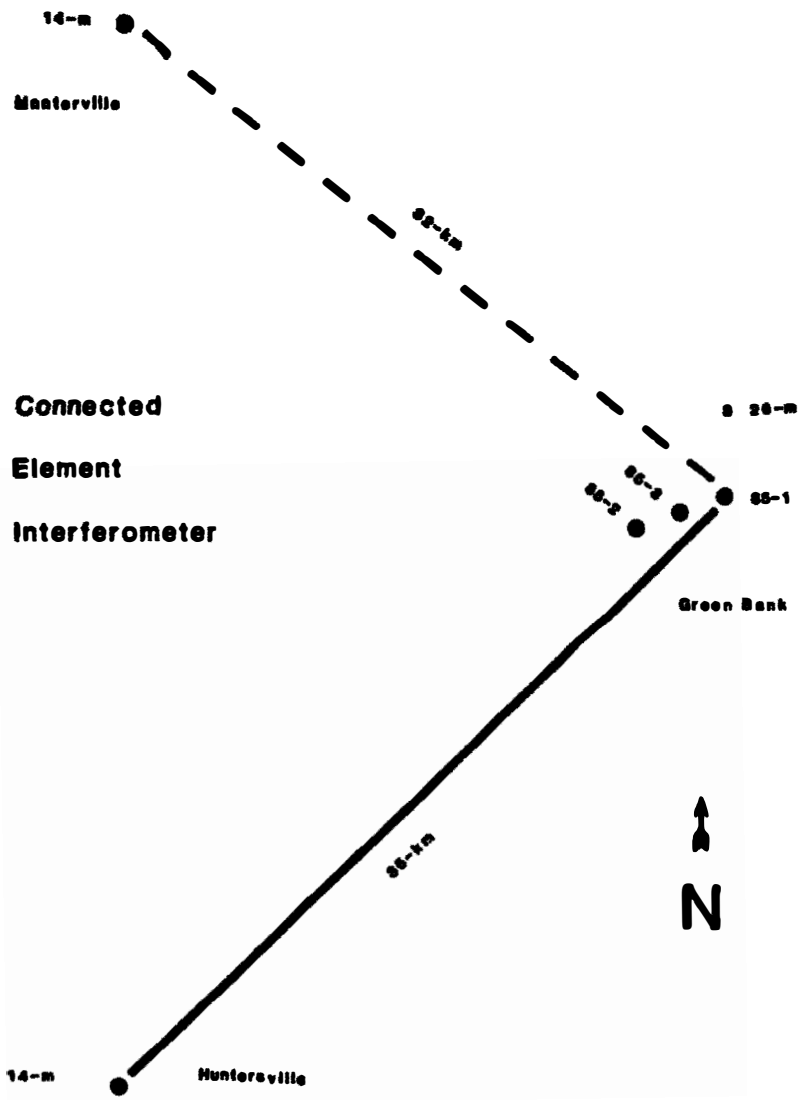

Fig. 4. Schematic Diagram of the Green Bank interferometer geometry.

C. NEW SOURCE CATALOG

nitially, the catalog used for the positions of all the quasars in the observing program was that of Wade and Johnston (1977). After a few months observations, several of the positions were slightly improved and some sources added and some dropped (Klepczynski, et al., 1980). Recently, Kaplan, et al. (1982) have constructed a catalog utilizing observations made from October 1979-February 1980. This catalog now forms the basis for the observing program.

In order to prevent a discontinuity in the values of UT and PM when the new catalog went into effect, an adjustment in the reference baseline was made. The amount of the adjustment was deduced from the observed changes in the positions of the quasars and verified by re-reducing selected solutions throughout the year.

During the formation of the new catalog, it had been found that the position of the quasar 1226+023 (3C273B), which determines the zero point of the catalog right ascensions, was not consistent with that of the other 15 quasars. Because of this, the right ascension system of the new catalog is effectively shifted 2.8 ms from the right ascension system of the old catalog. Because of the shift in the right ascension system, a compensating shift should be seen in the values of UT based on this new catalog when compared with values of UT based on the old catalog. Selected dates during 1981 were chosen and the data were re-reduced identically in all measures except for using the newly determined quasar positions. Table I summarizes the results of the comparison of the new values with the old values. It is seen that there is a systematic difference in UT of 2.8 ms, the amount by which the right ascension system of the new catalog was shifted. It can also be seen from Table I, that the introduction of the new catalog has reduced the mean error of the UT0-UTC determinations. From the interferometer data published in the BIH annual reports, it can be seen that the internal mean errors for the solution of UT based on three days of data range from 0.4 ms during the best observing period in winter to about 2.0 ms during the summer months.

The spatial distribution of quasars used in the current observing program is not sufficient to allow for reliable solution of UT and PM and other unknowns using less than three days of data. In order to remedy this deficiency, additional sources will be added to the observing program. Positions for these new sources will be determined during the coming year. Two new sources will be observed each month. Each source is brighter than one Jansky at both S and X

TABLE I - Comparison of UT and PM Based on Old and New Catalogs.

	UT_{old}	UT_{new}	Old-New
15 Jan 81	$-0^s.2121 \pm 0^s.0005$	$-0^s.2150 \pm 0^s.0004$	2.9 ms
15 Apr 81	-0.4390 ± 0.0008	-0.4416 ± 0.0007	2.6
31 Jul 81	$+0.3397 \pm 0.0012$	$+0.3369 \pm 0.0010$	2.8
15 Oct 81	$+0.2005 \pm 0.0008$	$+0.1977 \pm 0.0007$	2.8

	PM_{old}	PM_{new}	Old-New
15 Jan 81	$-0''.3202 \pm 0''.0068$	$-0''.3104 \pm 0''.0046$	$-0''.0098$
15 Apr 81	-0.2421 ± 0.0102	-0.2333 ± 0.0090	-0.0088
31 Jul 81	-0.1232 ± 0.0146	-0.1157 ± 0.0132	-0.0075
15 Oct 81	-0.3002 ± 0.0093	-0.2840 ± 0.0083	-0.0162

band frequencies and unresolved over the various baselines of the interferometers. The intent is to use these observations to improve their positions and thus put them on the system of Kaplan et al. (1982). At the end of 18 months a sufficient number of quasars on the system of Kaplan et al., should exist to allow for uniform sky coverage at eight hour intervals. We hope this will lead to daily estimates of UT and PM without diluting the precision presently obtained.

D. NEW ATMOSPHERIC MODEL

Figure 3 shows an approximately seasonal variation of the Green Bank residuals with respect to the BIH. It is probable that a large fraction of this variation is a consequence of the procedure used in modelling the neutral atmosphere. It is common to consider the refraction by the neutral atmosphere to consist of two terms; (1) a "dry" term and, (2) a "wet" or water vapor term. The procedure we have been following to calculate atmospheric phase delay is the ray tracing method adopted by Wade and Johnston (1977). This algorithm uses the dry component of the Air Research Defense Command Standard Atmosphere. This model is fixed, i.e., no seasonal changes in the structure of the atmosphere are considered. Also, the algorithm ignores the surface measurements of temperature and air pressure. The values of the model atmosphere

were assumed to be valid for the entire year. By not using surface measurements to determine the zero point of the refractivity curve and by ignoring seasonal variations in the structure of the dry atmosphere, errors with an annual signature are introduced into the calculation of the phase delay. The water vapor term is treated more realistically in that the wet profile is fixed by measurements of absolute humidity made at the surface. Thus, the large day-to-day variation in the water vapor content is taken into account. An exponential curve of fixed scale height is used to represent the wet component. Possible annual variations in the value of the scale height are not considered. Thus, the wet and dry components are both subject to unmodelled effects that would produce errors having an annual signature in the calculated phase delay. The net effect of these errors in the computed delay could produce a spurious rotation, having an annual period, of the interferometer baseline.

Currently at the U.S. Naval Observatory, research is underway to explore modifications to the ray tracing technique that take into account the above-mentioned difficulties. The surface weather measurements are being used to fix the wet and dry refractivity profiles. Various functional forms have been used to represent the wet and dry components. To date the most promising combination is as follows: the neutral atmosphere is considered to be three layers, the planetary boundary layer, the troposphere and the stratosphere. Near the surface, in the planetary boundary layer the dry and wet profiles are considered to be linear. The slopes of the two lines are based on monthly averages of radiosonde data. The refractivity N as a function of height in meters, h, is given by:

$$N(h) = D(h) + W(h)$$

where D and W denote the dry and wet terms, respectively.

At the surface, denoted by subscript s,

$$N_s = D_s + W_s$$

Within the planetary boundary layer $0 \leq h \leq BL$ ($BL \approx 500$ m)

$$N(h) = D_s + \frac{dD}{dh} h + W_s + \frac{dW}{dh} h$$

Let the subscript BL denote values at h = BL, then within the troposphere $BL < h \leq TP$

$$N(h) = D_{BL} \left[1 - \frac{6.7 \times 10^{-3}}{T_s} (h - BL) \right]^4 + W_{BL} \exp \left[-(h - BL)/h_w \right],$$

where T_s is the measured surface temperature, TP the tropopause height and h_w is the wet scale height. The latter two are determined from monthly averages of radiosonde data.

Let the subscript TP denote values at h = TP. In the stratosphere the wet component is negligible, and

$$N(h) = D_{TP} \exp\left[-(h - TP)/h_d\right],$$

where h_d is the dry scale height determined from monthly averages of radiosonde data.

The introduction of the planetary boundary layer was made because surface weather measurements are influenced by the air-ground interface and are not, without modification, indicative of conditions well above the surface. Since Green Bank is in a mountainous area, existing radiosonde data may not be strictly applicable. Possible empirical modifications to some of the above parameters may be necessary. This problem is currently being evaluated.

E. WATER VAPOR RADIOMETER

The degradation of the interferometer data during summer is reflected in the three to four fold increase in the mean errors associated with determinations of UT and PM. This is due to the increase in the scan-to-scan phase scatter. One important cause of these short-term irregularities is the highly variable water vapor content of the atmosphere. Each antenna is now fitted with a meteorological station which measures the temperature, pressure and water vapor content at each site. This is not adequate for modelling the wet atmosphere due to the variable and unknown distribution of the atmospheric water along the line-of-sight. Therefore, we have begun the construction of two water vapor radiometers, to be placed inside the antennas of our longest baseline and to monitor the atmospheric water content in the line-of-sight of each dish.

The water vapor radiometers are being constructed at the U.S. Naval Observatory, and will be operated at 20.6 GHz and 31 GHz, similar to those designed by Guiraud, *et al.*, (1979) at the National Oceanic and Atmospheric Administration in Boulder, Colorado, and independently by Resch (1980) at Jet Propulsion Laboratory (JPL) in Pasadena, California. They will have prime focus parabaloid dishes of 1 m size and their beam size of about 1^0 is only slightly larger than the beam size of the primary interferometer dishes. The radio brightness of the water vapor and liquid droplets is, within a reasonable range of atmospheric parameters, linearly related to the column density of the two water components. The differentially measured water vapor should therefore also be linearly related to the phase deviations in the interferometer. A test run of the JPL

water vapor radiometers, when installed on the Very Large Array (VLA), has shown that they can introduce a considerable improvement to the VLA phase data (G. Resch, private communication).

The current status of the radiometers is that all of their intermediate frequencies (IF) and back-end electronics are constructed and tested; a few front-end wave guide parts are still on order but can be quickly incorporated into this system when they arrive. After the radiometers are calibrated at the U.S. Naval Observatory, they will be installed at Green Bank during the fall of 1982. An evaluation period of about six months will follow. Their results will be compared directly with the actual data taken by the interferometer.

F. DISCUSSION

Since the beginning of its service as a dedicated astrometric instrument, the Green Bank radio interferometer has proven to be a reliable instrument, meeting all of its expected performance requirements in an extremely cost effective manner. During the 44 months of its operation through May 1982, the longest unscheduled, unforeseen down-time was two consecutive weeks. It is hoped that the developments outlined here will significantly improve the overall capabilities of the CEI technique.

G. BIBLIOGRAPHY

D.E. Hogg, G.H. Macdonald, R.G. Conway and C.M. Wade (1969), "Synthesis of Brightness Distribution in Radio Sources", in Astronomical Journal, 74, 1206.

F.O. Guirand, J. Howard and D.C. Hogg (1979), "A Dual-Channel Microwave Radiometer for Measurement of Precipitable Water Vapor and Liquid", in IEEE Transactions in Geoscience Electronics, GE-17, 129.

K.J. Johnston, J.H. Spencer, C.H. Mayer, W.J. Klepczynski, G.H. Kaplan, D.D. McCarthy, and G. Westerhout (1979), "The NAVOBSY/NRL Program for the Determination of Earth Rotation and Polar Motion", in ____ ___ _____ Rotation, edited by D.D. McCarthy and J.D. Pilkington, published by D. Reidel.

G.H. Kaplan, F.J. Josties, P.E. Angerhofer, K.J. Johnston, and J.H. Spencer (1982), "Precise Radio Source Positions from Interferometric Observations", in Astronomical Journal, 87, 570.

W.J. Klepczynski, K.J. Johnston, G.H. Kaplan, D.D. McCarthy, J.H. Spencer, F.J. Josties, and R.L. Branham (1980), "Progress Report on the USNO/NRL Green Bank Interferometer Program", in Radio Interferometry Techniques for Geodesy, edited by R. Coates, published by NASA-GSFC.

D.D. McCarthy (1981), "An Intercomparison of Connected Element Interferometer and Lunar Laser Earth Rotation Parameters", in IAU Colloquium 63, High Precision Earth Rotation and Earth-Moon Dynamics, Lunar Distances and Related Observations.

D.D. McCarthy, G.H. Kaplan, W.J. Klepczynski, F.J. Josties, D.N. Matsakis, P.E. Angerhofer, K.J. Johnston and J.H. Spencer (1980), "Earth Rotation Parameters from Connected Element Interferometric and Classical Techniques", in AIAA Guidance and Control Conference Proceedings, Paper No. 80-1755.

D.D. McCarthy, W.J. Klepczynski, G.H. Kaplan, F.J. Josties, G. Westerhout, K.J. Johnston, and J.H. Spencer (1979), "Variations of Earth Orientation Parameters from Changes in the Orientation of the 35 km Baseline of the Green Bank Interferometer", in Annual Report of the BIH 1979, 1980.

G.M. Resch (1980), "Mark III VLBI System - Tropospheric Calibration Subsystems", in Radio Interferometry Techniques for Geodesy, edited by R. Coates, published by NASA-GSFC.

C.M. Wade and K.J. Johnston (1977), "Precise Positions of Radio Sources. V. Positions of 36 Sources Measured on a Baseline of 35 km", in Astronomical Journal, 82, 791.

OBSERVATIONS OF SCINTILLATION AND CORRELATED FLUX USING THE REAL-TIME VLBI SYSTEM (K-2)

Nobuyuki Kawano, Taizo Yoshino, Fujinobu Takahashi and Kunimasa Koike

Kashima Branch, Radio Research Laboratories
Hirai, Kashima, Ibaraki, 314 Japan

and

Hiroshi Kumagai

Hiraiso Branch, Radio Research Laboratories
Nakaminato, Ibaraki, 311-12 Japan

ABSTRACT. A real-time VLBI system ,(K-2), with 47 km baseline connected by a terrestrial micro-wave link was developed. This system adopts the bandwidth synthesis technique which samples five channels. These five channels, each of 2 MHz bandwidth, are switched sequentially at every 10 ms. The measurement accuracies of phase and delay are about 3 degrees, and 0.1 ns respectively. Using this system, the phase scintillations on the path through the atmosphere, the visibility scintillations due to the solar wind and the correlated fluxes of 44 radio sources were observed at 4 GHz.

1. INTRODUCTION

Because of the potential for high capacity communications and the limitation to the integration time in VLBI, the atmospheric phase scintillations in microwave and millimeter wave regions are of considerable interest. Propagation effects resulting from atmospheric phenomena influence optimum utilization of these frequency regions and the minimum product of two antenna diameters in VLBI. There is another cause for the limitation to the integration time in VLBI. That is the phase scintillation due to the solar wind. In this paper, the phase scintillation derived from the difference between the phase variations of the signals from two satellites, and the visibility scintillation due to the solar wind measured when the propagation path of radio waves from QSO 3C273 approached the sun, are reported. We also observed 80 radio sources in order to investigate available radio sources to a VLBI measurement for geodesy. We could detect 44 sources of flux more than 0.32 Jy, which corresponds to the minimum detectable flux density in our system. This result is also reported in this paper.

2. DESCRIPTION OF K-2 VLBI SYSTEM

The main characteristics and the block diagram of K-2 system are

reported in the references,(Saburi et al. 1982) and (Kawano et al. 1980). Fig. 1 shows a phase noise at 4 GHz due to the atomic frequency standards (Cs and Rb) which are used in K-2 system.

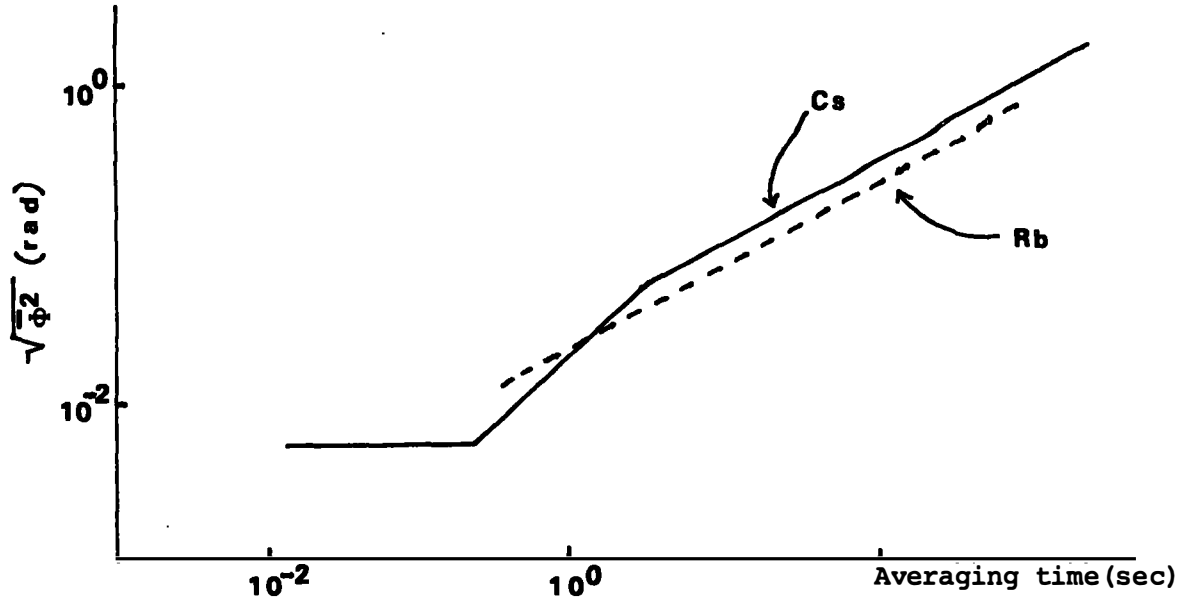

Fig. 1 Phase noise due to the atomic frequency standards (Cs and Rb)

3. MEASUREMENT OF ATMOSPHERIC PHASE SCINTILLATIONS

The phase scintillations along the path through the atmosphere were observed for the first time using the real-time VLBI system. We alternately received radio waves from synchronous satellites CS (Japanese Communications Satellite) at El=47.8 deg. and INTELSAT at El=1.7 deg. to obtain the atmospheric phase scintillations. The effects of secondary waves, which reflect on the ground, can be assumed to be far less than ones by phase scintillations at both elevation angles.

Assuming that the propagation path through the atmosphere, especially troposphere, is approximately proportional to 1/sin(El), the path length at El of 1.7 deg. is about 25 times as long as that at El=47.8 deg. On the other hand, the phase scintillation σ_ϕ^2 is directly proportional to propagation path length (Tatarski 1961). Therefore, the difference between phase variations of the signals from CS and INTELSAT can be regarded as the atmospheric phase scintillation.

Fig. 2 shows a square root of a difference of Allan variances $\sqrt{\sigma_\phi^2}$ derived from the phase variations of the signals from INTELSAT and CS. $\sqrt{\sigma_\phi^2}$ obeys approximately $0.2\times T^{0.7\sim 1.4}$ deg. at the zenith, where T denotes the averaging time in sec. This function $\sqrt{\sigma_\phi^2}$ is equivalent to the power spectral density $S(\nu)\propto \nu^{-1.4\sim -2.8}$ which is the results obtained through the path on the ground. Although the observations were carried out under the various meteorological conditions such as are

cloudy, of light rain and heavy rain, the effect of rain or other precipitation were not detected from these measurements. These results

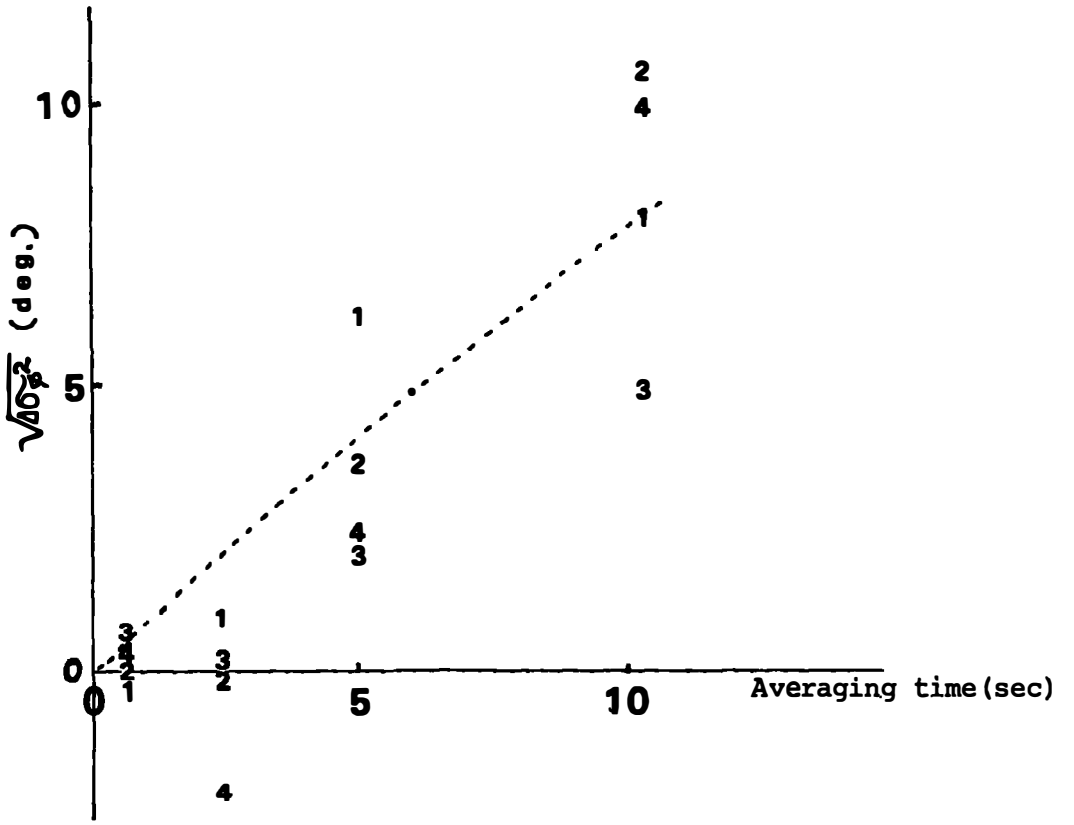

Fig. 2 Square root of the Allan variance of phase scintillations, $\sqrt{\sigma_\phi^2}$ (Square root of the difference of the Allan variances derived from the phase variations of the signals from INTELSAT and CS)

lead to the fact that $\sqrt{\sigma_\phi^2}$ at El=30 deg. may exceed one radian, and hence the coherence may decrease when the mean time or integration time becomes 300 sec. or more. This estimation suggests that the product of two antenna diameters in VLBI system should be more than 76 m^2 when the VLBI system with receivers of 50 K system noise temperature is used for geodesy, astrometry or other fields in Japan, even if an stable frequency standard such as H-maser oscillator is used. For example, if the main station has a 26 m antenna, the other station should have the antenna greater than 3 m.

4. MEASUREMENT OF VISIBILITY SCINTILLATION DUE TO THE SOLAR WIND

The observations of the visibility scintillation due to the solar wind were carried out by receiving QSO 3C273 from Sept. 18 to Oct. 14, 1980. The visibility scintillations increased when the wave propagation path

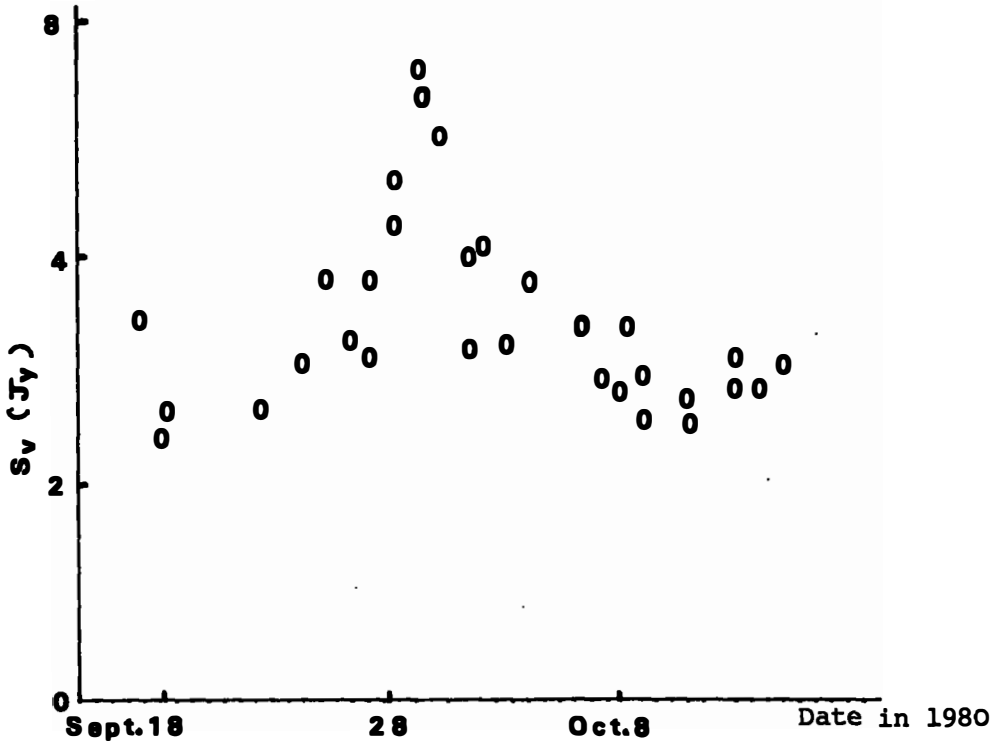

Fig. 3 Visibility scintillation S_ν due to the solar wind.

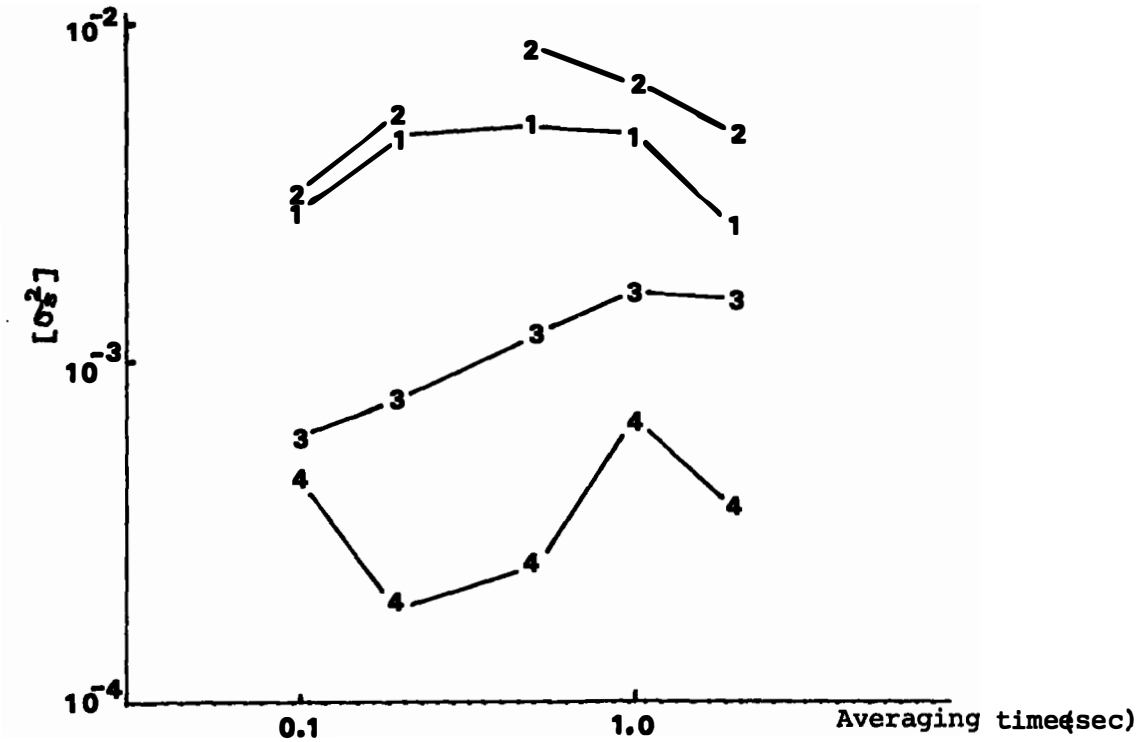

Fig. 4 Allan variances of the visibility scintillations for 3C273e
$[\sigma_s^2]$ denotes the normalized S_ν by the mean correlated fluxe

from QSO 3C273 approached the sun as shown in Fig. 3, and they reached 10 % of the mean correlated flux, higher than the normal level, when the distance between the path and the sun was the nearest of 0.08 AU. The Allan variance of the visibility, $[\sigma_s^2]$ became maximum in the mean time of 0.5∼1.0 sec. According to a theoretical investigation, the frequency range of the scintillations observed by a VLBI system is limited to the frequency higher than the baseline frequency given by Cronyn (Cronyn 1972), so that the averaging time 0.5 sec obtained by our observations is coincident with the reciprocal of the baseline frequency ν_b estimated from the Parker's solar wind model (Parker 1965). Furthermore, the visibility scintillations obey approximately the 3rd power law of the distance.

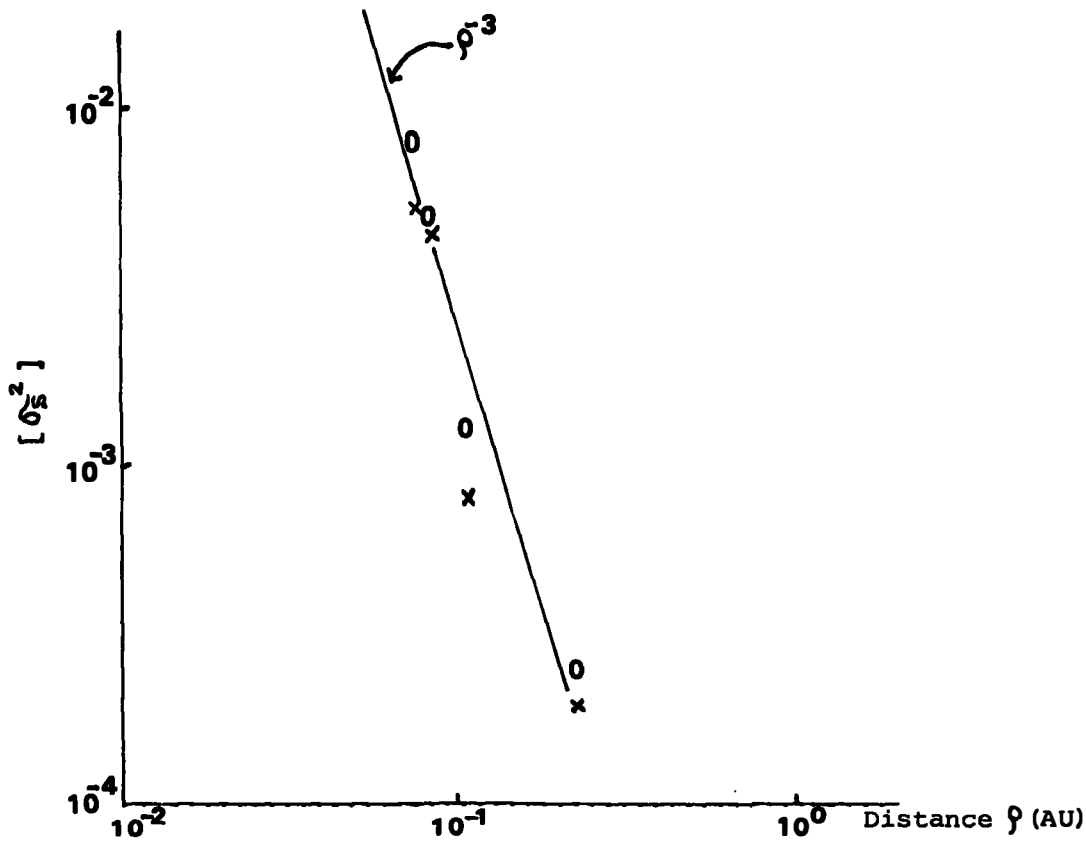

Fig. 5 Normarized visibility scintillation versus the distance between the path from 3C273 and the sun.

Fig. 4 and Fig. 5 show Allan variances of the visibility scintillations for 3C273 and relation of the scintillations with the distance between the path from 3C273 and the sun.

These results show that $[\sigma_s^2]$ becomes less than $10e^{-4}$ when the distance ρ exceeds 3×10^{-1}AU, and hence the effect of the interplanetary scintillations at 4 GHz diminishes over all scintillation frequencies in this case.

5. MEASUREMENT OF CORRELATED FLUX

We also observed 80 radio sources in order to investigate available radio sources to a VLBI measurement for geodesy. We could detect 44 out of 80 radio sources of flux more than 0.32 Jy, which corresponds to the minimum detectable flux density in our system. Table 1 is the result of this observation, and shows that the fluxes of 3C120, 3C123 and some others vary with an hour angle.

Source name	Flux (Jy)	Source name	Flux (Jy)
3C10	0.4	3C273B	26
3C20	0.4	3C274	1.0
3C28	0.4	3C279	4.0
3C29	0.6	3C286	4.4
3C31	0.4	3C287	1.2
3C66	0.4	3C295	1.0
3C75	0.4	3C380	1.4
3C84	34	3C382	0.4
3C105	0.6	3C386	0.4
3C119	1.2	3C391	<0.6
3C120	<1.8	3C397	<0.6
3C123	0.4~1.2	3C398	0.5
3C133	0.4	3C403	0.4
3C138	<1.8	3C410	<0.6
3C147	1.0~4.2	3C418	1.6
3C147.1	<0.6	3C452	0.4
3C192	0.4	3C454.3	5.2
3C196	0.4	3C461	<0.8
3C207	0.4	3C465	<0.6
3C237	0.6	4C39.25	3.0
3C268.1	0.4	DW1555+00	0.6
3C270	0.4	NRAO530	1.0

Table 1 List of correlated fluxes for 44 radio sources. (Frequency:4030MHz, bandwidth:1.3MHz, Integration time:30sec, rms error:0.32 Jy).

REFERENCES

Cronyn, W. M., (1972), "Interferometer visibility scintillation" Ap.J. 174, 181.

Kawano, N., Takahashi, F., Yoshino, T. and Kawajiri, N. (1980), "Phase scintillation measurement system using real-time VLBI", International IEEE/AP-S Symposium Digest, vol. 1, J.1/AP-6, p69-72.

Parker, E. J., (1965) Space Sci. Rev., 4, 666.

Saburi, Y., Yoshimura, K., Kato, S., Tsukamoto, K., Yamashita, F., Kawajiri, N. and Kawano, N., (1982) "Development of VLBI system and future experimental plan in the Radio Research Laboratories", in this issue.

Tatarski, V.I., (1961) "Wave propagation in a turbulent medium", MacGraw-Hill.

ON THE COMPUTATION OF IONOSPHERIC PATH DELAYS FOR VLBI FROM SATELLITE DOPPLER OBSERVATIONS

James Campbell, Franz Josef Lohmar
Geodätisches Institut, Universität Bonn

ABSTRACT. Two-frequency satellite Doppler observations carried out simultaneously with VLBI experiments on several European and one transatlantic baseline were used to determine ionospheric path delay corrections. In the first part the method applied is outlined and the problems and limitations are discussed. In the second part the ionospheric data obtained for an 18 cm VLBI campaign are presented.

1. INTRODUCTION

High accuracy geodetic applications of Very Long Baseline Interferometry require a careful calibration of the atmospheric effects on the measured quantities. In the radio frequency range wave propagation is affected both by the neutral atmosphere and by the ionized layers of the higher atmosphere (Hagfors 1976). In this paper only the contributions of the ionosphere to the measurements are discussed. The dispersive nature of the ionosphere can be used to eliminate the first order path errors if two widely spaced frequencies are observed simultaneously. In Doppler satellite tracking the dual frequency approach is an integrated part of the system and provides reliable ionospheric calibration (Guier et al. 1960).

In VLBI a dual frequency receiving system requires a considerable effort to be implemented, hence there are no more than a few stations adequately equipped to observe in the dual frequency mode. At present only the frequency pair 2.3/8.4 GHz (NASA S- and X-Band) is available for wider use, but stations with S-X-capability are mainly restricted to the territory of the U.S.A. In Europe other frequencies are favoured, such as 1.6, 5, 10 and 22 GHz (18, 6, 2.8 and 1.3 cm). For each of these frequency bands highly sensitive wideband receiving systems are available and commonly used for astronomical applications. In this situation it seems desirable to find alternative ways of collecting ionospheric data and to be able to apply ionospheric corrections to single frequency band VLBI measurements.

At present two approches have appeared in discussions more frequently:

1. Measuring the Faraday rotation of the radio signals of geostationary satellites (Davies et al. 1977).
2. Using dual frequency Doppler or pseudo range measurements to Earth satellites (Davies et al. 1977, MacDoran et al. 1982).

In both cases the ionosphere is probed at more or less widely spaced time intervals and generally not coinciding with the VLBI lines of sight. This is of course a serious drawback of both methods, especially if the high variablility both in time and in space of the ionospheric refraction is considered. It is fairly obvious that useful results can only be expected if spacial and temporal resolution is high enough to follow the more prominent ionospheric variations (i. e. the day-night effect and the latitude dependence). In order to investigate the value of satellite Doppler observations for correcting single band VLBI measurements several simultaneous VLBI- and Doppler-campaigns have been carried out with various stations in Europe and in the U.S.A. In this paper the adopted procedures are described and first results are presented.

2. DOPPLER COUNTS AS SOURCE FOR IONOSPHERIC INFORMATIONS

In geodetic applications Doppler measurements to the satellites of the Navy Navigation Satellite System are performed on both coherent frequencies emitted by the satellites, 149.988 MHz and 399.968 MHz (150 and 400 MHz) to eliminate the first order term of the ionospheric range error (IRE).

Taking only first order effects into account the refractive index of the ionosphere can be expressed by (e. g. Davies, 1977).

$$n = 1 - \frac{40.31}{f^2} \cdot EC, \qquad (1)$$

where EC = content of free electrons in $1m^3$.

Integrated along the line of sight with the assumption that the signal path is identical to the geometrical connection receiver (R) satellite (S) the IRE is

$$\Delta s = \int_R^S (1 - n)\, ds = + \frac{40.31}{f^2} \cdot \int_R^S EC\, ds = \frac{40.31}{f^2} \cdot TEC \qquad (2)$$

where the total electron content (TEC) represents the number of free electrons along the line of sight per m^2.

Writing down equation (2) for both frequencies it is possible to calculate the IRE from the difference in IRE at both frequencies

$$\Delta s_{400} = (\Delta s_{150} - \Delta s_{400}) \cdot \frac{f_{150}^2}{f_{400}^2 - f_{150}^2} \,. \qquad (3)$$

The observed Doppler counts N are defined as $N = \int_{t_1}^{t_2} (f^G - f^R)\, dt$, where

f^G = frequency of the receiver oscillator

f^R = received satellite frequency f^S, Doppler shifted and affected by the atmosphere.

Differencing the 400 MHz and the 150 MHz counts, after scaling the latter by $\frac{8}{3}$ $(= \frac{400}{150})$ we obtain:

$$\Delta N = \int_{t1}^{t2} (\tfrac{8}{3} f_{150}{}^R - f_{400}{}^R)\, dt \quad . \tag{4}$$

In a nondispersive medium the count difference ΔN would be zero (neglecting measurement errors of the receiver). ΔN may be interpreted as the change in the difference of the IRE's of both signals over the time span $t_2 - t_1$ divided by the 400 MHz wavelength.

$$\Delta N = \frac{f_{400}}{c_o} \cdot \left[\Delta s_{150}^{t_2} - \Delta s_{400}^{t_1} - \Delta s_{150}^{t_1} + \Delta s_{400}^{t_2} \right] \quad . \tag{5}$$

The change in IRE for the 400 MHz signal in the time span $t_2 - t_1$ is found using equations (3) and (5).

$$\Delta s_{400}^{t_2} - \Delta s_{400}^{t_1} = \frac{c_o}{f_{400}} \cdot \frac{f_{150}^2}{f_{400}^2 - f_{150}^2} \cdot \Delta N \quad . \tag{6}$$

Using the above equation it is possible to compute the changes in IRE along the satellite pass using the measured count differences ΔN.

To derive absolute values of the IRE, the initial range error $\Delta s_{400}^{t_0}$ at the beginning of each satellite pass has to be found.

In our data analysis we use a method developed by Leitinger et al. 1975. This method essentially relies on the fact that from two Doppler receivers located at a given North-South distance of about 1000 km the zenith angles of the lines of sight in the ionosphere will generally be significantly different (see fig. 1). This difference allows to solve for the constant biases at both stations.

Adding up the constant bias $\Delta s_{400}^{t_o}$ and all differences in the IRE calculated in equ. (6) the IRE referenced to the line of sight at epoch t_i is obtained.

3. INTERPOLATION MODEL FOR DOPPLER DERIVED IONOSPHERIC CORRECTIONS

The pointing directions of the radio telescopes will in general not coincide with the tracks of the NNSS satelliteso Therefore some sort of interpolation of the IRE values is required. Idially we have a three dimensional problem: azimuth and elevation in a local coordinate system and the time of observation. One way to attack the problem is to replace the actual ionosphere by a thin layer at a given constant altitude (e. g. 400 km in the mid-latitude zones) (Hartmann 1977)o The vertical IRE values are referenced to the ionospheric point (IP) which is defined as the intersection of the line of sight to the satellite with the ionospheric layer. The IP is described by only two parameters: Its geographic latitude and its local solar time. In this way one spacial parameter is combined with the parameter timeo Looking at the physics of the ionosphere, this approach seems reasonableo because the state of the ionosphere is strongly dependent on the hour angle of the sun (day-night-variations) and on the latitude. The values latitude, local solar time and also the ionospheric zenith angle can easily be calculated from the station-to-satellite geometryo

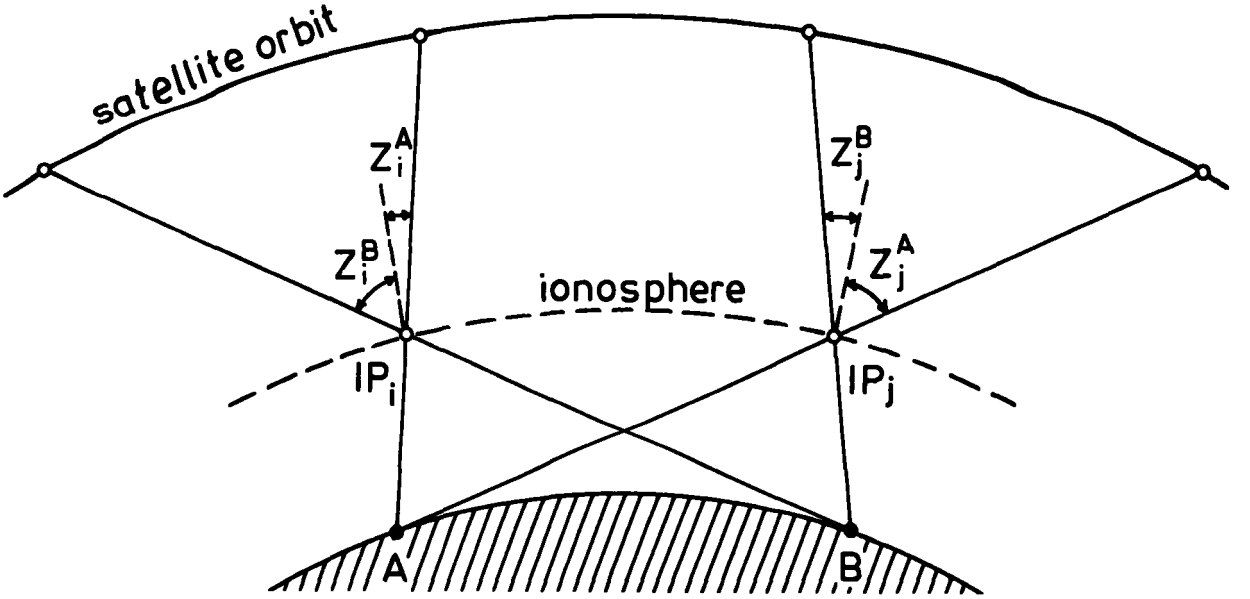

Figure 1: Geometry for two stations: For simplicity of drawing it is assumed, that the orbit of the satellite and the two stations A, B are in a common plane (Leitinger et alo 1975).

The actual interpolation of the vertical IRE is performed in the reference system defined above. The trace of the IPs for one satellite pass is approximately a North-South line and the vertical IREs of the pass form therefore a North-South profile of the ionosphere. A two dimensional representation of the Doppler derived vertical IREs can be given in contour maps using this coordinate system (figure 2).

4. IONOSPHERIC CALIBRATION OF VLBI OBSERVABLES

The three geodetically interesting VLBI observables, the group delay, the fringe phase and the fringe rate are independently estimated in the crosscorrelation function analysis (Moran 1976). All three quantities are affected differently by the ionospheric medium: the group delay, which is based on the phase response to frequency, is connected to the group velocity v_{gr} while the phase and the rate are connected to the phase velocity v_{ph} of the signal. In the presence of a dispersive medium the relationship between both velocities is (Bergstrand 1956)

$$\frac{1}{v_{gr}} = \frac{d}{df}\left[f \cdot \frac{1}{v_{ph}} \right] , \quad \text{where} \tag{7}$$

$$v_{ph} = \frac{c_o}{n} . \tag{8}$$

If (7) and (8) are combined with (1) we can verify that the ionospheric phase delay correction should be nearly equal in magnitude but opposite in sign from the group delay correction. Moreover the group delay must have the same sign as the tropospheric path correction, because $v_{gr} < c_o$ both in the ionosphere and in the troposphere.

The ionospheric mapping function we presently use in the baseline fitting program is similar to the one used for the troposphere (essentially a 1/cosz dependence), but instead of the ground based zenith angle z the zenith angle z (IP) at the height of the condensed ionospheric layer is introduced. At low elevations the ionospheric and the tropospheric mapping functions differ significantly, the latter showing a much steeper rise than the former. This in turn causes the rate correction, which is the time derivative of the delay correction, to be much less pronounced in the ionosphere than in the troposphere. Hence only a relatively small ionospheric signal may be expected in the fringe rates while the main contribution will be felt in the group delays and in the phases.

5. NUMERICAL RESULTS

Up to now three different VLBI campaigns have been accompanied

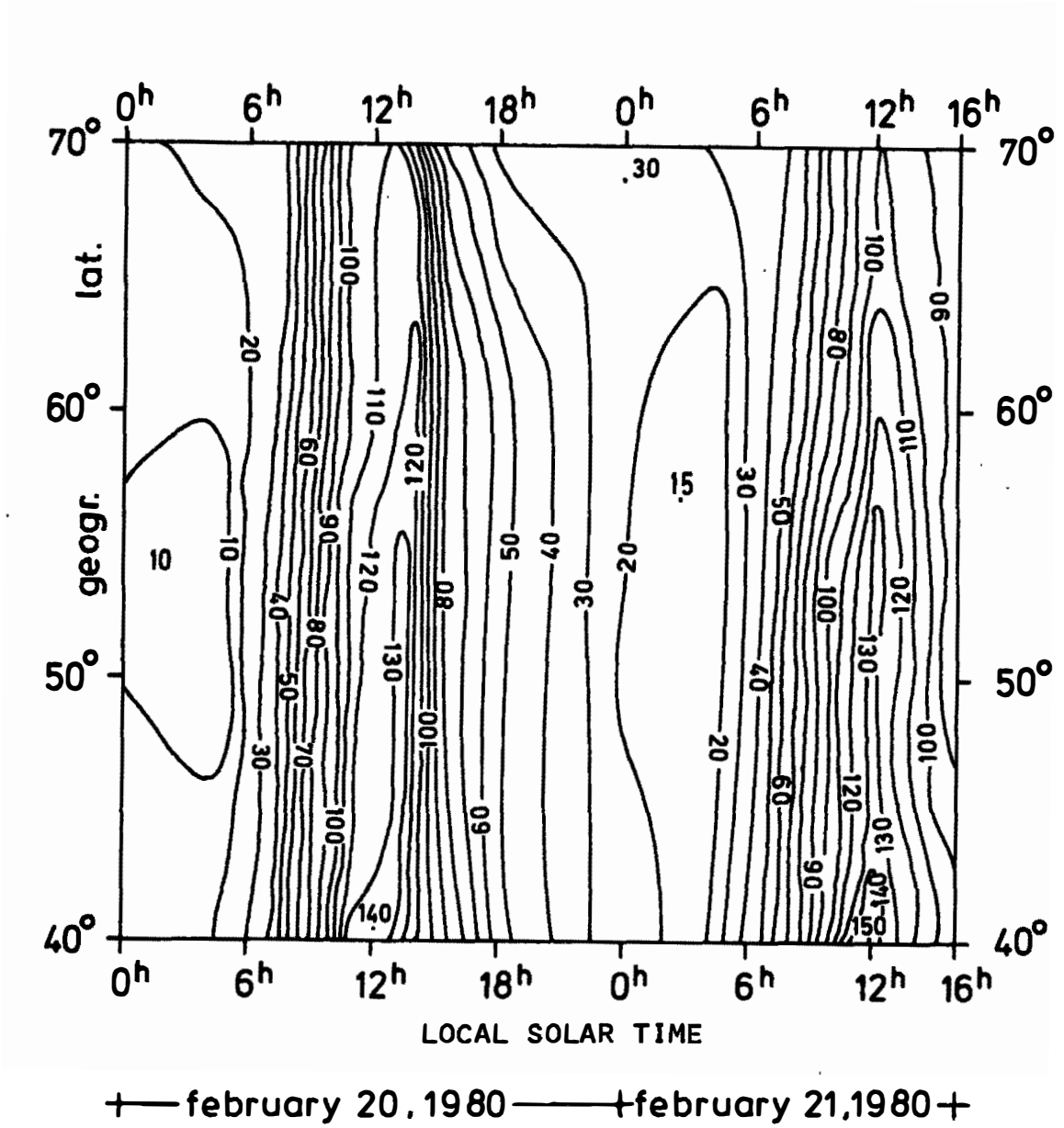

Figure 2: Ionospheric contour map derived from Doppler data of the stations Effelsberg and Onsala. The contour lines refer to the vertical IRE in meters at 400 MHz.

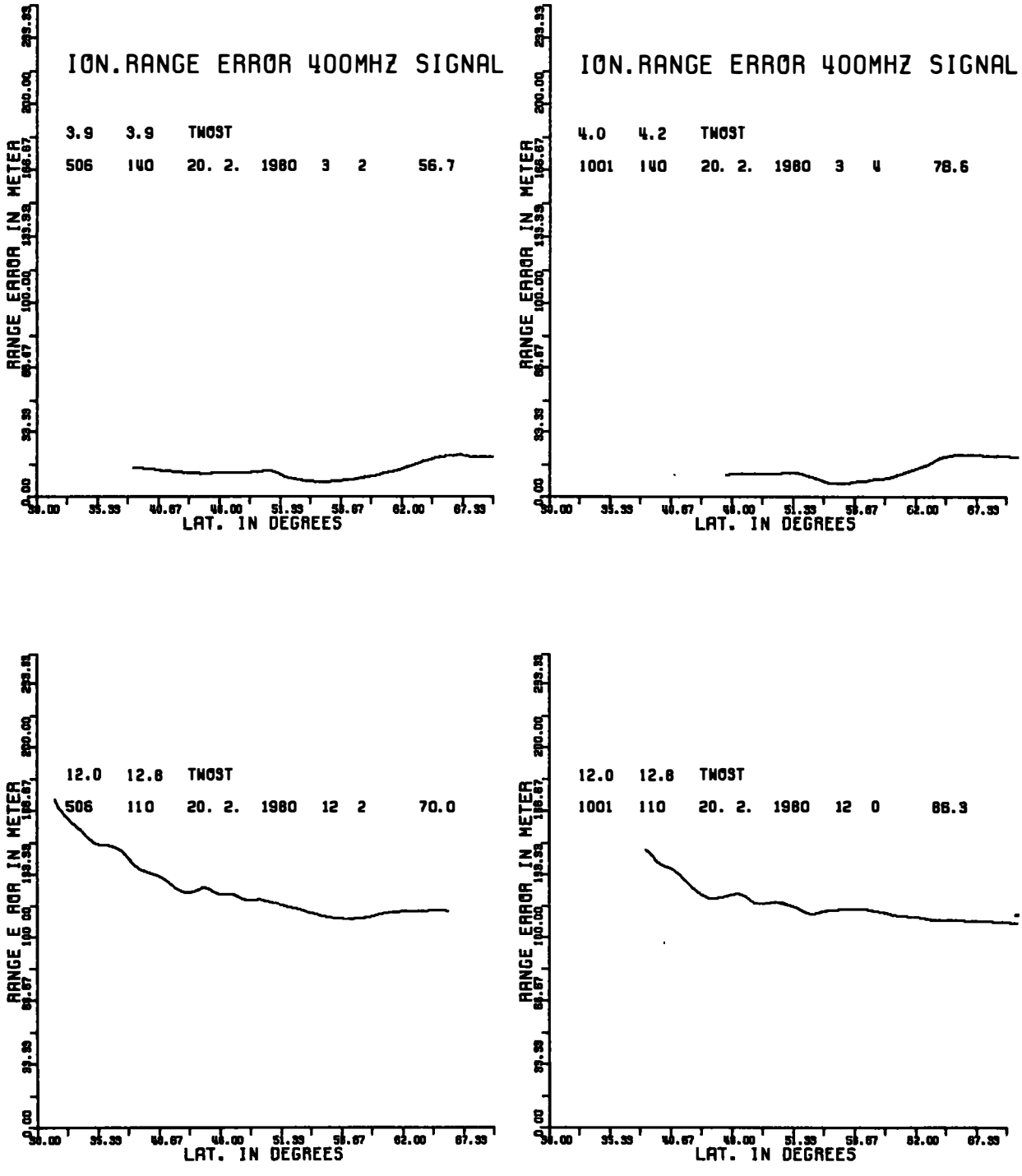

Figure 3 : Vertical IRE profiles derived from satellite passes on february 20, 1980 3h 2m UT (sat. 30100) and 12h 2m (sat. 30100) using Doppler data from station Effelsberg (left side) and from Onsala (right side).

by Doppler observations: The Nov. '79 MkoIII experiment at 2.3 and 8.4 GHz, the Febr. '80 Mk II experiment at 1.6 GHz and the April '81 ERIDOC Mk II experiment at 5 GHzo At this stage of the data processing (the ionospheric transfer model has just been completed) only a small part of the Febro '80 data have been used to obtain a first proof of concept before more effort is invested.

The Doppler data available for the dates of the experiment, the 20th and 21st of Febr. 1980, were taken at the stations of Effelsberg and Onsala with the Magnavox MX 1502 receiverso At NRAO Green Bank a Geoceiver was used while the receiver at Maryland Point apparently failed to produce any good datao For the first test we started to process the MX 1502 data and produced ionospheric profiles over Europe which served to interpolate the IRE's at the ionospheric points of the VLBI lines of sight and to draw the map in fig. 2. Four typical examples of ionospheric IRE-profiles at 400 MHz are shown in fig. 3. Two each are seen from Effelsberg and Onsala during the same satellite pass and represent the same portion of the ionosphereo The agreement at night time is very good, whereas at daytime small deviations can be seen. These reflect the inhomogeneities of the ionosphere and will set a limit to the applicability of the proposed methodo especially when short baselines are considered.

In order to test the effect of the Doppler derived ionospheric corrections on the VLBI group delays and fringe rates it appeared most efficient to run the baseline solutions with the option of

Dayo	Uncorrected data		Corrected data	
	Delay rms ns	Rate rms mHz	Delay rms ns	Rate rms mHz
51	14.0	3.6	5.2	3.0
52	12.0	2.0	5.3	1.6

Table 1: Effect of the Doppler derived ionospheric correction on best fit residuals of baseline solutions (Mk II 18cm data) (Baseline NRAO Greenbank - Effelsberg)

holding all parameters fixed except the three clock unknownso We used the best baseline coordinates and source positions presently available to us, i.e. the results from the November 79 Mk III experiment at 8.4GHz. The tropospheric parameters were set at their standard values of 2.10m extra zenital path. Under normal conditions these values only vary between 1.9 and 2.3 meters. Because of the lack of ionospheric data at the NRAO end of the baseline (the Geoceiver data have not yet been decoded) we chose a period of both days during which the NRAO site is still in night timeo while Effelsberg is already out in the daylighto In this case it is safe to assume a low mean night time value for NRAO and use the Doppler derived data for Effelsbergo The rms fitting errors shown in table 1 give a strong indication of the validity of the methodo The residual plots in figure 4 provide a more detailed illustration of the effectiveness of the applied correctionso

The solutions of the same data with the baseline and tropospheric parameters free indicate that the ionospheric bias tends to be absorbed by these parameters instead of blowing up the residuals, a fact which has been suggested by Robertson and Carter (1981)o In spite of a relatively high signal to noise ratio on the NRAO - Effelsberg baseline the data perform, helas, rather poorly, therefore more specific investigations will be carried out after reprocessing the crosscorrelation data with an improved software systemo

The preceding results are examples of particularly gross effects on an intercontinental baseline. It remains to be seen whether the method can keep its promise on shorter baselines with much more subtle effectso Some of the November 79 Mk III VLBI data which have been observed at both S and X bands will serve as excellent test data sets to validate the use of Doppler derived ionospheric information.

6. ACKNOWLEDGEMENTS

The authors would like to thank the Max-Planck-Institut für Aeronomie Lindau, Federal Republic of Germany and the Institut für Meteorologie und Geophysik der Universität Graz, Austria for supporting these studies and especially G.K.Hartmann and R. Leitinger for many valuable discussions.

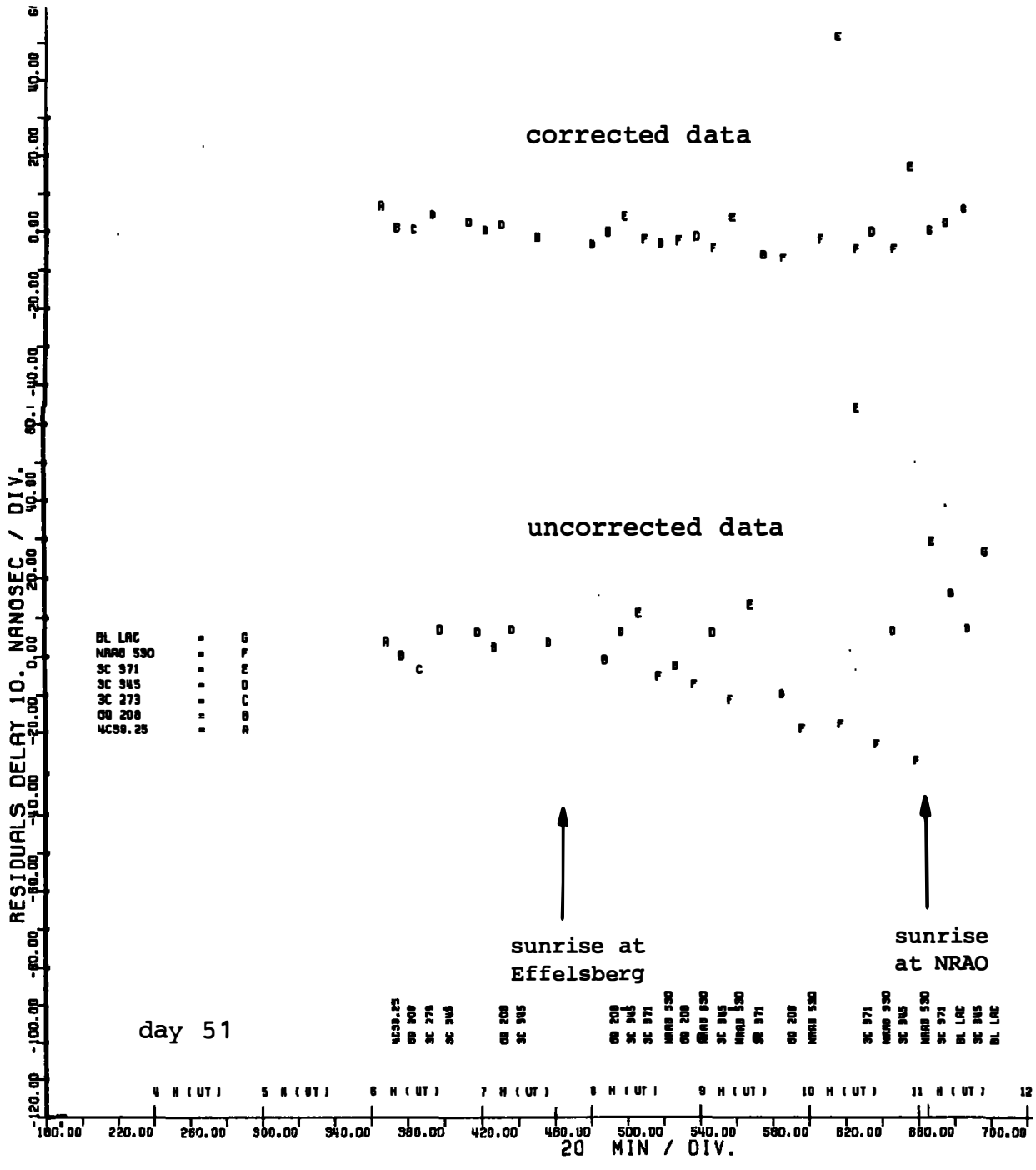

Figure 4: Residuals of least squares baseline fit with all parameters held fixed (except the 3 clock unknowns).

7. REFERENCES

Bergstrand, E. (1956) — Determination of the Velocity of Light. In: Handbuch der Physik, Vol. XXIV, Springer, Berlin.

Davies, K.; Degenhardt, W.; Hartmann, G. K.; Leitinger, R. (1977) — Electron Content Measurements over the U. S. Joint Radio Beacon Program NOAA/MPAE/Graz Station Report ATS-6 948 W.

Guier, W. H.; Weiffenbach, G. C. (1960) — A Satellite Doppler Navigation System, Proc. IRE 1, 507-516.

Hagfors, T. (1976) — The Ionosphere. In: Methods of Experimental Physics, Vol. 12, Part B: Radio Telescopes. Ed. M. L. Meeks, Academic Press, New York.

Hartmann, G. K.; Leitinger, R. (1977) — Zeit- und Breitenabhängigkeit von transionosphärischen Ausbreitungsfehlern. Kleinheubacher Berichte, 20, 267-276.

Leitinger R.; Schmidt, G.; Tauriainen, A. (1975) — An Evaluation Method Combining the Differential Doppler Measurements from Two Stations that Enables the Calculation of the Electron Content of the Ionosphere. J. Geophys., 41, 201-213.

MacDoran, P. F.; Spitzmesser, D. J.; Buennagel, L. A. (1982) — SERIES: Satellite Emission Range Inferred Earth Surveying. Proc. of the 3rd International Geodetic Symposium on Satellite Doppler Positioning, Las Cruces.

Moran, J. M. (1976) — Very Long Baseline Interferometric Observations and Data Reduction. In: Methods of Experimental Physics, Vol. 12, Part C, Radio Observations, Academic Press, New York.

Robertson, D. S.; Carter, W. E. (1981) — Earth Rotation Information Derived from MERIT and Polaris VLBI Observations. Presented at the IAU Colloquium No. 63 Grasse, France (DRAFT).

TECHNIQUES USED IN SAO HYDROGEN MASERS FOR INCREASED FREQUENCY STABILITY AND RELIABILITY

Edward M. Mattison
Robert F. C. Vessot

Smithsonian Astrophysical Observatory
Cambridge, Massachusetts 02138, U.S.A.

ABSTRACTo The major characteristics of frequency standards of concern to users are frequency stability, reliability of operation, and ease of transport. We describe approaches taken by SAO to fulfill these criteria in the VLG-11 series of hydrogen masers. They include receiver improvements for short-term stability, changes in resonant cavity construction and magnetic shield design for reduction of systematic effects, and redesign of the vacuum pumping system for longer life.

INTRODUCTION

Users of frequency standards -- and VLBI users of hydrogen masers in particular -- are interested in three major aspects of their standards' performance: frequency stability, reliability, and transportability. Currently, while masers are in short supply, VLBI puts an especially high premium on the ability to move a maser to an antenna site and have it operate with good stability precisely when it is needed: during a scheduled observing run. We describe here some of the factors that affect masers in these areas and discuss the approaches that the Smithsonian Astrophysical Observatory (SAO), in its program of research and development of masers for use in VLBI and space tracking programs, has taken to satisfy these requirements.

MASER FREQUENCY STABILITY

The frequency stability of hydrogen masers over intervals shorter than roughly 1,000 seconds is affected primarily by thermal noise, and is determined largely by the maser's power output and line Q and by the noise figure and construction of its receiver. With the aim of increasing reliability and short-term stability we have redesigned part of the VLG-11 receiver and reconstructed the entire unit. We have combined the successful rf design of the VLG-11B, which is based on a 100 MHz VCXO, with an improved phase-lock circuit that avoids the need for a separate sweep oscillator for acquiring lock. The receiver housing, which measures 6 x 20 x 29 cm, is machined from a solid aluminum block that provides mechanical ruggedness and thermal uniformity. It is shown in Fig. 1 with its covers removed. The method of assembly minimizes the number of coaxial connectors in high-frequency circuitso reducing a possible source of noise. In addition to providing the usual low-frequency outputs at 0.1, 1, 5, and 10 MHz, the receiver supplies signals at 100 MHz and 1,200 MHz. These are particularly

suitable for multiplication to higher frequencies in applications such as millimeter-wave VLBI.

Over intervals longer than about 1000 seconds, maser output frequency is influenced chiefly by systematic effects that include changes in the resonance frequency of the microwave cavity and variations in the external magnetic field.

Cavity frequency shifts, which result in pulling of the atomic line shape and consequently of the output frequency, can be caused by temperature-induced changes in the dielectric coefficient of the quartz storage bulb; by changes in cavity dimensions due to variations in ambient temperature, barometric pressure, or cavity mechanical properties; and by other mechanisms. Work at the Jet Propulsion Laboratory (Kuhnle, 1981), the U. S. Naval Research Laboratory (White, 1981), and SAO has shown that some masers display a regular long-term frequency drift on the order of parts in 10^{14} per day that is accompanied by a corresponding increase in the tuned cavity resonance frequency. The temporal behavior of these drifts is typically $1-e^{-t/T}$, with T on the order of 40 days. We believe that this effect is due to "bedding" of the ground surfaces of the low-expansion Cervit cavity at the joints between the cylinder. A similar effect has been observed in optically contacted joints in low- expansion materials (Jacobs, 1976). We have taken steps to reduce this drift by optically polishing the cavity endplates and cylinder end surfaces, and assembling the cavity under cleanroom conditions. We have observed that the frequency shift when the cavity is first assembled and clamped together is approximately 2 kHz for polished cavities, as compared with approximately 8 kHz for typical ground-joint cavities. Preliminary measurements indicate that the drift effect is much reduced, and we are in the process of tracking the tuning of two recently built masers to measure the effect accurately.

Other possible sources of cavity frequency drift are thermal expansion of the cavity material and relaxation of surface stress in the cavity's conductive coating. In an effort better to understand the properties of cavity materials and coatings we have collaborated with the University of Arizona Optical Sciences Center in a series of experiments. We measured the room-temperature thermal expansion coefficients of three low-expansion materials, ULE[1], Zerodur[2], and Cervit 101[3], before and after heating them to 700°C, the temperature at which the silver cavity coating is applied. The coefficients for Cervit 101 and ULE remained essentially unchanged following heating, while Zerodur's coefficient decreased in magnitude, as shown below.

Material	Expansivity x 10^8 ($^oC^{-1}$)	
	Before Heat Treatment	After Heat Treatment
ULE	+5.5	+5.5
Cervit 101	-14.5	-13.3
Zerodur	-12.3	-5.8

In a separate experiment we have measured the surface-stress induced curvature of rectangular silver-coated samples of cavity materials over a period of seven months. Preliminary results indicate that the peak- to-valley curvature of plates 100 mm long and 10 mm thick, coated with approximately 0.05 mm of silver, changed by less than the resolution of the experiment, approximately 1000 A°, over a period of six months. A temperature dependence of curvature was observed with a magnitude on the order of 2000 $A^{\circ}\ ^{\circ}C^{-1}$.

Certainly, one can never eliminate all systematic effects; as a major effect is reduced in magnitude, others will appear. Our approach to obtaining frequency stability is to make the maser as inherently stable as possible and then, if appropriate, to work at compensating for any residual perturbations. An example of this is our use of an extremely low mass quartz storage bulb to minimize temperature- dependent dielectric coefficient changes, and low-expansion cavity material to minimize thermally induced dimensional changes. Having minimized the cavity's thermal sensitivity, we stabilize the maser's internal temperature with a six-zone heat-added servo controller. To remove any long-term cavity drifts that remain, we are working on the development of an electronic cavity frequency stabilization system that will lock the cavity resonance to the atomic transition frequency with minimum perturbation of the atomic line.

To increase the effectiveness of the internal temperature control system we have installed in the maser cabinet a temperature controller that in effect turns the cabinet into a small environmental chamber. This provides constant temperature air for the maser electronics as well as for the physics package. Over an ambient temperature range of 21 to 28°C it yields an estimated temperature sensitivity $(1/f)(df/dT)$ of approximately $8 \times 10^{-16}\ ^{\circ}C^{-1}$. Exact values for the sensitivity await careful, lengthy measurements.

A maser's frequency can be altered by changes in the external magnetic field. Following our experience with shields designed by the Naval Research Laboratory (Gubser, 1981) for the small-cavity passive maser developed by SAO and NRL, we have designed and installed conical-ended magnetic shields in the latest VLG-11 masers. The innermost shield remains flat to provide suitable boundary conditions for the weak 0.5 G internally applied field. The conical shape of the three outer shields (Fig. 2) eliminates the "oil-canning" mechanical instability found in flat-ended shields and provides a mechanically stable structure that can be solidly supported without the hazard of localized stresses and resultant work hardening. This reduces the likelihood of changes in the permeability of the shields either during assembly of the maser or during transportation. Changes in ambient magnetic field can also affect the maser frequency by changing the distribution of atomic states in the atomic beam drift region, between the hexapole state-selector magnet and the low-field resonant cavity. To reduce this effect we have installed a band of low permeability material between the ion pump shield and the outer physics unit shield (Fig. 3). This band provides a low reluctance path across the gap between these shields and reduces the residual field in the beam drift region. A magnetic field coil mounted coaxially with the drift region generates a constant bias field. This

prevents large changes in ambient field from reducing the drift-region field to zero, which can alter the maser frequency or even quench maser oscillation by allowing the atomic states to become degenerate. The magnitude and direction of the bias field can be adjusted for operation of the maser in either northern or southern hemisphere. The measured shielding factor and magnetic sensitivity of a maser with the new magnetic shields are

$$\frac{dH_{ext}}{dH_{int}} = 18 \times 10^3$$

for $dH_{ext} = 0.44$ G

$$\frac{1}{f}\frac{df}{dH_{ext}} = 2 \times 10^{-13}\ G^{-1}$$

MASER RELIABILITY

Above all, the user of a frequency standard wants the standard to operate when he needs it. The major source of unreliability in masers in recent years has been the ion pump system used for pumping hydrogen and other gasses. Because this seems more serious than it was 10 years ago and is a problem with masers from several laboratories, it is possible that the metallurgy of the titanium plates used in the pumps has changed. At SAO we have developed a pumping system that eliminates the ion pump as the major pumping device. This system uses four Zr-Al sorption cartridges to pump hydrogen. The practicality of using this technique in masers was demonstrated in the NASA-SAO Gravitational Redshift Rocket Probe Experiment (Vessot, 1976), in which a single sorption cartridge pumped a rocket- borne hydrogen maser for over a year. In the current system a small multiple-anode ion pump designed and built by SAO scavenges residual gases such as nitrogen, argon, and hydrocarbons. The design of this pump permits switching to a fresh anode in case of shorting by screw dislocation ("whisker") growth from the cathode. The new system, which has an expected pumping lifetime of 5 years between reactivations of the cartridge, is retrofittable in all S.A.O. VLG-10 and VLG-11 model masers.

As part of our effort to improve maser vacuum systems we have designed and tested an in-vacuum hydrogen dissociator that uses no O-rings, thus eliminating a possible source of outgassing and leakage. A dissociator of this design has been operated in vacuum on a test stand for more than six months. Although the outside of the glass has darkened somewhat, apparently due to sputtering, the atomic hydrogen optical spectrum of the plasma has remained correct and the discharge has operated properly. A similar dissociator is being installed in our cryogenic maser for operation at 77K as a source of cold atomic hydrogen.

TRANSPORTABILITY

The ability to transport a standard depends upon its size, weight, and ruggedness. An important question is, can it be put on an airplane, and will it survive shipment? In VLBI applications masers must operate after being shipped to radio observatories, often in remote sites. SAO masers have been shipped successfully to Spain, Sweden, Germany, Australia, Japan, and throughout the United States. The VLG-11 maser is 124 cm high, 56 cm wide,

and 81 cm deep, and weighs 330 kg. When mounted on its shock-absorbing pallet it fits in the cargo compartments of DC-10 and L-1011 passenger planes. As witness to the effectiveness of its mechanical ruggedness, during a return trip shipment to SAO a maser was dropped with enough force to bend the cabinet frame, knock the meter needles off their pivots, and shift the ion pump magnets. When it was was turned on, it oscillated properly. (We do not, however, recommend this type of handling.) VLG masers can be trucked with full power, supplied by automotive batteries, and operated within minutes of arriving at the observing site. For air transport they are usually shipped with ion pump power only, supplied by high-voltage photoflash batteries with an expected life of many months. One such maser, which was "lost" enroute to an observing site and sat at an airport for almost a week, operated without difficulty. A maser shipped to Onsala, Sweden, with no power whatever took three days to reach its destination, was pumped down with an external ion pump power supply, and oscillated as soon as its temperature control system achieved equilibrium.

CONCLUSION

Since its invention in the early 1960's the hydrogen maser has come a long way from being a large, delicate laboratory instrument. Through the efforts of several groups the maser has emerged from the laboratory and has become a reliable, practical tool for the working scientist.

NOTES

[1] ULE is a registered trademark of Corning Glass Works, Inc.
[2] Zerodur is a registered trademark of Heraeus-Schott AG.
[3] Cervit is a registered trademark of Owens-Illinois, Inc.

ACKNOWLEDGEMENTS

We are pleased to acknowledge the support of the following agencies for the work reported here: Jet Propulsion Laboratory, U. S. Naval Research Laboratory, and NASA Marshall Spaceflight Center.

REFERENCES

Curtright, J. B., 1981: "A history and analysis of hydrogen maser reliability," Proc. 13th Ann. Precise Time and Time Interval Planning Meeting, p. 167. NASA conference publication 2220.

Gubser, D. U., S. A. Wolf, A. B. Jacoby, and L. D. Jones, 1981: "Magnetic shielding and vacuum test for passive hydrogen masers", Proc. 13th Ann. Precise Time and Time Interval Planning Meeting, p. 791. NASA conference publication 2220.

Jacobs, S. F., 1976: "Dimensional stability measurements of low thermal expansivity materials using an iodine stabilized laser," Proc. Second Freq. Standards and Metrology Symp., p. 269. Freq. and Time Standards Section, National Bureau of Standards, Boulder, CO, USA.

Kuhnle, P., 1981: Private communication. Jet Propulsion Laboratory, Pasadena, CA, USA.

Vessot, R. F. C., M. W. Levine, E. M. Mattison, et. al., 1976: "Space-borne hydrogen maser design," Proc. 8th Ann. Precise Time and Time Interval Planning Meeting, p. 277. Goddard Space Flight Center, Greenbelt, MD 20771, USA.

White, J., and K. McDonald, 1981: "Long term performance of VLG-11 masers," Proc. 33rd Ann. Freq. Control Symp., p. 657. USAERADCOM, Ft. Monmouth, NJ 07703, USA.

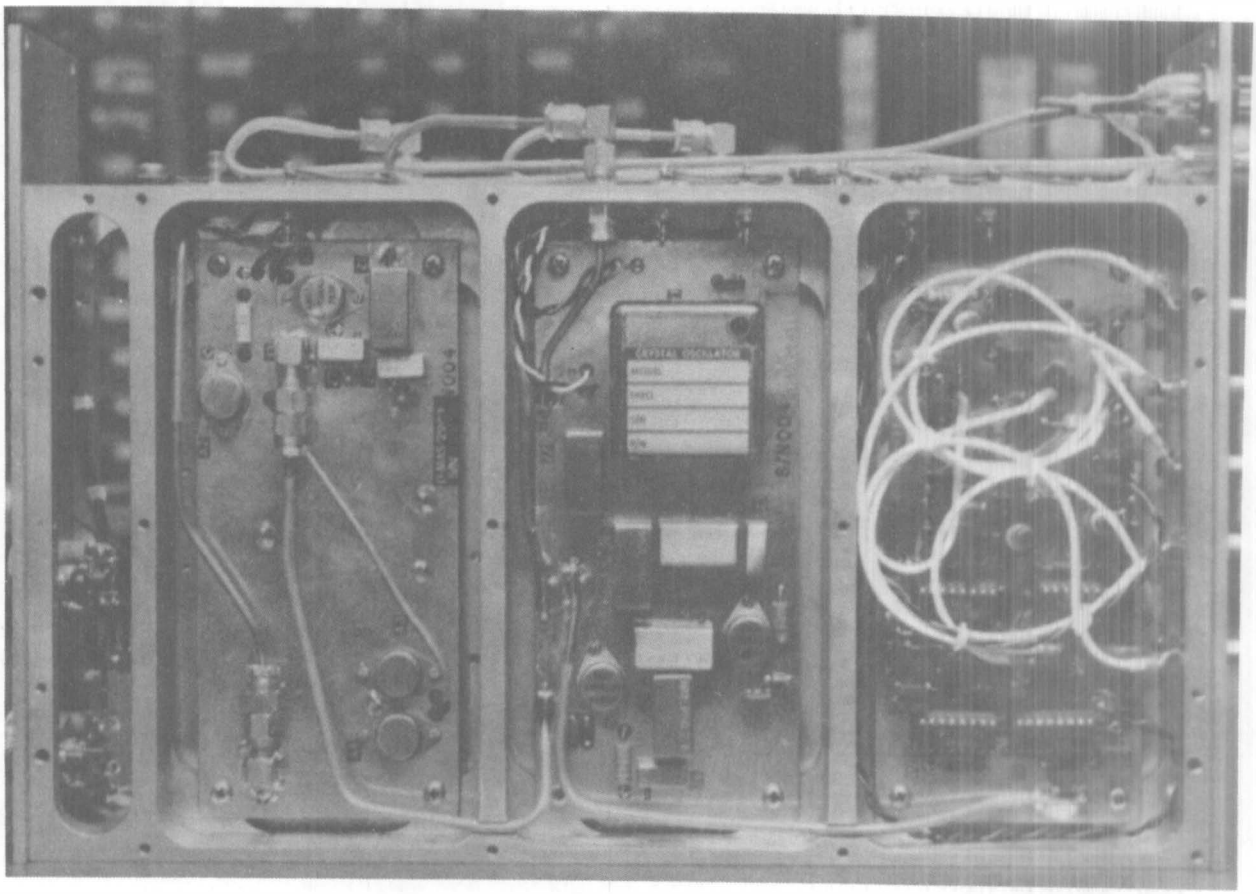

Fig. 1
Maser receiver with
side cover removed

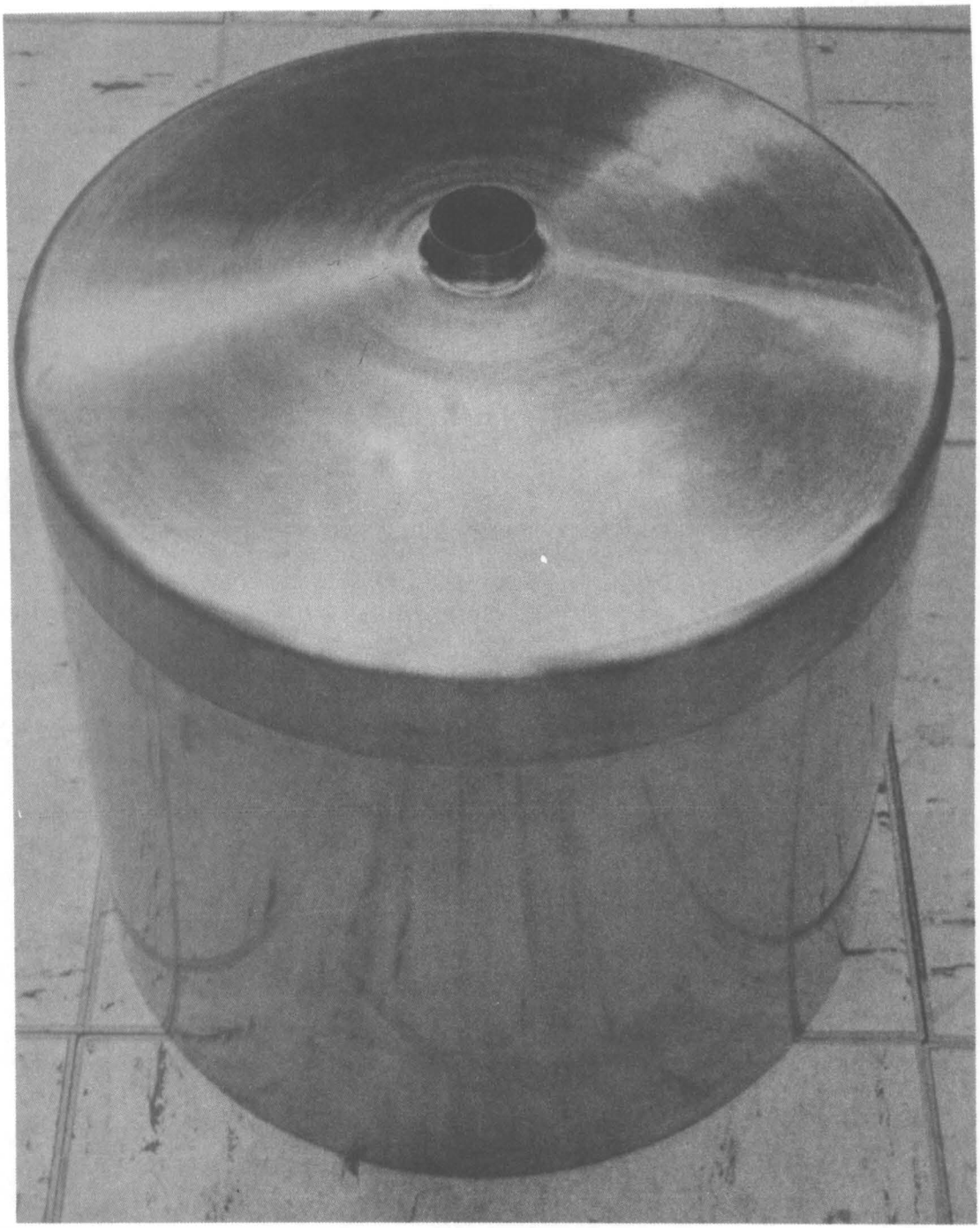

Fig. 2
Conical Magnetic Shield

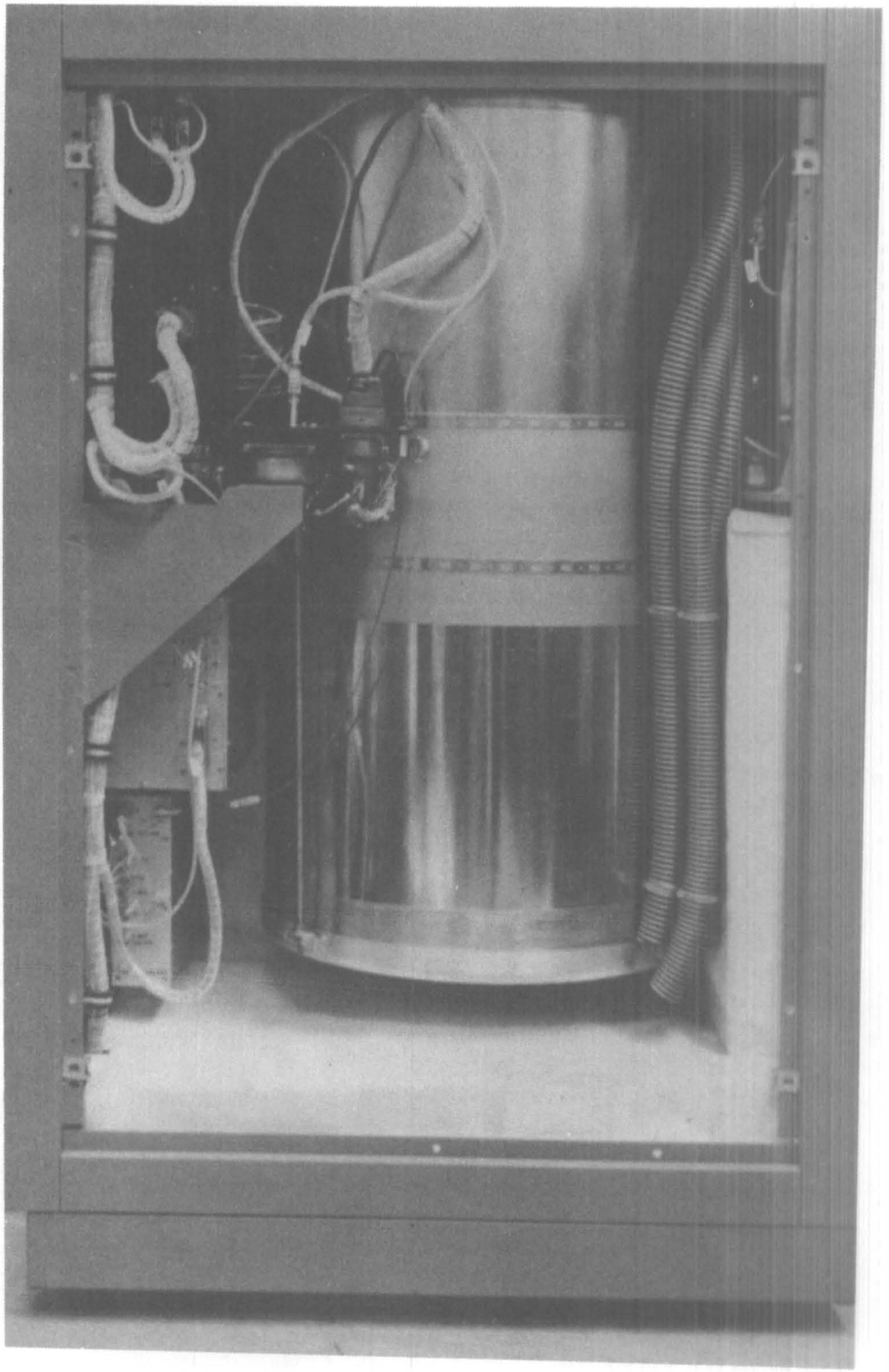

Fig. 3
Maser side view

DEVELOPMENT OF A PHASE-COHERENT LOCAL OSCILLATOR FOR A GEODETIC VLBI NETWORK

S. H. Knowles, W. B. Waltman,
E. O. Hulburt Center for Space Research
Naval Research Laboratory
Washington, D. C. 20375, U. S. A.

W. H. Cannon, D. Davidson, W. Petrachenko,
York University
Toronto, Canada

J. L. Yen,
University of Toronto
Toronto, Canada

J. Popelar,
Earth Physics Branch
Department of Energy Mines and Resources
Ottawa, Canada

and J. Galt,
Dominion Radio Astrophysical Observatory
Penticton, B. C., Canada

ABSTRACT: In most current VLBI experiments, use of the phase observable for geodetic measurements is sharply curtailed by the relative drift of the independent local oscillators at each station. A joint Canadian-U.S. experiment has been undertaken to demonstrate the possibility of making geodetic measurements where this oscillator drift, or clock correction, has been eliminated by using, effectively, a common local oscillator at widely separated stations. In order to do this, we have developed a high-precision phase-coherent link between VLBI stations in British Columbia, Ontario, and Maryland using the synchronous satellite ANIK-B. The system uses the 12/14 GHz transponder of ANIK-B, and makes only modest power and bandwidth demands on the satellite channel. A two-tone transmission format eliminates the necessity for a coherent satellite local oscillator, and two-way transmission enables elimination of satellite position changes as well as atmospheric effectse

Data obtained on link performance during a first experiment lasting several days show a measured phase stability of 2×10^{-15} for a period of one day. This is superior to typical VLB measurements of the performance of separated hydrogen masers. A complete measured Allen variance versus averaging interval curve has been computed, and clearly demonstrates the stability of the link. First results indicate verification of the ability of this technique to improve on the short-baseline interferometer method currently used to measure Universal Time. The potential of fully-coherent VLBI methods for geodetic and astrometric measurements will be discussed.

Introduction

Radio interferometry of natural sources has resulted in many advances in astrophysics, geodesy, astrometry, and related fields over the past 20 yearse Radio astronomers have succeeded via the technique of very long baseline interferometry (VLBI) in making interferometers with baselines as long as can be accommodated on the earth [Batchelor et al., 1976]. Although the VLBI technique does not require any real-time communications between the interferometer stations, two major technical problems are generated if this is not done. First, the data streams must be recorded on wide-bandwidth magnetic tapes and shipped to a central processing facility. A second limitation is that separate high-accuracy frequency standards are required at each station [Meeksę ed., 1976]. Our group has been studying the use of geosynchronous artificial satellites to eliminate these restrictions on VLBI technique. Using the Hermes satellite, some of us [Yen et al., 1977] demonstrated that real-time high-data-rate transmission of VLBI data via synchronous satellite is possible. Our latest effort using the Anik-B satellite has investigated the use of a synchronous satellite to link the oscillator systems at separate stations and eliminate the need for separate frequency standards. We report here on the successful link evaluation experiments, and comments on the implications for VLBI usagee

Theory Comparisons

The basic aim of the phase-coherent satellite experiment is to measure and compensate for phase differences between frequency standard oscillatorse This synchronization of two phase references is accomplished by transmitting a tone from station A to B through a satellite, and simultaneously transmitting an independent tone from B to A. At each station, the phase of the tone received from the other station is subtracted from the phase of the local reference. These differences measured at the two stations are again subtracted to produce a measure of the change in phase between reference oscillators at Beand A. A complication is introduced by the fact that the tone must be translated in the satellite to avoid regeneratione It is possible to achieve this translation in a coherent manner by means of a synthesizer locked to the incoming tone, as is done for certain deep-space probes. In a typical communications satellite, however, the satellite oscillator is incoherent with respect to transmitted signalse If the satellite also transmits a beacon that is derived from the same oscillator, this signal can be used to compensate for satellite oscillator drift. This was done in our earlier experiments with the Hermes satellite [Yen et al., 1977]e Alternatively, if no beacon is available one may simply transmit two tones, spaced as far apart in frequency as practical, and measure the phase difference between the twoe The effect of the satellite local oscillator is thus eliminated at the cost of reduced measurement precision, since the equivalent carrier frequency for this purpose is only the frequency difference between the two tonese

A two-tone method, with a frequency difference of 60 MHz, was chosen for our ANIK experiments (Fig. 1). Each station transmits two unmodulated tones, generated as different multiples of the same oscillator, which are retransmitted by the satellite to each other station. These tones are transmitted in one of six sub-bands near 14 GHz and are received in one of six sub-bands

near 12 GHz. Both tones pass through the same transponder circuitry. Each of our three stations receives three pairs of tones; one from each of the two other stations, and a signal transmitted through the satellite back to itself. These tones are then each coherently translated to form a comb of six tones, at frequencies from 1 to 7 kHz. The tones are each displaced very nearly the same amount by the frequency drift of the satellite translation oscillator and the satellite doppler shift, but each pair of tones remains separated by exactly 4 kHz. These tones are then combined with a 4 kHz reference tone generated at the receiving station, and recorded on audio tape for later analysis. When analyzed, the integrated phase difference between each tone pair and the reference represents the sum of the satellite motion along the analyzed path and the difference between the two station frequency standards. The phase difference between the two standards is obtained by subtracting the two complementary phase differences, as derived in the next paragraph. This system, since it uses only CW tones, is very economical of spectrum usage. The frequency excursion of each tone is determined by the diurnal drift of the satellite translation oscillator (±2 kHz) and by the satellite doppler (±100 Hz)e Each tone requires a bandwidth only wide enough to accommodate these shiftse

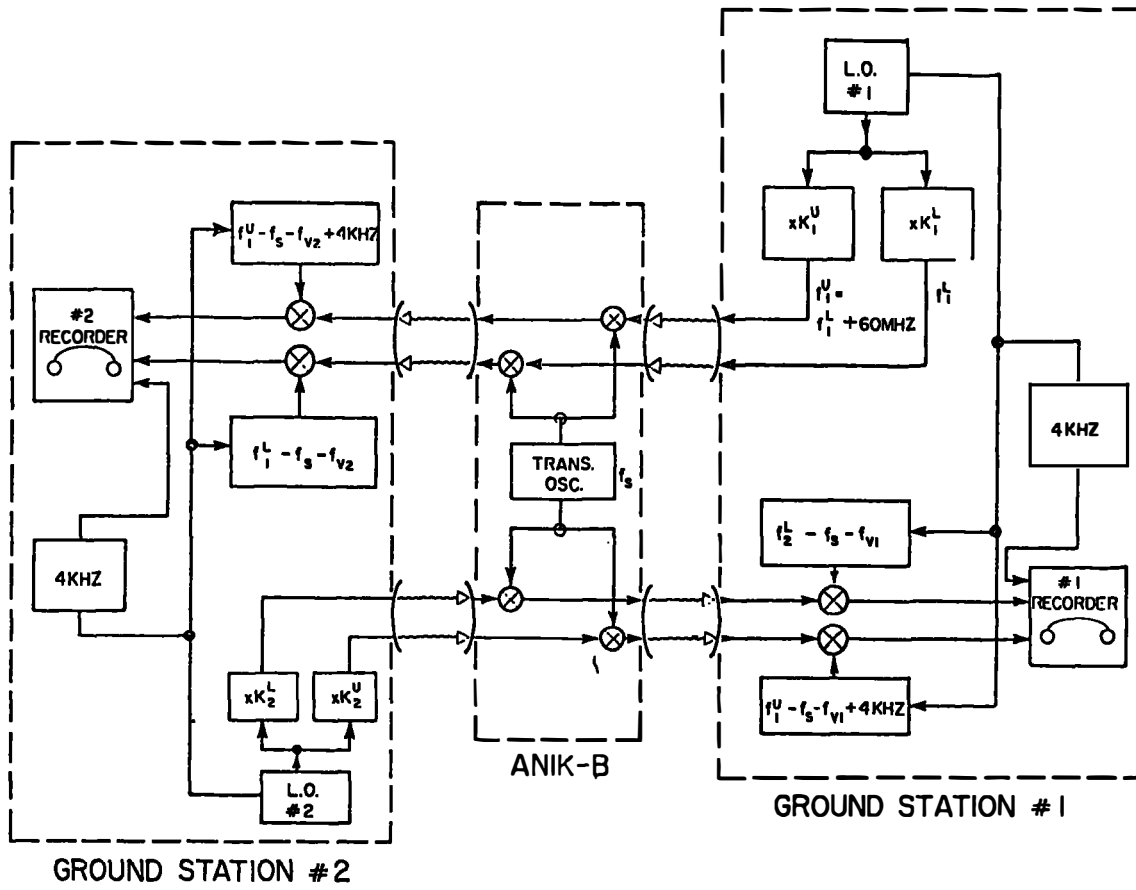

Figure 1 - Two-way link signal modulation-transmission-demodulation schemee f_v is the video offset appropriate to the particular statione

If the two complementary phase differences are added instead of subtracted, a high-precision measure of the path length change is obtainede This

relationship has been used by Knowles and Waltman (1980) to demonstrate the capabilityeof measuring a satellite'e motion to à precision of a few centimeterse

Description System

The detailed design used for the satellite-link system was somewhat different at each of our three stations, since each observatory built its link independently using existing hardware where possible. Anik-B is a multi-user communications satellite. The nominal uplink band which we use is centered at 14.24 GHz and the nominal downlink band is centered at 11.94 GHz. Our three links were not all assigned the same transponder because of antenna beaming constraints. For these reasons, we will concentrate on the basic principles used in system design. For the uplink, we first generate by means of appropriate synthesizers two phase-coherent tones separated by exactly 60.0 MHz, at a center frequency of about 150 MHz. These are then translated upwards in frequency so that each tone falls close to the edge of one of the Anik-B sub-bands. The two tones are then amplified by a traveling-wave-tube amplifier and sent up to the satellite through a diplexer. Tones returning from the satellite from all three stations are received on the same antenna, separated by the diplexer and translated downward to audio frequencies. The following protocols are observed. Firstly, the tone-pairs of different stations are arranged so that they are a nominal 1 kHz apart at the receiving station before satellite doppler is considered. Secondly, at video frequency the tones are mixed so that each pair of tones is separated by exactly 4 kHz, with the lower frequency of each pair at 1, 2 and 3 kHz. The major portion of the apparent satellite frequency change of about ±2 kHz is common to all three baselines, so all tones will shift in frequency by close to the same amount, and the drift may be compensated for by a single variable frequency synthesizer at each statione By using the dual-tone methode only the coherence of the oscillators needed to generate and demodulate the tone-pairs is important. None of the translation oscillators need be coherent, although in practice all except for the satellite translation oscillator are synthesized from a master station standard.

When each tone-pair is received, it must be demodulated by a phase detector. In principle, this phase-comparison can easily be done in real time, and the phase correction can then be applied to one of the station frequency standards to make a true phase-closed loop. We chose not to do this for the initial experiment; instead, the tones were recorded on an audio tape recorder at each station and analyzed later with a playback processor developed for the purposee Doing things this way made possible ex-post-facto decisions on link analysis parameters that would not have been possible if the loop had been closed in real time. However, we did need to introduce additional complexity to deal with the variable tape speed of standard audio tape recorders. On one of the two audio channels we recorded a time code. On the other we recorded the three tone-pairs mentioned above, plus a locally generated 4 kHz tonee

A block diagram of our playback machine is shown in Figure 2. In order to extract the differential phase information a special-purpose audio processor was constructede The processor first translates the six satellite tones upward about 10 kHz by means of a common local oscillator that is varied to

compensate for satellite doppler shifte Each individual tone is extracted in a separate filter; then each pair of tones is mixed together to extract a 4 kHz difference frequency. Each 4 kHz difference frequency is phase compared with the 4 kHz reference tone. Since the reference is also extracted from the tape, the tape recorder motion uncertainty is eliminated. For each tone pair we produce in-phase and quadrature phase outputs; these are then digitized at a 10 Hz rate and sent to a Hewlett-Packard 2116 minicomputer. The timing of the samples is controlled by interrupt from a time code extracted from the tapee The minicomputer, programmed in Forth, handles the subsequent tasks of measuring phase and counting turns. The phase data is then accumulated on disc; on final data reduction a software idling routine extends the phase over tape changes, dropouts, etc. This is made feasible by the fact that the measured phase, except for the integral revolution part, recovers exactly after a data gap.

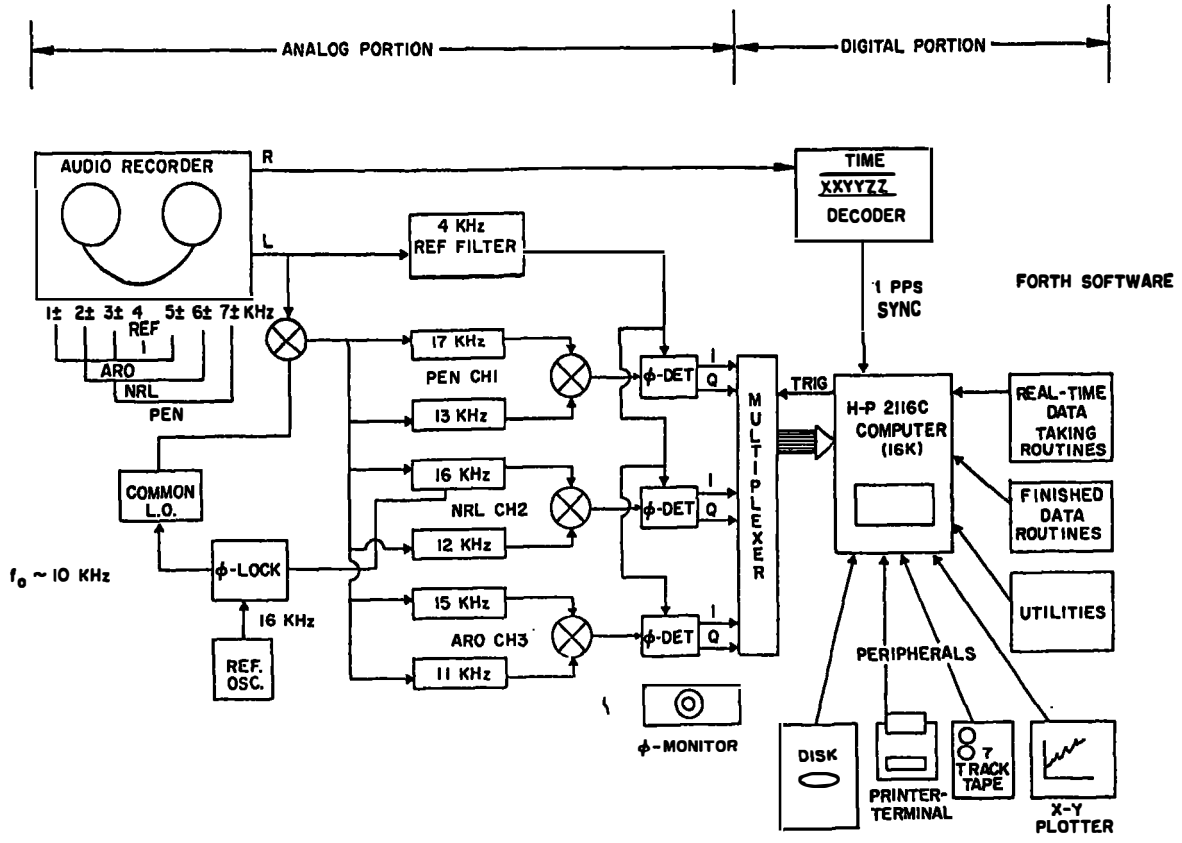

Figure 2 - Special-purpose satellite-link data processoe.

Experimental Procedure and Analysis

The work described here was undertaken to investigate the feasibility of operating an operational phase-link between North America observatories in order to establish a system for high precision geodesy and astrometry measurements. In addition, it is expected that our experience will prove valuable in the design of the various Long Baseline Arrays now underway.

In carrying out these studies, the Anik-B satellite was used to establish a phase link between the following observatories:

1. Algonquin Radio Observatory(ARO), Lake Traverse, Ontario, Canada
2. Dominion Radio Astrophysical Observatory(PEN), Penticton, B.C., Canada
3. Naval Research Laboratory(NRL), Nanjemoy, Maryland, U. S. A.

For the radio astronomy portion of the observations, we used antennas of 46 m diameter (ARO) and 26 m diameter (PEN and NRL)e Each of the three stations was equipped to observe astronomical sources at both 11 cm and 21 cm wavelengths to help compensate for ionospheric effectse Phase-link antenna diameters were 4.5 m(PEN)ę 10 m(ARO)ę and 25 m(NRL)e A hydrogen maser was available at NRL; rubidium standards were used at the other sites. The experiment described here took place during April 7-12, 1980 and provided an excellent evaluation of phase link performance over all time scales up to one day or longer. A similar experiment has been performed by van Ardenne et al. (1981); however, there are two important differences between their results and ours. Firstly, our link operated between separated stations, thus enabling more extensive tests of the potentialities of the method. Secondly, we obtained continuous phase-link data for a period of several days to study long-term effectse

Table I

Satellite Link Signal-to-noise Parameters for Penticton Link

	Uplink	Downlink
Nominal Frequency	14 GHz	12 GHz
Transmitter Power	20 watts	
Transmitting Antenna Gain	54 db	
Effective isotropic Radiated Power (P)	67 dbW	46e5 dbW
Modulation correctione for 4 tones	-6 db	
for bandwidth sharing 250Hz/70MHz		-26e1 db
Free Space Loss (L_{fs})	-206.6 db	-205e1 db
G/T	0 db/°K	25e4 db/°K
10 log B	24 db	24 db
C/N	59 db	45.3 db
C/N for NRL link	56.6 db	52.2 db
Carrier-to-interference ratio for satellite channel		32.1 db

Although the signal-to-noise ratio for the satellite link varied with each station, we present in Table I an analysis for the worst case as an example. Results expressed are carrier-to-noise ratios according to the standard satellite engineer's relationship [Reference Data for Radio Engineers, 1968]. We assume a ground transmitter power output of 20 watts and a receiving bandwidth of 250 Hz. which is set by our audio filters and clearly could be improved for better signal-to-noise ratio. We are limited in signal-to-noise ratio primarily by the satellite carrier-to-interference ratio. This and the additional loss factor of 26 db result because we were co-users of the satellite channel, so were only allowed to use part of the satellite output power. The signal-to-noise figures reported by van Ardenne et al. (1981) assume sole use of a satellite channele

The period from 12^h U.T. on April 8 to 12^h U.T. on April 9 was chosen as a period for thorough analysis of phase-link performancee Graphs and parameters will be primarily from the Algonquin-Penticton link; the other two baselines showed similar performance. Fig. 3 represents a sample of short-term path length measurements from a one-way link, illustrating the typical noise behavior of the link. As with all data in this section, the data actually represents degrees of observed phase at 60 MHz, which has been converted to a time representation. The noise has a white spectrum. The short-term variance of this noise is about 25 picoseconds (the curvature of the graph is an effect of the satellite motion)e

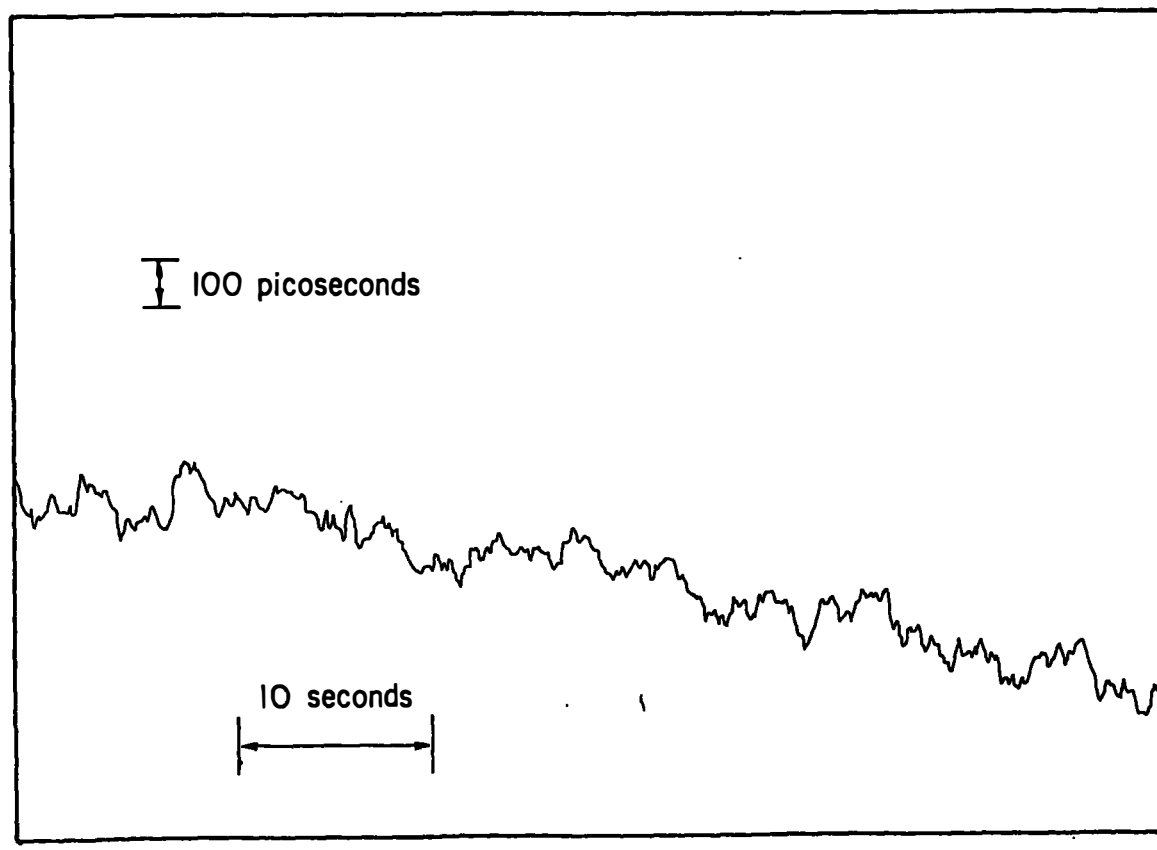

Figure 3 - Sample of short-term link noise (sampling interval 0.1 second)e Data is NRL at Pentictone

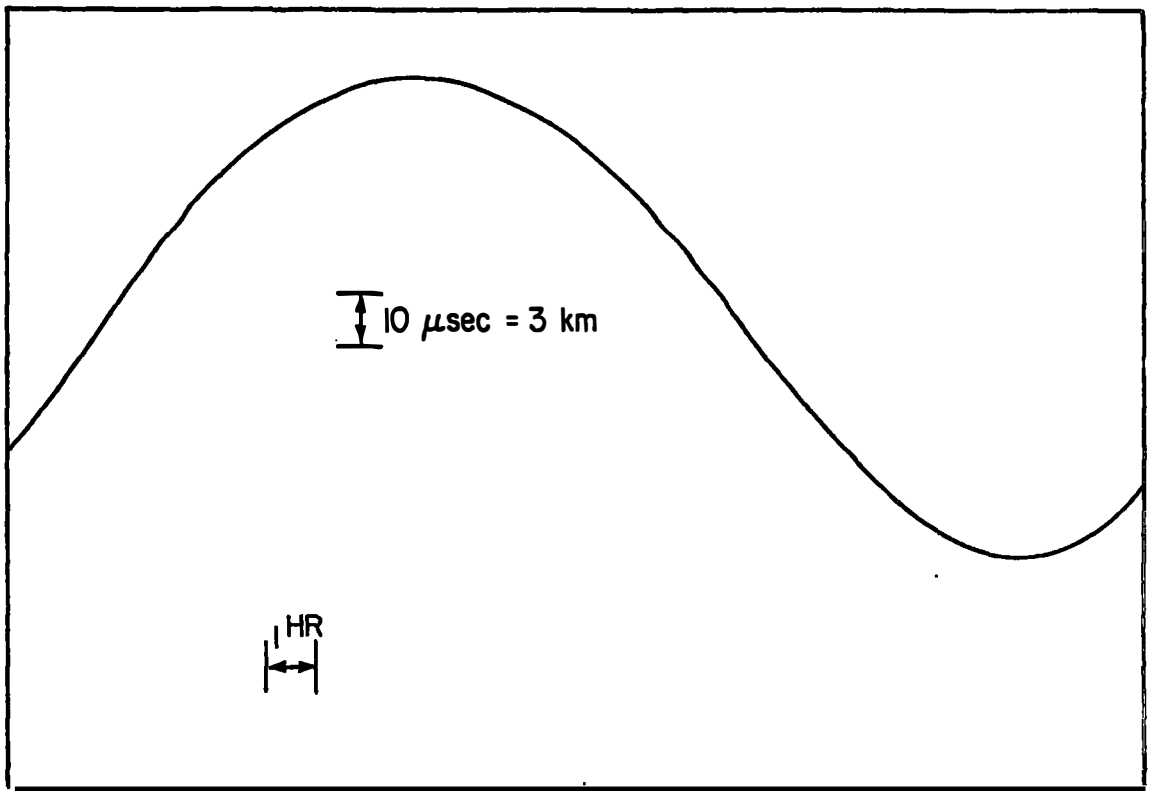

Figure 4 - Total phase excursion of Penticton signal received at Algonquin during the period from 12^h on April 8, 1980 to 12^h on April 9, 1980. Total peak-to-peak excursion is about 102 microseconds = 15.3 kilometers.

Since examination of the data at intermediate time scales showed no evidence of unexpected effects, a 24 hour sample of the link data was analyzed. The 24-hour period is a natural one for examining this sort of data because almost all perturbing effects, from whatever cause (e.g. satellite heating, ionosphere, satellite orbit, etc.) would be expected to appear on this time scale. Fig. 4 shows the integrated phase measured on the Penticton to Algonquin link. The large sine wave with a 24-hour period is the residual satellite motion, with a peak-to-peak amplitude of about 103 microseconds, corresponding to 15 kilometers of satellite motion. In order to determine the relative drift of two frequency standards the measurement of the phase at ARO from PEN is subtracted form the measurement at the phase of PEN from ARO, according to equation 10. The resultant appears as a straight line with a measured slope of -2.6870 microseconds/day. This corresponds to an error in rate of one rubidium standard upon the order of -3.15×10^{-11}. In order to determine the measurement errors in the double-subtracted data, the result must be examined on an expanded scale by subtracting the frequency standards slope. Fig. 5 shows the data from the Penticton-Algonquin baseline with this done. The remaining curvature is believed to represent the differential second derivative of the two standards.

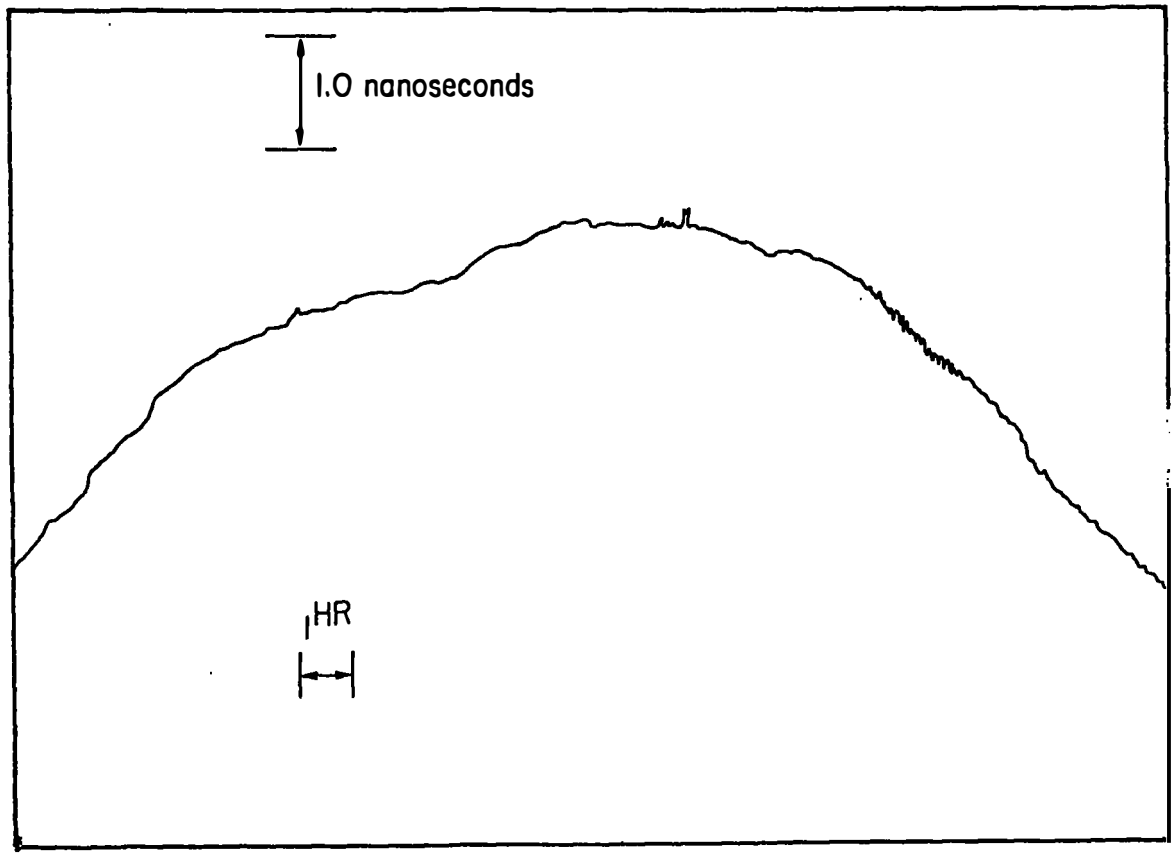

Figure 5 - Measured rate of advance of frequency standard at Penticton upon that at Algonquin, with scale expansion of 1000K and slope removed to show residual excursionse The parabolic compoonent is believed to represent the differential rate-of-change of the top frequency standards.

If we sum the phase differences from all three station pairs:

$$[\Phi_B - \Phi_A] + [\Phi_C - \Phi_B] + [\Phi_A - \Phi_C] = \varepsilon_{BA} + \varepsilon_{CB} + \varepsilon_{AC} \qquad (1)$$

we obtain a phase closure relationship which gives a measure of the link errors independent of the behavior of the station frequency standardse For the 24-hour period discussed here,

$t_A - t_B$ = -2.6870 μseconds
$t_N - t_A$ = +1.4079 μseconds
$t_B - t_N$ = +1e2809 μseconds
Sum +0.0011 μseconds

The closure error of 1.1 nanoseconds represents 23 degrees of phase at the 60 MHz difference frequency. At 03^h on April 9 a synthesizer adjustment at Algonquin apparently resulted in a phase jump of 0.4 turns which has been eliminated from Fig. 5. This adjustment does not affect the phase closure relationship.

We used the data from the sample period to estimate the Allen variance of the link, as is shown in the solid curve of Figure 6. The Allen variance for time intervals of less than 60 seconds was computed from a typical one-way

link; for intervals of one minute and longer it was computed from the phase-closure relationship of all three baselines. It was necessary to use the phase-closure relationship to measure the link parameters because over intervals of longer than about 10 minutes the two-way link variance is clearly dominated by the frequency drift rate of one rubidium standard upon the other, and levels off at about 3×10^{-13} for the Algonquin-Penticton pair. The Allen variance is about 3×10^{-10} for a sampling interval of 0.1 second, and decreases to about 1×10^{-14} at a sampling interval of 8 hours. The data points may be approximately represented by a straight line with a slope of -0.85; this compares with the slope of -1.0 to be expected from a link completely dominated by short-term noise. The most important qualitative conclusion to be drawn from this graph is that the variance is still decreasing rapidly at the longest sampling intervals. This is a necessary condition for a truly phase-stable link. The predicted phase stability based solely on these results is about 2×10^{-15} for a period of one day, and about 3×10^{-16} for a period of ten days.

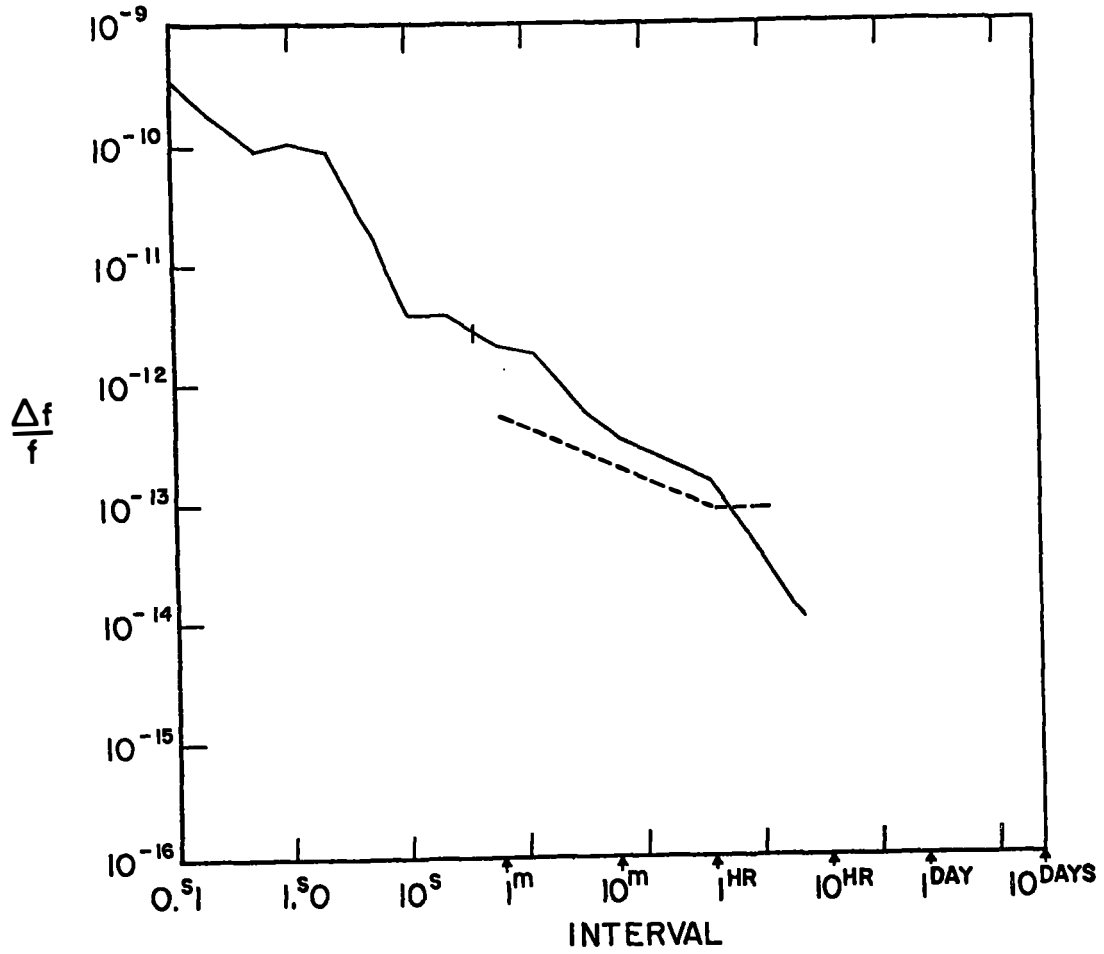

Figure 6 - Measured Allen variance of the satellite link as a function of averaging interavl for the sample period. Solid line is variance measured from three-baseline phase closure; dotted link is measured from comparison with radio astronomy data.

Figures for link stability expressed in time units are about 100 picoseconds for a one-second averaging time, and about 300 picoseconds for an 8-hour averaging interval. The latter represents about 13° of phase at the 60 MHz difference frequency. Although the Allen variance graph does not show this clearly, there are observed excursions in the phase in certain baselines with a quasi-period of seconds to minutes that are believed to be a result of cross-modulation effects in our link decoding circuitry. Reducing these will clearly improve the precision of the link.

Astronomical VLBI data was also recorded during the sample period using a selection of strong radio sourcese The radio source data was used to check the clock rate determined from the link, and for an independent computation of the Allen variance. The differential clock rate computed from the radio astronomy measurements [Cannon et al. 1981] for the ARO-PEN baseline was $+2e76 \pm 0.014 \times 10^{-11} + 6.39 \pm 0.27 \times 10^{-14}$/hr, which agrees satisfactorily within its error limits with the more precise satellite link value of $+2.8658 \pm 0.0014 \times 10^{-11} + 6.25 \pm 0.14 \times 10^{-14}$/hr. After using the link phase to correct the radio astronomy phase, an Allen variance was computed from 9 hours of astronomical data for the ARO-PEN baseline, and is plotted as the dotted line in Fig. 6.

The variance computed from the link data represents the internal consistency of measurement of the link proper, independent of the performance of the frequency standards. The phase closure test gives a true estimate of the random contribution to link error, and all systematic errors except those to which the link should be immune. Errors which are correlated between the two pairs of tones comprising a two-station link are not fully shown by the phase closure test, but all effects of this type should be fully cancelled by the two-tone differencing scheme used. The variance computed from the radio astronomy data should provide a more comprehensive test of the link, as well as including additional error sources associated with the radio astronomy receivers and atmospheric path. It is thus surprising to find the estimates for the one-minute time range somewhat below those for the link self-test. A possible explanation is that the medium-term noise was significantly worse on one of the baselines, since the phase-closure variance includes information from all three baselines. The radio astronomy variance slope is significantly different from -1; possible perturbative effects that could cause this include phase drifts in the long cables associated with transmitting oscillator phase to the radio astronomy receivers, and atmospheric delay changes that the link system has cancelled.

System Improvements

Modeling of system errors is made somewhat difficult by the variable conditions when transiting the satellite. The random component of the phase error should be governed by the standard relationship:

$$\sigma = \frac{\pi}{2(S/N)} \qquad (2)$$

for measurements of phase. Our signal-to-noise ratio is limited primarily by television-carrier interference. Using the value from Table I, our predicted random phase noise is about 0.°05. If one assumes that the noise behaves randomly, so that it can be averaged down, the estimate will improve further.

Our actual short-term noise is about 0.°5. This is significantly worse than the predicted value.

A large number of effects can cause systematic errors in the measured link output. In analyzing their importance it is helpful to keep in mind two principles of the double-tone method. In paths with two tones the information is extracted from the phase difference between the tones; thus these paths are not affected by operations which add a constant phase difference to each of the two tones such as frequency translation. In two-way paths the information is extracted from the difference in the path delays and is thus insenstive to symmetric changes in path length, as long as the time scale is not significantly shorter than the 0.25 second link transit time.

The troposphere causes an excess delay in signals transiting it in the X-band frequency range of about 5 meters. This delay is frequency independent, and should cancel completely except for the small component with period < 0.25 seconds. Total ionospheric effects are very small at X-band. At 12 GHz, the total of excess delay at zenith is about 15 cm, or 500 picoseconds for a typical daytime total electron content of 5×10^{17} m^{-2}, and about 10% of that at night. In analyzing the ionospheric effect, we should first note that any perturbation that is the same at station A and station B will appear identically in both the A-B link and the B-A link, and will appear as a change in link path length and thus cancel when considering frequency standards. Thus only various second-order differential effects need be considered. The most important of these occurs when the ionospheric electron content is different at station B than at station A. In this case, the full difference due to dispersion between the phase change on the uplink and that on the downlink appears as a phase change of the frequency standard. The uplink and downlink effects, in turn, are obtained by differencing the ionospheric effect at the two tone-pair frequencies separated by 60 MHz. For a normal daytime ionosphere at only one station, this double-differenced effect amounts to only 0.06 cm, or 0.°05 of 60 MHz phase. Another possible effect arises from the fact that the uplink and downlink frequencies are not exactly symmetrical. For typical daytime ionosphere values, this effect amounts to 0.°001. The expected effects from the ionosphere are thus small in comparison with our present link accuracy.

The satellite transponders can cause apparent path changes in two different ways. Group delay may be different in the satellite TWT amplifiers used in the forward and reverse paths. In the operation of the Anik-B satellite the same TWT is normally used for the forward and reverse paths between ARO and NRL, but two separate TWT's are involved on the paths to PEN. In addition, the group delay may differ within each TWT between high and low band edges. Both these effects might be expected to change with changes in the total TWT transmitter power, but no phase shifts attributed to this source have been seen in the data. At the ground stations similar effects may occur due to thermal changes in the operating point of the transmitting TWT amplifiers. Cable delay errors should be small since the transmit and receive cables, while separate, are identical types and in a similar environment. Errors in the frequency synthesizers used to generate the 60 MHz split on transmit and to remove it on receive will, however, be seen in the link output.

Most of the errors due to the tape recording of the tones are canceled by the use of the 4 KHz reference tone. One of the major sources of error in

the data shown here was found to be differential phase shifts in the audio electronics as the frequency of the entire ensemble of recorded tones shifts due to the satellite doppler shifts and the drift in the satellite translation oscillator. In future experiments this drift will be removed before recording. A second source of error which probably limits the short-term performance of the present link is insufficient separation of the tones in the audio filtering in the playback processing. The effect of this cross-modulation is seen as quasi-periodic "beats" in some of the link data.

Finally, the link only measures the performance of the frequency standards at its input terminals. Errors in the VLBI portion of the experiment will remain when the link data and VLBI data are combined and compared. While it is difficult to estimate exactly how much link performance can be improved, it seems reasonable that relatively simple improvements in the playback electronics to optimize noise performance and to reduce cross-modulation of tones can improve performance by one order of magnitude.

Conclusions

Interest in coherent oscillator links has been divided into two parts. First, the use of a link to provide a true phase-connected interferometer over long time intervals. Second, use of the satellite link over short-to-medium time intervals to eliminate the necessity for hydrogen masers as frequency standards.

Our experiment has already demonstrated the feasibility of using a satellite phase link to provide a phase-stable interferometer at moderate microwave frequencies. We see no evidence, in either the data presented here or in our other data samples, that phase error accumulates in other than a bounded fashion. Clearly, we can to first order eliminate all effects of the satellite's motion, as well as the effect of the incoherent satellite oscillator. Based upon the error analysis of the previous section, we can expect a stability of about ± 175 picoseconds over a one-day interval, and about ± 250 picoseconds over intervals of ten days or longer. For a one-day interval, this corresponds to ± 63° of phase at a frequency of one GHz. An improvement of one order of magnitude in the link performance, as discussed in the previous section, would make possible phase-stable performance at a frequency of 10 GHz.

When considering short-term variance, the picture is more complex. Experiments with hydrogen masers in the laboratory have shown a stabilty over a period of hours approaching 10^{-15}. Accepting these figures, our present link should be better than a hydrogen maser over periods of a day or longer; the improved link should be superior for periods of 3 hours or longer. However, the experimental experience of radio astronomers has not supported the hydrogen maser laboratory measurements. Water vapor long baseline interferometer experiments consistently indicate a maximum coherent integration time of about 5 minutes, which corresponds to a frequency stability of about 5×10^{-14}. This may be due to the effect of the atmosphere, in which case it represent a fundamental limit to the useful accuracy of frequency standards for this purpose. We achieve this stability in one hour with our present results, or in 6 minutes with proposed improvements. This indeed holds promise for replacing hydrogen masers. As mentioned earlier,

our experimental evidence shows clearly that we already exceed the performance of a rubidium standard over intervals of longer than several minutes. The improved level of performance holds significant promise for replacement of frequency standards in VLBI experiments (see Fig. 7). If the still higher precision of 1 x 10^{-14} claimed by van Ardenne et ale (1981) for a one-station experiment can be extended to a two-station link, this would still further improve the potential for a coherent link.

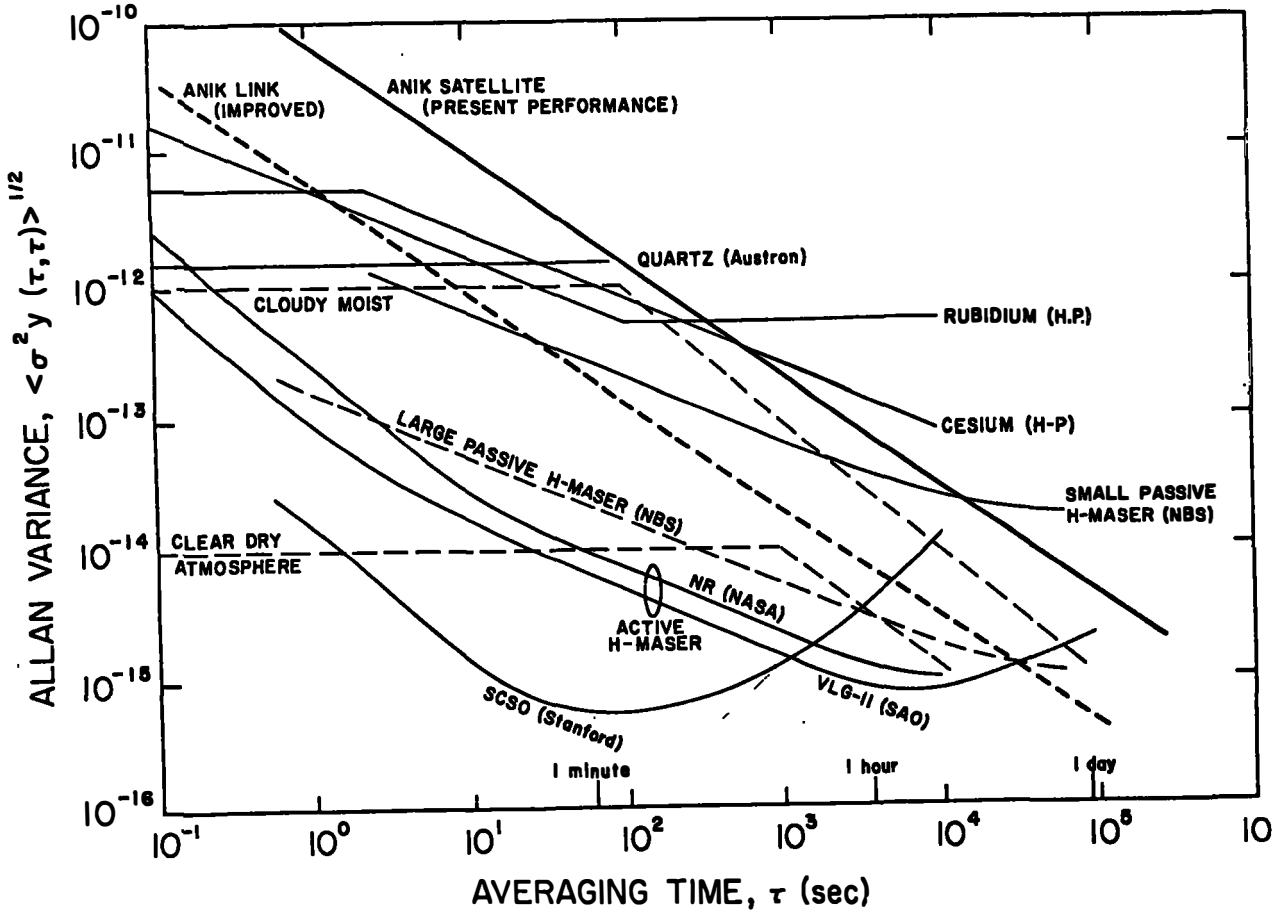

Figure 7 - Comparison of limiting performace of various frequency standards (and the atmosphere) for VLBI work. Presently achieved preformance of ANIK-B satellite link is shown as a solid line; possible improved performance as a dotted line.

Further improvement in accuracy may also be possible by using a "one-tone" method. This method basically eliminates the satellite oscillator by determining the exact time of satellite transit and comparing two signals that transited the satellite of the same noise. This method has the capability of more precise phase determination because the full carrier frequency is utilized. Work is underway to see if the one-tone method can indeed be utilizede effectively.

In making geodetic measurements using VLBI techniques it is not absolutely necessary to know the long-term phase correction between station oscillators,

as this can be separated and solved for in a least-square solution with the desired observables. However, knowledge of the clock correction clearly increases the weight and accuracy of the solution.

Phase-coherent connection between sources by rapid antenna slewing is a technique that provides optimuum astrometric accuracy. This technique has been attempted with at best partial success becuase of frequency standards initationse A link that enables phase-stable connection over intervals of 10-20 minutes, as this technique should in the improved mode, will enable this observing technique to be used effectively.

The economics of such a link involves the capital cost of satellite ground stations and the cost of satellite time. In both, the economics of this method are made quite favorable by the low information rate required. A standard earth-terminal antenna can be built for about $50,000. The bandwidth required from the satellite system is two narrow bands which can be utilized at the same time as a commercial television transmission. In addition, if only long-term phase information is required, continuous operation is not necessary. If an additional tone is added to take care of ambiguities, the link need be operated for only brief periods.

This type of multi-tone phase-measuring system should also be useful for accurate time comparisons. It is potentially more accurate than existing methods measuring group delay by some means, such as satellite time dissemination and VLBI group delay measurement.

Acknowledgements

The authors gratefully acknowledge Anik-B satellite time granted by the Department of Communications (Canada) under the Anik-B communications Program as Pilot Project 2T-3E. S. Weinreb prepared the data on other types of frequency standard performace in fig. 7.

References

Batchelor, R., D. L., Jauncey, K. J. Johnston, V. A. Efanov, L. R. Kogan, V. I. Kostenko, L. I. Matveenko, I. G. Moiseev, S. H. Knowles, A. Khe Papatsenko, R. Preston, J. Spencer, A. N. Timofeeve N. Fourikise and R. W. Schilizzi(1976), First global radio telescope, _____Zh., 2, 467-473.

Cannon, W. H., W. T. Petrachenko, D. A. Davidson, J. L. Yen, J. A. Galt, S. H. Knowles, W. B. Waltman, D. N. Fort, and J. Popelar(1981), "Development of Long Baseléne Interferometry for Monitoring of the Earth'es Rotation"e Final Report for Research Contract # 05SU.23235-0-0858, York University, Toronto, Canada.

Knowles, S. H. and W. B. Waltman(1980)e Application of coherent satellite link frequency standards to satellite position determénation, Record of the 1980 I.E.E.E. Position Location and Navigation Symposium, Atlantic City, N. J., Dec. 8-11, 1980, published by I.E.E.E., New York, Doc. # 80CH1597-4e 154-160e

M. L. Meeks, ed., Methods of Experimental Physics: Vol. 12 Astrophycis - Part C: Radio Observations(1976)e Academic Press, New York, 207e

Reference Data for Radio Engineers, Fifth Edition(1968), Howard W. Sams and Co. Inc., Indianapolis, Ind., 34-3e

van Ardenne, A.e J. D. O'Sullivan and A. de Dianous(1981), A high precision phase comparison experiment using a geostationary satellite, submitted to I.E.E.E. Transactions on Instrumentatione

Yen, J. L, K. I. Kellermann, B. Rayhrer, N. W. Broten, D. N. Fort, S. H. Knowles, W. B. Waltman and G. W. Swenson, Jr.(1977), Real-time, very-long-baseline interferometry based on the use of a communications satellite, Science, 198,e289-291e

CONCEPT AND REALIZATION OF A 20 M RADIOTELESCOPE FOR THE SATELLITE OBSERVATION STATION WETTZELL

Manfred Schneider
Lehrstuhl für Astronomische und Physikalische Geodäsie, Technische Universität München and SFB 78 *)

Richard Kilger, Klemens Nottarp, Ewald Reinhart
Institut für Angewandte Geodäsie (Abt. II DGFI), Frankfurt and SFB 78 *)

James Campbell, Hermann Seeger
Geodätisches Institut, Universität Bonn and SFB 78 *)

ABSTRACT. In November 1980 the Deutsche Forschungsgemeinschaft has adopted plans submitted by the SFB 78 to develop the Satellite Observation Station Wettzell into a fundamental geodetic station for global geodynamics programs. The most important step towards fulfilling these plans is to build a dedicated geodetic radiotelescope for Very Long Baseline and Satellite Interferometry. The telescope with a diameter of 20 m has been designed for optimal stability and will be equipped with a modern Mk III VLBI terminal as well as a hydrogen maser.

The installation of the new radiotelescope which will then be available for dedicated geodetic and geodynamic observing programs is scheduled for May to December 1982; routine operations should commence late in 1983.

1. GENERAL REMARKS

Since the early 1970's the geodetic satellite tracking efforts in the Federal Republic of Germany have been concentrated at the Satellite Observation Station Wettzell which is operated mainly by the Institut für Angewandte Geodäsie (Abt. II DGFI) acting on behalf of the Sonderforschungsbereich 78 Satellitengeodäsie (Special Research Group on Satellite Geodesy) of the Technische

*) SFB 78 = Sonderforschungsbereich 78 - Satellitengeodäsie - der TU München

Universität München (SFB 78)o Within this community of satellite geodesists the research activities of the following agencies have been joined together:

- Lehrstuhl für Astronomische und Physikalische Geodäsie der Technischen Universität München,
- Institut für Angewandte Geodäsie (Abt. II DGFI), Frankfurt a.M.,
- Abteilung I des Deutschen Geodätischen Forschungsinstitutes, München,
- Bayerische Kommission für die Internationale Erdmessung, München and only since 1980
- Geodätisches Institut of the Universität Bonno

Until now the activities at Wettzell have been concentrated on laser ranging to satellites with a short pulse Neodymium-YAG laser system (SRS), Doppler measurements, a limited period of C-Band Radar observations during the GEOS-III campaign and in the earlier years also optical observations with cameras. During the last years efforts have commenced to modify the SRS-system to add lunar laser ranging (LRS) capabilities by installing additional hardware and softwareo To satisfy the needs of all the tracking systems a dedicated precise time service with 4 rubidium and 3 caesium frequency standards has been established.

Until now geodetic VLBI has only been performed in this country by a VLBI group which was established in 1978 at the Geodätisches Institut in Bonn using the 100 m radiotelescope at Effelsberg, 30 km to the southwest of Bonno

It has already been recognized in 1979 that it would be necessary to make much more observation time available at a suitable radiotelescope, as the limited amounts of time available at the Effelsberg telescope are far too short to permit satisfactory participation in the international geodynamic programmes set up to determine intercontinental baselines, polar-motion and UT1 on a regular basis.

Original plans to equip another radiotelescope with the additional hardware necessary to participate in geodetic VLBI experiments (e. g. X- and S-band receivers, a Mark III data terminal and a hydrogen maser) were abandoned when plans were developed to upgrade Wettzell into a fundamental geodetic reference station equipped with all kinds of tracking systems used in international geodynamic programmes.

Following these general ideas plans have been worked out in 1979/1980 to procure and install a dedicated geodetic radiotelescope for installation in Wettzell in 1982/1983; the instrument was devised to include modern equipment such as e. g. a Mk III terminal, a HP 1000-F computer field system and a hydrogen maser frequency standardo

The project was approved and considered to be highly reasonable

as
- the necessary amount of observation time is not available at the 100 m telescope at Effelsberg,
- other radiotelecopes in the Federal Republic of Germany have to fulfill special requirements with permanently higher priority,
- all the existing antennae have been designed for other applications than geodesy which would mean that expensive modifications would be necessary;
- it is highly desirable to operate the different tracking systems in a co-location mode at one single station so that remaining systematic effects can be detected.

The proposal was accepted by the Deutsche Forschungsgemeinschaft (German Research Council) late in 1980 and the necessary funds were included in the budgets of the Institut für Angewandte Geodäsie and the Deutsche Forschungsgemeinschaft for the years from 1981 to 1984. Upon completion, the equipment will be available for VLBI experiments in cooperation with interested partners in Europe and overseas.

At this time an agreement is being worked out between the U.S. National Geodetic Survey and the Sonderforschungsbereich 78 to conduct co-operative programmes of observation between the U.S. POLARIS stations and Wettzell with the objective of improving the determination of polar motion and earth rotation parameters.

With the highly sophisticated tracking devices which will be available in Wettzell as soon as the lunar modifications of the Satellite Ranging System are completed and the new radiotelescope is operational - keeping in mind that all this equipment will be linked to a single precise time service -, the SFB 78 will be in a position to operate one of the few fundamental geodetic and geodynamic reference stations necessary to the fulfillment of the aims of future global geodynamic programmes.

2. THE CONCEPT OF THE NEW RADIOTELESCOPE

The main purpose of the new radiotelescope will be

- to monitor polar motion, earth rotation and earth tides,
- to measure and detect global plate motions and
- to serve as a reference station for regional projects in which base-line determinations will be carried out using mobile VLBI equipment in areas of particular geodynamic interest, e. g. in the Mediterranean region.

On the one hand the design had to be based on these applications, keeping in mind the financial restrictions on the other. Bearing in mind these two criteria which seem to be almost contradictory, the question to determine the size of the main reflector proved

to be the most predominant factor. It is possible to define aspects in favour of a large diameter for the antenna as well as setting up conditions which would be satisfied by a smaller reflector.

Some particular aspects seriously affected by the size of the main reflector are as follows:

a) operation with a partner radiotelescope requires that the diameter of the main reflector be large enough to enable observations of radio sources with a minimum correlated flux of
   $So_{corr} \geq 0.2$ Jy, when observing with a partner of similar size and
   $So_{corr} = 1.0$ Jy, when measuring together with a mobile antenna with a main reflector of e. g. D = 5 m (Orion).
b) The size of the main reflector has to be large enough to detect with standard receiving equipment (~ 125°K at X-band) at least compact 50 radio sources visible at the Wettzell latitude. To fulfill such a requirement a minimum flux of $s_{min} > 0.1$ Jy has to be detected in the X-band. On the other hand the diameter of the main reflector has to be small enough to keep the mechanical and thermal error sources as low as possible.
c) The total path covered by a wave front from a fictious plane at an arbitrary but constant distance from the telescope axis intersection point to an equally arbitrary but fixed mark on the feed horn will change due to distortion of the telescope structure under gravitational pull and wind load (see figure no. 1).
d) Similar changes of the described path will occur with temperature changes in the telescope structure.
e) Motions of the axis intersection point with respect to surrounding bench marks could arise if the azimuth mount is too large and not precisely guided.

In discussing c), d) and e) two philosophies may be followed:

1. The errors will be modeled.
2. The telescope's size will be kept small enough to keep these errors below the tolerable limit, i. e. below 2-4 mm in geodetic and geophysical applications.

In order to arrive at a conclusion the following preparatory computations were carried out:

$$T_A[K] = 10^{-26}\left[\frac{W}{m^2 \cdot Hz \cdot Jy}\right] \cdot \frac{S_{corr}[Jy]}{2 \cdot K\left[\frac{W \cdot sec}{K}\right]} \cdot \frac{\pi}{4} D^2[m^2] \cdot \eta_A ; \qquad (1)$$

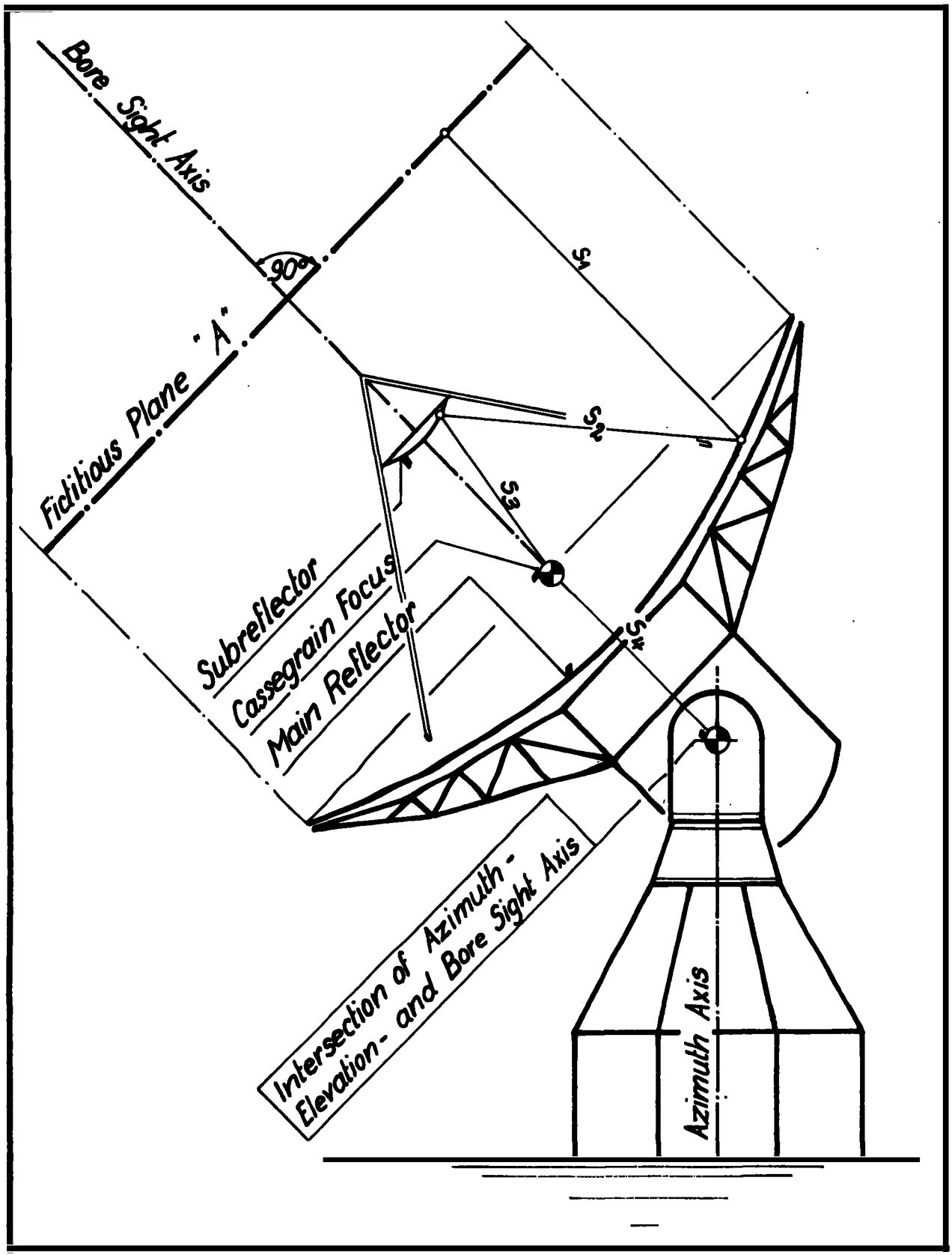

Figure 1.e-Ray path within the antenna $\sum_{i=1}^{4} S_i$.

for the antenna efficiency (Ruze 1966)

$$\eta_A = \eta_S \cdot \eta_B \cdot \eta_R \; ; \quad \text{with} \quad \eta_S = e^{-\left(\frac{4\pi\varepsilon}{\lambda}\right)^2} \; ; \qquad (2)$$

and for the signal-to-noise ratio (Renzetti 1980a)

$$SNR_{ch} = \frac{A}{\sqrt{2}} \cdot \frac{2}{\pi} \cdot \sqrt{\frac{T_{A1} \cdot T_{A2}\,[K]}{T_{S1} \cdot T_{S2}\,[K]}} \cdot \sqrt{2 \cdot B_{eff}\,[Hz] \cdot T_{coh}\,[sec]} \qquad (3)$$

equation 4 - defining the minimum flux S_{corr} of a radio-interferometer - can be derived:

$$S_{corr}[Jy] = 10^{26}\left[\frac{Jy \cdot m^2 \cdot Hz}{W}\right] \cdot \frac{4 \cdot SNR_{ch} \cdot K\left[\frac{W \cdot sec}{K}\right]}{A \cdot D_1 \cdot D_2\,[m^2]} \cdot$$

$$\cdot \frac{\sqrt{T_{S1} \cdot T_{S2}}\,[K]}{\sqrt{\eta_{A1} \cdot \eta_{A2}} \cdot \sqrt{B_{eff}\,[Hz] \cdot T_{coh}\,[sec]}} \; ; \qquad (4)$$

To carry out numerical computations the following assumptions are made:

Index 1 refers to the antenna in Wettzell, index 2 to the assumed partner radiotelescope which is here selected on the basis of the characteristics for Onsala and Orion (Renzetti 1980b):

K	= 1.38 • 10^{-23}	[J/K]	Boltzmann-constant
A	= 0.6		filter losses
D_1	= variable	[m]	diameter of the main reflector at Wettzell
	= 20.117	[m]	diameter of the main reflector at Onsala
	= 5.0	[m]	diameter of the main reflector at Orion
SNR_{ch}	= 10		signal-to-noise ratio per channel
B_{eff}	= 8 • 2 • 10^6	[Hz]	effective bandwidth in operating mode "B" with k=8 channels of each 2 MHz bandwidth in the X-band
T_{coh}	= param	[sec]	coherent integration period

$T_{S1} = T_{S2} = 75$	[K]	system temperature of the antennas
$T_{A1} = T_{A2}$	[K]	antenna temperature
$\eta_{S1} = 0.6823$		efficiency of the surface of the main reflector of the "Wettzell"-antenna
$\eta_{S2} = 0.6895$		corresponding value assumed for "Onsala"
$\eta_{S2} = 0.839$		corresponding value assumed for "Orion"
$\eta_{B1} = \eta_{B2} = 0.94$		aperture-blocking factor
$\eta_{R1} = \eta_{R2} = 0.60$		estimated efficiency for remaining losses

Figure 2 includes the diameter D_1 of the main reflector at Wettzell which is necessary in order to meet requirement a). The abszissa represents the correlated flux of the observed radio source at 8.4 GHz. The coherent integration period T_{coh}, which is primarily determined by the clock stability and the atmospheric conditions at a given observing frequency, is a parameter of the two families of curves. Observations are possible in the field to the right of each curve. Depending on the length of the coherent integration period VLBI-observations are feasible

- from $S_{corr} \geq 0.18$ Jy with $T_{coh} \geq 1000$ sec, respectively
  $S_{corr} \geq 0.58$ Jy with $T_{coh} \geq 100$ sec,

if one observes with a radiotelescope of similar size (as e. g. Onsala) and

- from $S_{corr} \geq 0.8$ Jy with $T_{coh} \geq 1000$ sec, respectively
  $S_{corr} \geq 2.5$ Jy with $T_{coh} \geq 100$ sec,

if one observes with a mobile radiotelescope (Orion).

Whereas the system noise error decreases with increasing diameter of the reflector, the mechanical and thermal deformations increase with growing antenna size. Therefore an optimization of the main reflector diameter is possible and necessary.

The system noise error (6) can be derived from equations (4) and (5):

$$\Delta S_{SNR}[m] = \frac{c\left[\frac{m}{sec}\right]}{const \cdot SNR_{ch} \cdot \sqrt{\sum_{k=1}^{N} (f_k - \bar{F})^2}\,[Hz]} \qquad (5)$$

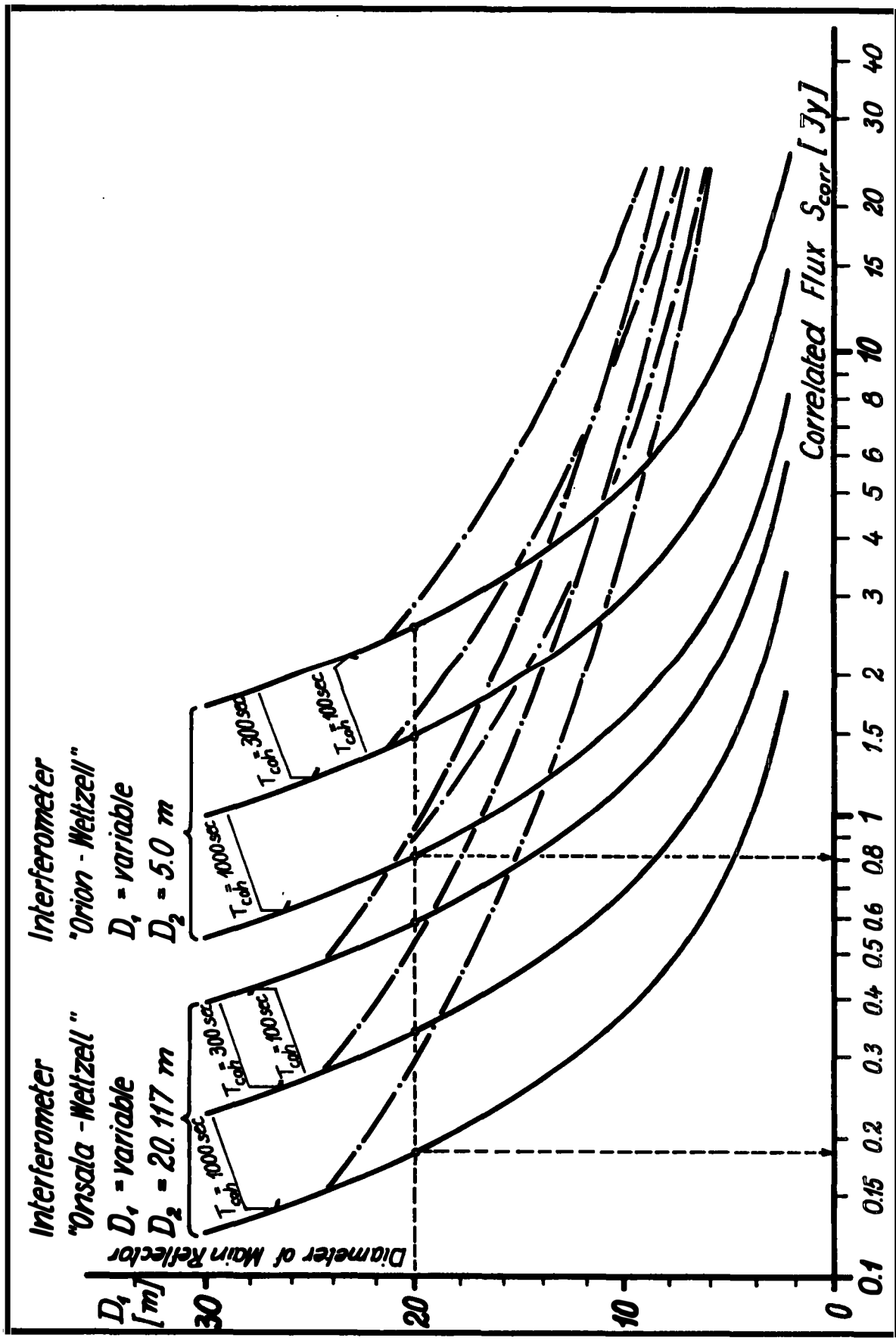

Figure 2.--Optimization diagram for diameter D_1 of main reflector.

$$\Delta S_{SNR}[m] = 10^{26}\left[\frac{Jy \cdot m^2 \cdot Hz}{W}\right] \cdot \frac{4 \cdot K\left[\frac{W \cdot sec}{K}\right] \cdot c\left[\frac{m}{sec}\right]}{A \cdot const \cdot D_1 \cdot D_2[m^2] \cdot S_{corr}[Jy]} \cdot$$

$$\cdot \frac{\sqrt{T_{S1} \cdot T_{S2}}\,[K]}{\sqrt{\eta_{A1} \cdot \eta_{A2}} \cdot \sqrt{\sum_{k=1}^{N} (f_k - \bar{F})^2[Hz^2] \cdot B_{eff}[Hz] \cdot T_{coh}[sec]}}; \quad (6)$$

where

const$\approx \frac{0.6}{2\pi}$ is the empirical constant referring to the correlation procedure.

$c = 3 \cdot 10^8$ [m/sec] is the velocity of electromagnetic waves

f_k [Hz] is the center frequency of each 2 MHz channel recorded by a Mk III-terminal; index k represents the number of registrated channels. Operating mode "B" is assumed with k = 8 channels, being located at the extreme edges of the 420 MHz passband.

$\bar{f}$ [Hz] is the center frequency of the 420 MHz-passband.

The path length within the antenna can be calculated rather exactly using the theorey of finite elements. In order to optimize the diameter D_1 of the main reflector equation 7, which represents the mechanical deformation of two antennae, has been used.

$$\Delta S_m[m] = k_m\left[\frac{1}{m}\right] \cdot \sqrt{D_1^4 + D_2^4}\,[m^2] \quad (7)$$

The parameter k_m is selected to be

$k_m = 10^{-5}\ \left[\frac{1}{m}\right]$ for the absolute deviations in the ray path,

$k_m = 3 \cdot 10^{-6}\ \left[\frac{1}{m}\right]$ for the RMS of the deviations in the ray path.

By a similar procedure the effect on the path length caused by temperature differences of the antenna structure can be estimated.

$$\Delta S_{th}[m] = k_{th}[-] \cdot \sqrt{D_1^2 + D_2^2}\,[m]; \quad (8)$$

making the following assumptions:

$k_{th} = 6 \cdot 10^{-5}$ the temperature coefficient, based on

$\alpha_{St} = 12 \cdot 10^{-6}\ \left[\frac{1}{K}\right]$ the termal coefficient of steel and

$\Delta t = 5^{o}\ [K]$ the assumed temperature difference.

Equation (9) is obtained by adding equations (6) and (7) to (8) followed by differentiation with respect to the reflector diameter D_1 of the Wettzell antenna

$$S_{corr}[Jy] = \frac{k_k\left[Jy \cdot m^3 \sqrt{sec}\right]}{D_2[m] \cdot \left(\frac{2 \cdot k_m \cdot D_1^5}{\sqrt{D_1^4 + D_2^4}} + \frac{k_{th}\ D_1^3}{\sqrt{D_1^2 + D_2^2}}\right)[m^2] \cdot \sqrt{T_{coh}[sec]}}; \qquad (9)$$

with the constant components k_k of equation (6)

$$k_k\left[Jy \cdot m^3 \cdot \sqrt{sec}\right] = 10^{26}\left[\frac{Jy \cdot m^2 \cdot Hz}{W}\right] \cdot \frac{4K\left[\frac{W \cdot sec}{K}\right] \cdot c\left[\frac{m}{sec}\right]}{A \cdot const} \cdot$$

$$\cdot \frac{\sqrt{T_{S1} \cdot T_{S2}}\ [K]}{\sqrt{\eta_{A1} \cdot \eta_{A2}} \cdot \sqrt{\sum_{k=1}^{N} (f_k - \bar{F})^2\left[Hz^2\right] \cdot B_{eff}\ [Hz]}};$$

Equation (9) is shown in figure 2 as a group of dash-dotted curves representing the zone, where the errors in geodetic VLBI, being a function of the main reflector diameter D_1, are minimized. In the field above these dash-dotted lines the increase of mechanical and thermal deformations predominates over the decrease of the system noise error and vice versa. It is felt that the finally selected diameter of 20 m is a good compromize between the four requirements a) to e). For cm-VLBI the 20 m-dish structure will not require any modeling of mechanical errors, which means that number 2 of the philosophies mentioned earlier in this paragraph has been adopted.

Based on these particular conclusions detailed specifications for the new radiotelescope including structural steel, reflector panels, subreflector, reflector and subreflector heating device, bearings, drive units and servo control but without feed cone, receiver, Mk III terminal and HP 1000-F computer have been written and submitted to 10 manufacturers considered in Europe, USA and Japan. 8 quotations were submitted by the companies addressed. They have been evaluated very carefully for their technical as well as their commercial aspects. Finally a consortium of two German companies - MAN and Krupp - were awarded to get the main contract which was signed in August 1981.

3. THE SPECIFICATION OF THE SELECTED TELESCOPE

The MAN/Krupp 20 m telescope selected for construction is designed as a coaxial Cassegrain "Turning-Head-Antenna". Azimuth-, elevation- and boresight axis intersect in one point located in the azimuth house and accessible without difficulty. Azimuth- and elevation-encoder are supplied with a boring thought to simplify the alignment and to support the control surveys. Attention should be called to the fact, that the azimuth- and the elevation bearings are situated as closely as possible to the intersection point of the axis. As a result, any deviation of this intersection point which is the reference point for geodetic VLBI will be produced mainly by thermal effects and will be relatively small. This may be the significant advantage of a "Turning Head Antenna" as opposed to the "wheel and track antenna".

The Wettzell radiotelescope as it is now under construction is characterized by the following technical details (see figure 3 and 4):

Main reflector

- unmodified mathematical rotational paraboloid
- diameter: D_1 = 20.0 m
- focal length: f_1 = 9.0 m
- f_1/D_1 = 0.45

Subreflector

- unmodified mathematical rotational hyperboloid
- diameter d = 2,7 m

Cassegrain focus

- seperation of vertex and main reflector: a = 2,55 m

Eigenfrequencies

- referred to the azimuth axis: 3.0 Hz
- referred to the elevation axis: 3,5 Hz

Tolerances

- _____ to the surface of the main reflector (design values) (compare figure 5 and 6)
  - error of a single panel surface: 0.25 mm RMS
  - mechanical deformation between elevation axis from 20° to 87°: 0.30 mm RMS
  - deformation due to wind forces: 0.05 mm RMS
  - deformation due to thermal changes of 2°K: 0.10 mm RMS
  - error due to adjustment of the main reflector: 0.15 mm RMS
  - total error for the surface of the main reflector: 0.38 mm RMS
- referred to the surface of the subreflector
  - total error (design value) achieved by mechanical machining of a cast aluminum reflector: 0.08 mm RMS

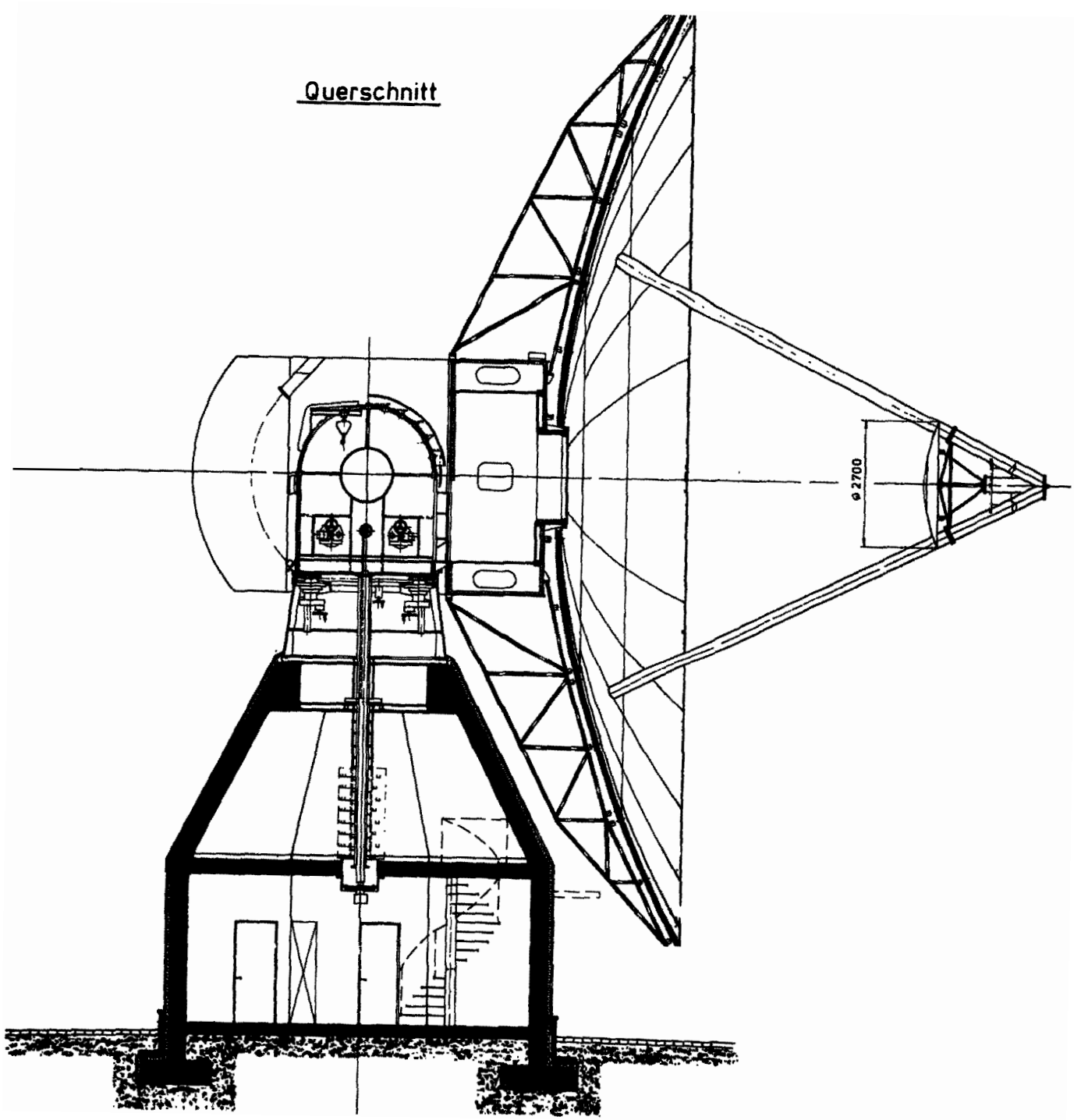

Figure 3: Cross Section of the Radiotelescope for Wettzell.

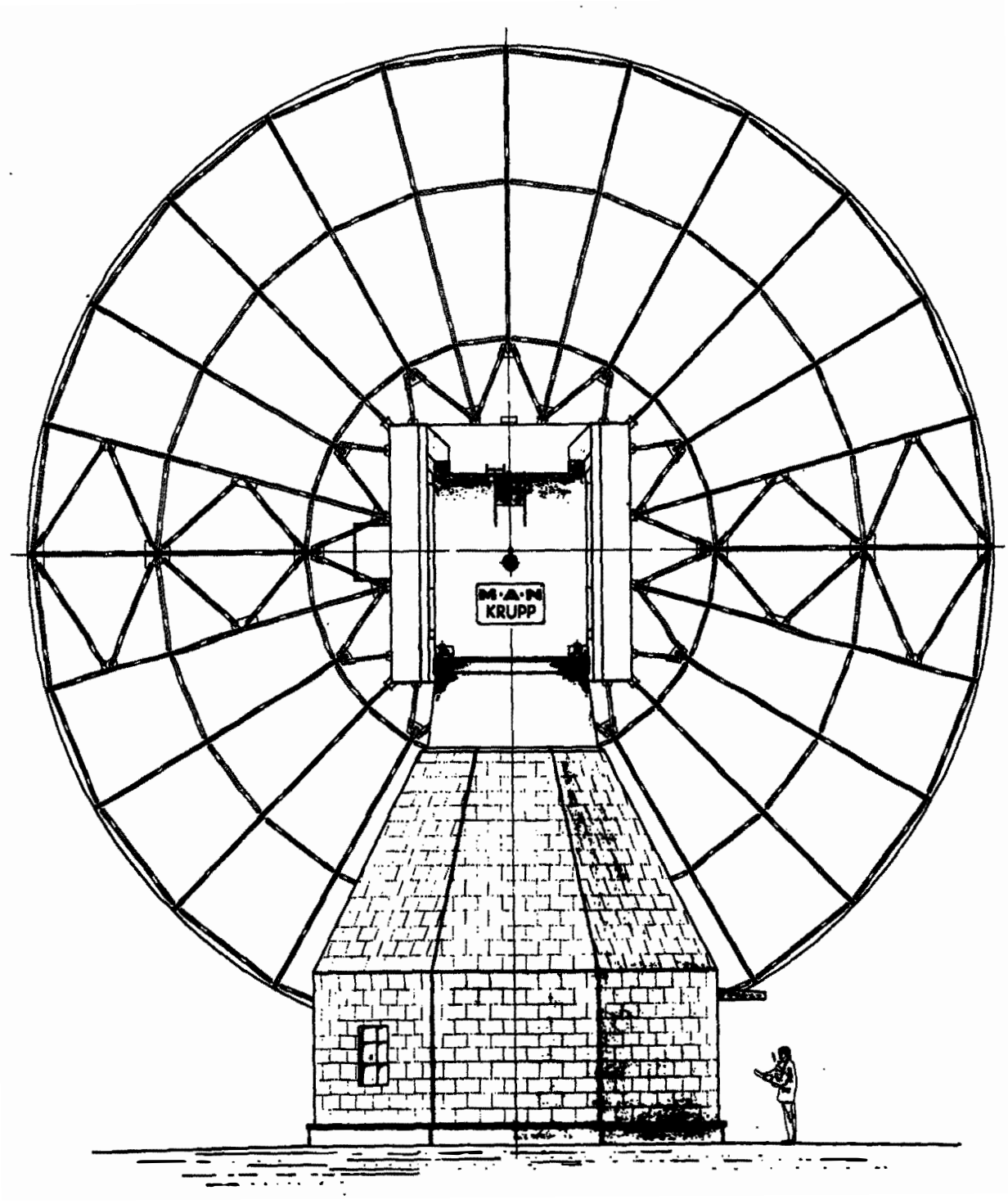

Figure 4: Rear View of the Radiotelescope for Wettzell

- referred to deviations of the wavefront within the antenna due to gravitational forces if the antenna is moved in elevation between 20° and 87°:
  - absolute differences between the longest and the shortest ray path: 2 mm
- referred to the accuracy of axial alignment (guaranteed values)
  - azimuth axis:
    deviation from the vertical direction: 5 "
    deviation of the azimuth bearing in radial direction: 0,2 mm
  - elevation axis:
    deviation from the horizontal direction: 10 "
    deviation of the elevation bearing in radial direction: 0,2 mm
- referred to the accuracy of antenna pointing
  - reproducible pointing error: 108 "
  - non-reproducible pointing error: 15 "

Kinematic data for the radiotelescope

- referred to the azimuth axis
  - tracking range: $\pm 270^{\circ}$
  - tracking velocity: from 0.001 $^{\circ}$/sec to 1 $^{\circ}$/sec
  - tracking acceleration: max $3^{\circ}/sec^2$
  - slewing velocity: 3°/sec
- referred to the elevation axis
  - tracking range: from 10° to 87°
  - tracking velocity: from 0.001 $^{\circ}$/sec to 1 $^{\circ}$/sec
  - tracking acceleration: max 1,5 $^{\circ}/sec^2$
  - slewing velocity: max 1,5 $^{\circ}$/sec

Following the award of the contract to MAN/Krupp in August 1981 preparations for construction commenced, which included selection of the optimal position of the radiotelescope (by investigating the subsoil at the site etc.). As soon as the properties of the selected site which is situated about 40 m to the west of the laser ranging system, were communicated to the IfAG and all the licenses were awarded for available the construction, the central building of the telescope was commenced. The building was completed in mid November 1981. About 300 cubic meters of concrete and 30 tons of reinforcing steel have been mounted to form an octogonal tower of approximately 8 m in height.

After the contract was signed MAN/Krupp immediately started to perform the final design, so that already a few weeks later it was possible to complete the final design review. During the same period the subcontractors to deliver the bearings, the gearings, the electric motors, the brakes, the encoders etc. were selected and confirmed. The subcontractor which has to supply the panels for the main reflector and the heating device for the panels - ZARGES - had already been determined before the contract was signed.

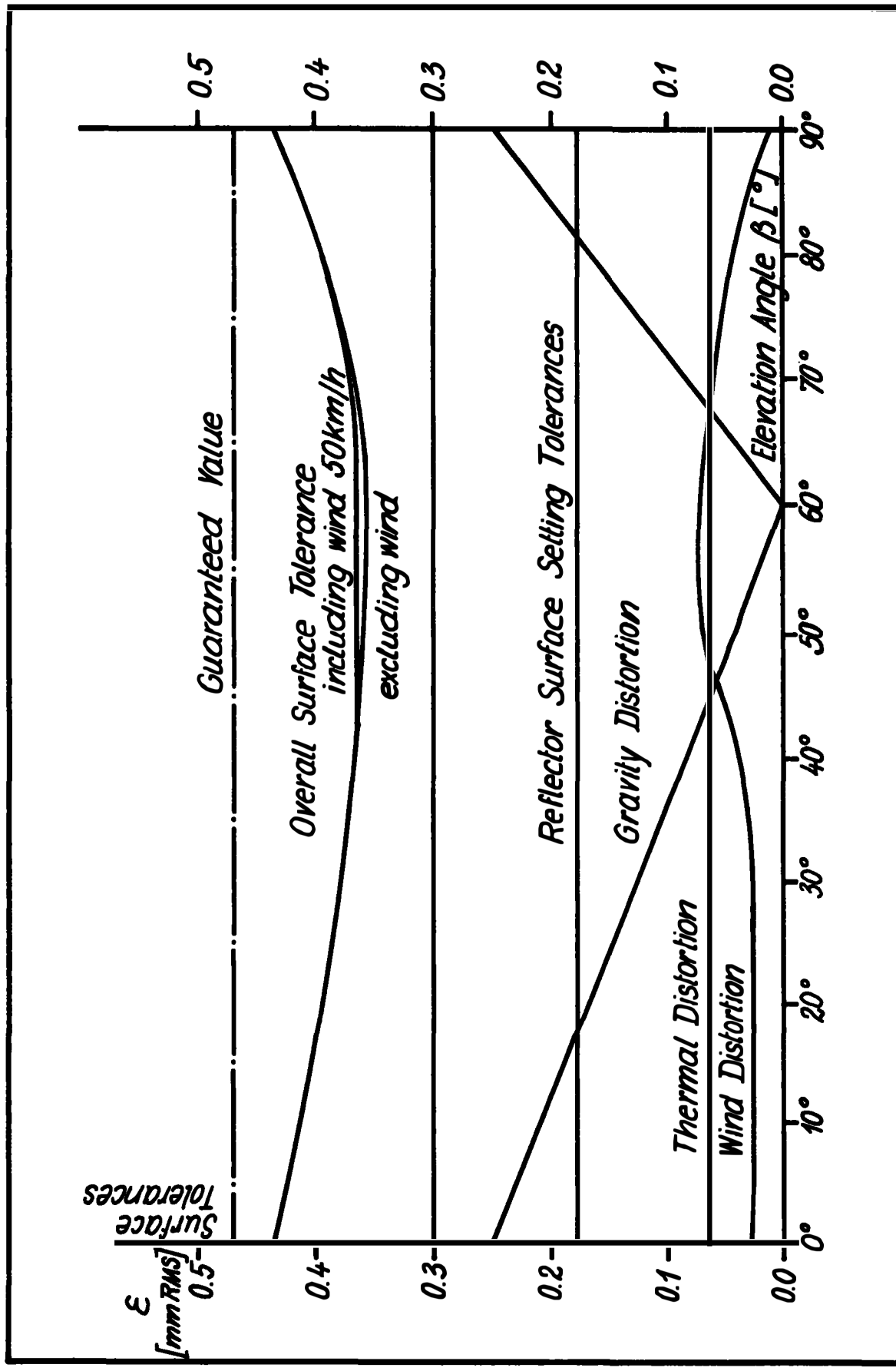

Figure 5.--Surface accuracy of main reflector (error budget).

The final drawings then were completed during the last days of November and in December MAN/Krupp began to manufacture the supporting ring to be mounted to the top of the concrete tower. During the first months of 1982 the subcontractors have supplied the bearings, the gearings, the electric motors and finally the panels after these part had passed the corresponding acceptance testso MAN/Krupp intend to prefabricate certain lots of the equipment at their plants as complete as possibleo The size of these lots is restricted only by transportation problemso Therefore only the main reflector has to be mounted at the site in Wettzello The contractors intend to start with the final installation during June 1982 by assembling the main reflector at the ground near the concrete tower. As soon as this task is completed two cranes will be installed in order to raise the prefabricated lots to their definitive level for final assembling, i. e.

- the supporting ring including the azimuth bearings and driveso
- the azimuth housing including the elevation bearings and driveso
- the elevation housing, prepared for assembling the main reflector and the
- two elevation arms with parts of the counter weighto

Because of the high rate of prefabrication already done at the contractors plants we expect to complete the raw installation at Wettzell about in October, starting final adjusting and alignment already before the winter period will commenceo

4. THE ELECTRONIC SUBSYSTEMSo

In order to define the feed system currently several concepts are considered as dual S/X-band concentric horns, S/X-band hybrid horns and a very ambitious three-frequency design to cover also the European 5 GHz-band without being forced to exchange the horn. This would highly facilitate the operation of the on-axis Cassegrain configurated telescopeo

The receiver front end probably will be a low-noise two stage GaAsFET amplifier installed in a Dewar at 20^{o} K which then is followed by another low-noise tri stage GaAsFET amplifier at a physical temperature of about 70^{o} K. The mixer and the broadband IF-amplifier will be operated at stabilized room temperature. The local oscillators for the two respectively three frequencies will be operated under phase coherent control of the Hydrogen Masero

A Mk III data acquisition system has been ordered from the Phoenix Corporation Mc Lean/Virg. (USA) to be delivered late 1982. In order to make use of the software already developed in the US a Hp 1000-F computer system will be ordered to be installed early in 1983.

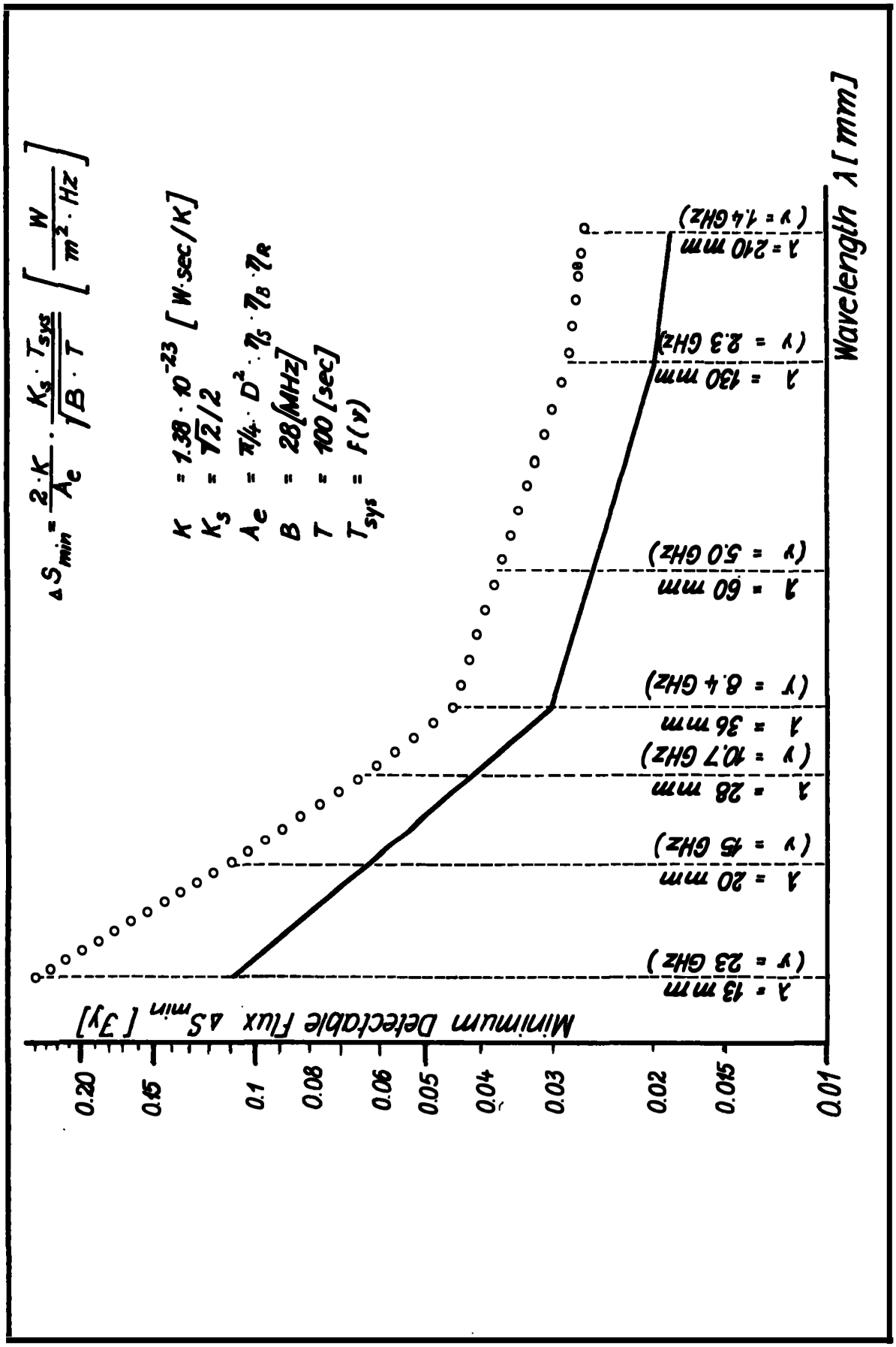

Figure 6.--Minimum detectable flux.

The time service of the Satellite Observation Station Wettzell comprehends three cesium standards (Oszilloquartz), 3 rubidium standards (Rhode and Schwarz) together with the corresponding time generators, counters, phase micro steppers and oszilloscopes (Schlüter et al., 1982). A computerized time comparing device is interogating all the station clocks every three hours. Time comparisons are performed by flying clocks travelling to the PTB (Braunschweig), BIH and USNO. A time transfer experiment between the PTB and Wettzell via METEOSAT is under preparation; a time comparison is expected every 3 hours with a resolution of about 30 nanoseconds (Schlüter et al., 1979). A Hydrogen Maser which is just now passing a test phase at the contractor's plant has been ordered from Oszilloquartz to be delivered mid 1982.

A noise adding radiometer and a S/X-band phase delay calibration system will be installed in 1983. It has still to be investigated which type of water vapour radiometer will be procured in the course of the following years.

5. REFERENCES

Kilger, R. (1980) — Eine Untersuchung zur Optimierung des für Wettzell vorgesehenen Radioteleskopes; Veröff. der Bayer. Komm. für die Interna. Erdmessung, astronomisch-geodätische Arbeiten, Heft Nr. 41, S.100-105

Renzetti, N. A. (1980a) — Operational Radio Interferometry Observation Network/Mobile Station Functional Requirements; Jet Propulsion Laboratory, California Institute of Technology, Pasadena, California, Sept. 22, 1980

Renzetti, N. A. et al. (1980b) — Orion Mobile Unit Design; the Telecommunication and Data Acquisition Progress Report 42-60, NASA and Jet Propulsion Laboratory, Institute of Technology, Pasadena, Calif., Sept./Oct. 1980, p. 6-32

Ruze, J. (1966) — Antenna Tolerance Theory - A Review; Proceedings of the IEEE, Volume 54, No. 4, April 1966, p. 633-640

Schlüter, W.; Nottarp, K.; Hübner, U. (1979) — One way time transfer via METEOSAT capable of 30 ns accuracy, Proceedings of the 11th Annual Precise Time and Time Interval Applications and Planning Meeting, Greenbelt, Nov. 27-29, 1979, p. 329-342

Schlüter, W.; Nottarp, K. (1981) — Applications of time and frequency in Geodesy, Journal of the Institute of Electronics and Telecommunication Engineers, Vol. 27, No. 10, 1981, p. 587-593

PRECISE SPACECRAFT TRACKING USING VLBI DIGITAL TONE EXTRACTION FOR THE PURPOSE OF GRAVITATIONAL WAVE DETECTION

Allen Joel Anderson

Joint Institute for Laboratory Astrophysics
University of Colorado
Boulder, Co. 80309

and

The University of Uppsala
Institute of Geophysics
Hälsby
S-755 90 Uppsala, Sweden

ABSTRACT

The prospect for the detection of a cosmic background of gravitational wave radiation is discussed. Experiments utilizing precise Doppler tracking of interplanetary spacecraft for the purpose of detecting this background are reviewed. Results of a recent experiment are presented which used facilities of NASA's Deep Space Tracking Network and Owens Valley Radio Observatory to track the Voyager spacecraft in an ultra precise manner using two independent hydrogen masers as frequency standards. The present limiting sensitivity of these experiments are believed to be tropospheric and plasma variations affecting the X band microwave signals at periods of between 10^3 - 10^4 seconds duration.

INTRODUCTION

Since the development of the general theory of relativity more than 50 years ago, there has been predicted the existence of gravitational waves. In the 1960's work was begun in an attempt to detect these waves using laboratory equipment. The names foremost among those early pioneers were those of Joseph Weber of the US and Vladimir Braginsky of

the USSR. A review of these experiments and their results is given in Davies (1980).

During the 1970's theoretical estimates of the energies and frequencies of various astrophysical sources for these waves have been calculated. Much of this work has been carried out at the California Institute of Technology in Pasadena, Ca. These calculations described the spatial strain amplitudes which might be expected near the earth, $\Delta h/h = \hat{\psi}$, produced by gravitational waves from known sources which would produce gravitational wave energy in various spectral bands. A summary of these results is depicted in Fig. 1, adapted from Thorne (1976).

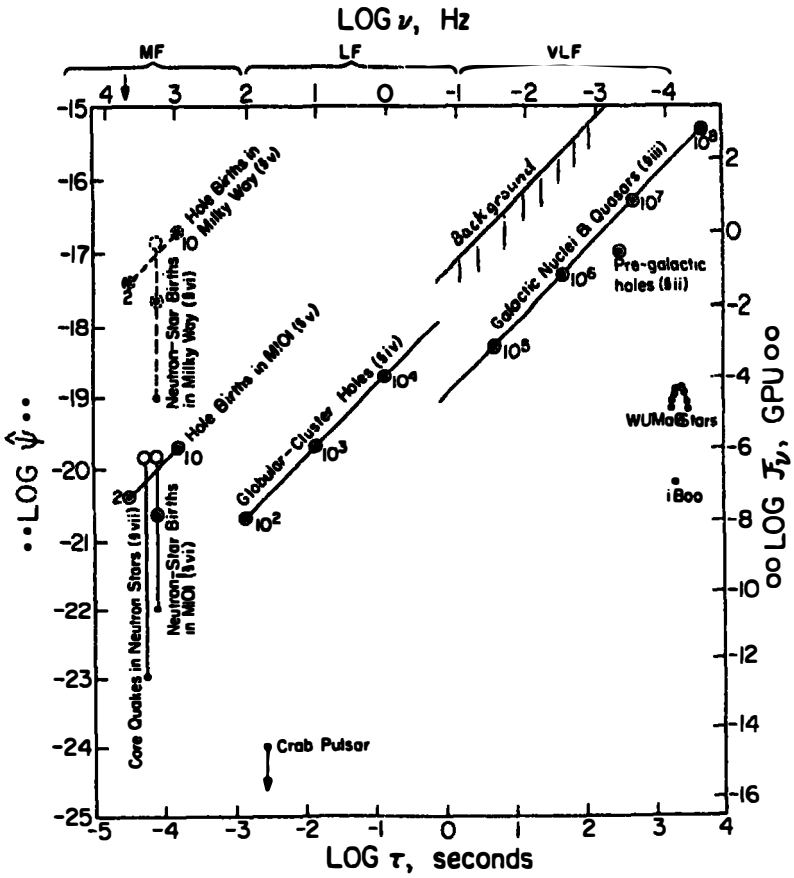

Figure 1. Spatial strain amplitudes near the earth Log $(\hat{\psi} = \Delta h/h)$ vrs Log τ for gravitational wave sources estimated in Thorne (1976).

The most noticable result is that the spectral region referred to as VLF (very low frequency), ranging from periods of 1 to 10^4 seconds, may contain the largest gravitational wave strain amplitudese Indeed, of all known sources, it is likely that the largest spatial strain amplitudes in the vicinity of the earth are caused by a cosmic isotropic background of low frequency. A number of recent theoretical studies have attempted to describe in some detail the varieus mechanisms in the early universe which would produce this isotropic gravitational wave background (Carr, 1979; Machhoon and Grishchuk, 1980; Bertotti and Carr, 1981). Several calculatiens have indicated that the prospects are good for the detection of a cosmic background of gravitational radiation in the foreseeable future.

DETECTION USING SPACECRAFT TRACKING TECHNIQUES

The method of accurately tracking interplanetary spacecraft for the purpose of detection of VLF gravitational waves began in the early 1970's (Anderson, 1971). With the introduction of hydrogen maser frequency standards, a search for the isotropic cosmic background of gravitational waves became astrophysically interesting (Anderson, 1977; Estabrook and Wahlquist, 1975; Anderson, 1978; Hellings, 1978; Hellings, 1981).

Doppler tracking of interplanetary spacecraft has been a main tool in space navigation and geodesy. The techniques used for gravitational wave detection are refinements and modificatiens of this now classical technique used in interplanetary spacecraft tracking. Thes data has been used for spacecraft navigation and controle planetary gravity field analysis, varieus refraction measurements, space plasma measurements and with other scientific experiments onboard spacecraft.

The wavelength of a gravitational wave is equal to the period, t, times the velocity of light, c. The gravitational wave background produces a special spectral signature, or autocorrelation signature, in the preciseeDoppler of the two-way signal, the technique most

often used in spacecraft tracking. As the wavelengths for periods > 10^3 seconds amount to > 3 x 10^{11} meters, outerplanet spacecraft missions are best suited for these types of investigations. Another significant factor which minimizes the sensitivity of the experiment is interplanetary plasma, and this also speaks favorably for an outerplanet mission where the plasma content is generally less than in the near earth environment.

A DESCRIPTION OF THE NOISE SOURCES

There are a number of significant noise sources which must be dealt with in order to maximize the sensitivity of the experiment for gravitational wave detection. Fig. 2 shows a schematic of the tracking system indicating the several media through which

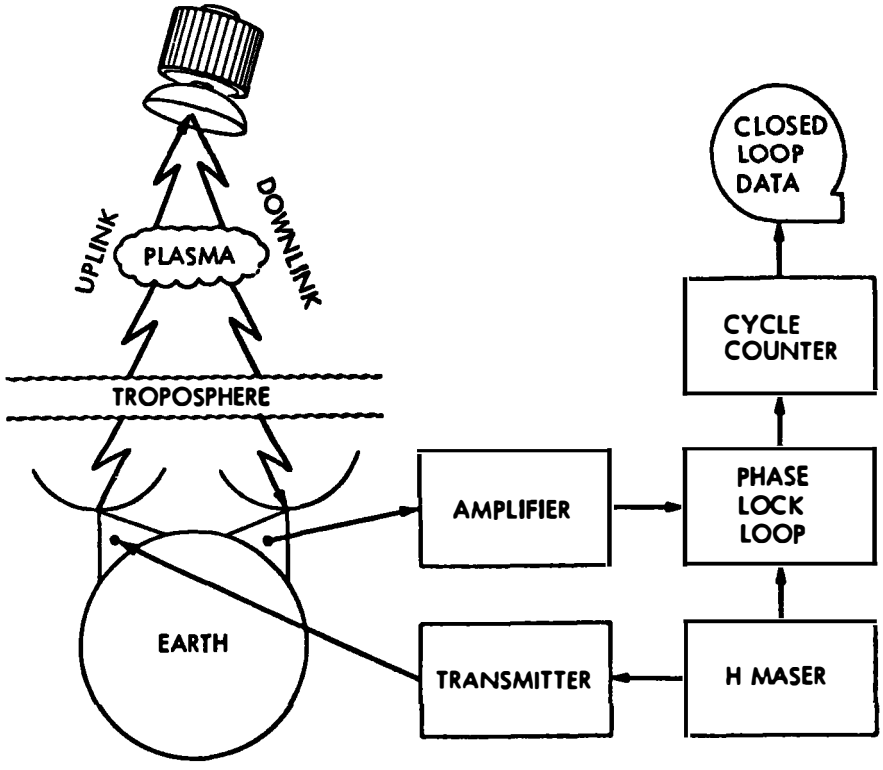

Figure 2.--Schematic of the Doppler spacecraft tracking system used for the gravitational wave cosmic background detection experiment.

the microwave signal must pass, all potential sources of noise to the experiment. The components are: 1) transmitting antenna system, 2) uplink troposphere (wet and dry), 3) uplink interplanetary plasma, 4) spacecraft antenna and transponder, 5) downlink plasma, 6) downlink troposphere (wet and dry), 7) receiving antenna, 8) hydrogen masers, 9) phase lock loop circuit, and 10) cycle counters.

The first source of noise is transmitting antenna accelerations. These can be monitored by accelerometers (recording gravimeters). At the present time this has not been the limiting factor for the experiment. The second factor, wet troposphere path length variations, have been observed to be significantly large enough to necessitate independent monitoring under bad tropospheric conditions. However, under favorable low wet troposphere variability conditions, measurements indicate this not to be the present limiting noise source (Anderson, 1979).

Interplanetary plasma variations can be monitored using dual S/X band tracking schemese Unfortunately a full two-way S/X band system is not in use with present spacecraft, lacking X band uplink capability. Future plans should eliminate this noise source, however at present this appears to be the limiting factor for the experiment. It has been found, however, that tracking spacecraft just after solar opposition, i.e. the spacecraft lie 180^{o} in the sky from the sun, reduces this noise source to near unmeasurable quantitiese Estimates indicate that using two-way X band tracking of spacecraft in the region of the outer planets at solar opposition would reduce plasma noise effects to well below 1 part in 10^{15}.

The limiting factor then becomes the frequency standards. Recent experiments by Mattison and Vessot (1982) at the Smithsonian Astrophysical Observatory have shown stabilities of a few parts in 10^{16} for periods of 3×10^{3} seconds should be obtainable with improved hydrogen maser systems.

A DESCRIPTION OF THE SIGNAL

The data produced by the experiment is a time series of frequency measurementse This set of frequency shift measurements, and its derivative, represents changes in the path length between the DSN transmitting antenna, the spacecraft antenna, and a receiving antenna when a separate receiving system is used.

The gravitational wave cosmic background produces a specific signature in the fourier transform or cross correlation of this time series (Anderson, 1977). A number of noise sources have different signatures and can thereby be separated from the gravitational wave response. Some noise sources, such as correlated white frequency clock noise, correlated troposphere and correlated ionosphere, have a signature that interfers with the gravitational wave cosmic background signature. Fig. 3 shows 5 noise signatures and the gravitational wave response in the autocovariance seriese The peaks in the series are at the round trip light time of the microwave signal which has been transponded from the spacecraft.

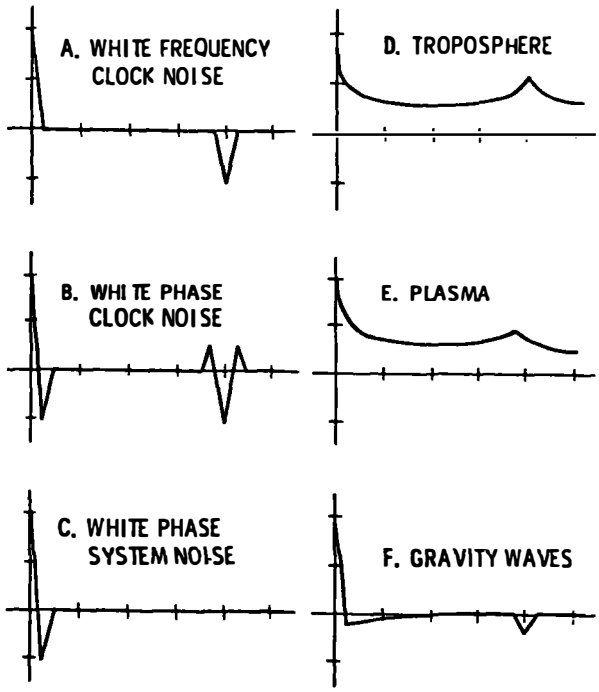

Figure 3.--Autocovariance functions for five known noise sources in a two-way tracking system (transmitting and receiving system the same) and the gravitational wave cosmic background response.

By using a separate receiving system with separate frequency standard and having an uncorrelated troposphere and ionosphere, i.e. sufficiently large separation between the transmitting and receiving stations, one is able to eliminate these correlated noise signatures and is left with the gravitational wave cosmic background signature (Anderson, 1977). It is this experiment that has been recently carried out using the Voyager spacecraft, a DSN Goldstone antenna, and the Owens Valley Radio Observatory facility (Hellings et al, 1981).

THE EXPERIMENTAL RESULTS

From March 6 to March 12, 1980, six days of tracking data were transponded from Voyager I while the spacecraft was near solar opposition. The S band uplink was generated using a hydrogen maser frequency standard at DSS-14, the 64 meter antenna at Goldstone, California. Two-way S/X band data were then received and recorded at DSS-14. Simultaneously, the 40 meter Owens Valley Radio Observatory (OVRO) antenna was used to receive the transponded X band signal from Voyager I. The data at OVRO used parts of the MK III VLBI receiver system and a digital tone extractor consisting of a frequency synthesizer locked to the OVRO hydrogen maser and phase measurement circuitry controlled by a FORTRAN program running on a HP-21 MX minicomputer. Frequency shift values were written on a floppy disk every 5 seconds.

This experiment represented the first time VLBI type spacecraft tracking data was acquired at an independent radio astronomy observatory using the MK III system and digital tone extractor. The operation proceeded without problem. The experiment was a successful demonstration of this capability which can easily be used in the future at several radio observatories in the US and Europe.

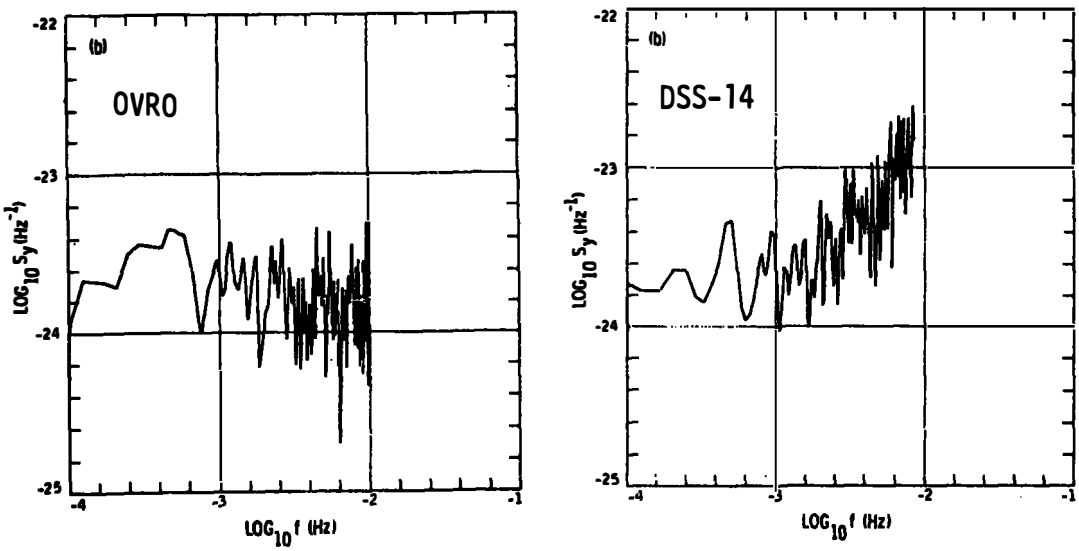

Figure 4.--Spectral analysis of OVRO and DSS-14 tracking data for 12 March 1980.

The data obtained from both stations was spectral analysed and autocorrelated using different filter lengths in an attempt to find the maximum sensitivity to gravitational wave cosmic background presently acheivable with these methods.

Fig. 4 shows the amplitude spectra of the data taken on the last day of the experiment, which also had the lowest contrie bution from plasma noise. A comparison between the Goldstone and OVRO spectra indicate generally a less noisy spectral content above 10^{-3}Hz for the OVRO data. The spectral noise below this frequency was approximately equivalent with some deviation in the detailed spectral content.

Fig. 5 is a composite of the autocovariance function for the best OVRO data set using 5 different filter lengths from 50 to 800 secondse The autocovariance function at the roundtrip light time, marked RTLT in the figure, is the significant portion which determines the sensitivity of the experiment to a gravitational wave cosmic background, as shown in Fig. 3. On the basis of the statistics of the autocovariance results, an upper bound on the limit of spatial strain produced by the

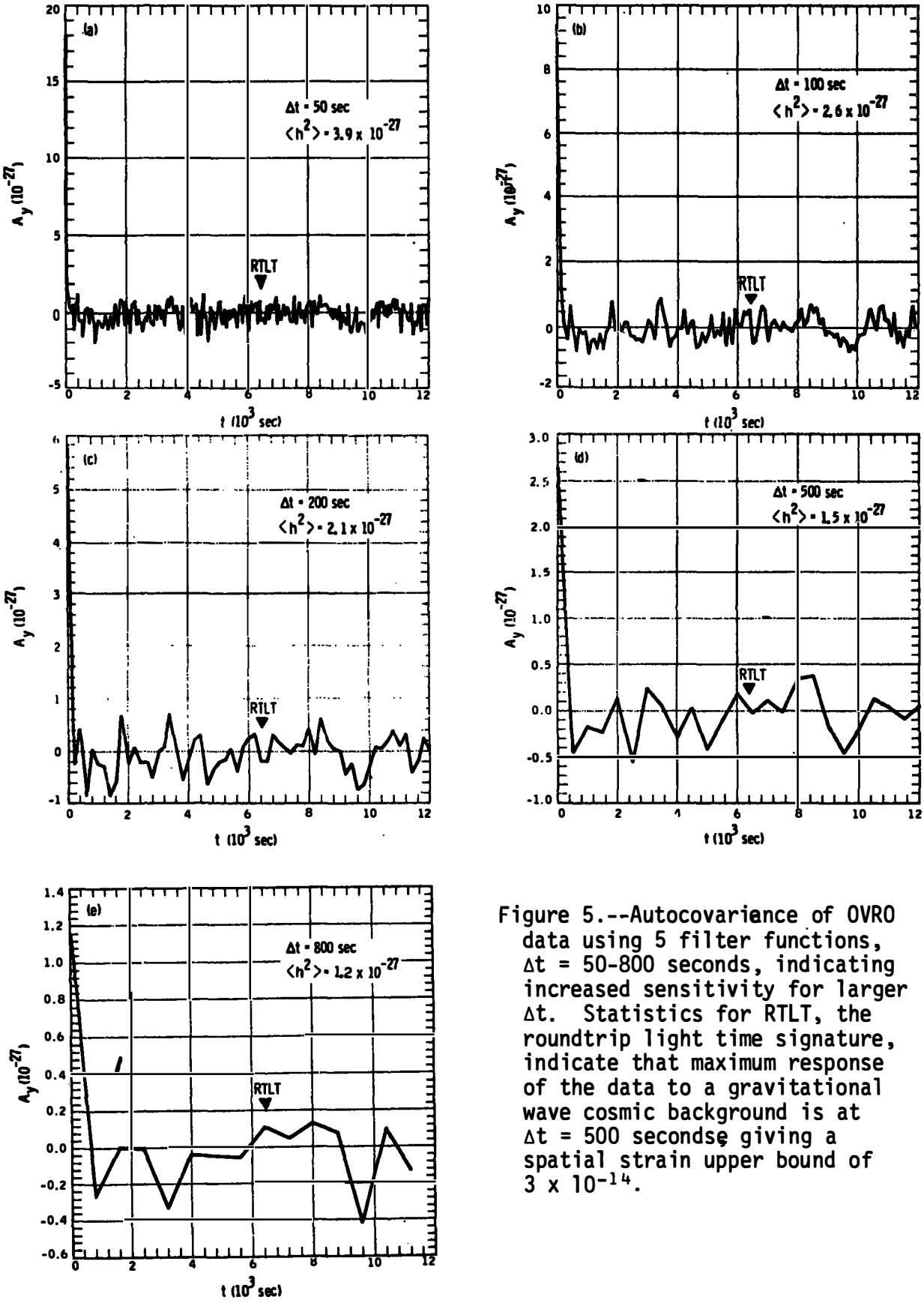

Figure 5.--Autocovariance of OVRO data using 5 filter functions, Δt = 50-800 seconds, indicating increased sensitivity for larger Δt. Statistics for RTLT, the roundtrip light time signature, indicate that maximum response of the data to a gravitational wave cosmic background is at Δt = 500 secondse giving a spatial strain upper bound of 3×10^{-14}.

presence of a gravitational wave cosmic background could be set at 3×10^{-14} for periods near the roundtrip light time, here $\sim 6 \times 10^{3}$ seconds. These results have first been reported by Hellings, et al (1981).

CONCLUSIONS

The successful application of presently available VLBI instrumentation to precisely track interplanetary spacecraft at an independent radio astronomy observatory has been demonstrated. It has been shown that independent radio astronomy observatory data is the most desirable from the standpoint of gravitational wave detection, as the data provided is free from correlated noise signatures which are close to the signature of the gravitational wave response.

The present detection system is limited because of the lack of a full X band deep space tracking system capability. With this improvement, the limiting sensitivity would then be the frequency standards in use and under unfavorable atmospheric conditions possibly the wet component of the troposphere.

With these conditions met, the measure of the upper bound to a gravitational wave cosmic background would be well below the limit presently set by astrophysical observations which are based upon assumptions of evolutionary cosmological models and would significantly contribute to gravitational wave research in the near future.

ACKNOWLEDGEMENTS

The experimental success of much of the work described here owes a great deal to the efforts of Ronald W. Hellings. Alan T. Moffet is gratefully acknowledged for the arrangements and use of the Owens Valley Radio Observatory. This experiment was carried out at the Jet Propulsion Laboratory, California Institute of Technology

with the assistance of the Owens Valley Radio Observatory. This work was sponsored in part by NASA contract NAS7-100 and in part by a grant from the Swedish Natural Science Research Council (NFR), FU 3114-114.

REFERENCES

Anderson, A.J., 1971. The probability of long period gravitational radiation and its detectione Nature, 229: 547-548.

Anderson, A.J., 1977. Detection of gravitational waves by spacecraft Doppler data. In: B. Bertotti (Editor), Experimental Gravitation. Accademia Nazionale dei Lincei, Rome, 235-246.

Anderson, A.J., 1978. Detection of gravitational wave background using Doppler tracking of the ISPM spacecraft. In: E. Grafarend and E. Livieratos (Editors), The mathematical structure of the gravity field. Proc. of the IAG special study group 4.45 symposium, Athense 61-67.

Anderson, A.J., 1979. Path length variations due to changes in tropospheric refraction. In: E. Tengström and G. Teleki (Editors), Refractional influences in Astronomy and Geodesye Proc. of IAU symposium No. 89, Uppsala. D. Reidel, pp. 157-162.

Bertotti, B. and Carr, B.J., 1981e The prospects of detecting gravitational wave background radiation by Doppler tracking interplanetary spacecraft. Preprint Cal Teche

Carr, B.J., 1979. Cosmological gravitational waves: Their origin and consequencese Orange aid preprint series in Astrophysics, 566, Cal Tech.

Davies, P.C.W., 1980. The Search for Gravity Waves. Cambridge University Presse

Estabrook, F.B. and Wahlquist, H.D., 1975. Response of Doppler spacecraft tracking to gravitational radiation. General Relativity and Gravitation, 6: 439-447.

Estabrook, F.B. and Wahlquist, H.D., 1978. Prospects for detection of gravitational radiation by simultaneous Doppler tracking of several spacecraft. Acta Astronautica, 5: 5-7.

Hellings, R.W., 1978. Testing relativistic theories of gravity with spacecraft Doppler gravity wave detection. Physical Review D, 17: 3158-3163.

Hellings, R.W., 1981. Spacecraft Doppler gravity wave detection. Physical Review D, 23: 834-843.

Hellings, R.W., Callahan, P.S., Anderson, J.D. and Moffet, A.T., 1981. Spacecraft Doppler gravity wave detection. Physical Review D, 23: 844-851.

Mashhoon, B. and Grishchuk, L.P., 1980. On the detection of a stochastic background of gravitational radiation by the Doppler tracking of spacecraft. Astrophysical Journal, 236: 990-999.

Thorne, K.S., 1976. General relativistic astrophysics. Orange aid preprint series in Astrophysics, 462, Cal Tech.

Mattison, E.M. and Vessot, R.F.C., 1982. Techniques used in SAO hydrogen masers for increased frequency stability and reliability. Paper presented at the IAG meeting, Tokyo. (See this symposium).

The U.S. National Crustal Motion Network

William E. Strange
National Geodetic Survey
National Ocean Survey, NOAA
Rockville, Maryland 20852, U.S.A.

ABSTRACT. As part of an interagency agreement, the National Geodetic Survey (NGS), NOS/NOAA, is responsible for establishing a National Crustal Motion Network (NCMN). The network will consist of 40 to 50 stations located throughout the United States, and will support future NGS requirements for maintenance and extension of the National Networks of Geodetic Control. Measurements at the NCMN stations will also support monitoring of crustal motion in the United States by the Crustal Dynamics Project of the National Aeronautics and Space Administration (NASA) and by NGS. Initial measurements at some of the stations of the NCMN were initated in 1981 by the NASA Crustal Dynamics Project.

Transfer of complete responsiblity for monitoring the National Crustal Motion Network from NASA to NGS is occurring in phases. At present, NGS is responsible for the implementation of stations, including site monumentation and ground survey measurements. NGS is currently training personnel to operate mobile Very Long Baseline Interferometry (VLBI) equipment and use existing VLBI reduction software for reducing and evaluating MARK III mobile VLBI data gathered under the NASA Crustal Dynamics Project. Current plans call for NGS to assume operational responsibility for one mobile VLBI system and a fixed VLBI base station in California in January 1984 and two additional mobile VLBI systems in January 1985. NGS plans to operate the three mobile VLBI systems to meet NGS geodetic control network and crustal motion requirements and, under NASA funding, to meet the requirements of the NASA Crustal Dynamics Project.

INTRODUCTION

The National Geodetic Survey (NGS), a component of the National Ocean Survey of the National Oceanic and Atmospheric Administration (NOAA), is responsible for the establishment and maintenance of the National Networks of Geodetic Control in the United States. The decade of the 1980's will see a dramatic transformation in the way in which NGS fulfills this responsibility. This transformation will result from the replacement of conventional ground based measurement systems (theodolites, geodimeters, etc.) with space measurement systems. The primary space measurement systems that will be used are Very Long Baseline Interferometry (VLBI) and geodetic receivers which make use of the Global Positioning System (GPS) satellites being launched by the U.S. Department of Defense.

The networks, established using VLBI and GPS systems, will have three basic components. First, there will be a network of three or four fixed VLBI stations. Second, there will be a network of 40 to 50 stations, distributed throughout the United States, which will be positioned relative to the fixed VLBI stations using mobile VLBI equipment. These stations will constitute the National Crustal Motion Network (NCMN)t Finally, there will be tens of thousands of stations whose positions will have been established relative to the stations of the NCMN using geodetic GPS receivers.

CONCEPT OF THE NATIONAL CRUSTAL MOTION NETWORK

The National Crustal Motion Network is expected to serve three important purposes. First, by using mobile VLBI the NCMN will extend and monitor a basic terrestrial coordinate system throughout the United States, which has been referenced to the inertial system defined by the fixed VLBI stations. The NCMN stations will serve as base stations for monitoring the remaining statibns of the National Networks of Geodetic Control using GPS geodetic receivers in a differential positioning mode. Second, these NCMN stations, which will be monitored by mobile VLBI, will serve as a check on and an intercomparison of the accuracy of the GPS geodetic receiver results. Finally, the NCMN will accurately monitor the crustal motions between points in the United States. For reasons discussed in the following paragraphs, the monitoring of the NCMN is expected to be carried out with both mobile VLBI systems and GPS equipmentt About 30 stations will be monitoried with mobile VLBI systems and an additional 10 to 20 stations monitored using GPS geodetic receivers.

A prerequisite for any geodetic control network is that it be referred to a well defined terrestrial reference system. The terrestrial reference system to which NCMN station positions will be referred will be defined by making use of the Polar motion by Analysis of Radio Interferometric Surveying (POLARIS) network. This network, consisting of fixed VLBI stations at Ft. Davis, Texas, Westford, Massachusetts, and Richmond, Florida, is described elsewhere in this volume (Robertson and Carter, 1982). A new adjustment of conventional geodetic data will be completed within the next few years. This control network will be designated the North American Datum of 1983 (NAD 1983). The NAD 1983 will also derive its orientation from the POLARIS stations. Thus, the NCMN stations will serve to maintain the NAD 1983 terrestrial coordinate system throughout the National Networks of Geodetic Controlt

The POLARIS stations will continuously monitor the orientation of the Earth in inertial space. This will provide the polar motion and earth rotation information required to separate motions of the earth in inertial space from motions of the stations when mobile VLBI and GPS geodetic receivers are used to monitor crustal motion. Because the POLARIS stations are all situated on the North American plate, the rotations of this plate will initially be absorbed in the solutions for polar motion and earth rotation. For this reason, the initial terrestrial coordinate system will be a coordinate system fixed with respect to the North American plate. However, through observations between the POLARIS stations and fixed VLBI antennas located on other continents, it will be possible to establish the differential movements of continents and ultimately to obtain a terrestrial coordinate system that is more nearly fixed with respect to the lower mantle.

Because the NCMN stations will be referenced to the POLARIS stations each time they are determined, the differential motion of the stations can be determined relative to the POLARIS coordinate system. Thus, the NCMN will provide a means of monitoring differential crustal motions throughout the United States with high accuracy.

The reference system used for GPS geodetic positioning is established by the orbits of the GPS satellites. Since the user is interested in accuracies at the few centimeter level, it is important that the VLBI stations account for changes in the GPS reference frame due to replacement of satellites or due to changes in the parameters (e.g., gravity field, polar motion) used when computing orbitst

STATUS OF NATIONAL CRUSTAL MOTION NETWORK

Mobile VLBI equipment has been developed by the Jet Propulsion Laboratory (JPL) of the California Institute of Technology for the NASA Crustal Dynamics Program. There are two mobile VLBI systems now operational: a 9-meter antenna system, designated MV-1, and a 4-meter antenna system, designated MV-2. JPL is currently constructing a second-generation mobile VLBI system, designated as MV-3, which is scheduled for completion late this year, and is modifying the MV-1 and MV-2 systems to operate with dual frequency for higher accuracy. Current plans call for placing MV-1 more or less permanently at Vandenberg Air Force Base in California and using MV-2 and MV-3 as mobile systems to carry out measurements at a number of stations in the western United States (primarily California) in support of the NASA Crustal Dynamics Program.

The United States has an integrated Federal program for the use of space systems for geodynamics and geodesy (ICCG, 1982), which involves NOAA, NASA, U.S. Geological Survey, National Science Foundation, and the Department of Defense (Defense Mapping Agency and U.S. Naval Observatory)t This Federal program calls for transfer of the MV-1, MV-2, and MV-3 mobile VLBI systems, as well as a fixed VLBI antenna (the Mojave antenna located at Goldstone, California) from NASA to the NGS. Current plans call for the MV-3 mobile system and the Mojave fixed antenna to be transferred in January 1984, and MV-1 and MV-2 to be transferred in January 1985.

Once the mobile VLBI systems are transferred to NGS, they will be operated by NOAA to meet the requirements of all Federal agenciest In particular, NGS will carry out observations required by the NASA Crustal Dynamics Project through 1988, the duration of the project. The NASA Crustal Dynamics Project is monitoring movement of stations in the western United States and Alaska to support earthquake and plate tectonic studies (Flinn, 1981). As a part of the NMCN, a number of these stations will continue to be monitoried by NGS after the NASA Crustal Dynamics Project is completed. In addition, NGS will establish additional regional coverage throughout the United States.

Because NGS will assume complete responsibility for NCMN observations beginning in 1985 and will continue to make observations at these stations after completion of the NASA Crustal Dynamics Project in 1988, NGS has already assumed responsibility for implementing the sitest Implemention includes

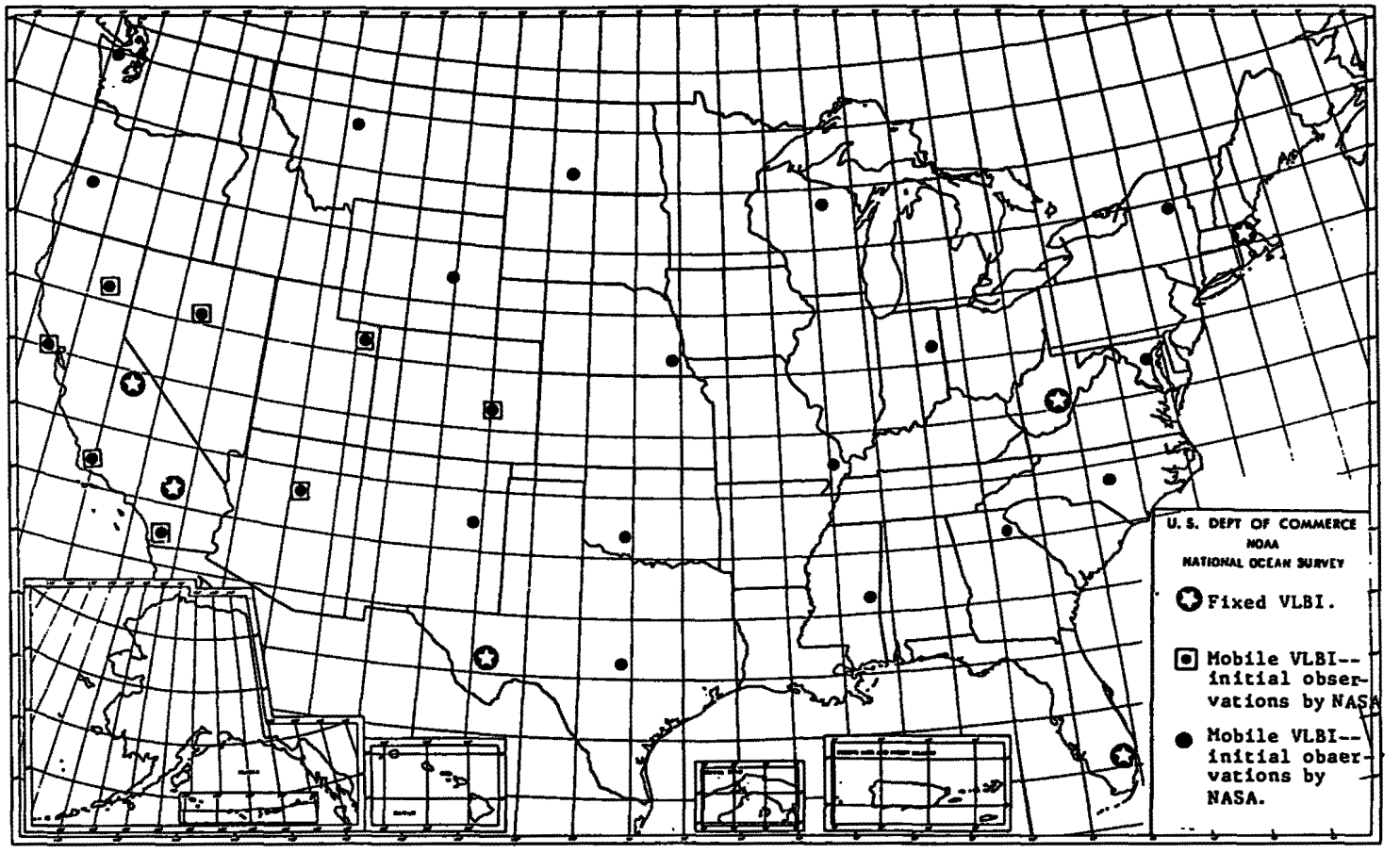

Figure 1.--NCMN sites to be monitored with mobile VLBI.

performing site reconnaissance, obtaining legal permission for use of the site, placing ground monumentation at the sites, and carrying out ground surveys to interconnect the monuments.

Future Plans

Currently the NCMN is expected to include 40 to 50 stationst The locations of 31 stations in the contiguous 48 States that NGS expects to monitor by means of mobile and fixed VLBI equipment are shown in figure 1. Shown here are six fixed stations and 25 stations thatt will be established using mobile VLBI equipmentt Positions of these 31 stations, and a fixed antenna at Fairbanks, Alaska, are currently planned for continued monitoring by NGS following completion of the NASA Crustal Dynamics Project. All of the fixed stations except Mojave and Richmond are currently operational. Mojave and Richmond are expected to become operational in 1983. Eight of the 24 stations that will be monitored using mobile VLBI will initially be positioned by NASA as a part of their Crustal Dynamics Project during the period 1982-1985. The remaining 16 stations are planned for initial positioning by NGS using mobile VLBI during the period 1984-1987.

An additional 10 to 20 stations will be established in California, Arizona, and Alaska as part of the NASA Crustal Dynamics Project using mobile VLBI. Positions of these stations will be monitored using Mobile VLBI systems until completion of the Crustal Dynamics Project in 1988. NGS expects to continue monitoring those stations of this group which are felt to provide valuable crustal motion information based on the results obtained during the lifetime of the NASA Crustal Dynamics Project. However, current plans call for NGS to monitor movement of these stations, as part of the NCMN, using differential GPS techniques, since these stations will be used entirely for purposes of crustal motion monitoring and not for coordinate system maintenance. Also, in the case of California, the stations are closely spaced, making them especially amenable to positioning using GPS geodetic receivers.

The National Crustal Motion Network will provide a continuing means of monitoring crustal motion and regional strain in the United States while at the same time maintaining the terrestrial coordinate system required by the National Networks of Geodetic Controlt

REFERENCES

Robertson, D. S., and W. E. Carter, Operation of the NGS POLARIS network (this volume).

Flinn, E. A., Applications of space technology to geodynamics, Science, Vol. 213, pp 89-96, July 3t 1981.

Interagency Coordinating Committee for Geodynamics, Federal Implementation Plan for the Application of Space Technology to Crustal Dynamics and Earthquake Research, 113 pp, Washington, D.C., June, 1982.

FUTURE PLANS FOR FRENCH VLBI PROJECT : SCIENTIFIC PERSPECTIVES AND TECHNICAL CAPABILITIES

François Biraud
Observatoire de Paris-Meudon
92190 Meudon, France

Claude Boucher
Patrick Hill
Institut Géographique National
2, Avenue Pasteur 94160 St-Mandé, France

Carlo Rosolen
Observatoire de Paris-Meudon

ABSTRACT: In 1981, the GRGS (Research Group in Spatial Geodesy), including CNES (National Space Center), IGN (National Geographical Institut), CERGA (Astronomy and Geodesy Research Center), and Observatory of Paris-Meudon, has worked out a VLBI program. The first step in that project would be to operate at the end of 1982 with EISCAT dishes in Kiruna (Sweden) and Sodankylä (Finland) at 935 MHz. The available VLBI recording system will be 2 MK II block, and a French H-Maser version should be operational at the end of 1983.

Scientific goal would be, later than 1983, to tend towards a S/X band and a MK III system working either in Kiruna or at other sites equipped with a new dish and its use for astrometric and geodetic experiments.

Presented at IAG Symposium No.5 : Geodetic applications of Radio Interferometry, Tokyo, May 7-8, 1982

1) INTRODUCTION

Since 1981, the GRGS (Groupe de Recherches de Géodésie Spatiale) has started a VLBI program. The principal scientific orientation is given towards global Geodynamics and Astrometry. In fact, the GRGS is coordinating all the French space geodetic programs since 1971, date of its creation. Member organizations are :

- The Bureau des Longitudes (BdL)
- The Centre National d'Etudes Spatiales (CNES)
- The Institut Géographique National (IGN)
- The Observatoire de Paris (including CERGA and BIH)

The radioastronomy group of the Observatory of Meudon has been involved since the beginning of the VLBI project in building the technical equipments. In the near future, this national program should be extended to the Observatory of Bordeaux (radioastronomy group) and to Nançay station.

The centimetric VLBI project, in its early stage, will establish a close relationship with radioastronomers interested by mm-VLBI, particularly IRAM (Institut de Radio-Astronomie Millimétrique)t

2) THE ERIC PROJECT

In 1981, with technical collaboration of the radioastronomy group of Meudon Observatory, GRGS has started the ERIC project (EISCAT Radio Interferometric Campaign). The primary goal of this project is to become familiar with the VLBI technique, and particularly to estimate the necessary resourcest The next step is devoted to study data reduction methods and to investigate some preliminary plans concerning the choice of a new VLBI dedicated antenna.

2.1) Present technical developments

The ERIC technical deve :onsists in the manufacturing of two Mk II recording systemst l be running by the end of 1982.

Video converters are those of the Mk III system, provided by Phoenix Corporation. A formatter has been built from the JPL drawings and has been adapted to the new video recorder VFT 250 (RCA).

Each terminal will work with two video converters and will therefore allow bandwidth synthesis observations (BWS). BWS is used to provide higher accurate results with VLBI observationst

At the same time, a technical collaboration was defined with the Laboratoire de l'Horloge Atomique (LHA) to realize a compact version of the H-maser running at the University of Orsay, since 1972. Basic specifications are given below :

size (m)	:	1.8 × 1.2
weight (kg)	:	
σ_τ (after one	:	$2.2\ 10^{-15}$ ($\tau = 10^3$ s)

2.2) EISCAT antennae

The first step of French VLBI program, ERIC, is characterized in using two of the three EISCAT (European Incoherent SCATtering Scientific Association) dishes, primarily installed in Scandinavia for ionospheric studies. Antennae of interest (because working in reception mode) are 32 metre paraboloids located at approximately 70° of latitude, in Kiruna (Sweden) and Sodankylä (Finland). Mounting system is an alt/az one. A receiver working at 935 MHz is presently equipping this network.

A detailed study has been started and is furthering actually to define technical improvements that we have to effect to observe at a frequency close to 10 GHz ($\sim$ X band). Problems encountered are :

- Determination of the accuracy of the actual surface
- Possibility to improve the paraboloid shape
- Tests on pointing and tracking systems
- Definition and realization of new feeders and receivers
- Control of local oscillators stability

We already have an idea of the efficiency of the Kiruna antenna. Technicians from Onsala Observatory have found a 12% efficiency at 86 Hz (1981). This value is very low and could be explained by uncertainties on the effective temperature of the noise tube, source flux densities, angular size of the observed sources, and also on misalignment of the secondary mirror, and finally by the actual misalignment of panels of the paraboloid (as it was seen during our last technical mission). However, it seems possible to improve the surface quality and line up the axis of the secondary mirror [1].

The present pointing and tracking systems are not sufficiently accurate to work at 10 GHz. TIW, manufacturer of these antennae, has been contacted to improve this accuracy eventually.

We also plan to study ionospheric scintillation effects quantitatively on VLBI experiments. At these latitudes, the scintillations may be strong and may disturb the phase stability of the recorded signal.

2.3) ERIC experiments

ERIC project may be divided into three main phases :

ERIC Ø is concerning electronic tests on the two Mk II recording systems. The Nançay radiotelescope will be used at a 18 centimetre wavelength. The two independent tracks of this receiver will provide a zero baseline VLBI observation. Two rubidium clocks will be utilised.

ERIC 1 will allow VLBI observations between the two EISCAT dishes at 935 MHzt The goal of these experiments will be technical essentially, and should probe the complete efficiency of our equipment and our capabilities to run such experimentst

ERIC 2 should be the actual improvement of one or two antennae to allow 10 GHz observations (S/X band)t This stage of ERIC should be considered only if all the tests defined above were positive and if expected scientific results are sufficient with respect to our future program.

3) FUTURE PLANS

At the same time when we are preparing ERIC 2, we are also working on new investigations, which seem of a major interest for future planning.

3.1) 30 metre antenna

Such an antenna would be dedicated to VLBI. It would be an alt/az mounting and would work between 1 and 22 GHz. Priority would be given to S/X band observationst

This antenna, of a diameter close to 30 metres, would be located either in France or in an overseas country (for example : Reunion, Guyane ...). This geographical location has not yet be definedt

3.2) 15 metre transportable antenna

Such a project is obviously of a great interest for geodetic studiest The main goal of this kind of equipment is to cover unsurveyed areast

French manufacturers have capabilities to build such a system with a diameter of approximately 15 metrest This antenna should be also equipped with feeders and receivers going from 1 GHz to 22 GHz (or at least S/X). For this purpose, our laboratories are making a particular effort in order to increase the portability of the VLBI equipments, including H-maserst

3.3) Scientific cooperation

French community has expressed a strong support towards geodynamical and astrometric activitiest Earth rotation study (polar motion, UT 1), geodesy (regional and global tectonics) have already been put in high priority by GRGS with participation to MERIT and Crustal Dynamics Projectst

Cooperation with networks dedicated to geodetic VLBI, such as POLARIS [2], is of prime interest to ust

Anyway, the French VLBI group has a will to cooperate with any other network, at S/X band or others. Other frequencies on our antenna would be utilized to study source structures and their evolution in time. These information are necessary to define and maintain a catalogue of radiosources.

4) CONCLUSION

The group intends to assert itself towards Geodynamics and Astrometry using S/X bands, but also displays a great effort for the millimetric VLBI, involving high frequency observations (226 Hz).

By approximately 1986, with the 30 metre radiotelescope in Spain and the interferometer of Plateau de Bures, near Grenoble, IRAM, with millimetre observations, will bring a large complementarity to the centimetric VLBI group.

References

[1] BIRAUD (F.), CHAMPION (M.), HILL (P.), ROSOLEN (C.) - (1982)
Projet ERIC - Etude de l'antenne de Kiruna
Notes Techniques NT/G n° 25 - IGN/SGNM/DTIG, Saint-Mandé

[2] ROBERTSON (D.S.), CARTER (W.E.) - (1982)
Operation of the National Geodetic Survey POLARIS network
Presented at IAG Symposium n° 5 : Geodetic Applications of Radio-Interferometry, Tokyo

DEVELOPMENT OF VLBI SYSTEM AND FUTURE EXPERIMENTAL PLAN IN THE RADIO RESEARCH LABORATORIES

Yoshikazu SABURI, Kazuyuki YOSHIMURA and Seiji KATO

Radio Research Laboratories
Koganei, Tokyo 184, Japan

Kenich TSUKAMOTO, Fujio YAMASHITA, Nobuhiro KAWAJIRI and Nobuyuki KAWANO

Kashima Branch, Radio Research Laboratories
Kashima, Ibaraki 314, Japan

ABSTRACT. The VLBI systems have been developed in Radio Research Laboratories (RRL) since 1974. The domestic experiments were made in 1977 and 1979 by using the first one (K-1) and the second one (K-2), respectively. The third system (K-3) has been developed since 1979 according to the five-year plan, which is compatible with Mark-III system in the U.S.A. The joint experiments between NASA and RRL will start at the beginning of 1984 and be continued at least for five years. In addition, RRL will make the domestic observations in cooperation with the Geographical Survey Institute (GSI) after 1984. The data analysis software in K-3 system will be completed in 1982 by RRL in cooperation with the International Latitude Observatory of Mizusawa (ILOM).

1. INTRODUCTION

Very Long Baseline Interferometer System makes use of many precise and modern techniques. Radio Research Laboratories (RRL) has experiemces in some of such techniques in its own research programs, such as those in the fields of Frequency standard, Space communications, Space and Atomospheric Sciences, Information processing and others. Putting these experiences together, high precision VLBI system (K-3) has been developed since 1979 under the five-year plan. This paper briefly summarizes the past and present developments of VLBI system in RRL, and some future observation plans both for intercontinental and domestic baselines.

2. HISTORY OF THE DEVELOPMENT OF VLBI SYSTEMS AT RRL

In 1974, a research group of radio astronomy in RRL started working on the first VLBI system (K-1) consisting of one-channel digital recording of 2 MHz bandwidth. After preparation for about two years, the first VLBI experiment was conducted in Japan with a baseline of 121 km.

From 1977, the second system (K-2) was developed for the purpose of measuring of phase scintillation in the received signal from the Experimental Communication Satellite (ECS) and from celestial radio sources. In this system,

the digital data sampled at the sub-station (Hiraiso Branch of RRL) was transmitted to the main station (Kashima Branch of RRL) via a microwave link. In 1979, the experiment using K-2 system proved itself to be a success in establishing techniques of real-time data processing and of five-channel bandwidth synthesis.

As the third stage, a five-year plan for the development of high precision VLBI system for geodesy (K-3) started in 1979 in relation to the Japanese national project of earthquake prediction techniques. At that time, VLBI joint experiment was proposed by NASA as one of the items of items of US-Japan technical cooperation. After the mutual agreement made between NASA and RRL in 1980, the original plan was revised to be compatible with Mark III system. The development of K-3 system has been conducted according to the revised plan, and the back-end part of the system and the most part of software will be completed in 1982. The first experiment between the U.S.A. and Japan is scheduled to be made early in 1984. Table 1 lists the history of VLBI developments in RRL.

Year	Item
1974 Sep.	Start of the first VLBI system (K-1) development
1977 Jan.	First VLBI experiment in Japan with a baseline of 121 km
Oct.	Start of the second VLBI system (K-2) development
1978 Dec.	Beginning of consultation about U.S.-Japan joint experiment
1979 Apr.	Start of five-year plan of high precision system development (K-3)
Sep.	K-2 system experiment in real-time data processing mode with a baseline of 47 km
1980 Feb.	Formal agreement between U.S.A. and Japan on joint experiment in 1983
1981 Apr.	Revised K-3 system development plan to be compatible with Mark-III
1982	Back-end and software will be completed
1984 Jan.	First U.S.-Japan joint experiment scheduled

Table 1. History of VLBI development in RRL

3. BRIEF DESCRIPTION OF K-1 AND K-2 SYSTEMS AND THEIR RESULTS

3.1 K-1 System

The K-1 system was designed referring to Mark II system in order to establish the basic VLBI techniques in RRL. It consisted of one-channel IF amplifier of 2 MHz bandwidth, 4 Mb/s sampler, digital diphase-modulation coding, VTR recorder, Cesium beam standard and correlation processor. The first VLBI experiment was made in Japan in January 1977 by using K-1 system with a baseline of about 121 km between RRL Kashima antenna (26 m in diameter) and NTT Yokosuka antenna (12.8 m in diameter). The signals at 4180 MHz from the geostationary satellite ATS-1 and those from 3C273B were observed. By reducing of ATS-1 data, a resolution of 5 ns in determining delay time with r.m.s. error of about

4 degrees for relative phase was attained. For the celestial object, 3C27B, the cross-correlation peak was detected by using the fringe rotation techniquer

The main characteristics of K-1 system are summarized in Table 2 together with those of K-2 and K-3 systemsr The details of K-1 system and the experimental results were reported in the references [VLBI special issue, Review of RRL, 1978] and [Kawajiri et al, 1979].

Items	K-1	K-2	K-3
Purpose	Basic techniques of VLBI	Real-time data processing and Bandwidth synthesis	Precision VLBI system compatible with Mark III
Receiving frequency	4180-4182 MHz	4030-4132 MHz	2200-2320 MHz and 8180-8600 MHz
Channels	1	5 (alternative)	28 (maximum)
Sampling rate	4 Mb/s	4 Mb/s	8, 4, 2, 1, 0.5 and 0.25 Mb/s
Recorder	Toamco VR489 (video)	(Real-time)	Honeywell M-96
Atomic standard	Cs clocks with regular tube	Cs with high performance tube and Rb	Hydrogen Masers
Computer	NEAC 3100	NEAC 3200	HP-1000: 10 L(System control) 45 F(Data analysis)
Calibration device	—	—	Water vapor radiometer and system delay calibrator
Precision	5 ns	0.1 ns	better than 0.1 ns

Table 2. Main characteristics of K-1, K-2 and K-3 system

3.2 K-2 system

The second VLBI system, K-2, was developed as a phase scintillationmeasuring systemrin Japanese Experimental Communications Satellite (ECS) Project. The technical emphasis was put mainly on a real-time data processing system and a bandwidth synthesis methodr The block diagram of K-2 system is shown in Fig. 1 and the characteristics are listed in Table 2.

The bandwidth synthesis is performed by five channels of 2 MHz bandwidth each, which are separated by 0, 10, 30, 60 and 100 MHz at 4 GHz and can be switched sequentially every 10 ms. The distance of the baseline between the main station at Kashima Branch of RRL and the sub-station at Hiraiso Branch of

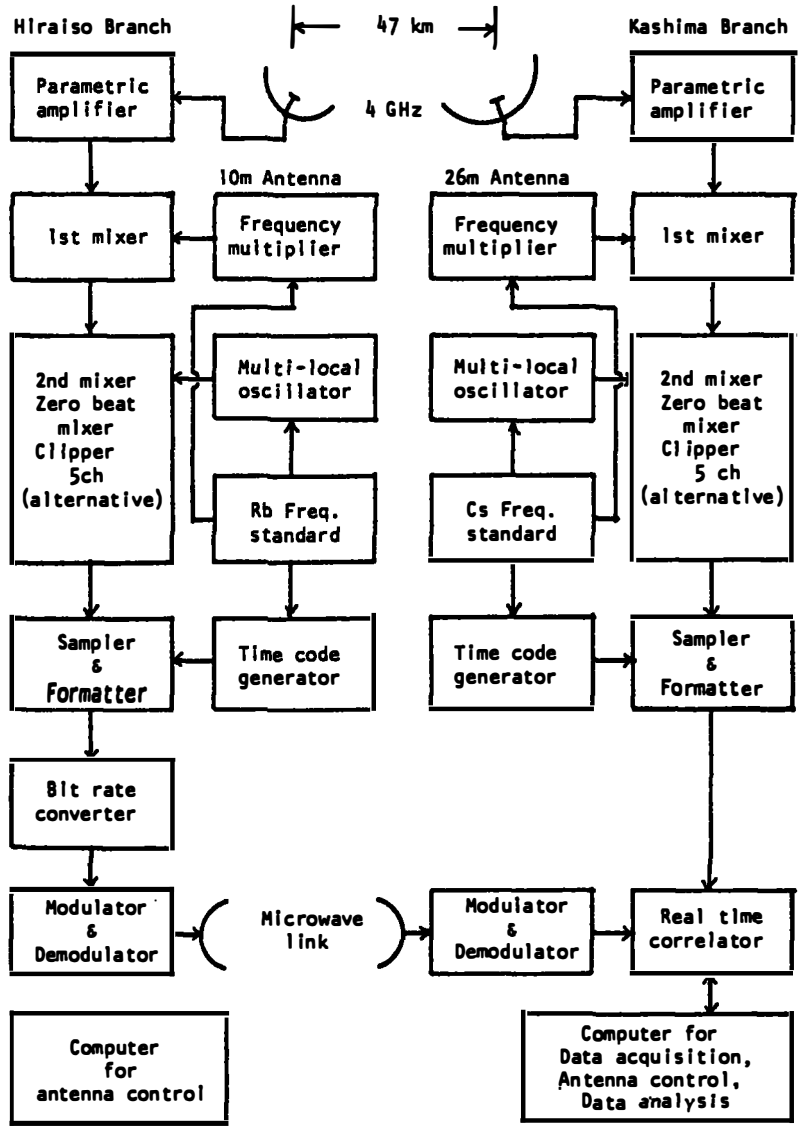

Fig. 1. Block diagram of K-2 system

RRL is 47 km. Digital data sampled at the sub-station were transmitted via a microwave link in order to make a real-time data processing at the main station.

Using this real-time VLBI system, three kinds of experiments were carried out. The first is the determination of the difference in time of arrival (delay time) by receiving wide-band noise from the geostationary satellite CS and QSO 3C273. In the case of CS, the estimation error of delay time was about 0.1 ns with the integration time of 0.1 sec for each channel, because of a strong flux density. In the case of QSO 3C273, the estimation error resulted in about 0.17 ns with the integration time of 2 sec. High precision of K-2 system was proved by these results, but the long-term observation was limited mainly due to the frequency instability of the atomic standards, Cs beam and Rb clocks.

The second is the measurement of phase scintillations in a signal from a satellite which occurs along the path through the atomosphere. As a result of the measurements on the signals from the satellites CS and Intelsat, it is shown that the Allan variance of the phase scintillations in the averaging time of 10 sec is about 16 deg. and it obeys the 1.4 - 1.8th power law of the averaging time.

The last one concerned with the phase scintillation by the solar wind. The measurements were made on the radio waves from QSO 3C273 at 4 GHz when its propagation path approached the sun at a distance of 0.08 AU. The intense visibility fluctuations were detected for 10 days and the maximum fluctuation exceeded 10 % of the total flux. The fluctuation obeys approximately the 3rd power law of the distance between the path and the sun. It was also confirmed that the scintillations decreased when the averaging time exceeds 0.5 sec. From these results, it is suggested that the effects of the phase scintillations at 4 GHz produced by the solar wind may disappear for the VLBI baseline distance of several tens km when the solar elongation angle exceeds 5 - 7 degr The details of K-2 system and the results are reported in the references, [Kawano et al, 1980] and [Kawano et al, 1982].

4. K-3 SYSTEM DEVELOPMENT

As the third stage, a five-year plan for the development of a high precision VLBI system (K-3) for geodesy started in 1979. After the conclusion of the agreement between NASA and RRL in 1980 as to JS-Japan joint VLBI experiment, the plan was revised thoroughly both in hardware and software in order to use K-3 system for intercontinental observation and to be compatible with the Mark III system.

The K-3 system includes not only hardware but also software for deriving physical quantities such as baseline vectors, time synchronization error, polar motion, earth rotation and others from the measured delay time and fringe rates. On the design and construction of the K-3 system, the following items are considered:

(1) The precision of delay time measurement is 1 ns for S-band and 0.1 ns for X-band;

(2) Compatibility with the Mark III system in software as well as hardware,

(3) IEEE 488 buses are used to control and monitor each module of the system with a computer,

(4) The measurement of relative instrumental delay using calibration signals can be made in real time by the correlator.

The block diagram of K-3 system is shown in Fig. 2 and its main characteristics are summarized in Table 2. The detail of K-3 hardware and that of K-3 software are reported in this issue, [Kawaguchi et al, 1982] and [Takahashi et al, 1982], respectively.

As to hardware system, the manufacture of the back-end part including hydrogen maser, water vapor radiometer, system delay calibrator and correlation processor will be completed in 1982. The overall system check and

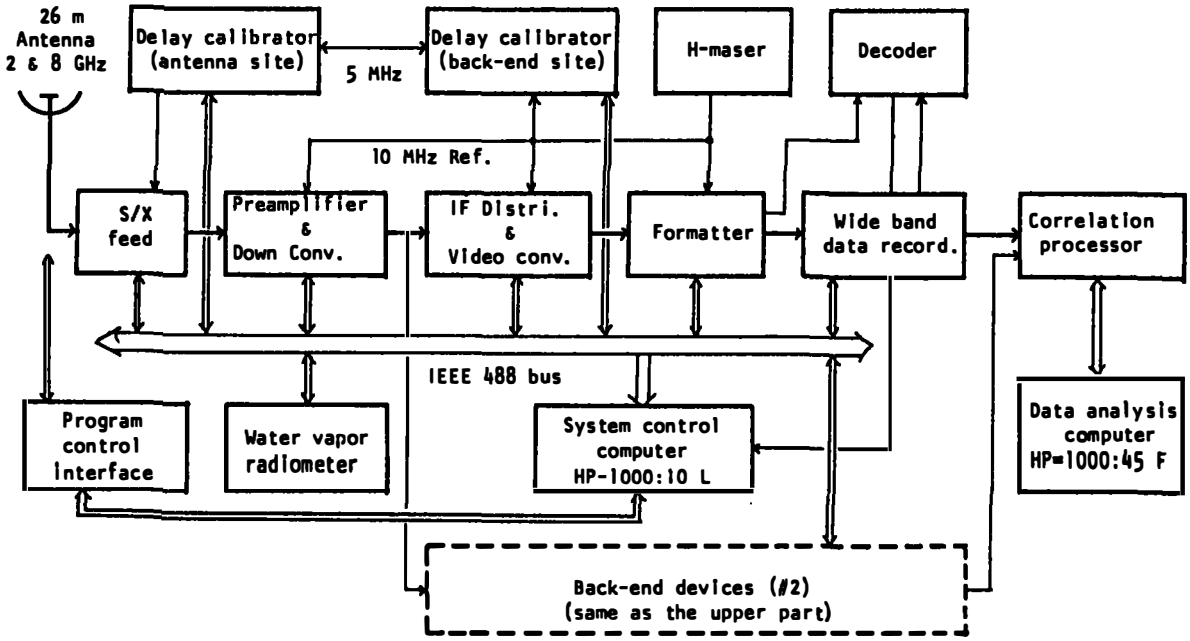

Fig. 2 Block diagram of K-3 system

evaluation will be made in 1983 immediately after the installation of S and X-band front-endr The software includes Automatic operation, correlator control, Bandwidth synthesis, Baseline analysis, Data-base management and Antenna tracking. The automatic operation software (KAOS) compatible with "Field system" of Mark III has been already developed and the others will be completed in 1983.

5. FUTURE EXPERIMENT PLAN

According to the mutual agreement between NASA and RRL mentioned in Section 2, RRL will undertake VLBI joint observations by using the 26-meter antenna at Kashima Branch with one or more of the antennas operated by the U.S.A. The objective is to demonstrate the capability and to contribute to establishing a global network of VLBI observations for the study of plate motion,polar motion and earth rotation.

The system level experiment, as the first one of U.S.-Japan joint experiments will be made at the beginning of 1984 as previously scheduledr The mutual agreement to continue the observations at least for five years beginning in late 1984 has been made. The data processing and analysis for those observations will be made by NASA and RRL by using their own software, which may give very useful information to the MERIT and the DELP programsr In futurer RRL intends to make international cooperations with as many stations as possible for various studies including time synchronizationr

In parallel with the U.S.-Japan joint experiment, the domestic experiments are also being planned by RRL and the Geographical survey Institute(GSI)r

The GSI started in 1981 to prepare a system with a transportable 5-meter antenna, the design of which is based on the techniques developed by RRL for K-3 system. For the purpose of system checking by both parties, such as precision, accuracy and reliability, the first experiment is expected to be made in 1984 on a baseline of about 52 km between the RRL Kashima 26-meter antenna and the GSI Tsukuba 5-meter antenna, [Kawaguchi, et al, 1982].The result will be compared with those measured by the traditional meansr The follow-on experiments will be continued by transporting the GSI 5-meter antenna to some places within a country for the readjustment of Japanese geodetic network established by the GSI, [Nishi, et al, 1982], and for monitoring the local crustual movements. These experiments will be performed as a part of the domestic program corresponding to DELP project.

Along with the observation plan, RRL will continue the development of the system in improvement of precision, in establishment of a transportable system suited to the physical features of Japan, in realization of real-time VLBI network, and in applications to satellite tracking and others. The RRL will continued further cooperations with the Japanese organizations concerned,such as the International Latitude Observatory of Mizusawa (ILOM) in software development, the Tokyo Astronomical Observatory (TAO) in Joint observation and the Maritime Safety Agency (MSA) in coordination with laser ranging observation. The future experiment plan is summarized in Table 3.

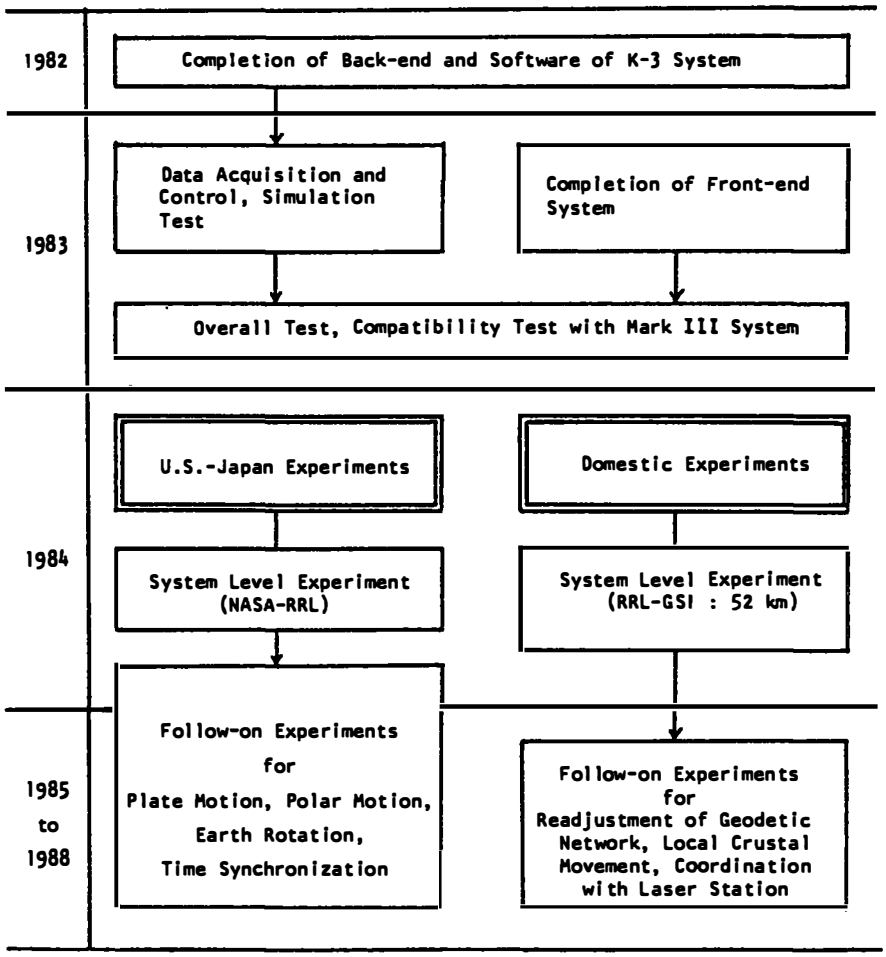

Table 3. Experiment Plan

6. CONCLUDING REMARKS

In this paper, the outline of the past and present VLBI system development and some future experiment plan is given. We are confident that our K-3 system may contribute to the international and domestic studies in many fields. We would like to express our sincere thanks to many persons concerned in RRL and the organizations in the U.S.A. and Japan during the stage of K-3 system development, especially to the members of geodynamics project in NASA Headquarter and GSFC for their close cooperation and assistancer

REFERENCES

Kawaguchi, N.; Sugimoto, Y.; Kuroiwa, H.; Kondo, T.; Hama, S.; Amagai, J., Morikawa, T. and Imae, M. (1982); "The K-3 hardware system being developed in Japan and its capability", in this issuer

Kawaguchi, N., Kawajiri, N., Kawano, N., Yoshimura, K., Ishii, H., Murakami, M., Nishimura, O., Yoshimura, Y. and Kaidu, M., (1982), "A baseline determination between Kashima 26m and Tsukuba 5m antennas in joint VLBI experiment plan of RRL and GSI", in this issue.

Kawajiri, N.; Ojima, T.; Kawano, N.; Takahashi, F.; Yoshino, T. and Koike, K. (1979), "The first VLBI experiment in Japan", Journal of the RRL, Vol. 26, No. 119, p13-64.

Kawano, N.; Takahashi, F.; Yoshino, T. and Kawajiri, N. (1980); "Phase scintillation measurement system using real time VLBI", International IEEE/AP-S Symposium Digest, Vol. 1, J.1/AP-6, p69-72.

Kawano, N.; Yoshino, T.; Takahashi, F.; Koike, K. and Kumagai, H. (1982); "Observations of scintillation and correlated flux using the real time VLBI SYSTEM (K-2)", in this issue.

Nishi, S., Yoshimura, Y. and Komaki, K. (1982), "Control of Japanese geodetic network by VLBI", in this issue.

Takahashi, F.; Yoshino, T.; Murakami, H.; Koike, K. and Kunimori, H. (1982), "K-3 VLBI software development for international experiments", in this issue.

"VLBI experiment special issue" (1978), Review of the RRL, Vol. 24, No. 130, p443-619. (in Japanese)

INVESTIGATION OF GEOPHYSICAL CONDITIONS AT KASHIMA VLBI STATION

T.YOSHINO AND F.TAKAHASHI
Kashima Branch, Radio Research Laboratories
Ministry of Posts and Telecommunications
Kashima-Machi, Ibaraki-Ken 314, Japan

ABSTRACT

New Measurement of intercontinental baseline length between Kashima in Japan and US-operated observatories in North America, Alaska and Hawaii for geodesy, will be performed with use of the K-3 (being developed in Japan, and compatible with Mark III) and Mark III (developed in U.S.A.), starting late in 1983. And this experiment will provide us the information of plate motion between the stations, which is very useful to Japan because it is relevant to the study of generation mechanism of big earthquakes.

Before starting this experiment, various geophysical environmental data around VLBI stations should be investigated. First of all, Japan is surrounded by three plates, which are Eurasian Plate, Pacific Plate and Phillipine Sea Plate. Boundary surfaces of these plates manifest important geophysical characters. Therefore we examined the relative position of Kashima Station, Japan Trench and other plate boundaries.

Secondly, geological features at Kashima VLBI station are examined by the boring samples which were gotten at the time of antenna construction.

Thirdly the characteristics of the climate and ionosphere at Kashima are clarified. Other conditions, such as radio interference is also reported.

INTRODUCTION

Starting later in 1983, Kashima station in Japan will take part in the global VLBI network. And the experiments will be performed to get the precise baseline length, clock error parameters, earth rotation parameters etc. Generally, VLBI data includes many contributions caused by geophysical and electrical factors, such as clock error, excess path in propagation, polar motion, crustal motion etc. Among these factors, some of them can be predicted correctly, but some can not. In particular, if we do not know the local surrounding conditions in VLBI stations, we may be lead to incorrect understanding of VLBI data. Therefore we investigated the surrounding conditions which may cause much contributions.

As Japan locates on the circum-Pacific seismic belt, the relative position between Kashima station and plate boundaries, where earthquakes originate, were examined, and also investigated the

geological condition at Kashima station. And we also examined the climate and ionosphere. And as Kashima locates near Tokyo which is a great source of radiation, the radio interferences in S and X band were investigated. We hope the investigations of each VLBI stations in the world will be reported about those things in this wayr

THE LOCATION OF KASHIMA VLBI STATION

In the beginning, Fig.1(Head 1981; Ref(1)) shows the world wide plates mapr And this figure also shows the location of VLBI stations and the baseline including Kashima station on its endr There are very long baselines between Kashima and other VLBI stations; Haystack Radio Observatory, Owens Valley Radio Observatory, and so on. And Kashima VLBI station locates on almost the same latitude as those in USA. And we can realize that Kashima locates on near the plate boundary. By looking this picture, you can realize that the position of Kashima station is very useful to investigate the plate motion. If Kashima station is rejected in this figure, the information taken by VLBI experiment will decrease considerably.

The magnified map of Fig.1 is shown in Fig.2. This map shows Japan main islandsr And Kashima locates at the center of those islands. Although this is a small area, we can see three plates together in this map. Pacificr Plate, Phillipine Sea Plate, and Eurasian Plate. Kashima station looks to lie on the Eurasian Plate, but we can not entirely say that
Japan islands and Eurasian Plate are connected completely. By using more VLBI stations in Asia, it will be determined in the future. And Kashima is only 150rkm apart from Japan Trenchr Japan Trench means the subduction of Pacific Plate. And it is believed that this motion triggers the big earthquakesr

To see the land and the sea together, bathymetric chart is used in Fig.3. Kashima is about 90 km east from Tokyo. And one more characteristic thing is that Kashima station is very near the seashorer only 1.5 km apart. As the ocean loading effects are expected in Kashima, we intend to use the tide data of the tide station at the port of Kashima to correct the VLBI data. The expected value of ocean loading effect is a few centi-metersr Instead of theoretical estimation of tide data, we will use this real data in Kashima station. Because the development of industrial area near our laboratory has been going on, and the shape of the sea-bottom changes slowly, some serious error between theoretical tide data and real data will always existr

THE FOUNDATION OF KASHIMA VLBI STATION

In the geodesy in the near future, the position of VLBI station will become a important reference point. This means that the antenna reference point should correctly reflect the crustal motion of that area. It is a problem of coupling between the foundation of antenna and the lithosphere. The lithosphere has about 100 km thickness in

case of land; and it is almost composed of rock. Then it is important to investigate the connection with the foundation of antenna and the rock or the hard stratum.

Fig.4 shows a 26m antenna structure in Kashima. In the case of 26m antenna, about 5m of the portion of foundation is put into the groundr. And thirty PC-piles are driven in. The piles are 26m long. So the piles reaches to 30m depth. As the top of 26m antenna in this figure is 31m high from the ground; the height of the antenna is almost the same as the depth of pilesr The bottom view of the antenna is shown in lower side. And the weight of 26m antenna over the ground is about 1221 ton, and the one under the ground is about 1278 ton.

The soil profile under the 26m antenna(Fig.5) is shown in Fig.5, and it was surveyed by boring before antenna construction. This map shows the history of crust. Because the seashore is near here, the surface is covered with sand. But sandy and very loose stratum is not thick.
Then we can see from the top, sand soil, loam, silt clay etc. They are mainly composed of sedimentary soils. Though the ground surface is sandy, 26m antenna is built on the Diluvium which is said relatively rigid for structuresr And the N-values; which mean the hardness of soils; immediately increases at about 30m depthr That means hard stratum. As the piles reach to 30m depth, we can understand that the piles reach to this hard stratum. And the weight of antenna is dispersed to this stratum.

Japan lies on the circum-Pacific seismic belt. And about 10% earthquakes in the world has been occurred near Japan. Fig.6(a) shows the vertical cross section of earthquake distribution, and Fig.6(b) shows the earthquakes mapr We can understand from these maps that the Pacific Plate reaches to 50-100 km under the ground of Kashima. And as the rocks in Japan has generally many clefts caused by the pressure of plates, relative movement inside Japan had better be also monitored to confirm the data of plate motion. We are now planning to measure the baseline length between Kashima and GSI(Geographical Survey Institute) in Tsukuba(see Fig.3) by Laser Ranging. It is 50km apart. And it will be also measured by the VLBI method(antenna diameter; Kashima:26m, Tsukuba:5mr) And we think that the finite element method is useful to analyze the coupling of the structures and the base because we can simulate the complicated response of base with use of real data by this methodr

OTHER CONDITIONS SURROUNDING KASHIMA

VLBI observation affects many geophysical conditionsr Next we consider about the ionosphere. Fig.7 shows the geomagnetic latitude in the northern hemisphere. Geomagnetic pole is slightly different from geographic pole. Though Kashima's geographic latitude is 35 deg.; the geomagnetic latitude is 25 deg. Because the geomagnetic storm occurs in high geomagnetic latitudes, the ionosphere over

Kashima station is relatively expected calm. So we may say that if the effect of the ionospheric disturbances of delay and delay rate are detected, it is mainly caused by another station. When Kashima is the one end of baseline, we may be able to separate this ionospheric disturbances. This means that Kashima can act as a reference station of the ionospheric effect.

Then we show the Kashima's climate. The climograph is shown in Fig.8(a). It is a mean value of 5 years. And it is a typical pattern of the east side of Japan. And Fig.8(b) is the relative humidity variation in a year. Mean value at each months exceeds 50%.
And the weather is relatively moderate here.

In Fig.9 we show the radio interference in Kashima. These graphs plot the number of times radio interferences were detected in S and X band. This measurement was done by the small horn antenna. And we scanned it in all azimuth direction at low elevation angle in several hours. Radio interferences are seen more in S-band than in X-band. But we can probably avoid them in K-3 VLBI system by tuning the receiving frequency. As we must coincide the receiving frequency at all the VLBI stations, the state about the radio interferences should be informed to the scheduler before experiments.

Now, we show the features of Kashima station.

1) Location	Longitude	140°39'45".634 E
	Latitude	35°57'15".132 N
	height	77.13 m
2) Geomagnetic	Latitude	about 25°
3) Climate	Mean Temperature	15°C
	Precipitation	1248 mm/yr
4) Crust	Eurasian Plate	
	Diluvium Platform	
5) 1.5 km apart from seashore		
150 km apart from Japan Trench		
90 km apart from Tokyo		

For correct understanding of the high precision VLBI data, we think all the VLBI stations had better report these local geophysical conditions.

ACKNOWLEDGEMENT

The authors wish to thank Dr.Kawajiri and Mr.Koike, RRL, for helping us to collect these data.

REFERENCES

(1) Head,J. and Solomon,S., 1981: Tectonic Evolution of the Terrestrial Planets, SCIENCE, Vol.213, pp.62-76
(2) Earthquake Research Institute, University of Tokyo, 1982:

Microearthquake Activity in and around the Kanto district(May, 1981-October, 1981); Report of the coordinating committee for earthquake prediction, Vol.27, pp.51-62, Edited by/Geographical Survey Institute, Ministry of Construction, Japan

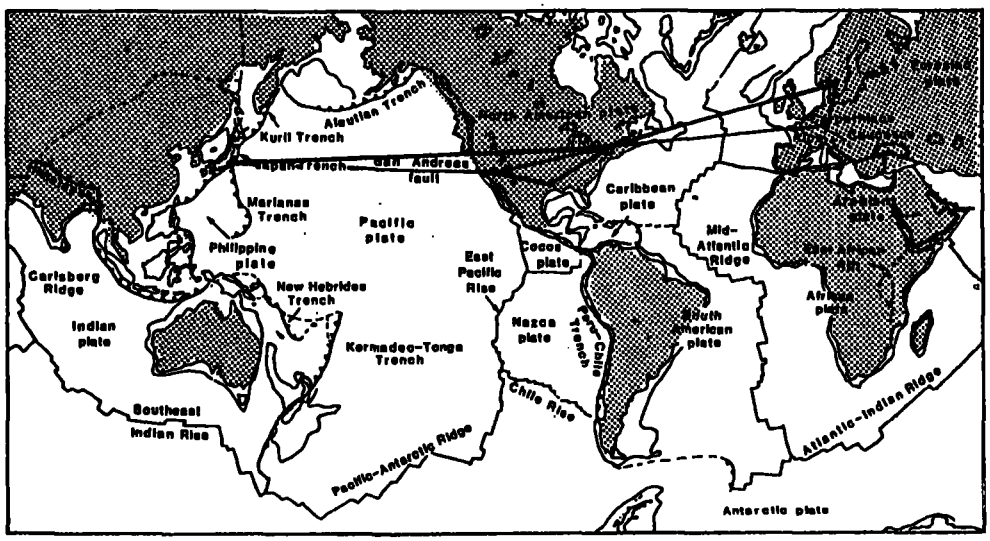

Fig.1 World Plates Map (some of baselines are drawn)

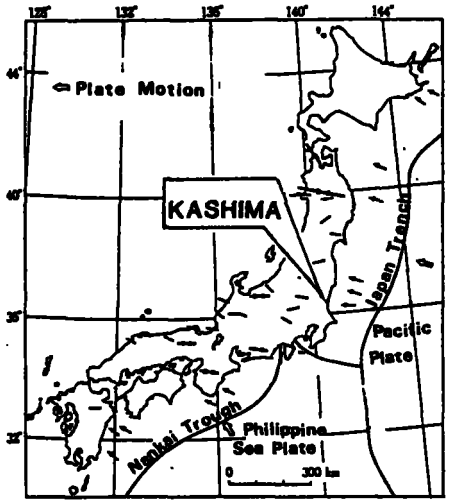

Fig.2 Japan Islands and the Plate Boundary

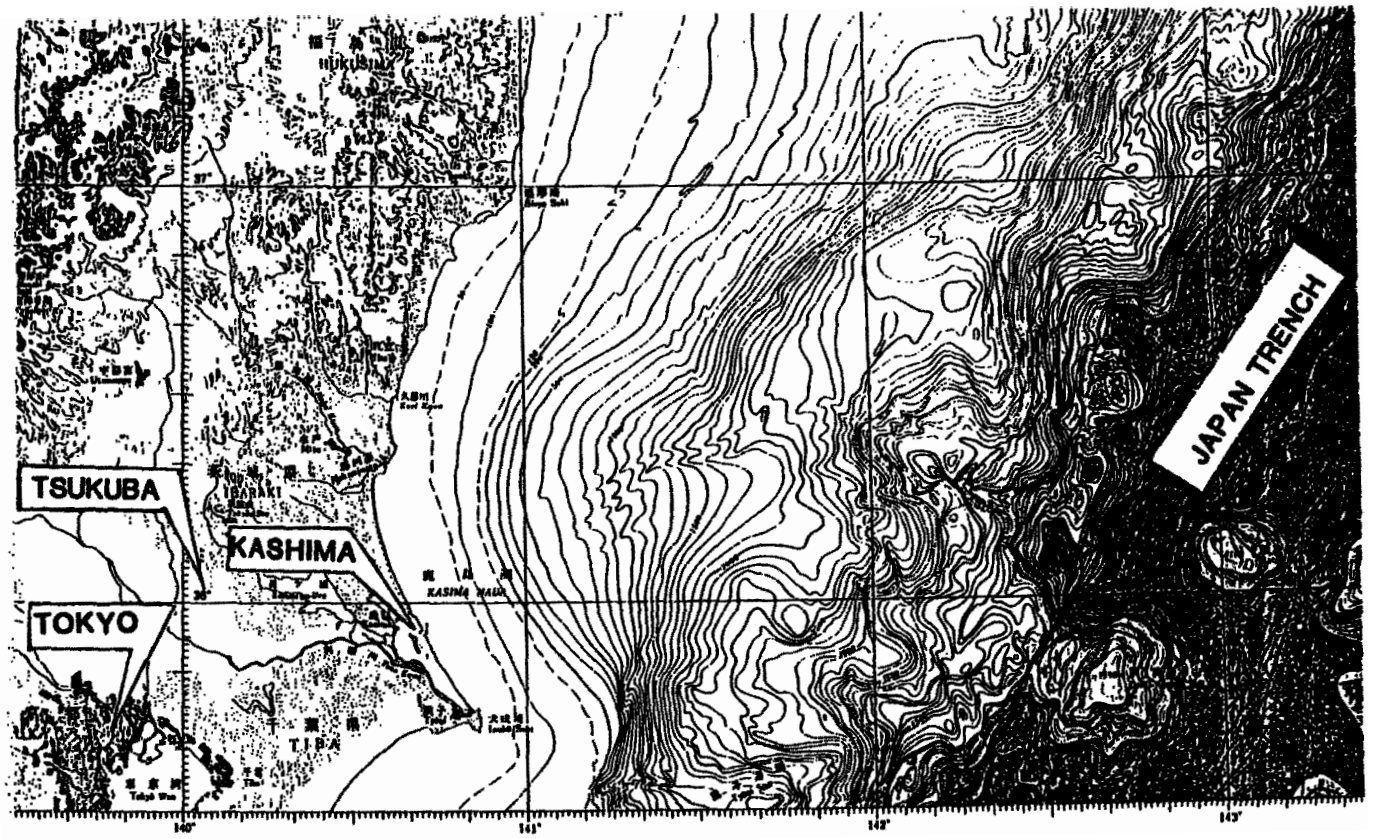

Fig.3 Bathymetric Chart

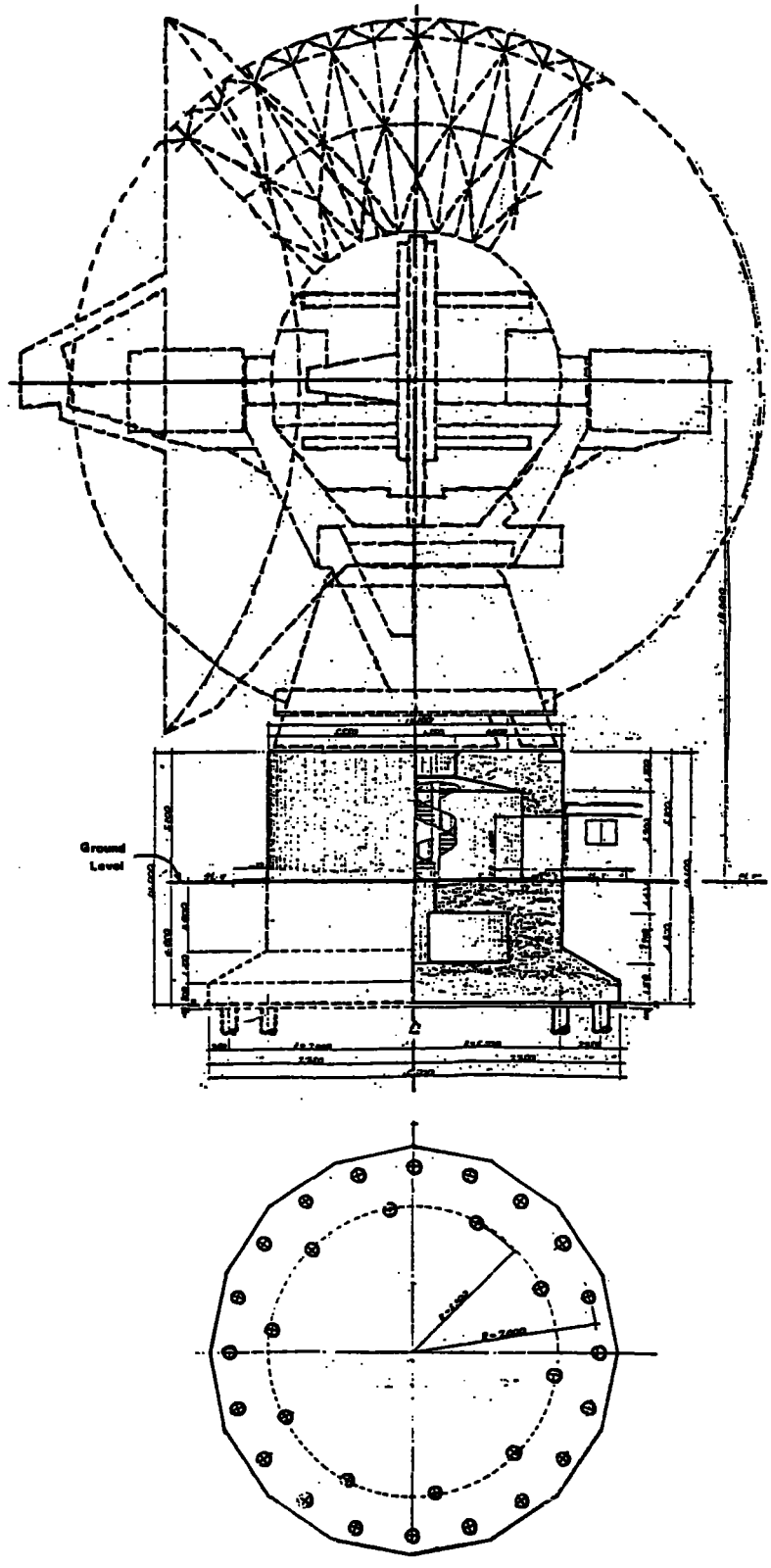

Fig.4 26m antenna structure in Kashima

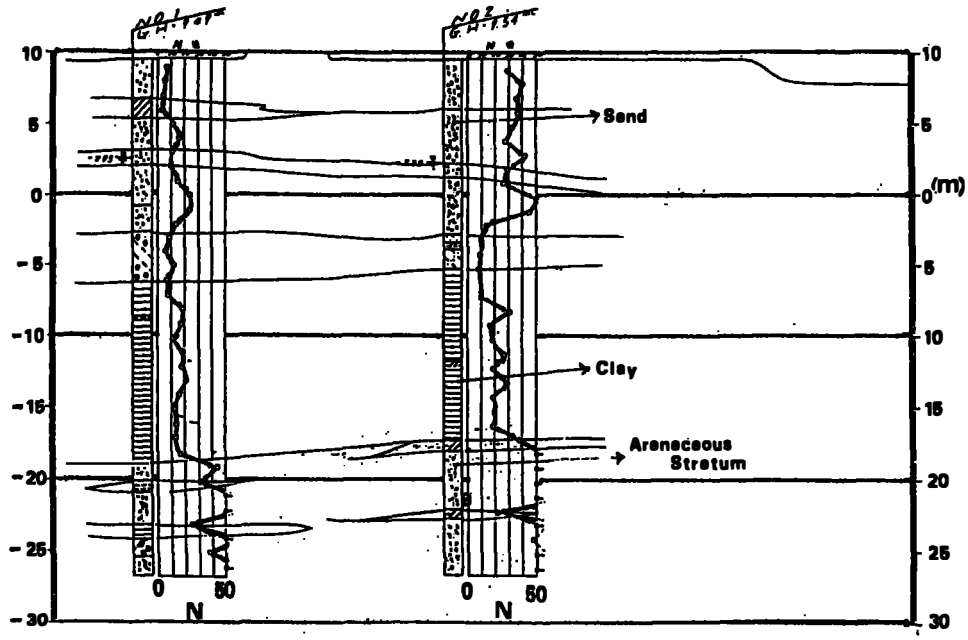

Fig.5 Soil Profile at Kashima Station

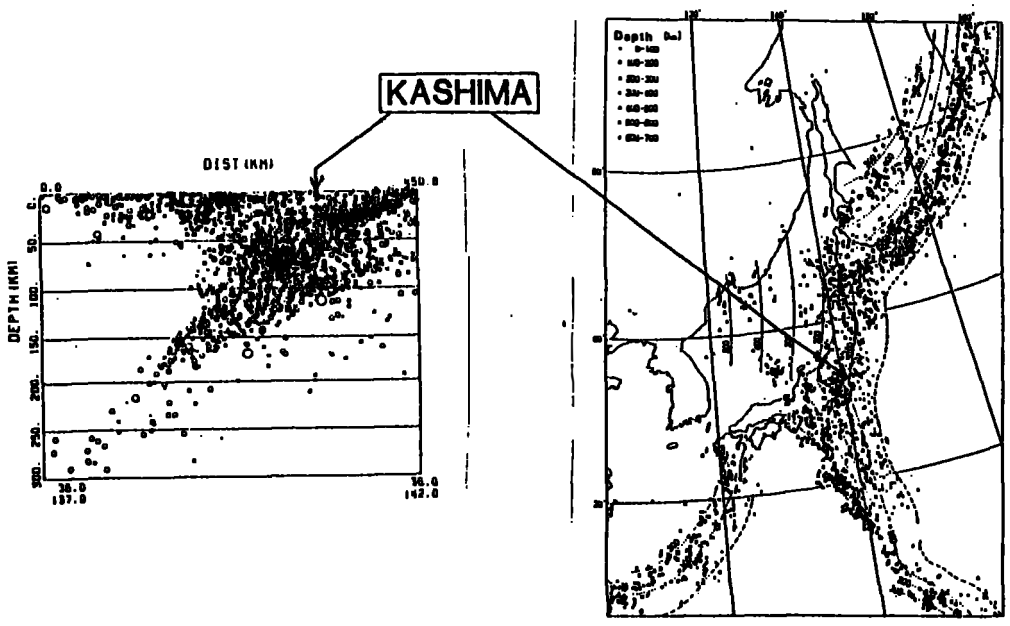

Fig.6 Earthquake Distribution Map
((a) Cross Section : Longitude 36.0°
(b) Depth of Hypocenters)

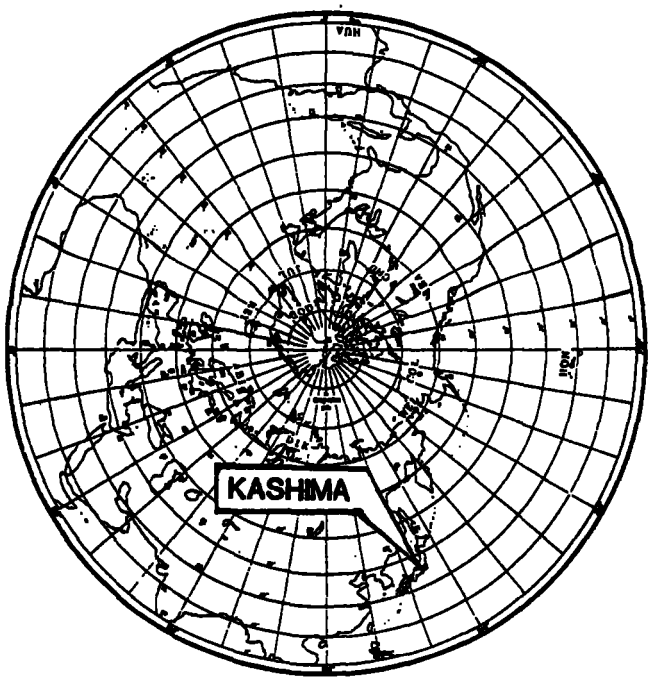

Fig.7 Geomagnetic Latitude
(geographic latitude of Kashima is about 36°,
geomagnetic latitude of Kashima is about 25°)

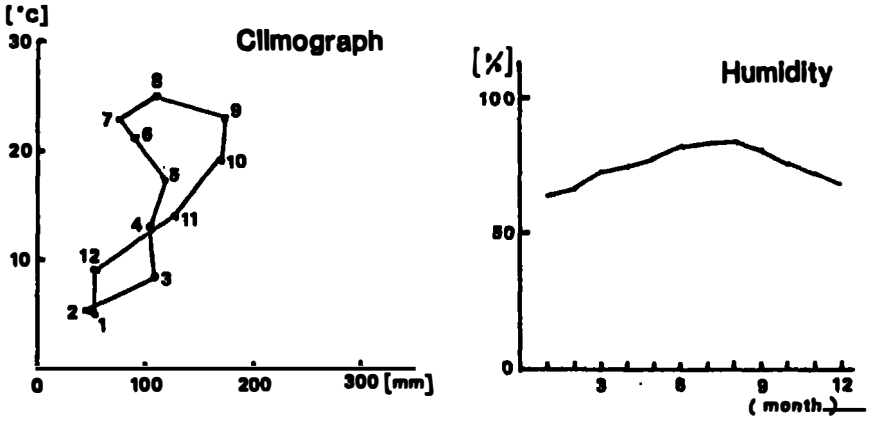

Fig.8 Climate ((a) Climograph, (b) Relative Humidity)

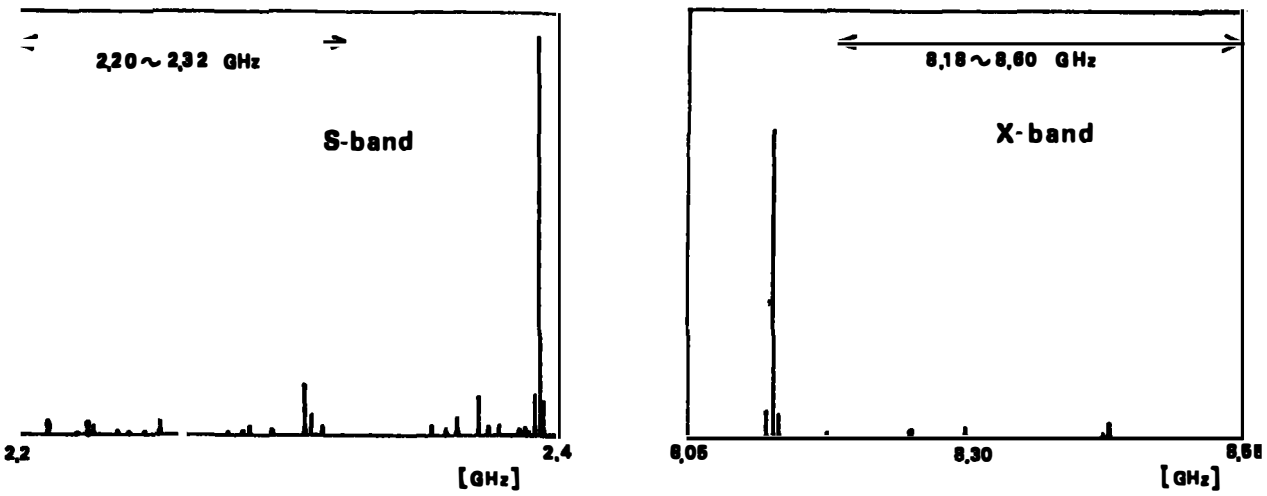

Fig.9 Radio Interference ((a) S-band, (b) X-bandr)

A BASELINE DETERMINATION BETWEEN KASHIMA 26 M AND TSUKUBA 5 M ANTENNAS IN JOINT VLBI EXPERIMENT PLAN OF RRL AND GSI

N.Kawaguchi, N.Kawajiri and N.Kawano
Kashima Branch, The Radio Research Laboratories
Kashima, Ibaraki 314 Japan

K.Yoshimura
The Radio Research Laboratories
Koganei, Tokyo 184 Japan

H.Ishii, M.Murakami, O.Nishimura, Y.Yoshimura and M.Kaidzu
Geographical Survey Institute
Yatabe, Tsukuba, Ibaraki 305 Japan

ABSTRACT. Joint VLBI experiments of RRL and GSI are planned on a baseline between Kashima and Tsukuba in 1984. The baseline of about 54 km in length will be determined in the accuracy of 2 cm or better, and compared with the data obtained seperately by laser ranging. A 26 meter antenna and a 5 meter antenna will be used in this experiment. After the establishment of the baseline between Tsukuba and Kashima, the 5 meter antenna will be transported to some principal points in Japanese islands and efficiently used for monitoring of crustal movement and adjustment of Japanese geodetic network.

INTRODUCTION

Joint VLBI experiments of RRL (The Radio Research Laboratories) and GSI (Geographical Survey Institute) are planned on a baseline length of about 54 Km between Kashima 26 m and Tsukuba 5 m antennas. This will become the first domestic VLBI experiment for geodetic application, and both institutes are preparing for their K-3 equivalent system, leading to commencement of the experiment in 1984. In this experiment, both 2 GHz and 8 GHz bands will be used for the correction against the ionospheric effects. Moreover, with use of water vapor radiometers at two frequency bands arranged at respective antenna sites, a high accuracy determination of three dimensional baseline vector will become possible, compensating for tropospheric effect. Accuracy and repeatability of the VLBI results will be confirmed, by comparison with the data obtained seperately by GSI in other means (e.g. laser ranging). After the experiments the 5 m antenna will be transported to domestic principal points for monitoring crustal movements, and adjustment of the Japanese geodetic network.

As the receiving system of 26 m antenna, including K-3 data acquisition terminal will be described in the other paper (Kawaguchi 1982), system design of 5 m antenna and the error estimation in joint VLBI experiment between RRL and GSI are mainly presented here.

BASELINE BETWEEN KASHIMA AND TSUKUBA

A geographical position of a baseline between the 26 m antenna of RRL, Kashima and the 5 m antenna of GSI, Tsukuba is shown in the Figure 1. This baseline is in Kanto district near Tokyo and is almost at the center of Japanese main islandr Estimated values of the baseline components in a fixed coordinate
system located on the earth are shown in Figure 2.

In the coordinate system, the z-axis is defined by an instantaneous rotation axis of the earth, the x-axis is on a equatorial plane and perpendicular to a local meridian surface and y-axis completes the right-handed Cartesian coordinate system. In Figure 2, Ω is lateral orientation angle of the baseline from due east, ξ complementaly angle of latitude, λ_0 longitude of middle point of the baseline, and φ_0 latitude of the middle point.

The baseline has about 54 km in length and almost east-west direction, and these values in Figure 2 will be refined by conventional surveys before and after VlBI experiments going on for one year in 1984. The surveys will be conducted by GSI and have the accuracy of about 5 cm by using a Laser Ranging method. The VLBI experiments will be conducted by RRL in coopora-tion with GSI, and the accuracy and repeatability of the VLBI experiments will be confirmed by comparison with the convensional survey resultsr

After a series of the VLBI experiments, the 5 m antenna will be trans-ported to some domestic principal points for monitoring crustal movement and adjustment of the Japanese geodetic network. The control of Japanese geodetic networkr by detail ishiyet al. 1982) in this issuer

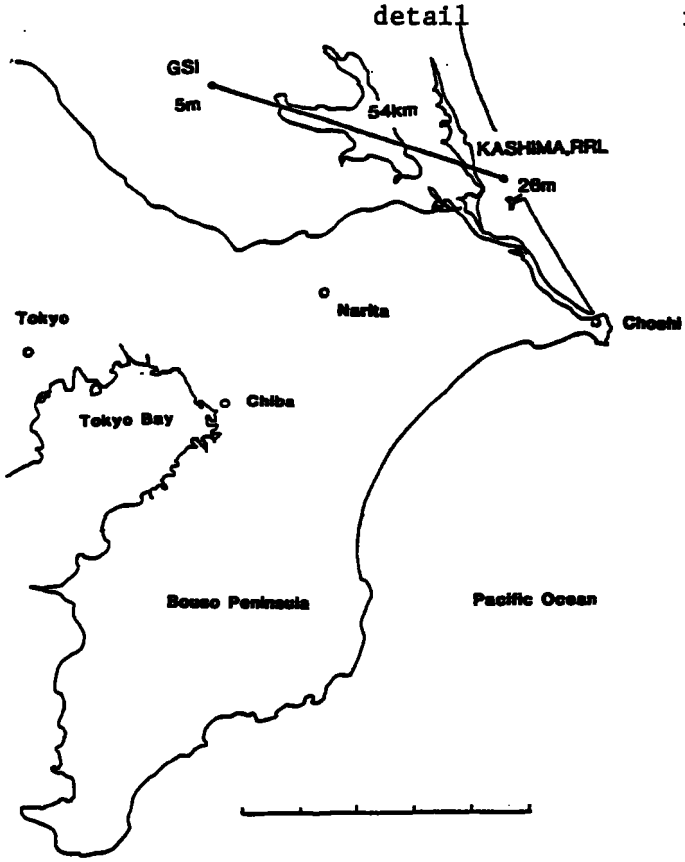

Figure 1. The geographical position of the RRL-GSI baseline

5M ANTENNA AT TSUKUBA

Geographical Survey Institute is responsible for the geodetic survey on whole land area in Japan. VLBI is considered to be able to contribute to improvement of the geodetic network of Japan and also be able to contribute to detection of tectonic plate motion in and around Japan.

As the first step of geodetic application of VLBI in Japan, joint VLBI experiment between GSI and RRL is planned. For geodetic application, it is desirable that the system has transportable receiving station. GSI has been developing transportable receiving station in three years program. In 1981, the first year of the program, GSI has designed and completed mechanical part of the antenna. The specifications of this antenna are listed in Table 1. Bandwidth, polarization and number of channels are selected considering compatibility with K-3 system.

To achieve high efficiency; there used shaped beam cassegrain antenna. As for transportability, the antenna can be devided into 3 parts, Antenna, Mount structure and Pedestal. The antenna (main dish) can be devided into 3 parts, so as to reduce the width of all the parts less than 3m. The side view of the antenna is illustrated in Figure 3. Three days at maximum are required to disassemble the antenna and three vehicles including 10-ton lolly and 10-ton crane will be used for transportation. At the next station, ten days at maximum are required to re-assemble the antenna and start observation. It is required there should not occur any significant failure in normal transportation.

Table 1. The specification of the 5m antenna

Items	specification
Antenna diameter	5 meter
Frequency range	X-band : 8180-8600 MHz S-band : 2220-2320 MHz
Polarization	RHCP X- and S-band
Antenna efficiency (Gain)	X-band 61 %(50.7 dB at 8390 MHz) S-band 32 %(36.5 dB at 2260 MHz)
Antenna noise temperature	X-band : 45 K (Elevation 45°) S-band : 120 Kr
VSWR	1.3 X and S-band
Axial ratio	3 dB X and S-band
Slew rate	Azimuth 0 to 1 deg/sec Elevation 0 to 0.5 deg/sec
Angle readout (resolution)	0.002 degree

26 M ANTENNA SYSTEM AT KASHIMA

A schematic sketch of the 26 m antenna together with the performance of the antenna and the S/X receivers are shown in Figure 4. For further details, refer to another paper (Kawaguchi,et al. 1982) in this issue.

DATA ACQUISITION

The VLBI data will be collected by a K-3 data acquisition terminal and a wideband data recorder at each station. The K-3 data acquisition terminal is mainly composed of an IF distributor, IF to video frequency converters (video converters), a formatter and a decoderr By video converters, two of seven video signals are frequency-converted from S-band and five from X-bandr These video signals of 2 MHz bandwidth are sampled in one bit at a rate of 4 Mbps and formatted together with a time code and a sync word. The formatted data at a rate of 4.5 Mbps (a parity bit is added to each 8 data bits) are recorded on seven tracks of tapes by a K-3 wideband data recorder. As a tape has 28 tracks, two round trips recording is possible for a reel of tape. A decoder is always used for monitoring the quality of data being obtained during the experiment.

Cable delay variation will be measured seperately by a K-3 delay calibrator, and tropospheric delay caused by water vapor will be estimated from sky noise measurements. The sky noise temperature due to water vapor along a ray path will be measured by a K-3 water vapor radiometer at two frequencies near the water-vapor-emission line of 22.2 GHzr

For a frequency standard in each station, a hydrogen maser oscillator will be used, and a cesium oscillator keeps the clock of each station and synchronized by a portable clock.

The VLBI experiments are fully automated under controls of a Kashima Automatic Observing Software (KAOS) and only two or three operators are needed at each station.

The detailed information about the K-3 hardware system is presented in the paper (Kawaguchi,et al. 1982) and the K-3 Automatic Observing Software is explained in the other paper (Takahashi,et al. 1982)r

ERROR ESTIMATION

The obtained data will be cross-correlated by a correlation processor at Kashima (Kawaguchi,et al. 1982) and analyzed by both institutes of RRL and GSI. Here, we will discuss a baseline determination error on this VLBI experiment.

The observation error due to system noise, tropospheric scintillation and clock instability, the correction error of cable delay and tropospheric delay, and the calculation error of the source position, polar motion and earth rotation are estimated as summarized in Figure 5. In the error due to system noise, the coherence loss of 50 percent is taken into account, the items of which are tabulated in Table 2. In the estimation, it is assumed that the integration time is 12 minutes for 12 weak sources and 4 minutes for 2 strong sources of 3C84 and 3C273. The correlated flux of these sources are cited from the reference (Wu 1980)r It is also assumed to use a bandwidth synthesis technique on five channels in X-band and two channels in S-band spanning 300 MHz and 100 MHz, respectively.

The tropospheric scintillation is calculated by using an empirical equation derived from observations of two strong satellite noise emission by a real-time VLBI (Kawano,et al. 1982).

The sensitivity of a sky noise error measured by a water vapor radiometer to a estimation error on a wet path length and of a surface pressure error measured by a pressure gauge to a estimation error on a dry path length are referred to the papers (Wu 1979) and (Moran,et al. 1976), and each estimation error is calculated on the assumption of 1 K and 0.2 mbar measurement error for each device.

As for other error sources, the errors listed in Table 3 are assumed. The total O-C error averagedr over one-day observations will be about 62 picoseconds and the resultant baseline determination errors on X,Y and Z components are estimated as shown in Figure 6. Each point in the figure represents the error when the three dimensional baseline components together with 12 clock offset parameters are determined from 32 observations. From the figure, it will be assured that the accuracy of about 2 cm or better may be attainable in the VLBI experiment on the baseline between Kashima and Tsukuba.

CONCLUSION

The VLBI results and the surveys by a Laser Ranging Method, each having the accuracy of about 2 cm and 5 cm, will be compared with each other and the geodetic referece baseline will be established between Kashima and Tsukuba in 1984. The repeatability of the VLBI experiments and the reliability of the K-3 VLBI system will also be confirmed on this baseline, and then the 5 m antenna will be transported to principal points in Japan and become a powerful tool for monitoring of crustal movement and adjustment of Japanese geodetic network.

ACKNOWLEDGMENT

We would like to thank many VLBI researchers in Jet Propulsion Laboratory, Haystack Observatory, Goddard Space Flight Center and NASA for their kind helps and encouragements in various fields of VLBI.

References

Kawaguchi,N.,Sugimoto,Y.,Kuroiwa,H.,Kondo,T.,Hama,S.,Amagai,J.,Morikawa,T. and Imae,M.,1982: The K-3 hardware system being developed in Japan and its capability, in this issue.

Kawano,N.,Yoshino,T.,Takahashi,F.,Koike,K. and Kumagai,H.,1982: Observation of scintillation and correlated flux using the real-time VLBI system, in this issue.

Moran,J.M.,Penfield,H.,1979: Test and Evaluation of Water Vapor Radiometers and Determination of their Capability to Measure Tropospheric Propagation Path Length, NASA Technical Report, NAS5-20975.

Nishi,S.,Yoshimura,Y. and Komaki,K.,1982: Control of Japanese geodetic network by VLBI, in this issue.

Takahashi,F.,Yoshino,T.,Murakami,H.,Koike,K. and Kunimori,H.,1982: K-3 VLBI software development for internationaloexperiment, in this issue.

Wu,S.C.,1979: Optimum Frequencies of a Passive Microwave Radiometer for Tropospheric Path-Length Correction,IEEE transaction,AP-27,No.2.

Wu,S.C.,1980: Error Estimation for ORION Baseline Vector Determination,TDA Progress Report,42-57,Page 16.

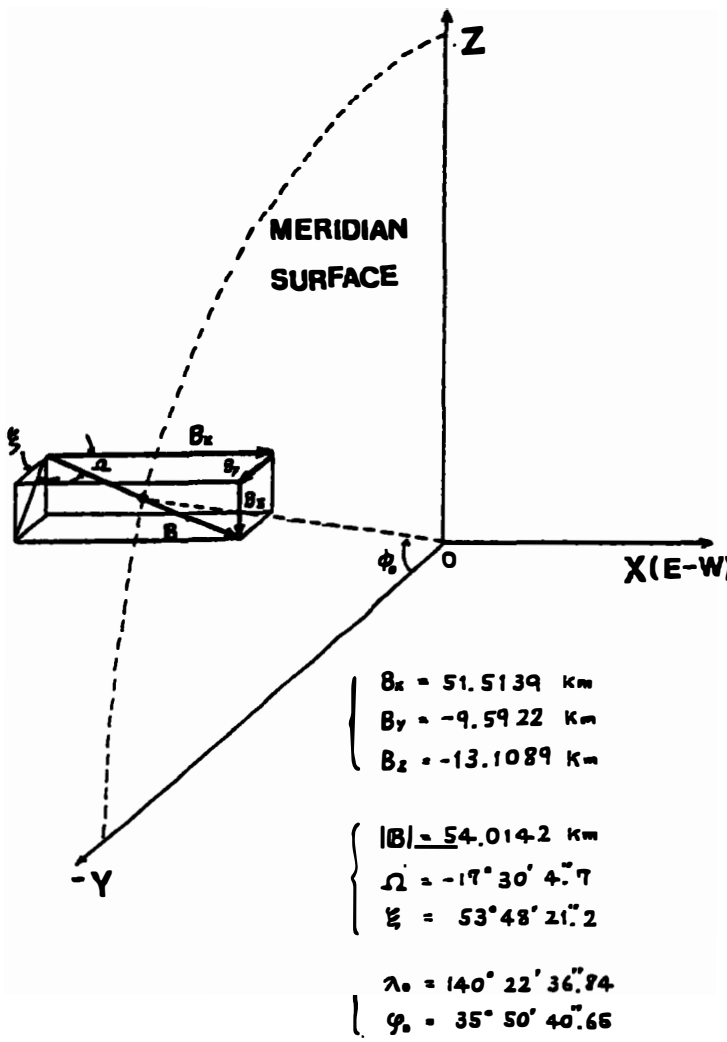

Figure 2. Predicted values of three dimensional baseline components

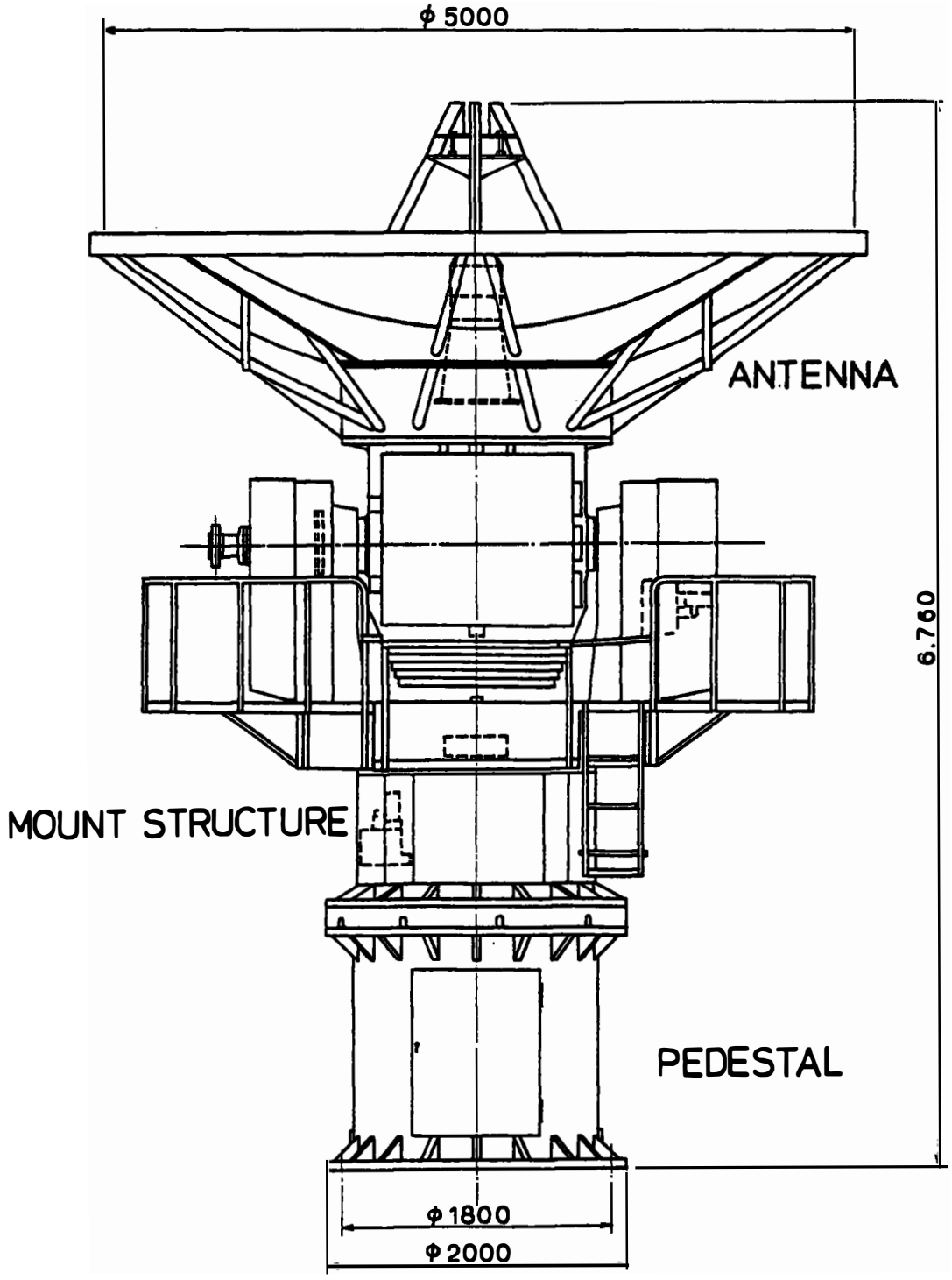

Figure 3. The schematic sketch of the 5m antenna

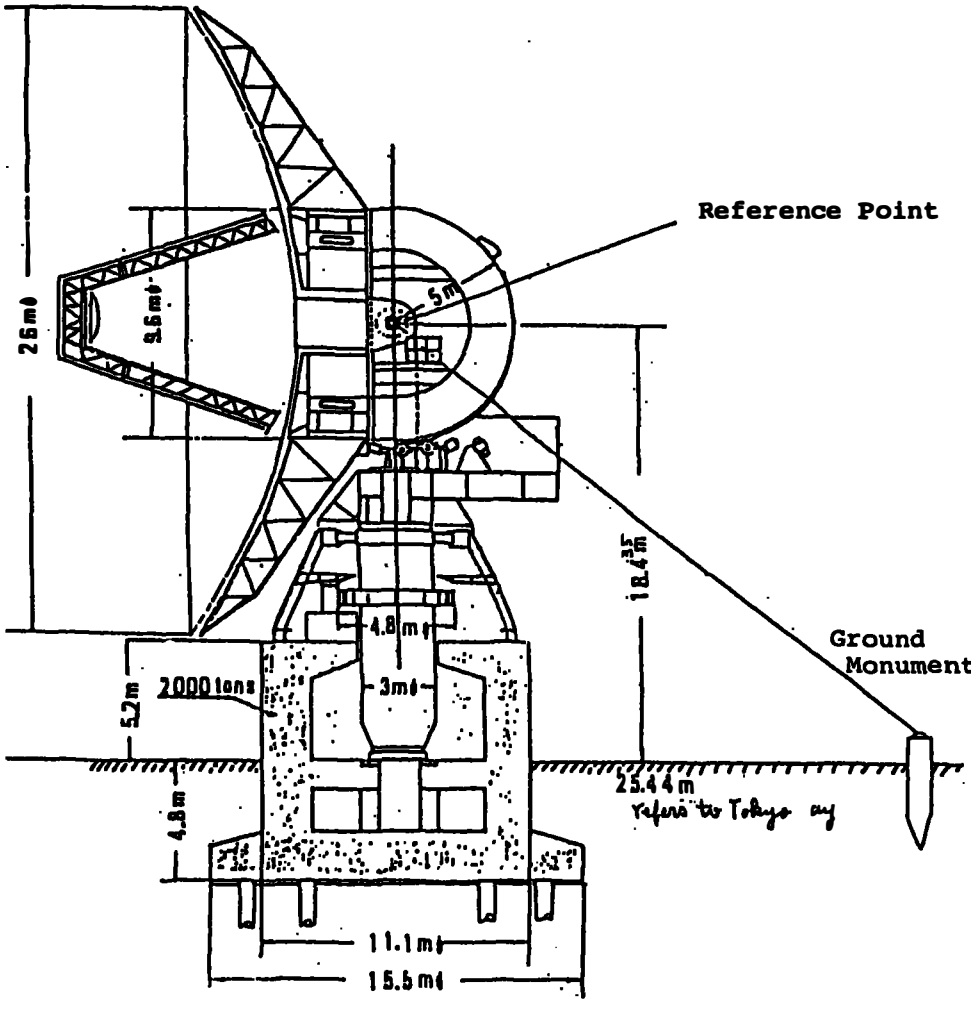

Frequency	2220-2320MHz	
Antenna Gain	52.8 dB	63.2 dB
(efficiency)	(53.6 %)	(45.2 %)
(feed loss)	(0.5 dB)	(0.4 dB)
Antenna noise temp.	70 K	60 K
Pre-amp noise temp.	100 K (FET)	100 K (parametric)
(NF)	(1.2 dB)	(1.0 dB)
(WG loss)	(6 K)	(25 K)
Total G/T	30.5 dBK	41.2 dBK

Figure 4. The schematic sketch of the 26 m antenna and performance of the antenna and S/X receivers

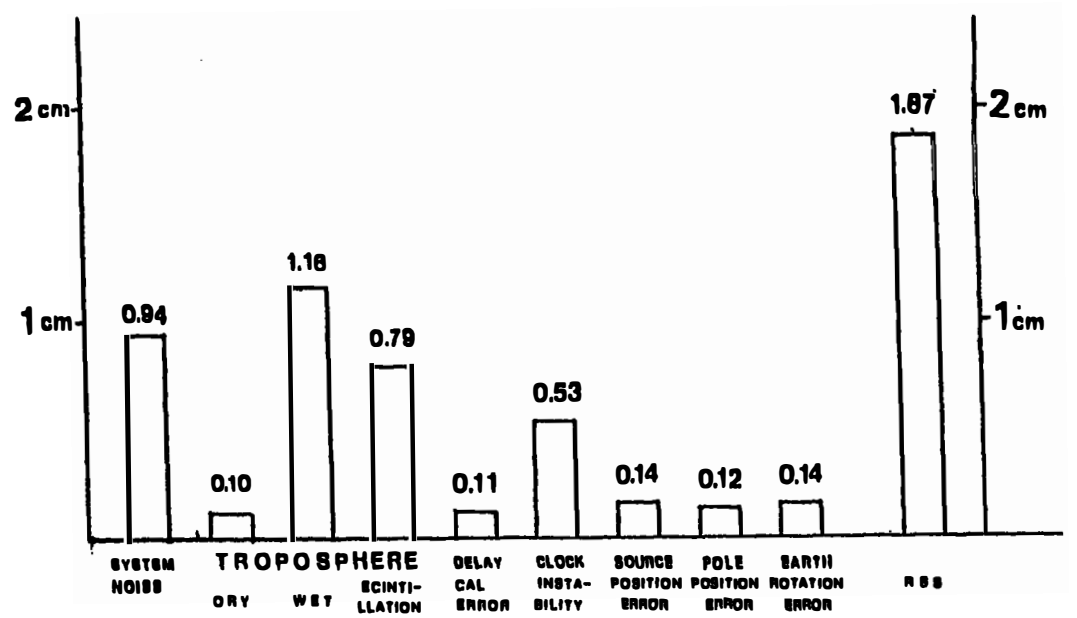

Figure 5. The estimated O-C error averaged over one-day observations

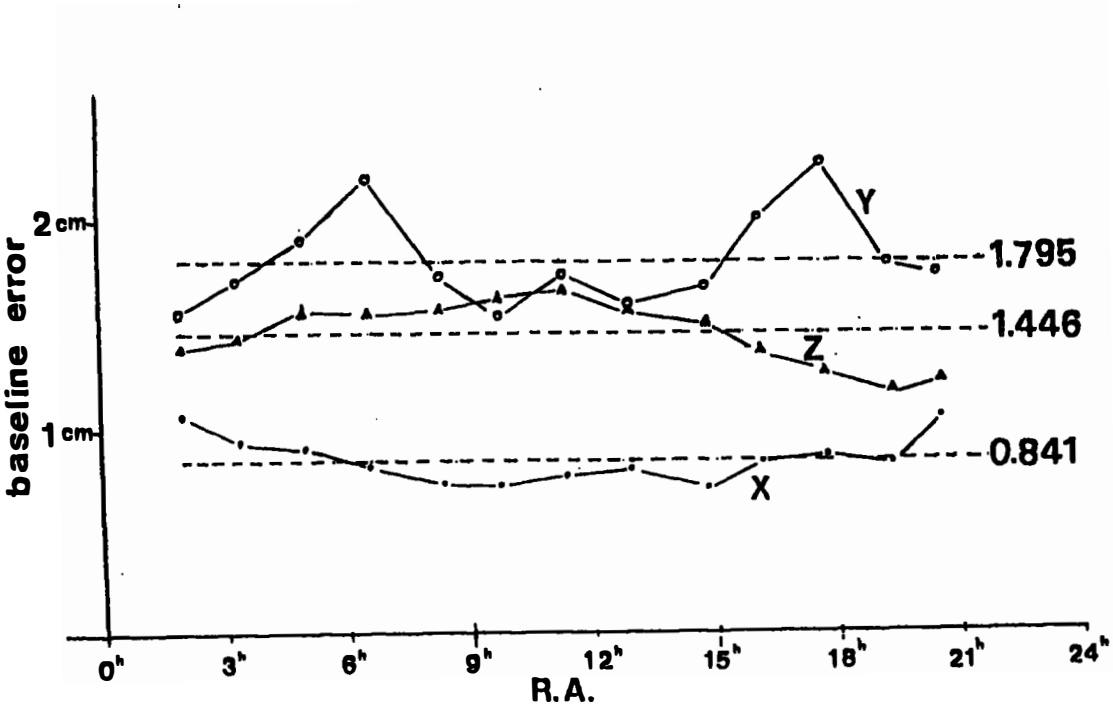

Figure 6. Three dimensional baseline determination error

Table 2. Items of coherence loss

Equipment	Loss Factor	Loss
Frequency Converter	Frequency instability	0.6 %
Image Rejection Mixer	Imperfect image rejection	1 %
Low Pass Filter	Imperfect filtering	3 %
Formatter	Imperfect clipping	1 %
	One bit sampling	36 %
Wideband Data Recorder	Bit error	1 %
Correlation Processor	Fringe stopping	4 %
	Fractional bit correction	3.4 %
Total Loss		50 %

Table 3. Items of error sources

Error sources	Error
For Calculation Error	
Source Position Error	0.01/SQRT(2)
Earth Rotation Error	0.6 msec
Pole Position Error	30 cm
For Correction Error	
Pressure Guage Error	0.2 mbar
Water Vapor Radiometer Error	1 K
Delay Calibrator Error	1 sec at 25 Hz
For Clock Instability	
Allan Variance of White Frequency Noise	10^{-13} at 1 sec
Allan Variance of Flicker Frequency Noise	10^{-14} over 100 sec

☆U.S. GOVERNMENT PRINTING OFFICE: 1983-380-997/2375